



PHD

**Novel methodologies for the synthesis and characterization of sulfinamides and vinyl esters**

Groleau, Robin

*Award date:*  
2021

*Awarding institution:*  
University of Bath

[Link to publication](#)

**Alternative formats**

If you require this document in an alternative format, please contact:  
[openaccess@bath.ac.uk](mailto:openaccess@bath.ac.uk)

Copyright of this thesis rests with the author. Access is subject to the above licence, if given. If no licence is specified above, original content in this thesis is licensed under the terms of the Creative Commons Attribution-NonCommercial 4.0 International (CC BY-NC-ND 4.0) Licence (<https://creativecommons.org/licenses/by-nc-nd/4.0/>). Any third-party copyright material present remains the property of its respective owner(s) and is licensed under its existing terms.

**Take down policy**

If you consider content within Bath's Research Portal to be in breach of UK law, please contact: [openaccess@bath.ac.uk](mailto:openaccess@bath.ac.uk) with the details. Your claim will be investigated and, where appropriate, the item will be removed from public view as soon as possible.



# **Novel methodologies for the synthesis and characterization of sulfinamides and vinyl esters**

**Robin Rupert Groleau**

*A thesis submitted for the degree of Doctor of Philosophy*

Department of Chemistry

University of Bath

May 2021

## **COPYRIGHT**

Attention is drawn to the fact that copyright of this thesis rests with the author. A copy of this thesis has been supplied on condition that anyone who consults it is understood to recognise that its copyright rests with the author and that they must not copy it or use material from it except as permitted by law or with the consent of the author. This thesis may be made available for consultation within the University Library and may be photocopied or lent to other libraries for the purposes of consultation.

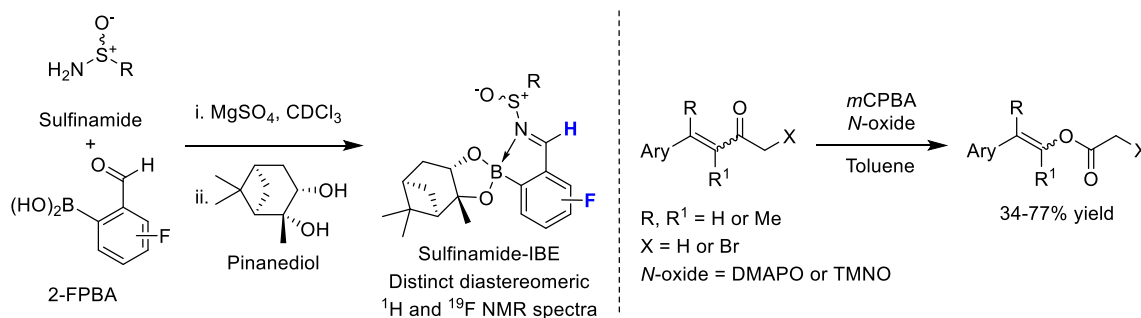
## ABSTRACT

The first chapter of this thesis begins by introducing methods for determining enantiopurity, followed by an in-depth discussion of how three-component self-assembly reactions between an amine, a chiral analyte, and 2-formylphenyl boronic acid (2-FPBA) can be used to produce stable iminoboronate ester (IBE) complexes. The extensive use of these three-component IBE assemblies for determining the enantiomeric excess of a range of chiral analytes using various analytical methods is discussed. A detailed review of the growing popularity of these supramolecular assembly motifs for formation of supramolecular stimuli-responsive materials and for the orthogonal derivatization of biomolecules is also described.

Chapter 2 describes how  $^1\text{H}$  NMR spectroscopic analysis of IBE complexes derived from 2-FPBA, *tert*-butanesulfinamide, and BINOL revealed previously unknown concentration- and enantiopurity-dependent anisotropic effects. Unlike previous IBEs, decreased  $\text{N} \rightarrow \text{B}$  coordination in BINOL-derived sulfinamide-IBE complexes results in their significant aggregation in solution. These aggregates contain mixtures of homochiral and heterochiral complexes, which means that chemical shift values in their  $^1\text{H}$  NMR spectra are dependent on the enantiopurity of the parent chiral sulfinamide, giving rise to a phenomenon termed in this thesis *diastereomer aggregation-induced anisotropy* (DAIA).

Chapter 3 describes the optimisation of a new stepwise Bull-James protocol for accurately measuring the enantiopurity of chiral sulfinamides using three-component complexes derived from chiral pinanediol and 2-FPBA. This derivatisation approach affords a highly reliable protocol to determine the enantiomeric excess of a wide range of sulfinamides by  $^1\text{H}$  NMR spectroscopic analysis. Use of a fluorinated 2-FPBA template also enables the enantiomeric excess of chiral sulfinamides to be determined by  $^{19}\text{F}$  NMR spectroscopic analysis. Preliminary results on development of a new Bull-James derivatisation protocol to determine the enantiomeric excess of sterically-demanding  $\alpha$ -quaternary amines are also described.

The fourth chapter describes investigations into using *N*-oxides (*e.g.* dimethylaminopyridine-*N*-oxide) as catalysts in Baeyer-Villiger (BV) oxidation reactions of ketones and  $\alpha,\beta$ -unsaturated ketones for the efficient production of esters and vinyl esters. Mechanistic studies have revealed that *N*-oxides act as proton and phase-transfer catalysts in the BV oxidation reactions of electron-rich ketones. These *N*-oxides function to accelerate nucleophilic delivery of *m*CPBA to the ketone carbonyl, whilst also suppressing epoxidation reactions of vinyl ester products. The discovery that *N*-oxides can catalyse degradation of the *m*CPBA oxidant resulted in trimethylamine *N*-oxide being identified as an improved 2<sup>nd</sup> generation catalyst for the BV oxidation of  $\alpha,\beta$ -unsaturated ketones.



## ACKNOWLEDGEMENTS

For their help, support, guidance, and everything else, I would like to thank a number of people, as well as apologise in advance for anyone I may miss out – you are neither forgotten nor unappreciated, you are an unlucky casualty of me writing my acknowledgments at the last minute.

First and foremost, I would like to thank my supervisor Prof. Steven D. Bull, without whom none of my accomplishments throughout my PhD would have been possible. From ‘nudging’ (grooming?) me towards the Catalysis CDT at the very beginning, to bringing me into his group and providing me with a wealth of advice, support, expertise, inspiration, and mentorship, Steve guided me through the last four years, and helped me along my first real steps into academia and scientific research. Add beer, banter, and the odd fancy meal, and I couldn’t have wished for a better PhD supervisor. Thank you Steve, for everything.

Working for Steve of course means working in the Bull and James groups, and my next set of thanks are owed to all of those I have worked with in and around 1S 1.28 over the years. I would like to thank past group members Dr Bill Cunningham, Dr Rob Chapman, Dr Maria Webber and Dr Maria Odyniec, who welcomed me into the group with open arms and made my time in the lab an enjoyable one. I would also like to thank the many members of the Cresswell group for taking me in as an honorary member, in particular Alison and Anna, who started their PhD journey at the same time as me. I would also like to thank my second supervisor Dr Marc van der Kamp, as well as Dr Natalie Fey, Dr Alex Cresswell, and Prof. Tony James whose advice and collaboration have been invaluable. Thank you also to Dr James Taylor and Prof. John Fossey for a thought-provoking, thorough, and thoroughly enjoyable PhD *viva*. I also want to acknowledge the many undergraduate students I supervised (Miles, Emma G, Emma P, David, Jack, Matteo, and Tommy).

Most importantly, I wish to thank Dr Josh Tibbetts and Ben Emery, (and Idris), the ‘Bull Boys’, for their support, friendship, HMLs, puns, and everything in between. I simply cannot imagine completing my PhD without them.

Thanks are of course due to the entirety of the research support team here in Bath. I would like to thank Dr Gabriele Kociok-Köhn for the crystal structures in this thesis, Dr Shaun Reeksting for his endless help and training in Mass Spectrometry, and of course Dr Catherine Lyall and Dr John Lowe, the most knowledgeable, helpful, and patient NMR team one could have asked for. Particular thanks to John, who seemed to be able to provide an endless stream of highly customisable and specific NMR experiments for whichever weird property of my molecules I wanted to probe next (most of which never even made it into my thesis!).

Thanks are also due to the EPSRC for funding my PhD work through the Bath, Bristol, Cardiff CDT in Catalysis, and I would also like to extend thanks to everyone involved in the CDT for their help. Particular thanks to the Bath cohort 3 Alba, Callum and Ioli. I also want to mention Dr Jon Hall, another CDT alumnus, whose company and support over the years has been invaluable.



I must also thank all of my friends and family, both for the support during my PhD, but also for everything that came before, and for putting up with my obsessive fascination with science. Special mention to Will, Alex, Chris, Rachel and Dean, thanks for always being there. I want to thank my parents Emma and Pierre Groleau for giving me the wonderful childhood and education that allowed me to reach this stage in my life, and for fostering my love of science from as early as I can remember.

And last but not least, my biggest thanks go to my wonderful fiancée Dr Grace Pearson, who deserves far more praise than I can put into words. Without her by my side none of this would have been possible - your constant reassurance was a lifeline during the hard bits, and your encouragement and love drove me forward. Thank you for always being there and for putting up with me for the last 7 years.

I've always wanted to be a scientist; I can't believe I get to be one now.

## ABBREVIATIONS

$\Delta\delta$ :	chemical shift difference	IBE:	iminoboronate ester
2-APBA:	2-acylphenylboronic acid	IR:	infrared
2-FPBA:	2-formylphenylboronic acid	LC:	liquid chromatography
3HQ:	3-hydroxyquinolin-2(1H)-one	LDA:	linear discriminant analysis
Aib:	aminoisobutyric acid	LDAO:	lauryl- <i>N,N</i> -dimethylamine <i>N</i> -oxide
ATRP:	atom transfer radical polymerization	LSR:	lanthanide shift reagent
BHS:	boron hot spot	<i>m</i> CBA:	<i>meta</i> -chlorobenzoic acid
BINAM:	1,1'-binaphthyl-2,2'-diamine	<i>m</i> CPBA:	<i>meta</i> -chloroperbenzoic acid
BINOL:	1,1'-bi-2-naphthol	MLCT:	metal-to-ligand charge transfer
Boc:	<i>tert</i> -butoxycarbonyl	MO:	molecular orbital
BV:	Baeyer-Villiger	MOF:	metal-organic framework
CAN:	ceric ammonium nitrate	MS:	molecular sieves
CAPE:	caffeic acid phenyl ester	<i>MW</i> :	molecular weight
CD:	circular dichroism	NMO:	<i>N</i> -methylmorpholine <i>N</i> -oxide
CDA:	chiral derivatizing agent	NMR:	nuclear magnetic resonance
CSA:	chiral solvating agent	nOe:	nuclear Overhauser effect
CSR:	chiral shift reagentCuAAc: Cu <sup>I</sup> - catalysed azide/alkyne cycloaddition	NOESY:	nOe spectroscopy
DAIA:	diastereomer aggregation-induced anisotropy	OEG:	oligo(ethylene glycol)
<i>de</i> :	diastereomeric excess	PAA:	peracetic acid
DIBAL-H:	diisobutylaluminium hydride	PBA:	perbenzoic acid
DLS:	dynamic light scattering	PCA:	principal component analysis
DMAP:	<i>N,N</i> -dimethyl-4-aminopyridine	PDRA:	post-doctoral research associate
DMAPO:	DMAP <i>N</i> -oxide	PE:	petroleum ether 40-60 °C
DNB:	1,4-dinitrobenzene	PEG:	polyethylene glycol
DOAP:	<i>N,N</i> -dioctyl-4-aminopyridine	PeT:	photoinduced electron transfer
DOAPO:	DOAP <i>N</i> -oxide	PGMA:	poly(glycerol methacrylate)
DOSY:	diffusion-ordered spectroscopy	pHEMA:	polyhydroxyethylmethacrylate
DPMS:	diphenylmethylsilyl	PNO:	pyridine <i>N</i> -oxide
<i>dr</i> :	diastereomeric ratio	PPGBC:	polypropylene glycol bis carbonateppm: parts per million
<i>ee</i> :	enantiomeric excess	PTC:	phase-transfer catalyst
equiv.	equivalents	<i>rac</i> :	racemic
<i>er</i> :	enantiomeric ratio	<i>R<sub>hyd</sub></i> :	hydrodynamic radius
ESDA:	enantioselective self- disproportionation on achiral phase	RNA:	ribonucleic acid
FI:	fluorescence intensity	RNS:	reactive nitrogen species
FRET:	Förster resonance energy transfer	ROS:	reactive oxygen species
FTIR:	Fourier transfer IR	<i>scf</i> :	scaemic
G:	guanosine	SDE:	self-disproportionation of enantiomers
GC:	gas chromatography	SIBE:	sulfiniminoboronate ester
HPLC:	high-performance liquid chromatography	SIDA:	self-induced diastereomeric anisochronism
HRMS:	high resolution mass spectroscopy	SIRE:	self-induced recognition of enantiomers
HWE:	Horner-Wadsworth-Emmons	Strp:	streptavidin
IB:	iminoboronate	<i>t</i> 3PGAME:	<i>trans</i> -3-phenylglyceric acid methyl ester
		TetMB:	1,2,4,5-tetramethylbenzene

TetMB: tetramethylbenzene  
TFA: trifluoroacetic acid  
TMB: trimethoxybenzene  
TMNO: trimethylamine *N*-oxide  
TMS: tetramethylsilane  
TPAP: tetrapropylammonium  
perruthenate

UV: ultraviolet  
UV-Vis: ultraviolet-visible  
VANOL: 3,3'-diphenyl-2,2'-bi-1-naphthol  
VAPOL: 2,2'-diphenyl-(4-biphenanthrol)

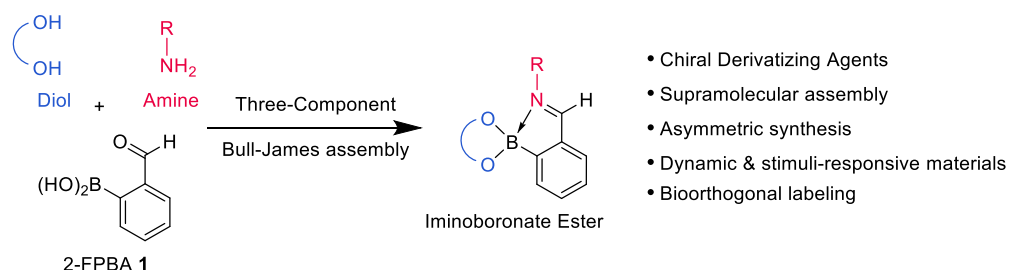
## TABLE OF CONTENTS

Abstract.....	II
Acknowledgements.....	III
Abbreviations.....	V
Table of Contents.....	VII
1. The Bull-James assembly: efficient iminoboronate complex formation for chiral derivatization and supramolecular assembly .....	1
1.1. Methods for determining enantiomeric excess.....	1
1.2. Inception of the Bull-James three-component derivatization approach.....	10
1.3. Discovery and structural features of the Bull-James assembly .....	12
1.4. Three-component assembly for determining <i>ee</i> by NMR spectroscopic analysis.....	17
1.5. Three-component assembly for determining <i>ee</i> by optical methods .....	37
1.6. Three-component assembly for electrochemical determination of the <i>ee</i> of BINOL .....	44
1.7. IBE assemblies as synthetic tools.....	45
1.8. Iminoboronate complexes for the formation of polymers and hydrogels .....	50
1.9. Iminoboronate derivatives for biological targeting and tagging .....	55
1.10. Conclusions and outlook on the Bull-James assembly .....	61
2. Diastereomer Aggregation Induced Anisochronism (DAIA) affects the <sup>1</sup> H NMR spectra of sulfiniminoboronate ester complexes derived from binol .....	63
2.1. Introduction .....	63
2.2. Scalemic assemblies using BINOL .....	74
2.3. The role of aggregation effects on the NMR spectroscopic analysis of BINOL-derived sulfiniminoboronates.....	80
2.4. Conclusions, future work, and outlook.....	100
3. The Bull-James assembly for determining the enantiopurity of sulfinamides by NMR spectroscopy .....	102
3.1. Bull-James assembly of sulfinamides for <sup>1</sup> H NMR analysis.....	102
3.2. Bull-James assembly of sulfinamides for <sup>19</sup> F NMR analysis .....	117
3.3. Bull-James assembly of non-sulfinamide analytes .....	125
3.4. Conclusions and future work .....	131

4.	<i>N</i> -oxide-catalysed Baeyer-Villiger oxidation reactions of ketones and $\alpha,\beta$ -unsaturated ketones	133
4.1.	The Baeyer-Villiger oxidation reaction and its use for the synthesis of vinyl esters.....	133
4.2.	Reoptimisation of DMAPO-catalysed BV oxidation reactions.....	145
4.3.	DMAPO-catalysed BV oxidation reactions of enones.....	154
4.4.	Mechanistic investigations into DMAPO-catalysed BV oxidation reactions .....	160
4.5.	Degradation studies on DMAPO and <i>m</i> CPBA in BV reactions.....	175
4.6.	Development of second generation <i>N</i> -oxide-catalysed BV oxidation conditions.....	179
4.7.	Conclusions.....	188
4.8.	Future work .....	189
5.	Experimental.....	191
5.1.	General experimental details .....	191
5.2.	Experimental details for Bull-James assemblies in chapters 1-3.....	192
5.3.	Synthetic and characterization details for chapter 3 .....	194
5.4.	Synthetic and characterization details for chapter 4 .....	207
6.	References .....	228
7.	Appendix A – X-Ray crystallographic data .....	248
8.	Appendix B – HPLC analysis of commercial samples of ( <i>R</i> )-129b.....	256
9.	Appendix C – $^1\text{H}$ NMR spectra of DMAPO + <i>m</i> CBA.....	258
10.	Appendix D – Representative NMR spectra for determining C-B $^{13}\text{C}$ NMR chemical shifts ...	259
11.	Appendix E –PhD Publications.....	261

# 1. THE BULL-JAMES ASSEMBLY: EFFICIENT IMINOBORONATE COMPLEX FORMATION FOR CHIRAL DERIVATIZATION AND SUPRAMOLECULAR ASSEMBLY

The research project described in the first half of this thesis describes the successful development of a new Bull-James three-component derivatization approach for determining the enantiomeric excess of chiral sulfinamides by NMR spectroscopic analysis. Consequently, this review chapter begins with a brief general introduction to methods for determining enantiomeric excess, followed by an in-depth discussion of how three-component self-assembly reactions between an amine, a chiral analyte, and 2-formylphenyl boronic acid (2-FPBA, **1**) template can be used to produce stable iminoboronate ester (IBE) complexes. These assemblies can be used to determine the enantiomeric excess of a range of chiral analytes, as general supramolecular assembly motifs, for the formation of supramolecular stimuli responsive materials, and for the orthogonal derivatization of biomolecules (Scheme 1).



Scheme 1: Three-component assembly of useful iminoboronate esters.

## 1.1. Methods for determining enantiomeric excess

Chiral compounds occur widely throughout chemistry and biology, comprising much of the biochemical machinery that underpins life, such as proteins, sugars, or DNA. As such, the stereochemistry of chiral biologically-active molecules is responsible for controlling their interactions with, and effects on, biological systems, with the availability of methods for their enantioselective synthesis critical to the fields of medicinal chemistry and drug design. Stereoselective synthesis is therefore paramount for the preparation of chiral molecules for numerous chemical and life science applications, with a range of chiral metal-containing catalysts, organocatalysts, biocatalysts, chiral auxiliaries, and chiral pool precursors routinely used to carry out enantioselective and diastereoselective syntheses. The importance of enantioselective catalysis was recognised in 2001 by the award of the Nobel Prize in Chemistry to K. B. Sharpless, W. S. Knowles, and R. Noyori for their work on “chirally catalysed reactions”.<sup>1</sup> Key to the successful development of enantioselective synthetic methodologies is the ability of chemists to determine the enantiopurity of chiral products, which is most often expressed as their enantiomeric excess (*ee*, equation 1).<sup>2</sup>

$$ee = \frac{[R] - [S]}{[R] + [S]} \times 100 \quad (1)$$

Many methods exist to determine the *ee* of small molecules, all of which rely on the action of a chiral inducer to create a diastereomeric environment which enables the enantiomers of a scalemic analyte to be distinguished. Chiral gas chromatography (GC) and liquid chromatography (HPLC/UPLC) are currently the most popular methods for determining the *ee* of small molecules, and have been the topic of many reviews.<sup>3–8</sup> Briefly, two approaches to determining *ee* by chromatography exist: (i) direct analysis, whereby a chiral mobile or stationary phase (CSP) forms transient diastereomeric interactions with the chiral analytes that results in their enantiomers having different retention times; (ii) indirect analysis, whereby prior chiral derivatization of the enantiomers of a chiral analyte is used to irreversibly produce diastereomeric derivatives that can then be separated using an achiral stationary phase.<sup>9</sup> Chiral stationary phases (CSPs) are typically preferred, and are usually composed of functionalised chiral materials derived from biopolymers, including cyclodextrin and cyclofructan CSPs for chiral GC analysis, and polysaccharide-, protein-, Pirkle- and crown ether-derived CSPs commonly used for chiral LC analysis.<sup>5,6</sup> Chiral GC/LC analysis of ‘clean’ mixtures of chiral compounds that achieve baseline resolution of enantiomers provides highly reliable and accurate results, boasting minimal errors and high reproducibility for many different classes of chiral compound.<sup>5</sup> However, extensive optimisation and screening is often required to achieve this, as each class of analyte will interact with each chiral system differently. Moreover, GC and LC equipment and their associated chiral columns are costly, with eventual degradation of the CSP over time leading to decreased resolving power and accuracy. Additionally, chiral chromatography can suffer from multiple additional sources of error, with separation processes potentially leading to degradation, racemisation, or epimerisation of analytes, whilst analysis of crude mixtures can result in co-elution of impurities with one or the other analyte stereoisomers. These effects can lead to spurious increases or decreases in peak integration, causing inaccurate ratios and thus incorrect *ee* determination.<sup>10,11</sup> Although thorough screening, benchmarking, and optimisation of chromatographic methods can minimise these risks effectively, these additional time and resource requirements to develop new chromatography conditions for different types of chiral analytes can add significant barriers to entry when using HPLC or GC techniques for determining enantiomeric excess.<sup>12</sup>

Generally less popular than chiral chromatography, optical methods provide a relatively low-cost rapid alternative to chromatographic techniques. Polarimetry was of course the first method capable of assessing enantiopurity and absolute configuration of chiral molecules, exploiting their ability to rotate the plane of polarised light (Figure 1).<sup>13</sup> The optical rotation of a chiral compound is dependent on their aggregation, conformation, and solvent, which often leads to widely temperature-, concentration-, and purity-dependent measurements. Consequently, the use of polarimetry to measure *ee* can only be carried out on purified chiral analytes, with the presence of any impurities often leading to inaccurate results. Polarimetry is now rarely used as a means of

determining the *ee* of chiral molecules from first principles, although comparison of the sign and magnitude of rotation with previously reported values is often used to assign the absolute configuration of chiral molecules isolated from enantioselective reactions or natural sources. Other optical methods such as circular dichroism (CD), UV-Vis, and fluorescence spectroscopy that enable either direct or indirect detection of chirality have become much more popular in recent times, in particular for high-throughput applications to screen for effective enantioselective catalysts (*vide infra*).<sup>14–22</sup>

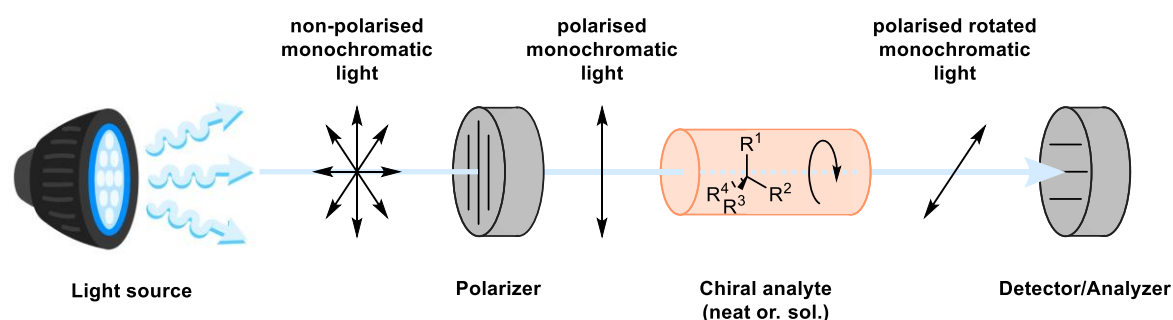


Figure 1: Basic principles of polarimetry, as illustrated by the basic function of a polarimeter.

Along the quest to develop new methods for determining enantiopurity (and absolute configuration), NMR has emerged as a convenient analytical technique.<sup>23,24</sup> The growing popularity of these methodologies for chiral analysis can be attributed to the same general properties that make NMR spectroscopy a popular characterisation tool: practical simplicity, rapid sample preparation and analysis, minimal resource requirements, ubiquity of NMR spectrometers, variety of NMR-active nuclei, and good accuracy, amongst others. The NMR-active nuclei of enantiomeric species are, of course, isochronous in achiral media, and so diastereomeric differentiation must be induced for enantiomers to produce differentiated signals. This is done either by creating an asymmetric system using either chiral solvating agents (CSAs), or by converting the enantiomeric analytes into diastereomers using chiral derivatizing agents (CDAs). The use of CSAs for NMR spectroscopic analysis allows for direct detection of enantiomers without the need for separation or functionalisation of the analyte, with a chiral environment created by addition to the analytical sample of a CSA that is capable of reversible diastereomeric interactions with each enantiomer of the chiral analyte.<sup>25</sup> This is illustrated well by the very first report of chiral solvation by William H. Pirkle in 1966 (Figure 2a), who observed that addition of (*rac*)-2,2,2-trifluoro-1-phenylethanol **2** to enantiopure  $\alpha$ -methylbenzylamine **3a** produced two sets of resonances in the  $^{19}\text{F}$  NMR spectrum.<sup>26</sup> Strong hydrogen bonding between the alcohol of the analyte and the basic amine of the solvent leads to the transient formation of distinct diastereomeric magnetic environments that results in each enantiomer experiencing anisochronous shielding/deshielding effects that lead to resolved chemical shifts for selected pairs of resonances. Following on from this initial discovery, Pirkle and others subsequently developed a range of related chiral solvating agents, including widely-used Pirkle's alcohol **4**, which can be used to determine the *ee* and absolute configuration (in some cases) of a wide range of analytes using  $^1\text{H}$ ,  $^{13}\text{C}$  and  $^{19}\text{F}$  NMR spectroscopic analysis (Figure 2b).<sup>26–33</sup> Since these developments, a broad range of functionalised small molecules have been discovered,



capable of inducing non-covalent interactions that enable them to act as chiral solvating agents. Selected examples are shown in Figure 2b, including BINOL-derived phosphoric acid **5** and chiral crown ether **6** that are commonly used as CSAs for amines;<sup>34,35</sup> phthalimide-derived amino alcohol **7** that is used for acids;<sup>36</sup>  $\alpha$ -hydroxy ketone **8** (in conjunction with 4-(dimethylamino)pyridine, DMAP) that can be used to determine the *ee* of secondary alcohols and acids;<sup>37</sup> and BINOL **9** for determining the enantiopurity of numerous analytes, including alcohols, amines, acids, amino alcohols, and sulfinimines.<sup>38,39</sup> This field of chiral analysis has also expanded to macrocyclic systems, adopting an approach similar to that of host-guest chemistry. In these instances, a macrocyclic CSA acts as a host, forming multiple non-covalent interactions with an analyte, thus creating a rigid chiral structure which induces significant chemical shift differences ( $\Delta\delta$ ).<sup>40–42</sup> For example, BINOL-derived macrocycle **10** is capable of forming multiple hydrogen bonding interactions with a variety of functionalities, enabling its use as a CSA for determining the *ee* of a range of analytes by <sup>1</sup>H NMR spectroscopy (see Figure 2c).<sup>40</sup> Computational study of optimised structures of the different enantiomers of sulfoxide **11** bound to CSA **10** clearly showed that hydrogen bonding of each analyte enantiomer to the host CSA affords diastereomeric complexes with significantly different 3D structures, which is responsible for the chemical shift differences that are observed.

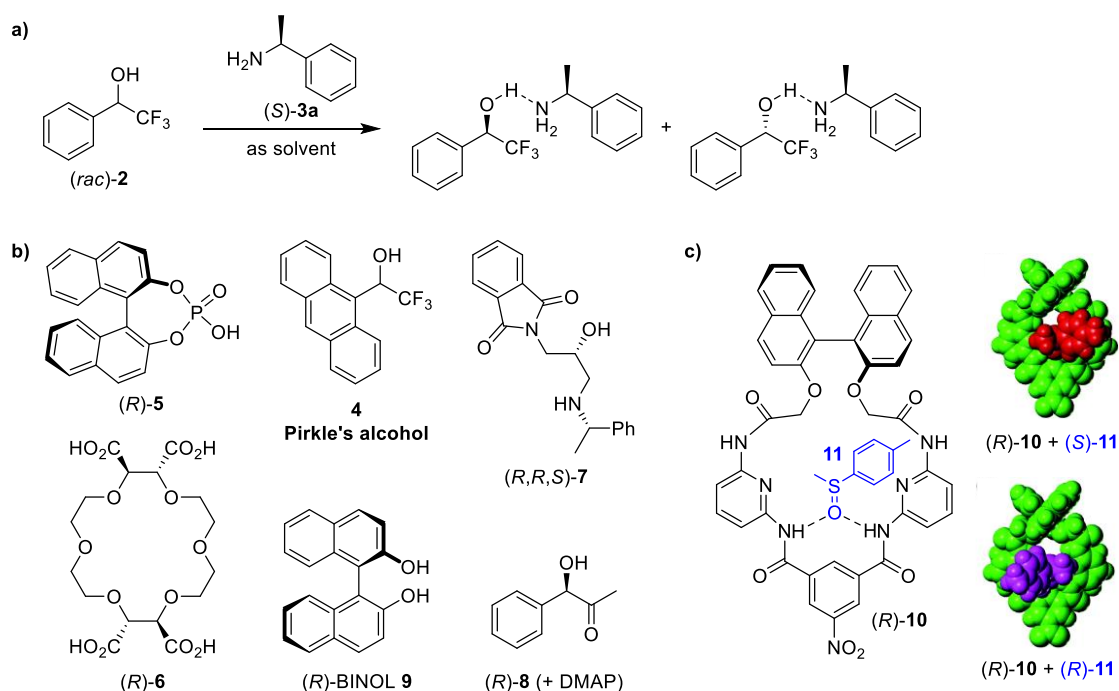
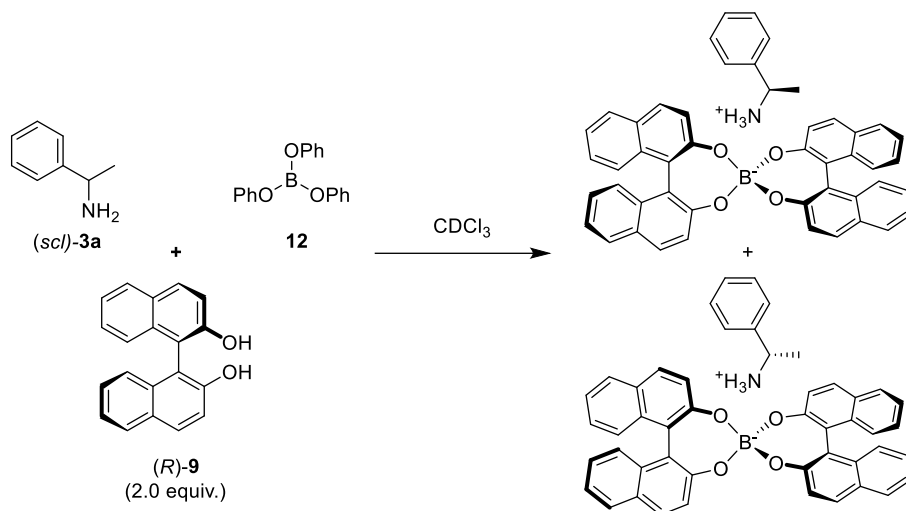


Figure 2: (a) Initial report of using a CSA to determine the *ee* of a chiral alcohol developed by W. H. Pirkle.<sup>26</sup> (b) Representative small molecule CSAs used to determine the *ee*'s of a range of chiral analytes. (c) Macromolecular CSA (R)-10 (green) that makes hydrogen bonds to chiral analyte **11**, with geometry-optimised structures bound to (S)-11 (red, top) and (R)-11 (magenta, bottom).<sup>40</sup>

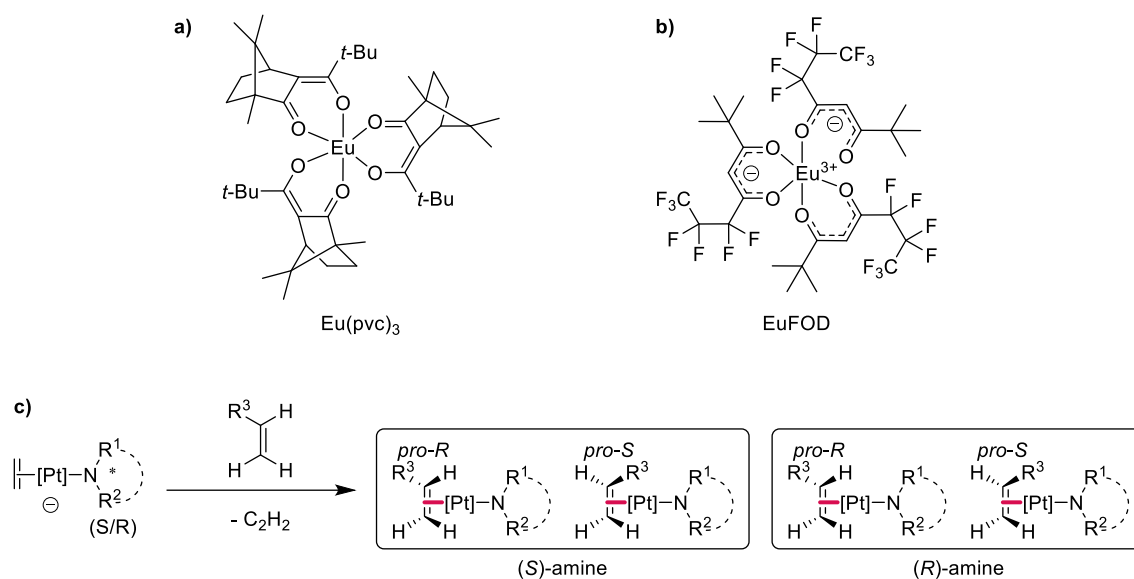
An alternative strategy involves the use of CSAs that can form strong ionic interactions with chiral analytes to produce diastereomeric ion-pair complexes, whose resonances are well resolved in their NMR spectra. For example, Suryaprakash and co-workers have shown that mixtures of (R)-BINOL **9**, triphenyl borate **12**, and a chiral amine (e.g.  $\alpha$ -methylbenzylamine **3a**) combine to

produce well-resolved diastereomeric salts comprised of a boronate anion containing two chiral BINOL ligands and the ammonium cation of the analyte (Scheme 2).<sup>43,44</sup>



Scheme 2: Suggested ion-pair complex CSA for determining the *ee*'s of chiral amine analytes developed by Suryaprakash *et al.*<sup>43,44</sup>

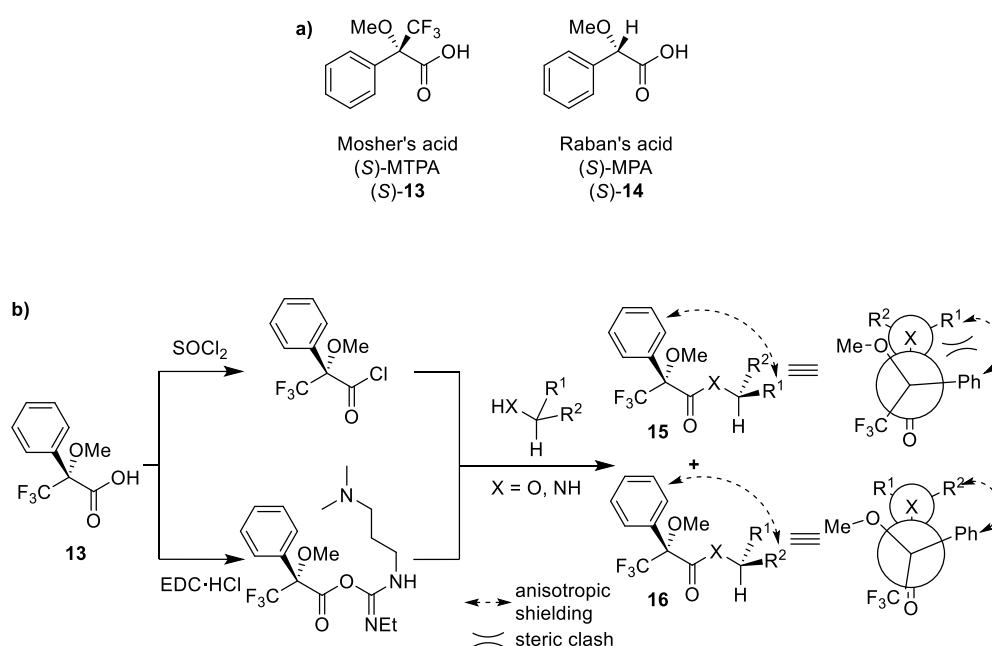
One additional term often used in the context of chirality and enantiopurity determination is that of “chiral shift reagents” (CSRs). The use of this term has been actively avoided by the author throughout this thesis, as its use throughout the chemical literature is somewhat sporadic and non-specific, in some instances being employed to generally describe any and all CDAs and CSAs,<sup>45–47</sup> whilst on other occasions referring more specifically non-covalent CSA-, ion-pairing-type or meta/ligand-based chiral differentiation systems. Most commonly, the term CSR is used to describe systems which form transient diastereomeric complexes (some similarity to the structures in Scheme 2 and Figure 2c), usually by complexation to metal ions. Metals from the lanthanide series are commonly used (*e.g.*  $\text{Eu}^{3+}$ ,  $\text{Pr}^{3+}$ ,  $\text{Yb}^{3+}$ ), which are sometimes referred to as “lanthanide shift reagents” (LSRs). These systems form rapidly equilibrating mixtures of diastereomeric analyte-lanthanide complexes and uncomplexed analyte, inducing a diastereomeric paramagnetic shift in the analyte. Due to the nature of these interactions, the results obtained from LSRs are concentration-, enantiopurity-, and magnetic field-dependent. An early example is  $\text{Eu}(\text{pvc})_3$  (Scheme 3a), reported by Whiteside and Lewis in 1970, which is capable of inducing an impressive  $\Delta\delta_{\text{H}}$  of approximately 0.5 ppm for the benzylic methine proton of  $\alpha$ -methylbenzylamine **3a**, leading to baseline resolved signals sufficient for its enantiopurity to be measured. Some degree chemical shift anisochrony was also observed for all other  $^1\text{H}$  NMR environments, but none sufficient for *ee* determination. Another common LSR is nonchiral  $\text{Eu}(\text{II})$  complex  $\text{EuFOD}$ , also known as  $\text{Resolv-Al}^{\text{TM}}$  or Siever's reagent (Scheme 3b), which is used in conjunction with other CSA/CSR reagents to amplify chiral shift behaviour by creating additional diastereomeric interactions, thus amplifying chiral shift by virtue of its paramagnetism. Other metal-derived CDA methods have also been developed, some of which function as CDA/CSA hybrids (Scheme 3c).<sup>48,49</sup>



Scheme 3: Examples of CSRs: (a)  $\text{Eu}(\text{pvc})_3$  for determining the ee of  $\alpha$ -methylbenzylamine **3a**;<sup>50,51</sup> (b) achiral LSR  $\text{EuFOD}$ ; (c) ethene-platinum(II) complexes for unsaturated analytes.<sup>49</sup>

The novel methodology for determining the *ee* of *S*-chiral sulfinamides described in this thesis falls within the category of CDAs, that rely on covalent modification of a chiral analyte to produce mixtures of diastereomeric species, in this case iminoboronates (IBs), whose ratios can be determined by NMR spectroscopic analysis.<sup>52,53</sup> This type of CDA approach was pioneered by Harry Mosher and Morton Raban in the 1960s<sup>54–58</sup> with the introduction of widely used eponymous Mosher's ( $\alpha$ -methoxy- $\alpha$ -trifluoromethylphenylacetic acid, MTPA, **13**) and Raban's ( $\alpha$ -methoxyphenylacetic acid, MPA, **14**) acids as CDAs for determining the *ee*'s of chiral amines and alcohols (Scheme 4a).<sup>24,59–61</sup> The general approach for Mosher-type CDA analysis is shown in Scheme 4b, which requires initial electrophilic activation of the acid through stepwise formation of its corresponding acyl chloride, or the use of stoichiometric amide/ester coupling agents such as EDC. Coupling an enantiopure CDA with a scalemic analyte results in the formation of diastereomeric mixtures of amide or ester products that can be distinguished by  $^1\text{H}$ ,  $^{13}\text{C}$  or  $^{19}\text{F}$  NMR spectroscopic analysis. This enables their diastereomeric ratio (*dr*) to be accurately determined by integration of pairs of diastereomeric resonances, with this *dr* value directly correlating to the *ee* of the parent chiral analyte. Extensive structural and computational investigations have been carried out on this class of CDAs to determine the origin of the chemical shift differences between their diastereomeric amides and esters.<sup>24,52,62–65</sup> It is now well understood that a key part of these reagents is their phenyl/aryl motifs, which are responsible for both conformational control by steric interaction and differential anisotropic shielding effects in each diastereomer. This is shown for Mosher's acid **13** in Scheme 4b, with specific conformational arrangements and intramolecular interactions dependent on the exact structures of the CDA and chiral analyte employed. In this instance, derivatization produces diastereomeric products whose analyte methine protons and  $\text{CF}_3$  group are positioned *syn* to the carbonyl group, which aligns the two  $\alpha$ -substituents of the analyte fragment *anti*- to the carbonyl group. The resultant steric clash between the phenyl substituent of diastereomer **15** and the largest substituent of the analyte ( $\text{R}^1$ ) leads to conformational distortion (relative to diastereomer **16**),

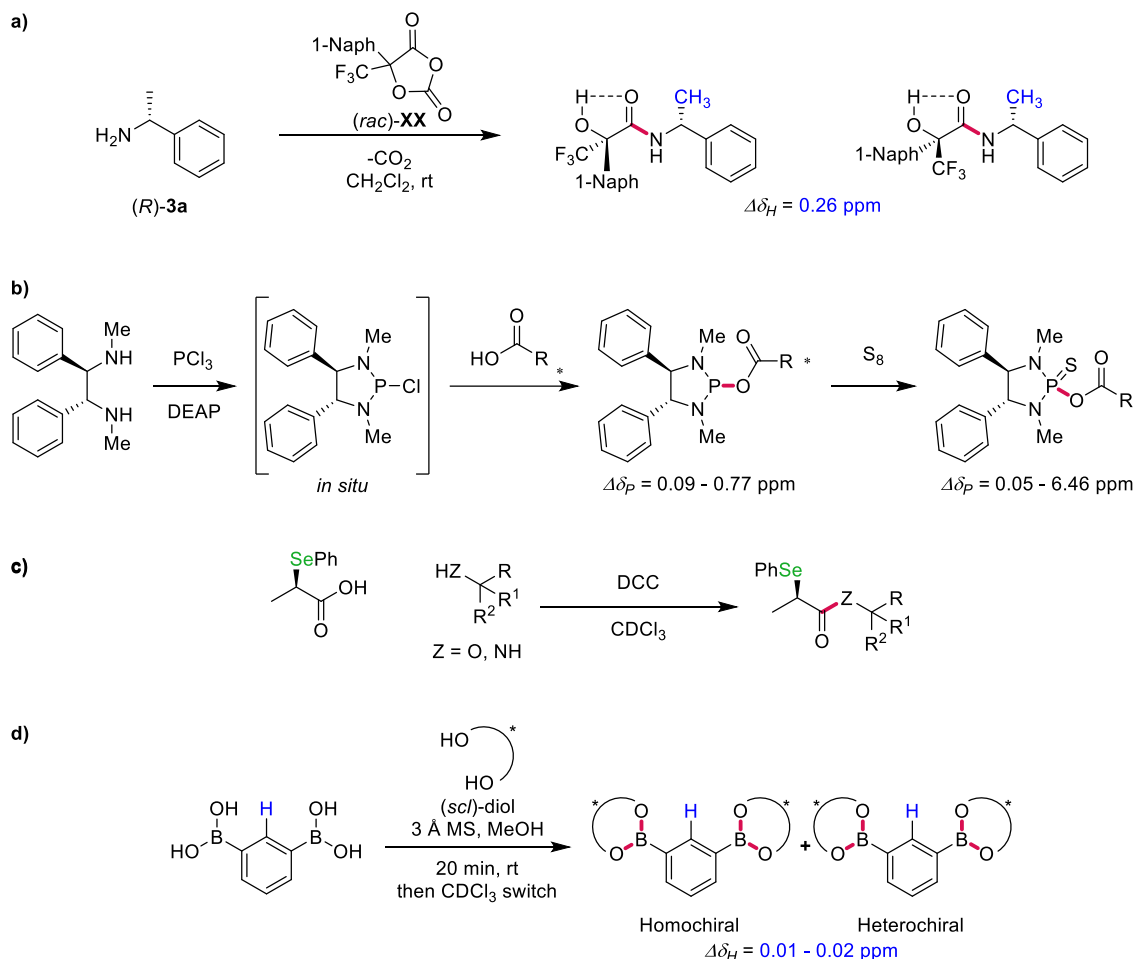
leading to each trifluoromethyl group experiencing different shielding environments that lead to distinct signals in their  $^{19}\text{F}$  NMR spectra. This difference in conformation between the two diastereomers **15** and **16** also results in chemical shift differences in diastereomeric pairs of resonances in their  $^1\text{H}$  (and sometimes  $^{13}\text{C}$ ) NMR spectra, whose relative integral ratios can then be used to determine the *ee* of the parent analyte. Though widely used, it must be noted that these classical CDA methods are time-consuming and often costly (*e.g.* **13** > £ 250/g from Merck), as pre-functionalisation, workup, and purification by chromatography is usually required, all of which increase the risk of unwanted racemisation/epimerisation or kinetic resolution effects that can produce inaccurate *ee* values.<sup>66</sup>



Scheme 4: (a) Common CDAs Mosher's and Raban's acids **13** and **14**. (b) Mosher's acid **13** for the chiral derivatization of alcohols and amines, with Newman-like projections showing chemically non-equivalent environments,  $\text{R}^1$  is the largest substituent.

Mosher-type and Bull-James CDAs are by no means the only types of chiral derivatizing agents, with many different classes of CDA reported in the literature, a selection of which is shown in Scheme 5. The reactions used for derivatization of chiral analytes with CDAs need to be rapid and complete, and so it is unsurprising that CDAs usually contain reactive units such as acyl chlorides, anhydrides, sulfonyl chlorides, phosphorus chlorides, or chloroformates (*e.g.* Scheme 5a,b).<sup>24,67–69</sup> Use of heteronuclear NMR to determine *ee* is becoming more common, moving beyond classical  $^1\text{H}$ ,  $^{13}\text{C}$  and  $^{19}\text{F}$  NMR analysis to include  $^2\text{H}$ ,  $^{31}\text{P}$ ,  $^{77}\text{Se}$ ,  $^{125}\text{Te}$ , or  $^{195}\text{Pt}$  nuclei (*e.g.* Scheme 5d, Scheme 3c above).<sup>49,70–74</sup> Achiral CDAs also exist, which employ bifunctional linkers to tether two molecules of analyte together, exploiting the principle of "statistical duplication" known as Horeau's principle.<sup>75</sup> These assemblies give rise to four possible stereoisomers (2 sets of diastereomers) which can be identified by NMR, and whose ratio is statistically dependent on the enantiopurity of the analyte. An example of this type of CDA developed by the Bull group is shown in Scheme 5e, which uses a bis-boronic acid to determine the *ee* of diols.<sup>76</sup> It is interesting to note that although Mosher-type

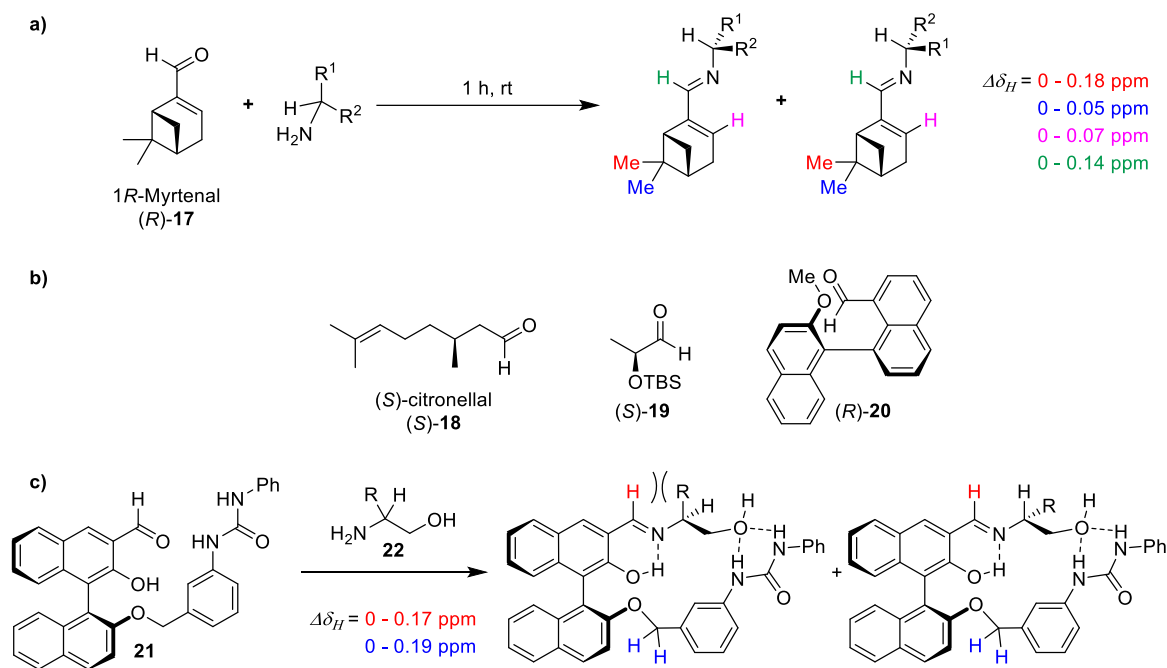
CDAs produce conformationally flexible diastereomers, most other approaches produce rigid diastereomeric products which maximise chemical shift differences that can be used to assign absolute configuration. Finally it should be noted that these same types of CDAs are also commonly used to generate diastereomers whose *dr*'s have been determined using other analytical techniques, such as circular dichroism, polarimetry, infrared spectroscopy and HPLC analysis.<sup>77–80</sup>



Scheme 5: Selected CDA examples illustrating functional variety: (a) anhydrides;<sup>68</sup> (b) phosphoryl chloride;<sup>69</sup> (c) selenide;<sup>74</sup> (d) bis-boronic acid Horeau-based template.<sup>76</sup> New bond between CDA and analyte in red.

The Bull-James three-component assembly used for determining the *ee* of amines (and other analytes) relies on the formation of an imine bond between their amino groups and the aldehyde of 2-FPBA **1** template, a general approach previously reported for a number of imine-derived CDA systems for chiral analysis of both aldehydes and amines.<sup>81</sup> These CDA systems rely on the relatively fast reactions between chiral aldehydes and amines to form diastereomeric imines, which allows rapid functionalisation of the chiral analyte. Imine condensation reactions between aryl amines and/or aryl aldehydes tend to be highly (*E*)-selective, producing imines with well-defined rigid structures, leading to diastereomeric imines with well-resolved NMR signals. Importantly, imine resonances in <sup>1</sup>H NMR spectra tend to be well-separated from other signals, allowing these characteristic peaks to be integrated to accurately determine *dr*, mostly irrespective of analyte structure. For example, Dufrasne *et al.* have reported the use of monoterpenoid myrtanal **17** as a

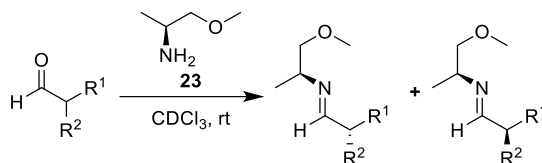
CDA for determining the *ee* of  $\alpha$ - and  $\beta$ -aryl amines and amino alcohols using  $^1\text{H}$  and  $^{13}\text{C}$  NMR spectroscopic analysis (Scheme 6a).<sup>82,83</sup> They found that the resultant diastereomeric imine complexes exhibited several well-resolved  $^1\text{H}$  NMR signals that could be integrated to determine *dr*. Similarly, methodologies for determining the enantiopurity of amines have been reported using citronellal **18**, lactate-derived **19**, and binaphthyl aldehyde **20** (Scheme 6b).<sup>84–87</sup> Larger systems that incorporate both imine condensation and hydrogen bonding interactions have also been developed, such as BINOL-urea CDA **21** developed by Kim and co-workers for chiral analysis of amino alcohol analytes **22** (Scheme 6c).<sup>88,89</sup> Initial condensation forms diastereomeric imine complexes, which form strong rigidifying intramolecular hydrogen bonding interactions that amplify the chiral environment, thus amplifying the chemical shift differences between matched pairs of diastereomeric resonances. In this instance the imine has a dual function, acting both as the analyte-CDA linker and as a strong Lewis base, hydrogen-bonding to the proximal phenolic proton to rigidify the system. Both the imine and the benzylic methylene protons could be used for chiral analysis in this system, affording good chemical shift differences of up to 0.19 ppm.



Scheme 6: (a) Myrtenal CDA developed by Dufrasne *et al.* to determine the *ee*'s of chiral amine analytes.<sup>82,83</sup> (b) Representative examples of aldehyde/imine CDAs.<sup>84–87</sup> (c) Dual functional aldehyde/imine CDA that incorporate both covalent and hydrogen-bonding.<sup>88,89</sup>

Conversely, reversibility of these pairs allows the *ee* of a scalemic chiral aldehyde to be determined *via* imine functionalisation with an appropriate chiral amine auxiliary. For example, Gellman *et al.* showed that derivatization of an  $\alpha$ -chiral aldehyde analyte with enantiopure (*R*)- $\alpha$ -methoxypropanamine **23** gave diastereomeric imines containing resolved resonances that could be used for *dr* analysis (Scheme 7).<sup>90</sup> This CDA was used to determine the *ee*'s of a range of chiral aldehydes that were in good agreement with chiral GC measurements. This method required no purification or workup, enabling it to be used for direct analysis of crude reaction mixtures/products, thus allowing for rapid “*in situ*” measurements of *ee*. It is important to note that

the acidity of aldehyde  $\alpha$ -protons could potentially lead to racemization over time, and so NMR spectra need to be recorded immediately after mixing in order to ensure accurate *ee* measurements.



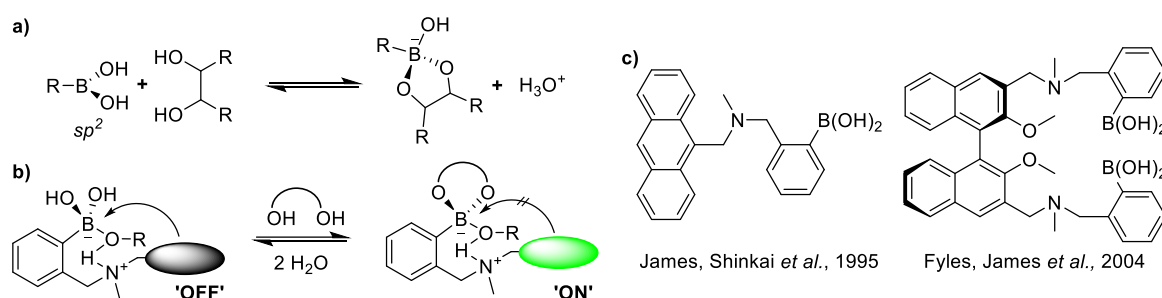
Scheme 7: CDA method for determining the *ee* of  $\alpha$ -chiral aldehydes using (*R*)- $\beta$ -amino-ether **23**.<sup>90</sup>

## 1.2. Inception of the Bull-James three-component derivatization approach

Development of the versatile three-component iminoboronate ester methodology described in the remainder of this review has been pioneered by the Bull and James groups at the University of Bath (UK) over the last two decades. Its success has led to its widespread use by numerous other research groups for different supramolecular applications resulting in this type of reaction now being termed the “Bull-James assembly”. To date, this self-assembly methodology has found a wide range of applications, including: CDAs for determining the enantiomeric excess of a range of chiral analytes using NMR, optical, and electrochemical techniques; as a supramolecular self-assembly reaction to produce boracycles, chiral auxiliaries and ligands for stereoselective synthesis; the production of new types of polymers and stimuli-responsive materials; and as the basis of a new type of “click” chemistry methodology for modifying/functionalising peptides and proteins.

The Bull group have had an interest in the development of asymmetric methodologies for the synthesis of chiral amines for many years, and have often needed to determine the *ee* of new types of chiral amines containing single stereocentres.<sup>91–96</sup> One approach that they have commonly employed involves reaction of a scalemic amine with a CDA such as Mosher’s acid chloride (expensive, moisture sensitive, multiple steps, *vide supra*) to afford diastereomeric amide derivatives whose *dr* could then be determined by NMR spectroscopic analysis.<sup>54,56</sup> Alternatively, the *ee*’s of these chiral amines (or their derivatives) could be determined using chiral HPLC analysis. The range of structures and functional groups present in the chiral amines produced in the Bull group meant that different CDAs or multiple expensive chiral HPLC columns often needed to be screened before a suitable system was identified to resolve the enantiomers of each different class of amine.<sup>3,7</sup> Therefore, the Bull group were interested in identifying a practically simple, cheap, and rapid CDA approach that could be used to rapidly analyse the *ee* values of a wide range of chiral amines using NMR spectroscopic analysis.

The James group have been interested in chemical sensing and supramolecular chemistry for many years, having developed a wide range of self-assembled fluorescent sensors that employ the reversible binding of boronic acids (planar  $sp^2$  boron) to diol fragments to produce boronate ester complexes (tetrahedral  $sp^3$  boron) to induce a change in fluorescence response (Scheme 8a).<sup>97–102</sup> They have described that *ortho*-aminomethylphenylboronic acid sensors are particularly effective for the fluorescent, optical, and electrochemical sensing of sugars, with this class of sensors recently finding commercial applications for continuous monitoring of glucose levels in critical care patients.<sup>103,104</sup> Diol complexation in this class of sensors is favoured by the presence of the proximal Lewis basic tertiary amino group,<sup>105</sup> which binds to the boron centre to produce stable intramolecular aminoboronate ester complexes. Orthogonal binding of both the diol analyte and the amine to the boron centre occurs in a cooperative manner, with complexation of the diol producing a boronate ester with a more Lewis acidic  $sp^2$  boron centre, and the intramolecular N→B interaction increasing the overall stability of the complex. Complexation of these types of aminoboronic acid sensors to diols in aqueous/alcoholic media has been shown to produce solvent-inserted aminoboronate complexes, whose formation results in fluorescence “turn-on” through elimination of “loose-bolt” internal conversion quenching of the fluorescence of the parent boronic acid probe (Scheme 8b).<sup>106,107</sup> The versatility and strength of this type of aminoboronic acid complexation process has been exploited to produce many sensors for the fluorescent detection of a wide range of diols and sugars, as well as sensors for pH, anion, and reactive oxygen species sensing (Scheme 8c).<sup>97,102,108</sup> The added stability of this type of aminoboronate ester complex has also been used as the basis of supramolecular assemblies for the generation of a wide range of hydrogels, boronic acid-appended porphyrins, amphiphiles, polymers, and covalent organic frameworks, amongst others.<sup>100,109,110</sup>

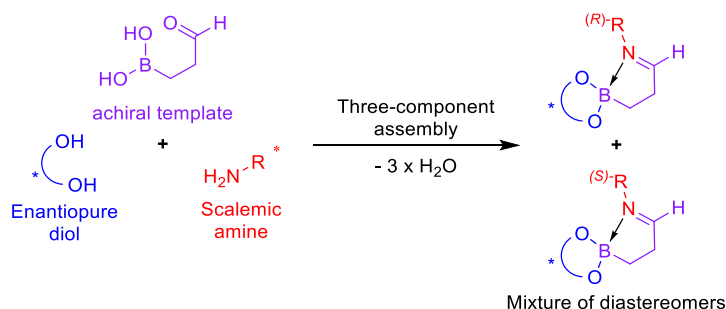


Scheme 8: (a) Rapid complexation of a boronic acid with a vicinal diol reversibly affords a cyclic boronate ester. (b) Complexation of a diol to a non-fluorescent *o*-aminomethylphenylboronic acid sensor in water or an alcohol solvent results in formation of a solvent-inserted fluorescent boronate ester complex. Diol binding results in fluorescence “turn-on” due to elimination of a “loose-bolt” effect that causes internal conversion quenching of the fluorescence of the uncomplexed boronic acid probe.<sup>106</sup> (c) Representative *o*-aminomethylphenylboronic acid glucose/diol sensors developed by the James group.<sup>102,108</sup>

Nomikai-inspired<sup>111</sup> conversations during a research trip to Japan in 2002<sup>112</sup> led James and Bull (and Arimori – PDRA in the groups) to realise that this type of boronate ester complexation chemistry could be exploited to develop a simple three-component protocol for determining the enantiopurity of chiral amines. Their simple idea was to react an achiral bifunctional template that contained a boronic acid and a proximal aldehyde group (purple) with a chiral 1,2-diol (blue) and a



scalemic amine (red) to selectively afford a pair of diastereomeric IBE complexes, whose *dr* could then be determined through the integration of pairs of diastereomeric signals in their  $^1\text{H}$  NMR spectrum. So long as no kinetic resolution occurred during the derivatization process, this *dr* value would be an accurate reflection of the *ee* of the parent scalemic amine. Moreover, the orthogonal three-component self-assembled nature of the protocol meant that it would be easy to adapt this derivatization approach to determine the *ee* of chiral diols and other chiral analytes (Scheme 9).

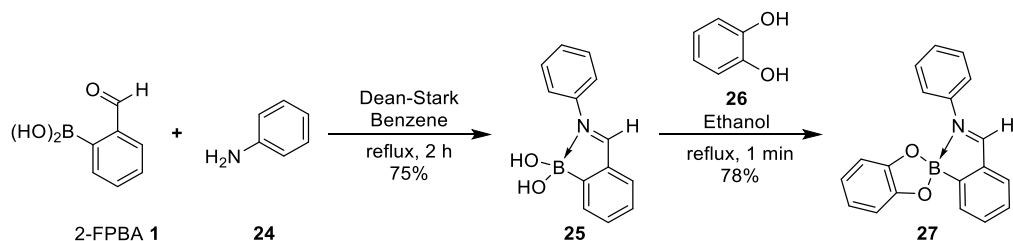


Scheme 9: Design principles for a three-component derivatization protocol to produce an IBE-based CDA for determining the *ee* of a scalemic amine.

### 1.3. Discovery and structural features of the Bull-James assembly

#### 1.3.1 *Discovery of the Bull-James assembly CDA for determining the ee of amines*

A review of the literature revealed a promising report by Dunn *et al.*,<sup>113</sup> who had described the stepwise synthesis of stable IBEs based on imine condensation of 2-FPBA **1**<sup>114</sup> with aniline **24** to afford an iminoboronic acid **25** intermediate that was then reacted with catechol **26** to afford iminoboronate ester **27** (Scheme 10). This precedent indicated that reaction of 2-FPBA **1** with a chiral diol and a scalemic amine could be used as the basis of a three-component derivatization protocol for determining the *ee* of chiral amines, as outlined in Scheme 9.



Scheme 10: Stepwise three-component self-assembly of an achiral IBE complex **4** by Dunn *et al.*<sup>113</sup>

This three-component assembly concept was initially investigated by mixing 2-FPBA **1**, (*S*)-BINOL **9** and (*rac*)-4-methoxy- $\alpha$ -methylbenzylamine **3b** in  $\text{CDCl}_3$  with 4 Å molecular sieves (MS) to drive the condensation reactions to completion. Fortuitously, this reaction led to quantitative formation of a 50:50 mixture of the diastereomeric IBE complexes ( $\alpha$ -*S,S*)-**28b** and ( $\alpha$ -*R,S*)-**29b** within 5 min (Figure 3a),<sup>115</sup> with complexation reactions of scalemic 4-methoxy- $\alpha$ -methylbenzylamine **3b** of known *ee*

indicating that no kinetic resolution was occurring. Examination of the  $^1\text{H}$  NMR spectra revealed that the *ee*'s of scalemic amines could be easily determined by integration of corresponding pairs of  $^1\text{H}$  NMR resonances originating from each of the IBE diastereomers that were formed. The imine (black, left),  $\alpha$ -methine (red, centre left), *p*-methoxy (green, centre right), and  $\alpha$ -methyl (blue, right) proton resonances of each diastereomer were fully baseline-resolved, exhibiting relatively large chemical shift differences  $\Delta\delta_{\text{H}}$  values of 0.11-0.21 ppm (Figure 3b). The presence of multiple well-resolved diastereomeric peaks in these  $^1\text{H}$  NMR spectra enabled the integral ratios of multiple pairs of diastereomeric resonances to be used to accurately measure high *ee* values (> 95 % *ee*), thus minimising any risk of inaccuracy caused by baseline noise or the presence of impurities (Figure 3b).

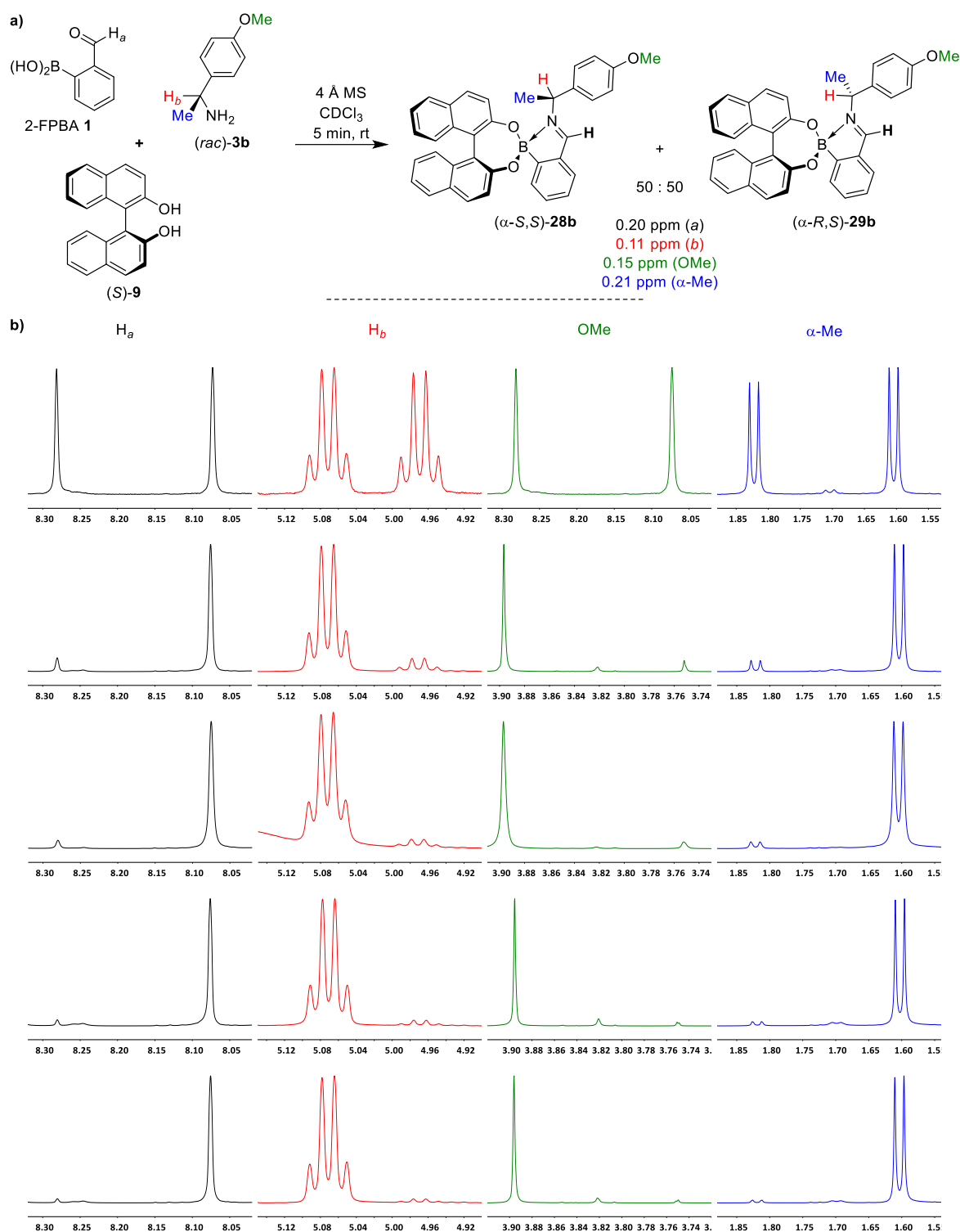


Figure 3: (a) Three-component assembly of 2-FPBA **1**, (S)-BINOL **9** and (*rac*)-4-methoxy- $\alpha$ -methylbenzylamine **3b** and observed  $\Delta\delta_H$ 's. (b) Expanded  $^1\text{H}$  NMR (500 MHz,  $\text{CDCl}_3$ , 100 mM) spectra of diastereomeric complexes produced from reaction of 2-FPBA **1** with (S)-BINOL **9** and (S)-**3b** of 0, 80, 90, 95 and 98% ee. Spectra prepared following published procedure.<sup>116</sup>

This three-component derivatization reaction was attractive from a practical standpoint, as it was moisture tolerant, employed cheap, commercially available, bench-stable reagents, and proceeded rapidly at room temperature ( $\sim 5$  min) in  $\text{CDCl}_3$  (common solvent for NMR spectroscopy), with no need for reaction workup or purification. Moreover, it produced diastereomeric IBEs whose  $^1\text{H}$  NMR

spectra exhibited multiple pairs of baseline-resolved diastereomeric proton resonances with large  $\Delta\delta_H$  values which meant that their *dr* could be analysed using low field NMR spectrometers (*e.g.* 250 MHz). Furthermore, the imine signals appeared in a region of the  $^1\text{H}$  NMR spectrum that was well removed from any other resonances, thus limiting the risk of overlapping peaks resulting in inaccurate integration values. These initial results indicated that this self-assembling CDA stood a strong chance of being applicable for determining the *ee* of a wide range of chiral amines, with its combinatorial three-component nature affording the opportunity to change the chiral diol component used for derivatization to maximise the signal resolution of pairs of diastereomeric peaks as required (*vide infra*). The modular nature of this CDA also afforded the opportunity to use an enantiopure amine as a chiral reporter to analyse the *ee* of chiral diols, or any other chiral analyte that might show orthogonal reactivity for either the boronic acid or formyl groups of the 2-FPBA template.<sup>109</sup>

### 1.3.2 Structural and mechanistic features of IBE complex formation

Since the initial reports describing the use of this three-component method to determine the *ee*'s of amines, significant structural and mechanistic work has been carried out to understand the efficiency of the self-assembling pathways leading to formation of these stable IBE complexes. X-ray crystallographic analysis of the diastereomeric IBEs ( $\alpha$ -*S,S*)-**28a** and ( $\alpha$ -*R,S*)-**29a** produced in the three-component assembly reaction of (*S*)-BINOL **9**, 2-FPBA **1**, and enantiopure  $\alpha$ -methylbenzylamine **3a** (Figure 4) revealed N-B distances of 1.656 Å and 1.642 Å respectively, clearly indicating the presence of strong N $\rightarrow$ B coordination bonds that confer structural rigidity.<sup>117</sup> This was further confirmed by  $^{11}\text{B}$  NMR spectroscopy which revealed upfield 'tetrahedral boron' signals for both complexes. This rigidity leads to the benzylic C-H bonds being positioned directly above the boronate centres to minimise steric interaction with the BINOL ligand. Differences in the  $^1\text{H}$  NMR chemical shifts of the  $\alpha$ -methyl protons of the diastereomers can be explained by the homochiral complex ( $\alpha$ -*S,S*)-**28a** experiencing anisotropic shielding effects from the BINOL naphthyl moiety that are not present in the heterochiral ( $\alpha$ -*S,R*)-**29a** complex. Similar variations in local anisotropic shielding effects between diastereomeric complexes are responsible for the different chemical shifts of multiple pairs of diastereomeric proton resonances observed in their  $^1\text{H}$  NMR spectra. The ease of crystallisation of Bull-James-assembled IBEs also provides the opportunity to determine the absolute configuration of a chiral amine (or diol) analyte through X-ray crystal analysis of a diastereomerically-pure IBE complex prepared from a chiral diol (or amine) of known absolute configuration.

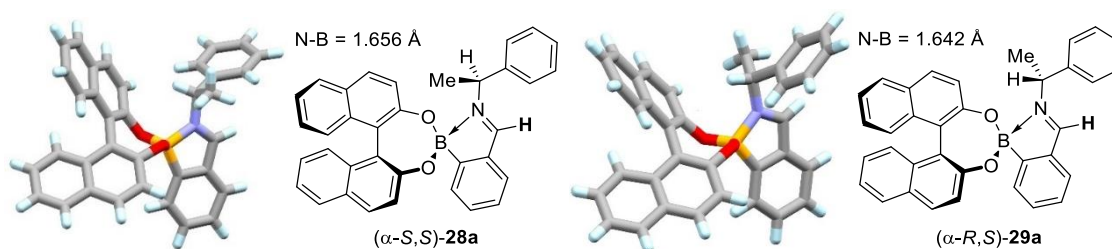
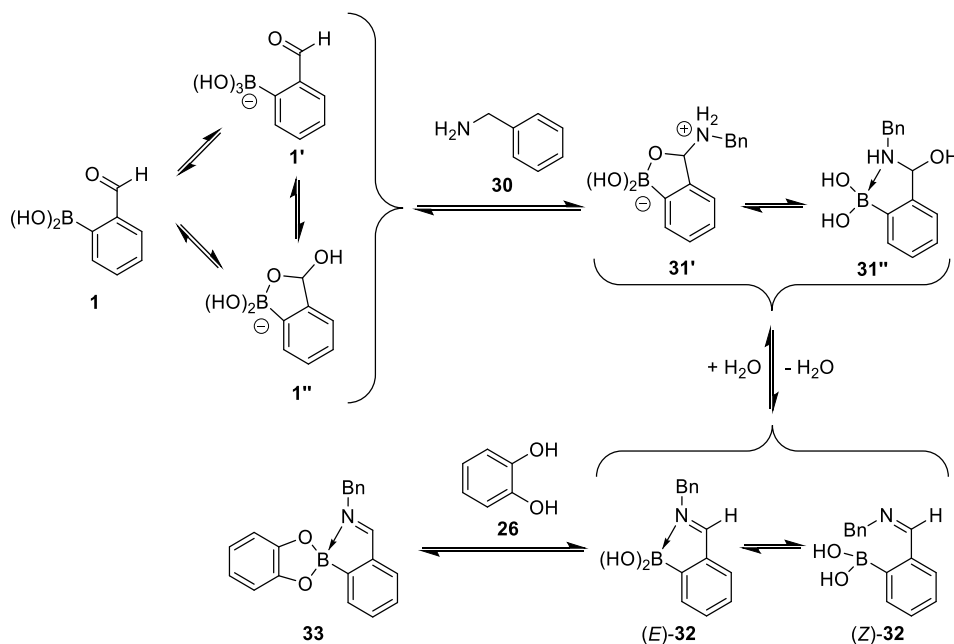


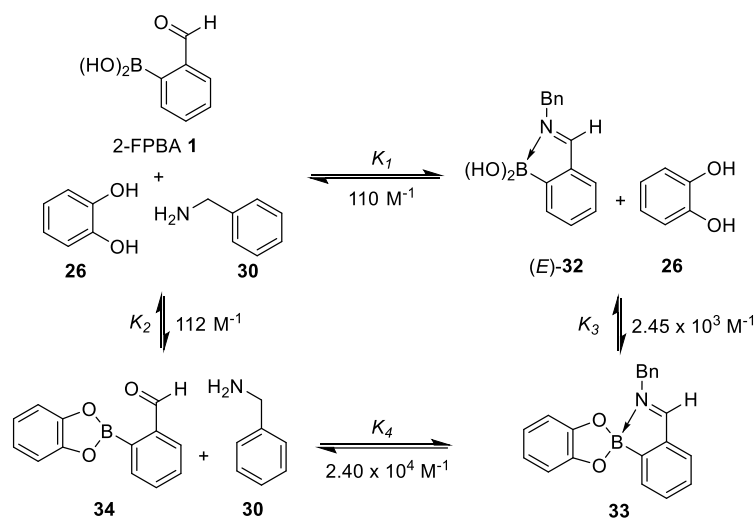
Figure 4: X-Ray crystal structures of IBEs ( $\alpha$ -S,S)-**28a** and ( $\alpha$ -R,S)-**29a**.<sup>117</sup>

A simplified achiral three-component system using 2-FPBA **1**, catechol **26**, and benzylamine **30** was used by Anslyn and co-workers to explore the mechanism and kinetics of the stepwise formation of these self-assembled IBE complexes.<sup>118</sup>  $^1\text{H}$  and  $^{11}\text{B}$  NMR spectroscopic analysis of two- and three-component reactions in acetonitrile -  $d_3$  (improved solubility of reagents/products) revealed the presence of a multistep reaction pathway leading to IBE complex formation (Scheme 11). These studies revealed that the 2-FPBA **1** template exists in equilibrium with its corresponding borate **1'** and benzoxaborole **1''** species, with strong intramolecular binding of a lone pair of its aldehyde group to the boron centre, activating the aldehyde towards nucleophilic attack.<sup>119–121</sup> Reaction of the aldehyde with an amine produces hemi-aminals **31'** and **31''** that then eliminate water to produce iminoboronic acid **32**. Subsequent addition of catechol then leads to formation of the desired achiral iminoboronate complex **33**. Interestingly, a small amount of the unproductive (*Z*)-imine **32** (no intramolecular  $\text{N} \rightarrow \text{B}$  coordination) was observed in the two-component complexation reaction, which is consumed through equilibration to (*E*)-IBE **33** upon addition of catechol. Similar reaction pathways and intermediates have been suggested and observed by others, including important works by Spozryński and Yatsimirsky.<sup>122–124</sup>



Scheme 11: Stepwise mechanism of the three-component assembly of 2-FPBA **1**, benzylamine **30** and catechol **26** in  $\text{CD}_3\text{CN}$ .<sup>118</sup>

In order to further evaluate the nature of the self-assembly processes operating in these complexation reactions, the observed binding constants for each individual two- and three-component assembly step in methanol were calculated (Scheme 12). These data clearly revealed that guest binding of the diol and amine to the 2-FPBA host is a cooperative process, as demonstrated by the dramatic increase in binding affinities when moving from two- to three-component assemblies. This difference in reactivity was observed upon binding of catechol **26** to the boron centre, as equimolar mixtures of the diol and 2-FPBA **1** did not lead to quantitative formation of formyl boronate ester **34** ( $K_2 = 112 \text{ M}^{-1}$ ), whereas addition of catechol **26** to iminoboronic acid **32** strongly favoured formation of iminoboronate ester **33** ( $K_3 = 2.45 \times 10^3 \text{ M}^{-1}$ ). Similarly, addition of benzylamine to boronate ester **34** to give iminoboronate ester **33** ( $K_4 = 2.40 \times 10^4 \text{ M}^{-1}$ ) was more favoured than addition of benzylamine **30** to 2-FPBA **1** to afford imine **32** ( $K_1 = 110 \text{ M}^{-1}$ ) by an order of magnitude. This further confirms that the strength of binding of the diol to the boron centre to produce a boronate ester complex is increased by the presence of a proximal imine functionality (and *vice versa*). These complexation results are consistent with results reported by Gillingham *et al.* to explain the efficiency of bioorthogonal iminoboronate complexation reactions (*vide infra*), as well as explanations provided to explain the reaction pathways of analogues of *o*-aminomethylphenylboronic acid complexes.<sup>125–127</sup>



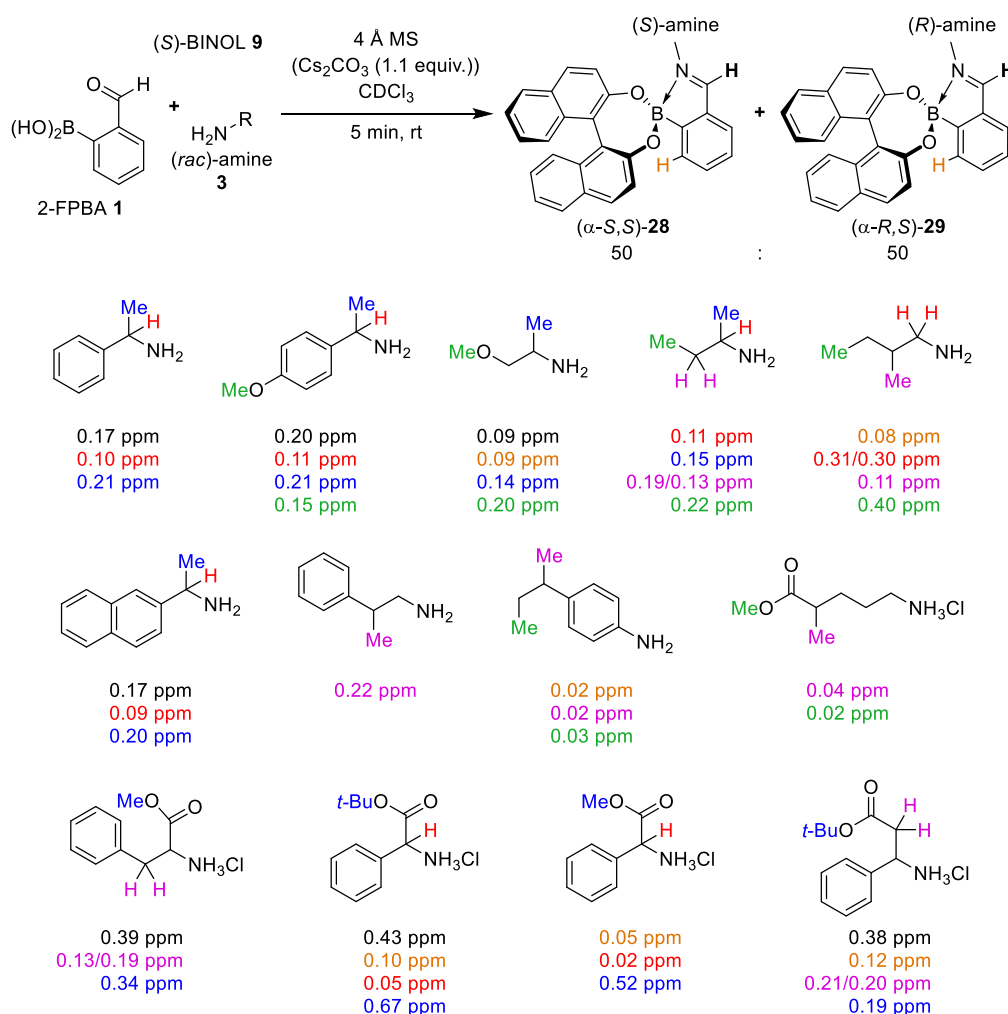
Scheme 12: Observed binding constants for intermediates generated in the three-component assembly reaction of 2-FPBA **1**, benzylamine **30**, and catechol **26** in  $\text{CD}_3\text{OD}$ .<sup>118</sup>

## 1.4. Three-component assembly for determining *ee* by NMR spectroscopic analysis

### 1.4.1 Primary amines

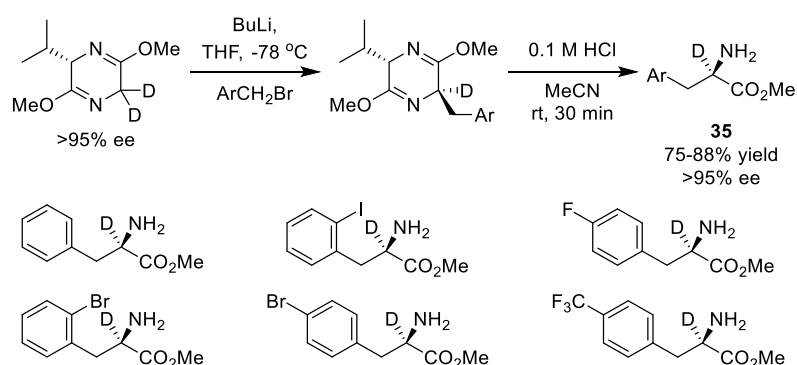
The optimal conditions (enantiopure BINOL,  $\text{CDCl}_3$ , 4 Å molecular sieves, 5 min) that were established to determine the *ee* of 4-methoxy- $\alpha$ -methylbenzene **3b** were then applied to determine the enantiopurities of a wide array of primary chiral amine analytes (Scheme 13).<sup>115</sup> This

derivatization approach shows good scope, affording a series of diastereomeric IBEs **28** and **29** whose  $^1\text{H}$  NMR spectra all exhibited at least one pair of well-resolved diastereomeric signals that could be integrated to determine their  $dr$ 's. Complexation using scalemic samples confirmed that none of these chiral amines underwent any kinetic resolution (or epimerisation) during the derivatization process, thus allowing this new CDA to be used to accurately measure the  $ee$ 's of a wide range of chiral amine analytes. Impressively, this derivatization method was found to be effective for analysing the  $ee$  of primary amines containing remote stereocentres up to 5 carbon atoms removed from the complexed amino group, and direct analysis of chiral ammonium salts could be achieved through incorporation of  $\text{Cs}_2\text{CO}_3$  (1.1 equiv.) as a base for neutralisation. A subsequent report by Urriolabeitia and co-workers described that derivatization of enantiopure phenylglycine methyl ester salts (more labile  $\alpha$ -stereocentre) resulted in formation of mixtures of diastereomeric IBEs when derivatization reactions were left for extended periods of time ( $> 1$  h).<sup>128</sup> This issue was subsequently solved by switching the base used for amine salt neutralisation from  $\text{Cs}_2\text{CO}_3$  to less-soluble  $\text{K}_2\text{CO}_3$ , which allowed racemisation-free derivatization of chiral amine salts containing potentially labile stereocentres to be carried out.<sup>129</sup>

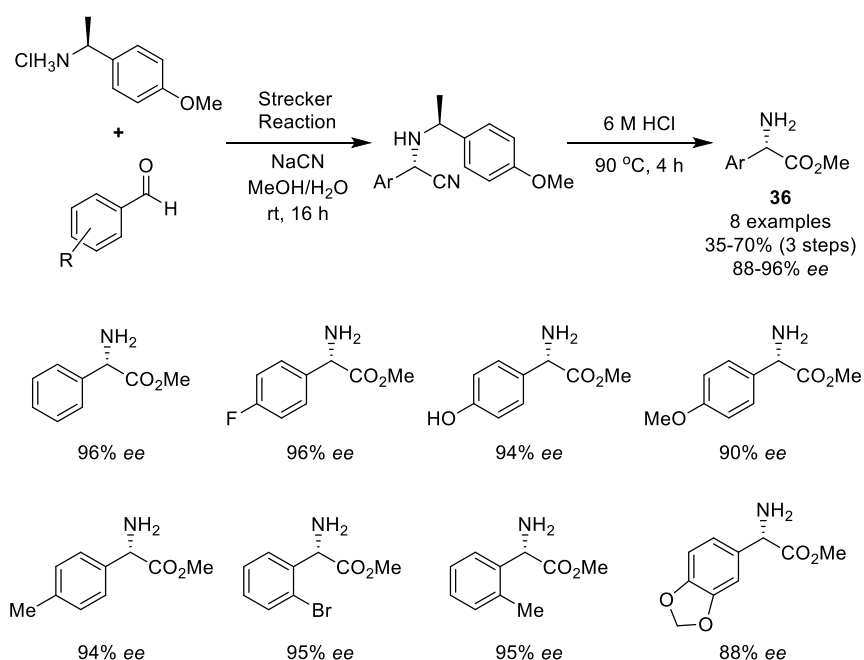


Scheme 13: Three-component assembly reaction of 2-FPBA **1**, (S)-BINOL **9** and (rac)-amines **3** to afford diastereomeric IBEs **28** and **29** with  $^1\text{H}$  NMR (300 MHz,  $\text{CDCl}_3$ , 66.7 mM)  $\Delta\delta_{\text{H}}$  values quoted for selected pairs of diastereomeric resonances.<sup>115</sup>

Since these initial reports, this CDA method has been published as a general procedure in *Nature Protocols*,<sup>116</sup> and has been used by the Bull group to validate the enantioselectivities of a number of new asymmetric methods for the production of chiral amines. Their first application was to confirm the enantiopurities of (*R*)-[ $\alpha$ -<sup>2</sup>H]-phenylalanine methyl esters generated by alkylation of the *aza*-enolate of deuterated Schöllkopf's *bis*-lactim ether **35** (Scheme 14).<sup>130</sup> This CDA method has also been used to confirm the enantiopurities of  $\alpha$ - and  $\beta$ -amino esters **36** and **37** prepared using asymmetric Strecker (Scheme 15) and enantioselective *aza*-conjugate addition reactions, respectively (Scheme 16).<sup>129,131</sup> It has also been used to confirm the enantiopurity of a chiral  $\alpha$ -methylbenzylamine-derived intermediate (*R*)-**38** that was used for the synthesis of a chiral ligand used in the preparation of a pseudo-C<sub>3</sub>-symmetric titanium alkoxide propeller-like complex (Scheme 17).<sup>132</sup>

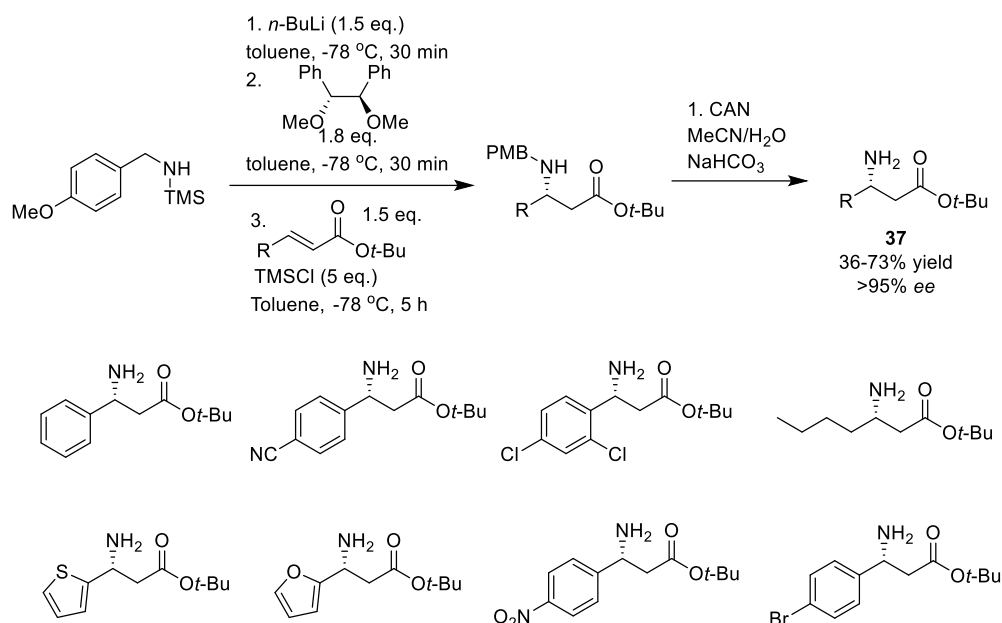


Scheme 14: Three-component CDA method (using enantiopure (*R*)-BINOL **9**) used to determine the *ee*'s of  $\alpha$ -deuterated- $\alpha$ -amino esters **35** produced in asymmetric enolate alkylation reactions.<sup>130</sup>

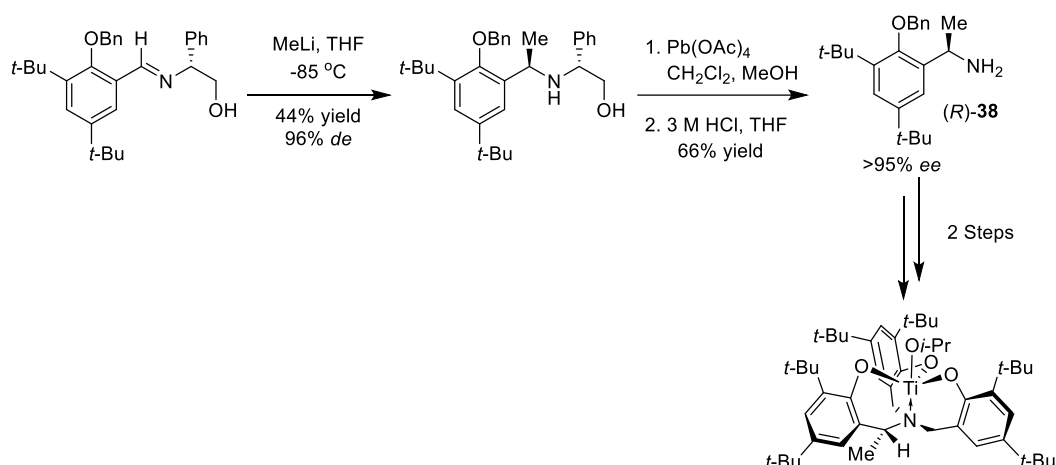


Scheme 15: Three-component CDA (using enantiopure (*S*)-BINOL **9**) used to determine the *ee*'s of  $\alpha$ -arylglycines **36** produced in asymmetric Strecker reactions.<sup>129</sup>



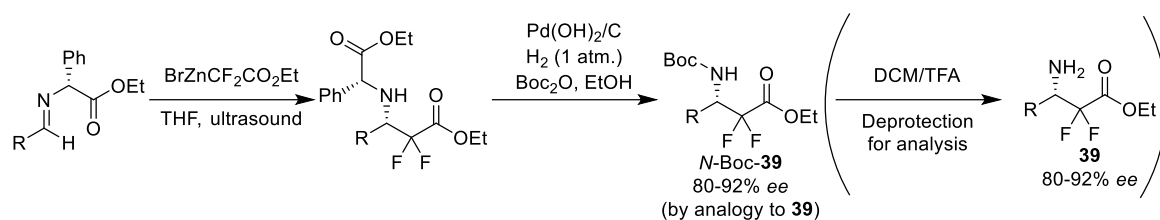


Scheme 16: Three-component CDA (using enantiopure (*R*)-BINOL **9**) used to determine the *ee*'s of *tert*-butyl β-amino esters **37** produced in enantioselective *aza*-conjugate addition reactions.<sup>131</sup>

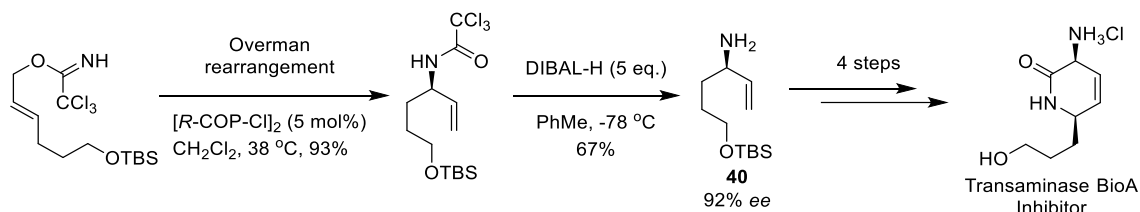


Scheme 17: Three-component CDA (using enantiopure BINOL **9**) used to determine the *ee* of a tetradentate amine ligand (*R*)-**38** used to prepare an enantiopure 'propeller-like' pseudo-C<sub>3</sub>-symmetric titanium alkoxide.<sup>132</sup>

Other research groups have also used the Bull-James assembly to determine the *ee* of amines produced in various stereoselective protocols. Duggan *et al.*, for instance, reported a novel synthesis of aliphatic α,α-difluoro-β<sup>3</sup>-amino esters **39** through addition of zinc enolates to chiral phenylglycine-derived imines (Scheme 18),<sup>133</sup> with the three-component CDA approach then used to demonstrate that the *N*-Boc-deprotected amine products had *ee*'s of 80-92%. The *ee* of a chiral allyl amine intermediate **40**, produced in an enantioselective Overman-rearrangement that was used to synthesise a transaminase BioA inhibitor (potential antitubercular agent), was also measured in this manner (Scheme 19).<sup>134</sup>

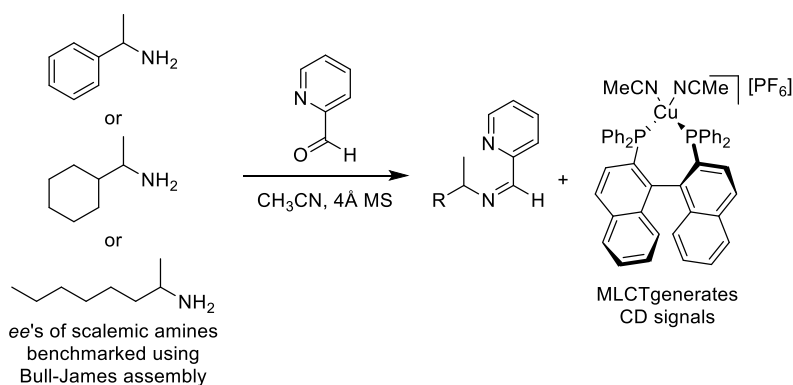


Scheme 18: Three-component CDA method (using enantiopure (*S*)-BINOL **9**) used to determine the *ee* of an  $\alpha,\alpha$ -difluoro- $\beta^3$ -amino esters **39** prepared using a sonocatalyzed Reformatsky reaction.<sup>133</sup>



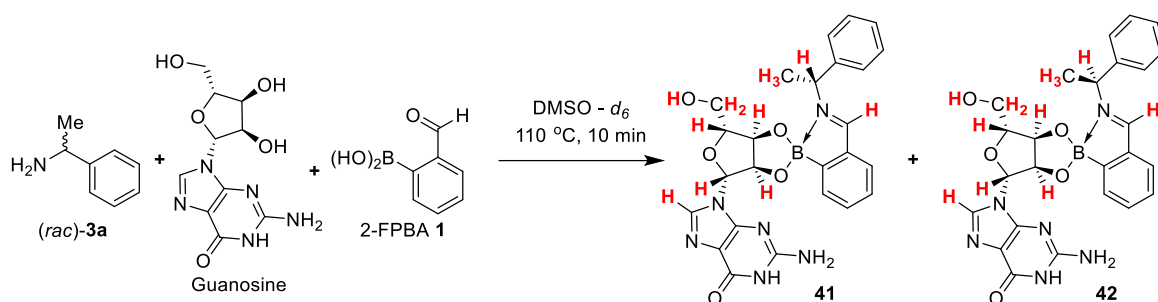
Scheme 19: Three-component CDA method (using enantiopure BINOL **9**) used to determine the *ee* of a chiral allylamine **40** produced in an enantioselective Overman rearrangement reaction.<sup>134</sup>

The Anslyn group have also employed NMR spectroscopic analysis of three-component IBE assemblies to benchmark the *ee*'s of amine analytes. These amines were subsequently used to develop a new CD method for high-throughput *ee* determination based on formation of diastereomeric chiral copper complexes that produce different metal-to-ligand charge transfer (MLCT) bands in the visible region of their CD spectra (Scheme 20).<sup>135</sup>



Scheme 20: Three-component analysis used to benchmark the *ee*'s of chiral amines used to develop a MLCT CD assay for high-throughput determination of the *ee*'s of primary amines (using (*S*)-BINOL **9**).<sup>135</sup>

Suryaprakash *et al.* have reported the use of the chiral diol fragments of RNA nucleosides as chiral selectors for determining the *ee* of a small range of amines,<sup>136</sup> as shown for the complexation reaction of guanosine, 2-FPBA **1** and (*rac*)- $\alpha$ -methylbenzylamine **3a** to produce the diastereomeric complexes **41** and **42** shown in Scheme 21. These complexation reactions required more forcing and solubilising reaction conditions (DMSO, 110 °C) to proceed to completion, and whilst the structural complexity of these diastereomeric IBEs afforded multiple resolved resonance pairs (red), 800 MHz  $^1\text{H}$  NMR spectra were required to fully resolve them.

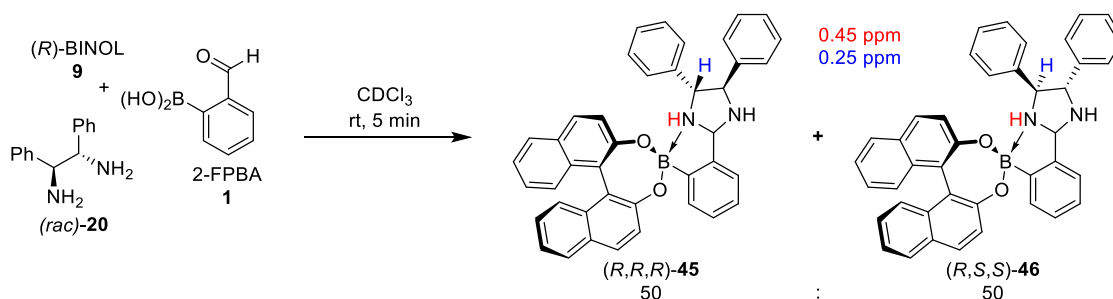


Scheme 21: Three-component assembly of 2-FPBA **1**, guanosine, and (*rac*)- $\alpha$ -methylbenzylamine **3a**. Pairs of diastereomeric protons that exhibited distinct resonances in a 800 MHz  $^1\text{H}$  NMR spectrum are shown in red.<sup>136</sup>

Fossey and co-workers have exemplified the experimental simplicity and reproducibility of this NMR derivatization protocol by successfully using it as the basis of a research-informed undergraduate teaching class that was used to train a cohort of > 100 2<sup>nd</sup> year undergraduate students at the University of Birmingham (UK).<sup>137</sup> An optimised iminoboronate protocol using 2-FPBA **1**, (*R*)-BINOL **9**, and  $\alpha$ -methylbenzylamine **3a** was used as an educational tool to introduce the students to the principles of dynamic covalent supramolecular chemistry and methods of determining the enantiopurities of chiral molecules, whilst reinforcing their knowledge of carbonyl condensation chemistry and fundamental Lewis acid/base coordination processes.

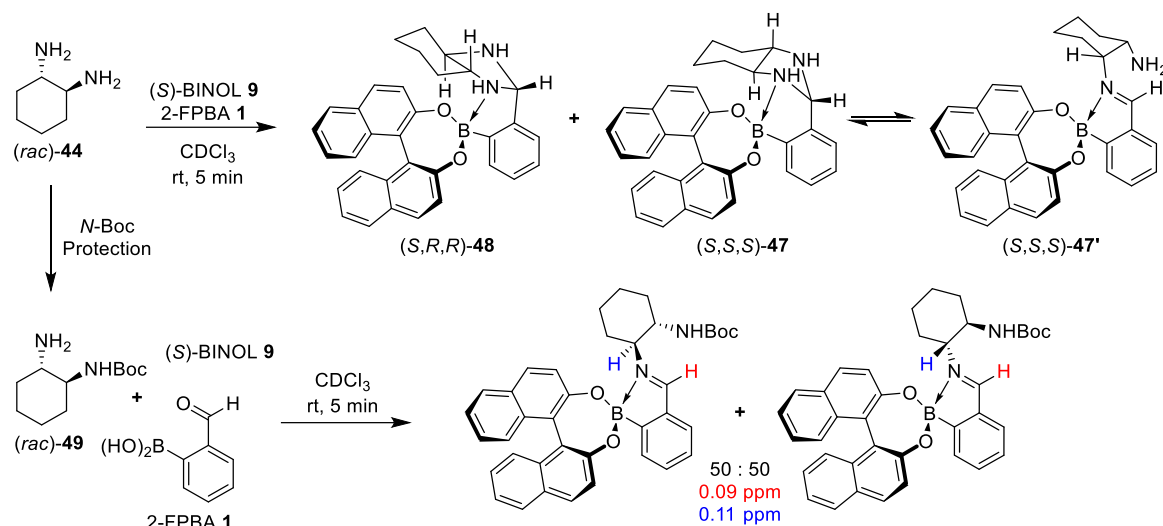
#### 1.4.2 Diamines

As alluded to previously, the Bull-James CDA protocol can be employed for a variety of analytes, and so was subsequently applied to determine the *ee*'s of two widely used *trans*-diamines: *trans*-1,2-diphenylethane-1,2-diamine **43** and *trans*-cyclohexane-1,2-diamine **44**.<sup>138</sup> Reaction of diamine (*rac*)-**43** with (*R*)-BINOL **9** and 2-FPBA **1** resulted in the formation of a pair of diastereomeric imidazolidines (*R,R,R*)-**45** and (*R,S,S*)-**46**,<sup>139–141</sup> which exhibited well-resolved pairs of diastereomeric signals for the amino (red) and benzylic (blue) protons proximal to their BINOL fragments being observed in their  $^1\text{H}$  NMR spectra (Scheme 22).<sup>138</sup> Furthermore, these diastereomeric IBE complexes were found to be stable enough for N-H deuteriation by addition of  $\text{D}_2\text{O}$ , which resulted in simplified  $^1\text{H}$  NMR spectra that enabled more accurate determination of *dr*'s.



Scheme 22: Three-component assembly of 2-FPBA **1**, (*R*)-BINOL **9** and (*rac*)-*trans*-diphenylethylene diamine **43** to produce a pair of diastereomeric imidazolidine boronate esters **45** and **46** with  $^1\text{H}$  NMR (500 MHz,  $\text{CDCl}_3$ )  $\Delta\delta_{\text{H}}$  of selected resonances.<sup>138</sup>

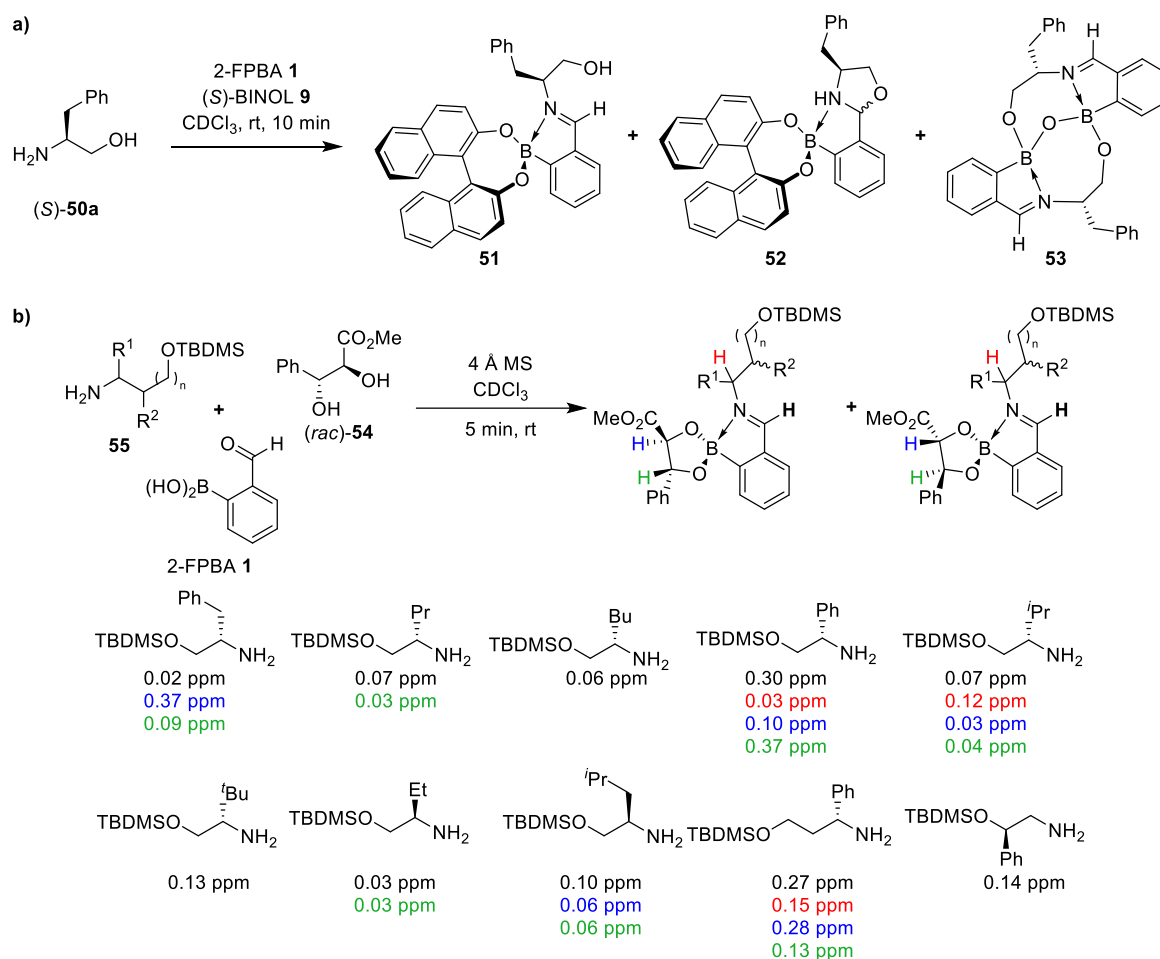
Unfortunately, applying this CDA approach to *trans*-cyclohexane-1,2-diamine **44** proved unsuccessful, with its derivatization with (*S*)-BINOL **9** and 2-FPBA **1** producing a mixture of products (Scheme 23). Although the heterochiral imidazolidine complex (*S,R,R*)-**48** proved stable, increased steric demands within the homochiral complex resulted in formation of a dynamically equilibrating mixture of imidazolidine (*S,S,S*)-**47** and its corresponding imine (*S,S,S*)-**47'**. A simple solution to this problem was achieved, through *N*-Boc-protection of the parent diamine **44** to afford *N*-Boc-diamine **49**, which then underwent IBE derivatization to afford the desired mixture of IBE diastereomers in the usual manner.



Scheme 23: Three-component derivatization of 2-FPBA **1**, (*S*)-BINOL **9** with (*rac*)-*trans*-cyclohexane-1,2-diamine **44** and (*rac*)-*N*-Boc-*trans*-cyclohexane-1,2-diamine **49** with  $^1\text{H}$  NMR (400 MHz,  $\text{CDCl}_3$ , 80 mM)  $\Delta\delta_H$  of selected resonances.<sup>138</sup>

### 1.4.3 Amino alcohols

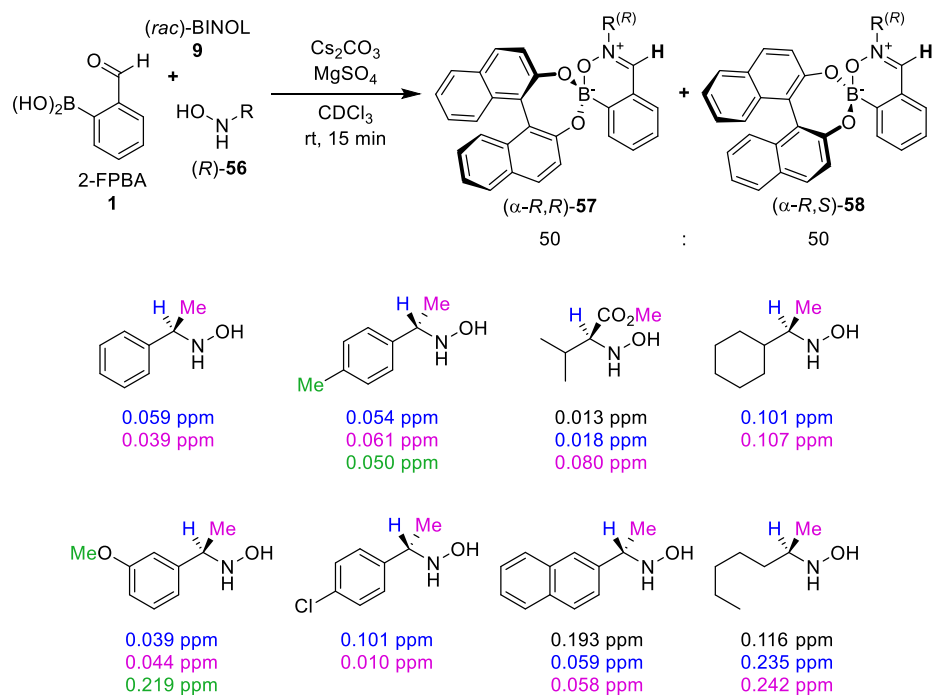
Attempts to apply the CDA methodology to 1,2-amino alcohols proved similarly problematic, with assembly of (*S*)-phenylglycinol **50**, 2-FPBA **1** and (*S*)-BINOL **9** producing complex equilibrating mixtures of products (Scheme 24), including the desired IBE **51**, oxazolidine boronate ester **52** and a larger polyboracycle **53**.<sup>142</sup> Once again, the problems caused by these competing complexations could be solved using a protection strategy, with *O*-silylation of the problematic alcohol functionality prior to assembly resulting in the three-component complexation proceeding smoothly to give the desired diastereomeric IBEs. A simple diol screen revealed that the best results were obtained when BINOL **9** was substituted by (*rac*)-(*syn*)-methyl 2,3-dihydroxy-3-phenylpropionate **54**, which was subsequently employed for the successful three-component derivatization of ten enantiopure *O*-silyl amino alcohol analytes **55**.



Scheme 24: (a) Problematic three-component assembly of (S)-phenylglycinol **50**, 2-FPBA **1**, and (S)-BINOL **9**. (b) Three-component derivatization of 2-FPBA **1**, (rac)-**54** and O-silylated 1,2-amino alcohols **55** with <sup>1</sup>H NMR (400 MHz, CDCl<sub>3</sub>, 80 mM)  $\Delta\delta_H$  of selected resonances.<sup>142</sup>

#### 1.4.4 Hydroxylamines

Bull-James assembly of chiral hydroxylamines **56** with 2-FPBA **1** and (rac)-BINOL **9** in the presence of a Cs<sub>2</sub>CO<sub>3</sub> base gave mixtures of diastereomeric nitrono-boronate esters **57/58** (Scheme 25).<sup>143</sup> Unlike amines, which form five-membered IBEs containing an intramolecular N → B bond, hydroxylamines gave more stable diastereomeric six-membered nitrono-boronate ester complexes whose formation was favoured by both strong N-O and O-B bonds.<sup>113,144</sup> These structures were confirmed by X-ray crystallography of (α-S,R)-**58f**, which revealed a bicyclic assembly containing a coplanar zwitterionic -C=N<sup>+</sup>-O-B<sup>-</sup> arrangement (Figure 5). This produces a rigid ring system that produces relatively large chemical shift differences for selected pairs of diastereomer resonances (up to 0.242 ppm) in their <sup>1</sup>H NMR spectra.



Scheme 25: Three-component assembly of 2-FPBA **1**, (*rac*)-BINOL **9**, and hydroxylamines **56** to form diastereomeric nitrono-boronate ester complexes **57** and **58** with  $^1\text{H}$  NMR (500 MHz,  $\text{CDCl}_3$ , 80-115 mM)  $\Delta\delta_H$  of selected resonances.<sup>143</sup>

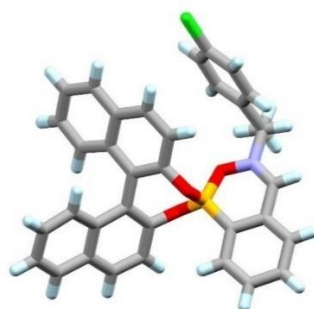
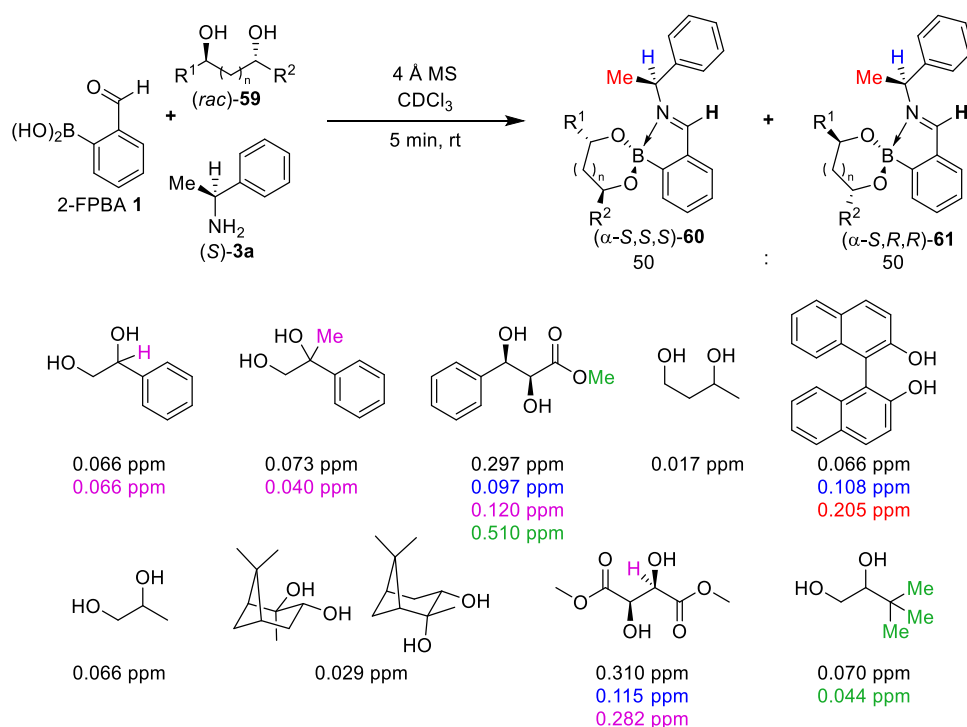


Figure 5: X-Ray crystal structure of ( $\alpha$ -*S,R*)-**58f**, from (*S*)-4-chloro- $\alpha$ -methylbenzylamine **56f**.<sup>143</sup>

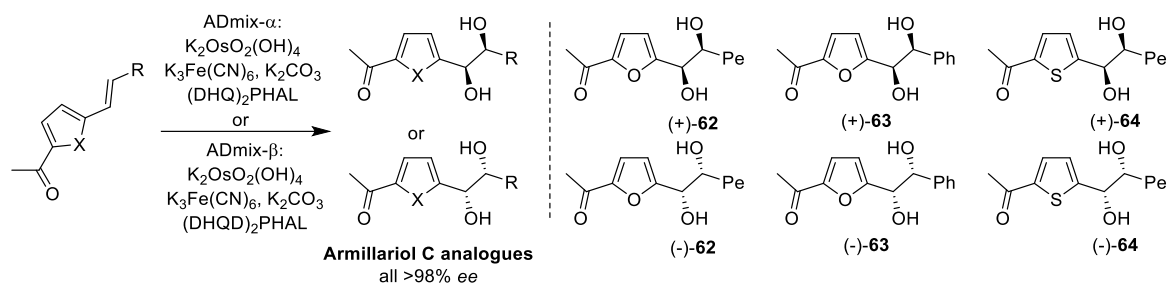
#### 1.4.5 Diols

The role of analyte and chiral reporter in the three-component CDA are broadly interchangeable, and so the Bull-James assembly has also been adapted to determine the *ee*'s of chiral 1,2- and 1,3-diol analytes through use of an enantiopure amine chiral reporter (Scheme 26).<sup>145</sup>  $\alpha$ -Methylbenzylamine (*S*)-**3a** was chosen as a cheap readily available chiral amine reporter for reaction with 2-FPBA **1** and a range of racemic chiral diols **59**, which produced diastereomeric complexes ( $\alpha$ -*S,S,S*)-**60** and ( $\alpha$ -*S,R,R*)-**61**, which exhibited one or more baseline-resolved pairs of signals for their IBE diastereomers in their  $^1\text{H}$  NMR spectra.

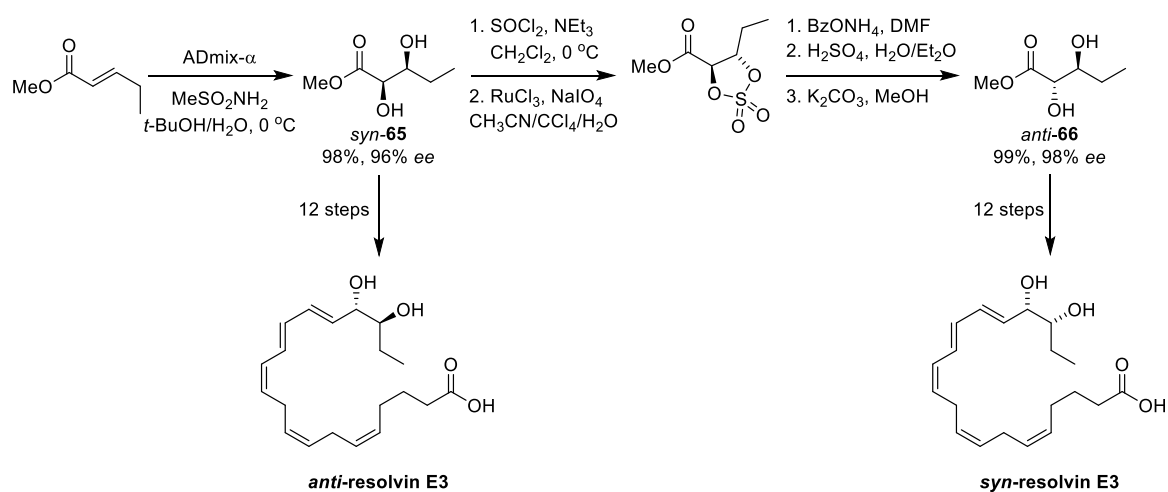


Scheme 26: Three-component assembly using 2-FPBA **1**, (S)-α-methyl benzylamine **3a** and (rac)-diols **59** with <sup>1</sup>H NMR (300 MHz, CDCl<sub>3</sub>, 66.7 mM)  $\Delta\delta_H$  of selected resonances.<sup>145</sup>

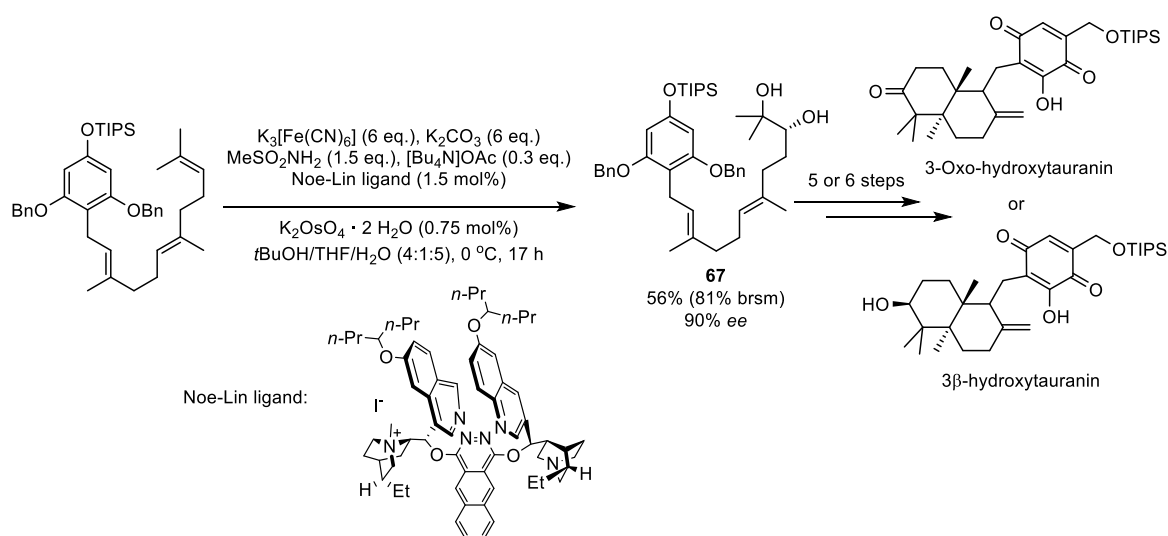
This method has also been published as a detailed general procedure in *Nature Protocols*,<sup>146</sup> and has subsequently been applied to determine the *ee* of a range of chiral 1,2-diols by a number of research groups. One elegant example is the work by Watkins *et al.*, who employed the CDA (using (S)-α-methylbenzylamine **3a**) to determine the *ee*'s of a range of chiral furan and thiophene diols (**62/63** and **64** respectively) prepared using Sharpless enantioselective ADmix dihydroxylation methodology, that were used for the first stereoselective synthesis of (+)-armillariol C **62** (Scheme 27).<sup>147</sup> Inoue *et al.* used enantioselective dihydroxylation reactions of α,β-unsaturated esters to prepare both enantiomers of *syn*-diol **65** (shown for ADmix-α), whose β-stereocentres were then inverted in two steps *via* cyclic organosulfate intermediates to afford their corresponding *anti*-diols **66**. The enantiopurities of all four diol stereoisomers were determined as 96-99% *ee* using three-component chiral derivatization (using α-methylbenzylamine **3a**), with these stereoisomers then transformed into the four corresponding stereoisomers of resolvins E3 (Scheme 28).<sup>148</sup> Similarly, this CDA approach has been used to determine the enantiopurity of diol **67** (90% *ee*, single stereocentre, using both (*R*)- and (*S*)-**3a**) that was also produced in an enantioselective dihydroxylation reaction and subsequently used to prepare 3-oxo and 3β-hydroxytauranin (Scheme 29).<sup>149</sup>



Scheme 27: Three-component CDA method (using enantiopure (*S*)- $\alpha$ -methylbenzylamine **3a**) used to determine the ee of both enantiomers of armillariol C **62** and analogues **63/64** that were produced using a Sharpless asymmetric dihydroxylation reaction.<sup>147</sup>



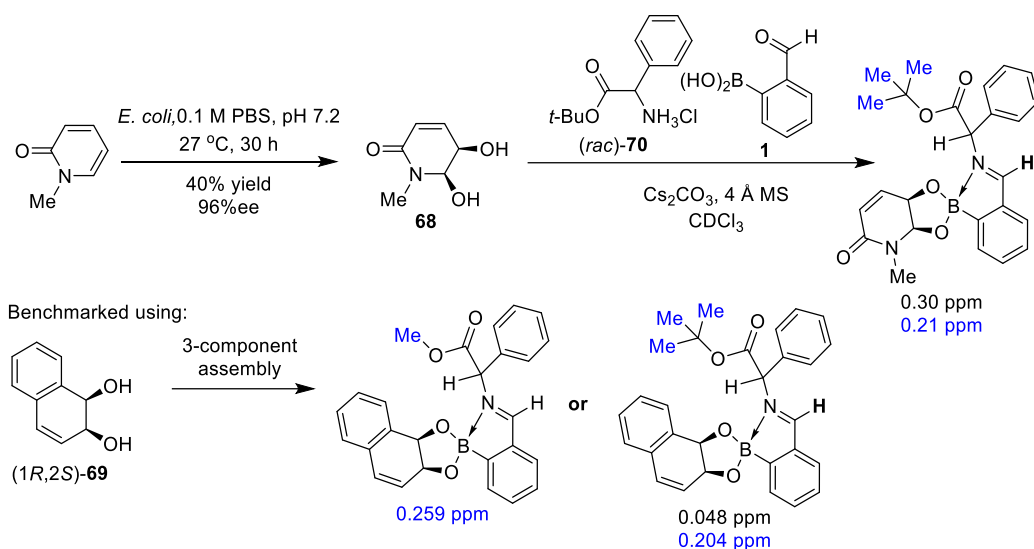
Scheme 28: Three-component CDA method (using enantiopure  $\alpha$ -methylbenzylamine **3a**) used to determine the ee's of *syn*- and *anti*-diols **65** & **66** that were subsequently used to synthesis all four possible stereoisomers of resolvin E3 (shown for ADmix- $\alpha$ ).<sup>148</sup>



Scheme 29: Three-component CDA method (using enantiopure (*R*)- and (*S*)- $\alpha$ -methylbenzylamine **3a**) used to determine the ee of diol **67** that was subsequently used for total syntheses of 3-oxo- and 3β-hydroxytauranin.<sup>149</sup>

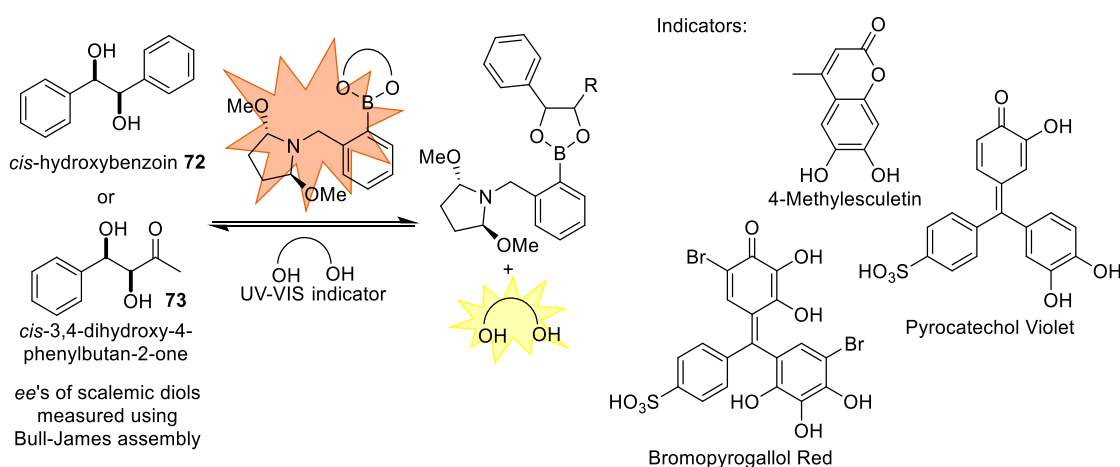


Chopard *et al.* have used the three-component CDA to determine the enantiopurities of *cis*-diols **68** and **69**, produced from the microbial *cis*-dihydroxylation of naphthalenes and pyridinones. In this instance, the chiral amine reporter used for derivatization was optimised, which identified phenylglycine *tert*-butyl ester **70** as the chiral reporter that gave diastereomeric IBEs with the best  $\Delta\delta_H$  values (Scheme 30).<sup>150</sup>



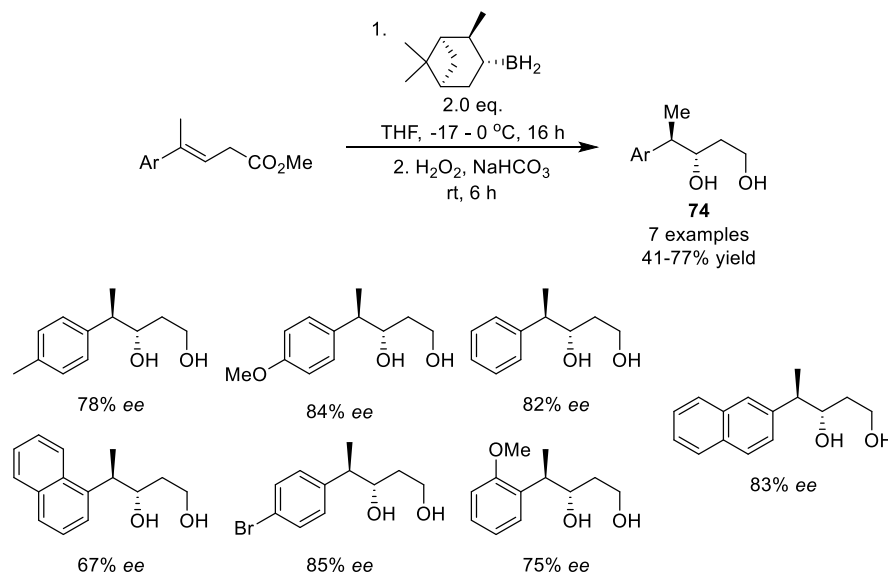
Scheme 30: Three-component assembly for determining the enantiopurity of *cis*-diol arenes using phenylglycine *tert*-butyl ester **70** and 2-FPBA **1** with  $^1\text{H}$  NMR (250 MHz,  $\text{CDCl}_3$ , 44 mM)  $\Delta\delta_H$  of selected resonances.<sup>150</sup>

The three-component CDA was also used to measure the *ee*'s of *cis*-diols **72** and **73** produced in Sharpless dihydroxylation reactions by Anslyn *et al.* (Scheme 31).<sup>151,152</sup> The *ee*'s of these diols were then used to benchmark indicator displacement UV-Vis assays for the high-throughput determination of yields and enantioselectivities of Sharpless dihydroxylation reactions. This approach employed reversible host/guest assemblies of an *o*-aminomethylphenylboronic acid sensor, in which the UV-VIS signal intensity is directly determined by the *ee* and concentration of the analyte.<sup>151,152</sup>

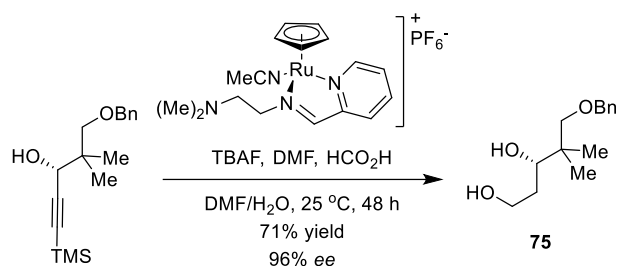


Scheme 31: Indicator displacement assay used for UV-Vis and colorimetric determination of enantioselectivity and yield of *cis*-diols **72** and **73** produced in Sharpless dihydroxylation reactions.<sup>152</sup>

The Bull group have applied the CDA method to determine the *ee* of a range of chiral 1,3-diols **74** synthesised in moderate to good *ee* by tandem hydroboration/reduction of  $\beta,\gamma$ -unsaturated esters (Scheme 32).<sup>153</sup> The three-component assembly CDA has also been used by Herzon *et al.* to determine the *ee* of 1,3-diol **75** (92%) that was synthesised by catalytic reductive hydration of a chiral alkynylsilane by sequential hydration/hydrogenation using a novel half-sandwich ruthenium complex and formic acid (Scheme 33).<sup>154</sup>



Scheme 32: Three-component CDA method (using enantiopure (S)- $\alpha$ -methylbenzylamine **3a**) used to measure the *ee*'s of chiral 1,3-diols **74** formed in tandem chiral borane-mediated asymmetric hydroboration/reduction reactions of  $\beta,\gamma$ -unsaturated esters.<sup>153</sup>



Scheme 33: Three-component CDA (using enantiopure  $\alpha$ -methylbenzylamine **3a**) to measure the *ee* of a 1,3-diol **75** formed in a stereoselective reductive hydration reaction of an alkynyl alcohol catalysed by a half-sandwich ruthenium complex.<sup>154</sup>

The three-component CDA has also been used to assess the enantiopurity of polymers containing diol fragments, with Kressler *et al.* reporting its application to determine the enantiopurities of poly(glycerol methacrylate)s (PGMAs, **76**) that were prepared from enantiopure solketal methacrylate monomers using atom transfer radical polymerization (ATRP) reactions.<sup>155</sup> Enantiopure and racemic polymer chains were derivatised with  $\alpha$ -methylbenzylamine **3a** and 2-FPBA **1** in DMSO - *d*<sub>6</sub>, to afford mixtures of iminoboronates ( $\alpha$ -S,S)-**77** and ( $\alpha$ -S,R)-**78** that exhibited several pairs of distinct diastereomeric resonances in their <sup>1</sup>H NMR spectra (Figure 6). Peak

broadening caused by the polymeric backbone meant that baseline resolution was not observed, however the  $\Delta\delta_H$ 's of the polymer's methine, *exo* methylene and *endo* methylene proton signals ( $H_a$ ,  $H_b$ ,  $H_c$ , respectively) were sufficiently different to enable qualitative assessment of the enantiopurity and absolute configurations of the PGMA side-chains of these polymers.

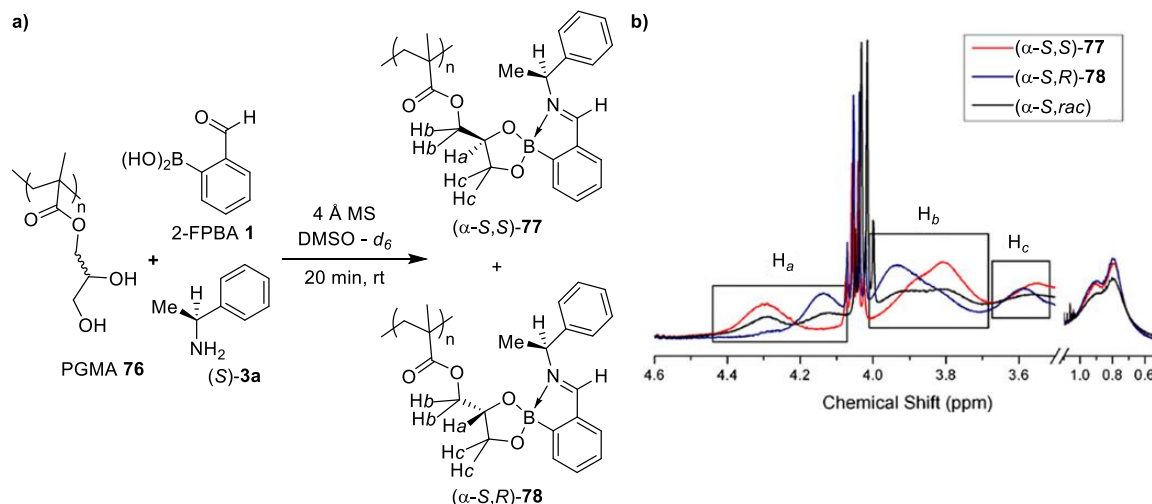
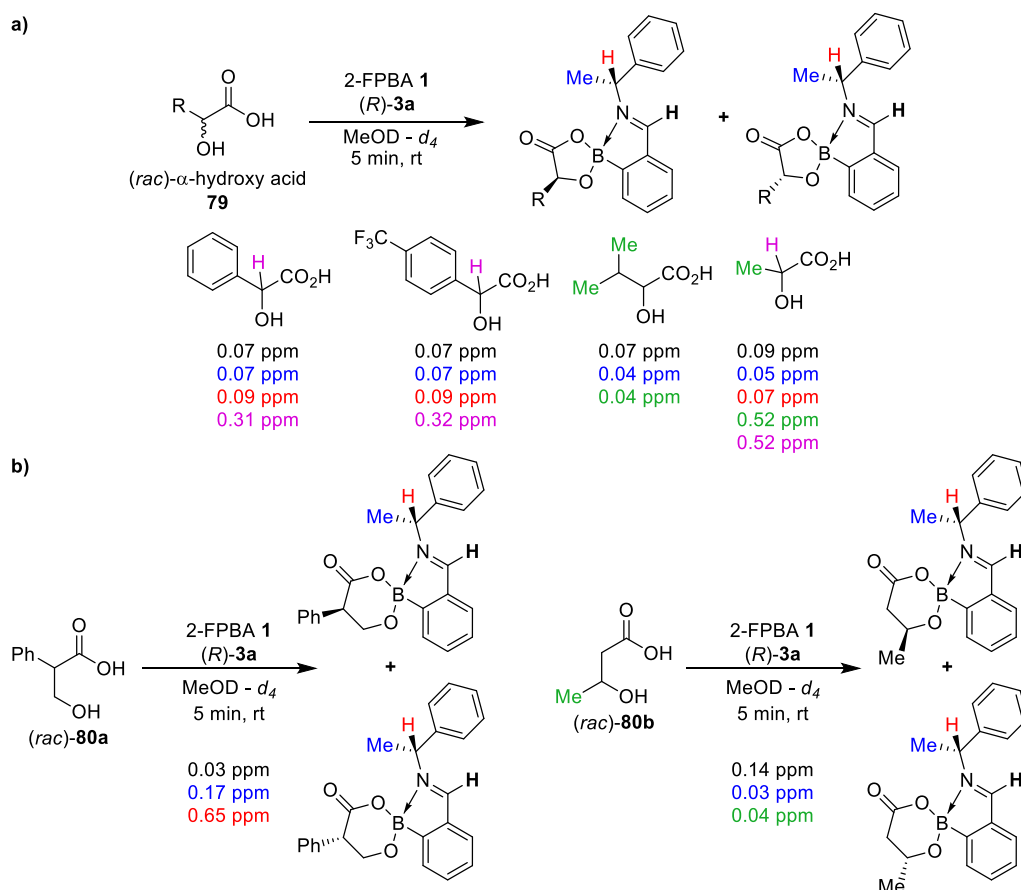


Figure 6: (a) Bull-James assembly used for derivatization of the diol side-chain of PGMA **76**. (b) Inset of <sup>1</sup>H NMR (400 MHz, DMSO – *d*<sub>6</sub>, ~ 6 mM) spectra showing chemical shift variation of  $H_a$ ,  $H_b$  and  $H_c$  resonances of complexes of (S)-PGMA (red), (R)-PGMA (blue) and (rac)-PGMA (black).<sup>155</sup> Reproduced with permission from Elsevier.

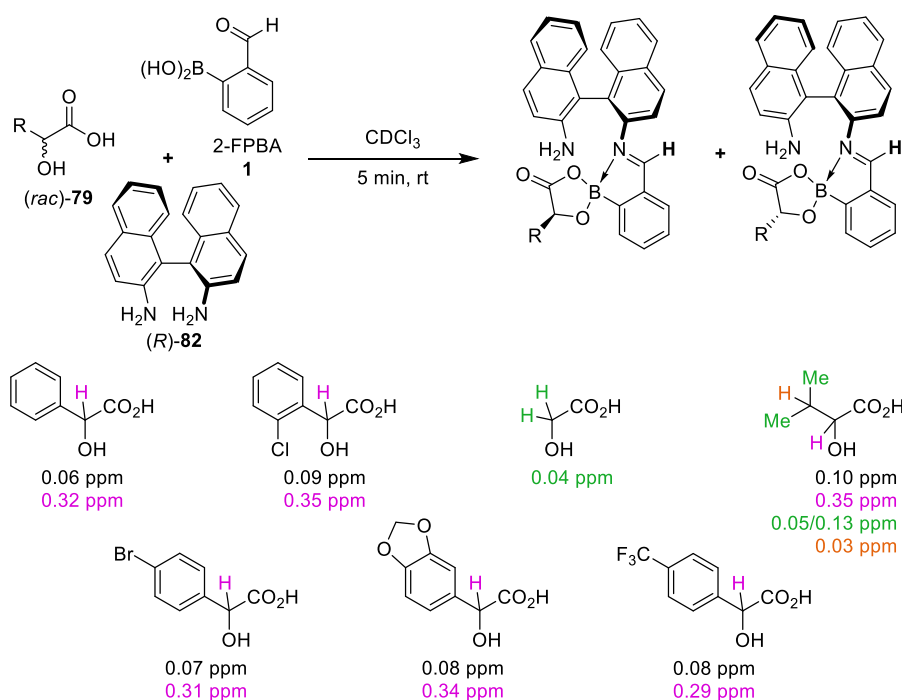
#### 1.4.6 Hydroxyacids and diacids

The groups of Chaudhari and Suryaprakash have also expanded the scope of the Bull-James assembly CDA by demonstrating that it can be used to determine the enantiopurities of hydroxyacids **79/80** and 1,4-diacids **81**.<sup>156–158</sup> Treatment of (rac)-α-hydroxyacids **79** (Scheme 34a) and (rac)-β-hydroxyacids **80** (Scheme 34b) with 2-FPBA **1** and α-methylbenzylamine **3a** in MeO-*d*<sub>4</sub> resulted in mixtures of diastereomeric iminoboronate esters which showed modest to excellent  $\Delta\delta_H$  (0.04-0.65 ppm) values in their <sup>1</sup>H NMR spectra. As in previous reports, the role of analyte and reporter in these IBE complexes was found to be interchangeable, and so corresponding use of an enantiopure hydroxyacid could be used to determine the *ee* of scalemic amines.



Scheme 34: Three-component CDA for determining the enantiopurities of (a)  $\alpha$ -hydroxyacids **79**; and (b)  $\beta$ -hydroxyacids **80** with  $^1\text{H}$  NMR (400 MHz,  $\text{MeOD-}d_4$ , ~300 mM)  $\Delta\delta_H$  of selected resonances.<sup>156–158</sup>

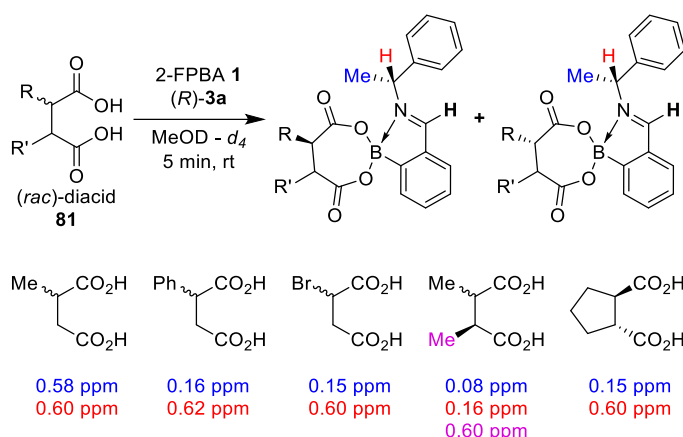
This methodology was optimised further to improve resolution and sensitivity, with the chiral amine reporter used for IBE complex formation changed from  $\alpha$ -methylbenzylamine **3a** to axially chiral diamine BINAM **82**.<sup>158</sup> Three-component assembly of  $\alpha$ -hydroxyacids **79**, 2-FPBA **1** and BINAM **82** produced diastereomeric IBEs which exhibited excellent chemical shift differences for pairs of diastereomeric resonances in their  $^1\text{H}$ ,  $^{13}\text{C}\{^1\text{H}\}$  and  $^{11}\text{B}$  NMR spectra (Scheme 35). Interestingly, the excellent chiral discrimination produced in this self-assembled system resulted in chemical shift differences being observed in an IBE complex derived from achiral substrate glyconic acid, which exhibited a  $\Delta\delta_H = 0.04$  ppm value for the prochiral  $\alpha$ -protons of its IBE complex.



Scheme 35: Three-component CDA for determining the enantiopurities of  $\alpha$ -hydroxyacids **79** using 2-FPBA **1** and BINAM **82** with selected  $^1\text{H}$  NMR ( $400\text{ MHz}$ ,  $\text{CDCl}_3$ ,  $\sim 300\text{ mM}$ )  $\Delta\delta_{\text{H}}$  of selected resonances.<sup>158</sup>

Simple conformational models of the IBE complexes formed in these systems were developed, allowing the absolute configuration of hydroxyacids to be predicted using either BINAM **82** or  $\alpha$ -methylbenzylamine **3a** as a chiral reporter.<sup>159,160</sup> Following benchmarking, analysis of the relative signs of the  $\Delta\delta_{\text{H}}$  values, broadness of signals and 2D nOe interactions enabled the absolute configuration of a range of hydroxyacids and primary amines to be assigned using BINAM **82** as a chiral reporter. In those cases where assignment was hampered by significant signal overlap in the  $^1\text{H}$  NMR spectra, these resonances could be successfully deconvoluted using simple 2D RES-TOCSY  $^1\text{H}$  NMR experiments.<sup>161</sup>

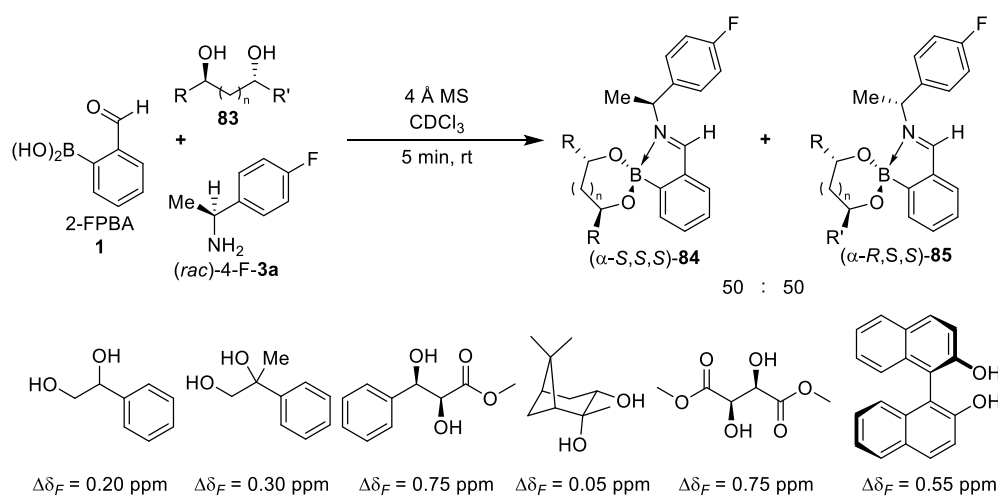
These three-component assembly protocols were also used to determine the *ee*'s of chiral 1,4-diacids **81** (Scheme 36), resulting in moderate to excellent chemical shift differences ( $\Delta\delta_{\text{H}} = 0.08\text{--}0.62\text{ ppm}$ ) in the  $^1\text{H}$  NMR spectra of the diastereomeric IBEs of five diacid analytes.<sup>157</sup> Once again, the components of this assembly could be switched, enabling chiral diacids to be used to produce diastereomeric IBE complexes to determine the *ee*'s of chiral primary amines. In some instances, the large chemical shift differences observed in these diacid/amine-derived IBE complexes even led to full resolution of certain  $^{13}\text{C}\{^1\text{H}\}$  NMR signals.



Scheme 36: Three-component CDA for determining the enantiopurity of 1,4-diacids **81** with <sup>1</sup>H NMR (400 MHz, MeOD – *d*<sub>4</sub>, ~300 mM)  $\Delta\delta_H$  of selected resonances.<sup>157</sup>

#### 1.4.7 <sup>19</sup>F NMR spectroscopic analysis

Fluorine was the first NMR-active heteronucleus to be studied for compatibility with the Bull-James assembly, due to the strength of its signal, its broad range of chemical shifts, and the simplicity of <sup>19</sup>F NMR spectra making it an excellent and widely-used NMR-active reporter. Bull and James first demonstrated incorporation of fluorine into their three-component assembly in 2009,<sup>162,163</sup> with initial work focusing on using a fluorinated chiral amine reporter in the three-component protocol (Scheme 37). A range of diols **83**, 4-fluoro- $\alpha$ -methylbenzylamine 4-F-**3a** and 2-FPBA **1** were derivatised to form <sup>19</sup>F NMR-active complexes ( $\alpha$ -S,S)-**84** and ( $\alpha$ -R,S,S)-**85**, which exhibited a  $\Delta\delta_F$  range of 0.05-0.75 ppm between diastereomers. A similar approach was subsequently employed by Suryaprakash *et al.* for analysis of hydroxyacid and diacid protocols, with CF<sub>3</sub>-appended chiral reporters and analytes affording diastereomeric complexes with non-equivalent <sup>19</sup>F NMR signals that could be integrated to determine their *dr*.<sup>156,157</sup>



Scheme 37: Three-component protocol using 2-FPBA **1**, 4-fluoro- $\alpha$ -methylbenzylamine 4-F-**3a** and chiral diols **83** to produce fluorinated diastereomeric complexes with good <sup>19</sup>F NMR (400 MHz, CDCl<sub>3</sub>, 66.7 mM)  $\Delta\delta_F$  values.<sup>162</sup>

A significant improvement to this fluororous approach was achieved by incorporating the fluorine reporter atom into the achiral 2-FPBA template to produce a generally applicable method for determining the *ee* of different classes of chiral analytes. 4-fluoro-2-formylphenylboronic acid (4-F-2-FPBA, 4-F-1) was synthesised and used in the three-component assembly protocol, producing fluorinated diastereomeric complexes **86/87** which afforded baseline-resolved signals in their  $^{19}\text{F}$  NMR spectra, allowing for *ee* determination of diols by both  $^{19}\text{F}$  and  $^1\text{H}$  NMR spectroscopic analysis (Figure 7). Similar results were reported by Suryaprakash *et al.* during their later work on applying this CDA to determine the enantiopurity of diacids (*vide supra*).<sup>157</sup>

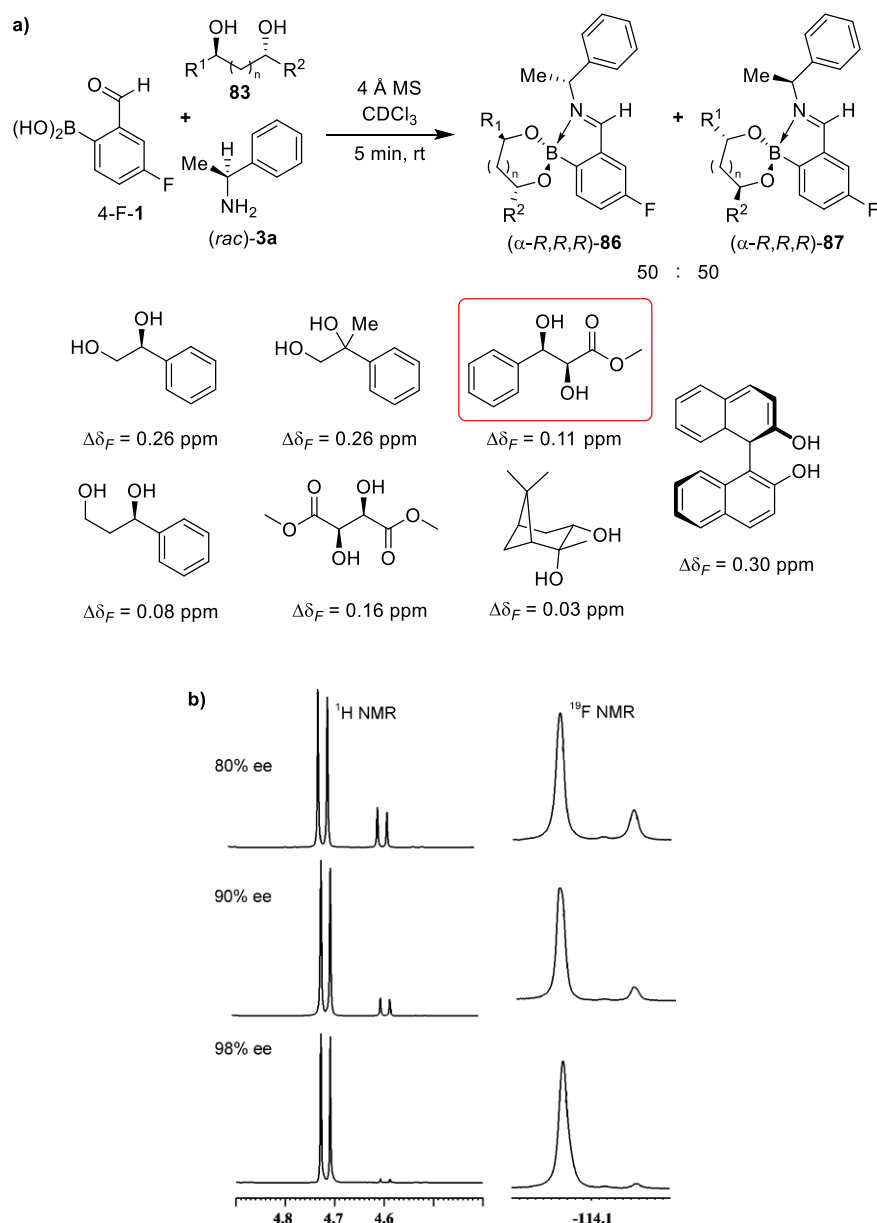
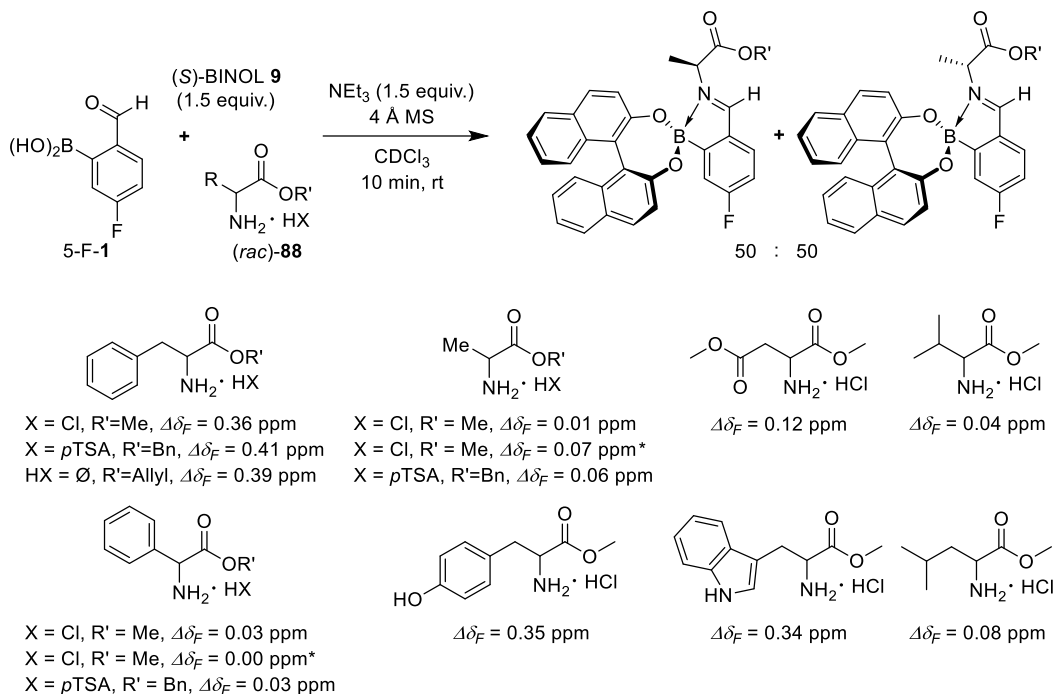


Figure 7: (a) Three-component protocol using 4-F-1, (*rac*)- $\alpha$ -methylbenzylamine **3a** and chiral diols **83**. (b) Expansion of  $^1\text{H}$  (500 MHz,  $\text{CDCl}_3$ , 66.7 mM) and  $^{19}\text{F}$  (470 MHz,  $\text{CDCl}_3$ , 66.7 mM) NMR spectra of three-component assembly of 4-F-1, (*R*)-**3a** and a scalemic diol (red) at 80%, 90% and 98% *ee*.<sup>162</sup> Adapted with permission from the American Chemical Society.

Recently, Oe *et al.* have also reported the three-component assemblies of fluorinated 2-FPBA derivatives 3-F-1, 4-F-1 and 5-F-1 with (*S*)-BINOL **9** and  $\alpha$ -methylbenzylamine **3a** with the aim of

identifying diastereomeric IBEs with the greatest  $\Delta\delta_F$  values (Scheme 38).<sup>164</sup> After establishing that 5-F-**1** was the best fluorinated template (93% conversion,  $\Delta\delta_F = 0.10$  ppm for their model system), this system was optimised using excess BINOL and triethylamine (1.5 equiv. each) to minimize kinetic resolution and/or epimerisation of  $\alpha$ -amino ester salts **88**.

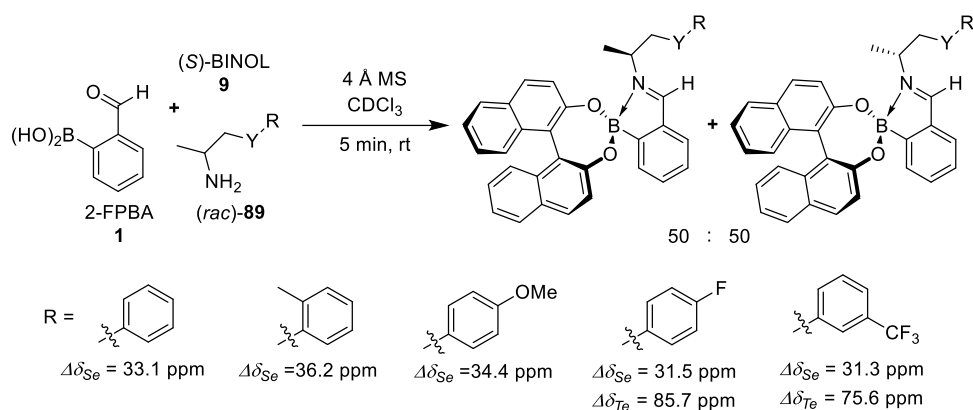


Scheme 38: Modified Bull-James assembly of amino ester salts **88** with 5-F-**1** and (S)-BINOL **9** with <sup>19</sup>F NMR (376 MHz, CDCl<sub>3</sub>, 30 mM)  $\Delta\delta_F$  of selected resonances. \*CD<sub>2</sub>Cl<sub>2</sub> used as solvent.<sup>164</sup>

#### 1.4.8 Chalcogen NMR spectroscopic analysis

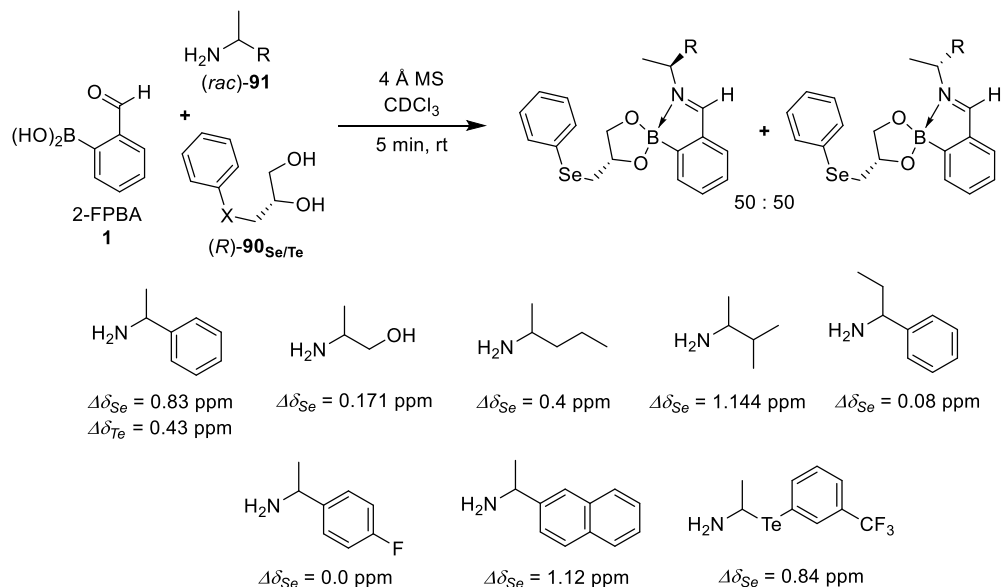
Silva *et al.* have shown that incorporation of NMR-active chalcogens <sup>77</sup>Se and <sup>125</sup>Te into the analyte or chiral reporting unit can also be used to determine *ee* using three-component assembly protocols.<sup>165,166</sup> Their initial report focused on derivatizing racemic chalcogen-containing amines **89** (Scheme 39) with 2-FPBA **1** and (S)-BINOL **9** to afford pairs of iminoboronate complexes. <sup>77</sup>Se{<sup>1</sup>H} and <sup>125</sup>Te{<sup>1</sup>H} NMR spectroscopy of these complexes showed excellent chemical shift anisochrony for the diastereomeric IBE complexes formed, with  $\Delta\delta_{Se}$  values ranging from 26.2–34.4 ppm and  $\Delta\delta_{Te}$  values ranging from 75.6–85.7 ppm. Although only racemic samples were employed in this work, the magnitude of chemical shift differences observed indicates that these systems would be useful for determining the *ee* of diol analytes.





Scheme 39: Three-component assembly of 2-FPBA **1**, (S)-BINOL **5** and chalcogen containing amines **89**, and the  $\Delta\delta_{Se}$  (99 MHz,  $CDCl_3$ ) and  $\Delta\delta_{Te}$  (132 MHz,  $CDCl_3$ , 20 mM) values of their diastereomeric IBE complexes.<sup>166</sup>

Subsequently, Silva *et al.* synthesised selenium-containing 3-phenylchalcogen-1,2-propanediol **90** for use as a chiral reporter with 2-FPBA **1** and chiral amines **91** which gave pairs of diastereomeric IBEs, the majority of which exhibited baseline-resolved diastereomeric signals in their NMR spectra with chemical shift differences for  $\Delta\delta_{Se}$  and  $\Delta\delta_{Te}$  of 0-1.144 ppm and 0.43 ppm, respectively. (Scheme 40).<sup>165</sup> Interestingly, the chemical shift differences observed in this instance were 100-fold smaller than in their previous work, implying that the chalcogen atoms occupy positions in space that are relatively remote from the amine stereocentres and so only experience small anisotropic shielding effects. Nevertheless, integration of diastereomeric  $^{77}Se$  NMR signals could be used to produce accurate measurements of the *ee*'s of scalemic samples of known enantiopurities ( $\pm 4\%$ ).



Scheme 40: Three-component assembly of 2-FPBA **1**, chalcogen containing diols (R)-**90**<sub>Se/Te</sub> and racemic amines **91** with  $\Delta\delta_{Se}$  (99 MHz,  $CDCl_3$ , 7.1 mM) and  $\Delta\delta_{Te}$  (132 MHz,  $CDCl_3$ , 7.1 mM) values of their diastereomeric IBE complexes.<sup>165</sup>

### 1.5. Three-component assembly for determining *ee* by optical methods

The Bull-James assembly has also been applied to the optical sensing of *ee* using methods that rely on CD, UV-Vis, or fluorescence spectroscopic analysis, with the aim of developing methods potentially applicable for high-throughput analysis.<sup>14,20</sup> All of these approaches rely on exploiting differences in the spectroscopic response of diastereomeric IBE complexes, whose *dr*'s correspond to the *ee* of the parent chiral analyte used for the IBE complexation.

#### 1.5.1 *Determining the *ee* of amines and diols using circular dichroism*

A collaboration between the Anslyn, Bull, and James groups in 2012 reported the use of circular dichroism spectroscopy to analyse diastereomeric IBE complexes formed from the three-component self-assembly of chiral amines **92**, chiral BINOL derivatives **93/94**, and 2-FPBA **1** (Figure 8a).<sup>167</sup> As with many multicomponent host-guest assemblies, a strong CD signal was observed (Figure 8b), with a maximum difference in signal response between diastereomeric complexes produced from the enantiomers of  $\alpha$ -methylbenzylamine **3a** observed at 253 nm (98,941 deg.cm<sup>2</sup>/dmol). This enabled BINOL and two brominated derivatives to be employed as chiral reporters in an array of sensing ensembles, whose CD signals were processed using Principal Component Analysis (PCA) and Linear Discriminant Analysis (LDA) to produce chemometric statistical models that were capable of differentiating between different  $\alpha$ -chiral amine analytes and determining their *ee*'s with an average error of  $\pm 5.8\%$  (Figure 8c, d). The use of PCA and LDA is widespread in the field of differential sensing as multivariate statistical tools which recognise and amplify patterns from large datasets.<sup>168</sup>

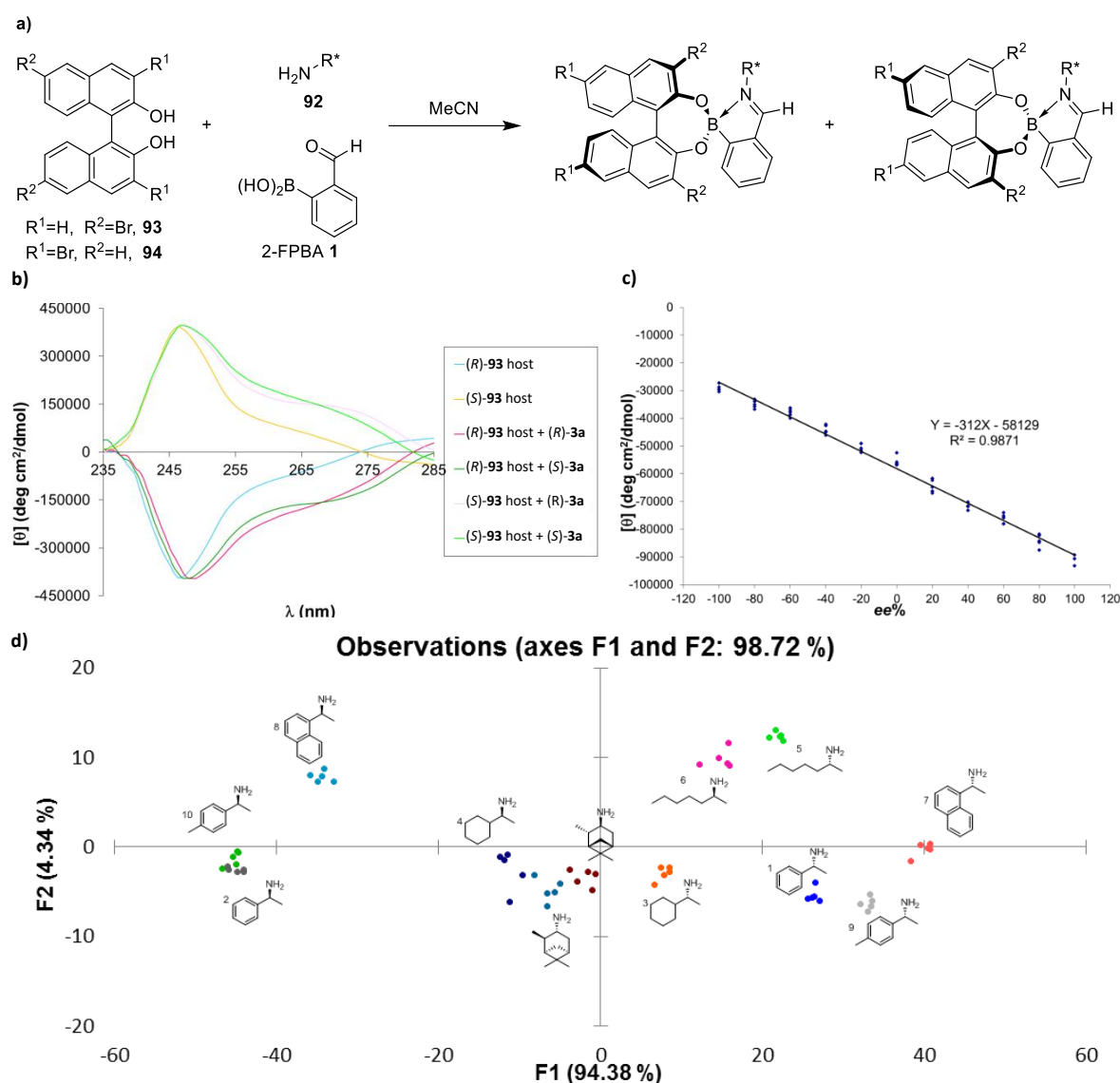


Figure 8: (a) Three-component assembly of 2-FPBA **1**, BINOL-derivatives **93/94** and a chiral amine **92**. (b) CD spectra of diastereomeric IBE complexes obtained from 2-FPBA **1**, 6,6-dibromo-BINOL **93** and  $\alpha$ -methylbenzylamine **3a**. (c) Calibration curve for CD outputs of complexes produced from mixing (*R*)-BINOL **9**, 2-FPBA **1** and (*scf*)-**3a** of known *ee*. (d) LDA plot of chiral amine analytes.<sup>167</sup> b, c, d Adapted with permission from the Royal Society of Chemistry.

Subsequent to this report, Wolf *et al.* described a self-assembling system based on host complexes derived from 4-methoxy-2-FPBA (4-OMe-**1**) and non-chiral 2,2'-binaphthol **95** (Figure 9a).<sup>169</sup> Two-component assembly of chiral amines (1-cyclohexylethylamine **96** and 1-aminoindane **97**) with 4-OMe-**1** gave iminoboronic acid complexes with only weak CD signals (dashed lines, Figure 9b). However, addition of **95** resulted in a large increase in the Cotton signals of the resultant IBEs, consistent with the self-assembly process controlling the helicity of its BINOL fragment (solid lines, Figure 9b). Although this system was not used for *ee* determination, the amplitude of signal change indicates this type of assembly is likely to be suitable for this purpose.

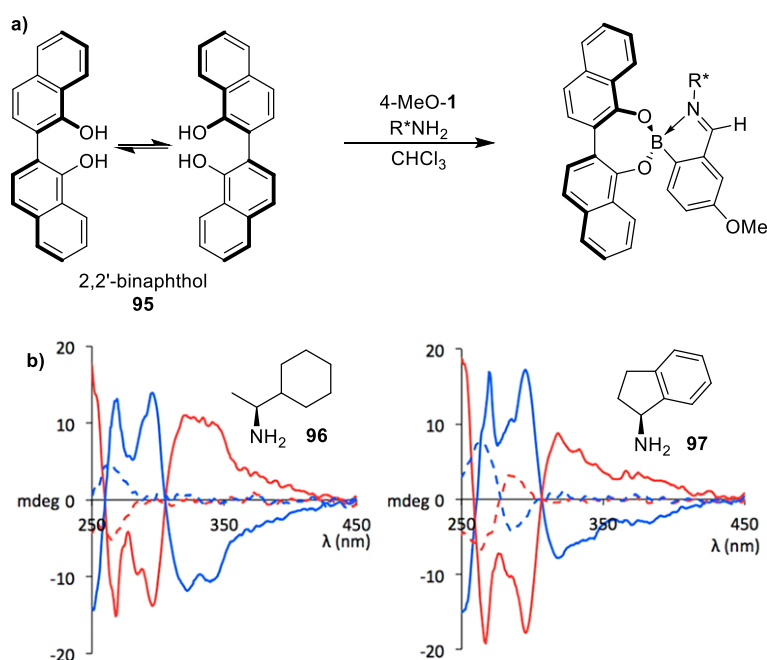


Figure 9: (a) Three-component assembly of 2,2'-binaphthol **95**, 4-MeO-**1** and a chiral amine to afford complexes for CD spectroscopic analysis. (b) CDA spectra produced from complexes derived from amines **96** (left) or **97** (right). Blue and red lines correspond to complexes produced from the (*R*)- or (*S*)-enantiomers of the amines, respectively. Dashed lines correspond to two-component complexes formed from 4-MeO-**1** and the enantiomers of the amines **96** and **97**. *C* = 37.5  $\mu$ M.<sup>169</sup> Adapted with permission from the American Chemical Society.

### 1.5.2 Determining the *ee* of amines, amino alcohols and diols using fluorescence

Collaborations between James and Anzenbacher have also led to the development of multiple Bull-James assembly-derived fluorescent assays,<sup>170–173</sup> with their practicality and versatility leading to their publication in *Nature Protocols*, validating its use as an effective method for the high-throughput analysis of the *ee* of chiral diols, amino alcohols and amines produced in stereoselective reactions.<sup>174</sup> Their first reports focused on the development of “turn-off” fluorescent assemblies using fluorescent host systems comprised of 2-FPBA **1** and 3,3'-diphenyl-2,2'-bi-1-naphthol (VANOL) or 2,2'-diphenyl-(4-biphenanthrol) (VAPOL) as chiral reporter diols for determining the *ee*'s of scalemic amines (Figure 10a).<sup>170–172</sup> Interestingly, these extended aryl systems exhibited the same NMR chiral shift behaviour as seen in previous BINOL-based systems, with several sets of baseline-resolved signals observed for each pair of diastereomeric complexes in their <sup>1</sup>H NMR spectra. This host system (2-FPBA **1** + chiral fluorescent diol) was found to be suitable for determining the *ee* of both amines and amino alcohols. In the case of amines (and amino acids/esters), IBE formation resulted in photoinduced electron transfer (PeT) quenching, leading to a “turn-off” fluorescence response (Figure 10b). As shown in Figure 10c, fluorescence intensity (FI) was dependent on the chirality of the amine analyte, which enabled *ee* values of amine samples to be correlated to changes in fluorescence intensity with good levels of accuracy ( $\pm 1$ -2%) (Figure 10d).

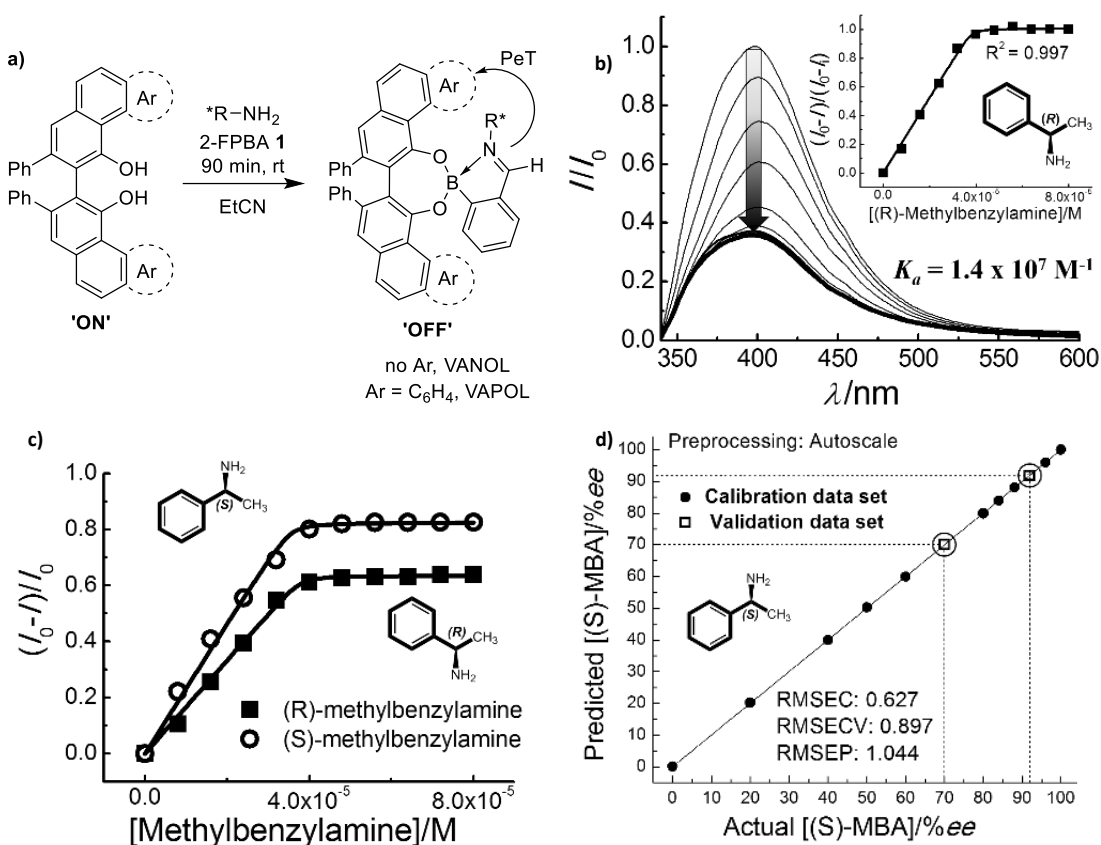


Figure 10: (a) Three-component assembly of 2-FPBA 1, a chiral primary amine and a fluorescent diol. (b) The fluorescence ( $\lambda_{\text{ex}}=335$  nm) of a mixture of (S)-VANOL (40  $\mu\text{M}$ ) and 2-FPBA 1 (40  $\mu\text{M}$ ) in anhydrous EtCN decreases on addition of (R)- $\alpha$ -methylbenzylamine 3a (0-80  $\mu\text{M}$ ). (c) Binding isotherms of (S)- and (R)- $\alpha$ -methylbenzylamine 3a to (S)-VANOL-2-FPBA host. (d) Qualitative LDA of amine, amino alcohol and amino acid enantiomers in EtCN.<sup>170</sup> b, c, d reproduced with permission from John Wiley and Sons.

This type of fluorescent three-component self-assembly platform was also applied to the analysis of the *ee*'s of amino alcohols, with formation of oxazolidine intermediates resulting in a red-shift of the fluorescence signal rather than PeT quenching (Figure 11a). Differential changes in fluorescent intensities were once again observed between the diastereomeric oxazolidine products produced (*vide supra*), thus allowing for the measurement of the enantiopurity of the parent amino alcohol analyte. This enabled ratiometric changes in fluorescence to be used to determine the *ee*'s of amino alcohols, as well as providing the ability to distinguish between amino alcohol and amine analytes. This is seen clearly in Figure 11b, with LDA affording large distances between clusters of enantiomers and functional groups of the parent analytes. Interestingly, these studies found that addition of polar/protic additives (water, citric acid, ethylene glycol, sucrose, glycerol) had a more pronounced effect on the equilibrium constants for formation of the heterochiral complexes over the homochiral complexes, indicating that the heterochiral complexes were less stable. This led to the discovery that these types of additives could be used to further discriminate between analyte enantiomers in these complexation reactions.

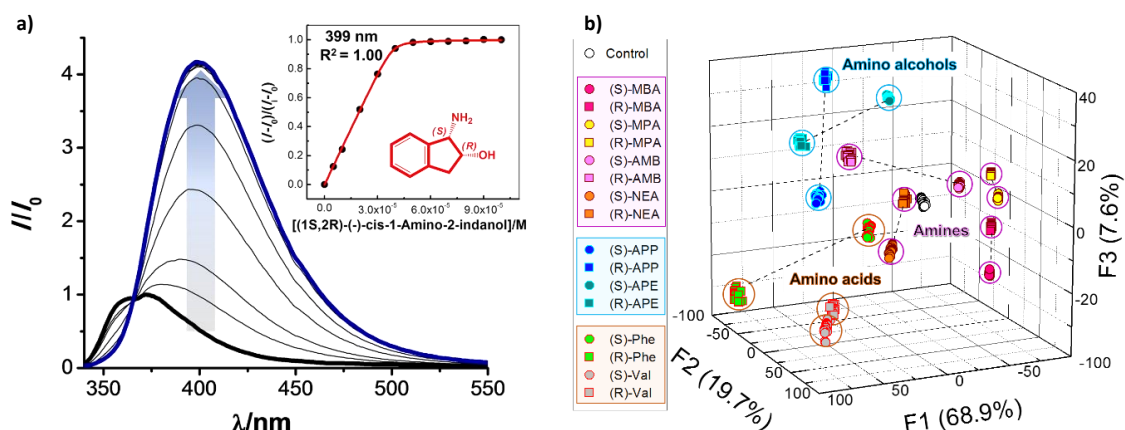


Figure 11: (a) Fluorescence spectra of the three-component assembly of 2-FPBA 1, (S)-VANOL and [(1S,2R)-(-)-cis-1-amino-2-indanol] (0-100  $\mu\text{M}$ ). (b) Qualitative LDA of chiral amine, amino alcohol and amino acid analytes.<sup>170</sup> Reproduced with permission from John Wiley and Sons.

Use of enantiopure L-tryptophan derivatives as fluorescent reporters for three-component complexation meant that these types of fluorescence assays could be adapted to determine the *ee*'s of scalemic diols (Figure 12) to within a 2% error limit.<sup>172</sup> As with amines and amino alcohols, the fluorescent profiles of the diastereomeric homochiral and heterochiral complexes produced from various classes of diols were sufficiently different to enable LDA to be used to accurately determine both their structures and *ee* values (Figure 12).

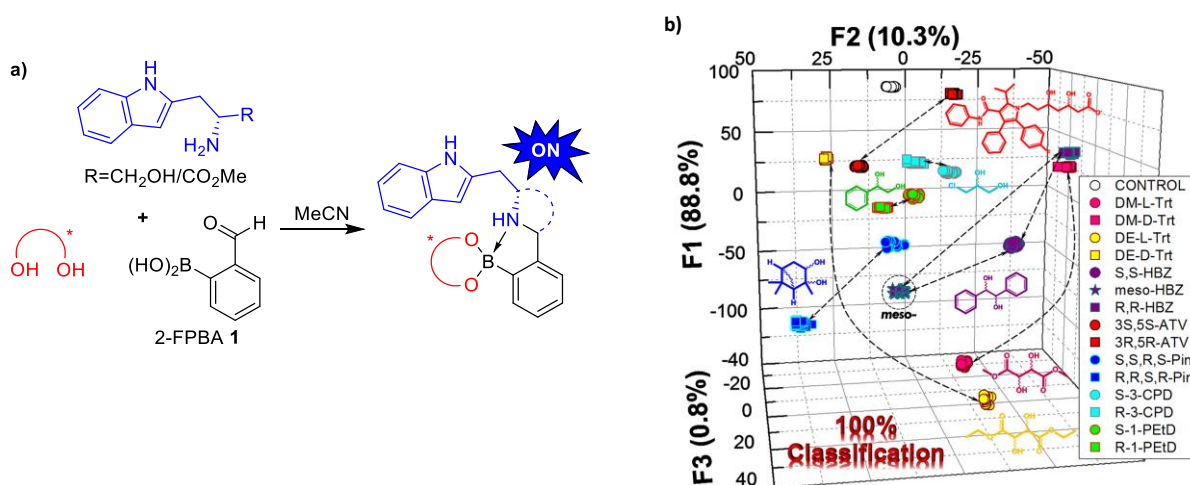


Figure 12: (a) Three-component assembly of 2-FPBA 1, a chiral diol and a fluorescent tryptophanol derivative. (b) Qualitative LDA of 16 chiral diols showing 100% correct structural classification.<sup>172</sup> Reproduced with permission from John Wiley and Sons.

The practicality of this fluorescence methodology for high-throughput screening was demonstrated by measuring the enantiopurities of 14 samples of Atorvastatin (a hypercholesterolemia drug) of unknown *ee*'s using a high-throughput assay (Figure 13a), with quantitative linear regression analysis revealing accurate enantiopurity determination in all cases ( $R^2=0.999$ ). This type of fluorescence assay was also employed to analyse the *ee* of diols produced in Noyori asymmetric transfer hydrogenation reactions of benzil to hydrobenzoin (diol). In this case, an artificial neural network was developed that was used to correctly determine the absolute configuration, *ee* and

concentration of hydrobenzoin products (both crude and recrystallised) with high levels of accuracy (Figure 13b, c).

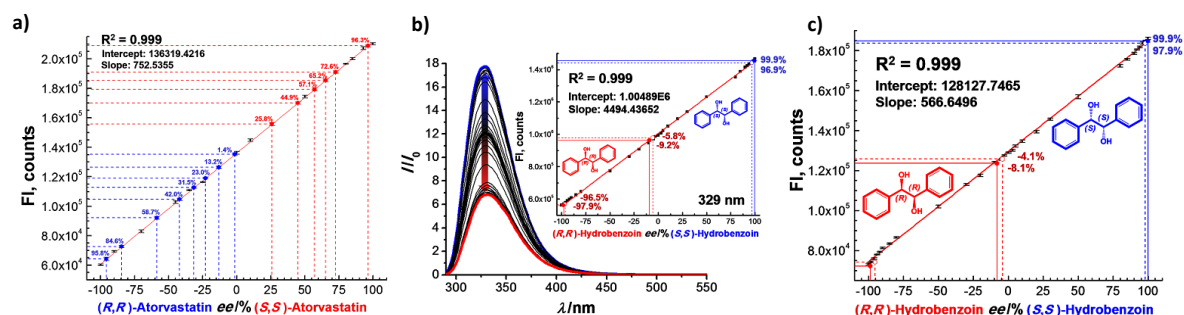
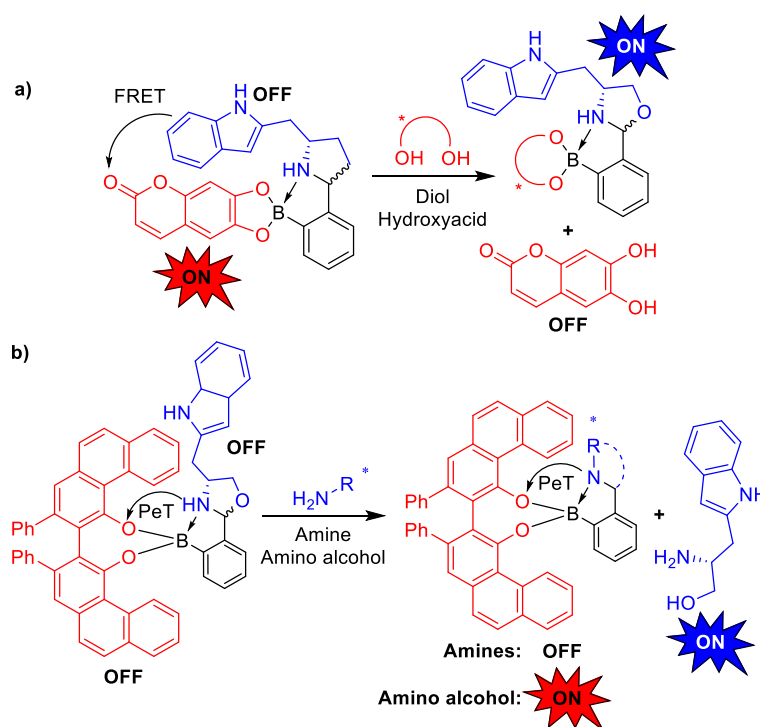


Figure 13: (a) Standard graph of FI vs. *ee* of L-tryptophanol and 2-FPBA **1** assemblies (1:1, 40 mM) of atorvastatin of known (black) and unknown (blue and red) *ee* values. (b) Fluorescence titration profile of L-tryptophanol–2-FPBA (1:1, 40 mM) complexes with hydrobenzoin standards (inset: Standard curve of FI vs. *ee*). (c) HT fluorescence assay standard curves for FI readings from mixtures of hydrobenzoin of known *ee* in comparison with six hydrobenzoin samples of unknown *ee* (red, blue circles).<sup>172</sup> Reproduced with permission from John Wiley and Sons.

Most recently, Anzenbacher *et al.* have reported a dual chromophore indicator displacement assay which proved to be more sensitive for determining *ee* than the aforementioned “turn-off” systems.<sup>173</sup> This approach employed a combination of two fluorescent dyes capable of orthogonal binding to the aldehyde and boronic acid fragments of the 2-FPBA template (Scheme 41). Initial assembly of L-tryptophanol and 6,7-dihydroxycoumarin produced a bichromophoric oxazolidine-boronate complex, with intramolecular Förster resonance energy transfer (FRET)<sup>175</sup> processes leading to weak fluorescence of its tryptophanol moiety and enhanced fluorescence of its coumarin fragment. Addition of a scalemic diol (or hydroxyacid) analyte results in displacement of the coumarin dye and separation of the FRET pair, which leads to fluorescent “turn on” of the tryptophanol fluorophore, and “turn off” of the dihydroxycoumarin (Scheme 41a). Since assembly of each enantiomer of the parent analyte proceeds diastereoselectively, each enantiomer leads to a different fluorescence response which can be used to determine the *ee*’s of a scalemic analyte.

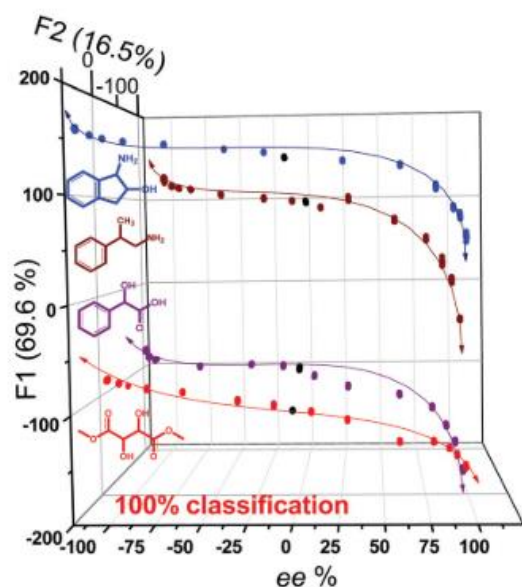


Scheme 41: Displacement assays using bichromophoric three-component assemblies for determining the enantiopurities of a range of scalemic analytes: (a) Use of 2-FPBA 1, L-tryptophan and 6,7-dihydroxycoumarin for the detection and *ee* analysis of diols and hydroxyacids. (b) Use of 2-FPBA 1, L-tryptophan and (S)-VAPOL for the detection and *ee* analysis of amines and amino alcohols.<sup>173</sup>

Alternatively, the use of (S)-VAPOL as a chiral reporter produced an IBE system suitable for determining the enantiopurity of amines and amino alcohols (Scheme 41b). In this case, the fluorescence of both fragments of the enantiopure oxazolidine sensor is likely to be quenched through PeT donation of the nitrogen lone pair of the oxazolidine fragment to the VAPOL fragment, although the exact mechanism of fluorescence and quenching was not determined. Addition of a scalemic amine analyte results in displacement of the L-tryptophan unit producing an IBE complex that results in a fluorescence "turn-on" response, with the fluorescence of the VAPOL remaining "turned off". Use of an amino alcohol analyte to afford an imidazoline-boronate ester complex also results in displacement and "turn-on" of tryptophan, however the ensuing PeT process leads to amplification of the (S)-VAPOL fluorescent signal which is also "turned-on". Since addition of the enantiomers of amine, amino ester, diol and hydroxyacid analytes to these chiral indicator displacement sensors result in different fluorescent responses, this bichromophoric Bull-James sensing system could be used to successfully classify the structures of 26 different analytes and accurately determine their absolute configurations and enantiopurities (Figure 14).



a)



b)

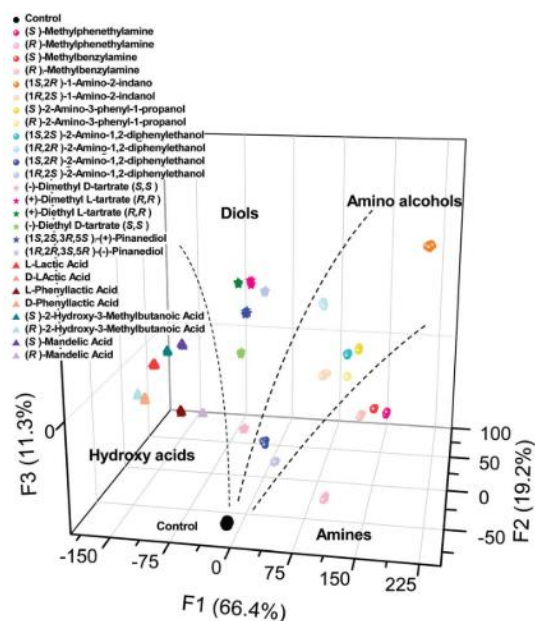


Figure 14: (a) Semi-quantitative LDA of fluorescence response data from displacement assays enables simultaneous determination of the *ee* values of four different types of amine, amino alcohol,  $\alpha$ -hydroxyacid and diol analytes. (b) Qualitative LDA of the fluorescence response of 26 chiral amines, amino alcohols, diols and hydroxyacids (+ controls) in the displacement assay enabled their structures to be predicted with a 100% success rate.<sup>173</sup> Reproduced with permission from the Royal Society of Chemistry.

### 1.6. Three-component assembly for electrochemical determination of the *ee* of BINOL

Finally, a collaboration with the Tucker group demonstrated that the *ee* of BINOL could be measured electrochemically through derivatization with a redox-active two-component iminoboronic acid complex derived from a ferrocene amine and 2-FPBA **1** (Figure 15a).<sup>176</sup> It was found that the resultant diastereomeric complexes ( $\alpha$ -*R,R*)-**98** and ( $\alpha$ -*R,S*)-**99** exhibited significantly different electropotentials of 614 mV and 665 mV, respectively (Figure 15b). This difference allowed the *ee* of BINOL **9** to be determined with an error of  $\pm 3\%$ , thus enabling minor enantiomers ( $< 5\%$ ) to be detected, even at low concentrations. Crystallographic and  $^1\text{H}$  and  $^{11}\text{B}$  NMR spectroscopic analysis showed that whilst the homochiral diastereomeric complex ( $\alpha$ -*R,R*)-**98** formed an intramolecular iminoboronate  $\text{N} \rightarrow \text{B}$  bond, the more sterically hindered heterochiral complex ( $\alpha$ -*R,S*)-**99** did not, once again indicating that heterochiral IBE complexes are generally less stable (*vide supra*).<sup>171</sup> This structural difference is responsible for the differences in their electrochemical behaviour, with the  $\text{N} \rightarrow \text{B}$  bond of the homochiral complex resulting in (*R*)-BINOL **5** being more tightly bound, with a ratio of binding strengths  $K_{(\alpha-R,R)}/K_{(\alpha-R,S)}$  of  $\approx 19$ . Electrochemical oxidation of these IBEs results in the binding strength ratio  $K_{(\alpha-R,R)^+}/K_{(\alpha-R,S)^+}$  dropping to only 2.5, thus indicating a much larger decrease in stability of the homochiral complex ( $\alpha$ -*R,R*)-**98**. This difference is proposed to be due to weakening of the  $\text{N} \rightarrow \text{B}$  coordination bond caused by the proximal positive

charge of its oxidised ferrocene fragment. Evidence for weakening of the N→B coordination bond of the homochiral ( $\alpha$ -*R,R*)-**98** complex was also provided by the larger positive shift in redox potential upon addition of (*R*)-BINOL **9** to iminoboronic acid (*R*)-**100** (+95 mV for ( $\alpha$ -*R,R*)-**98** vs. +44 mV for ( $\alpha$ -*R,S*)-**99**). This indicates that the ferrocene unit of complex ( $\alpha$ -*R,R*)-**98** is harder to oxidise than ( $\alpha$ -*R,S*)-**99**, in line with its imine-boron coordination bond withdrawing electron density from the ferrocene redox system.

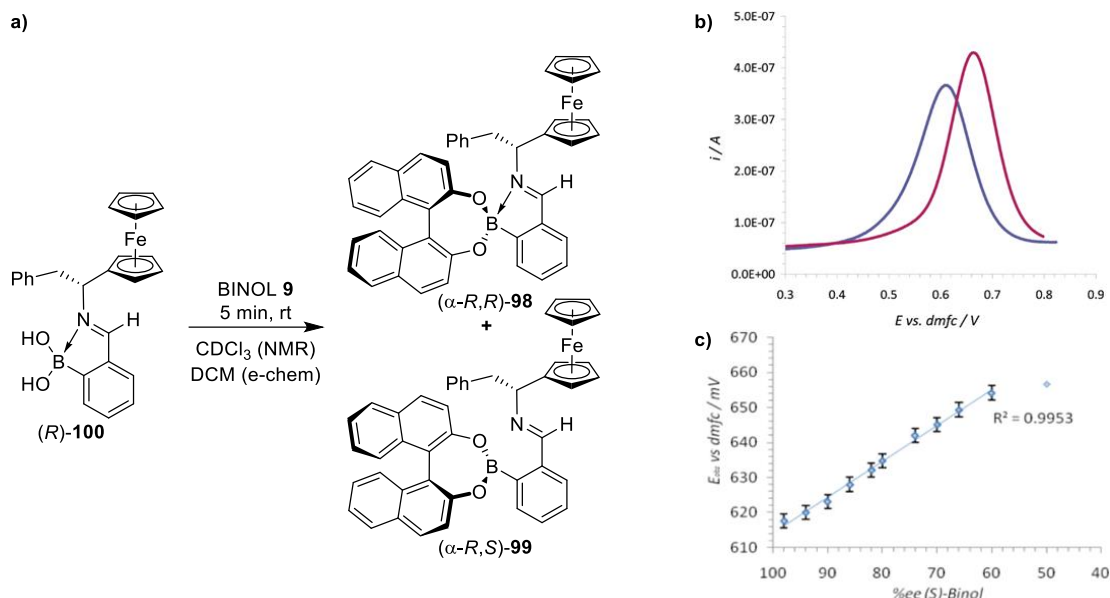


Figure 15: (a) Three-component assembly of 2-FPBA **1**, redox-active ferrocene amine (*R*)-**100** (pre-assembled) and BINOL **9**. (b) Square wave voltammograms of three-component ferrocene IBEs acquired in CH<sub>2</sub>Cl<sub>2</sub> (0.1 M TBA · PF<sub>6</sub>); (( $\alpha$ -*R,R*)-**98** shown in purple) and ( $\alpha$ -*R,S*)-**99** shown in blue). (c) Plot of *E*<sub>obs</sub> against *ee* for IBE complexes produced from (*S*)-BINOL **9** showing a linear dependence between 60% and 98% *ee*.<sup>176</sup> b, c Reproduced with permission from the American Chemical Society.

## 1.7. IBE assemblies as synthetic tools

The use of the Bull-James three-component assembly for determining enantiopurity is often credited as one of the first examples the use of orthogonal dynamic covalent bond formation to construct functional supramolecular assemblies.<sup>100,177–179</sup> The power of these chiral iminoboronate systems for self-assembly has led to supramolecular constructs of this type being used to prepare new types of boron-containing materials and as a mechanism to control reactivity and stereoselectivity.<sup>180–183</sup>

### 1.7.1 Self-assembled synthesis of polyheteroatomic boracycles

The three-component assembly reaction of 2-FPBA **1** with (*S*)-BINOL **9** and (*S*)-leucinol **50a** resulted in mixtures of imine and oxazolidine boronate products (*vide supra*),<sup>142</sup> however oxazolidine boronate ester (*S*,2*R*,4*S*)-**52a** fractionally crystallised out of solution after the crude reaction mixture was allowed to stand overnight (Figure 16a).<sup>184</sup> Carrying out a two-component assembly

using (*R*)-valinol **50b** and 2-FPBA **1** produced bridged iminoboronate (*R,R*)-**53b**, comprised of two fused boracycle rings containing two tetrahedral boron centres and a bridging oxygen atom linker (Figure 16b), in the same manner as related systems reported by Westcott *et al.*<sup>185,186</sup> Five additional chiral amino alcohols were used as substrates in this two-component self-assembly reaction in combination with either 2-FPBA **1** or 2-formyl furanylboronic acid **101**, which gave the respective boracycles in excellent 84-96% isolated yields. Achiral aromatic amino alcohols **50g** and **50h** were also shown to form boracycles in quantitative yields, although their decreased reactivity required heating under Dean-Stark conditions for complexation reactions to proceed to completion.

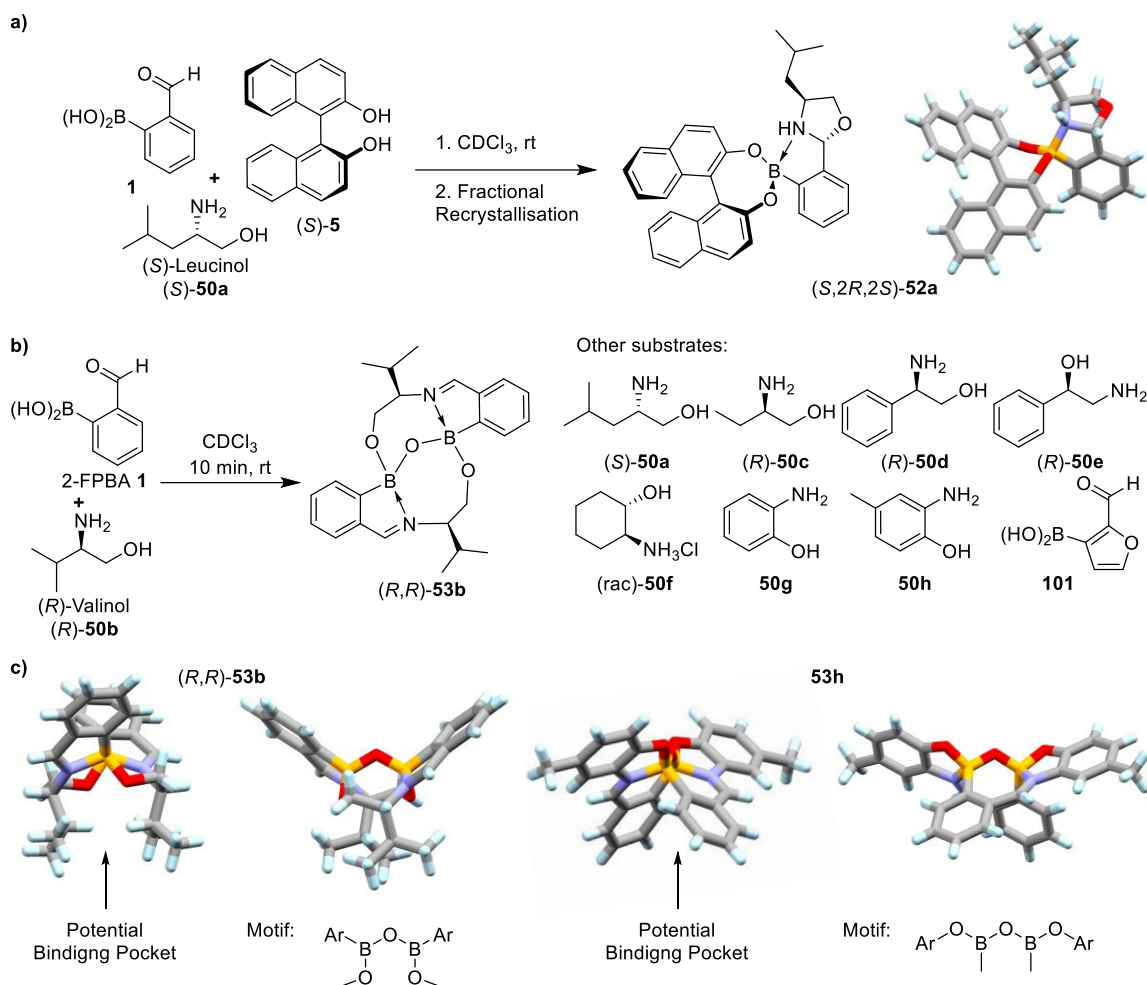


Figure 16: (a) X-Ray crystal structure of three-component assembly of (*S*,2*R*,2*S*)-**52a** formed from reaction of (*S*)-leucinol **50a**, BINOL **9** and 2-FPBA **1**. (b) Two-component assembly of formyl aryl boronic acids and 1,2-amino alcohols **50**. (c) X-Ray crystal structures of (*R,R*)-**53b** and **53h** viewed along and perpendicular to the boron-boron axis (left and right respectively).<sup>184</sup>

Both types of fused bridged bicycles were characterised using X-Ray crystallography (Figure 16c), which revealed interesting structural variation between the two-component products produced from chiral or achiral amino alcohols. In the case of (*R,R*)-**53b**, the B-O-B linkage is positioned on the opposite face to the two non-bridging *oxo*-substituents, which creates a binding pocket walled by the non-bridging oxygens and side-chains, and capped by a bridging B-O-B bond. Conversely, all of the atoms of the O-B-O-B-O motif are present in the same plane for complex **53h**, with all three

oxygen atoms sitting on the same side of the complex. These structural differences result in the pocket of the chiral complex containing two potentially coordinating oxygen atoms, whilst the pocket of the achiral complex is hydrophobic in nature.

### 1.7.2 IBE templates for the formation of miniamyloids

Geyer and co-workers have also reported the use of IBEs as bifunctional templating motifs for the controlled synthesis of A $\beta$ -miniamyloids.<sup>187,188</sup> A  $\beta$ -turn polypeptide mimic Hot=Tap composed of three *cis*-diol containing heterocyclic fragments (trimeric structure shown in Figure 17) was combined with excess amounts of 2-FPBA **1** and pentapeptide **102** under mild conditions to prepare three-component assemblies **103** containing three peptide fragments. This provided an excellent “one-pot” self-assembling alternative to previous methods for the synthesis of miniamyloids that previously required pre-functionalisation of the peptide prior to its attachment to the Hot=Tap backbone. Further work by the same group showed that this approach was broadly applicable to combine a wide range of peptides and Hot=Tap oligomers,<sup>188</sup> with a number of these supramolecular assemblies exhibiting similar structures to amyloid fibrils that contribute protein misfolding diseases such as to Alzheimer’s disease.

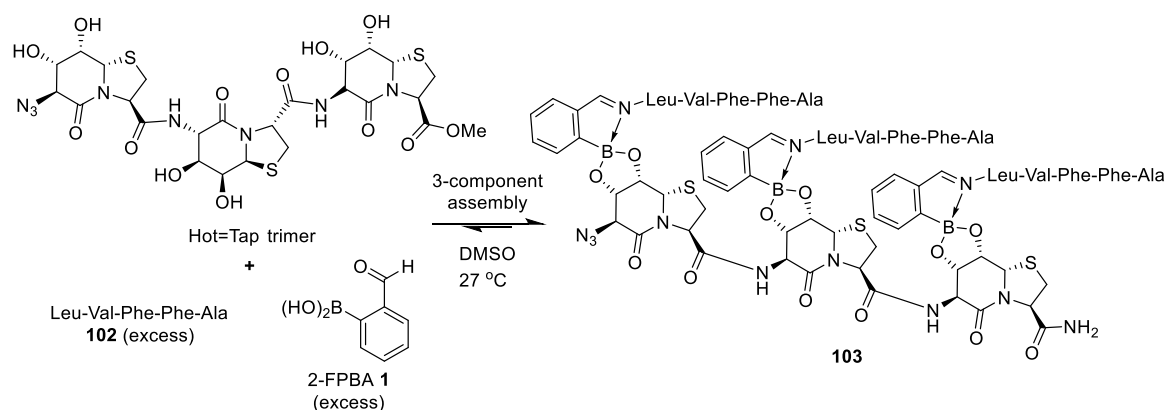
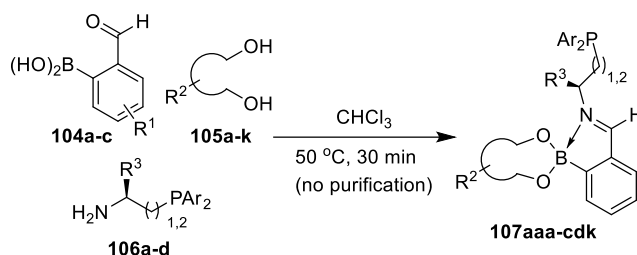


Figure 17: Synthesis of tripeptidic A $\beta$ -miniamyloid **103** from the three-component assembly of 2-FPBA **1**, pentapeptide **102**, and a trimeric Hot=Tap oligomer.<sup>187</sup>

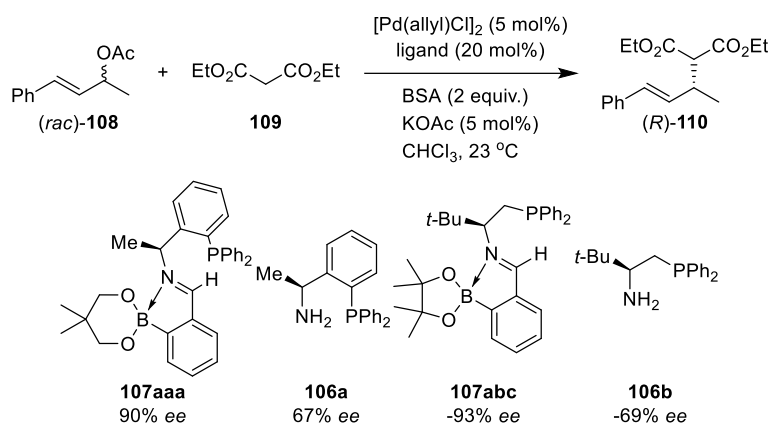
### 1.7.3 Chiral IBE ligands for asymmetric catalysis

Three-component assemblies have also been used by the Taylor group, who employed IBE bond forming reactions for the combinatorial synthesis of a library of chiral phosphine ligands for enantioselective palladium-catalysed allylic acetate substitution reactions.<sup>189</sup> They selected three achiral formyl boronic acid templates **104a-c**, eleven diol ligands **105a-k** (both chiral and achiral), and four chiral aminophosphines **106a-d** to create a library of 100 phosphinoiminoboronate ligands **107** (Scheme 42) that were individually screened as chiral ligands in palladium-catalysed allylic substitution reactions of (*rac*)-**108** with diethyl malonate **109** (Scheme 43). A wide range of enantioselectivities were observed, with the best results obtained for ligands **107aaa** and **107abc**

which respectively produced (*R*)-**110** in 90% *ee* and (*S*)-**110** in 93% *ee*, a significant improvement on the 67% and 69% *ee* values obtained using non-iminoboronate aminophosphine ligands **106a** and **106b**. The sheer volume of data acquired using this combinatorial approach enabled Taylor and co-workers to rapidly assign trends that would not have been so evident from a conventional stepwise ligand optimisation strategy. For instance, they were able to show that aliphatic diol ligands gave better stereocontrol as they decreased the Lewis acidity of the boron centre, which weakened the intramolecular N→B bond, thus facilitating stronger bidentate *P,N*-coordination of the ligand to the metal.



Scheme 42: Combinatorial IBE reactions used for the combinatorial synthesis of 100 chiral phosphine ligands.<sup>189</sup>

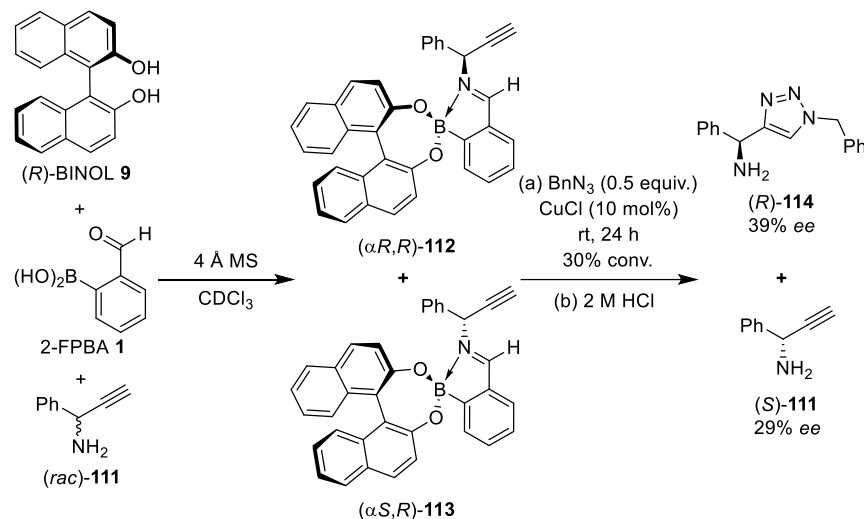


Scheme 43: Chiral phosphine-iminoboronate ligands afford enhanced enantioselectivities in palladium-catalysed allylic alkylation reactions.<sup>189</sup>

#### 1.7.4 IBE-derived chiral auxiliaries in CuAAC click reactions

Fossey and co-workers have reported use of the Bull-James assembly for asymmetric synthesis, employing it to construct a chiral auxiliary for the kinetic resolution of alkyne amines using a copper(I)-catalysed azide-alkyne cycloaddition (CuAAC) reaction (Scheme 44).<sup>47</sup> In this system, a racemic alkyne-containing primary amine **111** was self-assembled with 2-FPBA **1** and (*R*)-BINOL **9** to form a mixture of diastereomeric iminoboronate complexes **112/113** that were subjected to CuAAC conditions using 0.5 equiv. of benzyl azide. This resulted in the alkyne fragment of the ( $\alpha$ -*R,R*)-**112** diastereomer preferentially undergoing a stereoselective click reaction with a selectivity value of *S* = 4.1. Subsequent acid-catalysed hydrolysis of the IBE ester complexes then afforded

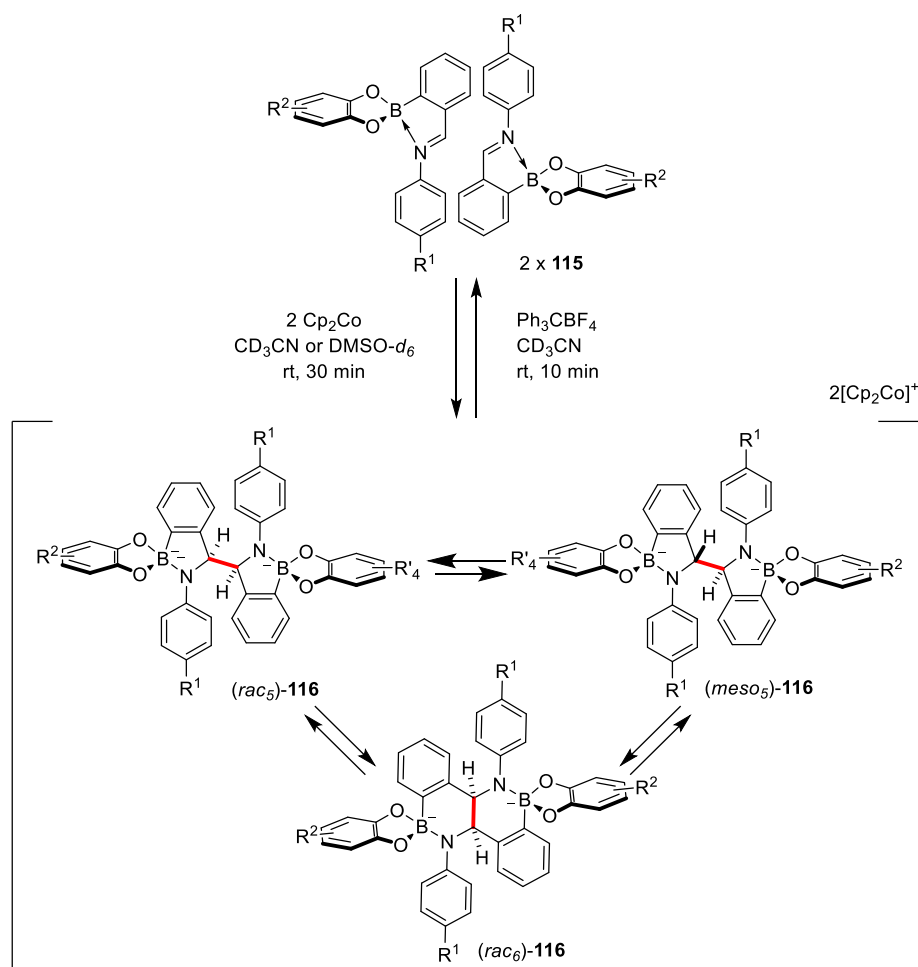
amino-azide (*R*)-**114** in 39% *ee* and recovered amine (*S*)-**111** in 29% *ee*. Although only moderate stereocontrol was achieved in this unoptimised ‘one-pot’ kinetic resolution reaction, the simplicity of installing and removing the chiral auxiliary in this type of system is noteworthy, particularly if more stereoselective transformations of these types of IBE complexes can be identified.



Scheme 44: Formation of diastereomeric IBE complexes from alkyne (*rac*)-**111** enables a CuAAC-catalysed click reaction to be used for their kinetic resolution.<sup>47</sup>

### 1.7.5 Reversible radical coupling of iminoboronates

McConnell *et al.* found that treatment of a pre-assembled *N*-aryl iminoboronate catechol ester **115** with the single electron reductant Cp<sub>2</sub>Co resulted in radical homocoupling of its imino benzylic groups to afford amido-boronates (*rac*<sub>5</sub>)-**116**, (*meso*<sub>5</sub>)-**116** and (*rac*<sub>6</sub>)-**116** (Scheme 45).<sup>190</sup> Kinetic analyses and structural studies revealed that 5-membered (*rac*<sub>5</sub>)-**116** and (*meso*<sub>5</sub>)-**116** were formed as kinetic products which then rearranged to 6-membered (*rac*<sub>6</sub>)-**116** under thermodynamic control, leading to mixed time-, temperature-, and substrate-dependent ratios of product **116**. These dimeric homo-coupled products were found to be less stable than their IBE precursors, with their treatment with an electron acceptor trityl cation (Ph<sub>3</sub>C)<sup>+</sup> resulting in regeneration of the original IBE monomers.

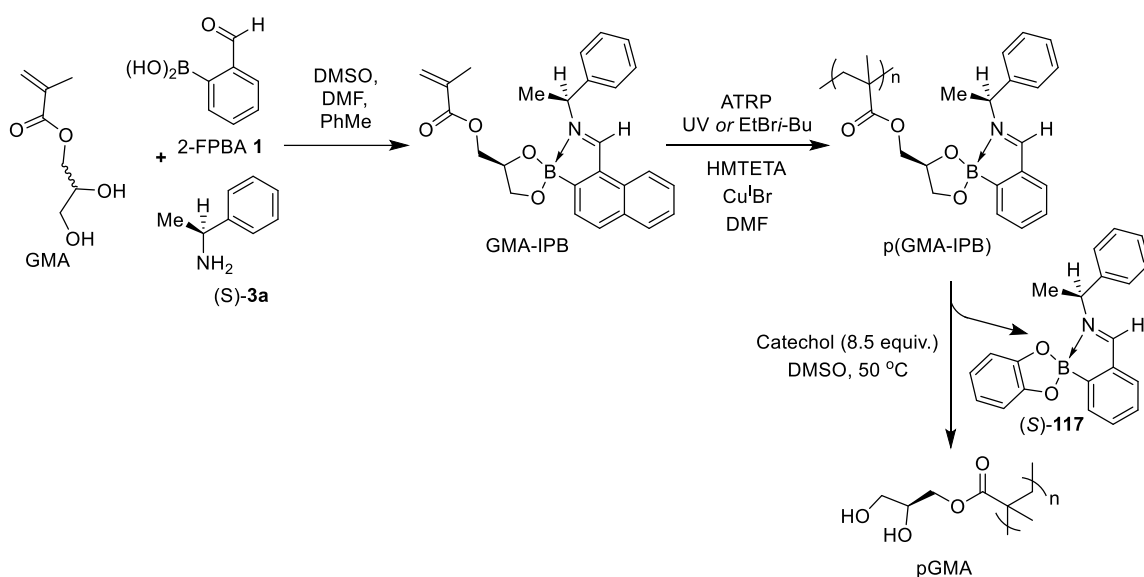


Scheme 45: Reversible radical coupling of iminoboronates **115** to afford amidoboronates **116** (radical-coupled bond in red) under thermodynamic control.<sup>190</sup>

## 1.8. Iminoboronate complexes for the formation of polymers and hydrogels

### 1.8.1 Iminoboronate polymers

Following their demonstration that the Bull-James assembly could be used to assess the chirality of polymers (*vide supra*), Kressler and co-workers have reported that derivatization of GMA monomers with 2-FPBA **1** and (*S*)- $\alpha$ -methylbenzylamine **3a** gave iminoboronate GMA-IPB monomers, which could undergo radical or UV-initiated low-temperature ATRP polymerisation to afford iminoboronate ester polymers in one pot (Scheme 46).<sup>191</sup> These polymers could then be decomplexed *via* treatment with a large excess of catechol **26** to afford simple p(GMA)s containing free diol units released by transesterification and elimination of catechol-iminoboronate (*S*)-**117**. A similar process could also be used to polymerise iminoboronate ester monomers containing two equiv. of 2-hydroxyethyl-methacrylate (HEMA), affording highly syndiotactic polymers (*rr* = 70.7–75.5% for pGMAs and 74.9–79.7% for pHEMAs).



Scheme 46: One-pot complexation and polymerisation of 2-FPBA **1**, (S)-**3a**, and GMA to afford iminoboronate ester functionalised polymers that are decomplexed by treatment with catechol to afford pGMA.<sup>191</sup>

### 1.8.2 Dynamic, self-healing and stimuli-responsive polymers and hydrogels

Iminoboronates have also been incorporated into polymeric systems as a structural element to facilitate cross-linking of polymer and hydrogel materials.<sup>192</sup> For example, Raquez *et al.* have developed self-assembled imine-coordinated boroxine polymeric systems that are produced from reaction of a diamine, a polyether-containing terminal bis-cyclic carbonate unit and a 2-FPBA boroxine trimer **118** (Figure 18a). Ring opening of the terminal cyclic anhydride groups by one of the diamine amines results in a urethane bond, with the other amino group then reacting to form a highly cross-linked iminoboroxine complex IBPU.<sup>193–195</sup> This self-assembly approach produces polymers with a high degree of stiffness (Young's modulus = 551 MPa) and tensile strength (11 MPa) despite the labile nature of iminoboronates. These dynamic iminoboronate covalent bonds were found to confer self-healing properties to these materials, with heating/cooling and wetting/drying enabling broken imine or boroxine bonds to be reformed (Figure 18b). Similarly, changes in temperature and humidity can be used as stimuli to make or break the bonds used to construct the iminoboronate-boroxine hubs, thus creating stimuli-responsive materials which are re-mouldable under mild treatment conditions. This provides a simple alternative to common isocyanate-derived polyurethane self-healing and stimuli-responsive polymers, which have been shown to have potential applications as solid polymer electrolytes.<sup>196</sup> Following these initial reports, functional variants of this core motif have been developed, based on substitution of the iminoboronate moieties with similar amino- and acrylamido-boronate motifs.<sup>197,198</sup>



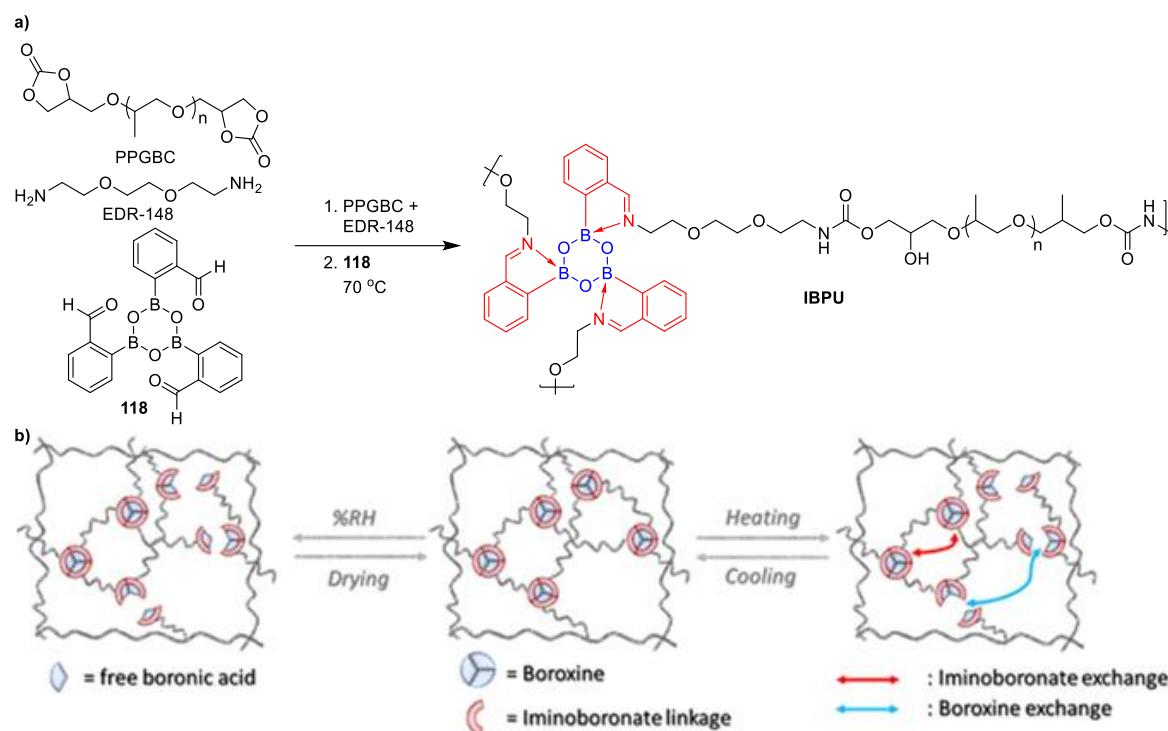


Figure 18: Three-component self-assembly of Iminoboroxine-containing self-healing polymers and hydrogels. (a) Synthesis of an iminoboroxine polyurethane network polymer. (b) Self-healing and modular behaviour of iminoboroxine-polyurethane polymers.<sup>192</sup> Reproduced with permission from the American Chemical Society.

This concept has been expanded further for the design of self-assembled IBE-containing polymers that are prepared from supramolecular assembly of 2-FPBA **1**, guanosine (G), aminoglycosides, and potassium chloride (Figure 19). These stimuli-responsive hydrogels contain a large network of hydrogen-bonded  $K^+$ -centred guanosine tetramers (G-quadruplexes), whose diol units are crosslinked through formation of iminoboronate ester groups with the amino groups of aminoglycoside units.<sup>199–203</sup> These hydrogels were found to be responsive to multiple stimuli, with an increase in temperature or addition of potassium-chelating crown ethers resulting in disruption of the G-quadruplex arrays and release of the aminoglycoside bis-iminoboronate guanosine units. The iminoboronate bonds of these complexes are also responsive to disruption by other stimuli, with addition of aqueous acid leading to their hydrolysis to the 2-FPBA **1**, amine, and diol components. Alternatively, the addition of glucose results in transesterification of the boronate ester, releasing a guanosine fragment and producing of new glucose-iminoboronate-aminoglycoside species. Finally, the reactivity of boronates towards reactive oxygen and nitrogen species (ROS/RNS) may be exploited, with addition of hydrogen peroxide triggering oxidative deborylation to produce an iminophenol and boric acid, and releasing the guanosine fragment.<sup>204–206</sup> This multi-responsive behaviour has been exploited for drug delivery for selective release of antibacterial aminoglycosides and the anticancer drug Doxorubicin.<sup>199,203</sup>  $CO_2$ -responsive iminoboronate poly(oligo(ethylene glycol)) polymers have also been reported by Jiang and co-workers, with bubbling of  $CO_2$  reversibly producing carbonic acid that triggers IBE bond hydrolysis, thus inducing depolymerisation processes that can be reversed by purging with  $N_2$  gas.<sup>207</sup> This  $CO_2$ -dependent behaviour has been demonstrated in multiple systems (*vide infra*) using both  $^1H$  NMR

and fluorescence assays to measure the fragmentation/re-complexation of IBE systems upon sequential CO<sub>2</sub>/N<sub>2</sub> bubbling.

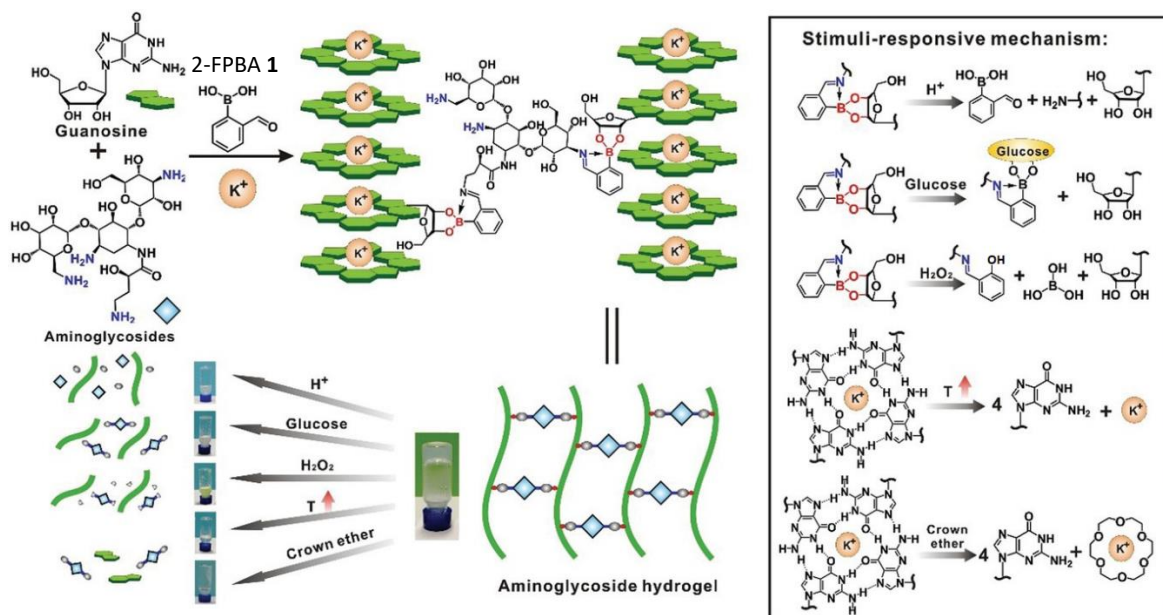


Figure 19: An aminoglycoside iminoboronate hydrogel assembled from guanosine, K<sup>+</sup>, an aminoglycoside and 2-FPBA **1**. These materials are responsive to multiple external stimuli such as acids, glucose, H<sub>2</sub>O<sub>2</sub>, heat and crown ethers, all of which act on different structural elements of the hydrogel network.<sup>199</sup> Reproduced with permission from John Wiley and Sons.

### 1.8.3 Stimuli-responsive aggregates and micelles

The Bull-James multicomponent approach has also been used to produce stimuli-responsive iminoboronate-containing nano-aggregates, micellar assemblies, and polymersomes that are stable in aqueous systems. Jiang and co-workers, for example, have reported the three-component assembly of poly(ethylene glycol) amine with 2-FPBA **1** and a nitrophenyl ethanediol (PEG-INEC) to produce amphipathic IBE complexes that self-assemble into nano-aggregates in aqueous systems (Figure 20).<sup>208</sup> These nano-aggregates were found to be responsive to three common stimuli: light - which results in release of a nitrosoaryl  $\alpha$ -hydroxy-ketone and an iminoboronic acid fragment; acid - which hydrolyses both the boronate ester and imine bonds to regenerate the original three-components; and hydrogen peroxide - which oxidatively cleaves the boronate ester to give boric acid, *o*-hydroxy-benzaldehyde and nitrophenyl ethanediol. Therefore, different external stimuli can be used to trigger controlled decomposition of these aggregates, which is potentially useful for the selective release of encapsulated hydrophobic guest molecules.

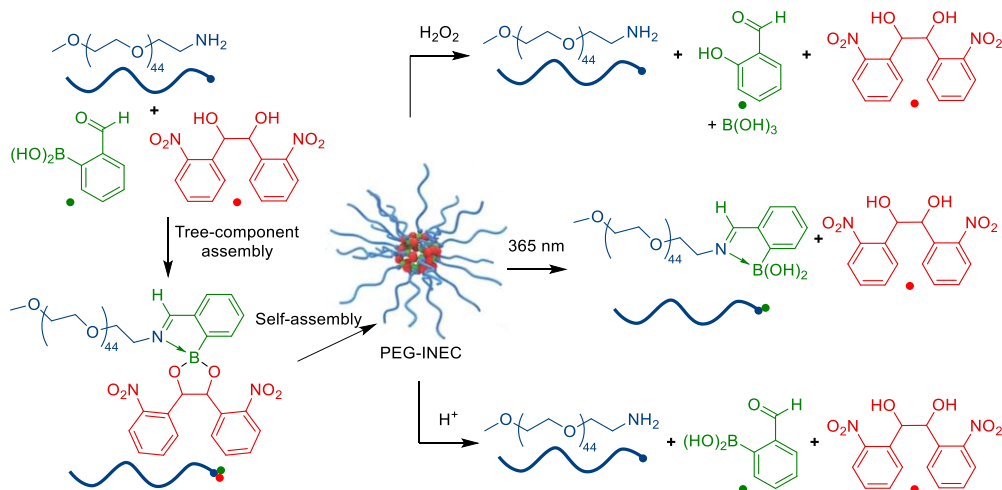


Figure 20: Self-assembled PEG-iminoboronate polymeric nano-aggregates and their stimuli-responsive degradation by light, acid, or  $\text{H}_2\text{O}_2$ .<sup>208</sup>

The same group have also reported the development of different iminoboronate aggregate systems, whose disassembly is triggered by the action of nucleophilic ROS or  $\text{CO}_2$ -induced solvent acidification.<sup>209,210</sup> For example,  $\text{CO}_2$ -responsive  $\text{N}_3\text{-(OEG-IBCAPE)}_4$  polymersomes are stable at physiological pH 7.4, however protonation of their tris-amine cores results in nano-aggregate disassembly at mildly acidic pH levels. This enabled iminoboronate ester linkers to be used to generate polymersomes attached to the diol unit of caffeic acid phenethyl ester (CAPE, anti-cancer drug, red) as a  $\text{CO}_2$ -responsive drug delivery system (Figure 21). These polymersomes exhibited improved transport properties that enabled their delivery to  $\text{CO}_2$ -rich HL-60 leukaemia cells that exhibit a mildly acidic environment. This acidity results in intracellular hydrolysis of the iminoboronate bonds of the polymersome aggregates, which leads to their disassembly and release of CAPE as a cytotoxic agent within the target cancer cells. Jiang *et al.* have most recently shown that that these structures are also responsive to tandem metalation of the triamine centre and ROS-cleavage of the iminoboronate linker.<sup>211</sup> The same transport principles have also been employed by Shi and co-workers for pH/GSH-responsive delivery of encapsulated capecitabine to HepG2 liver cancer cells.<sup>212</sup>

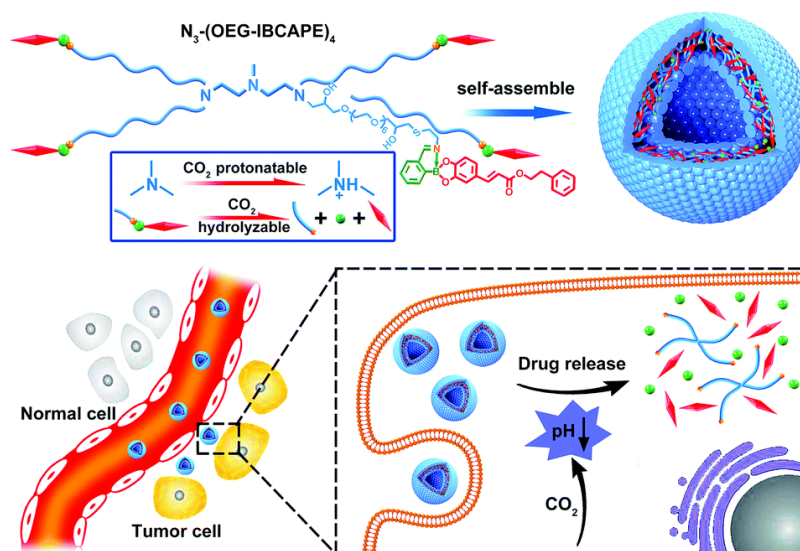
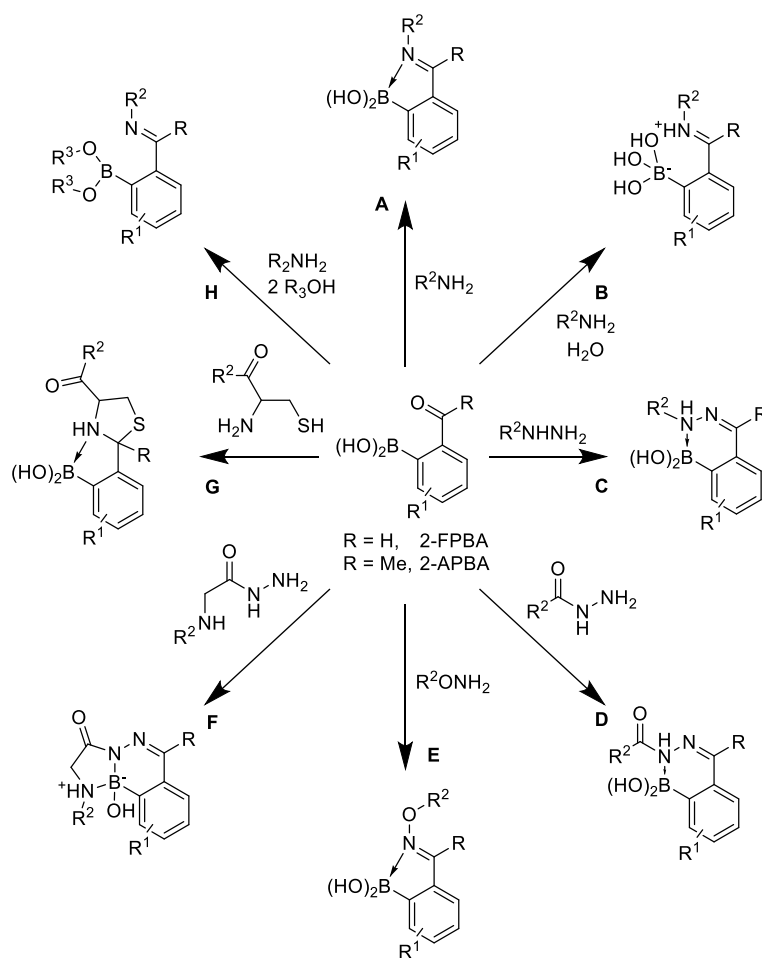


Figure 21: Self assembled prodrug  $N_3$ -(OEG-IBCAPE) $_4$  polymersomes and the stimuli-responsive  $CO_2$ -triggered release of CAPE in cancer cells.<sup>210</sup> Reproduced with permission from the Royal Society of Chemistry.

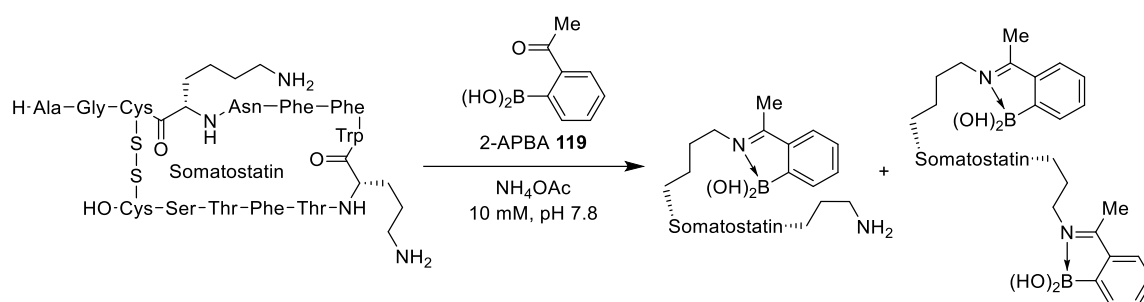
### 1.9. Iminoboronate derivatives for biological targeting and tagging

IB-type assemblies have also been employed for the functionalisation and tagging of the amino groups of peptides and proteins, with several recent specialised reviews having covered this topic in detail,<sup>213–216</sup> with only a general overview of this area provided herein. The majority of bioorthogonal labelling reactions that have been reported to date are two-component in nature, involving reaction of 2-FPBA **1** (or 2-acetylphenylformyl boronic acid, 2-APBA **119**) with amine or aminothiol residues of peptides or proteins to form imine/thioxazolidine bonds that are stabilised by the presence of a proximal boron centre (Scheme 47). These condensation reactions have been found to proceed with rate constants of over  $10^2$ – $10^3$   $M^{-1} s^{-1}$ ,<sup>217</sup> which is orders of magnitude faster than many traditional alkyne-azide ‘click’ coupling reactions. Gois, Gillingham and Anslyn have carried out binding studies that clearly demonstrate that the proximal boron centre accelerates imine condensation reactions and stabilises imine complex formation, with additives or external stimuli (*e.g.* changes in pH, ROS, nucleophiles...) normally required to achieve hydrolysis, degradation, or decomplexation.<sup>125,126,218,219</sup> For example, computational studies on the condensation of *n*-butylamine and 2-APBA **119** have shown that the adjacent boronic acid reduces the activation enthalpy for imine condensation drastically by 35–36 kcal/mol.<sup>218</sup>



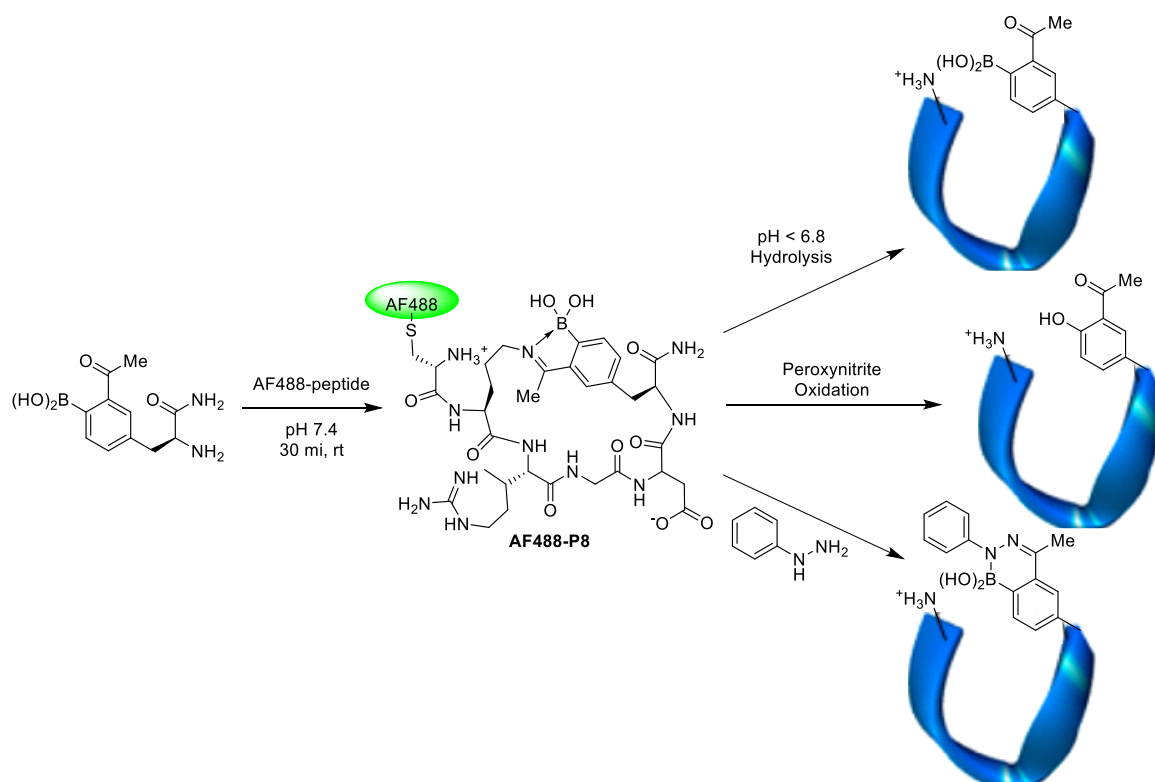
Scheme 47: Diverse bioorthogonal IB conjugation chemistries of 2-FPBA- and 2-APBA-derived linkers.

The most commonly employed amine-tagging systems involve generation of the two component iminoboronic acid assemblies **A** and **B** (pH interconvertible), both of which have been widely used to label the free  $\epsilon$ -amine groups of lysine residues in peptides and proteins. This approach was pioneered in 2012 by Gois *et al.* who reported formation of an iminoboronic acid complex between the hormonal neuropeptide Somatostatin and 2-APBA **119** in ammonium acetate buffer (20 mM, pH 5.0–7.0) (Scheme 48).<sup>218</sup> Following this success, they demonstrated that 2-APBA **119** could be used to successfully tag lysine groups present in lysozyme, cytochrome C, ribonuclease A, and myoglobin with a range of 2-formylaryl boronic acids. Improvements to this tagging approach have subsequently been reported based on the use of peptides/proteins containing  $\alpha$ -nucleophiles such as hydrazides, acylhydrazides and alkoxyamines which react more rapidly to afford hydrazone and oxime linkers (**C**, **D**, **E**, Scheme 47) that are more hydrolytically stable.<sup>217,220–223</sup> Similarly, multidentate coordination of bifunctional nucleophiles such as  $\alpha$ -amino hydrazides or 1,2-aminothiols to 2-FPBA/2-APBA templates have proved popular for producing stable bioconjugates containing tricyclic azadiborolidine boracycles (**F**, Scheme 47) and stabilised thioxazolidine linkers (**G**, Scheme 47).<sup>220,222,224–226</sup>



Scheme 48: Reaction of lysine groups in Somatostatin with 2-APBA **119**.<sup>218</sup>

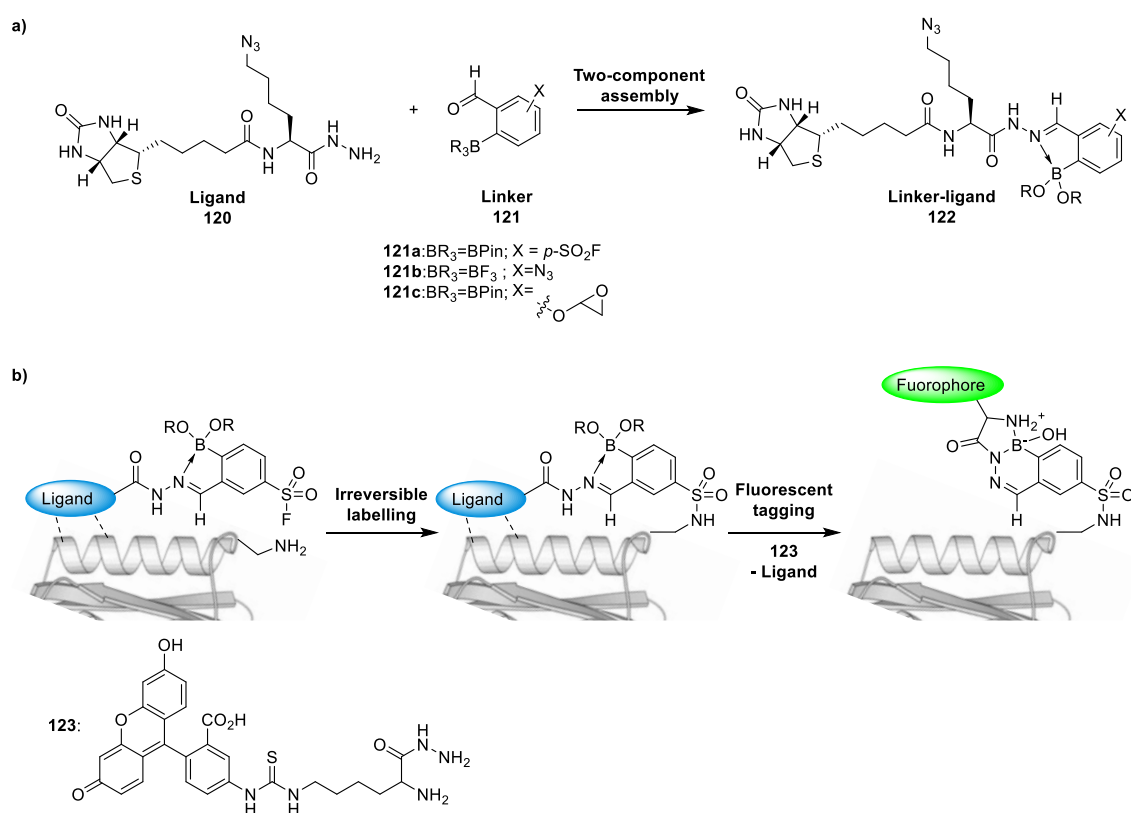
Proof of concept studies have shown that stimulus-triggered decomplexation of these types of protein-boracycle conjugates can be achieved through treatment with fructose, dopamine, glutathione, aqueous acid, ROS/RNS, *etc.*, with this reversibility exploited to induce partial or complete hydrolysis of intramolecular imine bonds to control ring-opening of cyclic peptides (Scheme 49). Since their inception, these types of stimuli-responsive two-component IB assemblies have been used to derivatize peptides, proteins, aminoglycosides, biological polyamines and amine-rich membrane lipids for fluorescent tagging, targeted fluorophore, biomolecule and therapeutic delivery, covalent protein inhibition, and reversible biomolecule functionalization.<sup>227–235</sup>



Scheme 49: A stimuli-responsive intramolecular iminoboronic acid bond can be used to control the cyclisation of an AF488 fluorophore-appended peptide.<sup>227</sup>

Witte *et al.* have very recently exploited the selectivity and reversibility of three-component hydrazone-derived assemblies to develop modular multicomponent chemical probes that can be used for protein tagging and/or labelling applications (Scheme 50).<sup>236</sup> In this approach, 2-FPBA-derived units containing amine-reactive “warhead” units (*e.g.* sulfonyl fluoride, epoxide, or azide,

**121a-c**) are reacted with a hydrazide ligand **120** containing a peptide recognition (e.g. streptavidin, Strp) to afford reactive ligand-linker IBE complexes **122**. Attachment of these IBE complexes to the target protein through the recognition domain results in selective reaction of the reactive warhead with an amino group of the desired protein, resulting in irreversible tagging of the protein surface. Subsequent treatment of these protein-bound complexes with  $\alpha$ -amino hydrazide fluorophores **123** then results in a fast transamination reaction displacing the hydrazide targeting ligand to selectively produce highly stabilised fluorescent tricyclic azadiborolidine protein complexes (**F**, Scheme 47) that can then be imaged fluorescently. Conveniently, these linker-ligand complexes could be prepared by simply combining equimolar amounts of ligand and linker prior to administration to the desired protein, or even be prepared *in situ* by adding the ligand and linker separately to the protein mixture.

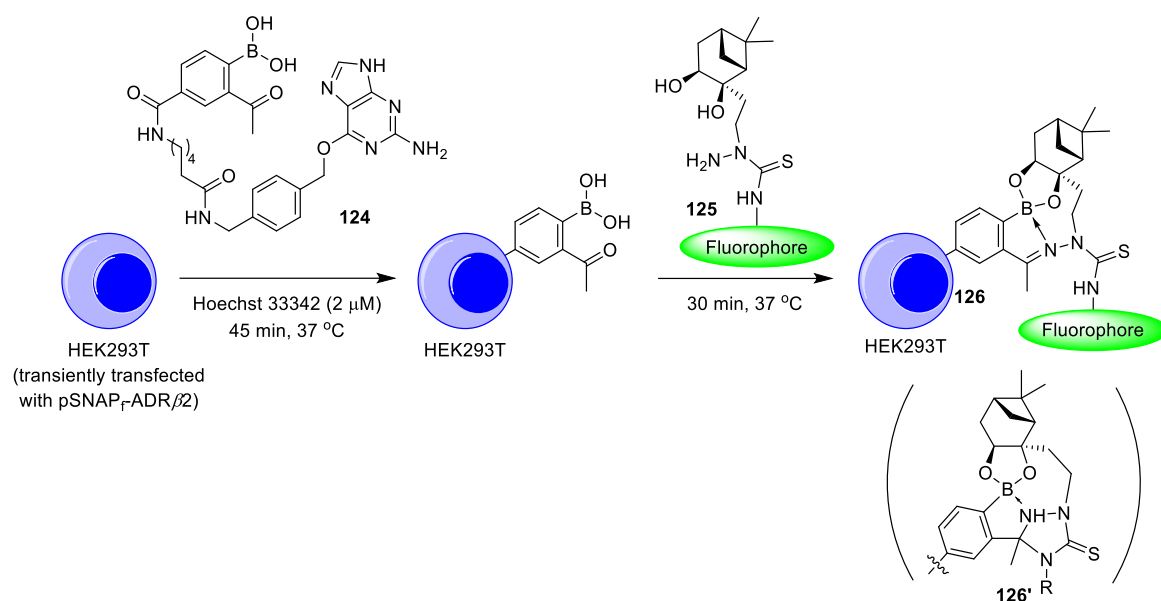


Scheme 50: (a) Modular assembly of a warhead-ligand iminoboronate-hydrazide complex **122**. (b) Ligand-directed covalent labelling of a protein by **122a** and ligand exchange with an  $\alpha$ -amino hydrazide fluorescent reporter **123**.<sup>236</sup>

The use of three-component strategies for tagging the amino groups of biomolecules has been less well explored (e.g. **H**, Scheme 42), although three recent reports demonstrate the potential of this approach for producing stable bioconjugates. In 2017, Hall and co-workers reported the development of a three-component-like click tagging approach, using a novel nopoldiol/arylboronate thiosemicarbazone/acyl (NAB-TAS) synergic system, where the thiosemicarbazide unit underwent rapid imine condensation to afford complex **126** that was stabilised by intramolecular formation of a boronate ester bond with the adjacent pendant nopoldiol (a popular “click” boronate motif). More recent characterisation work has shown that



these complexes undergo further intramolecular cyclization reactions, with the thiosemicarbazone nitrogen adding to the activated C=N, producing an additional triazolidine-thione ring as shown in structure **126'**.<sup>237</sup> This system was employed for live cell imaging by fluorescence microscopy using a SNAP-tag approach, in which HEK293T cancer cells were transiently transfected with the pSNAP-ADR62 plasmid, allowing 2-APBA-derivative **124** to be secured on the cell membrane, enabling 'click' fluorescent tagging of these cells with **125** for visualisation using fluorescence microscopy at concentrations as low as 10  $\mu$ M (Scheme 51).<sup>238</sup>



Scheme 51: 2-APBA modification of HEK293T cancer cells and subsequent "three-component click NAB-TAS" boronate/thiosemicarbazone fluorescent labelling.<sup>238</sup>

Further applications of this NAB-TAS approach have been very recently reported by the same group for *in vivo* targeting and imaging applications.<sup>237</sup> An APBA motif was first introduced locally into mice by intradermal injection of a boronate-*N*-hydroxysuccinamide (NHS) adduct **127** that was capable of reacting with exogenous nucleophiles to anchor the acyl-boronate motif to the extracellular matrix. A near-infrared (NIR) cyanine-appended nopoldiol-thiosemicarbazone derivative **128** was then administered systemically through retro-orbital injection, which resulted in production of a strong highly localised fluorescent signal after 24 h, indicating successful NAB-TAS-mediated targeted delivery of the fluorescent tag to the APBA-treated region.



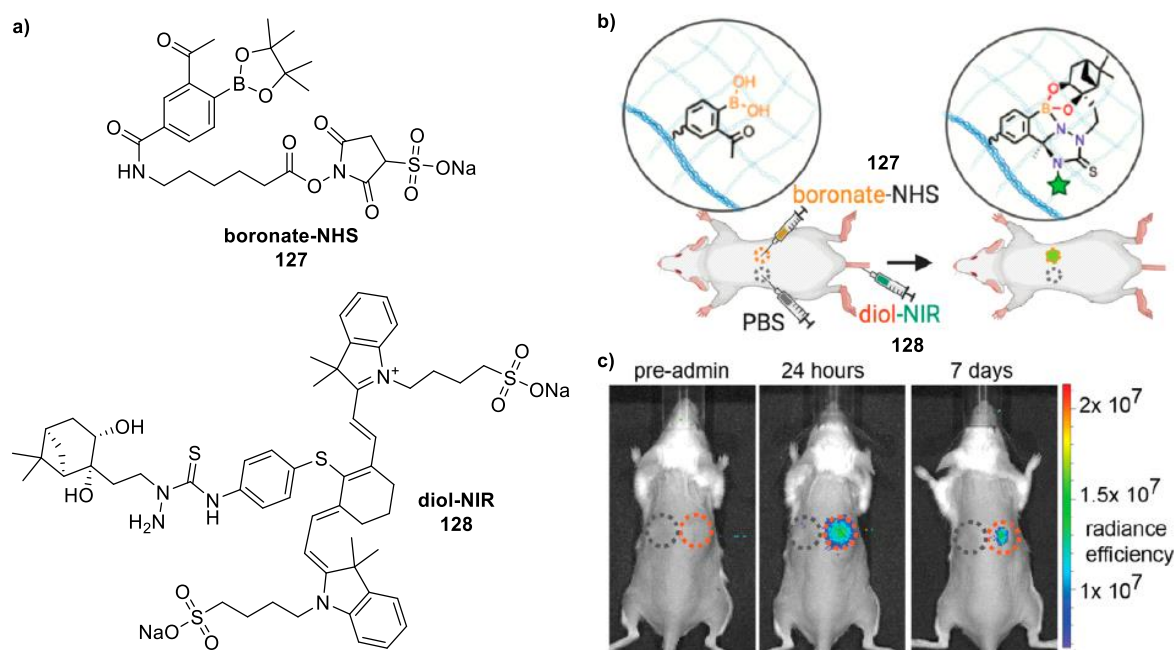
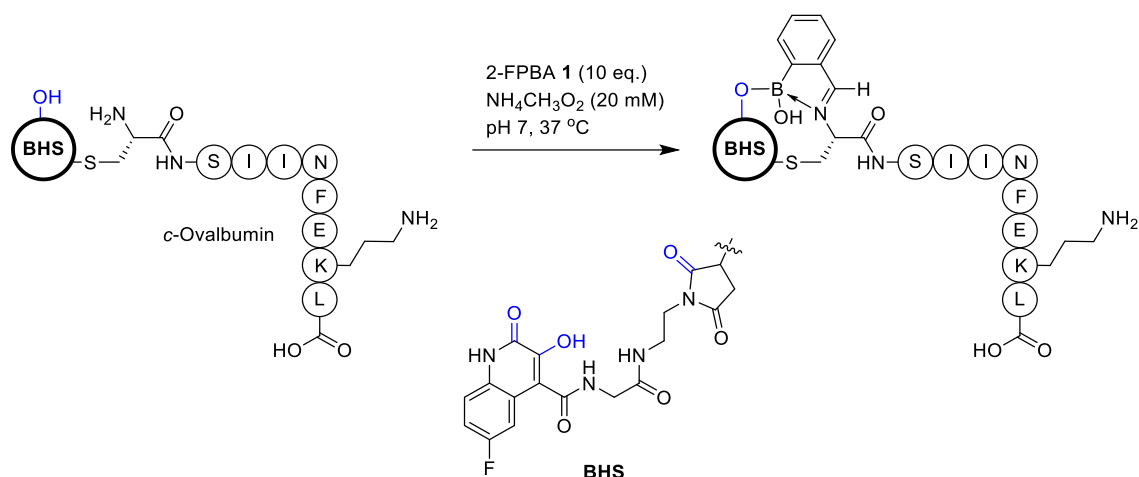


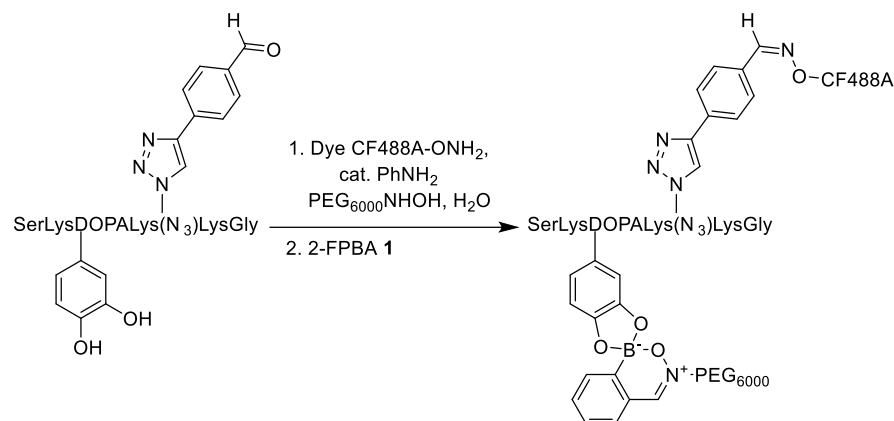
Figure 22: (a) Structures of boronate-NHS **127** and diol-NIR **128** used for *in vivo* NAB-TAS coupling bioorthogonal targeting. (b) Schematic representation of labelling experiments. **127** is first anchored to the tissue extracellular matrix, and **128** is then administered systemically for click capture. (c) Representative *in vivo* images of mice before, 1 day after, and 1 week after administration of **128**. Blue and red dashed circles indicate PBS and boronate-NHS injection sites, respectively.<sup>237</sup> Reproduced with permission from the American Chemical Society.

Gois *et al.* have reported a “boron hot spot” (BHS) approach to selectively target the amino groups of *N*-terminal cysteine residues, which was developed to address some of the promiscuity and reversibility issues that are often observed when two-component iminoboronic acid complexation reactions are used to functionalise biomolecules (Scheme 52).<sup>239</sup> They found that attachment of 3-hydroxyquinolin-2(1H)-one (3HQ)/succinimide groups to the thiol units of *N*-terminal cysteine residues resulted in selective imine condensation of the *N*-terminal amino group with 2-FPBA **1**. This was proposed to be due to the IB complex being stabilised by formation of an intramolecular B-O bond between the boronic acid and the BHS  $\alpha$ -hydroxy-amide fragment of the *S*-appended 3HQ fragment, with further hydrogen bonding stabilisation from the succinimide (blue, Scheme 52). This boron hot spot approach was used to selectively tag 2-FPBA-modified *c*-ovalbumin with an impressive  $K_a$  value of  $58,128 (\pm 2) \text{ M}^{-1}$ , thus allowing for site-selective labelling of its free *N*-terminal amino groups in the presence of other lysine residues despite a large excess of 2-FPBA **1**. This tagging approach was used to prepare glutathione-labile boron hot spot fluorescently-labelled protein conjugates that were capable of delivering their fluorescent payloads to HT29 cancer cells.



Scheme 52: Site-selective iminoboronate complexation of an *N*-terminal boron hot spot-modified *c*-ovalbumin.<sup>239</sup>

Finally, a collaboration with Anslyn has reported the use of 2-FPBA **1** and hydroxylamine to irreversibly functionalise the catechol fragment of an L-Dopa-containing peptide derivative. Fluorescent tagging of the peptide containing a Cu(I) Sharpless-Huisgen ‘click’ appended benzaldehyde group was achieved through imine bond formation with the *O*-functionalised hydroxylamine residue of the CF488A dye. Subsequent addition of 2-FPBA **1** then templated irreversible three-component formation of a highly stable nitrono-boronate linker (*vide supra*) that was formed from incorporation of the catechol unit of the L-Dopa residue and the *N*-functionalised hydroxylamine group of the solubilising PEG side-chain (Scheme 53).<sup>45</sup>



Scheme 53: Dual one-pot labelling of L-Dopa-containing peptide with a fluorescent dye and a solubilising PEG side-chain.<sup>45</sup>

## 1.10. Conclusions and outlook on the Bull-James assembly

The body of work presented in this review, which forms the basis of a publication in *Coordination Chemistry Reviews*,<sup>240</sup> clearly highlights the versatility and practicality of iminoboronate assemblies, with potential applications across many fields of chemistry and chemical biology. From its initial discovery as a CDA for determining the *ee*'s of chiral amines and diols, the Bull-James three-component assembly has now been developed into a wide-ranging method for the chiral analysis

of a broad variety of analytes using NMR, CD, fluorescence, and electrochemical methods. Beyond analytical applications, iminoboronate assemblies have also proven popular as orthogonal self-assembly tools for preparing boracycles, polymers, hydrogels and aggregates that exhibit stimuli-responsive properties. Similarly, bioconjugation applications have also been demonstrated, with ongoing development of two- and three-component dynamic labelling methodologies showing great promise as a versatile tool for “click” modification of the free amino groups (or diols) of biomolecules.

Although the original application of these IBE assemblies as analytical tools for determining enantiopurities continues to grow both in scope and popularity, it is likely that the potential chemical biology applications of these IB systems will be far wider ranging than was originally anticipated. Although it is expected that additional analytical IBE methods will be developed, some of which are reported in the chapters below, the future of these three-component iminoboronate ester assemblies clearly lies in their innate ability to act as reversible yet highly rigidified linkers. The prospect of expanding the use of these IBEs as easily ‘tuneable’ chiral auxiliaries for asymmetric synthesis is an exciting one and should lead to highly versatile, practically simple methodologies for a wide range of asymmetric transformations. It is also anticipated that the “click” and stimuli-responsive capabilities of these boron-coordination complexes will lead to further development of wide-ranging bioorthogonal and materials-based systems, with increasingly wide-ranging sensing, tagging, theranostic, and logic-based applications.

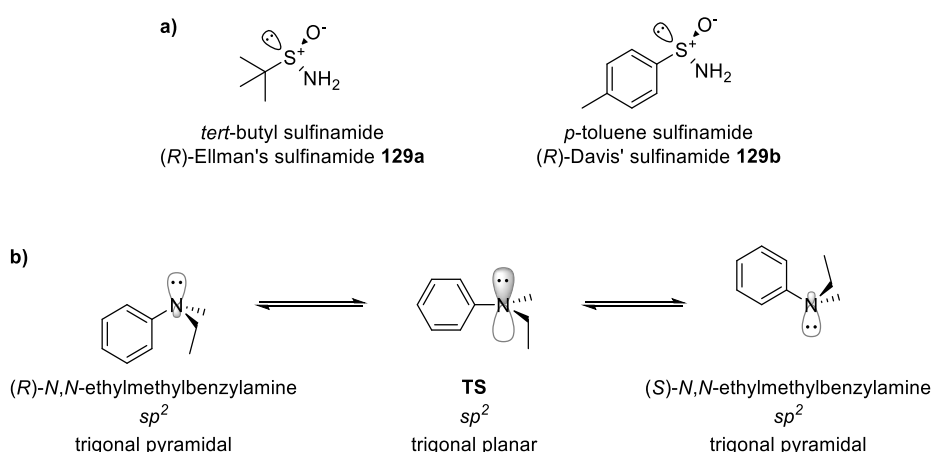
## 2. DIASTEREOMER AGGREGATION INDUCED ANISOCHRONISM (DAIA) AFFECTS THE $^1\text{H}$ NMR SPECTRA OF SULFINIMINOBORONATE ESTER COMPLEXES DERIVED FROM BINOL

### 2.1. Introduction

Having described how the Bull-James three-component assembly of iminoboronate esters can be used as a CDA to determine the *ee* of a wide range of chiral analytes by  $^1\text{H}$  and  $^{19}\text{F}$  NMR spectroscopic analysis, the Bull group were interested in investigating whether its scope could be broadened to other amine-type analytes. Of particular interest was assessing whether this method could be used to determine the *ee* of chiral primary sulfinamides, which are chiral at sulfur. Consequently, the following two chapters describe efforts to develop an effective Bull-James CDA method for determining the *ee* of sulfinamides, with this chapter beginning with a short overview of sulfinamides, looking at their asymmetric synthesis, applications, and reactivity. This chapter then moves on to detail how these studies led to the discovery that IBE assemblies derived from sulfinamides and BINOL form supramolecular aggregates in solution.

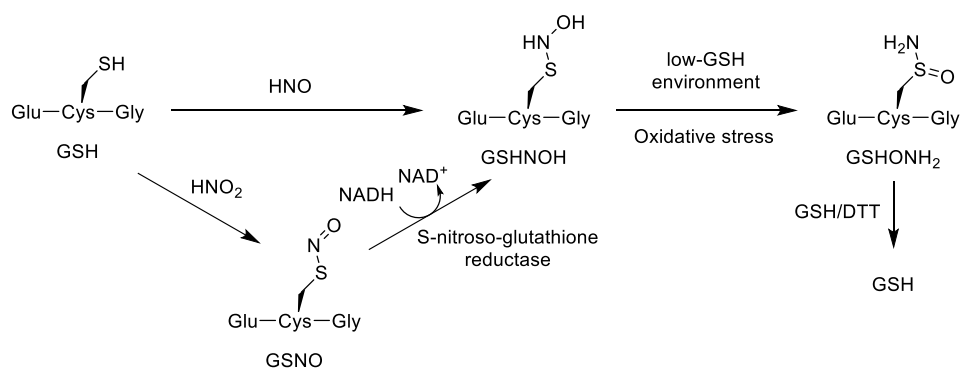
#### 2.1.1 *Sulfinamides*

Sulfinamides are most commonly employed as “chiral ammonia sources” for the asymmetric synthesis of chiral products (usually amines) using traditional chiral auxiliary approaches.<sup>241–245</sup> This is possible because sulfinamides are *S*-chiral, containing a stereogenic sulfur atom that complements more common carbon stereocentres that are found widely throughout Nature. Conserved chirality in sulfinamides arises despite their three-coordinate nature, with the presence of a configurationally stable  $sp^3$  hybridised lone pair enforcing a trigonal pyramidal structure at sulfur, as illustrated in the structures of Ellman’s and Davis’ sulfinamides **129a** and **129b** (Scheme 54a). These structures are analogous to those of amines, which also adopt a tetrahedral conformation with an  $sp^3$  lone pair occupying the fourth coordination site (e.g. *N,N*-ethylethylaniline, Scheme 54b).<sup>246</sup> Although this tetrahedral geometry can clearly lead to two distinct nitrogen chiral centres, the barrier to inversion of tertiary amines is very low, generally estimated at  $< 10$  kcal/mol,<sup>247</sup> proceeding *via* a trigonal planar  $sp^2$ -hybridised transition state (**TS**). Therefore, although individual tetrahedral conformations of amines may be chiral themselves, their rapid interconversion leads to non-conserved stereogenic centres, and so tertiary amines are not generally considered *N*-chiral molecules unless tetrahedrally enforced. This is much less of an issue for *S*-chiral structures such as sulfinamides, sulfoxides, and sulfonates, which experience a much higher barrier to pyramidal inversion, and therefore generally retain their stereochemistry unless exposed to forcing conditions. Inversion and racemisation of sulfinamides and sulfoxides will be discussed in more depth below in section 3.2.2.



Scheme 54: (a) Structures of Ellman's and Davis' sulfinamides **129a** and **129b**. (b) Chiral inversion of *N,N*-ethylmethylbenzylamine.

The natural occurrence of sulfinamides is very limited, seemingly arising exclusively from post-translational oxidative modifications of peptidic thiol residues.<sup>248</sup> Two similar pathways for their biological formation have been reported to date (Scheme 55). Thiol-containing peptides and proteins, such as GSH, can be directly oxidised by exogenous nitroxyl (HNO) to form an *N*-hydroxysulfenamide intermediate **130**. Alternatively, this *N*-hydroxysulfenamide intermediate can be formed *via* oxidation of GSH by nitrous acid (HNO<sub>2</sub>) to produce *S*-nitrosothiol GSNO,<sup>249</sup> which is then reduced by *S*-nitroso-glutathione reductase using NADH as a cofactor.<sup>248,250</sup> Under oxidative stress conditions, where the relative concentration of GSH is low, the *N*-hydroxysulfenamide GSHNOH intermediate rearranges to produce its corresponding primary sulfinamide GSHONH<sub>2</sub>.<sup>248</sup> These post-translational modifications can severely affect the structure and function of affected proteins and peptides, as shown by Keceli *et al.* in a series of papers exploring the structure and reactivity of these products.<sup>251–253</sup> Using a combination of <sup>1</sup>H and <sup>15</sup>N NMR spectroscopy, high-resolution MS, and macromolecular modelling techniques, they showed that these modifications are in fact reversible in the presence of excess GSH or dithiothreitol (DTT), regenerating free thiols through reductive/rearrangement processes.<sup>252</sup> The same studies also investigated the hydrolysis of these species to the corresponding sulfinic acids, concluding that protein environments and acidic conditions accelerated these processes. Following these and similar oxidation pathways, it is evident that the presence of sulfinamides in peptides and/or proteins can be considered as biomarkers of oxidative stress.<sup>254,255</sup>

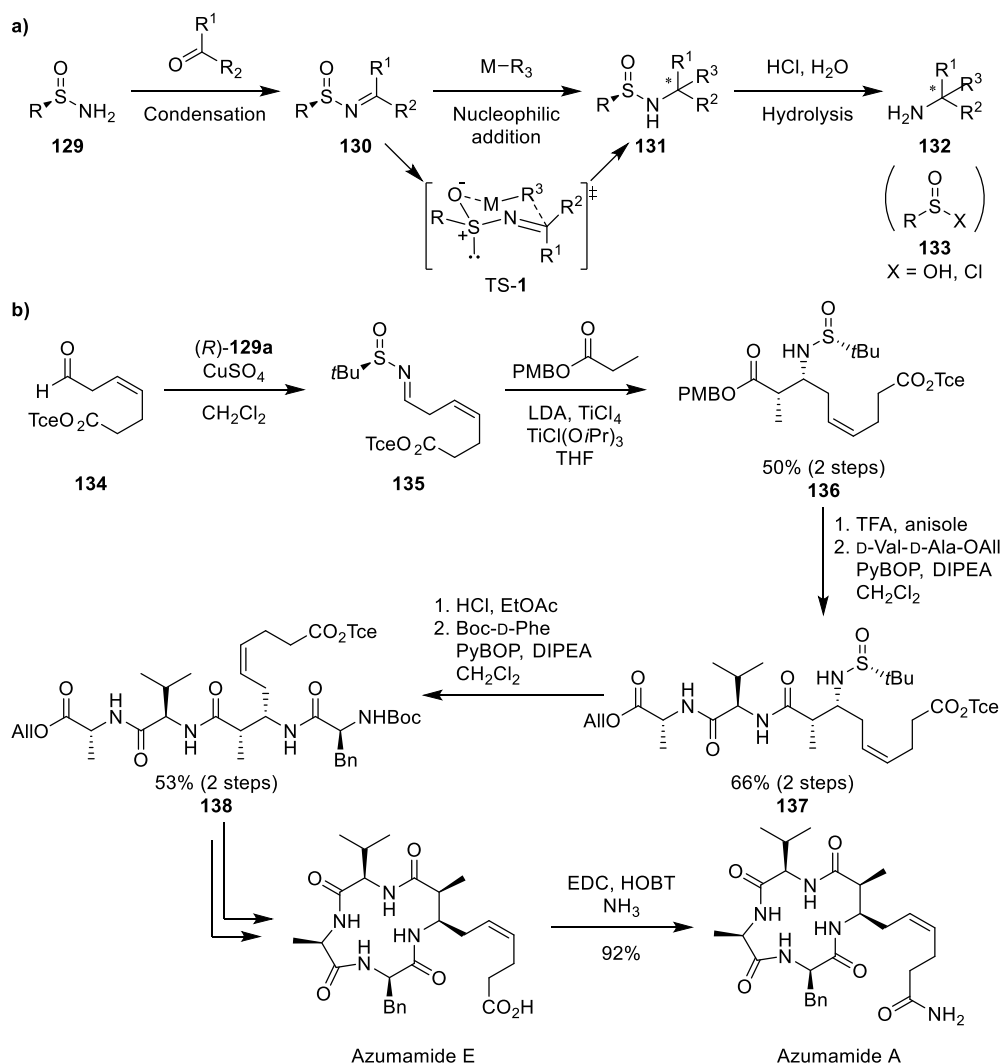


Scheme 55: Biosynthesis of sulfinamides by post-translational oxidative modifications of GSH.<sup>248</sup>

### 2.1.2 The use of chiral sulfinamides in asymmetric synthesis

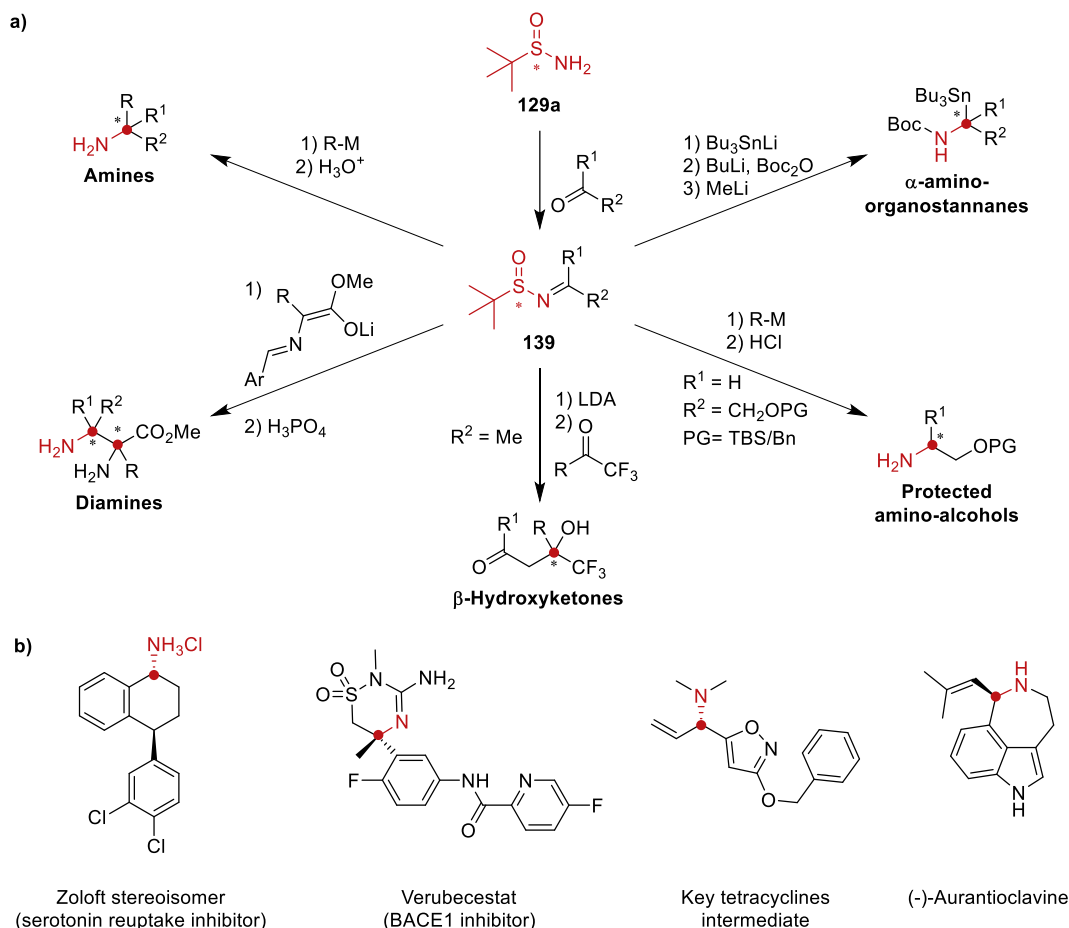
The most widespread use of primary sulfinamides is as chiral auxiliaries for the asymmetric synthesis of a wide range of chiral products, with the most popular Ellman's **129a** and Davis' **129b** sulfinamides having been used thousands of times by many different academic and industrial groups. The general synthetic strategy that is employed for these sulfinamide auxiliaries is presented in Scheme 56a. Firstly, a chiral sulfinamide **129** is condensed with the carbonyl group of an aldehyde (or ketone) to produce an *N*-sulfinyl imine (or sulfinimine) of general structure **130**, which can then serve as a "chiral ammonia building block". Nucleophilic attack by a suitable organometallic reagent results in its addition across the C=N bond to generate a substituted sulfinamide **131** containing a new  $\alpha$ -amino stereocentre with high levels of diastereocontrol. These additions generally proceed with excellent facial selectivity due to a combination of the steric demand provided by the *tert*-butyl fragment, and the metal-coordinating and facial directing ability of the S=O oxygen (TS-1). Finally, the desired enantiopure amine **132** can then be liberated through acid-catalysed hydrolysis of the diastereomerically-pure sulfinamide **131**. This final step results in racemisation of the stereogenic sulfur due to production of sulfinyl chloride/sulfinic acid cleavage products **133**, although methodologies have been developed to enable recovery of enantiopure sulfinyl species.<sup>243,256–258</sup> An example of the power of this approach is shown in the bidirectional peptide synthesis approach used in the total synthesis of the natural products azumamide A and azumamide E by Ganesan and co-workers (Scheme 56b).<sup>259</sup> Condensation of aldehyde **134** with chiral sulfinamide (*S*)-**129a** gave (*S*)-sulfinimine **135**, which was subjected to a stereoselective Mannich reaction using a propionate enolate to afford  $\alpha$ -substituted  $\beta$ -amino ester **136** containing two new stereocentres with excellent levels of diastereocontrol. The *O*-PMB ester group of  $\beta$ -amino ester **136** was then oxidatively deprotected to afford its free acid group that underwent amide bond coupling with dipeptide D-Ala-D-Val-OAll to give tripeptidic **137**. The *N*-sulfinyl group of tripeptide **137** was subsequently hydrolysed under strong acidic conditions to produce a free amino group that underwent a second amide bond coupling reaction with *N*-Boc phenylalanine to produce tetrapeptide intermediate **138**. This key tetrapeptide intermediate was then easily converted into

the macrocyclic peptides azumamide E and azumamide A using a series of cyclisation/deprotection reactions.



Scheme 56: (a) General strategy for using sulfinamides as chiral auxiliaries for the asymmetric synthesis of chiral amines and their derivatives. (b) Asymmetric total syntheses of azumamides A and E by Ganesan *et al.*<sup>259</sup>

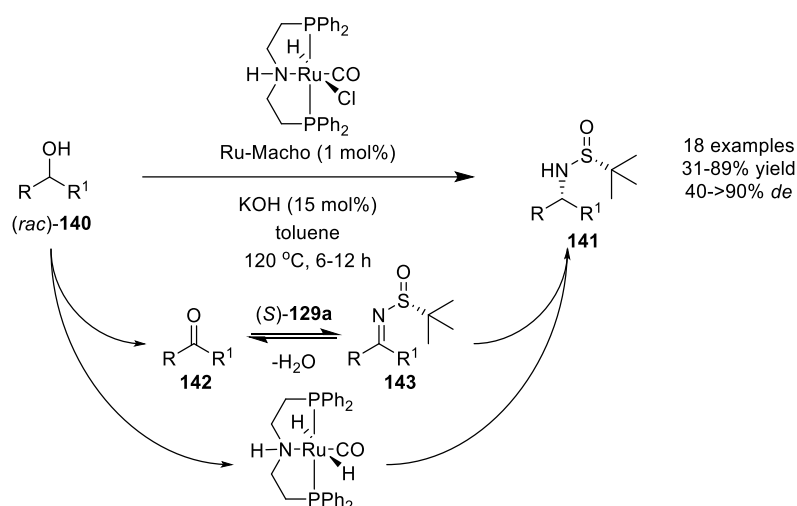
Ellman's sulfinamide is the most widely used chiral auxiliary in asymmetric synthesis, which has been used to prepare an impressive range of enantiopure amines, diamines, amino alcohols,  $\alpha$ -organometallic amines,  $\alpha$ - and  $\beta$ -amino acid derivatives, and  $\beta$ -hydroxy ketones, with all of these transformations proceeding *via* sulfinimine intermediate **139** (for representative examples see Scheme 57a).<sup>257,260–266</sup> This has led to its widespread use in large scale synthesis of chiral amines for the production of drugs and structurally challenging natural products (Scheme 56b, Scheme 57b).<sup>267–270</sup>



Scheme 57: (a) Representative examples of the use of enantiopure sulfinamides as chiral auxiliaries for asymmetric synthesis. (b) Useful/high-value products synthesised using these methodologies (sulfinamide-derived atoms and sulfinamide-directed stereocentres in red).<sup>267–270</sup>

In 2014 Guan *et al.* reported the use of Ellman's sulfinamide as a chiral ammonia source for the conversion of racemic secondary alcohols (*rac*)-**140** to enantiopure  $\alpha$ -secondary sulfinamides **141** (Scheme 58b) using a 'borrowing hydrogen' catalytic approach.<sup>271</sup> In their elegant approach, a ruthenium catalyst (Ru-Macho) first oxidises a secondary alcohol substrate to an achiral ketone intermediate **142** which then reacts reversibly with sulfinamide (*R*)-**129a** to form chiral sulfinimine **143**, that is then reduced by the Ru-Macho catalyst to produce a secondary sulfinamide containing a new stereocentre. This 'one-pot' method was used to prepare a range of 18 chiral sulfinamides **141** in moderate to good diastereoselectivities of 40–90% *de*, with acid catalysed hydrolysis of the S–N bonds of their purified major diastereomers then affording their corresponding enantiopure amines.

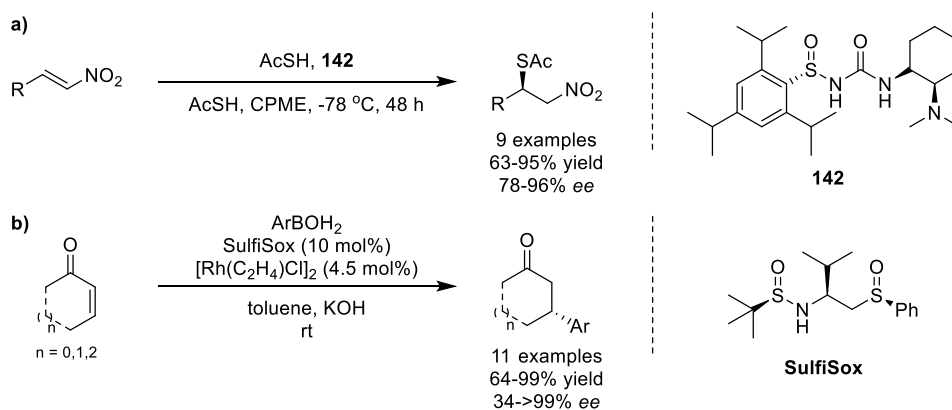




Scheme 58: “Borrowing hydrogen” approach for the diastereoselective synthesis of  $\alpha$ -secondary sulfinamides from racemic alcohols by Deng *et al.*<sup>271</sup>

### 2.1.3 The use of chiral sulfinamides as organocatalysts and chiral ligands

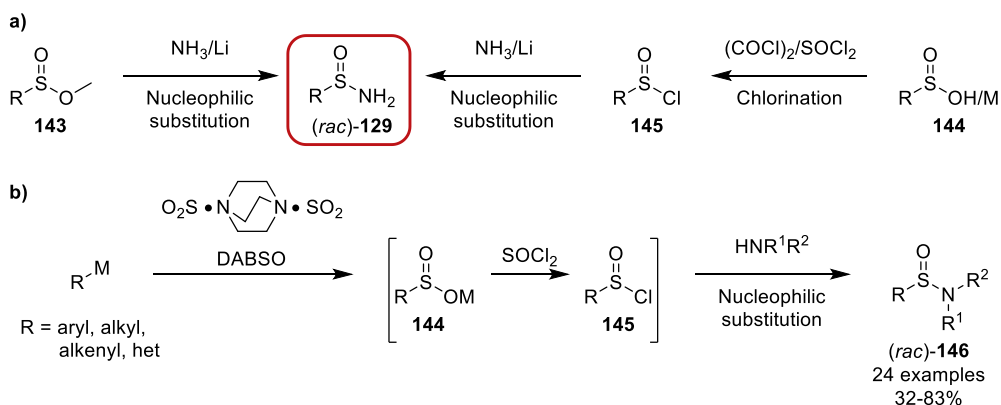
Aside from their widespread use in chiral auxiliary chemistry, sulfinamides have also found application as organocatalysts or as ligands/additives in enantioselective catalytic systems, with some representative examples shown in Scheme 59. For instance, Ellman’s group integrated the sulfinamide moiety into *N*-sulfinyl urea motifs to produce chiral organocatalyst **142**, which was used to catalyse the highly enantioselective conjugate addition of thioacetal acid to nitroalkenes (Scheme 59a).<sup>272,273</sup> This organocatalytic methodology has since been expanded to incorporate a wider range of substitution patterns and other types of nucleophile (*e.g.* Meldrum’s acid), with organocatalyst **142** used in other types of reactions, such as enantioselective *aza*-Henry reactions.<sup>272,274–276</sup> Increasingly, chiral sulfinamides have also been incorporated into ligands for metal-catalysed reactions, such as Fernández *et al.*’s recently published chiral SulfiSox ligand that was used for the enantioselective rhodium-catalysed 1,4-addition of arylboronic acids to  $\alpha,\beta$ -unsaturated ketones to produce  $\beta$ -aryl-ketones in good yields and up to > 99% *ee* (Scheme 59b).<sup>277</sup>



Scheme 59: Selected examples of enantioselective reactions catalysed by: (a) An *N*-sulfinyl urea organocatalyst **142**.<sup>273</sup> (b) A rhodium catalyst containing a SulfiSox chiral ligand.<sup>277</sup>

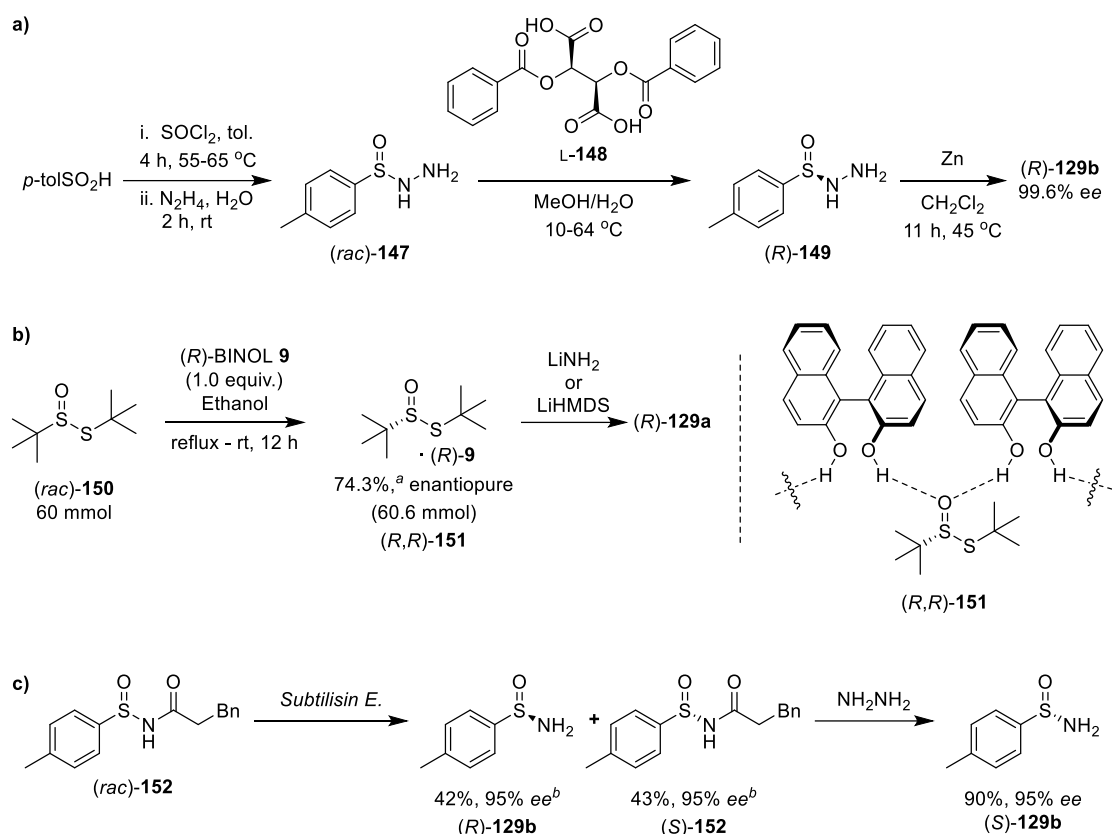
#### 2.1.4 Methods for preparing chiral sulfinamides in enantiopure form

Unfortunately, despite the popularity of primary sulfinamides for asymmetric synthesis requiring access to enantiopure materials, sulfinamide chiral auxiliaries are not available directly from the chiral pool. Consequently, multiple synthetic approaches have been developed for the preparation of chiral sulfinamides in enantiopure form.<sup>278</sup> The simplest approach is of course to prepare racemic sulfinamides in a non-stereoselective manner, which can then be resolved into their corresponding enantiomers. Primary sulfinamides are easily prepared through simple amination of racemic methyl sulfinate **143** using a lithiated ammonia source such as Li/NH<sub>3</sub> or LiHMDS (see Scheme 60a and section 3.1.4 for further discussion). Similarly, oxalyl chloride or thionyl chloride can be used to convert a sulfinic acid or metal sulfinate **144** into a sulfinyl chloride **145**, with amine displacement then affording a racemic sulfinamide (*rac*)-**129**. More tailored approaches, such as Willis' one-pot multicomponent strategy have also been used to prepare racemic sulfinamides,<sup>279</sup> with reaction of organometallic reagents with DABCO·(SO<sub>2</sub>)<sub>2</sub> (DABSO) producing metal sulfinate **144**, and thionyl chloride producing sulfinyl chloride **145** that can be reacted with different amines to afford racemic primary, secondary or tertiary sulfinamides **146** in high yields (Scheme 60b).



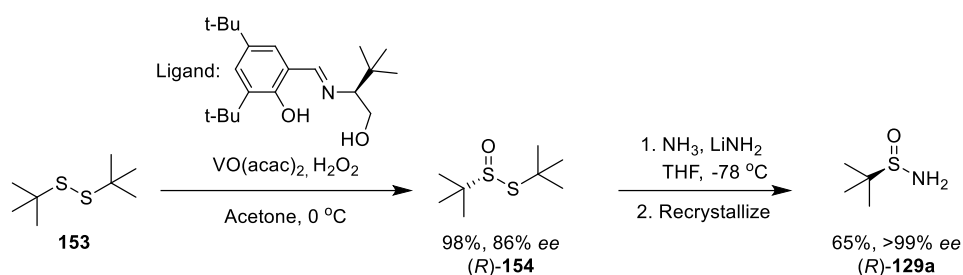
Scheme 60: Selected methods for the synthesis of racemic sulfinamides.

Racemic sulfinamides produced using these methods can be used when their enantiopurity is unimportant, however any biological or chiral auxiliary-based applications requires access to enantiopure sulfinamides. Resolution of racemic sulfinamides can be achieved using chiral preparative HPLC,<sup>280</sup> which although suitable for carrying out enantiomer separations on a small scale, is not generally applicable for the preparation of large amounts of a chiral sulfinamide. Few examples of the direct classical resolution processes are found for the direct resolution of racemic sulfinamides, however a number of resolution methods have been developed to prepare 'chiral at sulfur' precursors that may then be transformed into enantiopure chiral sulfinamides. Shanghai TTBME Co. Ltd have recently reported that racemic *p*-toluenesulfinyl hydrazine **147**, prepared from the corresponding sulfinyl chloride and hydrazine hydrate, can be resolved by co-crystallization with dibenzoyl-L-tartaric acid **L-148** to afford sulfinyl hydrazine (*R*)-**149** in 97.9% *ee* (Scheme 61a).<sup>281</sup> Subsequent reduction by zinc/acetic acid and recrystallisation afforded Davis' sulfinamide (*R*)-**129b** (99.6 % *ee*). Alternatively, Deng *et al.* reported that formation of inclusion complexes of *tert*-butanethiosulfinate **150** with (*R*)-BINOL **9** allowed for successful diastereoselective recrystallisation of homochiral diastereomeric complex (*R,R*)-**151** to be effected on a 60 mmol scale (Scheme 61b). Subsequent decomplexation of (*R,R*)-**151** affords enantiopure *tert*-butanethiosulfinate (*R*)-**150**, that could be converted into its corresponding *tert*-butanesulfinamide **129a** through treatment with LiNH<sub>2</sub>.<sup>282</sup> Kazlauskas *et al.* have reported that the protease *Subtilisin E*. can be used to for the kinetic resolution of (*rac*)-*N*-acyl arylsulfinamides (shown for Cbz-*p*-tolyl **152**), preferentially hydrolysing the amide bond of the (*R*)-**152** enantiomer over its opposite (*S*)-**152** enantiomer. Although this method suffered from substrate specificity limitations, this biocatalytic route was used to synthesise a small range of arylsulfinamide analogues of (*R*)-**129b** and *N*-acyl arylsulfinamide (*S*)-**152** in good yields and high enantiopurities (Scheme 61c), with the *N*-acyl arylsulfinamide (*S*)-**152** converted into their corresponding arylsulfinamide (*S*)-**129b** *via* treatment with hydrazine.<sup>283,284</sup>



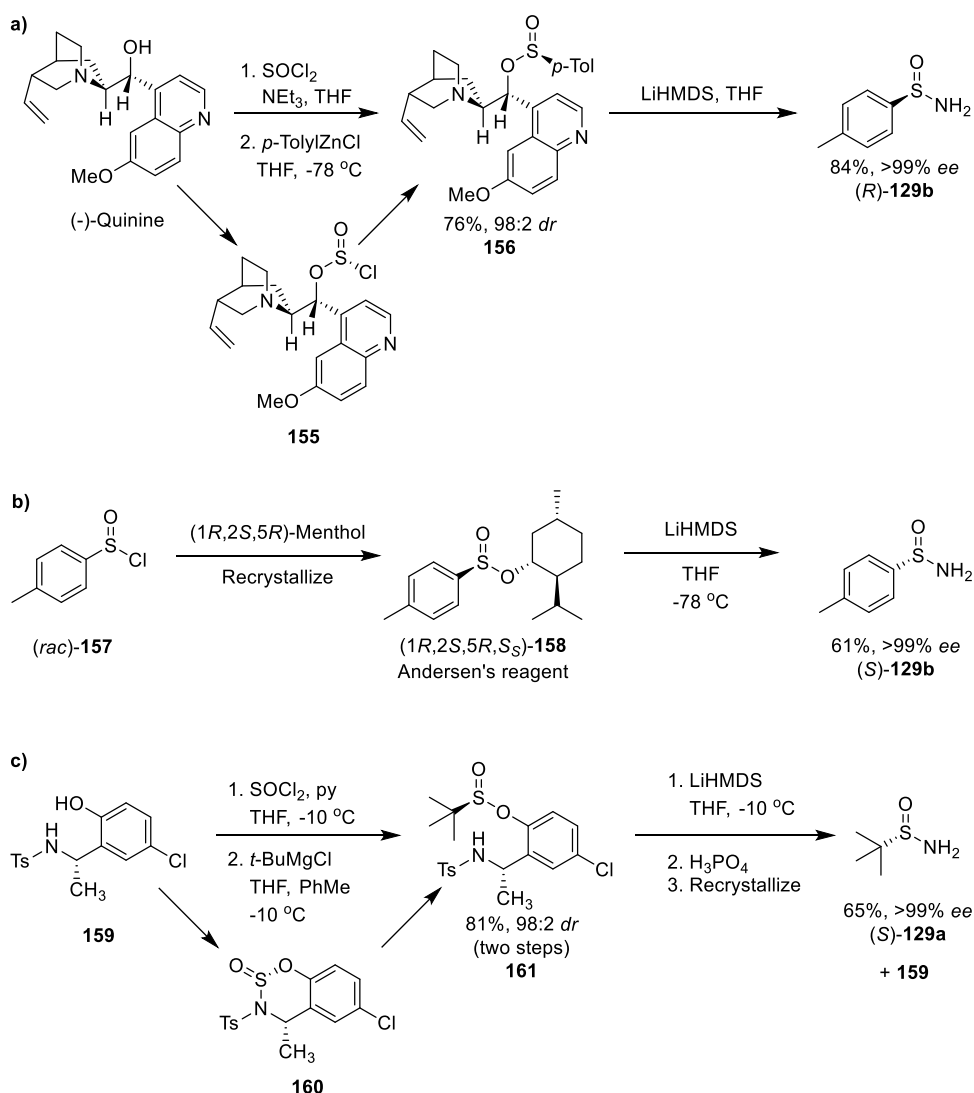
Scheme 61: Selected methods for the resolution of primary sulfonamide precursors: (a) Optical resolution of *p*-toluenesulfinyl hydrazine (*rac*)-**147** with **L-148**.<sup>281</sup> (b) Optical resolution of *tert*-butanethiosulfinate (*rac*)-**150** by co-crystallisation with (*R*)-BINOL **9**;<sup>282</sup> (c) *Subtilisin E*. biocatalysed kinetic resolution of *N*-Cbz-(*p*-tolylsulfonamide) **152**.<sup>283,284</sup> <sup>a</sup> Relative to the maximum 50% yield from racemic starting sample. <sup>b</sup> After recrystallization.

One of the most efficient approaches for preparing enantiopure *tert*-butanesulfinamide **129a** is the catalytic enantioselective sulfur oxidation methodology developed by Ellman to produce his widely used chiral auxiliary (Scheme 62).<sup>285,286</sup> Treatment of symmetric di-*tert*-butyldisulfide **153** with a chiral salen ligand, vanadium catalyst, and stoichiometric oxidants (*e.g.* H<sub>2</sub>O<sub>2</sub>) is used to produce a chiral thiosulfinate (*R*)-**154**, which is then subjected to nucleophilic reaction with lithium amide (with resulting stereoinversion at sulfur), to afford chiral sulfinamide (*R*)-**129a** in high enantiopurity on a kilogram scale. This enantioselective oxidative approach is generally limited to the production of chiral Ellman's sulfinamide **129a**, as good levels of enantiocontrol rely on both the steric bias and crucially the conformational stability of the thiosulfinate intermediate **154**, thus limiting this approach almost exclusively to *tert*-butyl substrates.<sup>278</sup>



Scheme 62: Ellman *et al.* synthesis of *tert*-butanesulfinamide (R)-129a through enantioselective oxidation of disulfide 153.<sup>285,286</sup>

Alternatively, chiral auxiliaries can be employed for the production of chiral sulfinamides (Scheme 63), an approach which is used widely for industrial and large scale production of these reagents. For example, the secondary alcohol group of chiral quinine can be reacted with thionyl chloride to afford quinine sulfinyl chloride **155** with high levels of diastereocontrol, with this intermediate then reacting with *p*-tolylzinc chloride to afford the corresponding quinine sulfinate **156** with clean inversion of configuration (Scheme 63a). This intermediate can then react with LiHMDS as a nucleophilic ammonia source, with displacement of the quinine chiral auxiliary fragment, to afford Davis' sulfinamide (R)-129b in excellent yield and enantiopurity.<sup>287</sup> Other auxiliaries can also be used, such as (1*R*,2*S*,5*R*)-(-)-menthol, used to prepare Andersen's reagent (1*R*,2*S*,5*R*,*S*<sub>5</sub>)-**158** from sulfinyl chloride (*rac*)-**157** (Scheme 63b).<sup>241,288–291</sup> This menthyl sulfinate diastereomer can be separated from its more soluble minor diastereomer by recrystallization, and then converted into enantiopure (*S*)-129b sulfinamide *via* treatment with LiHMDS. These chiral auxiliary approaches are not limited to the preparation of enantiopure Davis' *p*-tolylsulfinamide **129b**, with multiple reports of chiral auxiliary syntheses of chiral Ellman's sulfinamide as well, including many recent works by Senanayake and co-workers.<sup>290,292</sup> One such method is shown in Scheme 63c, in which a chiral phenol **159** is reacted with thionyl chloride, with the resulting sulfinyl chloride then being trapped intramolecularly by its *N*-tosyl group to produce benzo[1,2,3]oxathiazin-2-one **160** containing a defined sulfur stereocentre. Addition of *tert*-butyl Grignard to this intermediate then leads to formation of *tert*-butyl sulfinate **161** in high yield and diastereopurity, which is then reacted with LiHMDS to afford Elman's sulfinamide **129a** in high yield and enantiopurity. This method was shown to be highly effective and reproducible on > 10 kg scale, allowing for the synthesis of **129a** at scale, using mild conditions that allowed for facile recovery of the chiral auxiliary **159**.



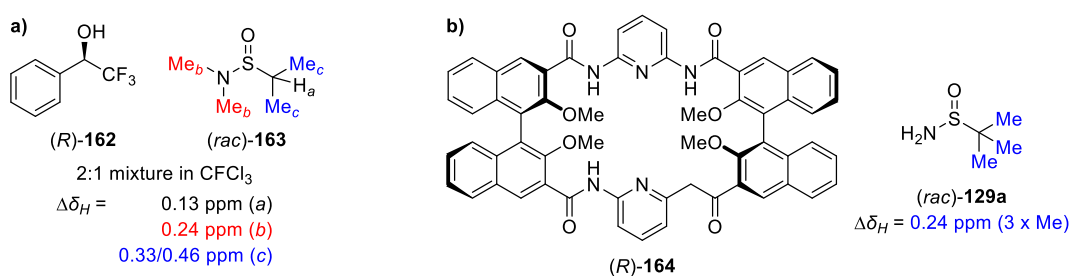
Scheme 63: Selected asymmetric syntheses of Davis' and Ellman's sulfinamides using chiral auxiliary approaches.<sup>287,288,290</sup>

### 2.1.5 Previous spectroscopic methods for determining the ee of sulfinamides

The chiral nature of sulfinamides, their predominant use as chiral auxiliaries, and their synthesis *via* kinetic resolution or enantioselective processes leads to a general need for techniques to accurately determine their enantiopurity. The enantiopurity of a primary sulfinamide chiral auxiliary is critical if it is to be used for the asymmetric synthesis of single enantiomer products, since the use of an enantiomerically impure sulfinamide will necessarily lead to a scalemic product. Although literature procedures and commercial sources report the preparation of chiral sulfinamides in high *ee*, it is prudent to confirm the *ee* of any chiral auxiliaries that are synthesised or purchased prior to use (see section 3.2.2 for an example of this). This can be achieved using chiral HPLC methodologies,<sup>293</sup> which although effective can require significant method development time and financial investment when determining the *ee* of a new chiral sulfinamide (*vide supra*). An array of chiral HPLC conditions and columns have been reported to determine *ee*'s of different type of chiral

sulfonamide, with a general preference for normal-phase separation conditions using coated polysaccharide columns (e.g. Daicel Chiralpak).<sup>293–295</sup>

Two reports on the use of chiral solvating agents that enabled the enantiopurity of sulfonamides to be determined by NMR spectroscopic analysis have also been reported previously in the literature.<sup>27,40</sup> The first, by Pirkle and co-workers,<sup>27</sup> employed enantiopure trifluorophenylethanol **162** (a variant of Pirkle's alcohol, *vide supra*), which induced anisochrony for all chemical shifts in the 100 MHz <sup>1</sup>H NMR spectrum of *N,N*-dimethyl isopropyl sulfonamide **163**, with significant chemical shift differences  $\Delta\delta_H = 0.13$ – $0.46$  ppm (1.3 – 4.6 Hz, reported in the original paper) for the diastereotopic methyl groups of its isopropyl functionality. Unfortunately, baseline resolution and determination of the *ee*'s of scalemic sulfonamides were not described in Pirkle's report. A second CSA for <sup>1</sup>H NMR spectroscopic analysis of the enantiopurity of chiral sulfonamides was reported more recently by Ema *et al.* (see Figure 2 for related work), who described the use of a chiral binaphthyl CSA (*R*)-**164**, which gave high chemical shift differences for the enantiomers of Ellman's sulfonamide (approx.  $\Delta\delta_H = 0.24$  ppm, data not described in original report).<sup>40</sup> As with Pirkle's report, this study served primarily as a proof of principle, focusing on the physical chemistry aspects of the system, rather than its potential application for accurately determining the *ee* of scalemic sulfonamides. An interesting report by Zhang, Liu *et al.* has demonstrated that the *ee* of Ellman's and Davis' sulfonamide can be determined by colorimetric and CD methods, using a L-glutamic acid amphiphilic diacetylene polymeric supramolecular gel as a spectroscopic reporter.<sup>296</sup> Strong hydrogen bonding between the polymer's glutamic acid moieties and the chiral sulfonamide functionality of the analyte resulted in significant CD and colour changes, with (*S*)-Ellman's sulfonamide **129a** turning the gel red, and the (*R*)-enantiomer maintaining the gel's blue colour, thus allowing for accurate UV-Vis determination of the enantiopurity of (*S*)-**129a** from 0–100% *ee*.

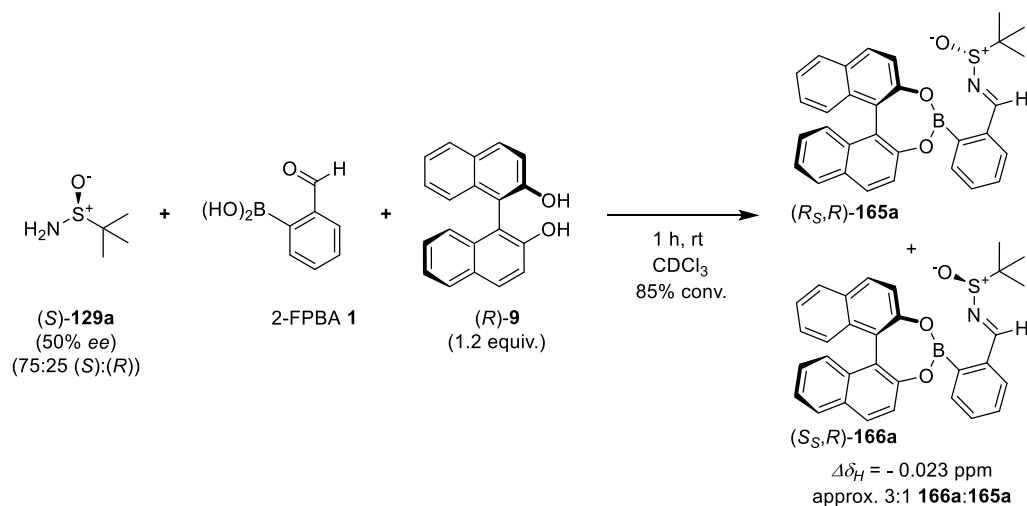


Scheme 64: Chiral CSAs that have been used to determine the *ee* of sulfonamides by NMR spectroscopic analysis.<sup>27,40</sup>

## 2.2. Scalemic assemblies using BINOL

With no previous CDA methods for determining the *ee*'s of sulfonamide chiral derivatizing agents the potential of the Bull-James assembly CDA methodology to determine the *ee* of this class of chiral amine analyte was explored. Though amine-derived and capable of similar reactivity, sulfonamides are far less nucleophilic, much bulkier, and generally less reactive than the traditional amine substrates of the Bull-James assembly, and so it was expected that additional optimisation

efforts would be needed to successfully produce sulfinamide three-component assemblies. Initial proof-of-concept experiments were carried out following a typical Bull-James three-component assembly procedure for the derivatisation of a simple primary amine (*e.g.*,  $\alpha$ -methylbenzylamine with 2-FPBA and BINOL, *vide supra*). Ellman's sulfinamide **129a** was chosen as the model sulfinamide substrate for these assembly reactions, due both to its popularity as a chiral auxiliary and the commercial availability of both its enantiomers (< £ 40 per gram for 25 g from Merck). Therefore, a simple one-pot assembly reaction of (*S*)-**129a** (50% *ee*), 2-FPBA **1** and (*R*)-BINOL **9** was carried out in deuterated chloroform for 1 h at room temperature (Scheme 65).  $^1\text{H}$  NMR spectroscopic analysis (Figure 23) revealed a new set of signals observed at 9.03 and 9.06 ppm, indicating that complexation had occurred to form a pair of sulfinamide-iminoboronate ester complexes **165** and **166** (or sulfiniminoboronate esters, SIBEs). The 73:27 ratio measured for the diastereomeric imine signals of this mixture of diastereomeric sulfiniminoboronate esters was consistent with the expected 3:1 heterochiral to homochiral ratio, indicating that no kinetic resolution had occurred. A promising chemical shift difference  $\Delta\delta_{\text{H}}$  of 0.023 ppm for the resonances of the diastereomeric imine peaks was observed. However, unlike conventional primary amines, the complexation reaction of the sulfinamide did not proceed to completion, halting at 85% conversion as indicated by the presence of 15% unreacted 2-FPBA **1** in the  $^1\text{H}$  NMR spectra (*cf.* aldehyde *CH* peak at 9.89 ppm). Additionally, although the imine protons of each SIBE diastereomer clearly exhibited distinct chemical shifts, these signals were broadened and were not completely baseline resolved in the 500 MHz  $^1\text{H}$  NMR spectra.



Scheme 65: One-pot three-component Bull-James assembly of Ellman's sulfinamide (*S*)-**129a** (50% *ee*), 2-FPBA **1** and (*R*)-BINOL **9** in  $\text{CDCl}_3$ .



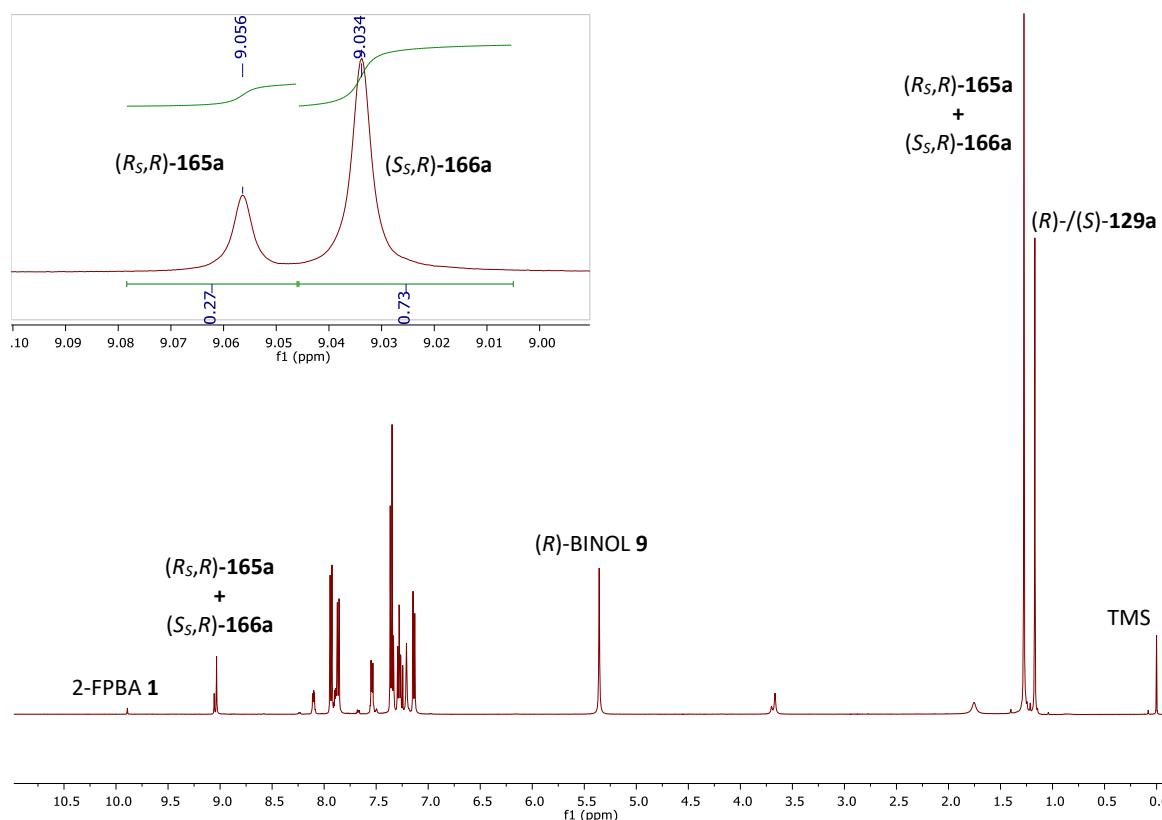


Figure 23:  $^1\text{H}$  NMR (500 MHz,  $\text{CDCl}_3$ , 100 mM) spectrum of the three-component assembly shown in Scheme 65. Inset: Expanded imine region.

These conversion issues were later resolved following a thorough optimisation process, as described later in chapter 3, however the lack of baseline resolution seen in these original assemblies was puzzling, as BINOL had in most previous cases resulted in sharp, well-resolved  $^1\text{H}$  NMR imine signals. In order to investigate this complexation reaction further, a simple scalemic screening study was carried out, involving reaction of 2-FPBA **1** and (*R*)-BINOL **9** with Ellman's sulfonamide **129a** of varying enantiopurity, ranging from enantiopure (*R*)-**129a** to (*S*)-**129a** in 20% *ee* increments. This resulted in 11 distinct  $^1\text{H}$  NMR spectra which displayed a relatively small but significant variation in chemical shift and chemical shift difference for the diastereomeric imine resonances from one sample to the next (Figure 24). Importantly, this change in chemical shift as the *ee* of the sulfonamide was varied had not previously been observed for Bull-James assemblies of other types of chiral amine analyte.

When enantiopure samples of either (*S*)- or (*R*)-sulfonamide **129a** were combined with 2-FPBA **1** and enantiopure (*R*)-BINOL **9** in  $\text{CDCl}_3$  at 0.1 M, sulfiniminoboronate complexes with  $^1\text{H}$  NMR imine signals at 9.041 ppm ((*S,S,R*)-**166a** heterochiral, blue, Table 1, entry 1) and 9.048 ppm ((*R,S,R*)-**165a** homochiral, blue, Table 1 Entry 11) were formed, respectively, implying a baseline  $\Delta\delta_{\text{H}}$  chemical shift difference between the two diastereomers of -0.007 ppm. This chemical shift difference value was comparable to the -0.010 ppm  $\Delta\delta_{\text{H}}$  observed between the imine signals in the 50:50 mixture of diastereomeric sulfiniminoboronate complexes produced when a sample of (*rac*)-sulfonamide **129a** was derivatised (Table 1, entry 6). Decreasing the *er* of the (*S*)-**129a** used in the derivatisation

process led to the imine resonance of the heterochiral complex (*S<sub>S</sub>*,*R*)-**166a** shifting incrementally downfield by 0.017 ppm (see Figure 2) from 9.041 ppm for enantiopure (*S*)-**129a** (Table 1, Entry 1) to 9.058 ppm for a 10:90 *er* of (*S*)-**129a**:(*R*)-**129a** (Table 1, Entry 10). This was accompanied by a corresponding incremental upfield shift of -0.026 ppm (see Figure 2) in the chemical shift of the imine proton resonance of the homochiral complex (*R<sub>S</sub>*,*R*)-**165a** from 9.074 ppm for 90:10 *er* (*S*)-**129a**:(*R*)-**129a** (Table 1, Entry 2) to 9.048 ppm for enantiopure (*R*)-**129a** (Table 1, Entry 11). The opposing chemical shift trend of the heterochiral and homochiral complexes as the *er* of (*S*)-**129a** is varied from 100:0 to 10:90 results in their imine peaks coalescing into a single broad resonance at 9.052 ppm when a sample of (*S*)-**129a** of 30:70 *er* is derivatised (Table 1, Entry 8). This *er/dr*-dependent chemical shift variation means that derivatisation of a sample of (*S*)-**129a** of 90:10 *er* produces an imine peak for the minor homochiral complex (*R<sub>S</sub>*,*R*)-**165a** that is downfield of the imine peak of the major heterochiral complex (*S<sub>S</sub>*,*R*)-**166a** (Table 1, Entry 2), with a large chemical shift difference  $\Delta\delta_H = -0.030$  ppm. Conversely, in a sample of (*R*)-**129a** of 90:10 *er* (*i.e.* 10:90 (*S*)-**129a**) the imine peak for the now major homochiral complex (*R<sub>S</sub>*,*R*)-**165a** is upfield of the peak for the minor heterochiral complex (*S<sub>S</sub>*,*R*)-**166a** (Table 1, Entry 10), albeit with a small  $\Delta\delta_H = +0.007$  ppm that results in significantly overlapping peaks. Interestingly, the imine chemical shifts of both SIBE diastereomer complexes present in a diastereomerically impure mixture were more deshielded than when in their pure diastereomeric form. These trends were confirmed by repeating the complexation study using scalemic samples of sulfinamide **129a** combined with the opposite diol atropisomer (*S*)-BINOL **9** (Figure 24b), which showed the same variation in chemical shift of the imine proton resonances of its heterochiral and homochiral complexes as the enantiopurity of the chiral sulfinamide **129a** analyte was varied. As expected, use of (*S*)-BINOL **9** enantiomer as a chiral reporter in this second study led to mirroring of the imine chemical shift differences observed when (*R*)-BINOL **9** was used in the initial derivatisation study (*cf.* Figure 24a and b).

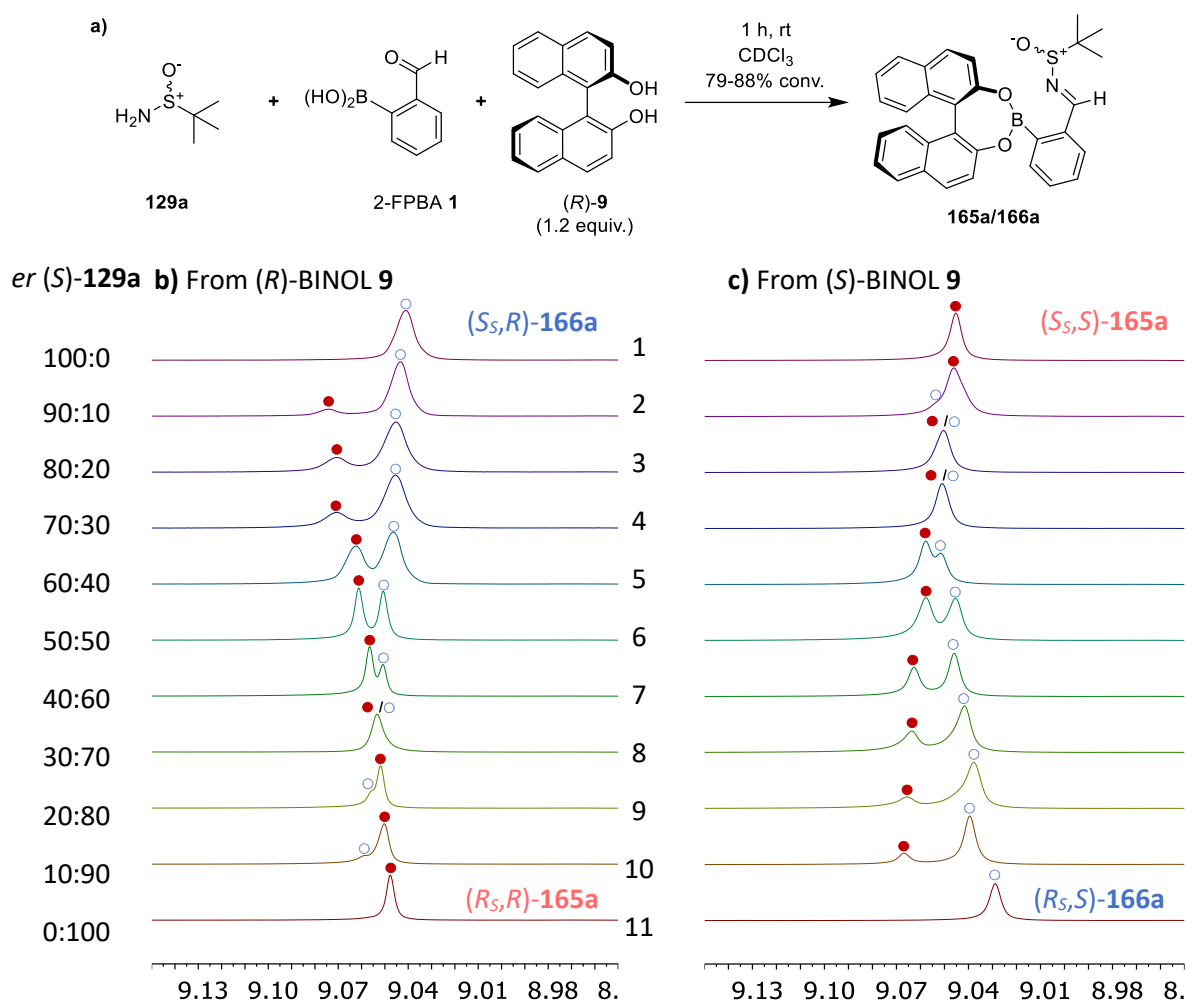


Figure 24: (a) Three-component assembly of 2-FPBA **1**, BINOL **9** and Ellman's sulfonamide **129a** (derivatisation reaction shown for (R)-BINOL **9**). (b,c) Expanded imine region of the <sup>1</sup>H NMR (500 MHz, CDCl<sub>3</sub>, 100 mM) spectra of homochiral and heterochiral sulfiniminoboronate complexes. (b) Complexes prepared using (R)-BINOL **9**; (c) Complexes prepared using (S)-BINOL **9**. Heterochiral diastereomers (*S<sub>s</sub>,R*)-/(*R<sub>s</sub>,S*)-**166a** labelled with hollow blue circles. Homochiral diastereomers (*R<sub>s</sub>,R*)-/(*S<sub>s</sub>,S*)-**165a** labelled with solid red circles. All chemical shifts referenced to TMS as an internal standard (~6 mM).

Table 1: <sup>1</sup>H NMR chemical shifts and chemical shift differences of the imine resonances of the homochiral and heterochiral sulfiniminoboronate ester complexes formed in the complexation reactions of 2FPBA **1**, (S)-BINOL **9**, and sulfinamide **129a** of varying *er* whose expanded NMR spectra are shown in Figure 24a (matched entry numbers).

Entry <sup>a</sup>	(S)- <b>129a</b> <i>er</i>	Chemical shift $\delta_H$ (ppm) <sup>b</sup>		$\Delta\delta_H$ (ppm) <sup>c</sup>
		(S,S)- <b>166a</b>	(R,S)- <b>165a</b>	
1	100:0	9.041	N/A	N/A
2	90:10	9.044	9.074	-0.030
3	80:20	9.045	9.071	-0.026
4	70:30	9.046	9.071	-0.025
5	60:40	9.046	9.063	-0.017
6	50:50	9.051	9.061	-0.010
7	40:60	9.051	9.057	-0.006
8 <sup>d</sup>	30:70	9.053	9.053	--
9	20:80	9.056	9.052	+0.004
10	10:90	9.058	9.051	+0.007
11	0:100	N/A	9.048	N/A

<sup>a</sup> Data extracted by MestReNova from spectra shown in Figure 24a. <sup>b</sup> Chemical shift of the imine proton of the corresponding three-component complex. <sup>c</sup> A negative value for  $\Delta\delta_H$  indicates that the imine proton resonance of the homochiral iminoboronate ester complex was more deshielded. <sup>d</sup> Diastereomeric signals coalesced, therefore chemical shifts are estimated and chemical shift differences could not be measured.

The unexpected nature of these enantiopurity-dependent chemical shift effects led to some concern that these effects might also be operating in previously reported Bull-James assembly reactions used to determine the *ee* of primary amines. Of particular concern was the fully coalesced imine signals present in the <sup>1</sup>H NMR spectra of the complexes formed from assembly of sulfinamide (R)-**129a** of 70:30 *er* with (R)-BINOL (Table 1, entry 8), which, taken in isolation, could potentially be misconstrued to suggest that the parent scalemic sulfinamide analyte was enantiopure! Moreover, the “crossover” in chemical shifts that occurs for the imine resonances of the heterochiral and homochiral sulfiniminoboronate complexes could also potentially lead to incorrect assignments of the absolute configuration of chiral analytes by misguided analogy. Therefore, a scalemic screen of the original Bull-James assembly of  $\alpha$ -methylbenzylamine **3a** (varying *er*), 2-FPBA **1** and BINOL **9** was carried out (Figure 25), which fortunately revealed that no variation in imine <sup>1</sup>H NMR chemical shift was observed upon varying the *er* of the parent amine. In all cases, the imine <sup>1</sup>H NMR signals of both diastereomeric heterochiral and homochiral complexes ( $\alpha$ -R,R)-**28a** and ( $\alpha$ -S,R)-**29a** remained at constant chemical shifts of 8.08 ppm and 8.25 ppm, as the *er* of the  $\alpha$ -methylbenzylamine **3a** was varied. This confirms that prior Bull-James assembly protocols do not suffer from the effects described in this chapter, and remain robust and accurate approaches for determining *ee*.

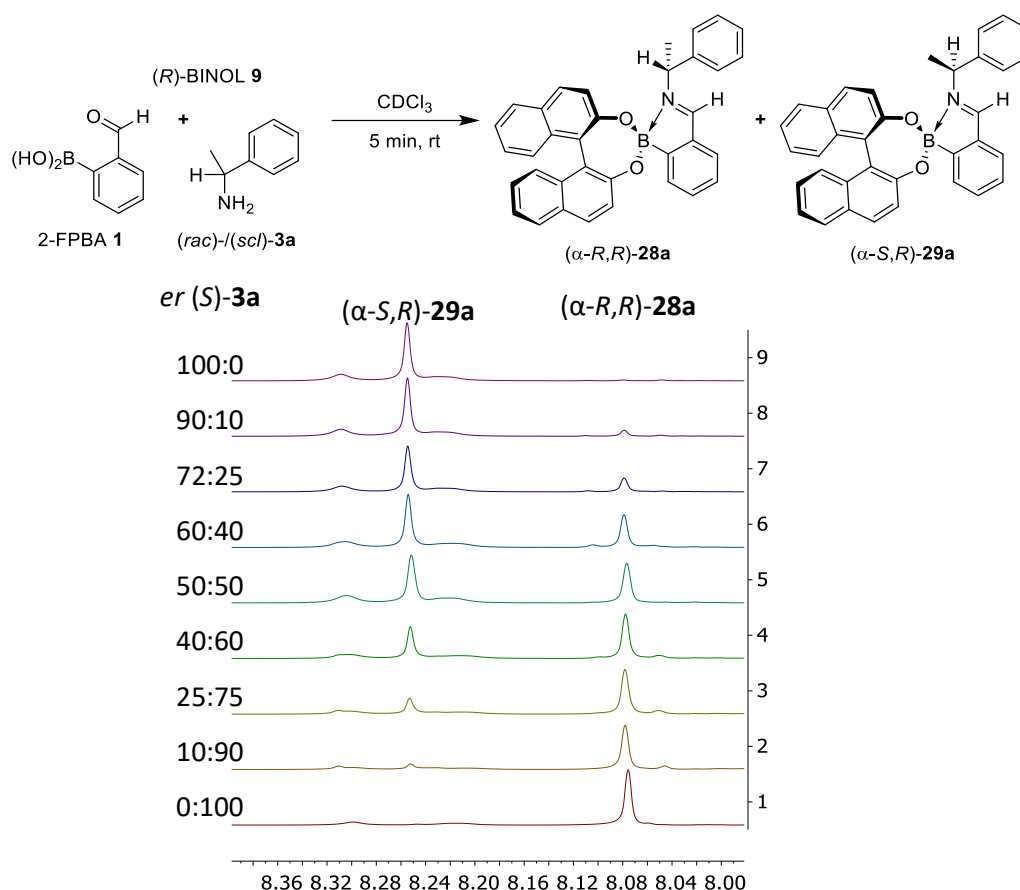


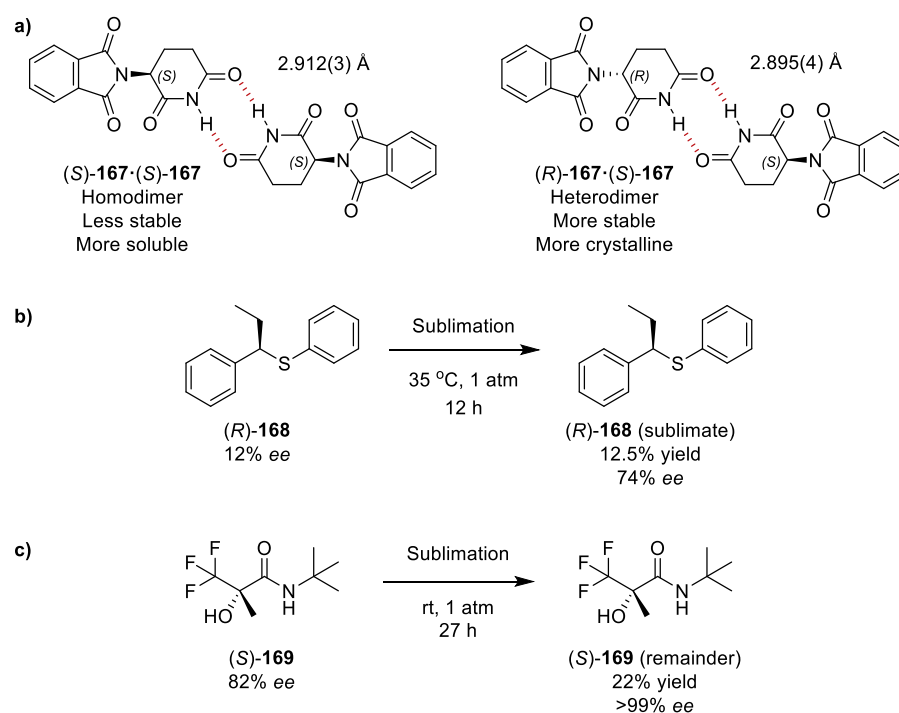
Figure 25: Expanded imine region of the  $^1\text{H}$  NMR (500 MHz,  $\text{CDCl}_3$ , 100 mM) spectra of the iminoboronate esters resulting from the three-component assembly of  $\alpha$ -methylbenzylamine **3a** of differing *er* ((*S*)-**3a** top left, (*R*)-**3a** bottom right), 2-FPBA **1** and (*R*)-BINOL **9**. Chemical shifts referenced to TMS internal standard (~6 mM).

## 2.3. The role of aggregation effects on the NMR spectroscopic analysis of BINOL-derived sulfiniminoboronates

### 2.3.1 *Diastereomer aggregation-induced anisochronism (DAIA)*

These results led us to propose that the unusual variation in chemical shift as the *er* of the sulfonamide analyte changed was being caused by dynamic solution-state equilibration between non-equivalent mixed aggregate states of diastereomeric homochiral and heterochiral sulfiniminoboronate complexes in solution. Although often overlooked, related variation in chemical shift values has been reported for scalemic mixtures of enantiomers in achiral environments, in a process that is commonly referred to as *Self-Disproportionation of Enantiomers* (SDE).<sup>297,298</sup> Simply put, SDE occurs when the enantiomers present in a scalemic sample self-associate to produce enantioenriched fractions/environments/aggregates, as first reported by Cundy and Crooks in 1983,<sup>299</sup> and named by Soloshonok in 2006.<sup>298</sup> In some cases this type of SDE events can be useful, such as when stereoselective aggregation events are exploited for the fractional crystallization of scalemic mixtures to produce enantiomerically-enriched crystalline products, underpinning Wallach's rule for instance.<sup>300–302</sup> For example, the crystal structures of

hetero-dimeric crystals of thalidomide **167** are denser and more stable than their corresponding heterodimeric crystals, which results in heterodimeric thalidomide crystals preferentially crystallising from solution. This means that the selective precipitation and solubility of heterochiral dimers over time can result in the enantiopurity of scalemic thalidomide in solution increasing over time, including *in vivo* (Scheme 66a).<sup>303</sup> SDE effects have also been found to facilitate *ee* enhancement in sublimation processes,<sup>304,305</sup> including an impressive early 1967 report of the enantioenrichment of (*R*)-**168** from 12% *ee* to 74% *ee* in the sublimate (Scheme 66b),<sup>306,307</sup> and more recent works by Soloshonok *et al.* studying relative rates of enantioenrichment by SDE sublimation,<sup>305,308</sup> such as the *ee*-dependent purification behaviour of hydroxyamide **169** (Scheme 66c).<sup>305</sup> These effects have also been shown to impact the behaviour and properties of a wide range of aggregating chiral compounds, influencing aspects of ultracentrifugation, sublimation, melting, and distillation processes to facilitate purification and analytical processes, or contribute towards inconsistent results.<sup>297,298,309</sup>



Scheme 66: Examples of SDE effects: (a) Inequivalent crystal packing of thalidomide **167** diastereomers.<sup>303</sup> (b) Enantioenrichment of (*R*)-**168** by sublimation.<sup>307</sup> (c) Enantiopurification of α-hydroxyamide (*S*)-**169** by sublimation.<sup>305</sup>

The effects of SDE have also been observed directly in preparative chromatography and HPLC, as well as solution- and solid-state NMR, where they are referred to as *enantioselective self-disproportionation on achiral phase* (ESDA) and *self-induced diastereomeric anisochronism* (SIDA), respectively.<sup>297,300,310</sup> As with the sublimation examples described above, SDE-derived *self-induced recognition of enantiomers* (SIRE) phenomena that give rise to ESDA and SIDA can be exploited for analytical NMR purposes, as recently reviewed by Soloshonok *et al.*<sup>311</sup> and Szántay *et al.*, respectively.<sup>312</sup> In a scalemic system, an enantiomer can exist either as a simple monomer, can self-associate to afford a homochiral dimer (or aggregate), or it can associate with its mirror enantiomer

to afford a heterochiral dimer (or aggregate). Since these association events are often highly concentration- and enantiopurity-dependent, the NMR spectra of non-enantiopure mixtures with different *ee*'s can sometimes appear different, with different enantiomers even exhibiting distinct spectra in scalemic samples in some cases. These effects have been extensively reviewed and explored,<sup>312</sup> with several recent works by Klika describing SIDA NMR effects for a range of chiral compounds.<sup>308,310,313</sup> These effects can potentially be a significant source of error and unreliability, leading either to inaccurate enantiopurity assessment, or unsuccessful chromatographic purification.<sup>24,310,314,315</sup> Selected examples of the consequences of these effects are shown in Figure 26. Trifluoromethylated amidoester (*R*)-**170** exhibits significant ESDA effects, with chromatographic purification of a scalemic sample of 66.6% *ee* using simple flash chromatography over unmodified silica, resulting in early fractions eluting with a significantly reduced 8.1% *ee*, with the enantiopurity of subsequent fractions gradually increasing to produce enantiopure (*R*)-**170** in the final eluted fraction (Figure 26a). Examples of SIDA NMR effects are shown in Figure 26b and Figure 26c, with the first example revealing distinct <sup>13</sup>C NMR signals for the minor and major isomers of non-enantiopure (*R*)-**171** that coalesce to a single peak in the racemate, and the second example showing distinctly different spectra and chemical shifts in the <sup>1</sup>H NMR spectra of samples of **172** of varying *ee*.

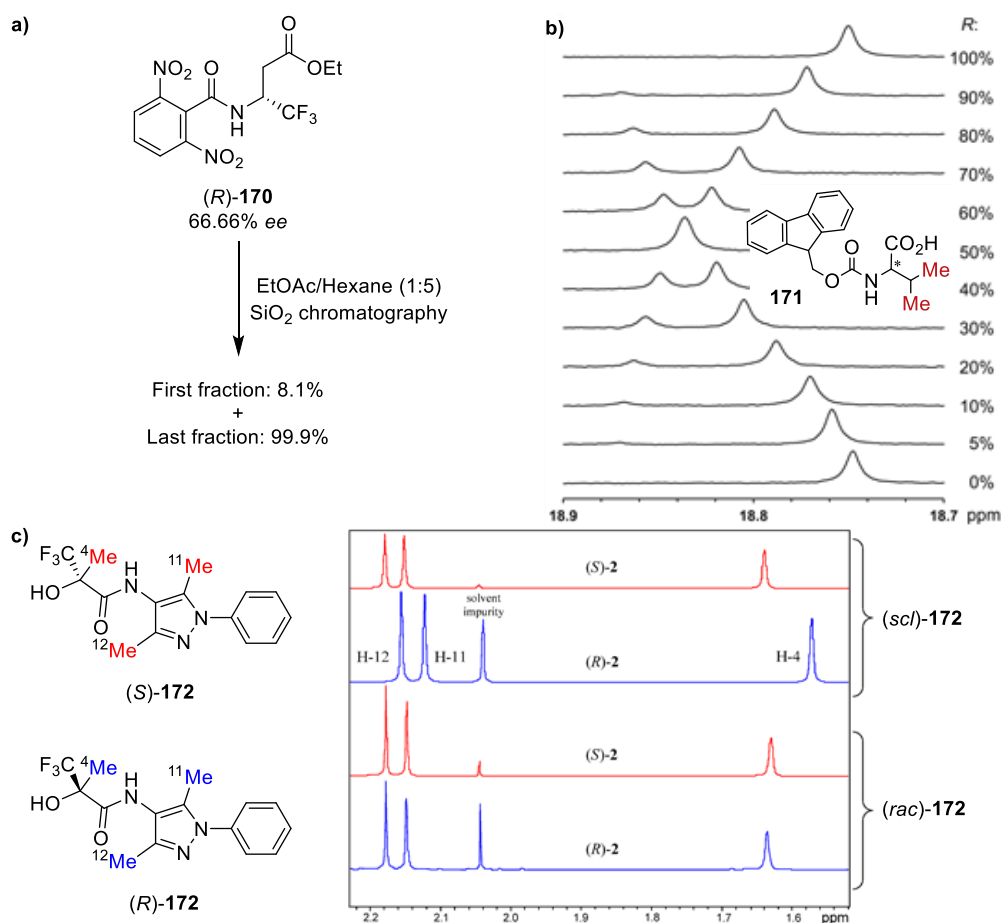
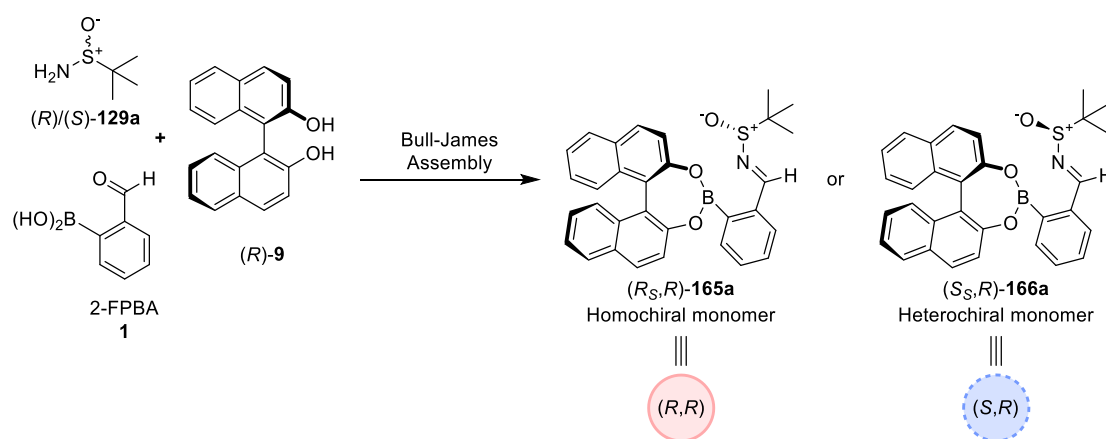


Figure 26: (a) ESDA-enabled enantiopurification of (*R*)-**170** by achiral chromatography.<sup>298</sup> (b) SIDA effects in the <sup>13</sup>C{<sup>1</sup>H} NMR (201 MHz, 10 °C, CDCl<sub>3</sub>, 200 mM) spectra of (*R*)-**171** at varying *ee*.<sup>312</sup> Reproduced with permission from Elsevier Ltd.

(c) SIDA effects in the  $^1\text{H}$  NMR spectra of **172**, showing spectra of arbitrary *ee* (top 2) and enantiopure (bottom two) samples.<sup>313</sup> Reproduced with permission from MDPI.

This work therefore proposes that the chemical shift drift observed in the  $^1\text{H}$  NMR spectra of the diastereomeric homochiral and heterochiral BINOL sulfiniminoboronate complexes in this study are also caused by SIDA-like aggregation effects, however this terminology has previously been reserved to describe NMR chemical shift variations caused by SIRE effects between enantiomers in achiral systems. As no reports of SIDA-type effects influencing the chemical shifts of diastereomeric complexes in solution could be found, this work now proposes a new term *Diastereomer Aggregation Induced Anisochronism* (DAIA) to describe this class of SIDA-like effect. At this stage it should be noted that the term “aggregation” used throughout this thesis refers to any assembly of molecules resulting from the aggregation of two or more “monomers”. This includes all aggregated states from simple dimers/trimers to larger aggregated species no longer in solution (e.g. small particles or droplets in suspension), as the exact nature of these supramolecular systems has not yet been determined. As it is clear that these DAIA phenomena have a pronounced effect on the shift and shape of the SIBE imine resonances of the diastereomeric homochiral and heterochiral SIBEs, this chapter will now consider the principles underpinning DAIA effects using the three-component Bull-James assembly as an exemplar. Three-component assembly of enantiopure (*R*)-BINOL **9**, 2-FPBA **1** and Ellman’s sulfinamide **129a** (varying *er*) will produce varying amounts of homochiral (*R<sub>S</sub>,R*)-**165** and heterochiral (*S<sub>S</sub>,R*)-**166**. These two diastereomeric complexes represent the monomeric species in the DAIA system, and are assigned as either a homochiral (*R<sub>S</sub>,R*)-monomer (red, solid edges) or heterochiral (*S<sub>R</sub>,R*)-monomer (blue, dashed edges) (Scheme 67). For simplicity, only this one pair of diastereomers, derived from (*R*)-BINOL **9**. Assemblies of the opposite enantiomeric system (from (*S*)-BINOL **9**) would exhibit the same properties and aggregation effects.



Scheme 67: Schematic abbreviation of diastereomeric sulfiniminoboronates present in the three-component assembly of (*R*)-BINOL **9**, 2-FPBA **1** and Ellman’s sulfinamide **129a**.

When enantiopure samples of sulfinamide (*R*)-**129a** (or (*S*)-**129a**) are used in the derivatisation process with 2-FPBA **1** and (*R*)-BINOL **9**, then monomeric (*R<sub>S</sub>,R*)-**165a** (or (*S<sub>S</sub>,R*)-**166a**) is formed that can reversibly aggregate to produce mixtures containing homomeric dimers, trimers and higher-order aggregates in solution (Figure 27). Rapid equilibration between these monomeric and



oligomeric complexes leads to partial broadening of the imine signals whose chemical shifts are determined by time-averaged contributions from all the monomer and aggregate forms that are present.

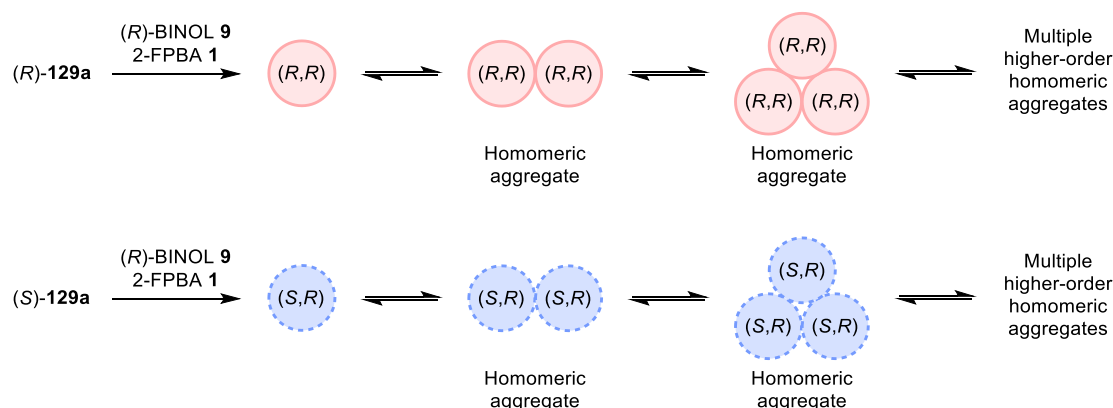


Figure 27: Reversible homomeric aggregation of enantiopure  $(R,S,R)$ -**165a** and  $(S,S,R)$ -**166a** complexes.

Conversely, when a scalemic sample of the sulfonamide is used as an analyte, then a mixture of diastereomeric sulfiniminoboronate esters  $(R,S,R)$ -**165a** and  $(S,S,R)$ -**166a** will be produced, with these monomeric species now aggregating to form either homomeric aggregates or mixed heteromeric aggregates that contain both types of monomer (Figure 28). The ratio of the different homomeric and heteromeric aggregates formed will be dependent on the *er* of the parent sulfonamide analyte that is derivatised. Use of a sulfonamide with a high *er* will favour formation of large amounts of homomeric aggregate (derived from the major enantiomer), with only small amounts of heteromeric aggregates formed that contain the majority of the minor sulfiniminoboronate diastereomer. Conversely, derivatisation of a racemic sulfonamide (or a sulfonamide with low *er*) will increase the amount heteromeric aggregate present in solution. The chemical shifts of the imine protons of the homochiral and heterochiral complexes formed from a scalemic sample will be determined by time-averaged contributions of all the rapidly interconverting monomeric and aggregate forms that are present, each of which will contribute its own distinct anisotropic shielding/deshielding effects. Therefore, diastereopurity-dependent variation in the ratio of monomeric species to homomeric/heteromeric aggregates in solution can result in significant changes in the chemical shifts of the imine protons of the homochiral and heterochiral complexes that are present. Examination of the  $^1\text{H}$  NMR data shown in Figure 24 indicates that the imine protons in a heterochiral aggregate (*e.g.* at high *dr*) are more deshielded than when they are part of a homochiral aggregate (*e.g.* at low *dr*). Some consideration was also given to possible variation in the rates of formation of each SIBE, which could lead to kinetic resolution effects, which could also affect chemical shifts and peak shape. This possibility was dismissed, however, as the *dr*'s measured throughout this and the next chapter remained consistent with the initial *er* of the analyte. Further discussion of kinetic resolution in SIBEs, as well as evidence showing it does not appreciably occur can be found later in chapter 3. Additionally, the rate/extent of aggregation was also considered, as it is conceivable that extended reaction times, delays prior to analysis, or longer

NMR experiments could lead to further equilibration or aggregation. Fortunately, no variation was seen between spectra of the same samples recorded at different times.

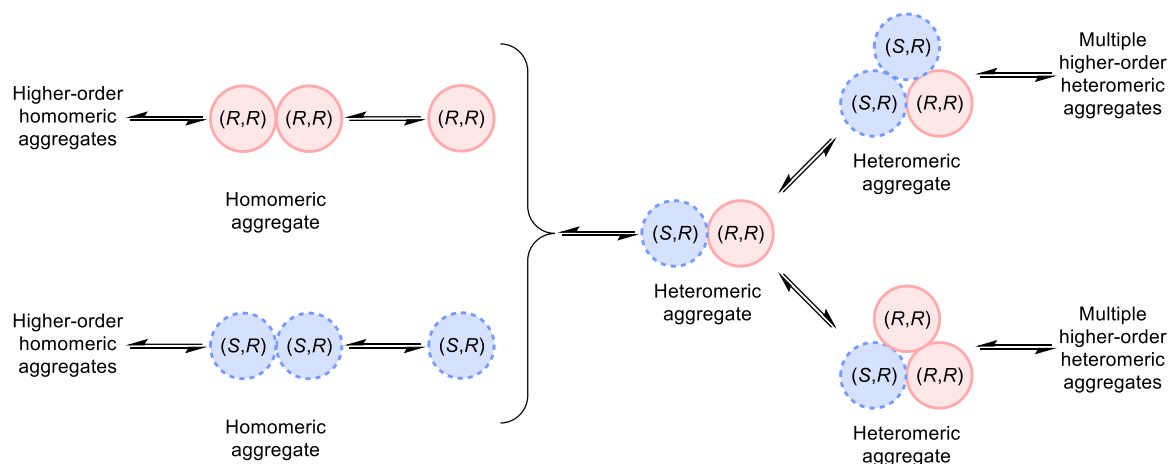


Figure 28: Reversible homomeric and heteromeric aggregation of scalemic  $(R,S,R)$ -165a and  $(S,S,R)$ -166a monomers.

### 2.3.2 Prior reports of concentration-dependent chemical shift variations

The presence of DAIA effects in these sulfinimine-BINOL boronate ester system is consistent with previous observations of SIDA effects in the literature, with SIDA-like behaviour previously reported for other BINOL and large conjugated  $\pi$ -systems.<sup>310,314,316</sup> Aggregation-induced effects have also been implicated once before other iminoboronate assemblies, with Silva *et al.* reporting that the chemical shift differences and variable peak shapes of diastereomeric BINOL-derived selenoiminoboronate complexes derived from *(rac)*-89b were improved on dilution enabling baseline resolution of diastereomeric  $\alpha$ -amino methyl signals in their  $^1\text{H}$  NMR spectra at 1.0 mM (Figure 29a, see resonances in blue).<sup>166</sup> In this instance, however, Silva *et al.* dismissed these minor aggregation effects as being caused by the presence of the chalcogen moiety, having previously seen similar effects in other chalcogen-based NMR assemblies, however the results presented in this chapter suggest that this may in fact have been an early sign of BINOL-IBE DAIA.

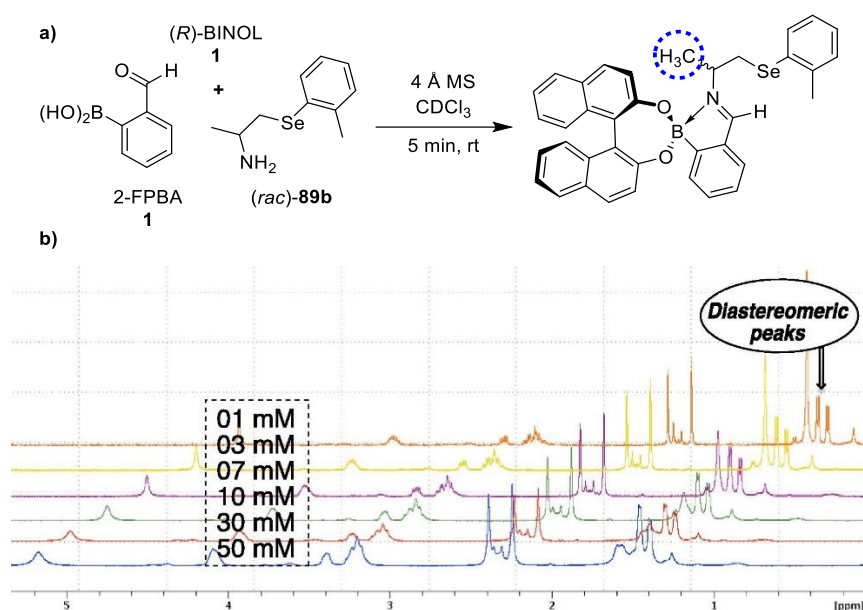


Figure 29: (a) Three-component assembly of 2-FPBA **1**, (*R*)-BINOL **9** and selenium containing amine (*rac*)-**89b**. (b) Expanded  $^1\text{H}$  NMR (500 MHz,  $\text{CDCl}_3$ ) spectra of the assembly three-component assembly shown in (a) at varying concentrations, with 'diastereomeric peaks' corresponding to the  $\alpha$ -amino methyl signals shown in blue dashed circle. Reproduced with permission from Elsevier Ltd.<sup>166</sup>

Although large concentration-dependent chemical shift drifts are often observed for resonances attributed to H-bonding protons, caused by increased/decreased rates of proton exchange and acid/base equilibria, these effects are less frequently observed for non-exchangeable protons.<sup>317–319</sup> To the best of our knowledge, only a handful of publications have previously reported these effects for aromatic/conjugated protons, with these reports describing concentration-dependent chemical shift variation of aromatic signals in pure samples (examples in Figure 30).<sup>320–325</sup>

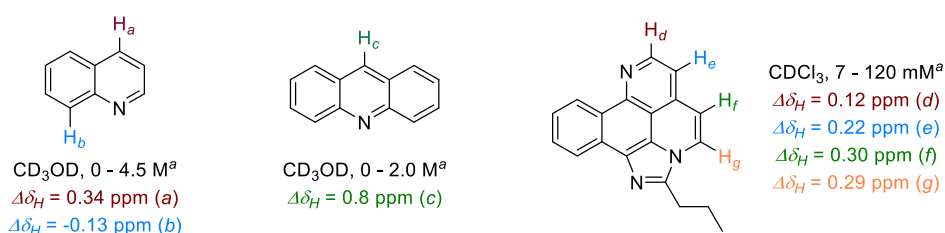


Figure 30: Selected examples of concentration-dependent  $^1\text{H}$  NMR chemical shift drift of non-exchangeable protons. A negative sign indicates a downfield shift at lower concentrations. <sup>a</sup> Estimated from figures, data not tabulated in original report.<sup>321,323</sup>

### 2.3.3 Concentration-dependent chemical shift variation of SIBEs

In order to provide further evidence for the DAIA hypothesis, the aggregation behaviour of BINOL sulfiniminoboronate complexes was further studied, by examining whether changes in concentration would significantly affect the chemical shifts of their imine protons.<sup>317,323,324,326</sup>  $^1\text{H}$  NMR spectroscopic analysis of samples of diastereopure (*R*<sub>s</sub>,*R*)-**165a** and (*S*<sub>s</sub>,*R*)-**166a** at different concentrations was carried out, which revealed a significant upfield shift in the chemical shift of their imine protons as their concentrations decreased (Figure 31, 31, Table 2). The chemical shift of

the imine proton of the heterochiral diastereomer (*S<sub>s</sub>,R*)-**166a** at a concentration of 100 mM appeared at 9.041 ppm, shifting incrementally on dilution, moving 0.345 ppm upfield to 8.696 ppm at a 100-fold lower 1.0 mM concentration of (*S<sub>s</sub>,R*)-**166a** (Figure 31b). Similarly, the imine signal of (*R<sub>s</sub>,R*)-**165a** at a concentration of 100 mM appeared at 9.041 ppm, moving 0.361 ppm upfield to 8.687 for a 1.0 mM concentration (Figure 31c). Variation in the chemical shift of the imine protons of the two diastereomeric complexes on dilution was found to be non-linear, leading to smaller changes in the chemical shift differences of their imine protons as more dilute solutions were analysed. This meant that a maximum base  $|\Delta\delta_H|$  value of 0.022 ppm for their imine protons was observed at a 50 mM concentration, whilst identical chemical shifts were observed at a lower 2.5 mM concentration. Interestingly, a crossover event was observed at the lowest 1.0 mM concentration, with a small  $\Delta\delta_H = +0.009$  ppm occurring, with the imine proton of the (*R<sub>s</sub>,R*)-**165a** diastereomer now resonating slightly upfield relative to the imine proton of its (*S<sub>s</sub>,R*)-**166a** counterpart. These large concentration-dependent variations in chemical shift indicate that both diastereomeric sulfiniminoboronate ester complexes aggregate significantly at high concentrations, with intermolecular anisotropic shielding effects within these aggregates responsible for their imine protons being more deshielded at higher concentrations. Changing sample concentration also leads to variation in the concentration of TMS and water, and so control experiments were carried out to ensure these incidental changes were not responsible for the results presented in this chapter. In all cases little to no change in the NMR spectra was observed, however for consistency and reproducibility TMS concentration is listed throughout this report whenever possible.

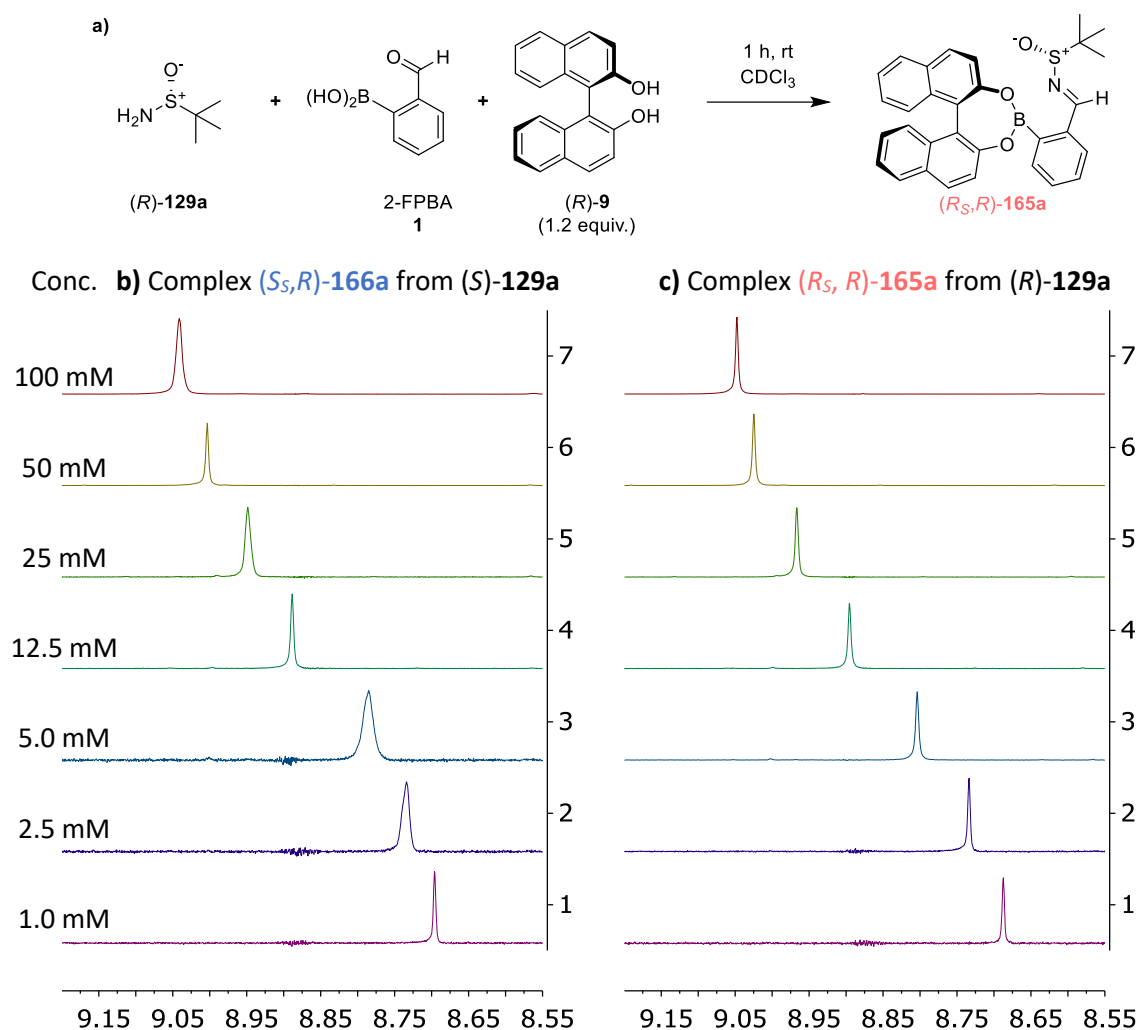


Figure 31: (a) Three-component assembly of 2-FPBA **1**, BINOL **9** and sulfinate **129a** (reaction shown for  $(R)$ -BINOL **9**). (b) Expanded imine region of the  $^1\text{H}$  NMR (500 MHz,  $\text{CDCl}_3$ ) spectra of heterochiral sulfiniminoboronate complex  $(S_S,R)\text{-}166a$  acquired at different concentrations. (c) Expanded imine region of the  $^1\text{H}$  NMR (500 MHz,  $\text{CDCl}_3$ ) spectra of homochiral complex sulfiniminoboronate  $(R_S,R)\text{-}165a$  acquired at different concentrations. Chemical shifts referenced to TMS internal standard ( $\sim 6$  mM in original 100 mM stock solution).

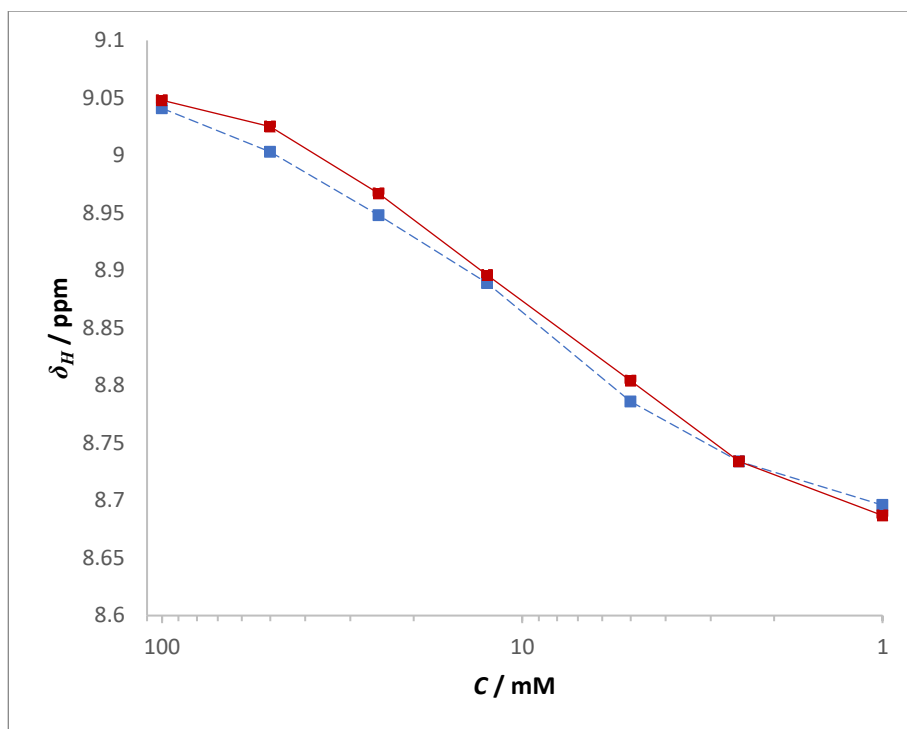


Figure 32: Plot of chemical shifts of imine protons versus concentration (log scale) of  $(R,S,R)$ -**165a** (red, solid line) and  $(S,S,R)$ -**166a** (blue, dashed line) (chemical shift data from Figure 31).

Table 2: Chemical shifts and “base  $\Delta\delta_H$ ” of the sulfiniminoboronate  $^1\text{H}$  NMR signals of Figure 31.

Entry <sup>a</sup>	Concentration	Chemical shift $\delta_H$ (ppm) <sup>b</sup>		Base $\Delta\delta_H^c$ (ppm)
		$(S,S,R)$ - <b>166a</b>	$(R,S,R)$ - <b>165a</b>	
1	100 mM	9.041	9.048	-0.007
2	50 mM	9.003	9.025	-0.022
3	25 mM	8.948	8.967	-0.019
4	12.5 mM	8.889	8.896	-0.007
5	5.0 mM	8.786	8.804	-0.018
6	2.5 mM	8.734	8.734	0.000
7	1.0 mM	8.696	8.687	+0.009

<sup>a</sup> Data extracted by MestReNova from spectra shown in Figure 31. <sup>b</sup> Chemical shift of the imine proton of the heterochiral and homochiral complexes. <sup>c</sup> A negative value for  $\Delta\delta_H$  indicates that the imine proton resonance of the homochiral iminoboronate ester complex was more deshielded.

The same dilution experiments were then carried out on a 50:50 mixture of  $(R,S,R)$ -**165a** and  $(S,S,R)$ -**166a** produced from the derivatisation of a racemic sample of Ellman’s sulfinamide **129a** with 2-FPBA **1** and  $(R)$ -BINOL **9** (Figure 33). The same general trend was again observed, with the imine signals of  $(R,S,R)$ -**165a** and  $(S,S,R)$ -**166a** shifting from 9.061 ppm and 9.051 ppm at 100 mM, respectively, to 8.693 ppm at 1.0 mM, or a 0.368 ppm and 0.358 ppm change, respectively. Interestingly, the partially overlapped peaks for the imine resonances of both the diastereomers were only distinguishable at concentrations of 100 mM and 50 mM, with both imines coalescing

into a single resonance at a concentration of 25 mM and below. One key observation can be made from these data: a chemical shift difference between the diastereomeric imine resonances only arises at higher concentration, becoming either negligible or vanishing entirely at lower concentrations. This suggests that the increased proportion of aggregate species at higher concentrations are almost entirely responsible for the observed chemical shift differences, whilst the monomeric forms which dominates at low concentrations exhibit indistinguishable  $\Delta\delta_H$  values for their imine resonances. Therefore, it can be deduced that the chemical shift differences are caused primarily by intermolecular shielding/deshielding interactions between molecules present within organised aggregates rather than classical intramolecular anisotropic shielding/deshielding effects. This highlights a sharp contrast between sulfiniminoboronate esters and other IBEs, which do not suffer from DAIA (see Figure 25).

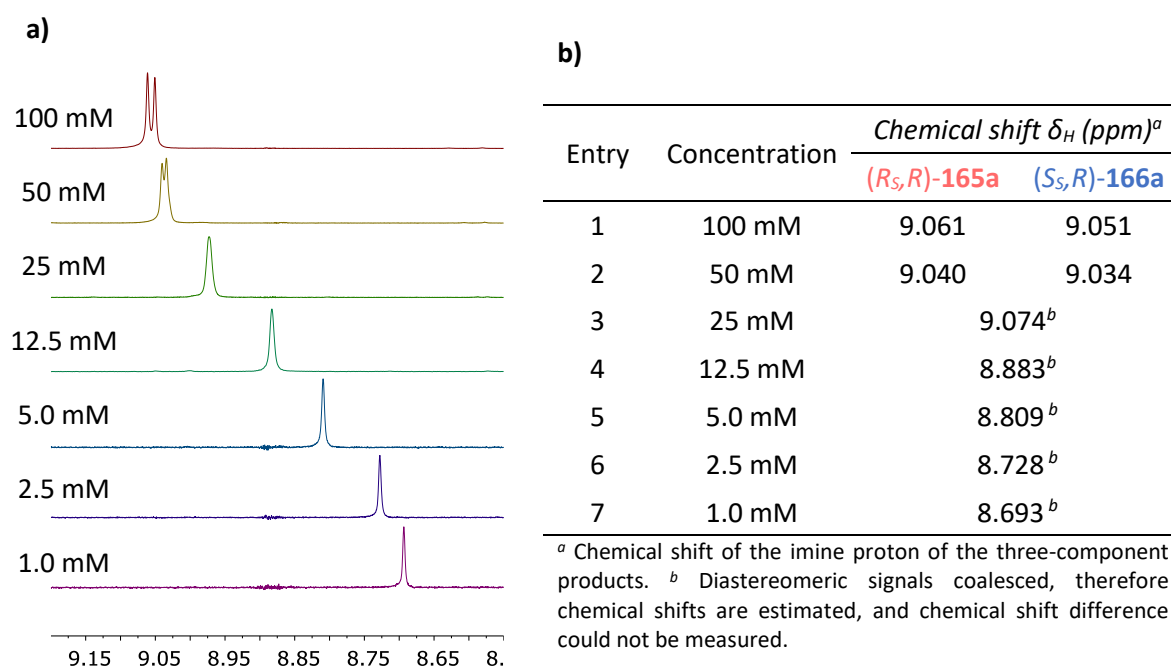


Figure 33: (a) Expanded imine region of the  $^1\text{H}$  NMR (500 MHz,  $\text{CDCl}_3$ ) spectra of three-component assemblies of 2-FPBA **1**, (*R*)-BINOL **9**, and (*rac*)-Ellman's sulfinamide **129a**, with samples diluted from 100 mM to 1.0 mM (top to bottom); chemical shifts referenced to TMS internal standard ( $\sim 6$  mM in original 10\0 mM stock solution). (b) Chemical shifts of the sulfiniminoboronate  $^1\text{H}$  NMR imine signals.

The observations in this chapter and the literature reports above raise potentially quite significant concerns about NMR spectroscopic protocols used to determine the *ee* and assign the configuration of chiral compounds, particularly those that contain functional groups that have the propensity to aggregated in solution. As already highlighted in the scalemic and concentration screening experiments, these DAIA effects could potentially lead to incorrect enantiomeric purity determination or incorrect assignments of absolute configurations. For example, looking at Figure 33a above, different conclusions would be drawn if the same three-component analysis of (*rac*)-sulfinamide **129a** were carried out at a concentration of 100 mM or < 50 mM. In the first case, two peaks of equal intensity for (*R,S,R*)-**165a** and (*S,S,R*)-**166a** are observed at 9.061 ppm and 9.051 ppm, respectively, as expected for derivatization of a racemic sample. On the other hand, at a concentration below 25 mM, only one imine signal is observed, which would lead to the incorrect

conclusion that only one diastereomeric complex was present, and that an enantiopure analyte had been used! Additionally, the absence of chemical shift difference at lower concentrations could have led to an entirely different research outcome, as had these experiments initially been carried out at lower concentrations, preliminary results would have indicated a complete lack of diastereomeric resolution, leading to the premature termination of the successful project detailed in this and the following chapter. This simple yet striking example highlights the significant risk of experimental error posed by DAIA-induced chemical shift variation.

Therefore, considering this example, and drawing on previous precedent for other SIDA-affected systems, the author now suggests that a simple set of dilution experiments should be carried out whenever NMR spectroscopy is used to determine the enantiopurity of new chiral compound is determined, which should easily identify any risk of DAIA-related misassignment occurring. Furthermore, considering the large  $> 0.35$  ppm concentration-dependent variation in chemical shifts observed in Figure 31-31, the author now recommends that the concentrations of NMR solutions of chiral compounds whose *ee*'s or configuration have been determined using CDA methods should be reported, as is currently the case when *ee* determination is carried out using other spectroscopic characterisation methods (*e.g.*, fluorescence, UV-VIS CD, polarimetry, *etc.*). Moreover, considering that in diastereopure samples each SIBE diastereomer is in essence just a stereopure compound, this chemical shift variation would also indicate that this precaution should be extended to all NMR spectroscopic data for any chiral compound, regardless of enantiopurity measurements, in order to avoid any potential structural misassignments between pure samples of different concentrations. For this reason, the concentration of all NMR samples throughout these first three chapters are listed where possible.

#### 2.3.4 DOSY NMR studies of BINOL-sulfiniminoboronate aggregation

In order to support the theory that that these concentration-dependent chemical shift effects were indeed due to aggregation-based changes,  $^1\text{H}$  NMR diffusion-ordered spectroscopy (DOSY) was used to calculate the diffusion coefficients (*D*) of (*R<sub>S</sub>,R*)-**165a** and (*S<sub>S</sub>,R*)-**166a** (see spectra in Figure 31). These DOSY experiments were based on a similar method to that employed previously by Klika *et al.* to show preferential heterochiral SIDA aggregation of enantiomers.<sup>313</sup> As shown in Figure 34 and Table 3, a diffusion coefficient of  $7.75 \times 10^{-10} \text{ m}^2/\text{s}$  was calculated for the highest 100 mM concentration of heterochiral (*S<sub>S</sub>,R*)-**166a**, increasing progressively to  $11.5 \times 10^{-10} \text{ m}^2/\text{s}$  as the concentration was decreased to 1.0 mM. A comparable change in diffusion constant was also observed on dilution of (*R<sub>S</sub>,R*)-**165a**, increasing progressively from  $7.89 \times 10^{-10} \text{ m}^2/\text{s}$  at 100 mM to  $11.2 \times 10^{-10} \text{ m}^2/\text{s}$  at 1.0 mM. These measurements are consistent with larger aggregated species being present at higher concentrations (slower diffusion), and smaller aggregated species being present at lower concentrations (faster diffusion). These data are also consistent with the premise that reversible aggregation events are responsible for the observed chemical shift variations of the imine proton resonances of both diastereomers. The *D* values of (*R<sub>S</sub>,R*)-**165a** were used to predict



the hydrodynamic radius ( $R_{hyd}$ ) and molecular weight ( $MW$ ) of the species present in solution.<sup>327,328</sup> These calculations confirmed a gradual decrease in predicted  $R_{hyd}$  from 7.56 Å at 100 mM to 5.94 Å at 1.0 mM, which corresponds to an approximate change in  $MW$  from 682.32 g/mol at 100 mM to 331.50 g/mol at 1.0 mM. Although the predicted  $MW$  of 331.50 g/mol for ( $R_S,R$ )-**165a** at a 1.0 mM concentration is clearly incorrect (*cf.* actual SIBE  $MW$  = 504.43 g/mol), this error in magnitude is to be expected, especially with ‘poorly-behaved’ aggregating compounds. This is because the model set used to develop the method employed for these calculations explicitly excluded compounds known to aggregate.<sup>327,328</sup> However, the relative change in the magnitudes of the measured hydrodynamic radii at different concentrations clearly indicate that a significant change in average aggregate size occurs as the sample is diluted. The calculated 20% decrease in hydrodynamic radius from 100 mM to 1.0 mM may not seem significant as a standalone figure, but as this implies an approximately 50% decrease in average aggregate volume, it is evident that BINOL-SIBEs aggregate at higher concentrations.

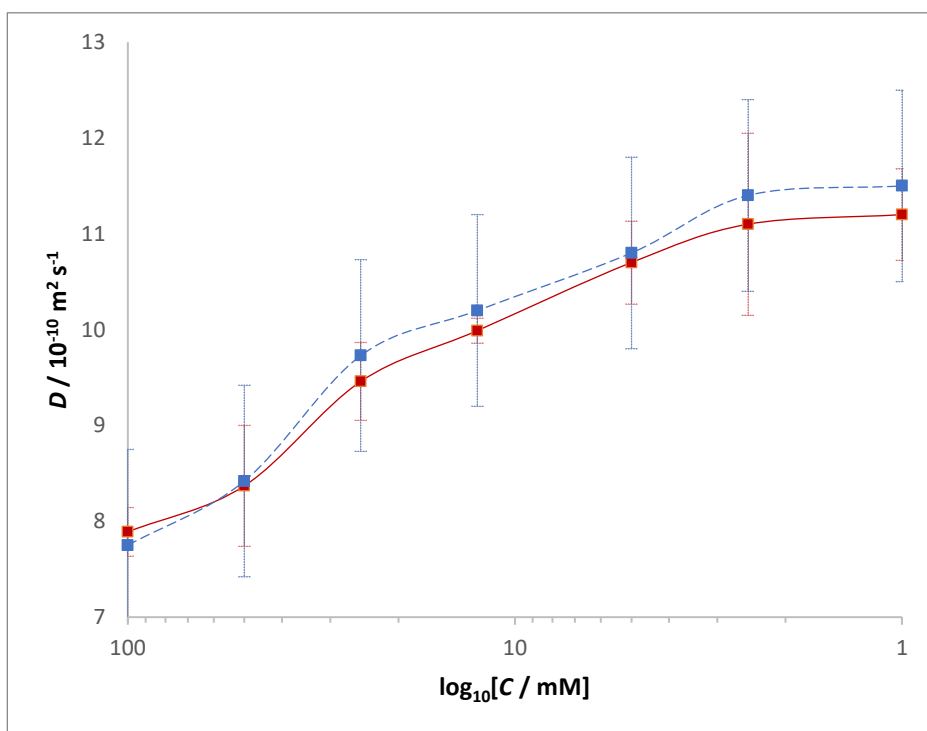


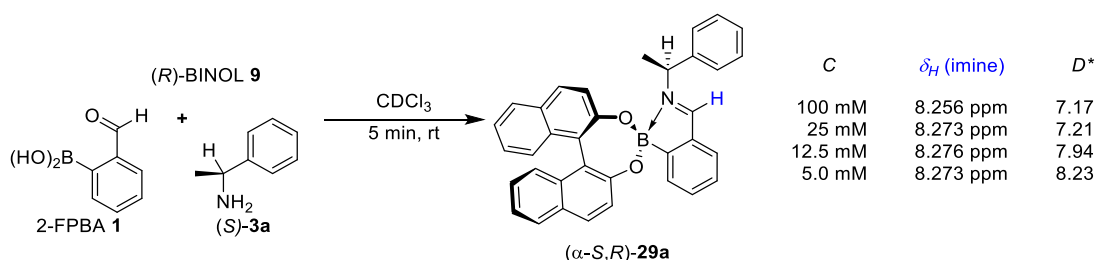
Figure 34: Plot of diffusion coefficient  $D$  versus concentration (log scale) of diastereopure sulfiniminoboronate derived from 2-FPBA **1**, ( $R$ )-BINOL **9**, and either ( $S$ )-**129a** (blue, dashed line) or ( $R$ )-**129a** (red, solid line) (500 MHz, 25 °C,  $\text{CDCl}_3$ , calculated using Bruker Dynamics Center software). Error bars represent 95% confidence interval.

Table 3: Diffusion coefficients and calculated predicted hydrodynamic radii and molecular weights for (*S<sub>S</sub>*,*R*)-**166a** and (*R<sub>S</sub>*,*R*)-**165a** derived from DOSY <sup>1</sup>H NMR at different concentrations.

Entry	Concentration (C)	Diffusion coefficient ( <i>D</i> / 10 <sup>-10</sup> m <sup>2</sup> /s) <sup>a</sup>		Predicted <i>R<sub>hyd</sub></i> ( <i>R<sub>S</sub></i> , <i>R</i> )- <b>165a</b> (Å) <sup>b</sup>	Predicted MW ( <i>R<sub>S</sub></i> , <i>R</i> )- <b>165a</b> (g/mol) <sup>b</sup>
		( <i>S<sub>S</sub></i> , <i>R</i> )- <b>166a</b>	( <i>R<sub>S</sub></i> , <i>R</i> )- <b>165a</b>		
1	100 mM	7.75	7.89	7.56	682.32
2	50 mM	8.42	8.37	7.24	602.27
3	25 mM	9.73	9.46	6.66	466.90
4	12.5 mM	10.2	9.99	6.42	417.58
5	5.0 mM	10.8	10.7	6.12	363.33
6	2.5 mM	11.4	11.1	5.98	337.51
7	1.0 mM	11.5	11.2	5.94	331.50

<sup>a</sup> Data extracted by MestReNova and Bruker Dynamics Center. <sup>b</sup> Calculated using Manchester NMR Methodology Group's SEGWE calculator.

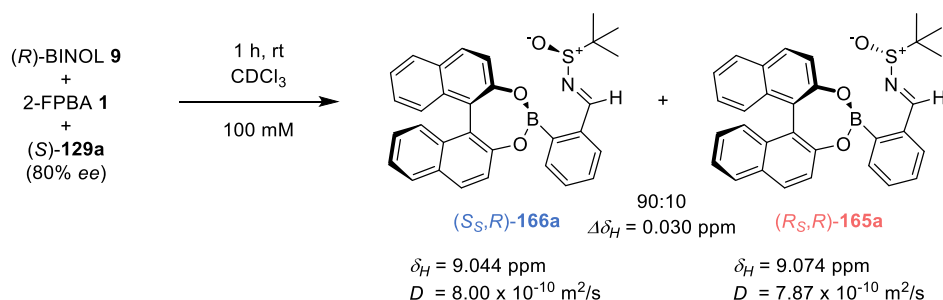
Having confirmed the aggregation behaviour of BINOL-derived sulfiniminoboronates, it was important to confirm that diastereomeric iminoboronate ester complexes produced from complexation of standard chiral amines with BINOL (that do not display enantiopurity-dependent DAIA effects, *vide supra*) were not aggregating in solution (Figure 25). Derivatisation of (*S*)-α-methylbenzylamine **3a** with (*R*)-BINOL **9** gave iminoboronate ester (α-*S*,*R*)-**29a** (Scheme 68), whose <sup>1</sup>H/DOSY NMR spectra were then acquired at different concentrations from 100 mM to 5.0 mM. These spectra revealed only a slight variation in the chemical shift of the imine proton resonance of (α-*S*,*R*)-**29a** as it was diluted, with only a slight increase in diffusion coefficient *D* upon dilution, from 7.17 × 10<sup>-10</sup> m<sup>2</sup>/s at 100 mM to 8.23 × 10<sup>-10</sup> m<sup>2</sup>/s at 5 mM. This small change in *D* is likely due to decreased viscosity upon dilution,<sup>329</sup> indicating that no significant concentration-dependent aggregation of 'conventional' amine-derived IBEs occurs, which is consistent with a lack of DAIA in the NMR spectra of their scalemic samples (Figure 25).



Scheme 68: Three-component assembly of α-methylbenzylamine (*S*)-**3a**, 2-FPBA **1** and (*R*)-BINOL **9**. Chemical shifts referenced to TMS internal standard (~6 mM in 100 mM stock solution). \* 10<sup>-10</sup> m<sup>2</sup>/s; data extracted by MestReNova and Bruker Dynamics Center, and calculated from an average of the imine, methine, and methyl signals.

A final set of DOSY NMR experiments was then carried out to investigate the diffusion coefficients of homomeric and heteromeric sulfiniminoboronate aggregates in samples from scalemic sulfonamide. Similarly to experiments described by Klika *et al.* during their work on SIDA effects (*vide supra*),<sup>313</sup> DOSY NMR was used to explore whether any differences in the diffusion behaviour of the major and minor diastereomeric species would be observed as their *dr*'s were varied.

Therefore, the diffusion coefficient of diastereomeric SIBEs were measured in a 100 mM sample prepared from 90:10 *er* (*S*)-**129a**, 2-FPBA **1** and (*R*)-BINOL **9** (Scheme 69). This *er* was chosen as it produced the largest chemical shift difference between the imine resonances of its diastereomeric complexes (see Table 1), and so would enable accurate comparisons of DOSY integration values derived from baseline-resolved imine peaks. Moreover, the large excess of heterochiral (*S<sub>S</sub>,R*)-**166a** in this sample meant that it would be primarily present in its homomeric aggregation state, whilst aggregates of the minor homochiral (*R<sub>S</sub>,R*)-**165a** would be dominated by its heteromeric aggregation state, thus allowing us to compare the diffusion of homomeric and heteromeric aggregates in the same sample. The *D* values of the diastereomeric complexes were found to be comparable, with  $D = 8.00 \times 10^{-10} \text{ m}^2/\text{s}$  for (*S<sub>S</sub>,R*)-**166a** and  $D = 7.87 \times 10^{-10} \text{ m}^2/\text{s}$  for (*R<sub>S</sub>,R*)-**165a**. It is interesting to note that in both cases the measured diffusion coefficients are comparable to the “baseline *D*” values for diastereomerically-pure mixtures of (*S<sub>S</sub>,R*)-**166a** and (*R<sub>S</sub>,R*)-**165a**. (*cf.* 7.75 and  $7.89 \times 10^{-10} \text{ m}^2/\text{s}$ , Table 3), indicating no significant preference for the formation of either heteromeric or homomeric aggregation in diastereomerically impure mixtures.

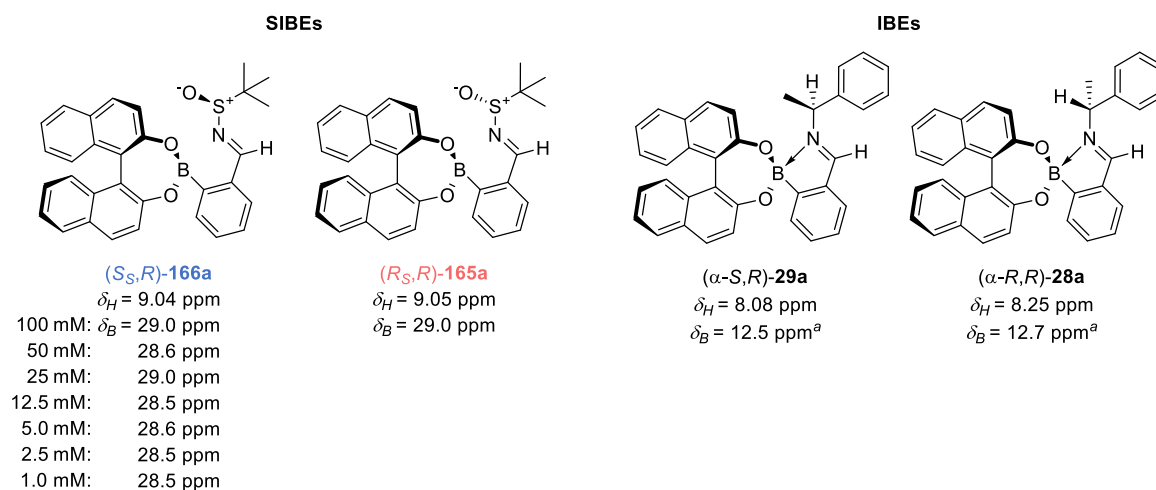


Scheme 69: Three-component assembly of (*S*)-**129a** (90:10 *er*), 2-FPBA **1** and (*R*)-BINOL **9**.  $^1\text{H}$  NMR (500 MHz,  $\text{CDCl}_3$ , 100 mM) chemical shifts referenced to TMS internal standard (~6 mM). Data extracted by MestReNova and Bruker Dynamics Center, and calculated from an average of the imine, methine, and methyl signals.

### 2.3.5 Structural rationale for DAIA of sulfiniminoboronates

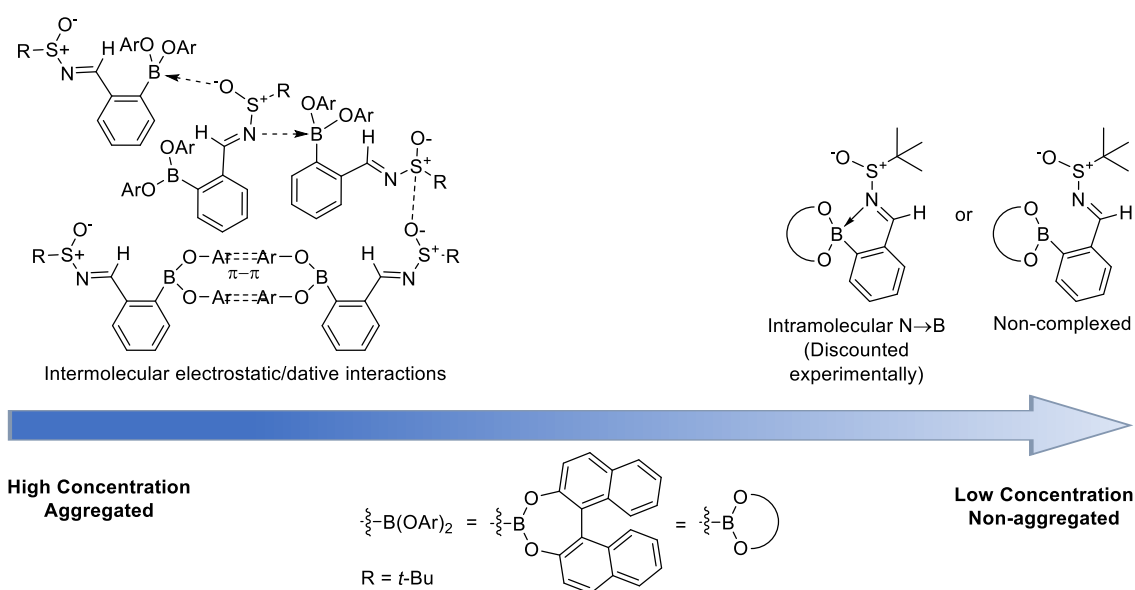
Attention was then turned towards what supramolecular aggregation phenomena might be responsible for the DAIA chemical shift variation effects that were only observed for the imine protons of the diastereomeric SIBE system. As discussed before, the availability of the sulfinamide nitrogen lone pair is decreased compared to amine analytes, with *tert*-butyl-sulfinamide **129a** being sterically hindered at its  $\alpha$ -amino position. It was reasoned that these structural features might be sufficient to seriously weaken the  $\text{N} \rightarrow \text{B}$  coordination bond in the corresponding sulfiniminoboronate complexes, allowing for free rotation around the aryl-boron and aryl-imine bonds of the complexes resulting in greater conformational flexibility that would favour aggregation.  $^{11}\text{B}$  NMR spectroscopic analysis revealed  $^{11}\text{B}$  chemical shifts of 29.0 ppm for both (*R<sub>S</sub>,R*)-**165a** and (*S<sub>S</sub>,R*)-**166a**, in stark contrast to the 12.5 ppm and 12.7 ppm normally observed for IBEs **28a/29a** derived from standard amines (*e.g.*  $\alpha$ -methylbenzylamine **3a**) (Scheme 70). These results indicate that the  $\text{N} \rightarrow \text{B}$  bond found in amine-derived BINOL IBEs ( $\delta_B$  ca. 10-15 ppm, tetrahedral) are not found in the corresponding BINOL SIBEs ( $\delta_B$  ca. 30 ppm, trigonal planar).

Looking at the  $^1\text{H}$  NMR chemical shift of the imine protons of all four species, the SIBE signals are significantly more deshielded (9.04 ppm, 9.05 ppm) than the corresponding IBE imine resonances (8.08 ppm, 8.25 ppm), which highlights the greater electron-withdrawing (*i.e.*  $\text{N} \rightarrow \text{B}$  destabilising) nature of sulfinimines over imines. These structural and NMR variations between SIBEs and IBEs support the conjecture that decreased availability of the sulfinamide amino lone pair impacts the ability of SIBEs to complex at the boron centre, resulting in non-coordinated SIBE species, as drawn throughout this thesis. This lack of intramolecular  $\text{N} \rightarrow \text{B}$  bonding is likely to impact strongly on the nature of the aggregation effects observed, affording greater conformational flexibility to SIBEs than conventional IBEs whose  $\text{N} \rightarrow \text{B}$  bonds mean they are much more rigid and compact, and so much less likely to aggregate. Conversely, lack of  $\text{N} \rightarrow \text{B}$  coordination in SIBEs leads to far more flexible structures, with multiple electron acceptor and electron donor sites that are then free to act cooperatively to produce the observed aggregates. Additionally, the SIBE sulfinimine/imine nitrogen lone pair remains free to coordinate to other species, whilst being tied up in in boron complexation in IBEs, affording SIBEs additional opportunities for intermolecular polar interactions.



Scheme 70: Imine  $^1\text{H}$  and  $^{11}\text{B}$  NMR (500/160 MHz,  $\text{CDCl}_3$ , 100 mM) chemical shifts of (*R*)-BINOL-derived SIBEs and IBEs.  
<sup>a</sup> Literature values.<sup>330</sup>

It was then considered whether the coordination/complexation boron centre might vary depending on its concentration, with intramolecular  $\text{N} \rightarrow \text{B}$  coordination favouring monomeric species at low concentrations, and intermolecular interactions favouring formation of aggregates at higher concentration (Scheme 71). However, measuring the  $^{11}\text{B}$  NMR chemical shift of (*S<sub>S</sub>*,*R*)-166a over the same range of concentrations as previous screening experiments revealed a consistent chemical shift  $\delta_{\text{B}} = 28.5 - 29.0 \text{ ppm}$  from 100 mM to 1 mM (Scheme 70), thus indicating that the  $sp^2$  hybridisation state of the boron centre remains predominantly uncoordinated in both its monomeric and aggregated form.



Scheme 71: Possible structural variation of BINOL-SIBEs at varying concentrations. Left: Aggregate state caused by various intermolecular interactions. Right: Monomeric form with (discounted experimentally) and without intramolecular N→B coordination.

The sulfinamide complexation reactions were then carried out in benzene -  $d_6$  and acetonitrile -  $d_3$  in order to determine what effect  $\pi$ -stacking and solvent polarity might have on the aggregation process (Table 4). As for the  $\text{CDCl}_3$  complexation experiments, the  $^1\text{H}$  NMR spectra of the diastereomeric SIBE ( $S_S,R$ )-**166a** complexes in deuterated benzene showed significant chemical shift drift of their imine resonances, with corresponding variation in their diffusion coefficients also observed. Interestingly, these variations did not mirror the chemical shift trend in  $\text{CDCl}_3$ , with the imine  $\delta_H$  value first increasing from 9.56 ppm to 9.60 ppm as the concentration dropped from 100 mM to 25 mM, before dropping to 9.40 ppm as the concentration fell to 5.0 mM. DOSY measurements revealed that the diffusion coefficient of the complex first rose as the concentration fell from 100 mM to 25 mM, then dropped significantly from 25 mM to 5.0 mM, with the hydrodynamic radius fluctuating between 6.39 Å and 6.89 Å. Previous studies have shown that aggregation-based chemical shift drift caused by solution-state  $\pi$ -stacking interactions in large conjugated systems can be suppressed by carrying out  $^1\text{H}$  NMR spectroscopic analysis in benzene -  $d_6$ .<sup>325</sup> As benzene itself is a  $\pi$ -system, its use as a solvent is expected to saturate any  $\pi$ -stacking sites of the SIBEs in solution, therefore preventing any significant intermolecular  $\pi$ -stacking aggregation events. Significant disruption to aggregation (*i.e.* larger  $D$ , smaller  $R_{\text{hyd}}$ ) would therefore indicate that SIBE aggregation was dominated by  $\pi$ -stacking interactions. These results, therefore, indicate that  $\pi$ -stacking interactions are not likely the driving force behind the overall aggregation/DAIA behaviour of these BINOL SIBEs, since benzene does not appear to have significantly decreased DAIA aggregation of ( $S_S,R$ )-**166a**. Carrying out the corresponding concentration-dependent NMR analysis of SIBE ( $S_S,R$ )-**166a** in more polar  $\text{CD}_3\text{CN}$  revealed no chemical shift variation as the concentration was decreased, with consistent imine proton resonances of 8.72-8.73 ppm obtained in all cases. Furthermore, the diffusion coefficients of ( $S_S,R$ )-**166a** in  $\text{CD}_3\text{CN}$  were higher than in  $\text{CDCl}_3$  or  $\text{C}_6\text{D}_6$  (even accounting for viscosity), implying

significantly smaller SIBE species (*cf.*  $R_{hyd}$  = 6.12 Å for 5.0 mM ( $S_S,R$ )-**166a** in  $CDCl_3$  vs  $R_{hyd}$  = 6.27 Å for 100 mM in  $CD_3CN$ ), thus indicating that ( $S_S,R$ )-**166a** is more monomeric in  $CD_3CN$  than in  $CDCl_3/C_6D_6$ . Since acetonitrile would not be expected to disrupt either hydrogen-bonding or  $\pi$ -stacking interactions, it therefore seemed fair to exclude both of these types of intermolecular interaction as the major drivers controlling aggregation. It was therefore concluded that polar/surfactant-type interactions are responsible for the aggregation of ( $S_S,R$ )-**166a** in  $CDCl_3$  and deuterated benzene, as they are disrupted by the increased polarity of the acetonitrile solvent ( $\epsilon$  = 35.688).<sup>331</sup> Therefore, it is proposed that the aggregation effects observed in BINOL-SIBEs reported in this chapter are driven primarily by polar interactions between their polar zwitterionic sulfinimine “head-group” moieties of the SIBEs, with the aryl rings of the BINOL and template acting as lipophilic “tail-groups” that are arranged in defined conformations that affect the magnetic environment of the imine protons, to influence their chemical shifts. This polarity and “headgroup” behaviour is consistent with other reports of sulfonamide crystal structures, as seen in Figure 35, which shows clustering of the sulfonamide functionality in the crystal structure of Davis’ sulfonamide ( $R$ )-**129b**, including an NH–OS hydrogen bond (see section 3.1.3 for another example).

Table 4: Imine  $^1H$  NMR  $\delta_H$ ,  $D$ , and  $R_{hyd}$  of ( $S_S,R$ )-**166a** in  $CDCl_3$ ,  $C_6D_6$  and  $CD_3CN$  assembled following the usual conditions.

(S)-**129a** + (HO)<sub>2</sub>B-C<sub>6</sub>H<sub>4</sub>-CHO (2-FPBA **1**) + (R)-**9** (1.2 equiv.)  $\xrightarrow[CDCl_3]{1\text{ h, rt}}$  ( $S_S,R$ )-**166a**

Entry	C	$CDCl_3$ ( $\epsilon$ = 4.7113) <sup>a</sup>			$C_6D_6$ ( $\epsilon$ = 2.2706) <sup>a</sup>			$CD_3CN$ ( $\epsilon$ = 35.688) <sup>a</sup>		
		$\delta_H^b$	$D^c$	$R_{hyd}^d$	$\delta_H^b$	$D^c$	$R_{hyd}^d$	$\delta_H^b$	$D^c$	$R_{hyd}^d$
1	100 mM	9.04	7.75	7.55	9.56	6.34	7.60	8.73	13.3	6.27
2	25 mM	8.95	9.73	6.66	9.60	8.09	6.39	8.73	15.6	5.58
3	5.0 mM	8.79	10.8	6.12	9.40	7.27	6.89	8.72	15.9	5.50

<sup>a</sup> Dielectric constants for the non-deuterated solvents, values from Gaussian reference.<sup>332</sup> <sup>b</sup> Referenced to TMS internal standard (~6 mM in 100 mM stock solution). <sup>c</sup> Data extracted by Bruker Dynamics Center, units:  $10^{-10}$  m<sup>2</sup>/s. <sup>d</sup> Calculated using Manchester NMR Methodology Group’s SEGWE calculator, units: Å.

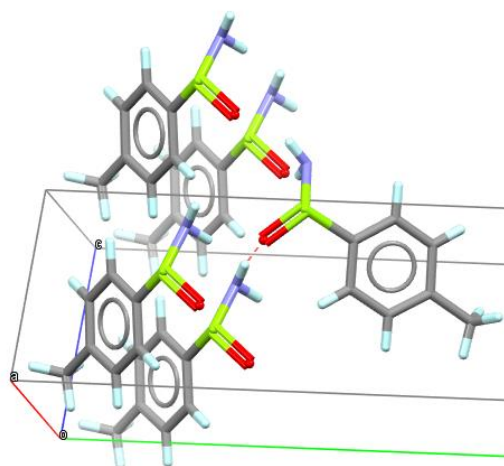


Figure 35: Crystal packing of Davis' sulfinamide (*R*)-**129b** showing clustering of polar sulfinamide "headgroup", including H-bonding (red dashed line).<sup>333</sup>

Since the concentration-dependent aggregation of BINOL-SIBEs appeared to be suppressed by carrying out their assembly and  $^1\text{H}$  NMR analysis in  $\text{CD}_3\text{CN}$ , a three-component assembly study of 2-FPBA **1**, (*R*)-BINOL **9** and scalemic Ellman's sulfinamide **129a** in  $\text{CD}_3\text{CN}$  was carried out (Figure 36). As is clearly visible in Figure 36, no distinct diastereomeric SIBE imine  $^1\text{H}$  NMR resonances were observed, with all five 500 MHz  $^1\text{H}$  NMR spectra showing a single singlet resonance at 8.73 ppm, regardless of their diastereomeric composition. Although slight broadening of the imine signal was observed in diastereomerically impure systems, it is clear that  $\text{CD}_3\text{CN}$  is unsuited as a solvent for determining the enantiomeric excess of sulfinamides using a BINOL-SIBE CDA approach. However, the fact that the imine signals of both non-aggregated diastereomers are fully overlapped in  $\text{CD}_3\text{CN}$ , once again suggests that the presence of aggregated complexes in  $\text{CDCl}_3$  and  $\text{C}_6\text{D}_6$  is responsible for the chemical shift anisotropy observed for the imine protons of the BINOL sulfiniminoboronate diastereomers in these systems. As before, this is concerning, as the use of  $\text{CD}_3\text{CN}$  as the solvent for this method could lead to the incorrect conclusion that the sulfinamide analyte is enantiopure. Additionally, early development of this method in  $\text{CD}_3\text{CN}$  could again potentially have led to the termination of the project.

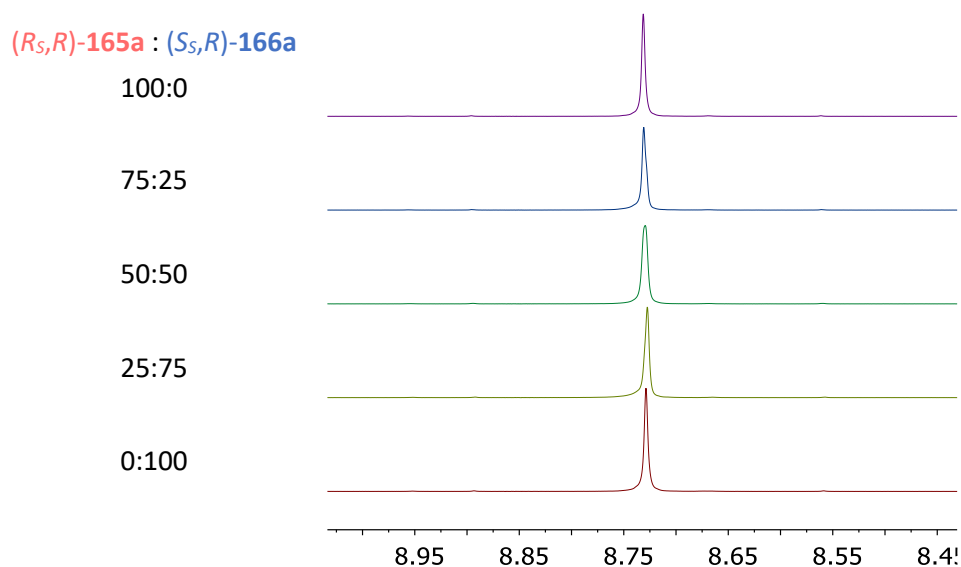


Figure 36: Expanded imine region of the  $^1\text{H}$  NMR (500 MHz,  $\text{CD}_3\text{CN}$ , 100 mM) spectra of homochiral and heterochiral sulfiniminoboronate complexes  $(R_S,R)$ -**165a** and  $(S_S,R)$ -**166a** at various ratios assembled in the usual manner.

### 2.3.6 Guidelines for avoiding SIDA and DAIA effects

The results presented in the previous few sections clearly paint a potentially concerning picture of inaccuracy and spurious errors when considering the NMR characterisation of chiral compounds. Of particular concern is the potential to incorrectly assign enantiopurity and absolute configuration when employing CDA NMR methodologies. Consequently, the author would like to put forward the following guidelines and control experiments to ensure accurate reporting of NMR characterisation data for chiral compounds, and reliable determination of enantiomeric excess by NMR spectroscopic methods.



DAIA/SIDA Effect	Risk	Control experiment/measures
Concentration-dependent $\delta$	Incorrect structural assignment	<ul style="list-style-type: none"> <li>- Report sample concentration in NMR characterisation data</li> <li>- Preferred: measure spectra at several concentrations, covering 2 orders of magnitude</li> </ul>
Enantio-/diastereo-purity-dependent $\delta$	Incorrect structural assignment	- Acquire spectra at enantiopure, scalemic, and racemic ratios
Overlapped/coalesced diastereomeric peaks	Incorrect enantiopurity measurement	- For new substrates/methods corroborate <i>er/dr</i> with additional methods ( <i>e.g.</i> other resonances/nuclei, $\alpha_D$ , HPLC, <i>etc...</i> )
Diastereomeric signal crossover	Incorrect <i>ee</i> or absolute configuration	<ul style="list-style-type: none"> <li>- For new substrates/methods corroborate with additional methods (<i>e.g.</i> other resonances/nuclei, <math>\alpha_D</math>, HPLC, <i>etc...</i>)</li> <li>- Avoid assigning absolute configuration by analogy or without additional structural data</li> </ul>

## 2.4. Conclusions, future work, and outlook

The research described in this chapter describes unexpected and unprecedented concentration- and *dr*-dependent chemical shift variations in the  $^1\text{H}$  NMR spectra of diastereomeric BINOL-derived sulfiniminoboronate esters. These studies revealed that the chemical shift differences between diastereomeric imine signals of BINOL-SIBEs varied between samples of different *dr*, with imine peak coalescence and cross-over being observed. This work has shown that this anomalous behaviour is caused by aggregation of diastereomeric BINOL-derived SIBEs, in a phenomenon newly termed *diastereomer aggregation-induced anisotropy* (DAIA). These DAIA effects have been carefully studied using a combination of  $^{11}\text{B}$ ,  $^1\text{H}$  1D and DOSY NMR spectroscopic studies, with these analytical results showing that significant SIBE aggregation occurs at high concentrations, with lower SIBE concentrations favouring monomeric species. Concentration and solvent studies strongly indicate that SIBE aggregation in non-polar solvents occurs primarily through polar interactions of their zwitterionic sulfinimine “head-groups”, with their more lipophilic aromatic tail groups aligning themselves to exert anisotropic shielding/deshielding effect on the imine protons of each diastereomer. Although the evidence for aggregation is fairly compelling, further work is now underway to better understand and characterise these features. Spectroscopic methods are currently being considered, such as UV-Vis to assess whether SIBEs are aggregating in solution or instead forming non-soluble species. Additionally, if this is the case dynamic light scattering (DLS) experiments will be carried out to attempt to characterise the size of these aggregate species. This aggregation process appears to be facilitated by the absence of  $\text{N} \rightarrow \text{B}$  coordination in sulfiniminoboronate esters, rendering these molecules more flexible, less coordinatively saturated,

and therefore more prone to intermolecular interactions. Reassuringly, conventional IBEs derived from amines do not aggregate to any significant extent in solution, and therefore do not suffer from DAIA-induced chemical shift variation. This observations raises some interesting questions on the nature and in particular the lability of  $N \rightarrow B$  bonds in IBEs and related species, and so further investigations using IR and  $^{15}\text{N}$  NMR spectroscopic methods are now being considered. Additionally, previously reported IBE structures are now being revisited to further understand the nature of the  $N \rightarrow B$  bond in different systems, and ensure correct characterisation and reporting of these complex structures.

Ongoing attempts to grow homomeric and heteromeric crystals of each of the BINOL-sulfiniminoboronate complexes are currently underway in order to better understand the exact nature of the aggregation process. The possibilities that DAIA affords for carrying out efficient diastereomeric purification through sublimation or recrystallisation processes will also be investigated, as has previously been done in SIDA-susceptible systems (*vide supra*). Finally, this case study of aggregation-induced anisotropy suggests that care should be taken in interpreting results when CDA NMR protocols are used to generate diastereomeric products to determine the *ee*'s of new types of chiral compounds, or even more generally any new class of analyte/solute. To quote a recent publication by Klika *et al.* discussing SIDA effects: "Due care should be taken with respect to conditions, particularly the concentration, when measuring NMR spectra of chiral compounds".<sup>313</sup> Similar advice was put forward by Mitra *et al.* in 1998 after observing concentration-dependent chemical shifts in quinolines (*vide supra*): "lack of consideration of the concentration of the NMR sample could lead to incorrect conclusions pertaining to the structural identity of a given molecule [...] it is thus important to give the solute concentration when reporting NMR spectra."<sup>323</sup> This advice resonates strongly with the results presented in this chapter, which highlight the need for more rigor and consistency in the reporting and interpretation of NMR data - in particular taking care to report concentration values when CDA NMR protocols are used to determine the enantiopurities of chiral compounds, and more generally when the structural characterisation of new chiral compounds is reported.

### 3. THE BULL-JAMES ASSEMBLY FOR DETERMINING THE ENANTIOPURITY OF SULFINAMIDES BY NMR SPECTROSCOPY

#### 3.1. Bull-James assembly of sulfinamides for $^1\text{H}$ NMR analysis

##### 3.1.1 *Diol chiral reporter optimization*

As shown in the previous chapter, BINOL **9** was found to be an unsuitable chiral diol reporter for use in the Bull-James CDA assembly of sulfinamides, due to a lack of baseline resolution and variable DAIA aggregation effects. Therefore, the first step towards developing a functional sulfinamide CDA protocol was to find an alternative chiral diol which would maximise baseline resolution and peak sharpness, whilst eliminating any problematic DAIA effects. To achieve this, eight commercially available chiral diols (including BINOL **9**, 1.2 equiv.) containing a range of steric and aliphatic/aromatic groups were screened in three-component reactions with *tert*-butanesulfinamide **129a** and 2-FPBA **1** (slight excess of diol, Table 5). All eight diols self-assembled with limited 3-85% conversion to produce diastereomeric sulfiniminoboronate complexes. All pairs of diastereomeric assemblies exhibited measurable chemical shift differences, again indicating the robustness and versatility of this type of Bull-James three-component derivatisation approach. Only diols **178**, **179** and **180** (Table 5, entries 6-8) led to full baseline resolution, with three-component assembly of analyte **129a**, 2-FPBA **1**, and pinanediol (1*R*,2*R*,3*S*,5*R*)-**180** resulting in an impressive  $\Delta\delta_{\text{H}}$  of -0.085 ppm, which was a 7-fold increase in  $\Delta\delta_{\text{H}}$  over the original BINOL-based assembly (*cf.* 0.012 ppm). Direct visual comparison of the imine regions of the  $^1\text{H}$  NMR spectra of BINOL- and pinanediol-derived SIBE complexes reveals this significant improvement in both chemical shift difference and line width on moving from BINOL to pinanediol as the chiral reporter (Figure 37). Thus, pinanediol was chosen as the most suitable diol chiral reporter to carry out further three-component derivatizations of sulfinamides. It is interesting to note the significantly higher conversion achieved for BINOL, which will be discussed in more depth in section 3.1.3.

Table 5: Chemical shift differences  $\Delta\delta_H$   $^1\text{H}$  NMR (500 MHz, dried  $\text{CDCl}_3$ , 100 mM) spectra of diastereomeric iminoboronate complexes of Ellman's sulfonamide **129a** (75:25 (*S*):(*R*)), 2-FPBA **1** and a range of enantiopure diols.

$\text{H}_2\text{N}-\text{S}^+(\text{CH}_3)_3 + (\text{HO})_2\text{B}-\text{C}_6\text{H}_4-\text{CHO} + \text{Diol} \xrightarrow[1\text{ h, rt}]{\text{CDCl}_3} \text{Complexes (75:25)}$

**129a** (75:25 (*S*):(*R*))      2-FPBA **1**      Diol (1.2 equiv.)

Entry <sup>a</sup>	Diol	Conv. <sup>b</sup>	$\Delta\delta_H$ (ppm) <sup>c,d</sup>
1	( <i>R</i> )- <b>9</b> 	85%	-0.012
2	( <i>S</i> )- <b>174</b> 	4%	+0.006
3	( <i>R,R</i> )- <b>175</b> 	15%	+0.027
4	( <i>S</i> )- <b>176</b> 	3%	+0.010
5	( <i>S</i> )- <b>177</b> 	10%	+0.014
6 <sup>e</sup>	( <i>S</i> )- <b>178</b> 	23%	+0.037
7 <sup>e</sup>	( <i>S</i> )- <b>179</b> 	9%	+0.047
8 <sup>e</sup>	(1 <i>R</i> ,2 <i>R</i> ,3 <i>S</i> ,5 <i>R</i> )- <b>180</b> 	30%	-0.085

<sup>a</sup> Reactions carried out on 0.1 mmol of sulfonamide at 0.1 M concentration. <sup>b</sup> Determined by  $^1\text{H}$  NMR integration of imine/aldehyde peaks. <sup>c</sup>  $\Delta\delta_H$  is the difference in chemical shifts of the imine protons of the pairs of diastereomeric iminoboronate ester complexes for each chiral diol. <sup>d</sup> A negative value for  $\Delta\delta_H$  indicates that the imine proton resonance of the homochiral iminoboronate ester complex was most deshielded. <sup>e</sup> Full baseline resolution observed for the imine resonances of their respective diastereomeric iminoboronate esters.

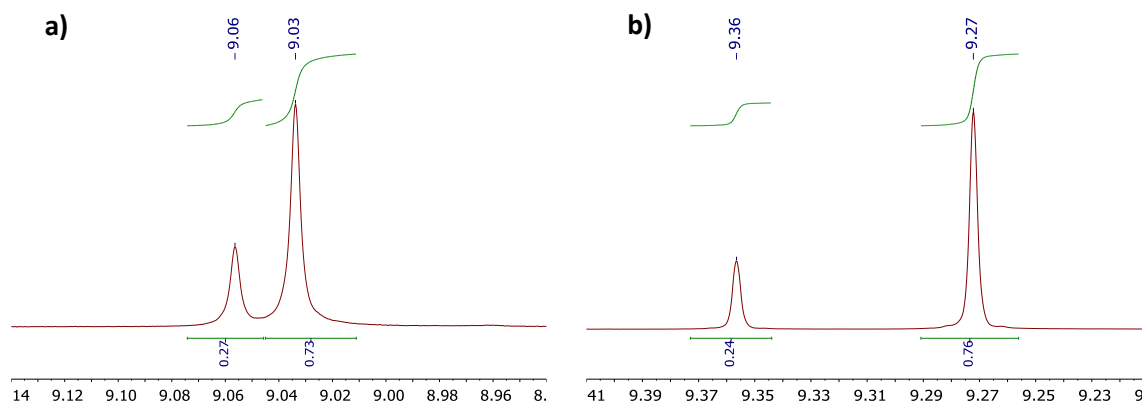
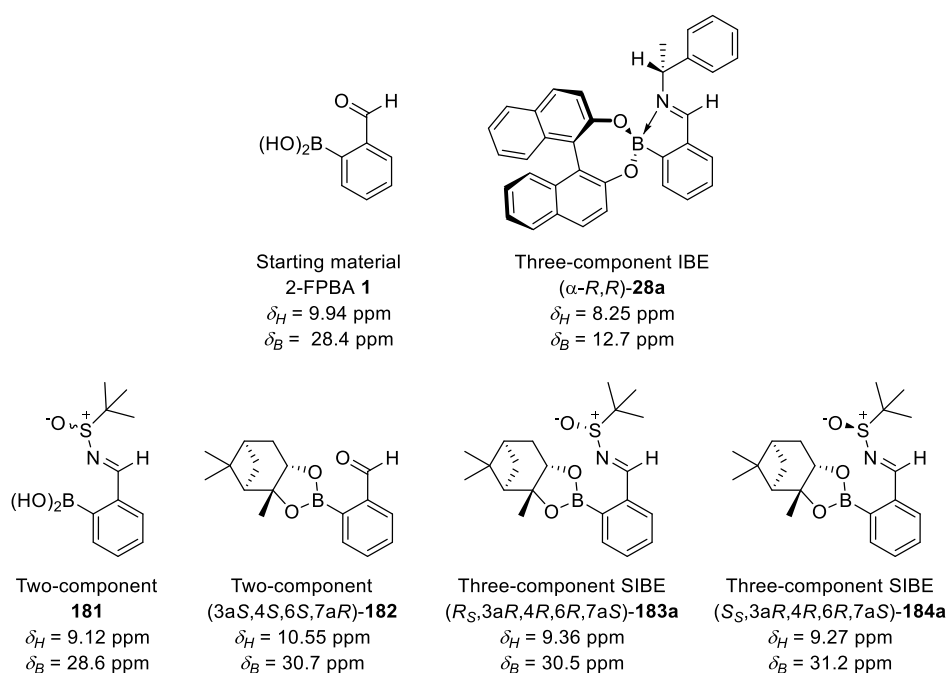


Figure 37: Expanded imine region of the  $^1\text{H}$  NMR (500 MHz,  $\text{CDCl}_3$ , 100 mM) spectra of complexes formed from the three-component assembly of 2-FPBA **1**, 75:25 *er* (*S*)-Ellman's sulfonamide **129a**, and (*R*)-BINOL **9** (a) or (1*S*,2*S*,3*R*,5*S*)-pinanediol **180** (b) (same scale)

### 3.1.2 Development of a stepwise process

With the issue of baseline resolution resolved, attention turned to addressing the issue of incomplete conversion. Unfortunately, despite the well-documented stability of pinanediol-boronate esters,<sup>334,335</sup> once again that the complexation reactions did not go to full completion, instead resulting in varying levels of completion which did not change over time. As described at length in chapter 1, two distinct condensation steps are involved in Bull-James three-component assemblies: imine condensation and boronate ester condensation. Considering the widespread use of the latter in the supramolecular assembly of analogous aminoboronate esters, and the success of many prior Bull-James assembly processes (*vide supra*), it appeared unlikely that the condensation of the diol chiral reporter with the boronic acid template was the problematic step. Sulfinimine condensations, on the other hand, are well known to be difficult to drive to completion, often requiring the addition of dehydrating agents, Lewis acids, or forcing conditions (*e.g.* Dean-Stark, heating, microwave).<sup>244,336–338</sup> This is due to the relatively low nucleophilicity of the sulfonamide nitrogen atom, which is isosteric to a primary amide functionality. For these assemblies, four products could potentially be formed upon simultaneous mixing of the three components (Scheme 72): a sulfiniminoboronic acid **181**, formed from two-component assembly of the sulfonamide **129a** and 2-FPBA **1**; a formyl boronate ester **182**, formed by two-component assembly of the diol **180** and 2-FPBA **1**; and the two desired three-component diastereomeric sulfiniminoboronate complexes **183a** (homochiral) and **184a** (heterochiral). To ensure that any mechanistic postulates were accurate, all four products were synthesised and characterised independently using NMR spectroscopy and high-resolution mass spectrometry. Pleasingly, the  $^1\text{H}$  NMR chemical shifts of the imine/aldehyde protons of all four species were found to be different, which meant that  $^1\text{H}$  NMR spectroscopy could be used to track formation of the two- and three-component assemblies.



Scheme 72: 2-FPBA-derived two- and three-component products and intermediates in the three-component assembly of **1**, **9** and **180**, and associated  $^{11}\text{B}$  NMR chemical shifts and diagnostic imine/formyl  $^1\text{H}$  NMR chemical shifts. 2-FPBA **1** and amine (*R*)-**3a**-derived IBE ( $\alpha$ -*R,R*)-**28a** also shown for comparison. Only diastereomers from (*R*)-BINOL **9** and (1*R*,2*R*,3*S*,5*R*)-**180** shown for clarity.

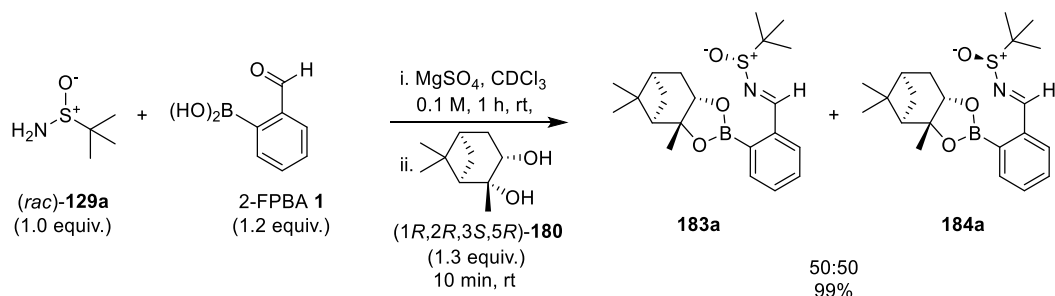
A series of experiments were therefore carried out to better understand this condensation process and identify conditions that would lead to complete conversion of Ellman's sulfinamide (*R*)-**129a** (33% *ee*), 2-FPBA **1**, and pinanediol **180** to the desired diastereomeric SIBE complexes (Table 6). Reaction of the three components in  $\text{CDCl}_3$  for 1 h gave a 70:30 mixture of two-component formyl boronate ester **182** and three-component sulfiniminoboronate esters **183a/184a** (Table 6, entry 1). Addition of  $\text{MgSO}_4$  as a drying agent only marginally increased the amount of **183a/184a** formed to 40% (Table 6, entry 2). The two-component reaction of 2-FPBA **1** with pinanediol **180** was found to give boronate ester **182** in 100% conversion after 10 minutes (Table 6, entry 3). No reaction was observed when sulfinamide **129a** was added to a solution of preformed boronate ester **182** in  $\text{CDCl}_3$  (Table 6, entry 4), indicating that boronate ester **6** is unreactive towards imine bond formation under these conditions. Two-component reaction of Ellman's sulfinamide **129a** and 2-FPBA **1** proceeded more slowly, affording sulfiniminoboronic acid **181** in 89% yield after 1 h, increasing to 94% in the presence of  $\text{MgSO}_4$  (Table 6, entries 5 and 6). Finally, premixing sulfinamide **129a**, 2-FPBA **1** and  $\text{MgSO}_4$  in  $\text{CDCl}_3$  for 1 h, followed by addition of pinanediol **180** gave 93% conversion to afford the desired three-component sulfiniminoboronate esters **183a/184a**, and the two-component boronate ester **182** in 7% yield (Table 6, entry 7).

Table 6: Optimization study of the three-component assembly reaction of Ellman's sulfinamide **129a** with 2-FPBA **1** and pinanediol **180**.

Entry <sup>a</sup>	Reagents	MgSO <sub>4</sub>	<b>1</b>	Product Ratios <sup>b</sup>		
				<b>182</b>	<b>181</b>	<b>183a/184a</b>
1	<b>129a</b> + <b>1</b> + <b>180</b>	-	--	70%	0%	30%
2	<b>129a</b> + <b>1</b> + <b>180</b>	+	--	60%	0%	40%
3	<b>1</b> + <b>180</b>	-	--	100%	--	--
4 <sup>c</sup>	Premix <b>1</b> + <b>180</b> , then add <b>129a</b>	-	--	100%	0%	0%
5	<b>129a</b> + <b>1</b>	-	11%	--	89%	--
6	<b>129a</b> + <b>1</b>	+	6%	--	94%	--
7 <sup>d</sup>	Premix <b>129a</b> + <b>1</b> , then add <b>180</b>	+	--	7%	0%	93%

<sup>a</sup> 2-FPBA **1** added to a premixed suspension of sulfinamide and diol to allow for accurate  $t_0$  starting point. <sup>b</sup> Determined by <sup>1</sup>H NMR spectroscopic analysis using imine/formyl signals in Scheme 72. <sup>c</sup> **1** and **180** premixed for 10 min. <sup>d</sup> **129a** and **1** premixed for 1 h.

These results prompted us to develop a new 'stepwise' three-component derivatization procedure, involving the reaction of (*rac*)-Ellman's sulfinamide **129a** and 1.2 equiv. of 2-FPBA **1** in CDCl<sub>3</sub> at room temperature for 1 h in the presence of MgSO<sub>4</sub> to maximize formation of reactive imine **181**. This was followed by addition of excess 1.3 equiv. of (1*R*,2*R*,3*S*,5*R*)-pinanediol **180** to give a 50:50 mixture of diastereomeric sulfiniminoboronate esters **183a/184a** in 99% conversion (Scheme 73).



Scheme 73: Two-step three-component assembly of 2-FPBA **1**, Ellman's sulfinamide (*rac*)-**129a**, and (1*R*,2*R*,3*S*,5*R*)-**180**.

To ensure that this novel stepwise three-component assembly afforded consistent results, free from the DAIA effects observed for BINOL-derived assemblies in chapter 2, scalemic samples of Ellman's sulfinamide were subjected to these optimised conditions, with *ee*'s ranging from

enantiopure (*R*)-**129a** to (*S*)-**129a** in eight increments (Figure 38). In all cases, the integration of the imine signals in the  $^1\text{H}$  NMR was consistent with the expected *dr*, with these  $^1\text{H}$  NMR spectra indicating this new pinanediol-derived system was free of DAIA-induced diastereopurity-dependent chemical shift drift.

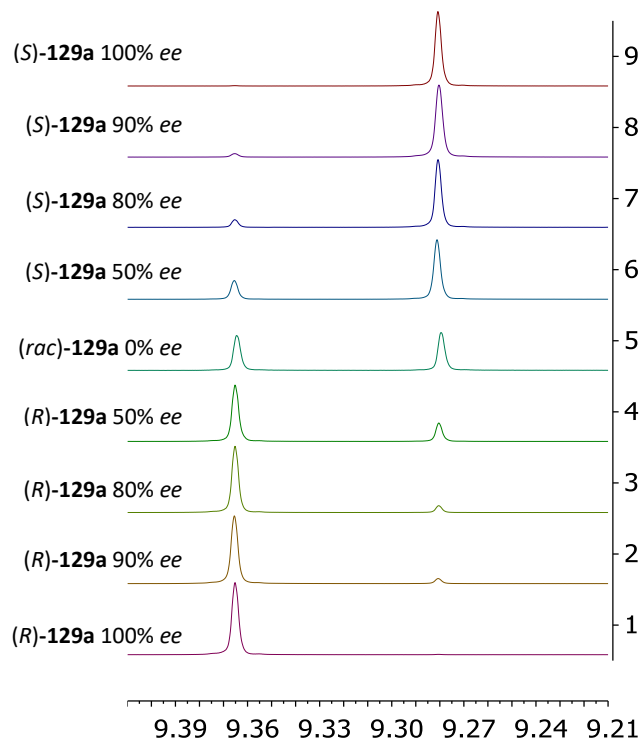


Figure 38: Expanded imine region of the  $^1\text{H}$  NMR (500 MHz,  $\text{CDCl}_3$ , 0.1 M) spectra of three-component assemblies of 2-FPBA **1**, (1*R*,2*R*,3*S*,5*R*)-pinanediol **180** and (*R*)-/(*S*)-Ellman's sulfinamide **129a** following the procedure in Scheme 73. Chemical shifts referenced to TMS internal standard ( $\sim 6$  mM).

To further ensure reliability and absence of DAIA effects, a set of concentration screening experiments was carried out for (*S*,3*aR*,4*R*,6*R*,7*aS*)-**184a**, which also failed to produce any significant chemical shift variation in either its  $^1\text{H}$  or  $^{11}\text{B}$  NMR spectra (Figure 39a-b), further indicating that no aggregation was occurring. Upon dilution from 100 mM to 25 mM and 5.0 mM the diffusion coefficient *D* of the sulfiniminoboronate was seen to only vary slightly from  $8.17 \times 10^{-10}$  to  $8.92 \times 10^{-10}$   $\text{m}^2/\text{s}$  and  $8.93 \times 10^{-10}$   $\text{m}^2/\text{s}$ , respectively. These concentration-dependent changes were significantly smaller than was observed for the BINOL-derived complexes reported in the previous chapter (*cf.*  $D = 7.89 \times 10^{-10}$   $\text{m}^2/\text{s}$  to  $10.7 \times 10^{-10}$   $\text{m}^2/\text{s}$  for (*R*,*S*)-**165a**), indicating significantly less aggregation of the new pinanediol-derived sulfiniminoboronates compared to those derived from BINOL (small change in *D* likely caused by the change in viscosity).<sup>329,339</sup> Moreover, following the findings that diastereomeric imine signals of BINOL-SIBEs were indistinguishable in  $\text{CD}_3\text{CN}$  (*vide supra*), a short series of scalemic screening experiments was carried out in  $\text{CD}_3\text{CN}$  to ensure the robustness of the new method (Figure 39c). The  $^1\text{H}$  NMR spectra of the assemblies of 2-FPBA **1**, (1*S*,2*S*,3*R*,5*S*)-**180** and sulfinamide **129a** at varying *er* clearly showed well-defined diastereomeric imine signals in pinanediol-derived SIBEs in  $\text{CD}_3\text{CN}$ . Interestingly, a slight increase in  $\Delta\delta_H$  was observed when compared to  $\text{CDCl}_3$ , with  $\Delta\delta_H = -0.109$  ppm for the imine



protons (*cf.* -0.085 ppm in CDCl<sub>3</sub>), however for reasons of consistency and cost, CDCl<sub>3</sub> was used for further development of this methodology for analysing the enantiopurity of sulfinamides.

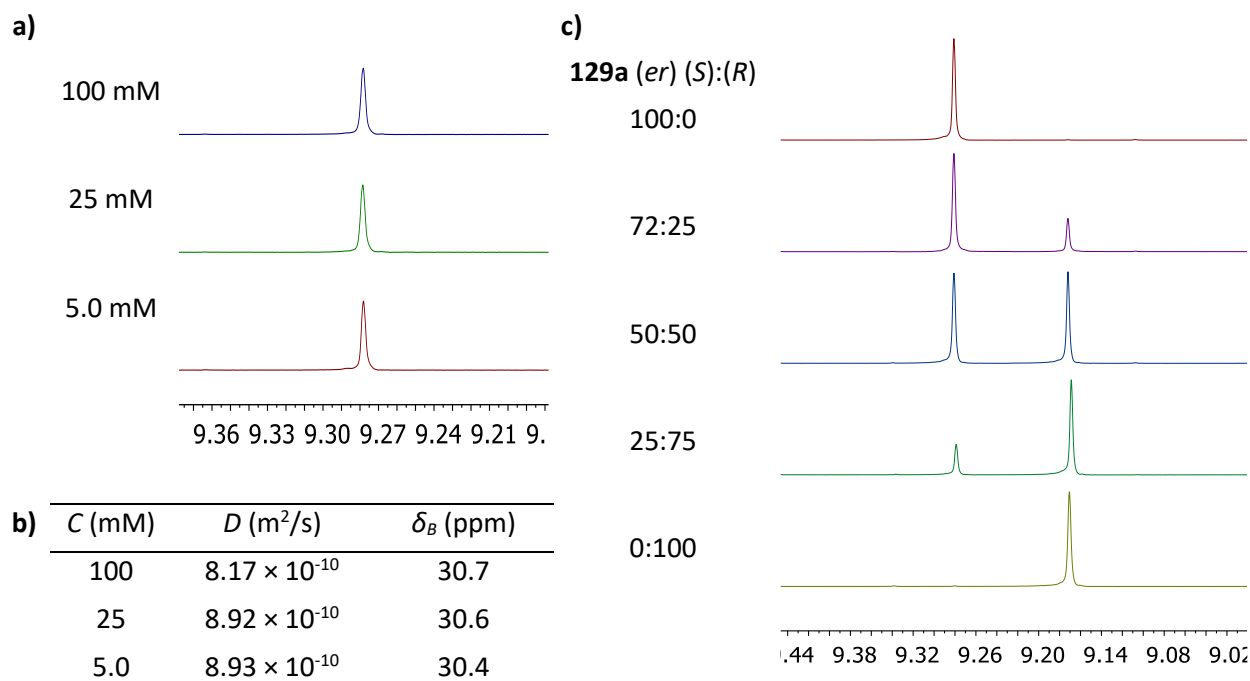
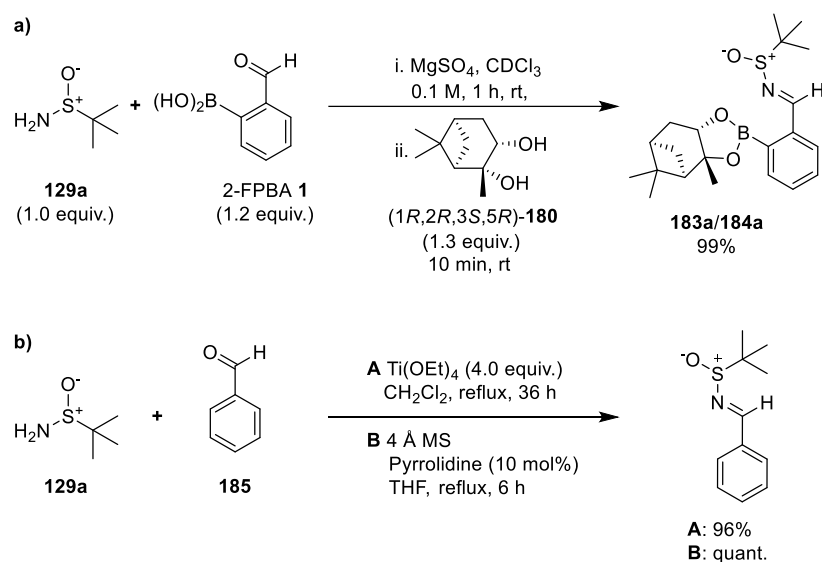


Figure 39: (a) Expanded imine region of the <sup>1</sup>H NMR (500 MHz, CDCl<sub>3</sub>) spectra of three-component assemblies of 2-FPBA **1**, (1*R*,2*R*,3*S*,5*R*)-pinanediol **180** and (*S*)-Ellman's sulfinamide **129a** at 100 mM, 25 mM and 5.0 mM concentrations following the procedure in Scheme 73. Chemical shifts referenced to TMS (~6 mM) internal standard. (b) <sup>1</sup>H DOSY diffusion coefficients and <sup>11</sup>B NMR chemical shifts of the same samples. (c) Expanded imine region of the <sup>1</sup>H NMR (500 MHz, CD<sub>3</sub>CN) spectra of three-component assemblies of 2-FPBA **1**, (1*S*,2*S*,3*R*,5*S*)-pinanediol **180** and Ellman's sulfinamide **129a** of varying *er*.

### 3.1.3 Mechanistic and structural considerations

The optimisation experiments described in Table 6 clearly suggest that quasi-irreversible formation of boronate ester **182** is significantly faster than reversible formation of imine **181**, with only sulfiniminoboronic acid **7** competent to react further to afford the desired SIBEs **183a/184a** in the three-component derivatization reaction (Table 6). This is in stark contrast to the observations by Anslyn *et al.* regarding the assembly of 2-FPBA **1**, benzylamine **30** and catechol **26** (see section 1.3.2), which showed that the boronate ester and imine condensation steps in traditional assemblies proceeded at a near-identical rate (112 M<sup>-1</sup> and 110 M<sup>-1</sup>, respectively).<sup>118</sup> Looking at the <sup>11</sup>B NMR chemical shifts of the four intermediates provides us with some explanation for these observations (Scheme 72). As in the BINOL-sulfinamide iminoboronates of the previous chapter, the <sup>11</sup>B NMR chemical shift indicates that pinanediol-derived SIBEs are also devoid of an iminoboronate N→B bond, since in all cases the <sup>11</sup>B chemical shifts of the boron atoms were *ca.* 30 ppm, which is indicative of a planar trivalent neutral *sp*<sup>2</sup> boronic species. This does not, however indicate that no coordination is possible, but rather that any N→B interactions are at best short-lived. This is for instance visible for the parent 2-FPBA **1**, which has a non-coordinated <sup>11</sup>B NMR chemical shift of 28.4 ppm, but nonetheless has clear O→B interactions, as indicated by the

formylboronic acid-benzoxaborole equilibrium and the significantly increased electrophilicity of the aldehyde (*vide supra*). Although many attempts were made to grow pinanediol-sulfiniminoboronate crystals, none were successful, and even upon evaporation to dryness these products remained oils, suggesting they may in fact not be crystalline in nature, which is likely due to their lack of N→B coordination and increased conformational flexibility. This structural information sheds some light on the difficulties faced in achieving high conversions in the sulfinimine condensation step. Despite the lack of permanent N→B coordination, it is evident that the proximal boron atom contributes to the sulfinimine condensation, as also occurs for conventional amine analytes. This is made apparent by the rapid high conversions achieved by the stepwise approach under mild nucleophilic conditions, compared to the harsh catalytic and/or water-scavenging conditions required for the same sulfinimine condensation reaction to occur with benzaldehyde **185** (*cf.* Scheme 74a & b).<sup>340,341</sup>

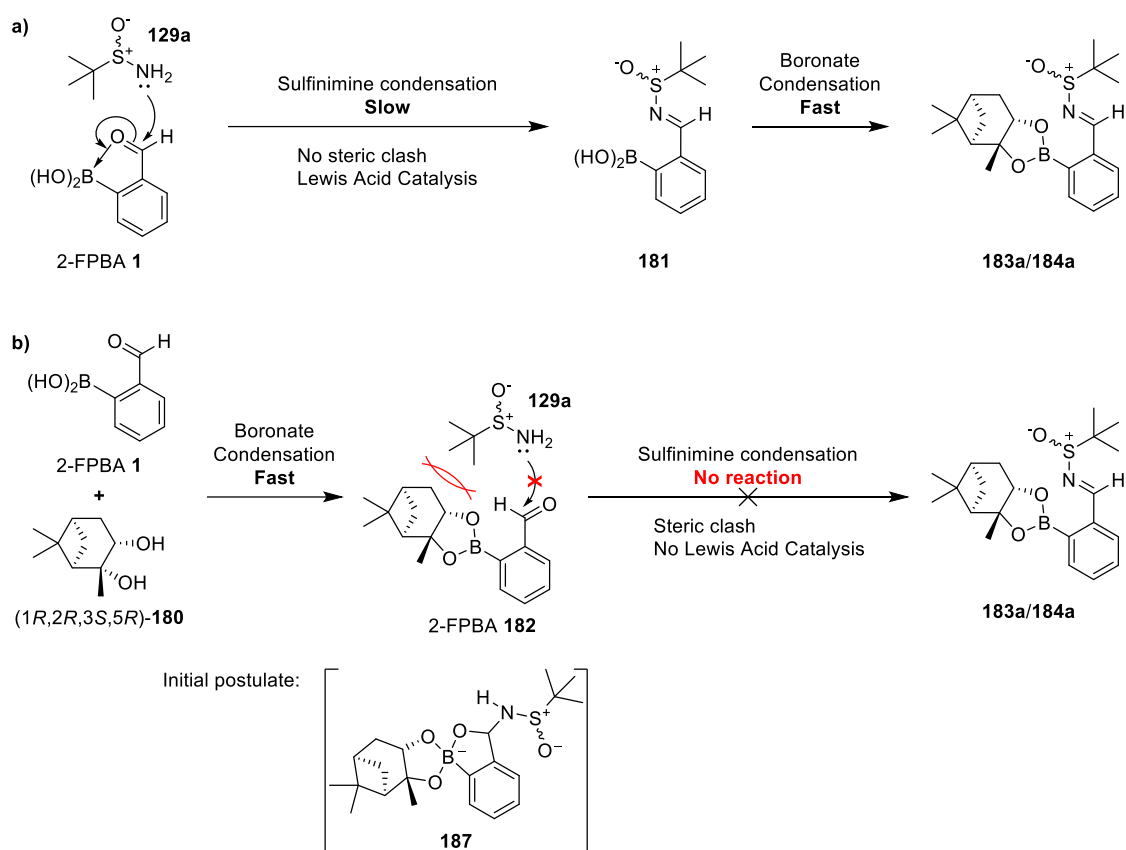


Scheme 74: (a) Optimised stepwise three-component assembly of **129a**, **2-FPBA 1** and **(1R,2R,3S,5R)-180** (*vide supra*). (b) Typical literature procedures for the sulfinimine condensation of Ellman's sulfinamide **129a** and benzaldehyde **185**.<sup>340,341</sup>

In the case of SIBE three-component assembly, reaction of **2-FPBA 1** with sulfinamides proceeds under milder conditions due to the adjacent boronic acid acting as an intramolecular Lewis acid catalyst to facilitate nucleophilic attack of the sulfinamide at the carbonyl group of **2-FPBA 1** (Scheme 75a). This condensation process is still relatively slow however, due to the inherently low nucleophilicity and steric demand of the sulfinamide nucleophile. Once two-component sulfiniminoboronic acid **181** formation has been achieved,  $^{11}\text{B}$  NMR spectroscopic data shows that no significant N→B coordination occurs, presumably due to the same factors of decreased Lewis basicity and steric bulk. Following NMR analysis, crystals of the sulfiniminoboronic acid **181** were grown by slow evaporation from  $\text{CDCl}_3/n$ -hexane, allowing us to further confirm this structural postulate. As shown in Figure 40a, no N→B coordination is seen in the crystal structure of (*S*)-**181**, be it intramolecular or intermolecular. Instead, the boronic acid, ring, and sulfinimine sit on the same plane, creating an extended O-B-C=C-N-S<sup>+</sup>-O<sup>-</sup> conjugated fragment (red, Figure 40a). The

opposite enantiomer (*R*)-**181** derived from (*R*)-Ellman's sulfinamide **129a** was also grown (see Appendix A). It is interesting to note that the crystal structures show strong "bidentate" hydrogen bonding interactions between the sulfinamide oxygen and the acidic boronic acid protons, illustrating the polarity of the sulfinimine functionality, as well as the ability of its O<sup>-</sup> group to donate electron density to form strong hydrogen bonds (Figure 40b). This observation provides some additional support for the previous suggestion that the sulfinimine functionality can act as a "polar headgroup" in non-coordinated BINOL-SIBEs to facilitate aggregation. Although N→B interactions in iminoboronic acids have been regularly assigned by NMR spectroscopy,<sup>118,217</sup> they are not regularly observed in crystal structures, with only one previous example of an X-ray crystal structure of a sulfiniminoboronic acid reported in the literature – a polyoxometalate (POM) **186**, which exhibited an alternative strong intramolecular hydrogen bonding interaction between its imine nitrogen lone pair and a boronic acid proton (Figure 40c).<sup>342</sup> In this case, the lack of N→B bonding was explained by a combination of weakened boronate Lewis acidity compared to its corresponding boronate ester, and general steric repulsion caused by the large POM group resulting in the 6-membered hydrogen bonded state dominating. It is particularly interesting that intermolecular hydrogen bonding is preferred in sulfiniminoboronic acid **181**, with no intramolecular bonding observed (good agreement with <sup>11</sup>B NMR data, *vide supra*), as this indicates how non-Lewis basic the lone pair of the sulfinimine nitrogen atom actually is.

Following the alternate pathway, if pinanediol boronate ester **182** forms first, the significantly increased steric bulk of the pinanediol ligand is simply too high for the bulky and weakly-nucleophilic sulfinamide to overcome, and so since no internal Lewis acid catalysis can occur, the sulfinimine condensation cannot proceed (Scheme 75b). An alternative explanation was originally suggested, proposing that the increased Lewis acidity of the boronate ester might be responsible, by over-stabilising reactive intermediate **187**, thus halting the sulfinamide reaction.<sup>294</sup> It must be noted that incomplete conversion was observed for all diols screened in Table 5, and that successful assembly of pinanediol-IBEs is known for other analytes/substrates,<sup>162,237,238</sup> and so it appears only slight steric bulk is sufficient to halt this sulfinimine condensation step, highlighting the sheer size of sulfinamides and weakness of the coordination in these systems. Boronate ester condensations are of course trivial for both 2-FPBA **1** and sulfiniminoboronic acid **181**.



Scheme 75: Suggested reaction pathways for the three-component assembly of 2-FPBA **1**, Ellman's sulfonamide **129a** and (1*R*,2*R*,3*S*,5*R*)-**180**, that are consistent with structural features and the data generated in the experiments described in Table 6.

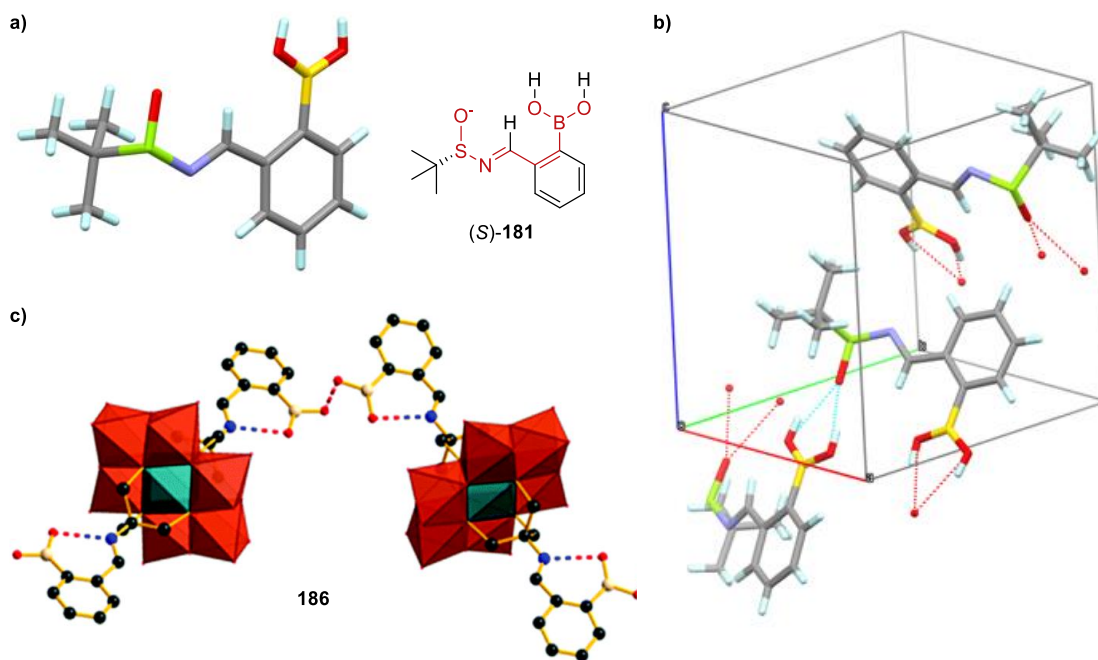
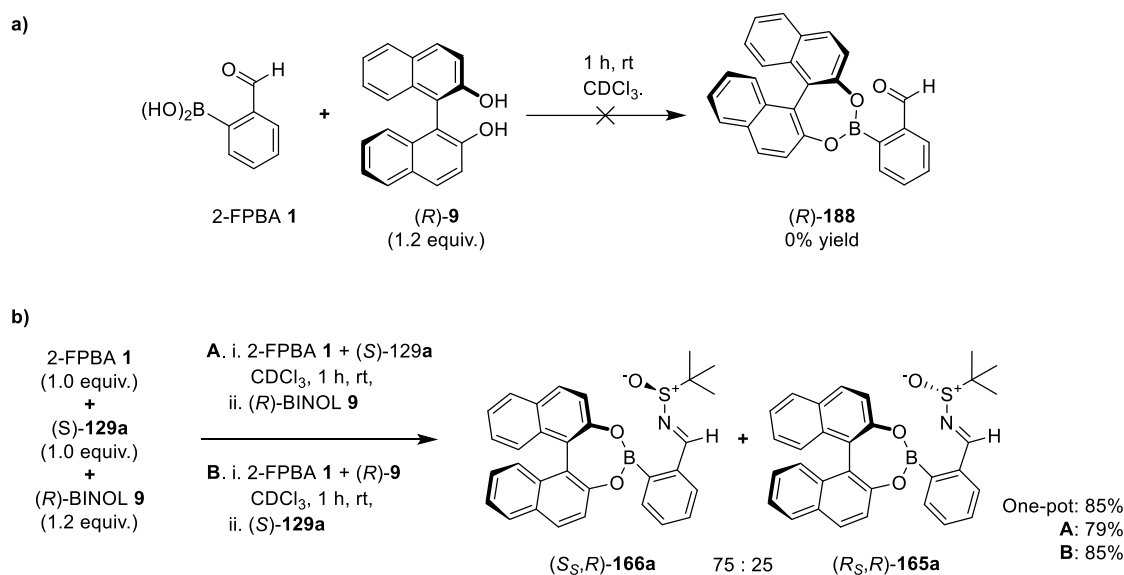


Figure 40: X-Ray crystal structure of iminoboronic acids: sulfiniminoboronic acid (*S*)-**181** (a) single molecule, (b) multiple molecules illustrating intermolecular H-bonding; (c) polyoxometalate IBE **186** showing hydrogen bonding interactions (dashed lines; H's omitted for clarity), adapted with permission from the Royal Society of Chemistry.<sup>342</sup>

These mechanistic proposals are consistent with the high 85% conversion observed in one-pot BINOL-sulfinamide Bull-James assemblies, as opposed to the 3-30% yields observed for other diols (see Table 5), which indicates a likely mechanistic deviation between the formation of BINOL-SIBE and other SIBE assemblies. The Bull and James groups have previously observed that BINOL does not condense to form boronate esters with simple boronic acids, instead requiring cooperative N→B coordination in order to produce stable BINOL boronate esters (unpublished), an observation supported indirectly by literature reports of donor-coordinated BINOL boronate esters.<sup>343</sup> It is believed that this is caused by the axial chirality of the BINOL diol, whose hydroxyl groups cannot readily achieve the planarity required to condense with a planar *sp*<sup>2</sup> boronic acid boron centre. These observations were confirmed for this assembly system by two-component assembly of 2-FPBA **1** and (*R*)-BINOL **9**, which showed no appreciable formation of boronate ester **188** under standard assembly conditions (Scheme 76a). This indicates either that the BINOL boronate ester is not stable, or that its formation incurs a significant kinetic barrier. Stepwise assembly reactions showed that comparable conversion to the expected BINOL-SIBEs occurred in all systems, regardless of order of addition or number of steps (Scheme 76b). This leads to the conclusion that the one-pot one-step three-component assembly of BINOL **9**, 2-FPBA **1** and Ellman's sulfinamide **129a** proceeds in an inherently stepwise manner, with initial sulfinimine condensation to produce sulfiniminoboronic acid **181** (*vide supra*) unobstructed by the presence of BINOL **9**, unlike for other diols. As this sulfiniminoboronic acid intermediate **181** contains a proximal Lewis basic nitrogen lone pair in the sulfinimine moiety, it is now capable of undergoing boronate ester complexation with BINOL **9** to produce SIBEs **165/166**. However, <sup>11</sup>B has shown that no lasting N→B coordination occurs in the assembled SIBE (*vide supra*), and so for all intents and purposes the sulfinimine and boronate esters of SIBEs exist as entirely separate functional groups in these complexes, exhibiting little to no IBE character. Therefore, these results suggest that BINOL boronate esters are not inherently unstable, and do not require stabilising IBE complexation to exist, but instead that their formation is kinetically/enthalpically limited. The proximal N→B donor of the sulfinimine provides sufficient interaction to induce transient tetrahedral character at the boron centre, serving to lower the activation energy barrier for BINOL-boronate ester formation, thus catalysing this process intramolecularly. <sup>11</sup>B NMR spectroscopy has been used in an attempt to observe the suspected transient N→B coordination of sulfiniminoboronic acid **181** by recording spectra with varying concentration (100 mM – 1.0 mM) and at variable temperatures (33 mM, -45 °C – 45 °C), but unfortunately no new *sp*<sup>3</sup> <sup>11</sup>B NMR resonances were observed.



Scheme 76: Two- and three-component assemblies of (R)-BINOL **9**, 2-FPBA **1** and Ellman's sulfonamide **129a** (75:25 (S):(R)).

One additional structural observation can be made regarding the lack of N→B coordination, in that it simplifies and eliminates some issues of structural complexity and divergence. Were a strong N→B bond present (e.g. **138a'**), the resulting tetravalent boronate centre would also define a chiral centre, leading to 8 possible stereoisomers of SIBE **183a'**, two of which are shown in Figure 41 (both derived from (R)-**129a** and (1*R*,2*R*,3*S*,5*R*)-**180**). Lack of N→B coordination instead allows for free rotation around the B-C bond, negating this issue entirely. Of course, this issue arises only from the use of non-symmetrical pinanediol **180**, and use of a symmetrical chiral diol such as BINOL **9** as in the previous chapter would not cause these types of issues. Interestingly, examples of standard IBEs with defined N→B bonds derived from non-symmetrical chiral diols are known (*vide supra*), which do not exhibit any issues of structural divergence at the chiral boron centre, with no additional stereoisomers observed. This implies IBE complexes may be more labile than currently assumed, with an N→B bond that is easily broken and reformed to rapidly equilibrate between both stereoisomeric forms of the boronate centre, either producing time-averaged NMR resonances of thermodynamic mixtures of both isomers, or equilibrating exclusively to the more favourable diastereomer to afford a single set of signals. Additionally, the formation of stable IBEs could simply be highly selective, producing exclusively one boron stereoisomer which does not equilibrate. To the best of our knowledge, these considerations have not yet been carefully studied or taken into consideration in functional IBE systems reported, and so future work will need to be carried out to gain a better understanding of the selectivity of equilibration of IBE boron centres.

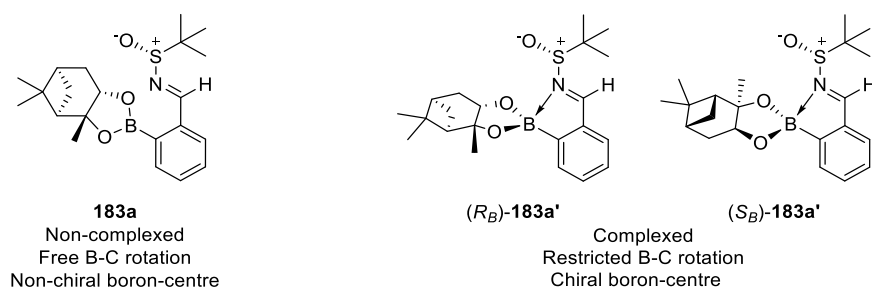
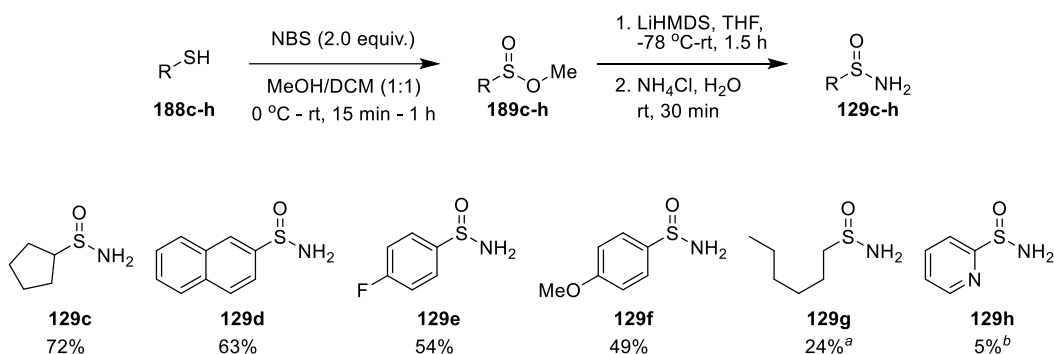


Figure 41: Comparison of SIBEs in the absence (**183a**) and presence (**183a'**) of an N-B coordination bond, producing chiral boron centres in the latter (assemblies derived from (S)-**129a** and (1*R*,2*R*,3*S*,5*R*)-**180**)

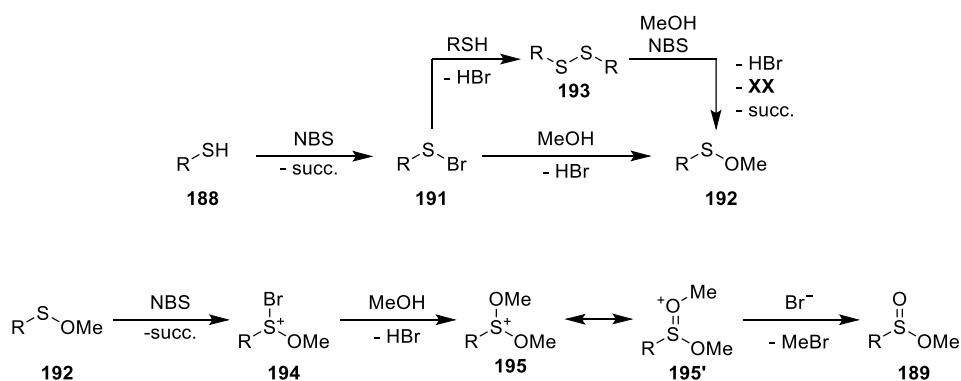
### 3.1.4 Sulfinamide analyte scope

Having developed an optimised two-step procedure for the Bull-James assembly of *tert*-butanesulfinamide **129a**, its general applicability was demonstrated on a range of sulfinamide substrates. As sulfinamides are used almost exclusively as chiral auxiliaries, only Ellman's and Davis' sulfinamides **129a** and **129b** are cheaply and readily commercially available, and so an additional six (*rac*)-sulfinamide substrates were synthesised. These were synthesised in two steps from commercial thiols following the well-established oxidation-amination route, using the synthetic procedures previously described by Liu, Qin and co-workers (Scheme 77).<sup>344</sup> First, a thiol **189** is oxidised by two equiv. of *N*-bromosuccinimide (NBS) in DCM/MeOH, to afford the corresponding methyl sulfinates **190** in near-quantitative yields and in high purity. Thus, this intermediate could be carried forward through the next step following a simple silica plug to remove the succinimide by-product. As shown in chapter 2 section 2.1.4, sulfinates are typically converted to primary sulfinamides by direct amination with lithium amide nucleophiles. In this case, LiHMDS was used as a practically-simple lithium amide, successfully effecting the amination of all six methyl sulfinates to afford the desired primary sulfinamides **129c-h** in 5-72% yield. It should be noted that in the case of **129g** and **129h**, poorer yields were obtained due to purification issues rather than poor yields at either stage of the reaction. For **129g**, the low melting point (41-42 °C) and lipophilic/surfactant nature of the hexanesulfinamide led to difficult and inefficient recrystallisation. In the case of 2-pyridine sulfinamide **129h**, although good mass retention and purity was observed for the crude products of each step, subsequent degradation was observed for both **190h** and **129h**, which may be due to homosubstitution/polymerisation of the product caused by the presence of the nucleophilic nitrogen of the pyridine ring.



Scheme 77: Two-step synthesis of sulfinamides **129** from thiols **188** via methyl sulfonates **189**. Procedure adapted from Liu, Qin and co-workers.<sup>344</sup> Lower yields caused by: <sup>a</sup> low crystallinity; <sup>b</sup> suspected self-polymerisation.

From a mechanistic standpoint, neither reaction in this process is novel, and so only a brief description of the mechanism of each step will be discussed here. Oxidation of the thiol to the sulfinate proceeds through multiple oxidation and substitution steps (Scheme 78). First, thiol **188** undergoes electrophilic bromination to form sulfenyl bromide **191** using an approach that is commonly used to synthesise sulfenyl halides in  $\text{CH}_2\text{Cl}_2$  in high yield.<sup>345,346</sup> In this case, since this reaction is carried out in methanol, the sulfenyl bromide **191** is quickly converted into methyl sulfenate **192**. An alternative pathway may also be envisaged, wherein sulfenyl bromide **191** reacts instead with thiol starting material **188** to afford symmetrical disulfide **193**,<sup>347</sup> that then undergoes oxidation and displacement by methanol to afford the required methyl sulfenate **192** and sulfenyl halide **191**.<sup>348</sup> Once methyl sulfenate **192** is formed, further electrophilic oxidation by NBS produces a cationic bromo-sulfenate **194**, which can undergo halo-substitution by methanol to produce dimethoxysulfenylum cation **195**. Bromide anions can then effect nucleophilic attack at the methyl group of the oxosulfenium resonance form **195'** to produce the desired methyl sulfinate **189** and bromomethane as a by-product.

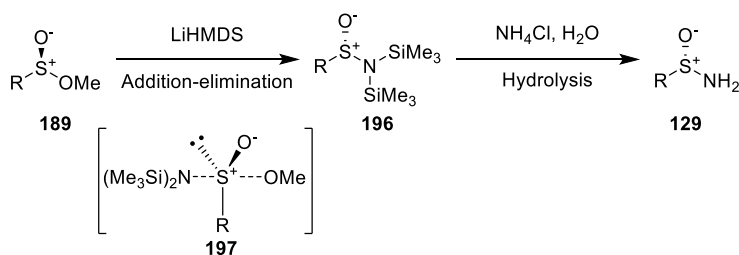


Scheme 78: Proposed mechanism for the oxidative synthesis of methyl sulfonates from thiols by NBS in methanol (adapted from Montelongo *et al.* and Hashemi *et al.*)<sup>347,349</sup>

The subsequent amination reaction proceeds in two reaction steps (Scheme 79). LiHMDS first adds to methyl sulfinate **189**, displacing methoxide to produce *N,N*-bis(trimethylsilyl)-sulfinamide **196**, with clean inversion of chirality at the sulfur centre. Although this type of transformation is often described as a simple  $\text{S}_{\text{N}}2$  substitution reaction, significant mechanistic and computational evidence



exists that indicate that these substrates undergo a two-step addition-elimination process, similarly to higher oxidation-state sulfonates and sulfonyl halides.<sup>350–353</sup> This reaction therefore proceeds *via* an unsymmetrical trigonal bipyramidal tetracoordinate intermediate **197** (not a transition state), with the nucleophile (HMDS) and leaving group ( $\text{MeO}^-$ ) at opposing apical positions, and the oxygen, R substituent, and lone pair positioned equatorially.<sup>350</sup> Once formed, *N,N*-bis(trimethylsilyl)-sulfonamide **196** is readily converted to the desired sulfonamide **129** through cleavage of its labile N-Si bonds by a mildly acidic aqueous workup.

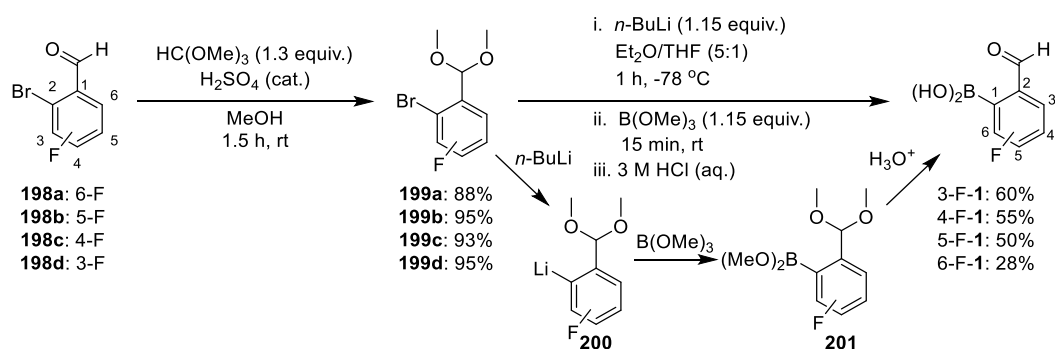


Scheme 79: Sequential amination and hydrolysis of methyl sulfonates by LiHMDS and  $\text{NH}_4\text{Cl}$  (aq.) to afford sulfonamides with full stereoinversion (shown for (*S*)-**129**).

With these six racemic sulfonamides **129c-h** in hand, they were subjected to the one-pot stepwise three-component assembly protocol, along with Davis' sulfonamide **129b** (racemate prepared from combining commercial enantiopure samples). In all instances, the analytes were converted to the corresponding sulfiniminoboronate esters **183b-h/184b-h** in good to excellent 55-99% yields, with analysis of the  $^1\text{H}$  NMR spectra of these mixtures revealing that the imine signals of all pairs of diastereomeric sulfiniminoboronate esters were fully baseline-resolved with good chemical shift differences  $\Delta\delta_{\text{H}} \geq 0.057$  (Table 7). The clear sulfonamide substrate-dependent degree of conversion to diastereomeric SIBEs meant it was crucial to confirm that no dynamic kinetic resolution was occurring. The measured *dr* of the SIBEs in each sample clearly demonstrated this, with *dr* values between 49:51 and 51:49, which is clearly well within experimental error of the 50:50 *dr* expected for a racemic analyte. General control experiments were also carried out (not shown), varying time, concentration, stoichiometry, and conversion, which returned the expected *dr* in all cases. Due to the stepwise nature of the process, kinetic resolution is not possible during the imine condensation step, and can only occur after addition of the chiral pinanediol. The boronate ester reaction is extremely fast and excess diol is used, and so the risk of any kinetic resolution occurring is minimised. Moreover, once the diol has been added, unreacted 2-FPBA **1** is quickly converted into boronate ester **182**, which has been shown to be unreactive towards sulfinimine condensation with either enantiomer of Ellman's sulfonamide **129a** (*vide supra*). This effectively "seals" the system, which is comprised of generally unreactive species, containing a fixed amount of sulfiniminoboronate with a fixed *dr*.

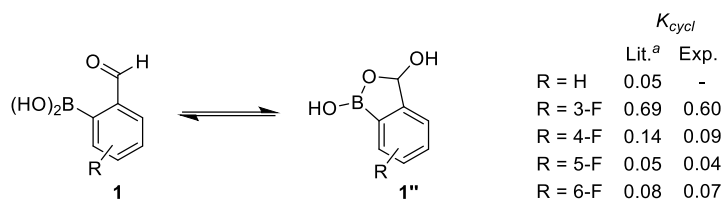


spectroscopic approach could also be applied to the chiral analysis of sulfinamides. Although the Bull and James groups originally reported the derivatisation of chiral amines with 4-fluoro-2-FPBA 4-F-**1**,<sup>162</sup> Oe and co-workers showed that in the case of amino acid ester hydrochloride analytes use of 5-fluoro-2-FPBA 5-F-**1** fluorinated template gave the best results, achieving the largest  $\Delta\delta_F$  and conversion (see section 1.4.7).<sup>164</sup> Given this divergent precedent, it seemed prudent to synthesise and screen all four possible regioisomers of fluorinated-2-FPBA for the formation of SIBEs (Scheme 80). As none were commercially available, these templates were synthesised in two steps from commercially available 2-bromo-fluorobenzaldehydes **198a-d** following the two-step method of Kowalska *et al.*, in a similar manner to the previous synthesis by the Bull group.<sup>120,162,354</sup> Firstly, the different fluoro-bromobenzaldehydes were stirred in methanol in the presence of trimethyl orthoformate and catalytic sulfuric acid to produce the desired dimethyl acetals **199a-d** in excellent 88-95% yield. In this instance, trimethyl orthoformate acts to both form the acetal and remove water from the system, driving the reaction to completion through formation of a methyl formate by-product. These acetals were then subjected to a lithiation/borylation step, by first effecting a lithium-halogen exchange with their bromide substituents using *n*-BuLi to produce lithiated fluorobenzene **200**, which was subsequently quenched with trimethyl borate to produce dimethoxy boronate ester **201**. Finally, a global deprotection step was then carried out, involving acid catalysed hydrolysis of both their acetal and boronic ester functionalities to produce all four formyl boronic acids F-**1** in 28-60% yield.



Scheme 80: Two-step lithiation/borylation synthesis of fluoro-2-FPBAs F-**1** from bromobenzaldehydes **198a-d**.

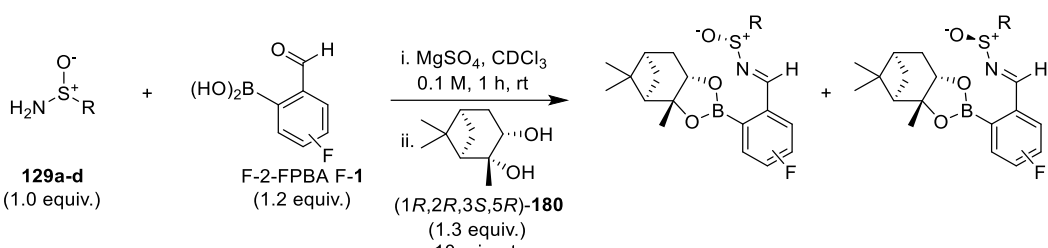
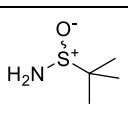
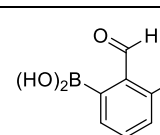
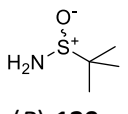
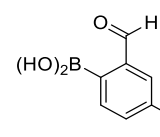
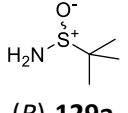
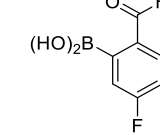
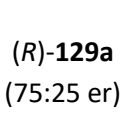
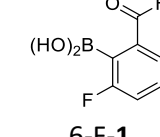
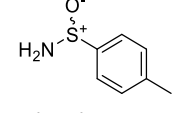
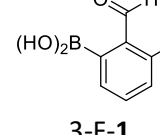
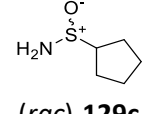
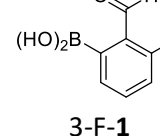
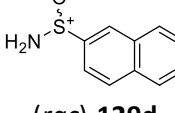
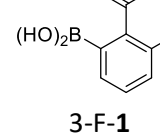
As previously shown when discussing the mechanisms of Bull-James assemblies (see section 1.3.2), 2-formylphenylboronic acids exist in an equilibrium with their tautomeric benzoxaboroles, in a process that is driven by the activation of the aldehyde towards nucleophilic attack by water. Benzoxaboroles were seen for all four isomers of F-2-FPBA, with the ratio of F-**1** to F-**1**' drastically affected by the location of the fluorine substituent, ranging from 60:40 for 3-F-**1** to 96:4 for 5-F-**1**. These values are comparable to those previously reported by Kowalska *et al.*,<sup>120</sup> with the slight variation easily accounted for by varying levels of water in the substrates or solvent (Scheme 81). However, reversible equilibration with their aldehydes meant that the presence of these benzoxaborole tautomers did not affect the ability of these fluorinated 2-FPBAs to function as effective templates in SIBE forming reactions, although this may account for the variable conversion observed by us (*vide infra*) and Oe (*vide supra*).<sup>164</sup>



Scheme 81: Tautomeric equilibrium of 2-FPBA derivatives. <sup>a</sup> Literature values from Kowalska *et al.*, 2016.<sup>120</sup>

With all four fluoro-2-FPBAs in hand, each was separately employed in a three-component assembly with Ellman's sulfinamide **129a** to assess their suitability as fluorinated templates for carrying out <sup>19</sup>F NMR analysis of *dr*'s (Table 8, entries 1-4). Pleasingly, use of the new stepwise one-pot derivatisation conditions resulted in reaction of all four fluorinated templates achieving 88-99% conversion to the corresponding diastereomeric fluorinated SIBEs when they were reacted in three-component reactions with sulfinamide **129a** and pinanediol **180**. The *dr* of the resulting complexes was determined by both <sup>1</sup>H and <sup>19</sup>F NMR spectroscopy, confirming once again that no kinetic resolution was occurring, with all *dr*'s found to be between 65:35 and 69:31, in good agreement with the known 33% *ee* of the parent sulfinamide analyte (expected 67:33 *dr*). Different baseline-resolved diastereomeric chemical shift differences  $\Delta\delta_H/\Delta\delta_F$  were observed for each of the four fluorinated templates, with 4-F-**1** consistently producing diastereomeric fluorinated SIBEs with the lowest chemical shift differences, exhibiting a  $\Delta\delta_H$  value for their imine resonances of -0.029 ppm and a  $\Delta\delta_F$  value of only 0.170 ppm, respectively (Table 8, entry 4). Conversely, use of 3-F-**1** produced fluorinated SIBEs with the biggest differences in chemical shift, producing a respectable  $\Delta\delta_H$  for their imine resonances of -0.064 ppm and a remarkable  $\Delta\delta_F$  of -2.328 ppm, respectively (Table 8, entry 1). Consequently, 3-F-**1** was selected as the fluorinated template to derivatize three further (*rac*)-sulfinamides **129b-d**, all of which afforded diastereomeric sulfiniminoboronates with consistently high  $\Delta\delta_H$  and  $\Delta\delta_F$  and conserved 50:50 diastereomeric ratio (Table 8, entries 5-7).

Table 8: Three-component assembly of sulfonamides **129a-d** with fluorinated FPBA derivatives and pinanediol **180**.

						
Entry	(rac)-Sulfonamide	2-FPBA	Conversion (%) <sup>a</sup>	dr <sup>b</sup>	$\Delta\delta_H$ (ppm) <sup>c,d</sup>	$\Delta\delta_F$ (ppm) <sup>d,e,f</sup>
1	 <b>(R)-129a</b> (75:25 <i>er</i> )	 <b>3-F-1</b>	88	68:32 68:32	-0.064	-2.328
2	 <b>(R)-129a</b> (75:25 <i>er</i> )	 <b>4-F-1</b>	99	65:35 66:34	-0.029	-0.170
3	 <b>(R)-129a</b> (75:25 <i>er</i> )	 <b>5-F-1</b>	99	66:34 67:33	-0.079	+0.197
4	 <b>(R)-129a</b> (75:25 <i>er</i> )	 <b>6-F-1</b>	94	69:31 68:32	-0.201	-0.578
5	 <b>(rac)-129b</b>	 <b>3-F-1</b>	37	49:41 49:41	-0.063	-1.188
6	 <b>(rac)-129c</b>	 <b>3-F-1</b>	87	50:50 50:50	0.042	1.457
7	 <b>(rac)-129d</b>	 <b>3-F-1</b>	40	51:49 51:49	0.070	1.365

<sup>a</sup> Conversion determined by <sup>1</sup>H NMR spectroscopy. <sup>b</sup> dr determined by both <sup>1</sup>H (top) and <sup>19</sup>F (bottom) NMR spectroscopy.

<sup>c</sup>  $\Delta\delta_H$  is the chemical shift difference between the imine protons of the diastereomeric sulfiniminoboronate esters in their <sup>1</sup>H NMR spectra. <sup>d</sup> A negative value indicates that the homochiral complex was most deshielded. <sup>e</sup>  $\Delta\delta_F$  is the chemical shift difference between the fluorine resonances of the diastereomeric sulfiniminoboronate esters. <sup>f</sup> Quantitative <sup>19</sup>F{<sup>1</sup>H} NMR experiments carried out using a *T*<sub>1</sub> relaxation time of 30 s.

The detection limits of this new dual proton/fluorous approach were then assessed by carrying out the self-assembly reaction of 3-F-**1** and enantiopure pinanediol (1*R*,2*R*,3*S*,5*R*)-**180** with Ellman's sulfinamide (*R*)-**129a** at relatively high *ee* levels of 75%, 90% and 96%, which were prepared from enantiopure commercial samples (Figure 42). Analysis of the resultant mixtures of sulfiniminoboronate esters revealed diastereomeric excesses (*de*) of 75%, 91% and 95% (<sup>1</sup>H NMR) and 73%, 89% and 95% (<sup>19</sup>F NMR), respectively, all of which were well within usual error limits when using chiral derivatizing agents to determine *ee*'s by NMR spectroscopy.

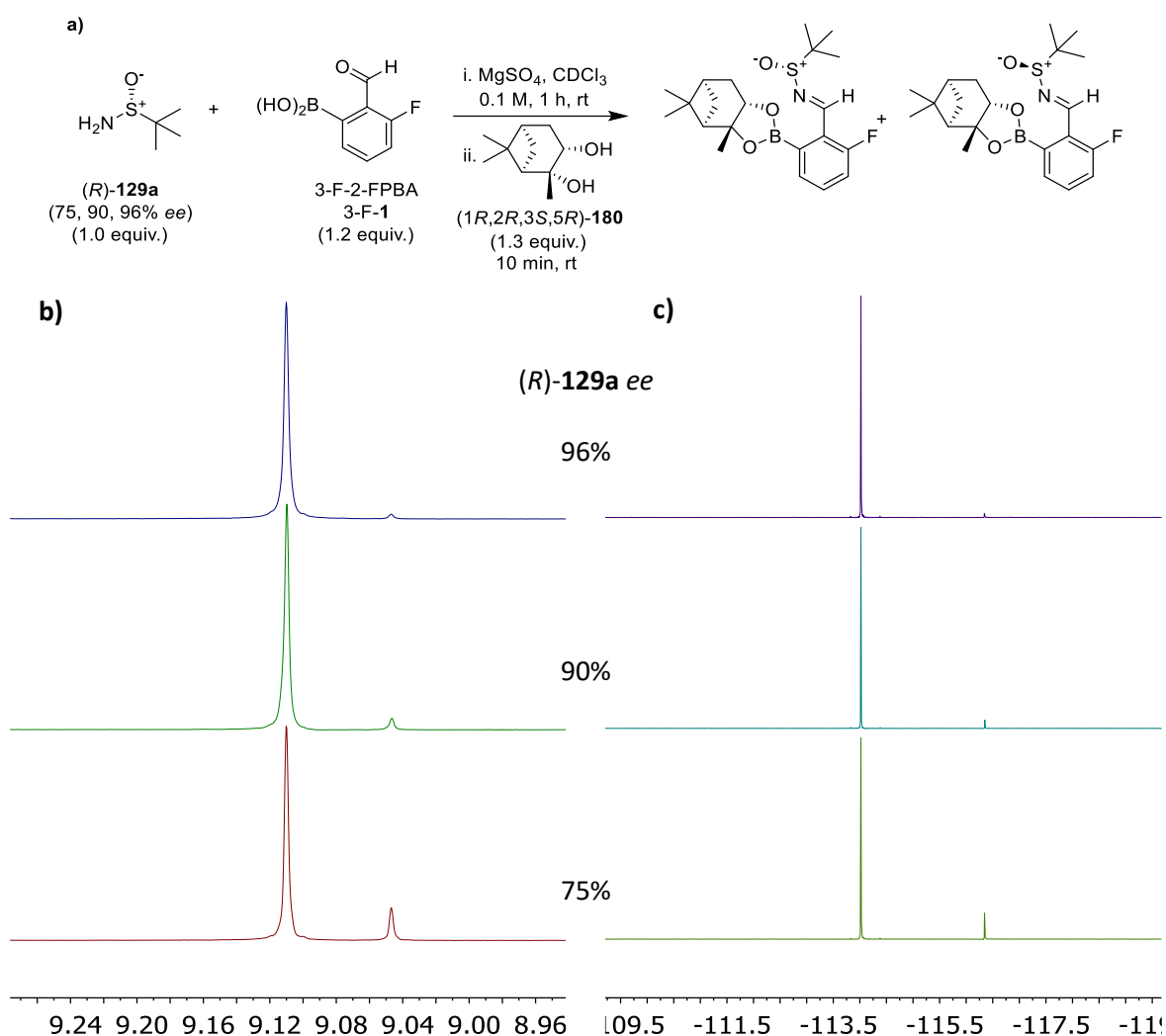


Figure 42: (a) Three-component assembly of 3-F-**1**, (1*R*,2*R*,3*S*,5*R*)-**180** and (*R*)-**129a** (75%, 90% and 96% *ee*). (b) Expanded <sup>1</sup>H NMR spectra of complexes formed from reaction the reaction in (a). (c) Expanded <sup>19</sup>F{<sup>1</sup>H} NMR spectra of diastereomeric complexes formed from reaction in (a).

### 3.2.2 Case example: Determining the *ee* of a commercial sample of 'enantiopure' Davis' sulfinamide

Having optimised and established the general applicability of the new CDA method, the new stepwise three-component CDA protocol was used to assess the enantiomeric excess of commercial samples of enantiopure (*R*)- and (*S*)-Davis' sulfinamide **129b** (purchased from Sigma-Aldrich). Both

$^1\text{H}$  and  $^{19}\text{F}\{^1\text{H}\}$  NMR analysis revealed that these “enantiopure” reagents were in fact scalemic, returning values of 90% *ee* for (*R*)-**129b** and 94% *ee* for (*S*)-**129b**, with both  $^1\text{H}$  and  $^{19}\text{F}$  NMR results in perfect agreement for each sample (Figure 43). Although the agreement between both nuclei strongly indicates these results are accurate, they were further confirmed by chiral HPLC analysis (see Appendix B). The discovery that these ‘sold as enantiopure’ sulfinamides were in fact scalemic was an important finding, as these ‘enantiopure’ Davis’ sulfinamide chiral auxiliaries are primarily employed as chiral auxiliaries for the asymmetric synthesis of chiral amines that are used in drug-discovery applications. Use of 90% *ee* sulfinamide **129b** as a chiral auxiliary would in most cases produce a 90% *ee* product, with the presence of the minor enantiomeric product having significant potential toxicity/regulatory issues if used to prepare drug molecules.

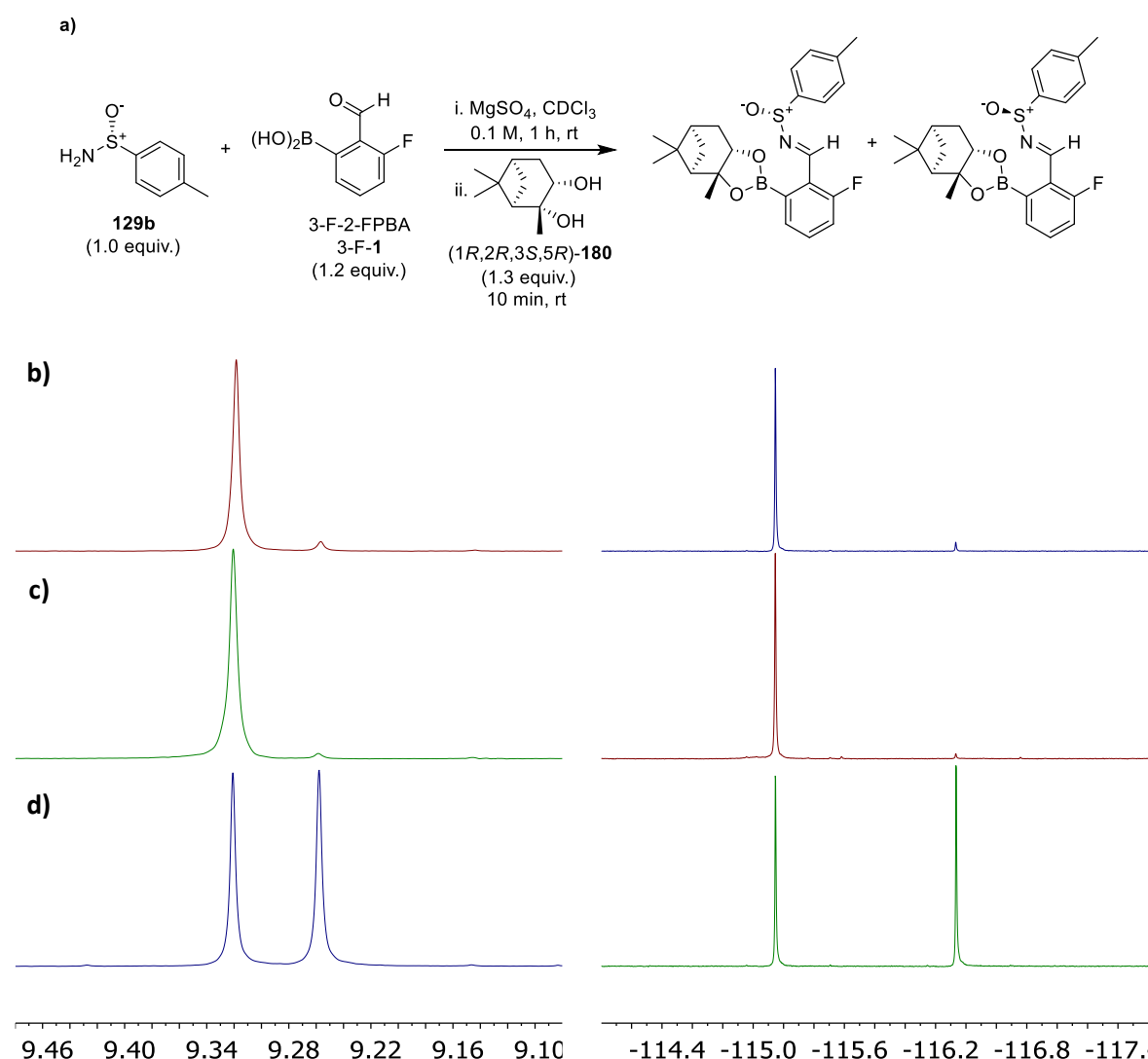
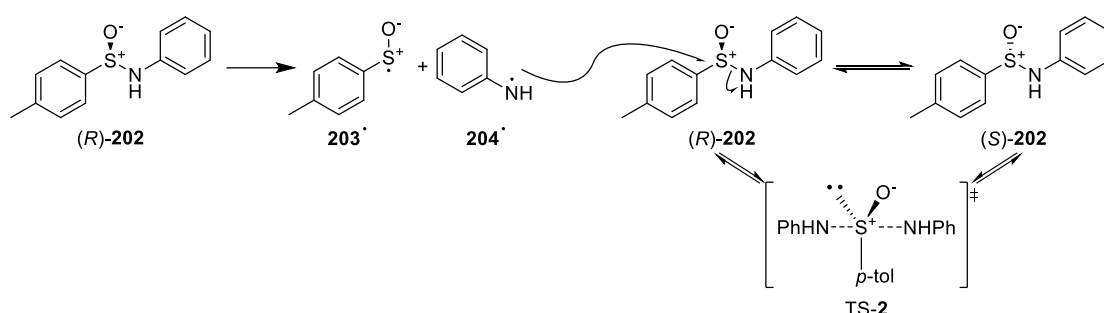


Figure 43: (a) Three-component assembly of 3-F-1, (1*R*,2*R*,3*S*,5*R*)-**180** and (*R*)-**129b** (varying *ee*). Expanded  $^1\text{H}$  (left) and  $^{19}\text{F}\{^1\text{H}\}$  (right) NMR spectra of diastereomeric complexes formed from the reaction in (a) using commercial ‘enantiopure’ samples of Davis’ sulfinamide (*R*)-**129b** (b) and (*S*)-**129b** (c), revealing ‘true enantiopurities’ of 90% and 94% *ee*, respectively. (d) Identical assembly with (*rac*)-**129b** for comparison purposes.

Sigma-Aldrich are a reputable chemical supplier who have rigorous testing procedures in place to determine the enantiopurity of any chiral compounds that they sell, so it was hypothesised that

'aged' samples of Davis' sulfinamide might have partially racemised over time. As discussed previously, these primary sulfinamides are considered to be configurationally stable, however only very limited work into their racemisation has been reported in the literature. The only significant aryl-sulfinamide racemization study found in the literature was carried out by Cram *et al.* in 1972, who reported that *S,N*-aryl sulfinamides such as **202** could racemise rapidly in solution at room temperature, through an *N*-aryl radical cleavage addition mechanism (see Scheme 82 for details).<sup>355</sup> This dissociative mechanism was supported by both kinetic and crossbreeding experiments, with no apparent indication of pyramidal inversion, despite the potential of the extended aniline-toluylsulfinamide conjugated system. However, since this racemization mechanism is heavily dependent on the generation of stable *N*-aryl radical **203**, it is unlikely to occur in primary sulfinamide systems due to the short lifetime and instability of the required amino radical  $\cdot\text{NH}_2$ .

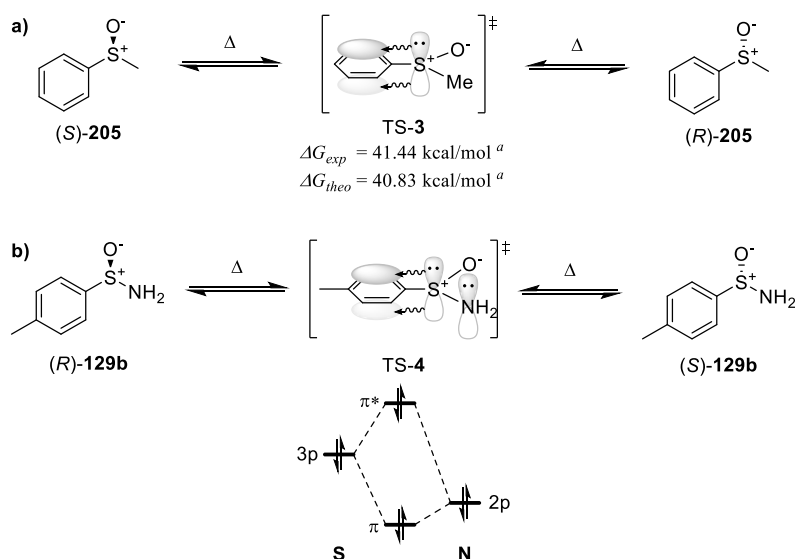


Scheme 82: Radical-chain racemization of aryl sulfinamides proposed by Cram *et al.*<sup>355</sup>

Studies on and exploitation of the racemization/inversion of chiral sulfoxides are far more common,<sup>356,357</sup> with aryl sulfoxides such as methyl phenyl sulfoxide **205** (most similar to Davis' sulfinamide **129b**) thought to racemize *via* a pyramidal *S*-inversion mechanism (Scheme 83a).<sup>358,359</sup> Experimental and theoretical works are in good agreement on this, reporting comparable experimental and theoretical activation energies  $\Delta G^\ddagger$  of 41.44 kcal/mol and 40.83 kcal/mol for **205**, respectively (very high barrier).<sup>358</sup> These inversion reactions proceed *via* an *S*-planar trigonal bipyramidal transition state TS-3, in which the sulfur lone pair resides in an axial p-orbital, with adjacent aromatic systems shown to stabilise the transition state through resonance stabilisation, with *para*-electron-withdrawing substrates racemising faster than *para*-electron-donating species. This inversion process has also been shown to be catalysed by the presence of acid, likely through reversible protonation of the sulfoxide  $\text{O}^-$  group, which further stabilises the transition state. Similar sulfur inversion processes are also known for related aryl thiosulfinates, with unwanted racemisation events the reason why enantioselective oxidation protocols are not generally used to synthesise Davis' auxiliary **129b** (see section 2.1.4).<sup>360</sup> Although no discussion of the pyramidal inversion of primary sulfinamides could be found in the literature, it seems plausible that aryl sulfinamides such as (*S*)-**129b** could also undergo the same racemisation process, proceeding *via* trigonal bipyramidal transition state TS-4, with resonance stabilisation from its *p*-toluyl substituent lowering the barrier to inversion (Scheme 83b). Unlike sulfoxides, however, sulfinamides contain an amino group, which will significantly disfavour formation of TS-4 by creating a disfavoured 4-electron system with a filled antibonding  $\pi^*$  orbital, as shown in the molecular orbital (MO)

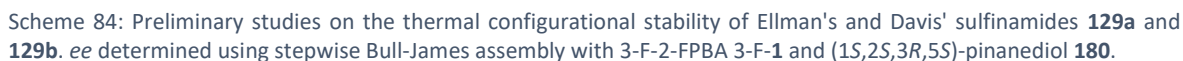


interaction diagram below. One would therefore expect sulfinamide pyramidal inversions to proceed *via* a higher energy transition state than their corresponding sulfoxide analogues, thus leading to more configurationally stable *S*-stereocentres.



Scheme 83: Racemisation by pyramidal atom inversion of chiral sulfoxide **205** (a), and sulfinamide **129b** (b, proposed) and disfavoured p-p MO interaction in TS-4. <sup>a</sup> Literature values.<sup>358</sup>

Since measurements of the *ee* of samples of both sulfinamides **129a** and **129b** carried out throughout this project over a period of many months returned consistent values, with no apparent change in enantiopurity over this period, it would appear that thermal racemisation of primary sulfinamides at room temperature is slow. Therefore, in order to investigate whether thermal racemisation in solution could potentially result in racemisation of the sulfur stereocentres of sulfinamides, commercial samples of Davis' sulfinamide (*S*)-**129b** (94% *ee*) and Ellman's sulfinamide (*S*)-**129a** (> 99% *ee*) stirred them in CHCl3 (0.1 M) at room temperature. Aliquots of these solutions were then removed over time, and their *ee*'s determined using the new stepwise Bull-James assembly method using template 3-F-**1** and pinanediol (1*S*,2*S*,3*R*,5*S*)-**180**, which revealed that no racemization was occurring over time. Crystalline samples of both sulfinamides were also heated at 65 °C in air (in a thermostated oven), with no racemisation of solid Ellman's sulfinamide (*S*)-**129a** (> 99% *ee*) observed after a week in the oven. However, the *ee* value of Davis' sulfinamide (*S*)-**129b** changed significantly over time at 65 °C, dropping from 94% to 44% *ee* (72:28 *er*) after just 48 h, and being completely racemised after days. Therefore, these results suggest that aryl sulfinamides are more stereo-labile than is appreciated in the chemical literature, with potentially serious implications for any synthetic procedures employing Davis' auxiliary for extended periods of time or at high temperature.



Reaction scheme for the synthesis of 206:

129a (a bis-sulfonamide derivative) reacts in toluene at 110 °C for 48 h to form 206 (a cyclic sulfonamide derivative) in 70% yield.

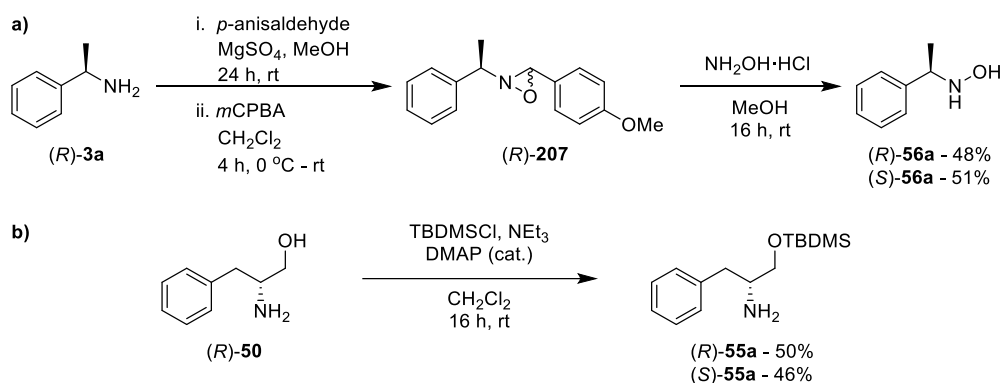
The reaction proceeds via a cyclic intermediate (shown in brackets) which loses  $\text{NH}_3$  to form the final product 206.

Scheme 85: Thermal rearrangement of (*R*)-*tert*-butanesulfinamide (*R*)-**129a** to sulfonamide **206** reported by Arava *et al.*, and proposed mechanism.<sup>361</sup>

### 3.3.1 Pinanediol as a general chiral reporter

125

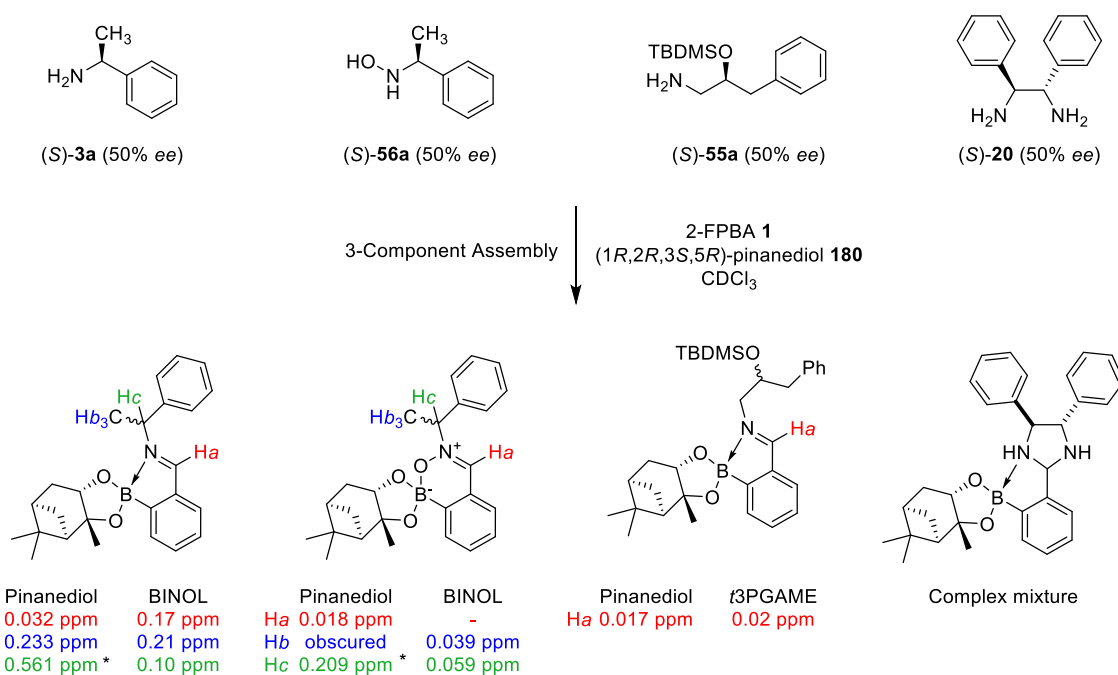
enantiomers of chiral *N*-phenylethyl hydroxylamine **56a** and *O*-TBDMS-phenylpropanamine **55a** needed to be prepared following known literature procedures. Both hydroxylamine **56a** enantiomers were prepared in two steps from the corresponding enantiopure  $\alpha$ -methylbenzylamine **3a** according to a previously published method by Wovkulich *et al.* (Scheme 86a).<sup>143,362</sup> Chiral amine **3a** was subjected to imine condensation with *p*-anisaldehyde to afford a chiral imine, that was then oxidised in one pot using *meta*-chloroperbenzoic acid (*m*CPBA) to afford oxaziridine **207**. The second step then involved ring opening of oxaziridine **207** with hydroxylamine to afford hydroxylamines (*R*)-**56a** and (*S*)-**56a** in 48% and 51% yields over two steps, respectively. The synthesis of *O*-TBDMS-phenylpropanamine **55a** was carried out in a single step from enantiopure 1,2-amino alcohol **50a**, which was treated with TBDMS-Cl in the presence of a catalytic amount of DMAP to afford the desired enantiopure protected products (*R*)-**55a** and (*S*)-**55a** in 50% and 46% yields, respectively (Scheme 86b).



Scheme 86: Synthesis of enantiopure hydroxylamines **56a** and *O*-TBDMS amino alcohols **55a** analytes (shown for (*R*)-starting materials for clarity).

All four classes of analyte were then subjected to one-pot three-component assembly with 2-FPBA **1** and (1*R*,2*R*,3*S*,5*R*)-pinanediol **180**, using scalemic amine samples of 50% *ee* (prepared from the enantiopure products, Scheme 87). Assembly of the amine **3a**, hydroxylamine **56a**, and *O*-silyl amino alcohol **55a** proceeded smoothly to afford the expected diastereomeric iminoboronate complexes, with well-conserved 3:1 *dr*'s. In the case of the amine analyte **3a**, the <sup>1</sup>H NMR signals for the imine and  $\alpha$ -methyl protons could be used to determine enantiopurity, with good chemical shift differences of 0.032 ppm and 0.233 ppm respectively, comparable to those observed with BINOL (*cf.* 0.17 and 0.21).<sup>142</sup> Although the  $\alpha$ -methine proton saw an impressive  $\Delta\delta_H = 0.561$  ppm (*cf.* 0.10 ppm for BINOL **9**),<sup>145</sup> these signals overlapped in part with pinanediol peaks, and so could not be used to determine enantiopurity. The assembly of hydroxylamines **56a** produced resolved signals for the imine protons of their IBE diastereomers, albeit with a relatively low chemical shift difference of 0.018 ppm. Once again, although the  $\alpha$ -methine <sup>1</sup>H NMR signal exhibited an impressive  $\Delta\delta_H = 0.209$  ppm (*cf.* 0.059 ppm for BINOL **9**),<sup>143</sup> overlap with unreacted pinanediol peaks meant these resonances could not be integrated to determine *ee*. The assembly of *O*-silylated amino alcohols **55a** with a pinanediol chiral reporter also resulted in several differentiated diastereomeric <sup>1</sup>H NMR signals, with the clear imine singlets exhibiting a baseline-resolved chemical

shift difference of 0.017 ppm, comparable to the 0.02 ppm achieved with the original *trans*-3-phenylglyceric acid methyl ester ligand (t3PGAME).<sup>142</sup> Although the vast majority of other signals seemed to be differentiated, the diastereotopicity of the analyte protons and the crowded nature of the aliphatic region of these spectra led to no additional clearly useable resonances for determining *ee*. Finally, the <sup>1</sup>H NMR spectrum resulting from the assembly of *trans*-diphenylethylene diamine **20** resulted in a complex mixture of products, with multiple overlapping peaks and no clearly defined diastereomeric complexes. The increased strain of this type of imidazolidine has already been discussed at length (see section 1.4.2), and it follows that the increased steric bulk of pinanediol over BINOL<sup>138</sup> leads to incomplete conversion and formation of complex mixtures of imidazolidine and imine products. Therefore, whilst derivatisation of sulfinamides, chiral amines, hydroxylamines, and *O*-silyl-amino alcohols using enantiopure pinanediol **180** and 2-FPBA **1** produces diastereomeric IBE complexes whose imine resonances are well resolved in their <sup>1</sup>H NMR spectra, the added steric demand of pinanediol means that it is probably wise to avoid its general use as a chiral selector when the *ee*'s of sterically demanding chiral substrates need to be determined. Use of the initially optimised diol is therefore still recommended for determining the *ee* of known Bull-James analytes.

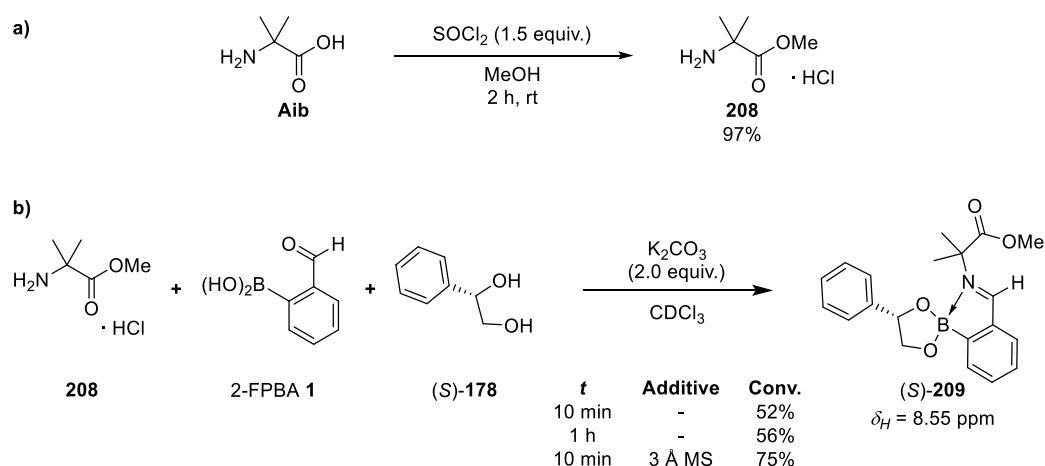


Scheme 87: Three-component assembly of 2-FPBA **1**, (1*R*,2*R*,3*S*,5*R*)-**180**, and various known analytes and previously reported and resulting  $\Delta\delta_H$ 's.<sup>138,142,143,145</sup> \* Not suitable for determining *ee* due to overlap with adjacent peaks.

### 3.3.2 Preliminary investigations into the Bull-James assembly of $\alpha$ -quaternary amino acids

Building on the successful Bull-James derivatisation of poorly-nucleophilic bulky sulfinamide analytes, attention was turned towards developing a method to measure the enantiopurity of sterically-demanding  $\alpha$ -quaternary amino esters, which are widely used as chiral building blocks in

the fields of medicinal chemistry, peptidomimetics/foldamer, are of interest to origin-of-life scientists, and are found in natural products.<sup>363–369</sup> Interestingly, despite the broad range of applications of the Bull-James assembly to determine the *ee* of chiral amines, its use to measure the *ee* of  $\alpha$ -quaternary species has never been reported to date. Although the nucleophilicity of these substrates should be comparable to other types of amine analytes, it was anticipated that the sterically-encumbered nature of the  $\alpha$ -amino position could lead to decreased reactivity, with possible disruption of  $N \rightarrow B$  coordination as seen for sulfinamides. Unfortunately, chiral  $\alpha$ -quaternary amino esters are expensive (*e.g.* > £200/g for 500 mg  $\alpha$ -methyl-L-valine), and so preliminary assembly studies were carried out using achiral 2-aminoisobutyric acid methyl ester hydrochloride **208** (synthesised in-house from Aib, Scheme 88a) to assess whether this class of quaternary amine substrates would successfully assemble with the template (Scheme 88b). Pleasingly, equimolar reaction of **208** with 2-FPBA **1** and (*S*)-**178** in CDCl<sub>3</sub> achieved 52% conversion to a new  $\alpha$ -quaternary IBE product (*S*)-**209**, as indicated by the presence of a new <sup>1</sup>H NMR singlet imine resonance at 8.55 ppm. A quick series of experiments demonstrated that an increased reaction time of 1 h only led to a marginal increase in conversion to 56%, however addition of 3 Å molecular sieves afforded (*S*)-**209** in 75% yield after only 10 min.



Scheme 88: (a) Synthesis of **208** from Aib. (b) Three-component assemblies of **208**, 2-FPBA **1** and (*S*)-**178**.

Following these promising preliminary results, the assembly of commercially-available (*rac*)- $\alpha$ -methyl phenylalanine methyl ester hydrochloride (*rac*)-**210** with 2-FPBA **1** and (*S*)-**178** in the presence of K<sub>2</sub>CO<sub>3</sub> was carried out (Table 9). Again, limited 52% conversion to the desired IBEs **211a** and **212a** was observed. However, to our delight, two singlet peaks at 8.249 ppm and 8.292 ppm were produced with a chemical shift difference  $\Delta\delta_H = 0.043$  ppm for the imine resonances of the diastereomeric IBE complexes. As for Aib methyl ester hydrochloride **208**, conversion could be significantly improved to 81% by addition of 3 Å MS (Table 9, entry 1). Unfortunately, small amounts of overlap were observed between the diastereomeric resonances, and so a short diol screen was carried out in an attempt to further maximise  $\Delta\delta_H$ . Pleasingly, most diols reacted to form the desired IBEs in limited 28–52% yield, with measurable chemical shift differences in all but two instances (BINOL **9** and 1,3-butanediol **176**, Table 9, entries 4 and 6). 1-Phenylpropane-1,3-diol **128** was the

only chiral reporter to produce fully baseline-resolved diastereomeric imine resonances in the  $^1\text{H}$  NMR spectrum (Table 9, entry 8). Interestingly, this screen supports the earlier observation that pinanediol **180** appears generally unsuitable as a chiral reporter for sterically-crowded analytes, as it was found to only produce a small  $\Delta\delta_{\text{H}} = 0.010$  ppm with no baseline resolution. Although a smaller chemical shift difference was produced by phenylpropanediol **179** than by original diol **128**, its noticeably sharper singlet peaks led to baseline resolution where the latter did not (Figure 44). Therefore, having optimised the diol chiral reporter and demonstrated that conversion could be improved to high levels, it is clear that the Bull-James assembly CDA approach is likely to be a viable method for determine the *ee* of  $\alpha$ -quaternary amino acids/esters, and by extension sterically-demanding  $\alpha$ -quaternary amines and amine derivatives.



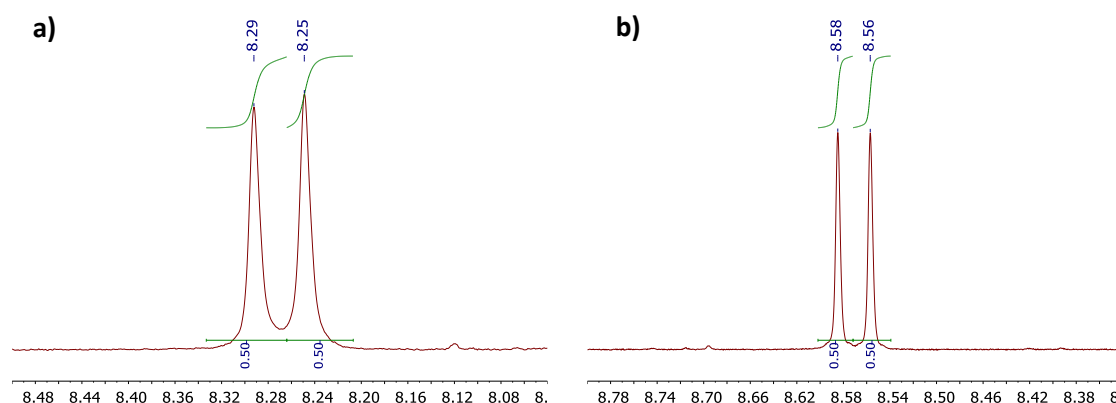


Figure 44: Expanded imine region of the  $^1\text{H}$  NMR spectra of complexes formed from the three-component assembly of 2-FPBA **1**, (*rac*)-**210**, and (*rac*)-phenylethanediol **128** (a) or (*R*)-phenylpropanediol **179** (b). Same scale for both spectra.

### 3.4. Conclusions and future work

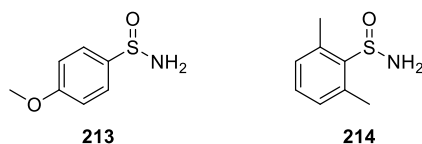
In conclusion, the third chapter of this thesis describes the successful optimisation, development and testing of a novel three-component stepwise Bull-James assembly chiral derivatizing agent methodology for determining the *ee* of chiral primary sulfinamides by  $^1\text{H}$  NMR spectroscopic analysis. The popularity of primary sulfinamides, predominantly employed as chiral auxiliaries, leads us to believe that this novel CDA method, that was published in *The Journal of Organic Chemistry*,<sup>294</sup> will be of use to many synthetic research groups.

Building on results arising from formation of the DAIA-affected BINOL-SIBE complexes described in chapter two, a diol chiral reporter screen was carried out to maximise the chemical shift difference between diastereomeric imine resonances, which identified pinanediol as the optimal ligand for the three-component assembly of sulfinamides and 2-FPBA **1**. Next, a series of optimisation experiments determined that optimal conditions for these assemblies required a modified two-step process, wherein the analyte and 2-FPBA template were first combined in a high-yielding two-component assembly, followed by addition of the pinanediol reporter to produce the desired SIBE products. The unexpected revelation that N $\rightarrow$ B coordination was absent in SIBEs, along with the optimisation studies, provided key insights into the likely mechanisms behind formation of these assemblies. The scope of this new methodology was demonstrated by successfully derivatizing a series of eight chiral sulfinamides. Further expansion of the methodology to  $^{19}\text{F}$  NMR spectroscopy was achieved by incorporation of a fluorine atom into the 2-FPBA template, with screening experiments revealing that 3-F-**1** was the optimal fluorinated template for these sulfinamides, achieving excellent  $\Delta\delta_F$  values in all cases. Throughout this work, great care has been taken to ensure that no racemisation, kinetic resolution, or DAIA-effects occur, thus ensuring that this novel stepwise protocol for the derivatization of sulfinamides is robust, accurate, and reliable.

The excellent detection limits of this method were illustrated for analysis of the *ee* of commercial samples of Davis' sulfinamide **129b**, which revealed both enantiomers were not in fact enantiopure as advertised, instead ranging from 90-96% *ee*. A brief investigation into the thermolability of Davis



sulfinamide showed it was not as configurationally stable as the wider chemical literature might imply, racemizing fully over a period of 7 days at 65 °C. Since the enantiopurity of chiral auxiliaries is crucial for the successful development and implementation of asymmetric syntheses, this is a potentially very important observation, with work now underway to better understand this racemization process and design analogues of Davis' sulfinamide with increased configurational stability by introducing either electron-donating groups or *ortho*-substituents (*e.g.*, **213** or **214**, Scheme 89).



Scheme 89: Proposed structures of Davis' sulfinamide analogues with increased chiral stability.

Finally, preliminary results have been reported for the three-component assembly of  $\alpha$ -methyl phenylalanine methyl ester hydrochloride, with a diol screen revealing that (*R*)-phenylpropanediol **179** was the best chiral reporter, producing a chemical shift difference for the corresponding diastereomeric IBE imine resonances of 0.028 ppm with full baseline resolution. Further optimisation of this method should yield a versatile CDA approach suitable for determining the enantiomeric excess of a range of  $\alpha$ -quaternary amine derivatives, which are known to often be ill-suited to more classical Mosher-type CDA analysis. Structural work will also provide interesting insight into the absence, presence or strength of an IBE N $\rightarrow$ B bond in these systems, building on these new discoveries on the behaviour of sterically-demanding and non-coordinated IBEs.

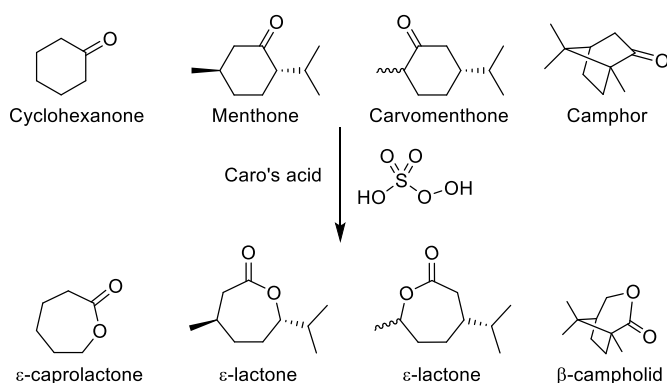
## 4. *N*-OXIDE-CATALYSED BAEYER-VILLIGER OXIDATION REACTIONS OF KETONES AND $\alpha,\beta$ -UNSATURATED KETONES

The remaining research and discussion chapter in this thesis describes a project looking at using *N*-oxides as catalysts for carrying out Baeyer-Villiger (BV) oxidation reactions, which was carried out in parallel to the work on Bull-James IBE assemblies described in the preceding three chapters. The work presented focuses on the optimisation of new catalytic BV oxidation protocols for the oxidation of ketones and  $\alpha,\beta$ -unsaturated ketones that produce esters and vinyl esters in good yields. It begins with a brief introduction to the Baeyer-Villiger oxidation reaction of ketones and  $\alpha,\beta$ -unsaturated ketones, discusses the reactivity profiles of vinyl esters, before providing a summary of previous work on the development of *N*-oxides as catalysts for BV reactions in the Bull group. This section is then followed by a discussion of new investigations into optimising these catalytic BV reactions for the synthesis of vinyl esters in good yields, with mechanistic investigations into the role of the *N*-oxide catalyst in these BV reactions, and their unexpected degradation effects on *m*CPBA leading to identification of new 2<sup>nd</sup> generation conditions for carrying out *N*-oxide catalysed BV reactions.

### 4.1. The Baeyer-Villiger oxidation reaction and its use for the synthesis of vinyl esters

#### 4.1.1 *The Baeyer-Villiger oxidation reaction*

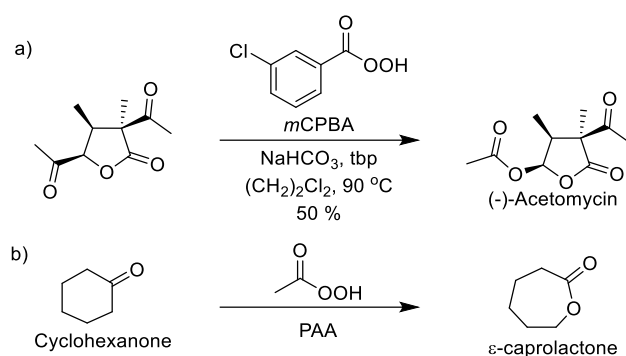
Now a staple of organic synthesis, Baeyer-Villiger oxidation reactions of ketones were first described in 1899 by Adolf von Baeyer and Victor Villiger.<sup>370</sup> In their seminal paper, they reported the solvent-free conversion of cyclic ketones to lactones using Caro's acid (peroxymonosulfonic acid, H<sub>2</sub>SO<sub>5</sub>), demonstrating its use for the BV oxidation of cyclohexanone and a range of terpenoid ketones (Scheme 90).



Scheme 90: Original report of the Baeyer-Villiger oxidation of terpenoids and cyclohexanone by Caro's acid.<sup>370</sup>

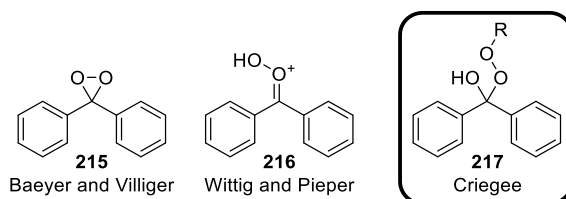
Since this initial report, the scope of the BV oxidation reaction has been expanded widely, so that it is now one of the most useful synthetic reactions available in the organic chemists' larder of

chemical transformations. A wide range of oxidants and/or catalysts are available to carry out a variety of BV reactions, including peroxides, peracids, peroxyimidic acids, Baeyer-Villigerase enzymes, MOFs, and zeolites. This means numerous BV protocols are available to oxidise many classes of ketone, with many of these methods demonstrating good functional tolerance, tuneable selectivity, and high levels of stereocontrol.<sup>371–374</sup> This versatility means the BV oxidation is now a ubiquitous reaction in organic synthesis, with applications ranging from its use for lab-scale total syntheses of natural products such as (-)-acetomycin,<sup>375</sup> through to industrial production of bulk chemicals such as  $\epsilon$ -caprolactone that is produced using peracetic acid on a 50,000 tonne scale annually (Scheme 91).<sup>376</sup>



Scheme 91: Representative applications of the Baeyer-Villiger oxidation reaction. (a) Total synthesis of (-)-acetomycin.<sup>375</sup> (b) Industrial production of  $\epsilon$ -caprolactone.<sup>376</sup>

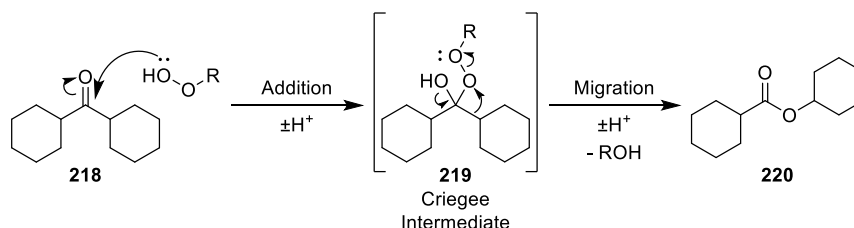
Many mechanisms were initially proposed for the Baeyer-Villiger oxidation, with all but three mechanisms discounted by 1950, with the three remaining intermediates for the BV oxidation of benzophenone shown in Scheme 92.<sup>377</sup> Both Baeyer and Villiger's dioxirane **215** and Wittig and Pieper's peroxide intermediates **216** require initial transfer of an oxygen atom from the peroxide to the ketone carbonyl oxygen, whilst the Criegee intermediate **217** requires nucleophilic attack of the peracid at the carbonyl carbon atom. This latter mechanism was eventually confirmed in 1953 by Doering and Dorfman, who studied the product distribution resulting from BV oxidation of <sup>18</sup>O-labelled benzophenone, with the resultant isotopic distribution confirming that the BV oxidation reaction proceeds *via* a Criegee intermediate.<sup>378</sup>



Scheme 92: Three potential intermediates proposed for the Baeyer-Villiger oxidation of benzophenone, as suggested by Doering and Speers.<sup>377</sup>

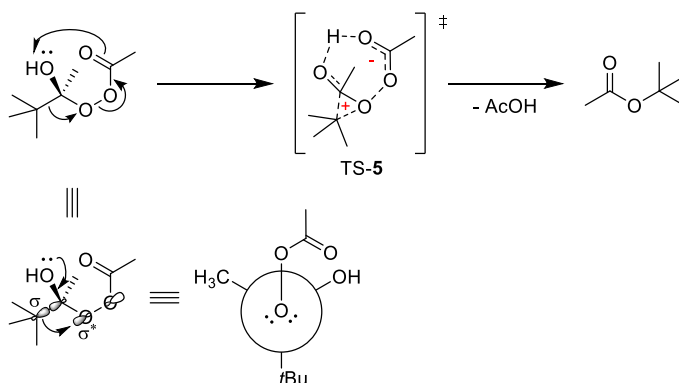
It is now widely accepted that classical Baeyer-Villiger reactions proceed *via* a two-step mechanism, which involves nucleophilic attack of the carbonyl by the peroxyacid, with associated proton transfer, resulting in a Criegee intermediate **217/220**. One of the carbon substituents then migrates

to the proximal oxygen atom, with concomitant cleavage of the weak peroxide bond occurring to produce an ester product (Scheme 93).



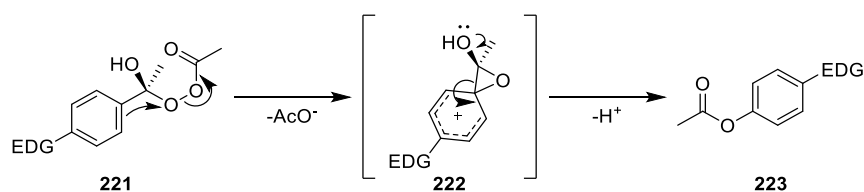
Scheme 93: Simplified mechanism of the Baeyer-Villiger oxidation reaction.

BV oxidation of a symmetric ketone such as **218** will produce a symmetric-substituted ester **220**, however, non-symmetric ketones can potentially form two distinct ester products (depending on which group migrates), with ester product ratios dependent on the migratory preference of the ketone's substituents. Work by Friess, Doering and Speers established the following migratory aptitude: tertiary alkyl > cyclohexyl > secondary alkyl > benzyl > phenyl > primary alkyl > methyl. Further investigations into the migration of substituted phenyl/aryl groups led to a secondary scale of migratory preference for substituted aryl groups: *p*-OMe > *p*-Me > *p*-H > *p*-Cl > *p*-Br > *p*-NO<sub>2</sub>.<sup>377,379</sup> As shown in Scheme 94, migration of non-aromatic groups occurs in a concerted manner, which is triggered by anti-periplanar alignment of the peracid and the migrating group (different mechanism for aryl migration, *vide infra*). The ensuing alignment of the C-C bonding  $\sigma$ - and O-O antibonding  $\sigma^*$ -orbitals allows electron migration from the former to the latter, with the migratory process driven by cleavage of the weak peroxide bond to produce stable ester and carboxylate/carboxylic acid products. These migration steps proceed *via* transition states such as TS-5, which contains a significant partial positive charge that is delocalised over the forming ester group and the migrating fragment. The ability of the migrating group to stabilise this charge is therefore crucial to lowering the overall energy of the transition state, leading to the observed trend whereby 'stabilising' tertiary alkyl groups migrate preferentially over 'non-stabilising' primary methyl groups. This explanation was originally postulated by Doering *et al.* nearly 70 years ago, and it has impressively stood the test of time, with this mechanistic proposal verified by more recent experimental and computational studies.<sup>380–382</sup>



Scheme 94: Migration step for the Baeyer-Villiger oxidation of pinacolone using peracetic acid as oxidant.

Migratory aptitude trends become even more pronounced when an aromatic group migrates, as  $\pi$ -participation from electron-rich systems can lower the transition state energy through a two-step migration process (Scheme 95).<sup>383</sup> In this instance, the aromatic  $\pi$ -system present in Criegee intermediate **221** can act as an internal nucleophile to attack the peroxide in an intramolecular fashion to eliminate a carboxylate leaving group. The resulting formal positive charge is now delocalised across the 5-atom conjugated system of stabilised arenium intermediate **222**, resulting in significant stabilisation of this intermediate (not a transition state). This non-aromatic phenonium intermediate can then collapse to afford ester **223**, resulting in rearomatisation and overall migration of the aryl unit. From these mechanistic considerations, it is evident that electron-rich aromatic systems will produce a more stabilised transition state intermediate, whilst electron-poor systems will tend to destabilise the transition state, thus explaining the reactivity trends observed in the 1950s.



Scheme 95: Mechanism of the migration of aromatic substituents in the Baeyer-Villiger reaction.<sup>383</sup>

#### 4.1.2 Syntheses and applications of vinyl esters

The synthetic versatility of vinyl esters and their presence as fragments in medicinally-active natural products (Figure 45) makes the availability of high yielding Baeyer-Villiger oxidation methodologies for their production highly desirable.<sup>384–386</sup>

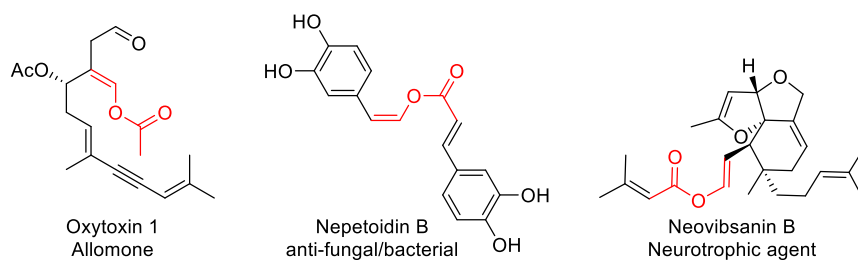
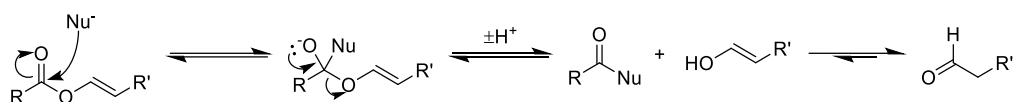
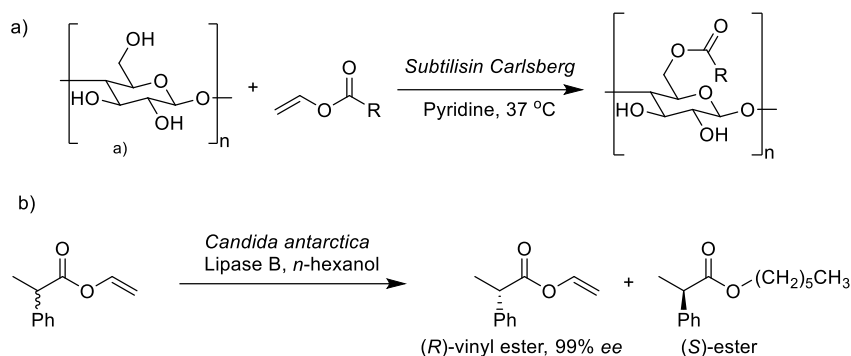


Figure 45: Examples of medicinally active natural products containing vinyl ester functionalities.<sup>384–386</sup>

The vinyl ester functionality is also synthetically useful, as its carbonyl group readily reacts with water or alcohol nucleophiles to produce new acid or ester products, respectively. However, contrary to classical ester groups, these reactions do not produce acid and alcohol by-products, as the resulting enol/enolate cleavage product rapidly tautomerizes to its corresponding aldehyde. This has the key benefit of rendering vinyl ester hydrolysis/alcoholysis processes essentially irreversible (Scheme 96), with vinyl esters commonly used as transesterification agents in polymerisation reactions and enzyme-catalysed kinetic resolution reactions that require irreversible reactions (Scheme 97).<sup>387,388</sup>

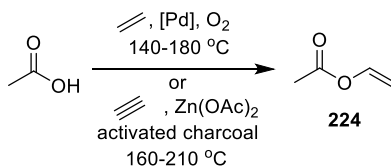


Scheme 96: General mechanism of nucleophilic attack of vinyl esters that produces aldehyde cleavage products.

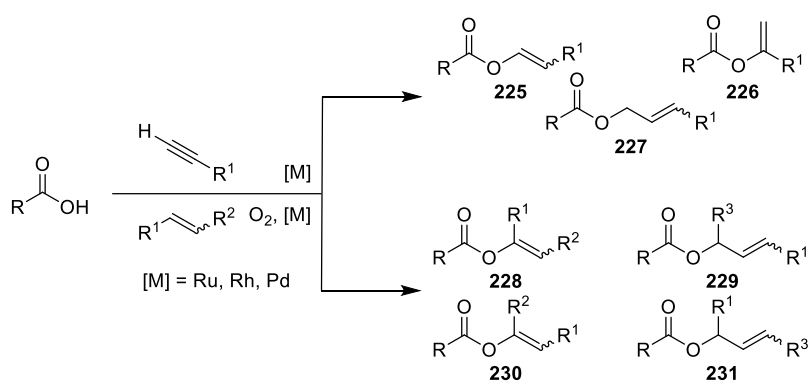


Scheme 97: Representative uses of vinyl esters – (a) Enzyme-catalysed transesterification of vinyl esters for the selective acylation of cellulose.<sup>387</sup> (b) Irreversible lipase-catalysed kinetic resolution of (*rac*)- $\alpha$ -aryl-carboxylic acids.<sup>388</sup>

Vinyl acetate **224** is by far the most widely produced vinyl ester, with an estimated annual production of over 6,000,000 tons (> \$7b per year), that is produced through of two different gas-phase processes (Scheme 98). The most widely used method employs palladium/alkali metal complexes to catalyse addition of acetic acid to acetylene using dehydrogenative/oxidative processes (80% production), whilst a  $\text{Zn}(\text{OAc})_2$ /activated charcoal catalyst is also used to add acetic acid across acetylene (~20% production).<sup>389,390</sup> Catalytic coupling of carboxylic acids with alkynes or alkenes (in the presence of an oxidant) has also been used for the synthesis of more complex vinyl esters, however these reactions often produce unwanted mixtures of (*E*)- and (*Z*)-vinyl esters **225**. Use of terminal alkynes can also lead to formation of Markovnikov products **226**, whilst terminal alkenes can undergo allylic ‘inner-sphere’ reactions to produce allylic esters **227**. Even greater complications arise when disubstituted alkene substrates are employed, often leading to formation of complex mixtures of products (*e.g.* **228-231**, Scheme 99).<sup>391–394</sup>



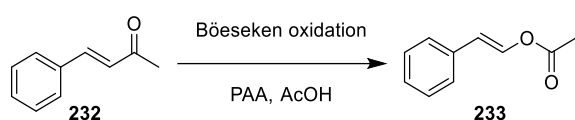
Scheme 98: Industrial-production of vinyl acetate from acetic acid.<sup>389</sup>



Scheme 99: Metal-catalysed syntheses of vinyl esters from carboxylic acids.<sup>391–394</sup>

#### 4.1.3 Early Baeyer-Villiger oxidation reactions of enone systems

An alternative method for preparing vinyl esters is to use a peroxide/peroxyacid to carry out a Baeyer-Villiger oxidation reaction of an  $\alpha,\beta$ -unsaturated ketone, which is the approach that will be investigated in this chapter. This BV method was first described in 1925 by Jacob Böeseken at the University of Delft (Figure 46).<sup>395,396</sup> Building on alkene/enone epoxidation approaches published earlier that century (*i.e.* Prilezhaev/Prileschajew and Weitz-Scheffer electrophilic and nucleophilic oxidation reactions, respectively),<sup>397,398</sup> Böeseken reported that reaction of benzalacetone (*E*)-**232** with peracetic acid (PAA) resulted in the formation of a new oxidised product, which he eventually identified as vinyl ester (*E*)-**233** after 5 years of pain-staking characterisation/mechanistic work (Scheme 100b).<sup>399–403</sup> This transformation was referred to as the “Böeseken oxidation”,<sup>404</sup> although like many of Böeseken’s methods this name is no longer in widespread use, with this transformation now subsumed under the broader umbrella of Baeyer-Villiger oxidations.



Scheme 100: (a) Böeseken oxidation of benzalacetone (*E*)-**232** to afford vinyl ester (*E*)-**233**.

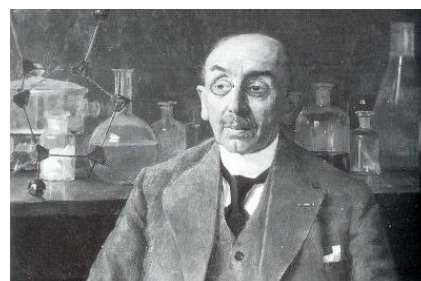
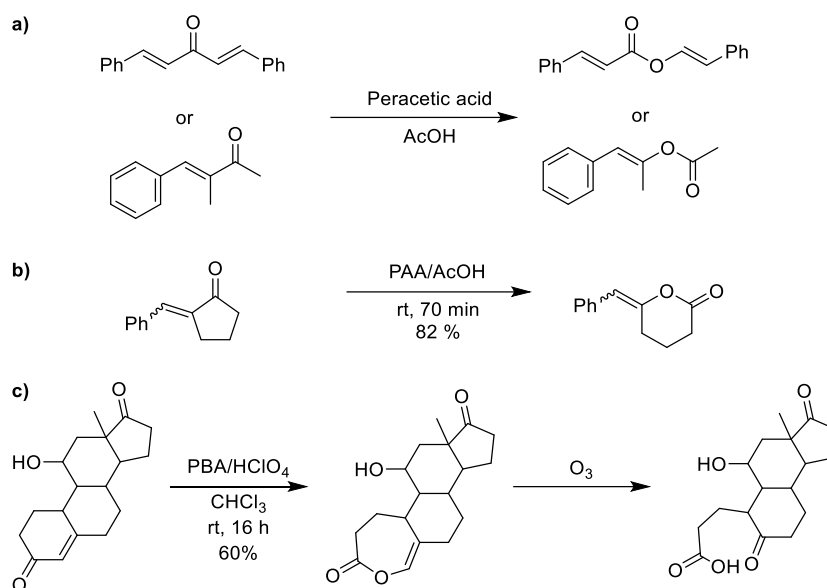


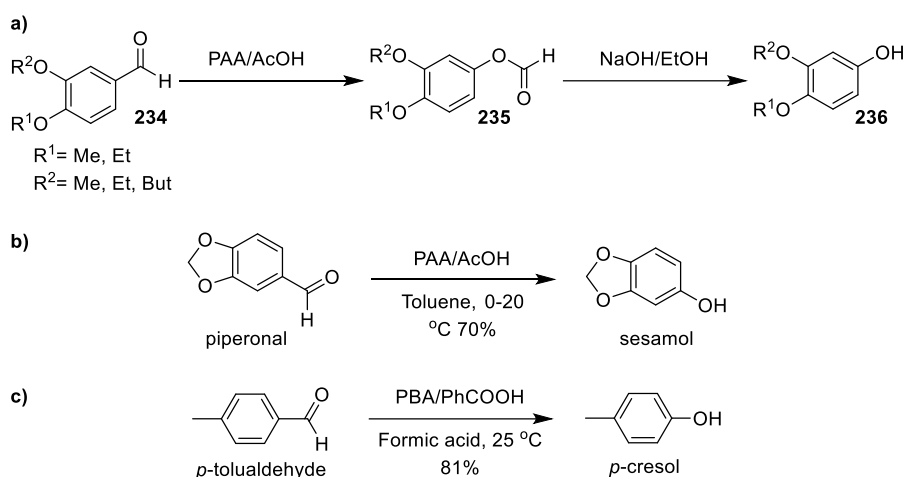
Figure 46: Prof. Jacob Böeseken at the University of Delft (source: Ernst Homburg collection)

Böeseken subsequently demonstrated that these peracid conditions could be used to successfully oxidise dibenzalacetone and  $\alpha$ -methyl benzalacetone to their corresponding esters (Scheme 101a),<sup>399,401</sup> with this BV reaction used regularly during the mid-20<sup>th</sup> century for both synthetic and structural elucidation purposes (Scheme 101b,c).<sup>405,406</sup>



Scheme 101: (a) Original Böeseken oxidation of a variety  $\alpha,\beta$ -unsaturated ketones.<sup>399,401</sup> (b) Böeseken oxidation of benzylidene cyclopentanone by Walton,<sup>405</sup> (c) Böeseken oxidation for structural elucidation of corticosteroids.<sup>406</sup>

Although this type of BV approach has not found widespread popularity for transforming conventional  $\alpha,\beta$ -unsaturated ketones into vinyl esters, the synthetic potential of this type of BV oxidation reaction has been realised for transforming aryl aldehydes and aryl ketones into their corresponding formyl and acyl esters, respectively. For instance, Böeseken showed that BV oxidation oxidations of benzaldehyde and acetophenone derivatives **234** could be used to produce their corresponding phenol esters **235** (Scheme 102),<sup>407,408</sup> with these esters then commonly hydrolysed to produce their corresponding phenols **236**. This alternative to the Dakin oxidation reaction (acid used instead of base, better functional group tolerance) has been applied to transform a range of aryl aldehydes for the synthesis of commercial phenol products (after hydrolysis of formate ester intermediates) such as sesamol and *p*-cresol (Scheme 102b,c).<sup>409–411</sup>

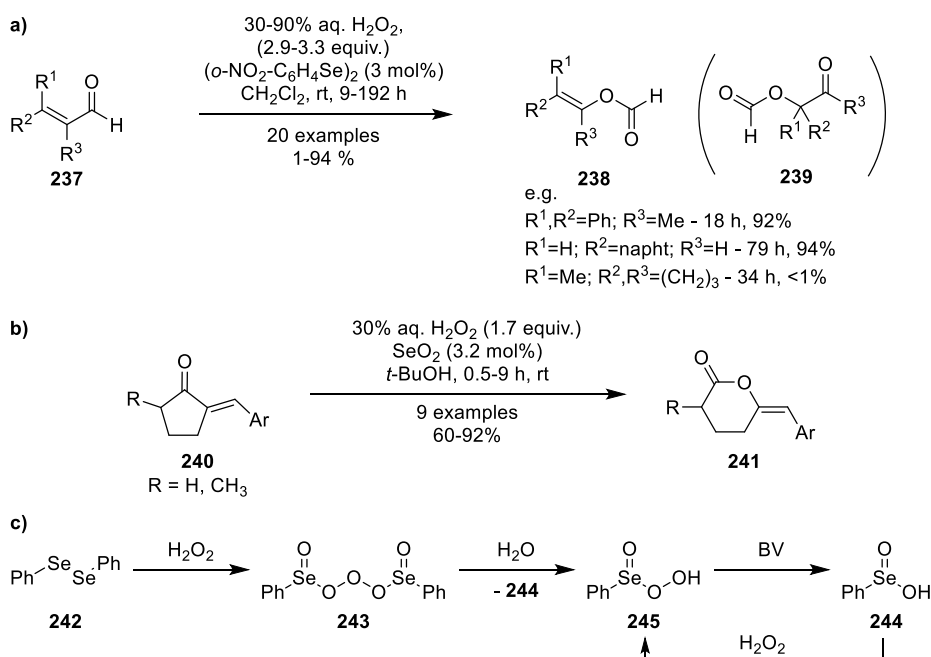


Scheme 102: (a) Original Böeseken oxidation and hydrolysis of vanillin derivatives **234** for the synthesis of phenols **236**.<sup>407,408</sup> (b,c) Patented Böeseken oxidations of benzaldehyde derivatives for: (a) BV oxidation of piperanal to sesamol,<sup>410</sup> (b) BV oxidation of *p*-tolualdehyde to *p*-cresol.<sup>411</sup>



#### 4.1.4 Baeyer-Villiger methods for the synthesis of vinyl esters

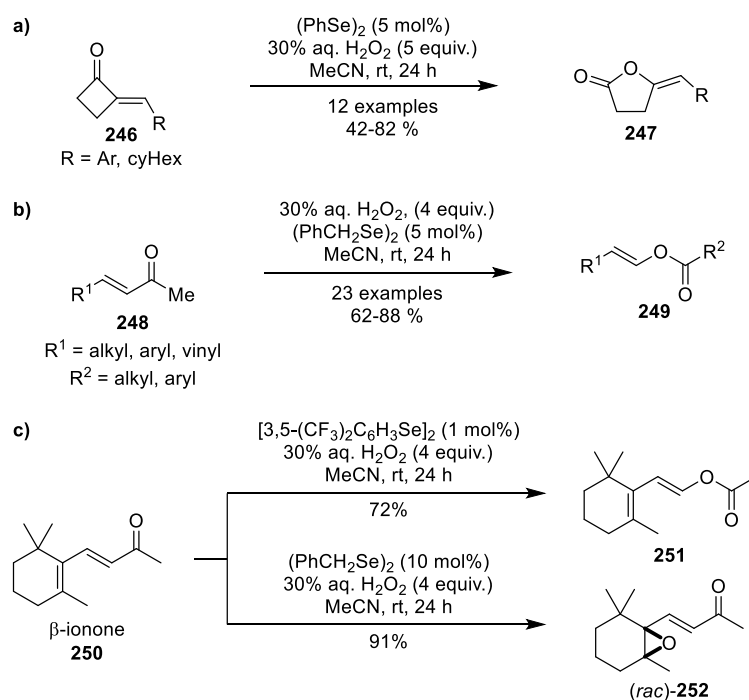
Excluding these early reports by Böeseken and subsequent sporadic reports in the literature, only a handful of other approaches describing the Baeyer-Villiger oxidation of  $\alpha,\beta$ -unsaturated ketones have been reported in the literature, both of which suffer from significant practical and/or substrate scope limitations. In 1987, Syper and co-workers reported the use of benzeneselenenic acid as a catalyst for the BV oxidation of  $\alpha,\beta$ -unsaturated aldehydes **237** using hydrogen peroxide as an oxidant (Scheme 103a).<sup>412</sup> Syper reported that bis(2-nitrophenyl) diselenide and  $\text{H}_2\text{O}_2$  (aq. 30-90%) could be used to produce a range of vinyl formate esters **238** in poor to good yields, with significant amounts of rearranged  $\alpha$ -O-formyl ketones **239** produced in a number of cases. Building on this work, Guzmán and co-workers later reported use of catalytic amounts of selenium dioxide for the oxidation of  $\beta$ -aryl substituted  $\alpha,\beta$ -unsaturated cyclic ketones **240** to produce cyclic vinyl esters **241** (Scheme 103b),<sup>413</sup> with low loadings of  $\text{SeO}_2$  and a small excess of hydrogen peroxide required to achieve good yields. Subsequent  $^{77}\text{Se}$  NMR spectroscopic studies revealed that the selenide precatalyst (e.g.  $(\text{PhSe})_2$ , **242**) is first oxidised to the corresponding benzeneseleninoperoxoic anhydride **243** by  $\text{H}_2\text{O}_2$ , which is then subsequently hydrolysed *in situ* to form benzeneseleninoperoxoic acid **245** (active species) and benzeneselenenic acid **244**.<sup>414</sup> This latter species **244** is also formed as the reduced by-product of the Baeyer-Villiger oxidation reaction, and is then re-oxidised by  $\text{H}_2\text{O}_2$  to reform the active oxidant **245** (Scheme 103c).



Scheme 103: Early examples of organoselenium-catalysed BV oxidation reactions of  $\alpha,\beta$ -unsaturated ketones. (a) BV oxidation of  $\alpha,\beta$ -unsaturated aldehydes **237** by Syper.<sup>412</sup> (b) BV oxidation of  $\beta$ -aryl substituted  $\alpha,\beta$ -unsaturated cyclic ketones **240** Guzmán *et al.*<sup>413</sup> (c) *In situ* generation and recycling of seleninoperoxoic acid **245** from diselenide precatalyst **242**.<sup>414</sup>

More recently (between 2014-2016), Yu *et al.* have published several new reports of organoselenium-catalysed BV oxidation reactions of vinyl ketones,<sup>414-416</sup> employing 5 mol% phenyl diselenide  $(\text{PhSe})_2$  to carry out BV oxidation of a range of twelve 2-methylenecyclobutanones **246**

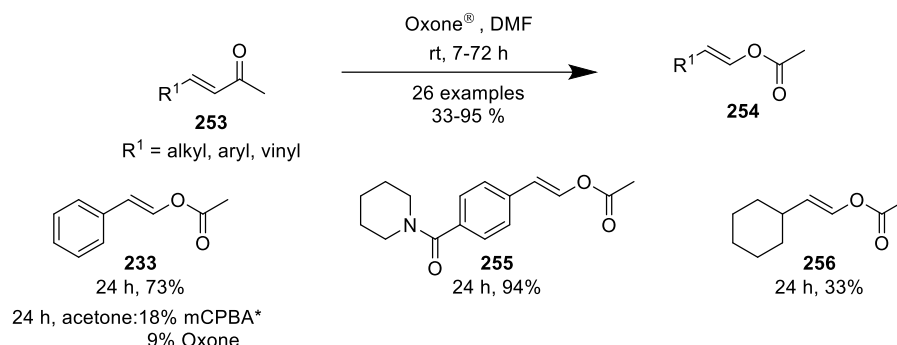
using a large excess of  $\text{H}_2\text{O}_2$  (5.0 equiv.) to synthesise twelve alkylidene lactones **247** in 42–82% yields (Scheme 104a).<sup>414</sup> Yu *et al.* subsequently reported that dibenzyl diselenide  $(\text{PhCH}_2\text{Se})_2$  could be employed for the synthesis of a broad range of vinyl esters **249** from their corresponding enones **248** in good yields (Scheme 104b).<sup>416</sup> Finally, their most recent report described oxidation of the terpenoid  $\beta$ -ionone **250**, which features an extended  $\alpha,\beta,\gamma,\delta$ -unsaturated diene system (Scheme 104c).<sup>415</sup> Careful optimisation of the diselenide precatalyst revealed that a  $(\text{PhCH}_2\text{Se})_2/\text{H}_2\text{O}_2$  system could be used to selectively carry out a Baeyer-Villiger oxidation reaction to afford vinyl ester **251**. Conversely, use of bis-trifluoromethylated diaryl diselenide  $[3,5-(\text{CF}_3)_2\text{C}_6\text{H}_3\text{Se}]_2$  resulted in epoxidation of the more electron-rich  $\gamma,\delta$ -alkene bond of  $\beta$ -ionone **250** to form epoxide **252**. Although good selectivities and impressive yields were achieved in these oxidative processes, extended reaction times (24 h) were necessary for full conversion, and a large excess of oxidant was required in all cases (4–5 equiv.). Moreover, the selenium reagents used in these Baeyer-Villiger reactions are toxic, relatively expensive, and are infamously associated with noxious odour issues that make them notoriously unpleasant to use.



Scheme 104: Organoselenium-mediated BV oxidation reactions reported by Yu *et al.*<sup>414–416</sup>

One other general Baeyer-Villiger method for the oxidation of  $\alpha,\beta$ -unsaturated ketones **253** has been reported, with Concellón *et al.* describing use of Oxone® (potassium monopersulfate triple salt,  $\text{KHSO}_5 \cdot \frac{1}{2}\text{KHSO}_4 \cdot \frac{1}{2}\text{K}_2\text{SO}_5$ ) as a BV oxidant (Scheme 105).<sup>417</sup> Although capable of good to high yields for a range of vinyl esters **254**, this method is restricted to the synthesis of *trans*-vinyl acetates, with reactions performed in DMF under an inert/dry  $\text{N}_2$  atmosphere. Many of these BV reactions required extended reaction times (up to 72 h), as well substrate-dependent reoptimisation of the amount of oxidant used in each case. Interestingly, this study reported that

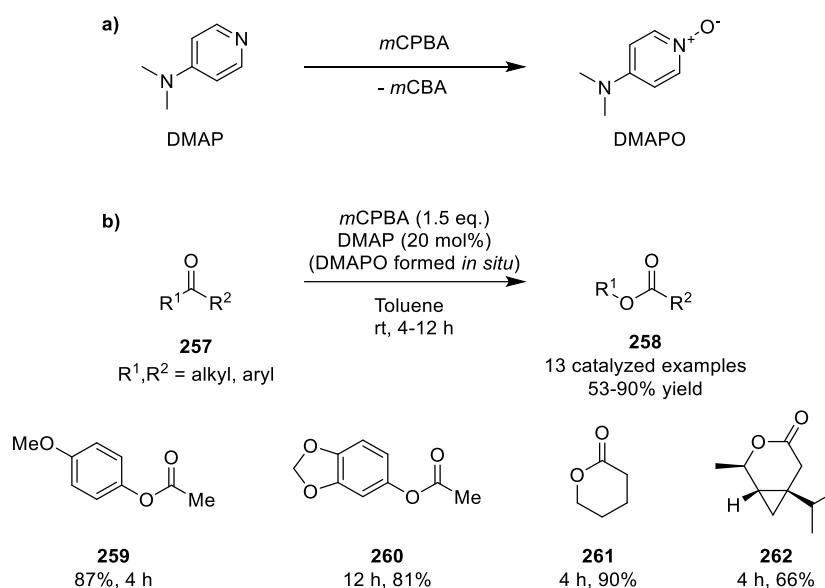
*m*CPBA was a more reactive oxidant than Oxone® in some of these BV reactions (*vide infra*), however Oxone® was found to be more selective for vinyl ester formation.



Scheme 105: Oxone-mediated Baeyer-Villiger oxidation of *trans*- $\alpha,\beta$ -unsaturated methyl ketones by Amo *et al.* \* 9%  $\alpha,\beta$ -epoxyketone also produced.<sup>417</sup>

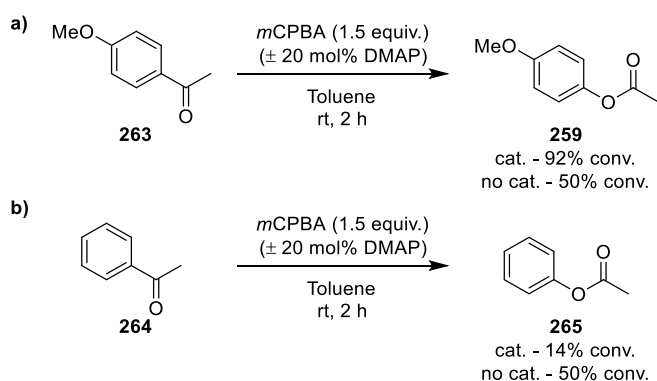
#### 4.1.5 *N*-oxide catalysed BV reactions

Concurrent to these selenide and Oxone®-mediated Baeyer-Villiger oxidation reactions of enones, the Bull group had previously investigated the use of *N*-oxides as catalysts in BV oxidation protocols for the production of esters and vinyl esters. The results of these previous studies are reported in full in Dr Ruth Lawrence's 2016 PhD thesis entitled '*N*-Oxides as Organocatalysts for the Baeyer-Villiger Oxidation and Bromination Reactions'.<sup>418</sup> These studies revealed that addition of 20 mol% DMAP to standard *m*CPBA-mediated Baeyer-Villiger reactions of ketones led to formation of DMAP *N*-oxide (DMAPO) *in situ* (Scheme 106a), which was found to be a competent organocatalyst for facilitating these types of BV oxidation reaction. Therefore, a novel catalytic BV oxidation protocol was established, whereby addition of catalytic amounts of DMAP/DMAPO to standard *m*CPBA mediated Baeyer-Villiger reactions could be used to facilitate conversion of electron-rich ketones **257** into their corresponding esters **258** under mild reaction conditions in relatively short reaction times (Scheme 106b, unpublished).



Scheme 106: (a) *m*CPBA-mediated oxidation of DMAP to DMAPO. (b) Novel DMAPO-catalysed BV oxidation methodology previously developed by the Bull group (unpublished).

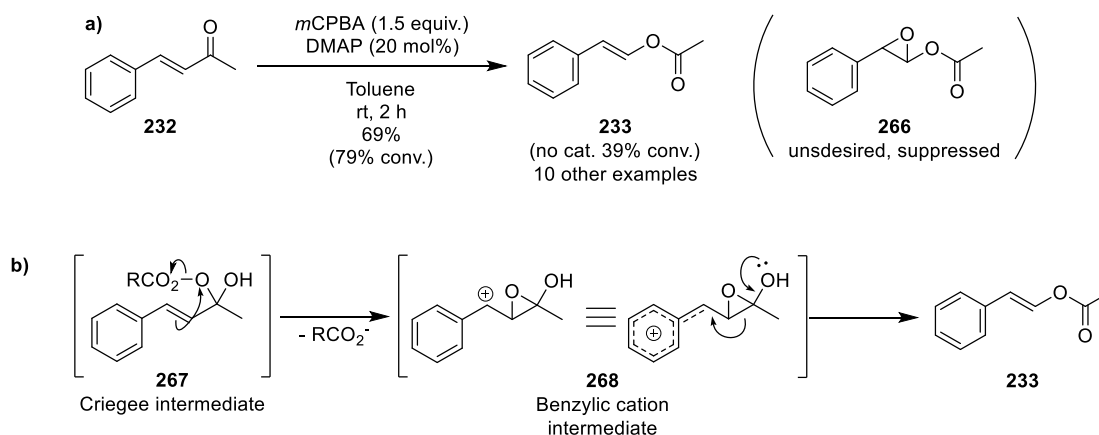
Some mechanistic investigations were carried out as part of this work, which determined that *N*-oxide-mediated rate acceleration of BV oxidation reactions only occurred for electron-rich ketones (*e.g.* *p*-methoxyacetophenone **263**, Scheme 107), whilst addition of DMAP to BV oxidation reactions of electron-deficient ketones (*e.g.* acetophenone **264**) resulted in slower BV reactions (see Scheme 107). As discussed, the presence of electron-rich ketone substituents resulted in a more facile migration step, whilst electron-deficient ketone substituents resulted in slower migration of the Criegee intermediate. These trends were used to confirm that DMAPO acts as an organocatalyst to catalyse the initial addition step of BV reactions that involve nucleophilic attack of *m*CPBA at the ketone carbonyl, meaning that *N*-oxides only catalyse BV reactions of ketone substrates whose peracid addition step is rate-limiting.



Scheme 107: Effects of DMAPO on the Baeyer-Villiger oxidation of different types of ketone: (a) DMAPO catalyses the Baeyer-Villiger reactions of ketones whose initial peracid addition step is rate-limiting; (b) DMAPO suppresses the Baeyer-Villiger reactions of ketones whose second migration step is rate-limiting.

Following this discovery, these DMAPO-catalysed conditions were applied to the Baeyer-Villiger oxidation of a range of arylidene  $\alpha,\beta$ -unsaturated ketones to successfully produce a range of 11 vinyl esters in 53-90% yields (Scheme 108a). *N*-oxide-mediated catalysis of the BV oxidation

reactions of these arylidene substrates are consistent with the postulate that the DMAPO catalyst acts predominantly to accelerate the initial *m*CPBA addition step. Firstly, it is expected that addition of a peracid to a conjugated  $\alpha,\beta$ -unsaturated ketone substrate would be relatively slow, as alkene-ketone conjugation decreases the reactivity of the carbonyl carbon towards nucleophilic attack. Secondly, as discussed for the aryl phenonium BV oxidation reactions above,  $\pi$ -participation from the aryl-vinyl benzyldiene ketone substituent in the Criegee intermediate **267** has the potential to generate a stabilised benzylic cationic intermediate **268** with partial aromatic character (Scheme 108b, cf. aryl stabilisation mechanism shown in Scheme 95). To the best of our knowledge, this possible migration mechanism has never been explored systematically, with only a brief suggestion of this type of stabilisation mechanism reported in a 1952 report by Wenkert and Rubin.<sup>419</sup> One of the key limitations of the BV oxidation reactions of  $\alpha,\beta$ -unsaturated ketones is the capacity of the alkene bonds of the vinyl ester products they produce to undergo further epoxidation reactions. Furthermore, the epoxides that are generated are also susceptible to further rearrangement/oxidation reactions which can all combine to produce complex mixtures of products (*vide infra*). Therefore, one of the key benefits of the new *N*-oxide-catalysed BV methodology is the ability of DMAPO to suppress formation of undesired epoxyesters **266** and their decomposition products. Unfortunately, although successful in affording good yields of ester and vinyl ester products in short reaction times, the catalytic role of the *N*-oxides in these BV reactions remained unclear. This also meant that it was still unclear whether fully optimised BV conditions had been identified for the BV oxidation of ketones/ $\alpha,\beta$ -unsaturated ketones in these systems.



Scheme 108: (a) DMAPO-catalysed Baeyer-Villiger oxidation of arylidene mono-ketones. (b) Suggested stepwise migration step in the BV oxidation reaction of benzylideneacetone **232**.

## 4.2. Reoptimisation of DMAPO-catalysed BV oxidation reactions

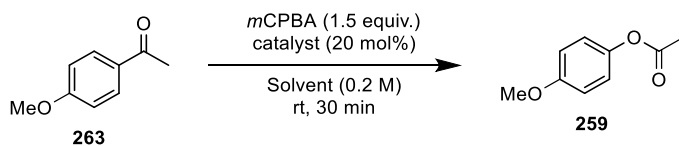
### 4.2.1 *Reinvestigation of the DMAPO-mediated BV oxidation reaction of *p*-methoxyacetophenone 263*

The general instability and explosive nature of pure peroxides and peroxyacids means that commercially-available *m*CPBA is traditionally sold/used as a 70-80 wt% mixture, with its remaining content comprised of approximately 15-25 wt% *meta*-chlorobenzoic acid (*m*CBA) and water (approximately 5 wt%).<sup>420</sup> This means that unless otherwise explicitly stated, the *m*CPBA used in the BV experiments throughout this thesis was approximately 75 wt% pure, as confirmed by iodometric titration on receipt from the supplier (and regularly throughout the course of this study).<sup>421</sup> Initial reinvestigation of the DMAPO-mediated BV oxidation reactions revealed that the sampling procedure previously used to calculate ketone conversion values was flawed.<sup>418</sup> Repeating some of these BV reactions revealed inconsistencies/reproducibility issues with the yields of vinyl esters and ketones produced, which was traced to issues associated with the reaction work-up procedure used to monitor substrate conversion levels. In the original experimental design, ketone (non-enone) substrate conversion levels were calculated by removal of solvent *in vacuo* at 40 °C (on a rotary evaporator), followed by analysis of the crude reaction product by <sup>1</sup>H NMR spectroscopic analysis. The DMAPO-catalysed BV reactions carried out proceed over relatively short periods of time at room temperature (*vide supra*), and so the increased temperature of the rotary evaporator water bath (between 40-50 °C), combined with the increasing concentration of the reaction mixture as evaporation proceeded, meant that the BV reaction was still occurring (and likely being accelerated) during the work-up/sampling process. Therefore, these original sampling conditions meant that BV conversion values were not only dependent on the temperature of the rotary evaporator water bath and length of evaporation, but also dependent on the initial concentration, reagent stoichiometries, and degree of conversion. Therefore, a combination of these variables was contributing to incorrect/unrepeatable conversion levels when the original crude BV reactions were repeated.

Consequently, it was necessary to redetermine the conversion levels of the DMAPO-catalysed BV reactions using a new 'direct' reaction sampling procedure based on removal of an aliquot from the reaction mixture (approx. 20 µL), followed by dilution with CDCl<sub>3</sub> and immediate analysis (within 30 min, control experiments carried out to ensure reaction stopped on dilution) by <sup>1</sup>H NMR spectroscopy (Table 10). This new sampling regime was initially demonstrated for the BV oxidation reaction of *p*-methoxyacetophenone **263** to *p*-acetoxy anisole **259**, which proceeded with a clean reaction profile (no side-reactions or degradation products), and so an internal standard was not required. This new monitoring procedure largely confirmed the data from the original DMAPO-catalysed BV study of *p*-methoxyacetophenone **263**, except that slightly decreased conversion values were found in most cases (as expected). A screen of amine/amine-*N*-oxide catalysts (Table 1, Entries 2-8) confirmed that the DMAPO-catalysed BV oxidation reactions of **263** were indeed effective in a range of solvents (Table 1, Entries 9-15). Use of DMAP or preformed DMAPO

(monohydrate, commercial) gave comparable conversion values of 61% and 59% respectively (Table 10, entries 7-8), confirming that amine precatalysts underwent *in situ* oxidation to form active *N*-oxide organocatalysts. A quick catalyst loading screen using this new monitoring method (Table 10, entries 7 and 16-19) also confirmed that an increase in catalytic activity up to 20 mol% DMAPO was followed by a sharp drop-off in conversion values from 61% to 22% when DMAP loading was increased from 20% to 50%, thus confirming lower conversion rates in BV oxidation reactions at higher DMAPO catalyst loadings (*vide infra*).

Table 10: Comparison of the conversion levels determined for the DMAPO-catalysed BV oxidation of *p*-methoxyacetophenone **263** using different sampling methods (evaporation or aliquoting).



Entry <sup>a</sup>	Catalyst/Precatalyst (mol%)	Solvent	Conversion (%) <sup>b,c</sup>	
			Evaporation <sup>418</sup>	Aliquot
1	None	Toluene	20	18
2	Trimethylamine <i>N</i> -oxide TMNO (20)	Toluene	65	61
3	NEt <sub>3</sub> (20)	Toluene	40	38
4	DIPEA (20)	Toluene	44	53
5	<i>N</i> -methylpiperidine (20)	Toluene	55	54
6	Pyridine (20)	Toluene	54	17
7	DMAP (20)	Toluene	87	61
8 <sup>d</sup>	DMAPO (20)	Toluene	89	59
9	DMAP (20)	Hexane	80 (25)	69 (25)
10	DMAP (20)	DCM	86 (20)	38 (20)
11	DMAP (20)	Trifluorotoluene	86 (63)	65 (63)
12	DMAP (20)	Acetonitrile	87 (55)	71 (55)
13	DMAP (20)	EtOAc	30 (50)	59 (50)
14	DMAP (20)	EtOH	89 (33)	80 (40)
15	DMAP (20)	Et <sub>2</sub> O	41 (14)	70 (14)
16	DMAP (5)	Toluene	- <sup>e</sup>	55
17	DMAP (10)	Toluene	- <sup>e</sup>	56
18	DMAP (30)	Toluene	- <sup>e</sup>	41
19	DMAP (50)	Toluene	- <sup>e</sup>	22

<sup>a</sup> *m*CPBA and catalyst/precatalyst were premixed for 15 min. <sup>b</sup> Values in brackets correspond to conversions for uncatalysed BV reactions. <sup>c</sup> Remaining mass balance comprised of unreacted ketone **263**. <sup>d</sup> DMAPO monohydrate used. <sup>e</sup> Experiments not carried out in previous work.

Further consideration revealed that the design of the previous BV screening experiments used to identify optimal catalyst loading conditions for *N*-oxide-catalysed BV reactions was also potentially flawed. For example, the BV screening results shown in Table 10 employed 1.5 equiv. of *m*CPBA in



all cases, regardless of the precatalyst loading (which mirrored the original BV study). This meant that a full 1.5 equiv. of *m*CPBA oxidant was available in catalyst-free systems (Table 10, entry 1), and when preformed *N*-oxides were used (Table 10, entries 2 and 8). However, those BV protocols that employ an amine precatalyst require initial consumption of *m*CPBA to produce the corresponding *N*-oxide catalyst *in situ*. For instance, use of 20 mol% DMAP as a catalyst (100% conversion to DMAPO) meant that only a maximum 1.3 equiv. of *m*CPBA would be available to carry out the desired BV oxidation reaction (*cf.* 1.5 equiv. *m*CPBA available in preformed *N*-oxide catalyst BV reactions). This disparity in the amount of *m*CPBA available between BV reactions using different precatalyst loadings had the potential to cause inaccuracies when comparing conversion data. However, since use of 20 mol% DMAP and DMAPO catalyst under otherwise identical conditions produced comparable 59% and 61% conversion levels (Table 10, entries 7 and 8), it appeared that small variations in the amount of excess *m*CPBA present in these BV reactions had little effect on overall ketone consumption rates. Nevertheless, a quick set of screening experiments were carried out, where the stoichiometry of the *m*CPBA oxidant was adjusted to allow for the amount of *m*CPBA consumed for precatalyst oxidation (Table 11). In all instances, 1.3 equiv. of *m*CPBA was added to the BV reactions, along with an extra 'dose' of *m*CPBA to account for the amount of oxidant consumed to oxidise the DMAP precatalyst to DMAPO *in situ*, with this approach classified as "catalyst-corrected" BV conditions. For example, a 10 mol% DMAP catalysed BV reaction was carried out using 1.4 equiv. *m*CPBA, with 0.1 equiv. of the *m*CPBA consumed to oxidise DMAP into DMAPO, leaving 1.3 equiv. of *m*CPBA available to carry out the BV reaction (Table 11, entry 3).

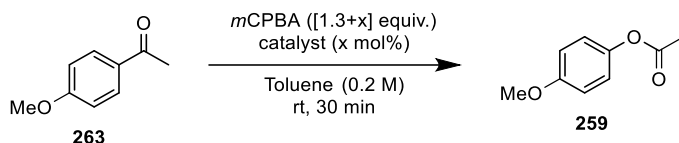
These catalyst-corrected studies confirmed the following observations:

- Addition of the *N*-oxide catalyst resulted in an increase in BV conversion levels, with maximum rate acceleration occurring at 20 mol% DMAPO catalyst loadings (Table 11, *cf.* entries 1-4).
- Only small differences in conversion levels were observed between 'standard' and 'catalyst-corrected' BV conditions, thus demonstrating the catalytic efficiency of the DMAPO catalyst in these reactions (Table 11, *cf.* entries 2-7).
- A decrease in conversion was observed as catalyst loadings were increased above 20 mol% (Table 11, *cf.* entries 4-6).
- Use of preformed 20 mol% DMAPO (1.3 equiv. *m*CPBA) for 30 min gave a lower 51% conversion than the 61% conversion obtained when 20 mol% DMAP precatalyst (1.5 equiv. *m*CPBA  $\equiv$  1.3 equiv. *m*CPBA for BV reaction) was used (Table 11, *cf.* entries 4 and 7).

The observations that DMAP-catalysed BV reactions (*in situ* DMAPO) gave slightly better conversion rates than pre-formed DMAPO-catalysed reactions led us to consider whether the extra 20 mol% *m*CBA generated as a by-product from rapid *in situ* conversion of DMAP to DMAPO might be generating a more acidic reaction mixture that was leading to a faster BV oxidation reaction. This hypothesis was explored by repeating the BV oxidation reaction using 20 mol% preformed DMAPO

and 1.3 equiv. *m*CPBA, in the presence of 20 mol% *m*CBA as an additive (Table 11, entry 8), which only gave a small increase in conversion levels from 51% to 54%.

Table 11: *m*CPBA stoichiometry studies for the optimisation of reaction conditions for the DMAPO-catalysed BV oxidation of *p*-methoxyacetophenone **263**.



Entry <sup>a</sup>	Catalyst/Precatalyst (mol%)	<i>m</i> CPBA (equiv.)	Conversion (%) <sup>b,c</sup>
1	None	1.3	9 (18)
2	DMAP (5)	1.35	50 (55)
3	DMAP (10)	1.4	52 (56)
4	DMAP (20)	1.5	61 (N/A)
5	DMAP (30)	1.6	43 (41)
6	DMAP (50)	1.8	27 (22)
7 <sup>d</sup>	DMAPO (20)	1.3	51 (59)
8 <sup>d</sup>	DMAPO (20) + <i>m</i> CBA (20)	1.3	54
9 <sup>d</sup>	DMAPO (20)	1.3 (pure)	42
10 <sup>d</sup>	DMAPO (20) + <i>m</i> CBA (20)	1.3 (pure)	53
11	None	1.3 (pure)	27
12	None + <i>m</i> CBA (20)	1.3 (pure)	21
13	None + H <sub>2</sub> O (5 wt%)	1.3 (pure)	10
14 <sup>e</sup>	None + <i>m</i> CBA (20) + H <sub>2</sub> O (5 wt%)	1.3 (pure)	13
15 <sup>d</sup>	DMAPO (20) + H <sub>2</sub> O (5 wt%)	1.3 (pure)	53
16 <sup>d,e</sup>	DMAPO (20) + <i>m</i> CBA (20) + H <sub>2</sub> O (5 wt%)	1.3 (pure)	55

<sup>a</sup> *m*CPBA and catalyst/precatalyst were premixed for 15 min. <sup>b</sup> Values in brackets correspond to conversions with uncorrected 1.5 equiv. *m*CPBA, from Table 10. <sup>c</sup> Remaining mass balance comprised of unreacted ketone **263**. <sup>d</sup> DMAPO monohydrate used. <sup>e</sup> Systems designed to approximate the composition of commercial *m*CPBA.

A batch of 75 wt% commercial *m*CPBA was then carefully purified by multiple washings with phosphate buffered saline (0.1 M, pH 7.5, (PBS)) to remove any *m*CBA that was present, followed by drying under vacuum to afford pure *m*CPBA (> 95%).<sup>422</sup> This purified *m*CPBA (1.3 equiv.) was then used to carry out the BV oxidation of *p*-methoxyacetophenone **263** using preformed DMAPO (20 mol%) which resulted in a clear drop in conversion levels to 42% (Table 11, entry 9). This 42% conversion level was less than the 51% conversion achieved using commercial *m*CPBA and 20 mol%

DMAPO (Table 11, entry 7) and the 61% conversion obtained when 20 mol% DMAP was used with commercial *m*CPBA (*cf.* Table 10, entry 4). Inclusion of 20 mol% *m*CBA as an additive in a pure *m*CPBA reaction led to an increase in conversion from 42% to 53% (Table 11, *cf.* entries 9-10), thus providing good evidence of a co-catalytic role for *m*CBA in accelerating the rate of these *N*-oxide-catalysed BV oxidation reactions.

A series of control reactions was then carried out to further determine the effect of *m*CBA and water on uncatalysed BV reactions of *p*-methoxyacetophenone. Carrying out the BV oxidation of **263** using purified *m*CPBA under catalyst-free conditions (Table 11, entry 11) achieved 27% conversion, which was three times the 9% conversion level obtained using commercial *m*CPBA (Table 11, entry 1). Addition of 20 mol% *m*CBA as an additive to a pure *m*CPBA reaction led to a slight decrease in conversion to 21% (Table 11, entry 12), whilst addition of 5 wt% water to a pure *m*CPBA reaction also caused conversion levels to decrease to 10% (Table 11, entry 13). Inclusion of both 20 mol% *m*CBA and 5 wt% water in a pure *m*CPBA reaction (still no *N*-oxide catalyst) led to 13% conversion (Table 11, entry 14), with both water-doped reactions achieving low conversion levels similar to the 9% conversion level seen with commercial *m*CPBA. These control reactions indicate that whilst water has a clear suppressive effect on the uncatalysed BV oxidation of **263** in toluene, *m*CBA was more catalytically active in the presence of water. We reasoned that the greater accelerating effect of *m*CPBA in aqueous systems might be due to more efficient ionisation of *m*CBA at water/toluene interfaces serving to produce localised acidic environments that could more efficiently promote the BV oxidation reaction. These water-doping experiments were then repeated in the presence of 20 mol% DMAPO (preformed, pure *m*CPBA, Table 11, entries 15-16), which showed that DMAPO efficiently catalyses the BV oxidation reaction of **263** in toluene in the presence of 5 wt% water, resulting in 53-55% conversion levels for the selective formation of ester **259** after 30 min.

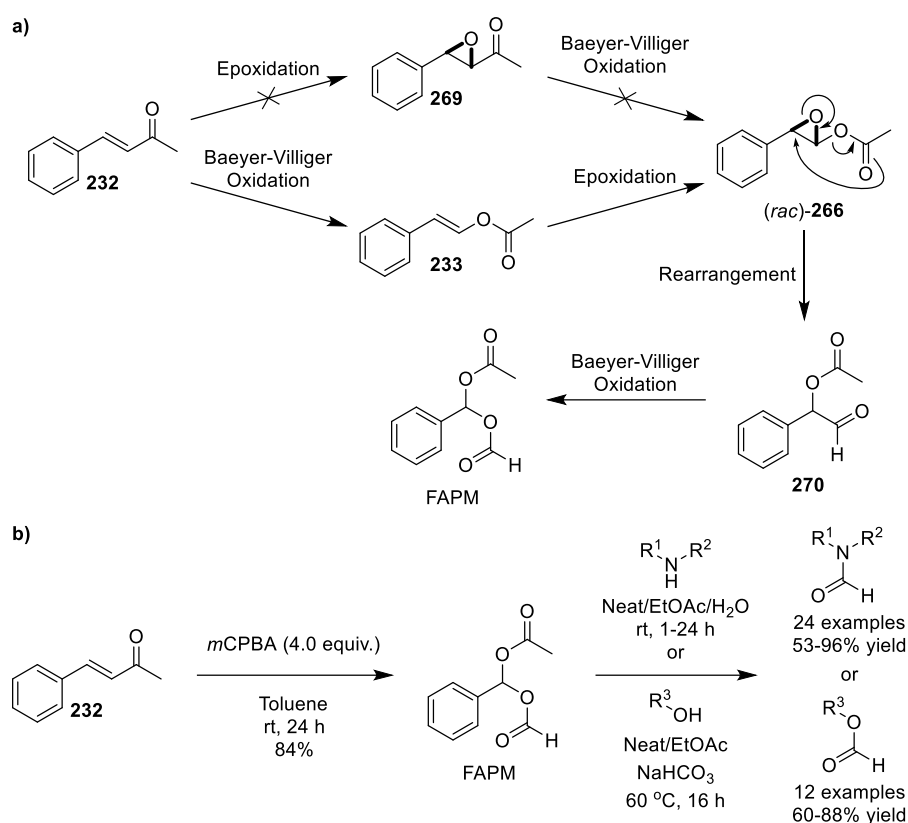
These series of simple screening experiments provided us with a clearer picture of the roles that DMAPO, *m*CBA, and water play in the *m*CPBA-mediated BV oxidation reactions of *p*-methoxyacetophenone **263** in toluene, which allowed the following conclusions to be drawn:

- DMAP and other amines are oxidised by *m*CPBA *in situ* to produce *N*-oxide species that are catalytically-active in BV reactions where initial nucleophilic attack of the *m*CPBA peracid is rate-determining.
- Low loadings of DMAPO (< 20 mol%) were catalytic in all the BV reactions explored, regardless of *m*CPBA purity, *m*CBA/water content, or *m*CPBA loading levels used.
- Increased loadings of DMAPO (> 20 mol%) led to a corresponding drop in conversion rates, even when higher loadings of *m*CPBA oxidant were used.
- Slightly faster BV reactions occurred when both DMAPO and *m*CBA were present as cocatalysts.
- Water and *m*CBA were inhibitory in the absence of any DMAPO catalyst.

- Optimal conversion levels after 30 min were achieved when DMAPO, *m*CBA and water were present in the BV reaction mixture (*e.g.* when commercial 75 wt% *m*CPBA was used).

#### 4.2.2 Reoptimisation of the DMAPO-catalysed oxidation of benzalacetone **232**

Having demonstrated the co-catalytic role and synergistic effect of DMAPO and *m*CBA in the BV oxidation reaction of conventional electron-rich ketones, attention was then turned to reinvestigating the conditions used in the DMAPO-catalysed BV oxidation reactions of  $\alpha,\beta$ -unsaturated ketones. As for the catalytic BV reactions of conventional ketones, it was necessary to redetermine conversion values using the new 'direct' sampling regime. Unlike the ester **259** produced from *p*-methoxyacetophenone **263**, the vinyl ester **233** produced from BV oxidation of benzylideneacetone **232** using *m*CPBA is capable of undergoing a variety of side-reactions that can further affect the overall yield of its BV reaction (Scheme 109a).<sup>418,422,423</sup> No direct epoxidation of enone **232** to  $\alpha,\beta$ -epoxyketone **269** is observed, however benzylideneacetone **232** readily undergoes BV oxidation to produce  $\beta$ -phenyl vinyl ester **233**, whose alkene functionality can react further with *m*CPBA to produce a relatively unstable  $\alpha,\beta$ -epoxyester (*rac*)-**266**. Since epoxide **266** is synthetically equivalent to an *O*-acylated hemi-acetal, it can then rearrange *via* an acyl transfer/epoxide ring-opening mechanism to produce formyl acetate **270**. Furthermore, formyl acetate **270** can then undergo a further Baeyer-Villiger oxidation reaction to produce formyloxyacetoxymethylmethane FAPM (Scheme 109b, also see Scheme 103).<sup>412,423,424</sup> Indeed, use of excess *m*CPBA (4.0 equiv. *m*CPBA, no DMAPO) and extended reaction times (24 h) can be used to produce FAPM in a high 84% yield, which the Bull group has shown can be used as a versatile *N*- and *O*-formylating agent.<sup>423,425–427</sup>

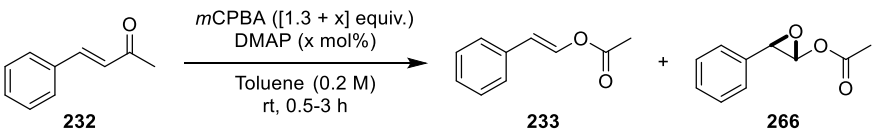


Scheme 109: (a) Oxidation and rearrangement products of benzylideneacetone **232**. (b) Bull group synthesis of FAPM, a versatile formylating agent.<sup>423,424</sup>

Given the range of products that can potentially be formed in the BV reactions of benzylideneacetone **232**, all of its BV reactions were carried out in the presence of 1,2,3,5 tetramethylbenzene (TetMB) as an internal NMR standard to calibrate product yields. A catalyst loading screen was first carried out using increasing amounts of DMAP precatalyst (0-100 mol%) and 1.3 equiv. loadings of BV-available *m*CPBA (1.3-2.3 equiv. *m*CPBA initially) (Table 4). The uncatalysed BV reaction proceeded relatively slowly, achieving only 40% consumption of enone **232** after 30 min, with 30% selectivity for the formation of vinyl ester **233**, with 10% of the unwanted epoxide **266** side-product also being formed (Table 12, entry 1). This lack of selectivity proved to be problematic when extended reaction times were used to try and drive the BV reaction to completion, with a 3 h reaction time resulting in 70% conversion to an almost equimolar mixture of vinyl ester **233** (33%) and epoxide **266** (37%) (Table 12, entry 2). Addition of 20 mol% DMAP precatalyst led to a significant acceleration of the BV reaction of enone **232**, which now gave 92% conversion to mixed products after 30 min. The selectivity of this BV reaction was also greatly improved, with a 79% yield of vinyl ester **233** observed, with only 13% undesired epoxyster **266** now present (83.5:16.5, approx., ~6:1, Table 12, entry 3). Further increases in DMAPO catalyst loading led to a drop in conversion levels with use of 40% and 50 mol% DMAP only affording 80% and 61% conversion, respectively, whilst only 31% conversion levels were observed when 100 mol% DMAPO was used (Table 12, entries 5, 7, 9, 11). Despite a drop in total conversion levels down to only 61%, increasing catalyst loadings had the benefit of increasing reaction selectivity, with use of 50 mol% DMAPO loadings producing a 59% vinyl ester **233** and only 2% epoxyster **266**, equating

to a 96.6:3.4 ratio of **233**:**266**, a five-fold increase in selectivity level over 20 mol% DMAP/DMAPO (Table 3, Entry 9). Carrying out catalytic BV reactions of **232** for 3 h confirmed that although increasing DMAPO catalyst loadings from 20 to 100 mol% resulted in lower conversion values, higher catalyst loadings resulted in less epoxide side-product being produced (Table 12, *cf.* entries 4, 6, 8, 10). Therefore, these results appeared to demonstrate that the DMAPO catalyst exhibited a dual function in producing better yields of vinyl ester **233**. Firstly, the DMAPO was acting as an organocatalyst (optimal for 20 mol% catalyst loading) to facilitate the initial rate determining step of the BV oxidation of enone **232** to produce vinyl ester **233**. Secondly, DMAPO was also serving to suppress the undesired epoxidation pathway that converts vinyl ester **233** to epoxyester **266** (and its decomposition/rearrangement products). These data led to the conclusion that catalyst loadings of between 20-50 mol% were optimal for carrying out DMAPO-catalysed BV oxidation reactions of  $\alpha,\beta$ -unsaturated ester **232** that reliably gave vinyl ester **233** in good isolated 70-80% yields.

Table 12: DMAPO-catalysed BV oxidation of benzalacetone **232**.

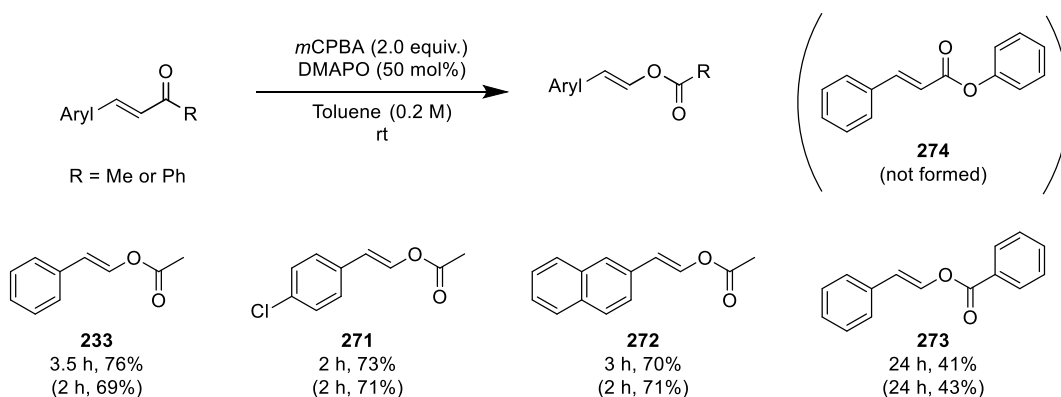
						
Entry <sup>a</sup>	DMAP loading	<i>m</i> CPBA loading	Time	Product distribution <sup>b</sup>		
				Enone <b>232</b>	Vinyl ester <b>233</b>	Epoxyester <b>266</b>
1	None	1.30 equiv.	30 min	60%	30%	10%
2			3 h	30%	33%	37%
3	20 mol%	1.50 equiv.	30 min	8%	79%	13%
4			3 h	-	82%	18%
5	30 mol%	1.60 equiv.	30 min	12%	79%	9%
6			3 h	5%	84%	11%
7	40 mol%	1.70 equiv.	30 min	20%	74%	6%
8			3 h	13%	81%	6%
9	50 mol%	1.80 equiv.	30 min	39%	59%	2%
10			3 h	33%	65%	2%
11	100 mol%	2.30 equiv.	30 min	69%	31%	-
12			3 h	65%	35%	-

<sup>a</sup> *m*CPBA and catalyst/precatalyst were premixed for 15 min. <sup>b</sup> All distributions were referenced to a TetMB internal standard to ensure integration accounted for the entire mass balance.

### 4.3. DMAPO-catalysed BV oxidation reactions of enones

#### 4.3.1 DMAPO-catalysed BV oxidation of $\alpha,\beta$ -unsaturated ketones

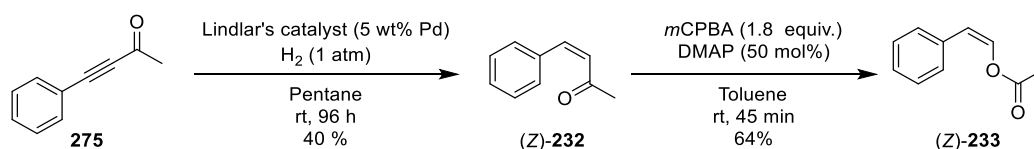
Armed with a better understanding of the catalytic/suppressive mode of action of the DMAPO organocatalyst, the reaction conditions for the BV oxidation of a range of  $\alpha,\beta$ -unsaturated ketones were reinvestigated. Therefore, use of a 50 mol% loading of DMAP and 2.0 equiv. *m*CPBA for the BV oxidation reaction resulted in complete consumption of benzalacetone **232** after 2.5 h, reproducibly affording 76% isolated yields of vinyl ester **233**. The utility of these improved conditions was then confirmed by carrying out BV oxidation of three additional  $\alpha,\beta$ -unsaturated ketones to produce arylidene esters **271**, **272**, and **273** (Scheme 110), with comparable yields observed in all instances when compared to the original BV conditions (20 mol% DMAP, 1.5 equiv. *m*CPBA). Most importantly, increasing DMAP loadings to 50% resulted in less epoxide by-product being formed, and so chromatographic purification of the hydrolytically-sensitive vinyl esters was much easier than under the previous reaction conditions. Chalcone-derived phenyl vinyl ester **273** was still only produced in a moderate 41% yield, which is due to the lower reactivity of the doubly conjugated ketone carbonyl of chalcone requiring extended reaction times to proceed to completion, which also led to greater epoxidation of chalcone over time. Importantly, no evidence of any phenyl acrylate ester **274** that could potentially be produced from competing phenyl migration was observed, thus indicating a strong migratory aptitude for the benzylidene moiety over the phenyl group in this sluggish BV reaction (*cf.* benzylic cationic intermediate BV mechanism shown in Scheme 108).



Scheme 110: DMAPO-catalysed BV oxidation of  $\beta$ -aryl enones. Values in brackets show results for previously reported reaction conditions (20 mol% DMAP, 1.5 equiv. *m*CPBA) by the Bull group.<sup>418</sup>

To further demonstrate the synthetic versatility of this method, it was then decided to apply the DMAPO-catalysed protocol to carry out BV reactions of some other  $\alpha,\beta$ -unsaturated ketones which had not previously been oxidised using this method. The first substrate chosen was (*Z*)-benzalacetone (*Z*)-**232**, to confirm that its BV reaction would afford vinyl ester (*Z*)-**233** diastereoselectively as a single diastereomer with complete retention of its alkene geometry. (*Z*)-benzalacetone **232** was synthesised in a single step *via cis*-hydrogenation of commercially available

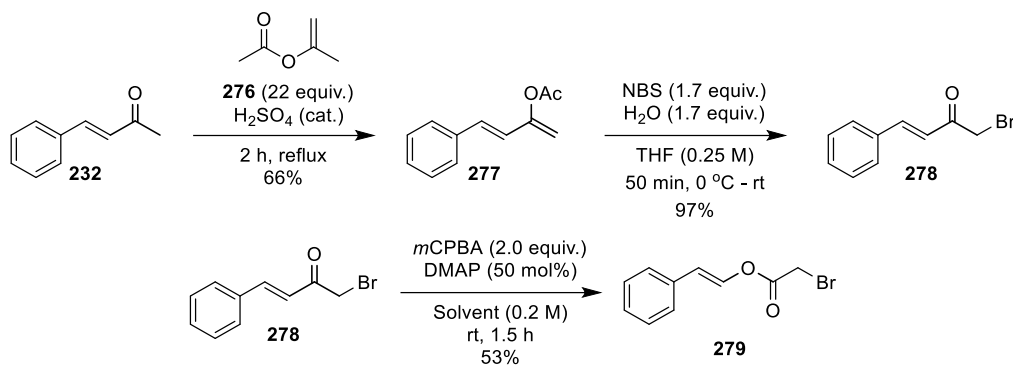
$\alpha,\beta$ -ynone **275** using Lindlar's catalyst (5 wt% Pd/CaCO<sub>3</sub> poisoned with lead) under H<sub>2</sub> (1 atm, balloon) in pentane in 40% isolated yield.<sup>428</sup> Subsequent BV oxidation of (Z)-**232** using standard DMAPO-catalysed conditions gave (Z)-styryl acetate **233** in 64% yield, with no evidence of any of the thermodynamically more stable (E)-**233** being formed. The increased rate of BV reaction of (Z)-benzalacetone over (E)-benzalacetone **232** (cf. 45 min vs. 2.5 h for full consumption) implies a faster rate of nucleophilic addition of *m*CPBA to the ketone carbonyl of (Z)-**232**. This is consistent with the more sterically-hindered ketone group of (Z)-**232** being distorted out of plane to its alkene functionality, thus decreasing conjugation and increasing the electrophilicity of its carbonyl. Evidence for this rationale comes from IR spectroscopic analysis, with the carbonyl stretching frequency of (Z)-**232** measured at 1691 cm<sup>-1</sup>, whilst the (E)-**232** diastereomer exhibits a strong absorption at 1655 cm<sup>-1</sup>, thus indicating decreased conjugation in (Z)-**232**. No competing alkene epoxidation of enone (Z)-**232** or vinyl ester (Z)-**233** to their corresponding epoxyketone or epoxyester products was observed under these BV conditions.



Scheme 111: Synthesis of (Z)-**233** by hydrogenation of ynone **275** and DMAPO-catalysed BV oxidation of (Z)-**232**.

The catalytic BV reaction conditions were then used for the synthesis of  $\alpha$ -bromo-vinyl ester (E)-**279**, as a potentially useful synthetic intermediate for use as a *N*-, *O*-, *C*-, or *P*-alkylating agent, or as a precursor to generate zinc enolates for use in Reformatsky-type reactions. The parent  $\alpha$ -bromo-ketone **277** was prepared in two steps *via* a literature procedure involving sulfuric acid-catalysed *O*-acylation of benzalacetone (E)-**232** with isopropenylacetate **276** to produce dienol acetate **277** in 66% yield, followed by  $\alpha$ -bromination using NBS to give benzylidene bromoacetone **278** in 97% yield.<sup>429</sup> Subsequent DMAPO-catalysed BV oxidation of bromoenone **278** afforded the novel  $\alpha$ -bromo vinyl ester **279** in 53% yield, that will be explored as a potential intermediate for the synthesis of nepetoidin B natural product analogues (see Figure 45 above and conclusion below). Attempts to carry out the *N*-oxide-catalysed BV oxidation of ynones and aliphatic enones were also made, however no unsaturated esters were obtained, further indicating the privileged nature of arylidene substrates in these type of *N*-oxide-catalysed BV reactions.



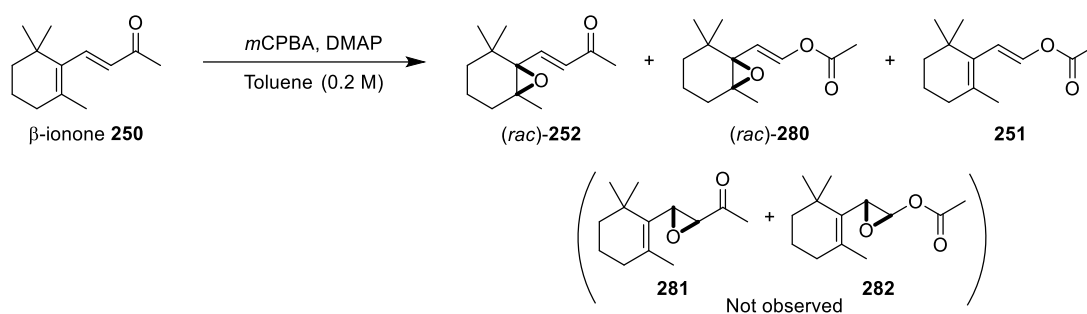


Scheme 112: Three-step synthesis of styryl bromoacetate (*E*)-**279** from benzalacetone (*E*)-**232**.

#### 4.3.2 DMAPO-catalysed regioselective BV oxidation of $\beta$ -ionone **250**

This new *N*-oxide-catalysed BV protocol was then benchmarked using  $\beta$ -ionone **250** as a substrate for the synthesis of vinyl ester **251** (*cf.* selenium-based BV methodology shown in Scheme 105). Use of standard DMAPO-catalysed conditions initially produced three products:  $\gamma,\delta$ -epoxyketone **252**; vinyl ester **251**; and  $\gamma,\delta$ -epoxyester **280** (Table 13). Interestingly,  $\alpha,\beta$ -epoxide products **281** and **282** were not produced, which is consistent with previous reports that only the more substituted electron-rich  $\gamma,\delta$ -alkene of  $\beta$ -ionone **250** is epoxidized.<sup>430</sup> Standard reaction conditions (rt, 1 h) led to 76% consumption of  $\beta$ -ionone **250**, affording a 20% yield of the desired vinyl ester **251**, along with 19% and 37% yields of epoxyketone **282** and epoxyester **280**, respectively (Table 13, entry 1). Total consumption of  $\beta$ -ionone **250** was achieved by increasing the *m*CPBA loading to 3.0 equiv., which afforded a mixture of epoxyketone **251** and epoxyester **280** in a 23:77 ratio (Table 13, entry 2). Carrying out these BV reactions at lower temperatures improved selectivity for formation of epoxyester **280** to 88% and 93% selectivities at 0 °C and -20 °C, respectively (Table 13, entries 3-4). Further cooling to -41 °C did not improve selectivity, with 66% consumption of  $\beta$ -ionone **250** after 1 h resulting in formation of 23:43 epoxyketone **252**: epoxyester **280** (Table 13, entry 5). Attempts to suppress  $\gamma,\delta$ -epoxidation further by increasing the loading of DMAPO to 100 mol%, whilst using 3.5 equiv. of *m*CPBA as oxidant) led to a significant drop in conversion and the production of mixtures of products (Table 13, entry 6). Conversely, simple removal of the DMAPO catalyst led to formation of a 92:8 mixture of epoxyketone **252** and epoxyester **280**, with epoxyketone **252** being isolated in 84% yield (Table 13, entry 7). This result further confirms the ability of DMAPO to drastically suppress alkene epoxidation reactions. Attempts to drive this epoxidation selectivity further by cooling to 0 °C resulted in 71% consumption with no improvement in selectivity (65:6 **252**:**280**, *i.e.* 91:9, *cf.* 92:8 at rt) (Table 13, entry 8). Addition of  $\text{NaHCO}_3$  (2.5 equiv.) also failed to improve selectivity for  $\gamma,\delta$ -epoxyketone **252**, instead resulting in only 77% conversion, with 23% epoxyketone **252**, 34% epoxyester **280** and 20% vinyl ester **251** (Table 13, entry 9) produced in a similar ratio to the initial DMAPO-catalysed run.

Table 13: *m*CPBA-mediated oxidation of  $\beta$ -ionone to epoxides **252** and **280**.



Entry <sup>a</sup>	Conditions	Product distribution (isolated yields)			
		Enone <b>250</b>	Epoxyketone <b>252</b>	Epoxyester <b>280</b>	Vinyl ester <b>251</b>
1	<i>m</i> CPBA (1.8 equiv.) DMAP (50 mol%) rt, 1 h	24%	19%	37%	20%
2	<i>m</i> CPBA (3.0 equiv.) DMAP (50 mol%) rt, 2 h	-	23%	77%	-
3	<i>m</i> CPBA (3.0 equiv.) DMAP (50 mol%) 0 °C, 1.5 h	-	12%	88%	-
4	<i>m</i> CPBA (3.0 equiv.) DMAP (50 mol%) -20 °C, 1.5 h	-	7%	<b>93% (81%)</b>	-
5 <sup>b</sup>	<i>m</i> CPBA (3.0 equiv.) DMAP (50 mol%) -41 °C, 1.5 h	34%	23%	43%	-
6	<i>m</i> CPBA (3.5 equiv.) DMAP (100 mol%) rt, 1.5 h	23%	17%	46%	14%
7	<i>m</i> CPBA (1.3 equiv.) rt, 1 h	-	<b>92% (84%)</b>	8%	-
8	<i>m</i> CPBA (1.3 equiv.) 0 °C, 2 h	29%	65%	6%	-
9	<i>m</i> CPBA (1.3 equiv.) NaHCO <sub>3</sub> (2.5 equiv.) rt, 1 h	23%	23%	34%	20%

<sup>a</sup> *m*CPBA and DMAP were premixed for 15 min. <sup>b</sup> Reaction carried out at 0.1 M concentration due to low-temperature solubility issues.

Therefore, two complementary protocols were identified that enabled selective oxidation of  $\beta$ -ionone **250**, with treatment with 1.3 equiv., *m*CPBA (no DMAPO) affording an 84% yield of epoxy ketone **252** (cf. 84% yield of **252** using Yu's complex selenide catalyst H<sub>2</sub>O<sub>2</sub> system),<sup>415</sup> whilst inclusion of 50 mol% DMAPO as an additive results in sequential BV oxidation and  $\gamma,\delta$ -alkene

epoxidation to produce epoxyster **280** in 81% yield as a major product (previously reported as a side-product in low yields only).<sup>431,432</sup> Attempts to develop a BV protocol that gave vinyl ester **251** as the major product proved unsuccessful, with cooling to 0 °C, decreasing the amount of *m*CPBA oxidant to 1.0 equiv., or use of 100 mol% DMAP leading to complex mixtures of the vinyl ester **351** (max 34%) along with  $\beta$ -ionone **250**,  $\gamma,\delta$ -epoxyketone **252**, and epoxyster **280** by-products (Table 14).

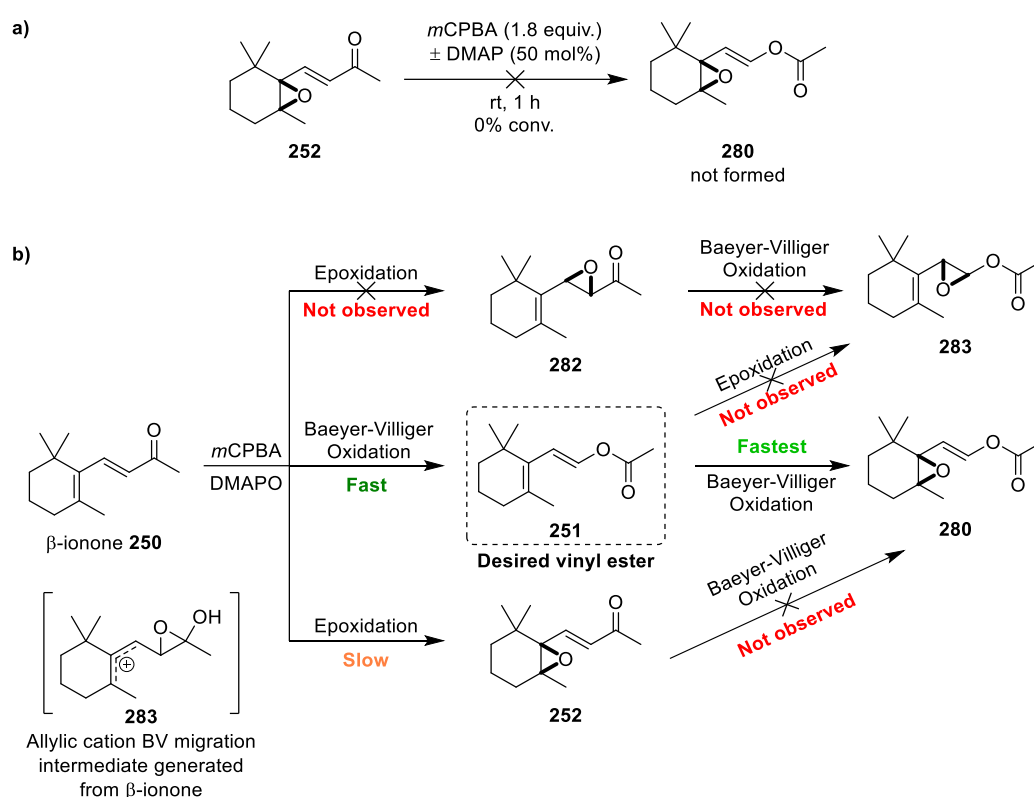
Table 14: *m*CPBA-mediated BV oxidation of  $\beta$ -ionone **250**.

Entry <sup>a</sup>	Conditions	Product distribution (isolated yields)			
		Enone <b>250</b>	Epoxyketone <b>252</b>	Epoxyster <b>280</b>	Vinyl ester <b>251</b>
1 <sup>b</sup>	<i>m</i> CPBA (1.8 equiv.) DMAP (50 mol%) rt, 1 h	24%	19%	37%	20%
2	<i>m</i> CPBA (1.8 equiv.) DMAP (50 mol%) 0 °C, 1 h	20%	8%	38%	34%
3	<i>m</i> CPBA (1.5 equiv.) DMAP (50 mol%) rt, 1 h	44%	11%	29%	26%
4	<i>m</i> CPBA (2.0 equiv.) DMAP (100 mol%) rt, 6 h	65%	6%	25%	4%
5	<i>m</i> CPBA (2.0 equiv.) DMAP (100 mol%) 0 °C, 6 h	64%	4%	29%	4%

<sup>a</sup> *m*CPBA and DMAP were premixed for 15 min. <sup>b</sup> See Table 13, entry 1.

These product distributions, in conjunction with the absence of  $\alpha,\beta$ -epoxides **281** and **282**, provide some insight into the relative reactivities of the different functionalities of  $\beta$ -ionone **250** in these BV oxidation reactions. Firstly, the more nucleophilic  $\gamma,\delta$ -alkene group of  $\beta$ -ionone **250** is clearly much easier to epoxidize than its  $\alpha,\beta$ -alkene bond due to its increased substitution pattern and remoteness from the deactivating carbonyl group. Secondly, the uncatalysed background rate of the Baeyer-Villiger oxidation reactions of  $\beta$ -ionone **250** and epoxyketone **252** are slow, only occurring significantly in the presence of the DMAP/DMAPO catalyst. Thirdly, treatment of epoxyketone **252** with *m*CPBA (with or without DMAP/DMAPO) does not result in any BV reaction to produce

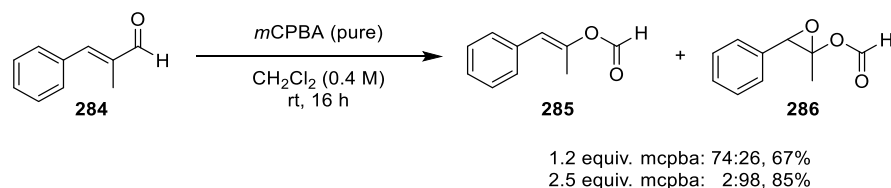
epoxy vinyl ester **280** (Scheme 113a), which means epoxyester **280** must be formed exclusively *via* BV oxidation of  $\beta$ -ionone **250** to vinyl ester **251** first, followed by epoxidation of the electron-rich  $\gamma,\delta$ -alkene bond. This is consistent with the  $\gamma,\delta$ -alkene bond of the vinyl ester **251** being more activated towards epoxidation by *m*CPBA than the corresponding  $\gamma,\delta$ -alkene bond of  $\beta$ -ionone **250**, and also explains why dienyl ester **251** could not be isolated as a major product from these reactions (see Scheme 113b for mechanistic summary). Furthermore, it is suggested that the BV oxidation of  $\beta$ -ionone **250** occurs *via* a stabilised allylic cation migration intermediate **283**, similar to the benzylic intermediate proposed in benzylidene systems (*vide supra*). Finally,  $\gamma,\delta$ -epoxyketone **252** does not undergo a BV oxidation because its ‘non-stabilised’ migratory transition state/intermediate is much higher in energy than the stabilised allylic species **283** generated in the BV oxidation reaction of  $\beta$ -ionone **250**.



Scheme 113: (a) Unreactive DMAPO-catalysed BV oxidation of epoxyketone **252**. (b) Reaction map of DMAPO-catalysed/suppressed oxidation reactions of  $\beta$ -ionone **250**.

These *N*-oxide-catalysed *m*CPBA-mediated BV reactions of  $\alpha,\beta$ -unsaturated ketones complement the recent work by Kazmaier *et al.*, who showed that  $\alpha$ -methyl  $\alpha,\beta$ -unsaturated aldehyde **284** (more nucleophilic, more stabilised) could be oxidised with purified *m*CPBA to produce  $\alpha,\beta$ -unsaturated formate ester **285**, or  $\alpha,\beta$ -epoxyformate **286** as required (Scheme 110). They found that use of 1.2 equiv. of purified *m*CPBA afforded a 74:26 mixture of vinyl ester **285** and epoxyester **286**, for a 67% isolated yield of vinyl formate ester **285**. Increasing the oxidant loading to 2.5 equiv. of *m*CPBA drove the epoxidation further to produce epoxyester **286** in 98% selectivity, allowing it to be isolated in 85% isolated yield. Investigations are currently underway to determine whether the

inclusion of an *N*-oxide catalyst into the BV reaction of  $\alpha,\beta$ -unsaturated aldehydes can be used to improve the yield of vinyl-formate ester **285**.



Scheme 114: Kazmaier *et al.*'s synthesis of  $\alpha,\beta$ -unsaturated formate ester **285** and  $\alpha,\beta$ -epoxyformate **286** using purified *m*CPBA.<sup>422</sup>

## 4.4. Mechanistic investigations into DMAPO-catalysed BV oxidation reactions

### 4.4.1 Mechanism of acid-catalysed BV oxidation reactions

Following these synthetic developments, a better understanding of the mechanism of action of the *N*-oxide catalyst was needed, which led us to review previous approaches that had been developed to catalyse peracid-mediated BV reactions. Two general approaches have been investigated for the catalytic activation of BV oxidation reactions: electrophilic activation approaches and nucleophilic activation strategies (Figure 47).<sup>373,433</sup> Electrophilic activation approaches employ a Brønsted or Lewis acid to coordinate to the carbonyl oxygen of either: (i) the ketone substrate, to activate it towards nucleophilic attack by the peracid (**287**); (ii) or the acid leaving group of the Criegee intermediate which promotes cleavage of the peroxide bond during the second migration step (**288**). Conversely, nucleophilic activation approaches are usually facilitated by a Lewis/Brønsted base that can: (iii) coordinate to (or deprotonate) the most acidic OH proton of the peracid during the addition step to increase its nucleophilicity (**289**); or (iv) deprotonate the alcohol group of the Criegee intermediate to trigger the migration step (**290**). Two examples of catalytic systems that have been developed are shown in Figure 47, with their mode of catalytic activation indicated. Note that in many cases multiple modes of activation are involved, and determining the exact mechanism is often not possible.

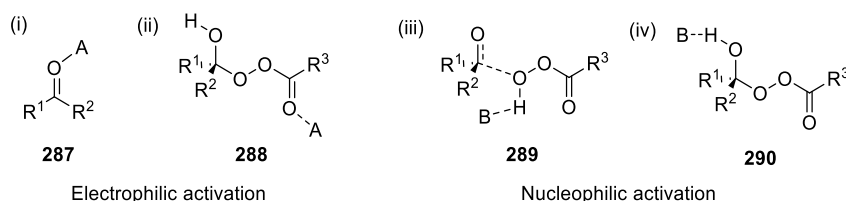
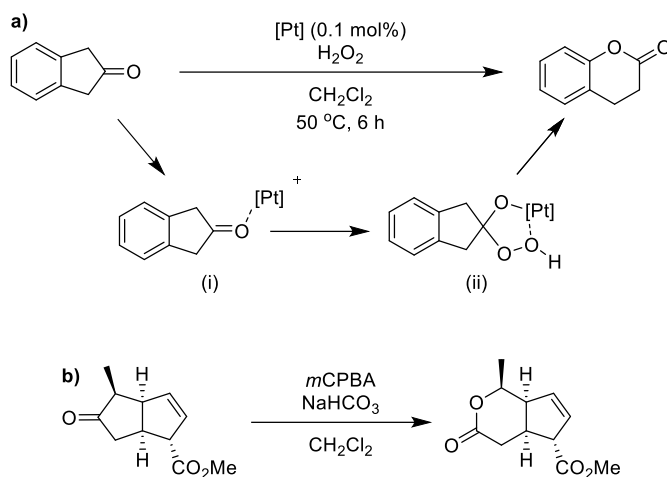


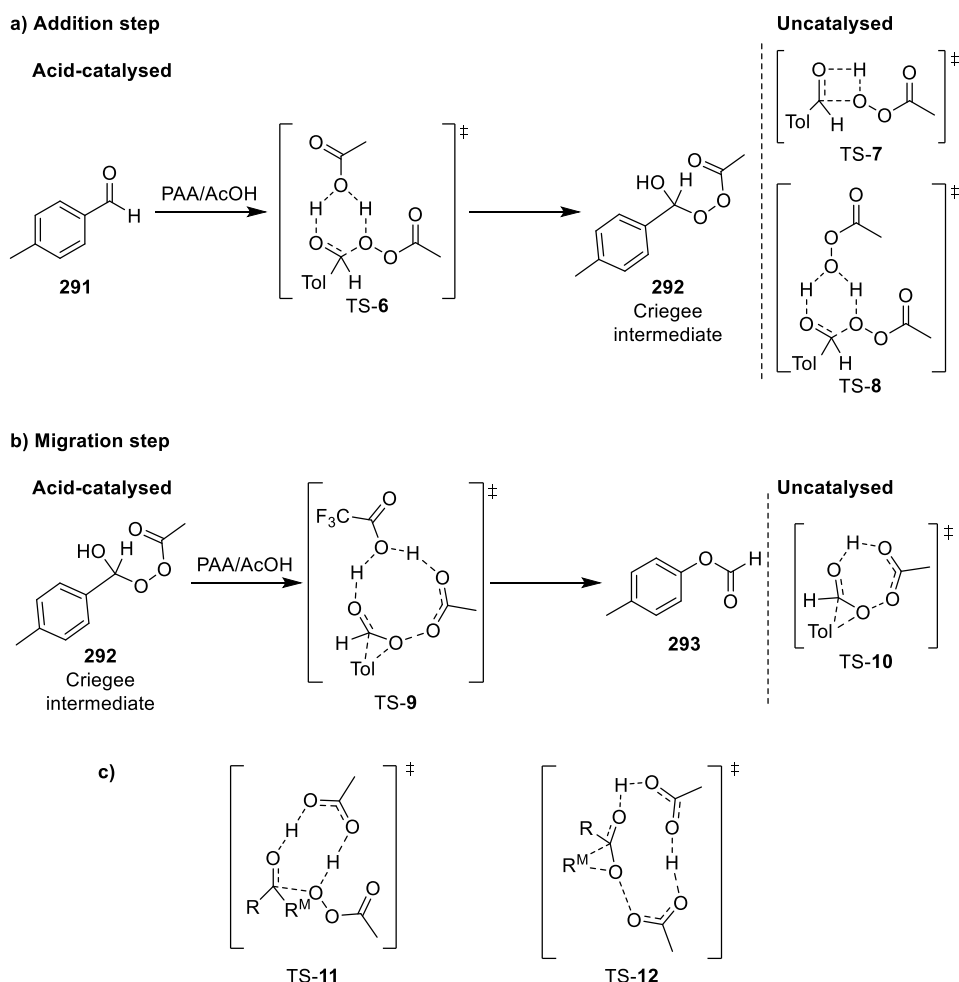
Figure 47: Electrophilic and nucleophilic catalytic activation of the BV oxidation reaction.



Scheme 115: Representative examples of catalytic BV oxidation reactions. (a) BV oxidation of cyclic ketones catalysed by electrophilic activation of the substrate (i) and intermediate (ii) by Lewis-acidic [((dppe)Pt(CF<sub>3</sub>)CH<sub>2</sub>Cl<sub>2</sub>)ClO<sub>4</sub>].<sup>434</sup> (b) NaHCO<sub>3</sub>-mediated nucleophilic activation (iii, iv) of cyclic ketones.<sup>435</sup>

Previous studies had revealed that the *N*-oxide catalyst only accelerated BV reactions of ketones where initial nucleophilic addition of *m*CPBA to the ketone was known to be rate determining, and so it appeared that the *N*-oxide catalyst must be operating by either pathway (i) or pathway (iii). Experimental and computational mechanistic investigations into peracid-mediated BV reactions of ketones have previously shown that the addition step is catalysed by carboxylic acids (*e.g.* *m*CBA), and that dynamic hydrogen bonding and proton transfer events are crucial in lowering the transition state energy of the initial peracid addition step to the ketone carbonyl.<sup>381,382,436–438</sup> For example, a study in 1997 by Okuno showed that BV oxidation of *p*-anisaldehyde and *p*-tolualdehyde **291** in non-polar solvents could be catalysed by either acetic acid or trifluoroacetic acid (TFA), with relatively weak AcOH only catalysing the initial addition step, whilst stronger TFA could catalyse both the addition and migration steps.<sup>436</sup> This study revealed that acid-catalysed BV reactions proceed *via* general acid catalysis, meaning that no formal protonation of the ketone substrate occurs prior to nucleophilic attack by the peracid. Interestingly, this was also suggested to be the case in aqueous media (where acid dissociation would be expected), indicating that this mode of catalysis is driven by discreet assemblies rather than non-specific pH/media effects.<sup>439</sup> Okuno proposed that carboxylic acid-catalysed addition of the peracid to the ketone occurs *via* a concerted 6-membered hydrogen bonded transition state TS-6 (Scheme 116a), with the bifunctional carboxylic acid acting to protonate the carbonyl of the ketone whilst simultaneously accepting the terminal OH proton of the peracid. Therefore, this ‘proton shuttling’ mechanism enables the carboxylic acid catalyst to increase the nucleophilicity of the peroxide whilst simultaneously activating the ketone carbonyl group towards nucleophilic attack. This transition state is highly favoured over non-catalysed transition states such as the forbidden 4-atom TS-7 that is often shown in textbooks, or the peracid-mediated TS-8 that is less effective at shuttling protons in the transition state (*cf.* *pK<sub>a</sub>* of *m*CPBA of 7.5 vs. *pK<sub>a</sub>* of *m*CBA of 3.82).<sup>440,441</sup> However, there is some controversy regarding these non-acid-catalysed multimeric transition states, with Alvarez-Idaboy and co-workers calculating prohibitively large energy barriers of 25 kcal/mol or more.<sup>381,437,438,442,443</sup> These

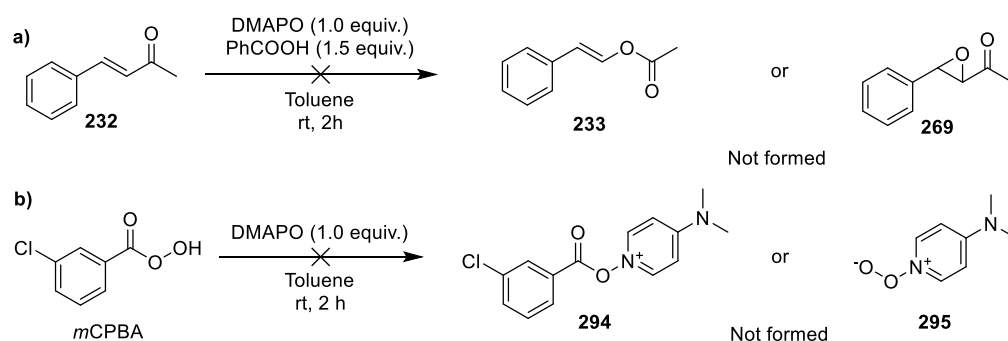
findings have since been corroborated by other studies, which have confirmed that acid catalysis is highly effective at activating the initial addition step of BV oxidations, even when only mild acids are employed.<sup>437,442</sup> Acid catalysis can also activate the migration step of BV reactions, although this appears to occur only when the migration step is relatively slow, and usually requires strong acid catalysts (*e.g.* TFA).<sup>377,436,437</sup> This is because carboxylic acid-catalysed migration proceeds *via* a 9-membered transition state TS-9, whose formation is only favoured when strong acids are employed (Scheme 116b). In the absence of a strong acid catalyst, migration occurs *via* a concerted 7-membered hydrogen bonding transition state TS-10 in which the Criegee hydroxyl proton migrates intramolecularly to the carboxyl group of the acid by-product. Other acid-catalysed transition states for BV reactions have also been calculated, in which carboxylic acids catalyse the addition or migration steps through more complex proton shuttling effects in which the hydrogen bond acceptor of the acid is the carbonyl oxygen (Scheme 116c). This leads to larger 8- and 11-membered hydrogen-bonded transition states TS-11 and TS-12, which are some of lowest transition energies for standard BV oxidation reactions that have been calculated to date.<sup>381,442,443</sup>



Scheme 116: (a,b) BV oxidation reaction of *p*-tolualdehyde **291** by peracetic acid according to Okuno.<sup>436</sup> (c) Proton-shuttling transition states proposed by Alvarez-Idaboy and co-workers.<sup>381,442,443</sup>

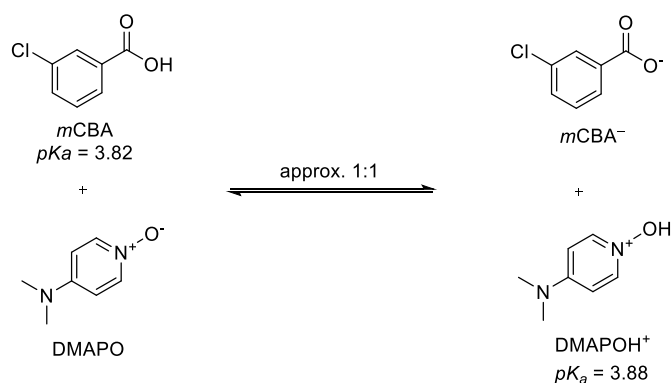
Although *N*-oxides are known to be capable of acting as direct oxidants in other types of oxidative reaction,<sup>444</sup> the Bull group have previously demonstrated that treatment of benzalacetone **232** with

stoichiometric amounts of DMAPO does not produce any vinyl ester **233** (or epoxide **269**) product (Scheme 117a).<sup>418</sup> Furthermore, <sup>1</sup>H NMR spectroscopic studies have also demonstrated that treatment of DMAPO with *m*CPBA does not produce any detectable *N*-oxy-acyl-pyridinium **294** or *N*-hydroperoxy-pyridinium **295** species that could potentially be acting as a more reactive *in situ*-generated BV oxidant (Scheme 117b). It was also confirmed that any hydrogen peroxide that might be formed as a by-product of the reaction of *m*CPBA and DMAPO (*vide supra*) was not a competent oxidant in these BV reactions.



Scheme 117: (a) DMAPO does not catalyse BV oxidation or epoxidation of benzalacetone (*E*)-**232**. (b) Treatment of *m*CPBA with DMAPO did not produce any new DMAPO-derived oxidants.

BV reactions of ketones that employ *m*CPBA (weaker acid) as a stoichiometric oxidant generate increasing amounts of *m*CBA (stronger acid) as the BV reaction proceeds towards completion. Since carboxylic acids such as *m*CBA are known to catalyse BV reactions, this meant that these BV oxidation reactions are potentially autocatalytic.<sup>437</sup> As discussed, commercial *m*CPBA was used in initial studies of *N*-oxides as BV catalysts, which contains ~75% pure *m*CPBA with the remaining mass made up of *m*CBA (20%) and H<sub>2</sub>O (5%). Therefore, *m*CBA is always available as a potential cocatalyst in these DMAPO-catalysed reactions, with the similar *pK<sub>a</sub>* values of *m*CBA (*pK<sub>a</sub>* = 3.82) and DMAPOH<sup>+</sup> (*pK<sub>aH</sub>* = 3.88) meaning that a near 1:1 equilibrium between DMAPO/*m*CBA and DMAPOH<sup>+</sup>/*m*CBA<sup>−</sup> is likely to be present in these biphasic BV reactions.<sup>441,445</sup>



Scheme 118: Quaternary equilibrium mixture formed from mixing *m*CBA with DMAPO.<sup>445,446</sup>

Having established that the *N*-oxide catalysts catalyse the first nucleophilic addition step of the BV reaction, it followed that DMAPO could be functioning as a Lewis base to increase the nucleophilicity of *m*CPBA (Figure 48a). In this respect, it should be noted that recent



computational and experimental work has shown that *N*-oxides (such as trimethylamine *N*-oxide, TMNO) are excellent H-bond acceptors that are capable of making strong hydrogen bonding interactions with weak acids such as HCN or acetylene ( $pK_a$  of 9.2 and 25, respectively).<sup>447</sup> Alternatively, it is possible that the protonated DMAPOH<sup>+</sup> equilibrium species could be acting as a Brønsted acid catalyst to activate the ketone carbonyl towards nucleophilic attack by the *m*CPBA nucleophile (Figure 48b). Either of these mechanisms would likely proceed *via* polarised/charged transition state/intermediates, and so any catalysed BV reaction would preferentially occur in the vicinity of the polar water-toluene interface, rather than proceeding in the non-polar toluene solvent. Some evidence for the formation of equilibrium mixtures in these systems was observed by carrying out <sup>1</sup>H NMR spectroscopy of DMAPO/*m*CBA mixtures, which showed downfield shifts ( $\Delta\delta_H = +0.05$  ppm, methyl resonances) for DMAPO resonances and upfield shifts for *m*CBA resonances ( $\Delta\delta_H = -0.06$  ppm, 4-H) that were consistent with protonation of DMAPO (decreased shielding) and deprotonation of *m*CBA (increased shielding) (see Appendix C for spectra). This equilibrium process could also explain the apparent suppression of BV oxidation reactions of electron-poor systems (*vide supra*), since complexation would decrease the availability of the acid catalyst, which would then be less available to catalyse the rate determining migration step.

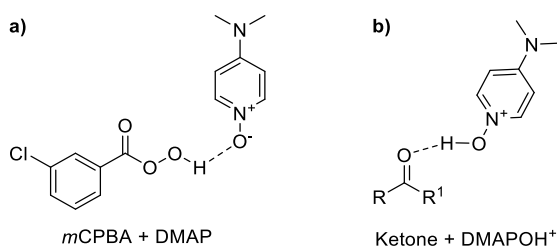


Figure 48: Possible modes of action of *N*-oxides for the catalysis of BV oxidation reactions. (a) Nucleophilic activation of *m*CPBA by DMAPO. (b) Electrophilic activation of the ketone by DMAPOH<sup>+</sup>.

Further evidence that formation of catalytically active DMAPOH<sup>+</sup> species might be important in these BV oxidation reactions came from the difference in BV reactivity that was observed when different types of *N*-oxides were used as catalysts.<sup>418</sup> Use of 20 mol% of electron-deficient 4-nitropyridine *N*-oxide **298** ( $pK_{aH} = -1.7$ ) and pyridine *N*-oxide **299** ( $pK_{aH} = 0.79$ ) in the BV oxidation reaction of *p*-methoxybenzophenone **296** (relatively unreactive ketone, facile migration) gave only 9 and 11% conversion to its corresponding ester **297** after 7 h, respectively. Conversely, use of more electron-rich DMAPO ( $pK_{aH} = 3.88$ )<sup>448</sup> resulted in 36% conversion to **297** after only 2 h, thus demonstrating its much greater catalytic activity (Figure 49). The significantly lower  $pK_{aH}$  values of *N*-oxides **298** and **299** ( $< 1.0$ )<sup>448</sup> means that they are likely to be essentially unprotonated by the *m*CBA ( $pK_a = 3.82$ )<sup>441</sup> under the BV reaction conditions, and so are unlikely to form the type of protonated *N*-oxide species (or quaternary mixtures) that can be formed when DMAPO is used as a catalyst.

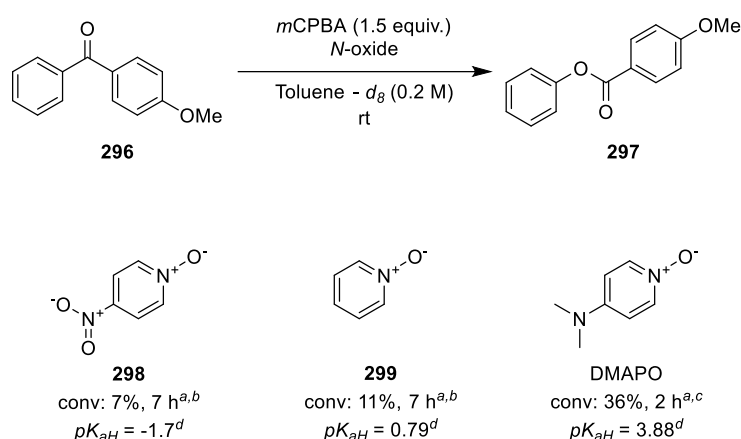


Figure 49: Substituted pyridine *N*-oxides. <sup>a</sup> Conversion achieved when the corresponding *N*-oxide (formed *in situ*) is used as the catalyst for the BV oxidation of *p*-methoxybenzophenone **296**. <sup>b</sup> Conversions from Dr Lawrence's thesis. <sup>c</sup> See Table 10, entries 6-7. <sup>d</sup> *pK<sub>aH</sub>* values from Makowski *et al.*<sup>448</sup>

Given the established role of carboxylic acids in catalysing BV oxidation reactions, it seems likely that DMAPOH<sup>+</sup> might be acting as a more catalytically active replacement for the *m*CBA cocatalyst that had previously been proposed to be present in BV transition states. Incorporation of DMAPOH<sup>+</sup> would create a favourable 6-membered hydrogen bonding ternary transition state TS-**13** that could promote the first addition step of the BV reaction *via* a similar proton relay mechanism to carboxylic acids (Figure 50). In this case, DMAPOH<sup>+</sup> would act as a Brønsted acid to protonate the lone pair of the ketone to activate it towards nucleophilic attack by *m*CPBA, whilst simultaneously acting as a Brønsted base to accept a proton from the incoming *m*CPBA to increase its overall nucleophilicity. Therefore, the DMAPOH<sup>+</sup> catalyst would serve to create a concerted proton relay pathway that would minimise charge build up in the transition state and decrease the overall energy barrier of the *m*CPBA nucleophilic addition step (Figure 50). This mode of action is clearly directly analogous to the well-established catalytic mode of action of mild acids elucidated by Okuno (*vide supra*, TS-**6**). Once again, the charged nature of the proposed DMAPOH<sup>+</sup> catalyst would mean that that its involvement as proton relay catalyst would most likely occur at the toluene-water interface.

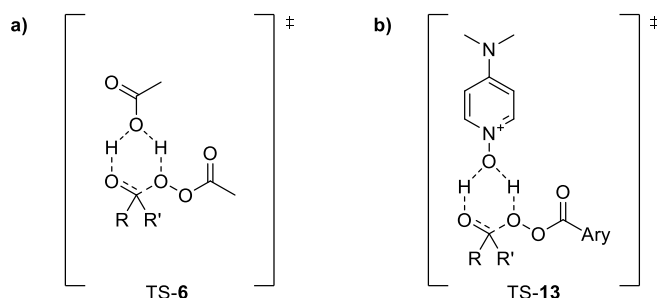
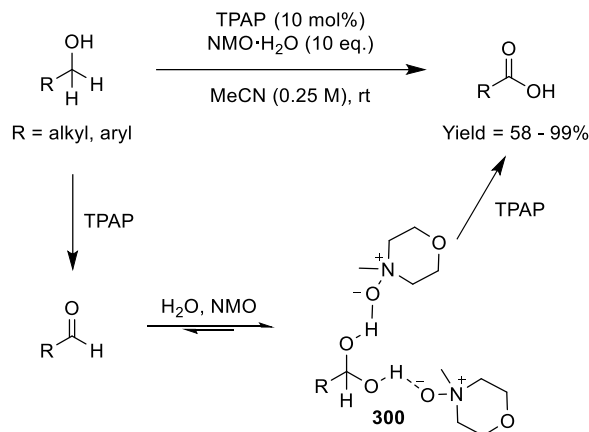


Figure 50: (a) Previously proposed transition state showing how a carboxylic acid can act as a bifunctional proton relay catalyst to promote nucleophilic addition of *m*CPBA to ketones in BV reactions.<sup>436</sup> (b) New transition state showing how DMAPOH<sup>+</sup> might function as proton transfer relay catalyst in BV reactions

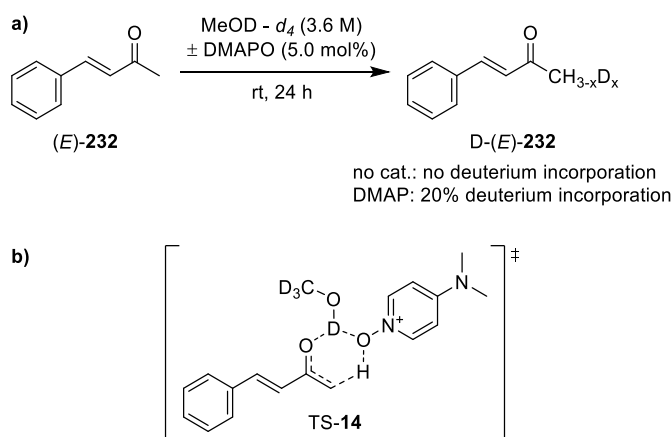
Precedent for the ability of *N*-oxides to participate in catalytically-relevant hydrogen bonding networks comes from a report by Stark *et al.* who described that *N*-methylmorpholine *N*-oxide (NMO) could be used to catalyse tetrapropylammonium perruthenate-mediated (TPAP) oxidation

of alcohols to carboxylic acids (Scheme 119).<sup>449,450</sup> They proposed that the high efficiency of this oxidative system was due to the water and NMO catalyst combining to form an *N*-oxide stabilised hydrogen bonding network that stabilised formation of the vicinal diol group of an aldehyde hydrate intermediate **300** that is then oxidised to its corresponding carboxylic acid.



Scheme 119: NMO-catalysed oxidation of alcohols to carboxylic acids by TPAP in the presence of water.<sup>449,450</sup>

Further evidence that DMAPO might be functioning as a proton transfer catalyst was obtained previously from deuterium labelling experiments, which revealed that treatment of  $\alpha,\beta$ -unsaturated ketone (*E*)-**232** with 5.0 mol% DMAPO in deuterated methanol resulted in significant deuterium incorporation into its methyl group over time (Scheme 120a).<sup>418</sup> This contrasts with the uncatalysed system where no deuterium incorporation into  $\alpha,\beta$ -unsaturated ketone **232** was observed, thus suggesting that DMAPO facilitates deuterium incorporation into benzalacetone **232** by acting as a Brønsted base to promote enolization *via* TS-14.



Scheme 120: (a) Deuterium incorporation studies of benzalacetone (*E*)-**232** with DMAPO and MeOD - *d*<sub>4</sub>. (b) DMAPO/DMAPOD<sup>+</sup> acting as a catalyst to promote enol tautomerization.<sup>418</sup>

#### 4.4.2 Evidence that DMAPO can act as a phase-transfer catalyst in BV reactions

These proposed mechanistic hypotheses for the catalytic activity of DMAPO in BV reactions would all proceed through polarised transition states, most likely to occur at the polar toluene-water

interfaces that are present in these biphasic BV oxidation reactions. Consequently, the relative solubilities of the different reactive components in toluene and water were studied to try and gain a better understanding of their effect on these BV oxidation reactions. The overall solubility of commercial *m*CPBA (containing approx. 20% *m*CBA and 5 wt% water) in toluene was relatively poor, leading to cloudy suspensions when added to toluene (and other BV reaction mixtures) (Figure 51A). Direct comparison of the relative solubilities of pure *m*CPBA and *m*CBA in toluene revealed that whilst *m*CPBA was soluble in toluene (Figure 51B), *m*CBA was completely insoluble which persisted as an unchanged crystalline solid (Figure 51C). The solubility of zwitterionic DMAPO in toluene was also found to be low, remaining crystalline as for *m*CBA (Figure 51D). However, addition of mixtures of DMAPO and commercial *m*CPBA (containing 20-25% *m*CBA, Figure 51E) or DMAPO and *m*CBA (Figure 51F) to toluene resulted in rapid dissolution/dispersion of all components to produce cloudy surfactant-like mixtures. This suggests that surfactant/phase-transfer-like quaternary mixtures are formed when DMAPO and *m*CBA interact in these systems (see acid-base mechanism shown in Scheme 118). Interestingly, whilst all three individual components were white solids, combination of mixtures of DMAPO/*m*CPBA/*m*CBA in toluene resulted in suspensions that exhibited a yellow hue that was localised around water droplets that were dispersed throughout the toluene solvent, which coalesced on standing (Figure 51E, commercial *m*CPBA). This observation indicates that toluene-soluble *m*CPBA is interacting with the quaternary DMAPO/*m*CBA mixtures present at the toluene-water interface. Supporting this hypothesis, mixing pure *m*CPBA and DMAPO in toluene resulted in a faint yellow homogenous solution (Figure 51G), thus indicating that intermolecular hydrogen bonding interactions between DMAPO and *m*CPBA were occurring. Addition of 5 wt% water to a pure mixture *m*CPBA and DMAPO produced a cloudy mixture with a significantly increased yellow colour, as seen previously for the mixture of DMAPO with commercial *m*CPBA (Figure 51H, *cf.* E). These observations strongly support the suggestion that solubilising hydrogen bonding interactions are formed between DMAPO and *m*CPBA (and *m*CBA), which is consistent with a previous report describing that *trans*- $\alpha$ -sillbazole *N*-oxide **301** can reversibly generate stable crystalline hydrogen bonded complexes with peracetic acid.<sup>451</sup>

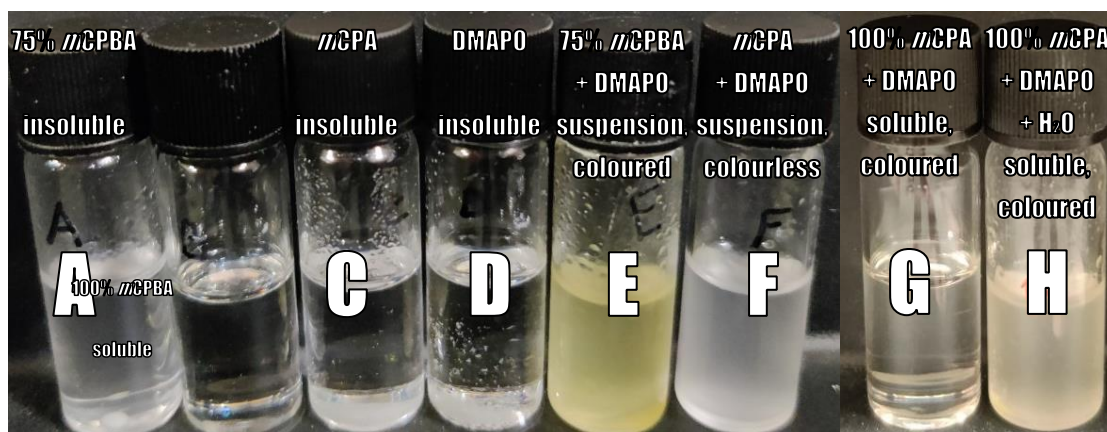
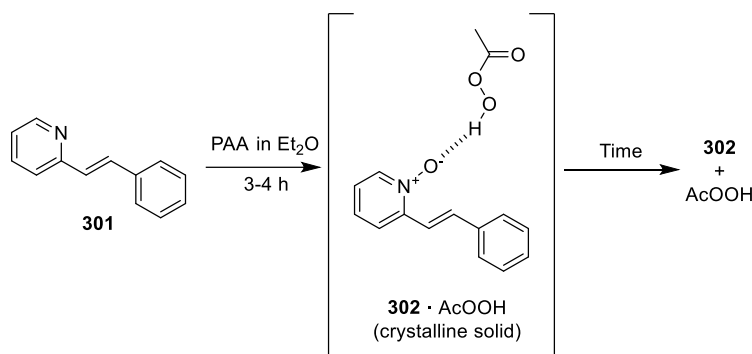


Figure 51: Various DMAPO-catalysed BV reaction components added to 1 mL toluene: A – 75 wt% *m*CPBA (61 mg, partially soluble); B – pure *m*CPBA (44 mg, soluble); C – *m*CBA (6.3 mg, insoluble); D – DMAPO (6.2 mg, insoluble); E – 75 wt% *m*CPBA + DMAPO (61 mg + 6.2 mg, cloudy dispersion, yellow after 15+ min); F – DMAPO + *m*CBA (6.2 mg + 6.3 mg, cloudy dispersion); G – DMAPO + *m*CPBA (6.2 mg, 44 mg, slightly coloured solution); H – DMAPO + *m*CPBA + H<sub>2</sub>O (6.2 mg, 44 mg, 5  $\mu$ L, slightly coloured cloudy dispersion). DMAPO monohydrate used.



Scheme 121: Oxidation of *trans*- $\alpha$ -stilbazole **301** to its corresponding *N*-oxide **302** forms a reversible complex with peracetic acid.<sup>451</sup>

Initial addition of *p*-methoxyacetophenone **263** to a cloudy suspension of commercial *m*CPBA and DMAPO in toluene led to no initial change in appearance (Figure 52A). However, once approximately 65% BV oxidation of *p*-methoxyacetophenone **263** had occurred (~45 min), large amounts of a crystalline white solid was found to precipitate out (Figure 52B). This precipitate was filtered off and analysed by <sup>1</sup>H NMR spectroscopic analysis, which revealed that it was essentially pure *m*CBA. This is consistent with consumption of *m*CPBA in the BV reaction resulting in generation of large amounts of *m*CBA by-product, whose concentration eventually reaches a saturation point where it precipitates out and so is no longer available to act as a catalyst in the BV reaction.

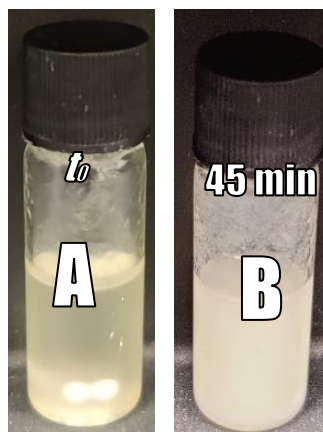
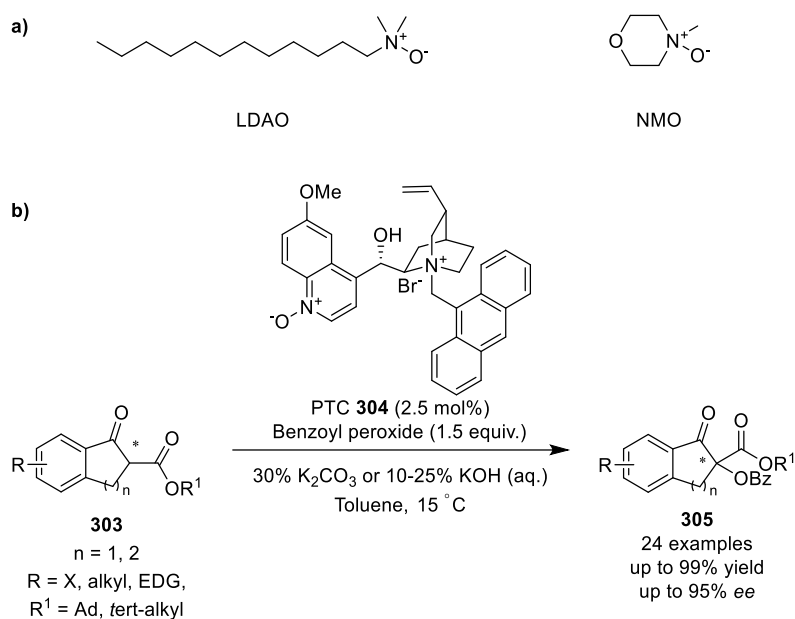


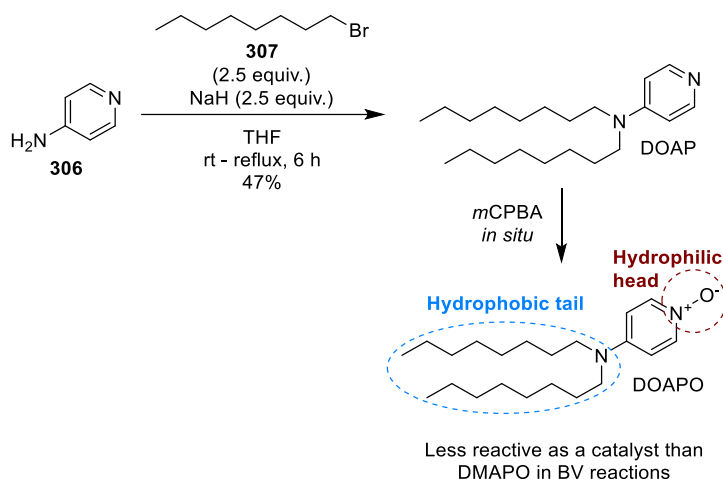
Figure 52: DMAPO-catalysed BV oxidation reaction of *p*-methoxyacetophenone **263** by *m*CPBA at  $t_0$  (A) and 45 min (B).

The ability of *m*CPBA to facilitate dissolution of DMAPO in toluene provides evidence that DMAPO could potentially be acting as a hydrogen bonding phase transfer catalyst (PTC) to promote the BV reactions. Unfortunately, due to complexity arising from the bi-/tri-phasic nature of this reaction, and the complicated side-reactions later discovered (see section 4.5), conclusive conclusions could be drawn at this stage, however the author feels the results presented throughout this chapter are consistent with the proton- and phase-transfer mechanisms suggested. Moreover, this hypothesis is consistent with the amphoteric surfactant-like properties of *N*-oxides whose hydrogen bonding properties have previously been exploited to prepare lubricant and cosmetic products.<sup>452</sup> For example, lauryldimethylamine *N*-oxide (LDAO) is used as a detergent to solubilise aggregating proteins, whilst the antimicrobial surfactant properties of *N*-oxides means they are widely used as antimicrobial components in detergents.<sup>453,454</sup> Similarly, NMO is widely employed as an ionic solvent on an industrial scale in the Lyocell process, with the hydrogen bonding properties of NMO facilitating pulp solubilisation to generate cellulose fibres that can then be processed into fabrics.<sup>455</sup> Precedent for the use of *N*-oxides as PTCs in catalysis also exists, with Meng and co-workers having reported use of 2.5 mol% cinchona-alkaloid-derived *N*-oxide **304** as a chiral PTC to catalyse the enantioselective  $\alpha$ -benzoylation of enolates of  $\beta$ -keto-esters **303** (or amides) to afford  $\alpha$ -benzoyloxy  $\beta$ -keto esters **305** in high yields and high enantioselectivities (Scheme 122).<sup>456,457</sup>



Scheme 122: (a) Examples of surfactant amine *N*-oxides. (b) Enantioselective  $\alpha$ -benzoyloxylation of  $\beta$ -keto esters by chincona-derived *N*-oxide phase transfer catalyst **304**.<sup>456</sup>

Given this precedent, it was hypothesized that a more lipophilic surfactant-like 4-dioctylaminopyridine *N*-oxide (DOAPO) analogue might be a better ‘phase-transfer’ *N*-oxide catalyst in BV reactions. It was reasoned that the zwitterionic *N*-oxide fragment of DOAPO would act as a polar headgroup, whilst its two *N*-octyl chains would provide lipophilic tail groups, thus conferring DOAPO with good surfactant-like properties (Scheme 123). After a variety of unsuccessful  $S_NAr$ -based attempts, it was found that treatment of 4-aminopyridine **306** with 2.5 equiv. of sodium hydride and 2.5 equiv. of 1-bromooctane **307** at reflux in THF successfully afforded DOAP in 47% yield (Scheme 123c) (*cf.* 14% yield for DOAP obtained using an  $S_NAr$  between 4-chloropyridine and dioctylamine).<sup>458</sup> Use of this surfactant-like DOAPO as a catalyst in the BV oxidation reaction of *p*-methoxyacetophenone **263** gave similar selectivity profiles to those observed for DMAPO, however its decreased reactivity levels (45% after 30 min with 20 mol% DOAP, *vs.* 61% with DMAP) meant that it appeared to provide no benefit over existing *N*-oxide catalysts (*e.g.* TMNO) that had been identified previously.



Scheme 123: Successful synthesis of DOAP from 4-aminopyridine **306** and 1-bromooctane **307**.

The implications of these reactions and observations on the mechanism of the DMAPO-catalysed BV oxidation reactions were then evaluated, which enabled us to propose an improved mechanistic hypothesis that seemingly explains these experimental results. It is proposed that DMAPO interacts with the *m*CBA at the toluene water droplet interface, resulting in an acid-base equilibrium being established that generates both DMAPO and protonated DMAPOH<sup>+</sup> species in the vicinity of the boundary layer. The more polar environment at the aqueous droplet-toluene interface means that any *N*-oxide catalysis of these BV reactions will occur preferentially in this boundary region (as suggested by the yellow hue observed at the surface of dispersed water droplets). The presence of both DMAP (Brønsted base) and DMAPOH<sup>+</sup> (Brønsted acid) species at this interface can then combine to establish hydrogen bonding networks that function to shuttle protons between the *m*CPBA nucleophile and the *m*CBA by-product to minimise charge build up in the BV transition state, thus lowering the energy of the initial addition step of the BV pathway (see Figure 53).



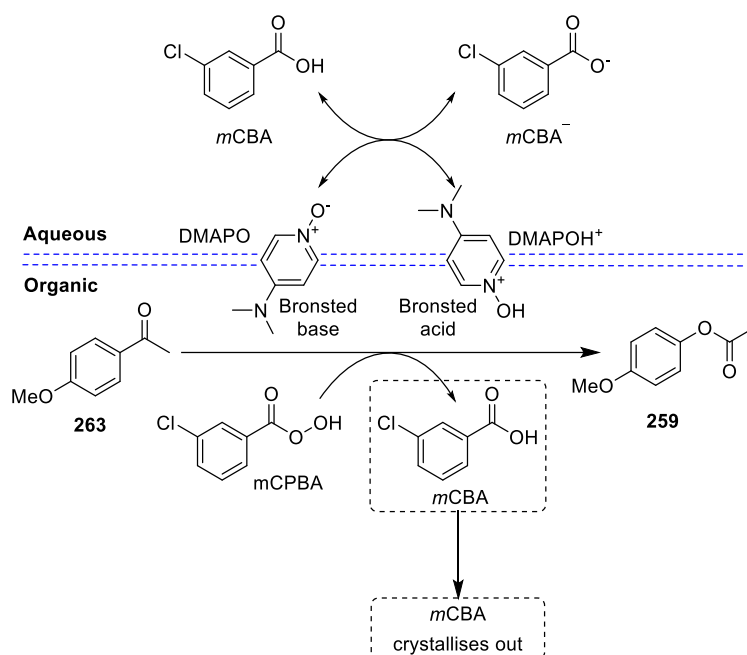
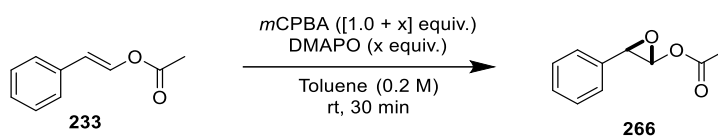


Figure 53: Schematic representation of the proposed mechanism of biphasic DMAPO-catalysed aqueous/toluene BV oxidation reactions of *p*-methoxyacetophenone **263** to *p*-acetoxy anisole **259**. The DMAPO and/or the DMAPOH<sup>+</sup> species produce a hydrogen bond network that lowers the transition state energy of the BV reaction. The DMAPO component may potentially act through coordination to the acidic hydrogen of the hydroxyl group of *m*CPBA to increase its nucleophilicity. The DMAPOH<sup>+</sup> component can potentially act as a Brønsted acid to protonate the carbonyl lone pair of ketone **263**, thus increasing its reactivity towards nucleophilic attack by *m*CPBA. Incorporation of DMAPOH<sup>+</sup> into the BV transition state may also facilitate proton transfer from the *m*CPBA nucleophile to the ketone substrate to form the Criegee intermediate.

#### 4.4.3 DMAPO acts as a proton transfer catalyst to suppress epoxidation of vinyl esters

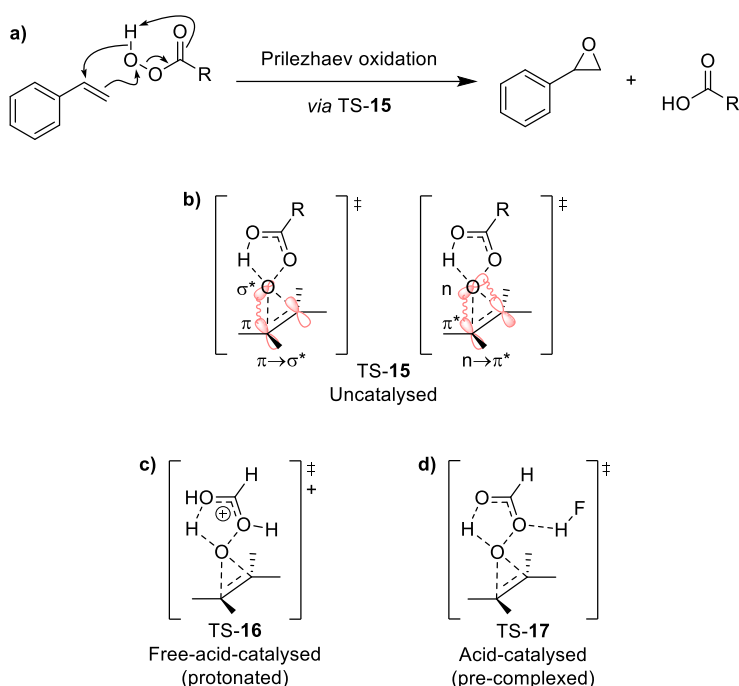
Next, this study focused on the observation that DMAPO exhibited a dual catalytic and suppressive role in the BV reactions of  $\alpha,\beta$ -unsaturated ketones, acting both as a catalyst to promote the BV reaction and as an inhibitor to suppress competing epoxidation reactions of vinyl ester (*E*)-**233** (see Table 12). This was done in a series of experiments using *m*CPBA and vinyl ester (*E*)-**233** as starting material to confirm that epoxidation of vinyl ester was suppressed by DMAPO (Table 15). In the absence of DMAPO, treatment of vinyl ester **233** with 1.0 equiv. of *m*CPBA in toluene at room temperature resulted in epoxidation of vinyl ester **233** to produce epoxyster **266** in 26% yield after 30 min (Table 15, entry 1). As predicted, this epoxidation reaction was suppressed by addition of *in situ*-formed DMAPO, with 20 mol% catalyst loading resulting in epoxyster **266** being formed in a decreased 17% yield, whilst use of stoichiometric amounts of DMAPO resulted in only 3% epoxyster **266** being formed (Table 15, entries 2-4).

Table 15: DMAPO-mediated  $\alpha,\beta$ -epoxidation of vinyl ester **233**.

Entry <sup>a</sup>	Additive (mol%)	<i>m</i> CPBA loading	Product distribution <sup>b</sup>		
			Vinyl ester <b>233</b>	Epoxyster <b>266</b>	Rearrangement products
1	None	1.00 equiv.	74%	26%	-
2	DMAP (20)	1.20 equiv.	83%	17%	-
3	DMAP (50)	1.50 equiv.	92%	8%	-
4	DMAP (100)	2.00 equiv.	97%	3%	-

<sup>a</sup> *m*CPBA and catalyst/precatalyst were premixed for 15 min. <sup>b</sup> All distributions were referenced to a TetMB internal standard to ensure integration accounted for the entire mass balance.

The mechanism of alkene epoxidation reactions using peracids is well known,<sup>397</sup> with electron-rich alkene bonds acting as nucleophiles to attack the peracid's most electrophilic oxygen atom, which triggers a concerted elimination/proton transfer/oxidation pathway that produces the epoxide and an acid by-product. These reactions are accepted to proceed *via* a spiro/spiro-butterfly transition state TS-**15** in which the alkene and peroxide are oriented orthogonally to each other (Scheme 124b).<sup>459,460</sup> This favours two key MO interactions: the primary  $\pi_{C=C} \rightarrow \sigma^*_{O-O}$  interaction responsible for the formation of epoxide, and a stabilising secondary  $n_O \rightarrow \pi^*_{C=C}$  electronic interaction between the distal oxygen lone pair and the alkene antibonding  $\pi^*$  orbital. Relevant to the work in this chapter is the fact that these electrophilic epoxidation reactions can be catalysed by strong acids (*eg.* TFA),<sup>461</sup> with specific acid catalysis (*cf.* general acid catalysis in first step of BV reaction) resulting in formal protonation of the peracid carbonyl oxygen which triggers nucleophilic attack of the peracid by the alkene (Scheme 124c).<sup>462,463</sup> Computational and experimental studies have shown that prior protonation of the peracid significantly decreases the activation barrier of alkene epoxidation, with Bach *et al.* calculating a 12.4 kcal/mol decrease in activation barrier (from 18.8 to 6.4 kcal/mol) for the epoxidation of ethene by performic acid (PFA) *via* TS-**16** when fully protonated performic acid was modelled in a polar environment.<sup>462</sup> However, formal protonation of *m*CPBA is unlikely to occur in non-polar hydrophobic solvents such as toluene, although peracid protonation could potentially occur at the toluene-water interfaces present in these BV reactions. On the other, strong hydrogen bonding between the carbonyl of the peracid and performic acid (general acid catalysis) is likely, and would produce TS-**17** (Scheme 124d) that was calculated to decrease the energy barrier for the epoxidation reaction of ethene by 3.0 kcal/mol.



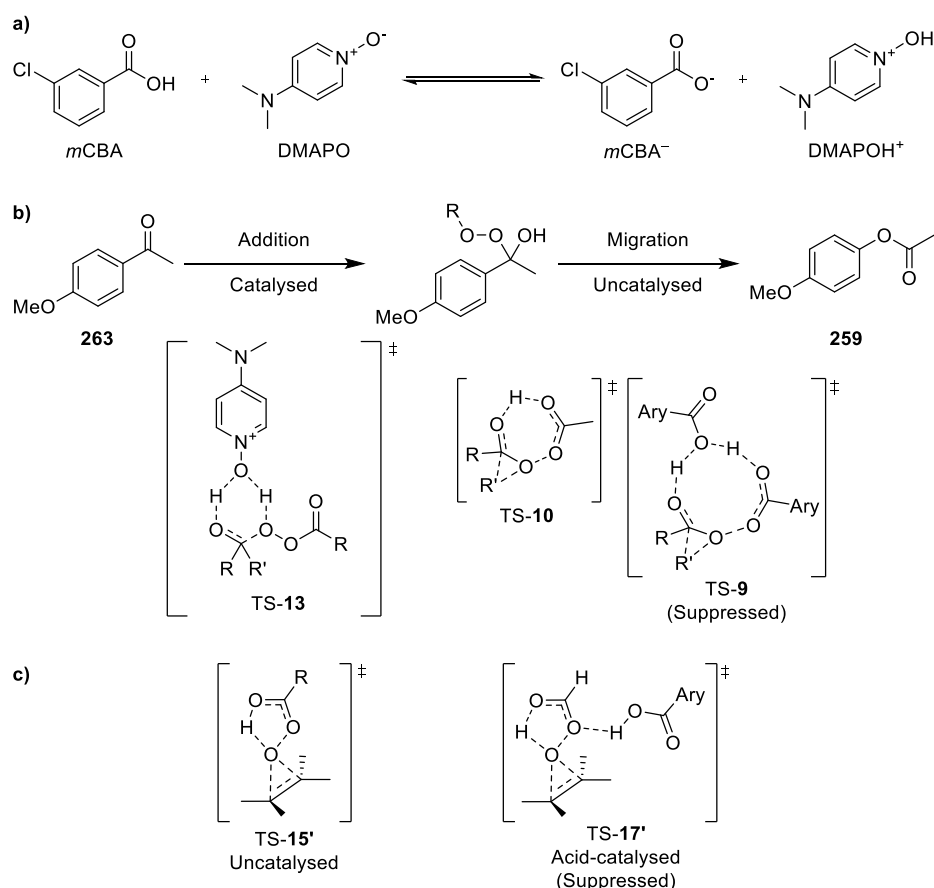
Scheme 124: (a) General mechanism of the Prilezhaev electrophilic epoxidation of styrene by peracids. (b) Spiro butterfly transition state TS-15 showing key MO interactions. (c) TS-16 of the specific acid-catalysed epoxidation of alkenes by PFA. (d) TS-17 of the acid-catalysed epoxidation of alkenes by a pre-formed PFA-HF hydrogen-bonded complex.

Increasing the concentration of DMAPO in these epoxidation reactions will result in preferential coordination of DMAPO (good hydrogen bond acceptor) to the acidic proton of undissociated *m*CBA, thus suppressing its ability to act as an acid catalyst of *m*CPBA-mediated alkene epoxidation reactions. Furthermore, coordination of DMAPO to the acidic proton of the *m*CPBA oxidant could also potentially disrupt formation of the intramolecular hydrogen-bond required for the spirocyclic TS of the alkene epoxidation to form. Importantly, *m*CPBA acts as an electrophilic oxidant in alkene epoxidation reactions, whilst it functions as a nucleophilic oxidant in BV reactions. This means that coordination of DMAPO to the most acidic hydroxyl proton of *m*CPBA will increase its nucleophilicity in the addition step of BV reactions of  $\alpha,\beta$ -unsaturated ketones to catalyse formation of vinyl ester products. Conversely, coordination of DMAPO to the most acidic terminal *m*CPBA peracid proton will decrease the electrophilicity of the proximal peroxidic oxygen to suppress epoxidation of the vinyl ester alkene bond, thus allowing better yields of vinyl ester to be obtained.

A general summary of these numerous observations and mechanistic postulates for the catalytic activity of DMAPO/DMAPOH<sup>+</sup> is shown in Scheme 125. These experiments and literature searches suggest that:

- DMAPO forms acid/base equilibrium mixtures with *m*CBA to produce Brønsted acidic DMAPOH<sup>+</sup> (a).
- DMAPO/DMAPOH<sup>+</sup> acts as a PTC to promote BV oxidation at the aqueous/toluene interface.

- DMAPOH<sup>+</sup> can act as a dual-function hydrogen bonding organocatalyst, as a Brønsted base for electrophilic activation of the peracid, and as a Brønsted acid for nucleophilic activation of the ketone, resulting in 6-membered TS-13 (b).
- Coordination of the *N*-oxide to the acid suppresses migration-limited reactions by reducing the availability of acid for catalysis, suppressing TS-9 (b).
- DMAPO-acid coordination suppresses epoxidation by decreasing the availability of/weakening the acid required to catalyse this undesired process (c).



Scheme 125: Summary of the proposed role of DMAPO in the BV oxidation reaction of *p*-methoxyacetophenone **263** and (*E*)-benzalacetone (*E*)-**232**.

#### 4.5. Degradation studies on DMAPO and *m*CPBA in BV reactions

Having established a robust working hypothesis for the mechanism of action of DMAPO in the BV reactions of ketones and  $\alpha,\beta$ -unsaturated ketones, the fact that catalyst loadings of > 20 mol% DMAPO resulted in lower ketone conversion levels was till puzzling. Further investigations into the DMAPO-catalysed BV oxidation reactions of *p*-methoxyacetophenone **263** using 1.3 equiv. *m*CPBA revealed that they slowed significantly at around 60-65% conversion levels, essentially halting at around 70-80%. Consequently, this decrease in conversion rate over time was investigated by

carrying out time-course monitoring of conversion levels of BV reactions of *p*-methoxyacetophenone **263** under different conditions (Figure 54). Use of 20 mol% DMAPO with 1.3 equiv. of commercial *m*CPBA in the absence/presence of water (or additional *m*CBA) all gave essentially the same conversion levels after 1 h. Use of pure *m*CPBA initially led to a slightly increased reaction rate, but this BV reaction once again slowed at around 30 minutes, ultimately achieving the same overall conversion levels seen when commercial *m*CPBA was used.

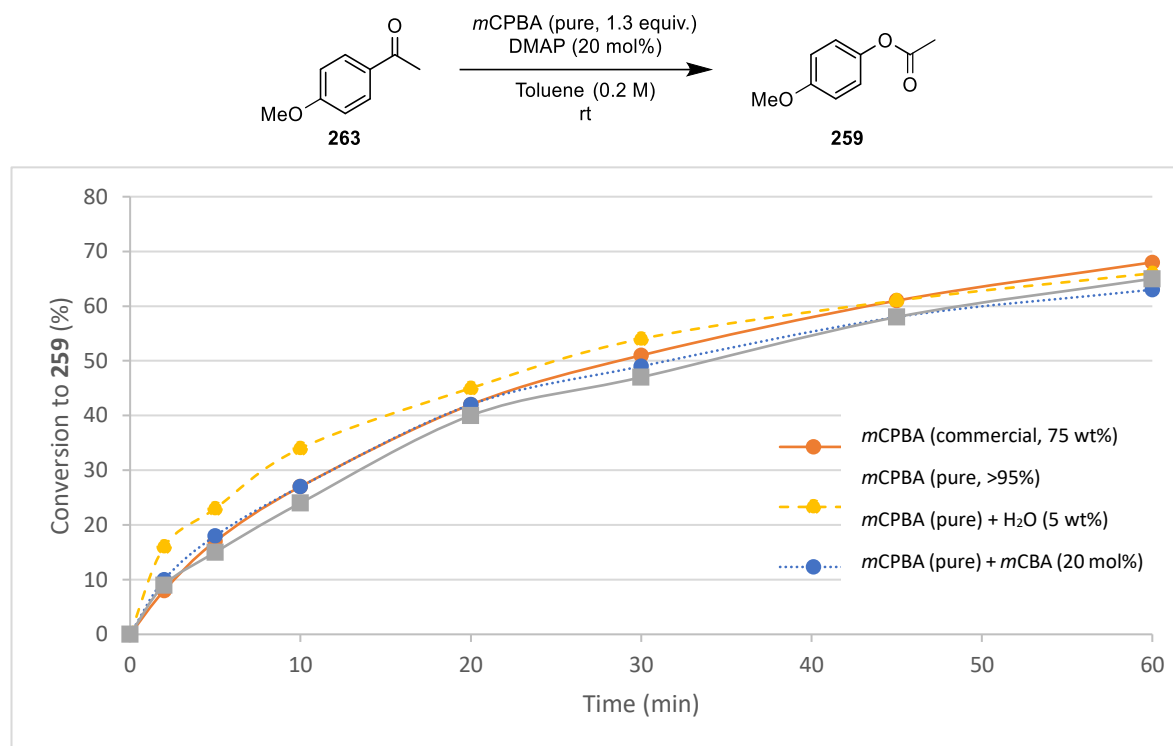
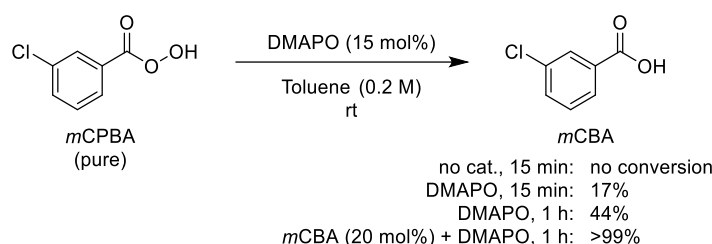


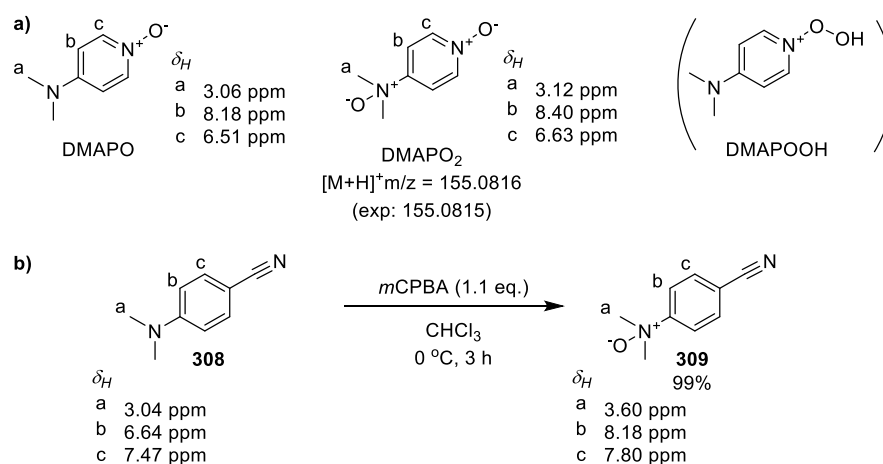
Figure 54: Reaction profiles of DMAPO-catalysed BV oxidation reactions of **263** in toluene using 1.3 equiv. *m*CPBA (commercial or purified) with and without H<sub>2</sub>O and *m*CBA. See 5.4.1 for example reaction conditions.

Close examination of the <sup>1</sup>H NMR spectra of crude reaction products revealed that no remaining *m*CPBA oxidant was present in any of these BV reactions after a couple of hours, which was surprising as at least 0.3 equiv. of *m*CPBA should be present even after total conversion. This led us to consider the fate of the ‘missing’ *m*CPBA in these BV oxidation reactions, whose degradation was confirmed by reacting 15 mol% preformed DMAPO with 1.0 equiv. of purified *m*CPBA in toluene (no ketone substrate) in the presence/absence of *m*CBA (20 mol%) (Scheme 126). <sup>1</sup>H NMR spectroscopic analysis revealed that 17% conversion of *m*CPBA to *m*CBA occurred after 15 min, rising to 44% consumption of *m*CPBA after 1 h. Addition of just 20 mol% *m*CBA alongside the DMAPO in this reaction (comparable to commercial *m*CPBA composition) led total conversion of the *m*CPBA component in just 1 h. These results clearly indicated that mixtures of DMAPO and *m*CBA accelerated decomposition of *m*CPBA, thus providing a simple explanation for the incomplete conversion levels observed in BV reactions when higher DMAPO catalyst loadings were used, with reactions simply running out of *m*CPBA oxidant before they could reach completion.



Scheme 126: Stability of *m*CPBA towards standard DMAPO-catalysed BV oxidation reactions

Close inspection of the  $^1\text{H}$  NMR spectra of these DMAPO/*m*CPBA control reactions revealed the presence of variable amounts of a new DMAPO-related species (~10-50% depending on reaction time and composition) that was identified as 4-(dimethylamino)pyridine *N,N*-bis-oxide DMAPO<sub>2</sub>. This assignment was based on the general downfield shift of all the signals of DMAPO<sub>2</sub> relative to DMAPO, with a significant 0.22 ppm difference in the aryl  $^1\text{H}$  resonances ( $\text{H}_b$ ) that are proximal to the dimethylamine oxide fragment (Scheme 127a). This postulate was further supported by HRMS analysis of the crude reaction mixture, which identified a new mass ion with a molecular ion of  $m/z = 155.0816$ , which is consistent with the expected  $m/z$  value of 155.0815 for the protonated cation of DMAPO<sub>2</sub>  $[\text{M}+\text{H}]^+ \text{C}_7\text{H}_{11}\text{N}_2\text{O}_2^+$ . The NMR spectroscopic data for *N,N*-bis-oxide DMAPO<sub>2</sub> were also found to match previously-reported data for DMAPO<sub>2</sub> which was previously produced through oxidation of DMAP using heterogeneous RuO<sub>2</sub> graphene nanoplatelets.<sup>464</sup> Although not anticipated, there is precedent for the oxidation of dimethylaniline nitrogen atoms to tertiary amine oxides, including examples of electron-poor systems such as 4-cyano-dimethylaniline *N*-oxide **309** (electronically analogous to DMAPO<sub>2</sub>), that can be synthesised in high yield through treatment of **308** with *m*CPBA at 0 °C (Scheme 127b).<sup>465</sup>

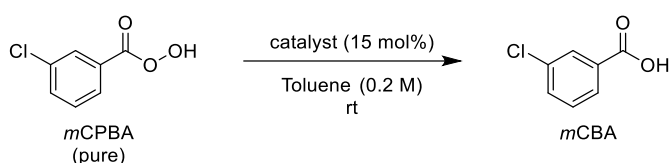


Scheme 127: (a) Structures of DMAPO catalyst, observed DMAPO<sub>2</sub> bis-*N*-oxide, and unobserved *N*-peroxo DMAPOOH. (b) Efficient *N*-oxidation of *p*-cyano dimethylaniline **308** by *m*CPBA by Jones *et al.*<sup>465</sup>

Importantly, the degree of degradation of *m*CPBA by DMAPO in these BV reactions proceeded well beyond the levels that would be required for stoichiometric oxidation of 15 mol% DMAPO to DMAPO<sub>2</sub>, and so it became clear that DMAPO (or DMAPO<sub>2</sub>) must be catalysing *m*CPBA degradation. To further investigate this *m*CPBA consumption process, its stability was monitored in the presence of 15 mol% pyridine-*N*-oxide (PNO), trimethylamine-*N*-oxide (TMNO) and *N*-methyl-morpholine-*N*-

oxide (NMO) (*vide supra*).<sup>418</sup> As expected, a control reaction involving simply stirring *m*CPBA in toluene led to no appreciable degradation (Table 16, entries 1-2). Mixing 15 mol% PNO with pure *m*CPBA also resulted in no reaction occurring after 1 h with all the *m*CPBA remaining intact after 1 h (Table 16, entry 6). Conversely, some *m*CPBA degradation was observed when both TMNO and NMO were exposed to *m*CPBA, with TMNO reducing *m*CPBA levels by ~25% after 1 h (Table 16, entry 8), whilst use of NMO resulted in 13%-24% *m*CPBA consumption after 1-2 h (Table 16, entry 10).

Table 16: Stability of pure *m*CPBA and various *N*-oxide catalysts under standard *N*-oxide catalyst reaction conditions (no ketone substrate).



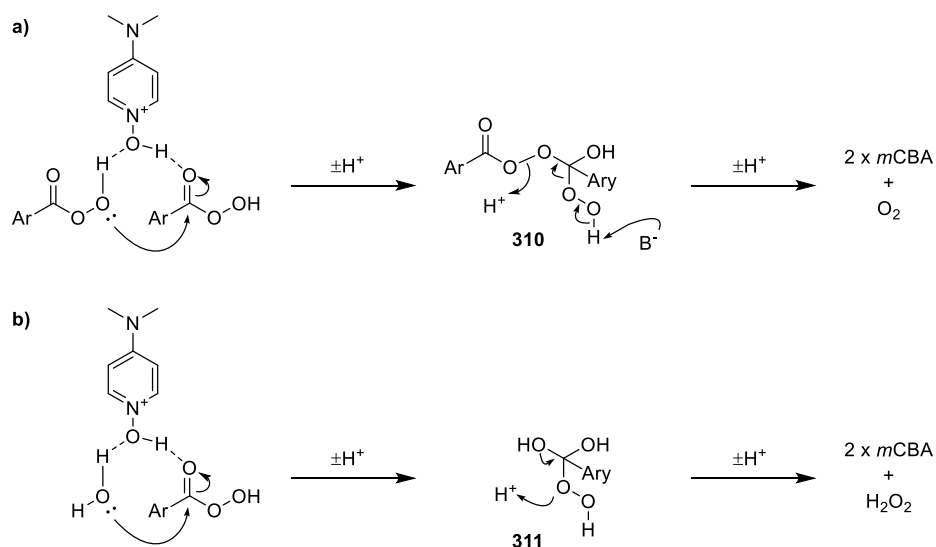
Entry	Catalyst	Time	Conversion (%) <sup>a</sup>
1	None	15 min	0%
2		1 h	1%
3 <sup>b</sup>	DMAPO	15 min	17%
4 <sup>b</sup>		1 h	44%
5	PNO	15 min	0%
6		1 h	0%
7 <sup>c</sup>	TMNO	15 min	24%
8 <sup>c</sup>		1 h	25%
9 <sup>c</sup>		2 h	45%
10	NMO	1 h	13%
11		2 h	24%

<sup>a</sup> Remaining mass balance comprised of unreacted *m*CPBA. <sup>b</sup> See Scheme 126. <sup>c</sup> TMNO dihydrate used.

The fact that 15 mol% DMAPO, TMNO and NMO resulted in consumption of > 15 mol% *m*CPBA oxidant indicated that they were all competent catalysts for producing *m*CBA. Consequently, a mechanistic hypothesis was proposed based on the ability of DMAPO/DMAPOH<sup>+</sup> (or DMAPO<sub>2</sub>/DMAPO<sub>2</sub>H<sup>+</sup>) to act as a proton-shuttling organocatalyst to catalyse the decomposition of *m*CPBA (Scheme 128a). It is mechanistically plausible that DMAPOH<sup>+</sup> would serve to catalyse nucleophilic addition of the OH group of one *m*CPBA molecule to the carbonyl of another *m*CPBA molecule to form a tetrahedral *bis*-peroxy intermediate **310**. The peroxy fragment of intermediate **310** would then eliminate oxygen with concomitant cleavage of the other peroxide bond to produce two molecules. of *m*CBA and one molecule of O<sub>2</sub>. This type of mechanism has previously been

shown for the decomposition of peracetic acid under mildly basic conditions,<sup>466</sup> however it is possible that the hydrogen-bonding catalysis provided by DMAPO could allow this decomposition pathway to proceed in organic acidic media.

An alternative mechanism for *N*-oxide-catalysed *m*CPBA degradation processes could be due to DMAPOH acting as a catalyst to facilitate simple hydrolysis of *m*CPBA by water. This pathway would involve DMAPOH<sup>+</sup> acting as a proton transfer catalyst in the same way to facilitate nucleophilic attack of water at the carbonyl group of *m*CPBA (Scheme 128b). This would generate an unstable tetrahedral intermediate **311** that would then collapse to produce *m*CBA through elimination of hydrogen peroxide as a leaving group. Evidence for this type of acid-catalysed degradation/hydrolysis mechanism occurring for peracetic acid can be found in the chemical literature.<sup>467</sup> Unfortunately, attempts to observe evolution of gaseous oxygen (bubbles/pressure build-up), or use of starch/iodide paper to identify the formation of aqueous hydrogen peroxide have so far both proven unsuccessful, and so further work is currently ongoing to elucidate the mechanism of DMAPO-catalysed *m*CPBA degradation.



Scheme 128: (a) A DMAPOH<sup>+</sup>-catalysed dimerization mechanism for the degradation of *m*CPBA into *m*CBA and O<sub>2</sub>. (b) A DMAPOH<sup>+</sup>-catalysed hydrolysis mechanism for the degradation of *m*CPBA into *m*CBA and H<sub>2</sub>O<sub>2</sub>.

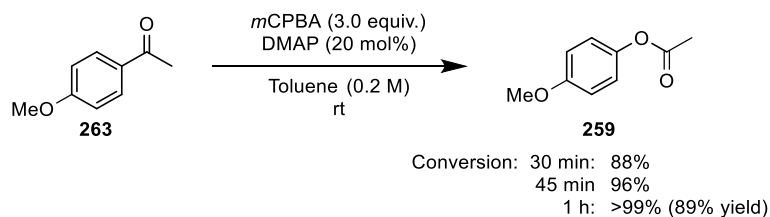
## 4.6. Development of second generation *N*-oxide-catalysed BV oxidation conditions

### 4.6.1 *New N-oxide organocatalyst screens*

Although that *N*-oxides can catalyse competing decomposition of *m*CPBA oxidant in these BV reactions, it was apparent that the *N*-oxide initially catalysed BV reactions at a faster rate than it catalysed *m*CPBA decomposition. This meant that increasing the amount of *m*CPBA oxidant used in the *N*-oxide-catalysed BV reactions of standard ketones should result in their complete consumption to afford higher yields of ester products. This hypothesis was confirmed by carrying



out DMAPO catalysed BV oxidation of *p*-methoxyacetophenone **263** using 3.0 equiv. of *m*CPBA and 20 mol% DMAP, which gave *p*-acetoxy anisole **259** in > 99% conversion after 1 h (> 95% mass recovery and purity of crude **259**). <sup>1</sup>H NMR analysis revealed that ~1.0 equiv. of *m*CPBA was present at the end of the BV reaction, indicating that ~2.0 equiv. of oxidant had been consumed (1.0 equiv. for the BV reaction, 1.0 equiv. *m*CPBA for the degradation pathway) (Scheme 129). This result represented a significant improvement on the previously reported conditions (20 mol% DMAP, 1.3 equiv. *m*CPBA) for BV oxidation which took 4 h to produce 87% conversion to ester **263**, with significant variability depending on batch, premixing time, *m*CPBA purity, etc...<sup>418</sup>

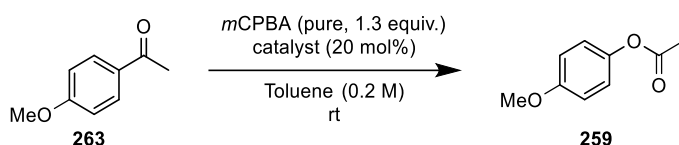


Scheme 129: DMAPO-catalysed BV oxidation of *p*-methoxyacetophenone **263** using excess *m*CPBA to overcome *m*CPBA degradation pathway.

Unfortunately, this *N*-oxide-catalysed protocol using excess *m*CPBA oxidant was not suitable for carrying out BV oxidation reactions of  $\alpha,\beta$ -unsaturated ketones because of the propensity of their vinyl ester products to undergo further epoxidation reactions (see synthesis of FAPM above, Scheme 109). Having established that *m*CPBA was stable to PNO under the BV reaction conditions, its use as a less catalytically-active *N*-oxide, but more stable *N*-oxide catalyst for the BV oxidation of *p*-methoxyacetophenone **263** (*vide supra*) was reinvestigated, which might allow use of near-stoichiometric amounts of *m*CPBA, rather than a three-fold excess. Pleasingly, use of 20 mol% preformed PNO (using 1.30 equiv. of purified *m*CPBA to simplify reaction profile analysis) led to good conversion of *p*-methoxyacetophenone **263** to ester **259**, with conversion levels reaching 40% after 1 h and rising steadily over time to reach 88% conversion after 5 h (Table 17, entries 3-7). These values compare with 33% and 75% conversion obtained for the uncatalysed BV reaction of *p*-methoxyacetophenone **263** after 1 h and 5 h, respectively, thus demonstrating that use of PNO has a beneficial (if limited) effect on BV reactions of *p*-methoxyacetophenone **263** - despite its low overall catalytic activity. TMNO and NMO were also used as *N*-oxide catalysts for the BV reaction of *p*-methoxyacetophenone **263**, which resulted in greater catalytic activity, with TMNO achieving 63%, 78% and 83% conversion levels after 1, 2 and 3 h, respectively, whilst NMO produced slightly lower 54%-69% conversion levels over 1-2 h (Table 17, entries 8-12). The plateauing of conversion levels for the NMO catalyst is consistent with previous observations that NMO degrades the *m*CPBA oxidant, and so after a couple of hours little oxidant remains to carry out the desired BV reaction. In order to illustrate that the 2<sup>nd</sup> generation TMNO catalytic protocol was practically useful, 20 mol% TMNO and 1.3 equiv. of commercial *m*CPBA were used to produce *p*-acetoxy anisole **259** in 91% isolated yield (as before, mass recovery and purity after workup were > 95%). This was a clear improvement on both the previous DMAPO method,<sup>418</sup> as well as the excess oxidant method that used 3.0 equiv. *m*CPBA. These new 2<sup>nd</sup> generation protocols were highly promising, as they

provided highly reproducible *N*-oxide-catalysed BV oxidation conditions that could be used to convert standard electron-rich ketones into ester products in good yields.

Table 17: *N*-oxide catalysed BV oxidation reactions of *p*-methoxyacetophenone **263** using pure *m*CPBA.



Entry <sup>a</sup>	Catalyst	Time	Conversion (%) <sup>b,c</sup>
1	PNO	1 h	40 (33)
2		3 h	64 (61)
3		5 h	88 (75)
4 <sup>d</sup>	TMNO	1 h	63 (33)
5 <sup>d</sup>		2 h	78 (45)
6 <sup>d</sup>		3 h	83 (61)
7	NMO	1 h	54 (33)
8		2 h	69 (45)
9 <sup>d</sup>	TMNO + 75 wt% <i>m</i> CPBA	1 h	56
10 <sup>d</sup>		3 h	79
11 <sup>d</sup>		5 h	97 [91% yield] <sup>e</sup>

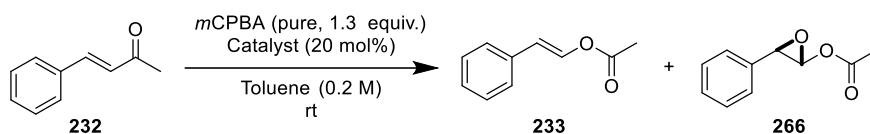
<sup>a</sup> *m*CPBA and catalyst pre-stirred for 15 min. <sup>b</sup> Conversions relative to initial stoichiometry of relevant components.

<sup>c</sup> Values in brackets correspond to conversions for uncatalysed BV reactions. <sup>d</sup> TMNO dihydrate used. <sup>e</sup> Isolated yield.

These new “2<sup>nd</sup> generation” *N*-oxide-catalysed BV oxidation conditions for the *N*-oxide catalysed BV oxidation of benzalacetone (*E*)-**232** using 1.3 equiv. pure *m*CPBA (Table 18). Clear catalysis was observed in all cases, with some degree of selectivity observed for formation of vinyl ester **233** in all cases, thus indicating that varying degrees of *N*-oxide-mediated epoxidation suppression was occurring. As expected, PNO-catalysed BV reactions of benzalacetone **232** was sluggish, resulting in 42% consumption of enone **232** in 30 min, which gave a 37:5 (86.5:13.5) ratio of vinyl ester **233** to epoxyster **266**, rising to 64% conversion with a poorer 51:13 (74.5:25.5) selectivity for **233** over **266** after 1.5 h, (Table 18, entries 1-2). TMNO and NMO proved to be more catalytically-active (Table 18, entries 3-6), achieving 66% and 75% consumption levels after 30 min, producing 61:5 and 67:8 (91.8:9.2 and 88.1:11.9) selectivity levels for formation of vinyl ester **233** over epoxyster **266**, respectively. These conversion levels increased over time, achieving 77% for TMNO and 89% for NMO after 3 h. Selectivity remained high when TMNO was used as the catalyst, producing an approximate 10:1 mixture of vinyl ester **233** to epoxyster **266** (71:7 = 90.1:9.9), whilst selectivity in the NMO-catalysed reaction dropped slightly to around 6:1 (76:13 = 82.9:17.1). Therefore, it

appears TMNO is not only competent at catalysing the initial BV oxidation reaction, it also suppresses most of the competing epoxidation reaction of vinyl ester **266** (as observed for DMAPO).

Table 18: *N*-oxide catalysed BV oxidation reactions of (*E*)-benzalacetone **232** by pure *m*CPBA.

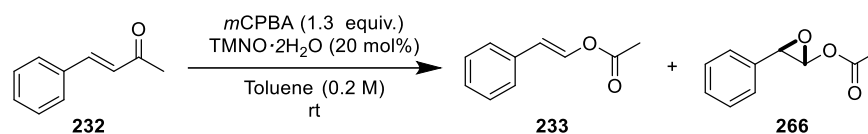


Entry <sup>a</sup>	Catalyst	Time	Product distribution <sup>b</sup>		
			Enone <b>232</b>	Vinyl ester <b>233</b>	Epoxyester <b>266</b>
1	PNO	30 min	58%	37%	5%
2		1.5 h	36%	51%	13%
3 <sup>c</sup>	TMNO	30 min	34%	61%	5%
4 <sup>c</sup>		1.5 h	22%	71%	7%
5	NMO	30 min	25%	67%	8%
6		1.5 h	11%	76%	13%

<sup>a</sup> *m*CPBA and catalyst pre-stirred for 15 min. <sup>b</sup> All distributions were referenced to a TetMB internal standard to ensure integration accounted for the entire mass balance. <sup>c</sup> TMNO dihydrate used.

A TMNO catalyst loading screen for the BV oxidation reaction of benzalacetone **232** was then carried out using 1.30 equiv. commercial *m*CPBA, with consumption levels increasing to a maximum level as the catalyst loading was raised from 0-20%. Promisingly, only a slight drop-off in conversion rates were observed as catalyst loadings were raised to 100 mol%, with higher levels of TMNO suppressing competing epoxide formation (albeit less effectively than DMAPO).

Table 19: TMNO-catalysed BV oxidation reactions of (*E*)-benzalacetone **232** by commercial *m*CPBA.



Entry <sup>a,b</sup>	TMNO loading	Time	Product distribution <sup>c</sup>		
			Enone <b>232</b>	Vinyl ester <b>233</b>	Epoxyester <b>266</b>
1 <sup>d</sup>	None	30 min	60%	30%	10%
2 <sup>d</sup>		1.5 h	30%	33%	37%
3	5%	30 min	49%	46%	5%
4		1.5 h	30%	57%	13%
5	10%	30 min	36%	58%	6%
6		1.5 h	19%	69%	12%
7 <sup>e</sup>	20%	30 min	24%	70%	7%
8 <sup>e</sup>		1.5 h	10%	75%	15%
9	50%	30 min	39%	58%	3%
10		1.5 h	22%	72%	6%
11	100%	30 min	48%	49%	3%
12		1.5 h	30%	66%	4%

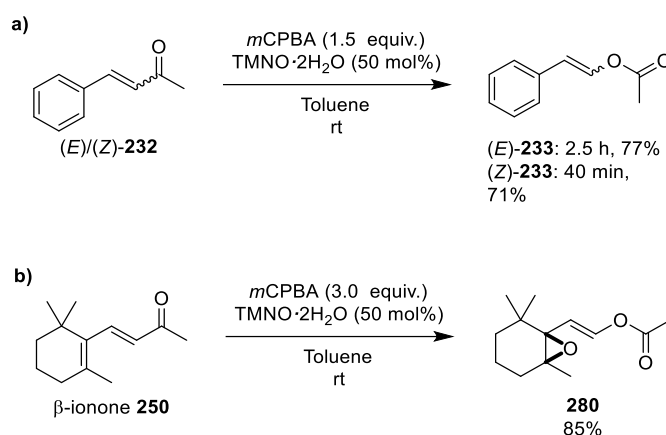
<sup>a</sup> *m*CPBA and catalyst pre-stirred for 15 min. <sup>b</sup> TMNO dihydrate used. <sup>c</sup> All distributions were referenced to a TetMB internal standard to ensure integration accounted for the entire mass balance. <sup>d</sup> See Table 12. <sup>e</sup> See Table 18.

Considering these catalyst screening results as a whole, it can be seen that TMNO is slightly less catalytically active towards the BV oxidation of benzalacetone **232**, and slightly less effective as an inhibitor of the competing epoxidation pathway than DMAPO. This may be due to the decreased acidity of TMNOH<sup>+</sup>, which has a *pK<sub>a</sub>* of ~4.7 when compared to DMAPOH<sup>+</sup> which has a *pK<sub>a</sub>* of 3.88.<sup>445,468</sup> This order of magnitude difference in acidity will perturb the equilibrium that exists between the different protonated *N*-oxide species and *m*CBA in these BV reactions (more TMNOH<sup>+</sup> than DMAPOH<sup>+</sup>). Therefore, the lower levels of TMNO species present in BV reactions of α,β-unsaturated ketones means that this catalytic system is less effective at suppressing competing epoxidation reactions than DMAPO. The fact that the most rapid DMAPO-catalysed BV reactions are likely to contain more unprotonated DMAPO species suggest that unprotonated *N*-oxides play a critical role as hydrogen bond acceptors to increase the nucleophilicity of *m*CPBA in these *N*-oxide catalysed BV reactions. However, the lower reactivity of PNO (*pK<sub>aH</sub>* of 0.79,<sup>448</sup> very little PNOH<sup>+</sup>

present) in these BV reactions suggests that the presence protonated *N*-oxide species (such as DMAPOH<sup>+</sup>) also play a key synergistic role in facilitating these catalytic BV reactions.

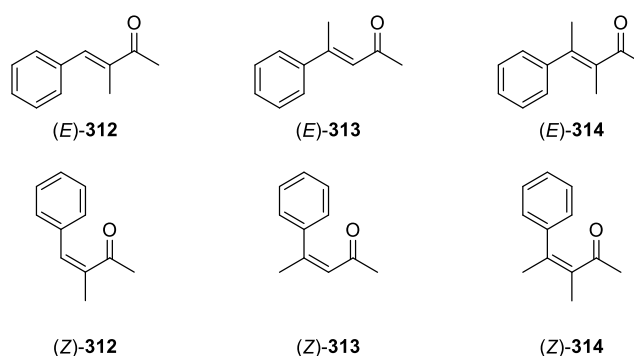
#### 4.6.2 Second generation TMNO-catalysed BV oxidation reactions of $\alpha,\beta$ -unsaturated ketones

Having demonstrated that TMNO was a more stable catalyst in the presence of *m*CPBA (unlike DMAPO which forms DMAPO<sub>2</sub>) which also resulted in less *m*CPBA decomposition over time, the potential of this slightly less reactive second generation *N*-oxide catalyst for the BV oxidation of a range of  $\alpha,\beta$ -unsaturated ketones for the synthesis of a small series of vinyl esters was explored. Treatment of (*E*)-benzalacetone **232** with 1.5 equiv. *m*CPBA and 50 mol% TMNO dihydrate gave a good 77% isolated yield of (*E*)-styryl acetate **233** was achieved after 2.5 h. Similarly, applying these BV reaction conditions to (*Z*)-benzalacetone **232** led to 71% yield of (*Z*)-**233** after 40 min, thus producing comparable results to those found in DMAPO-catalysed reactions (Scheme 130a). 50 mol% TMNO was also found to be an effective ‘drop-in’ catalyst replacement for the *bis*-oxidation of  $\beta$ -ionone **250** with use of 3.0 equiv. of *m*CPBA affording the corresponding  $\gamma,\delta$ -epoxyester **280** with 94% selectivity and in 85% yield (*cf.* 93% selectivity and 81% yield with DMAPO) (Scheme 130b).



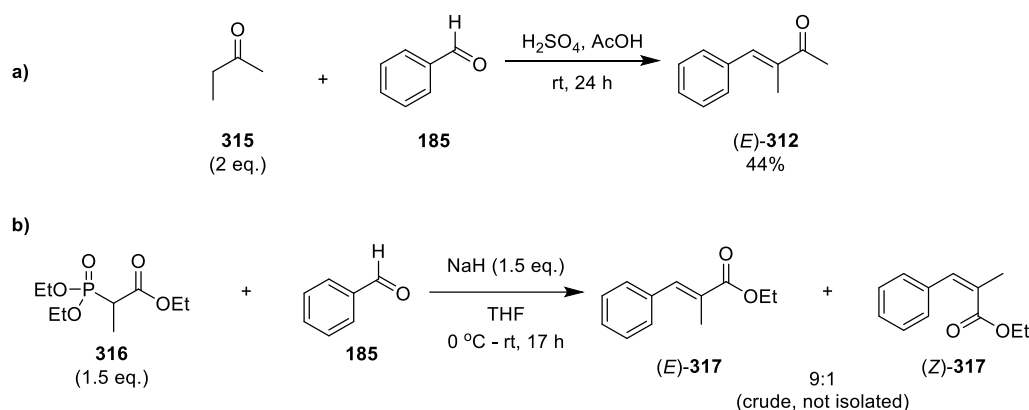
Scheme 130: (a) TMNO-catalysed BV oxidation reaction of (*E*)- and (*Z*)-**232** to the corresponding vinyl esters. (b) sequential BV oxidation and epoxidation of  $\beta$ -ionone **250**.

The applicability of these TMNO-catalysed Baeyer-Villiger oxidation conditions was then demonstrated for the BV oxidation of a range of geometric isomers of methyl substituted benzalacetone analogues **312-314** containing different trisubstituted and tetrasubstituted alkene substitution patterns. Consequently, a series of  $\alpha$ -methyl benzylidene acetone (*E*)-**312**/*Z*-**312**,  $\beta$ -methyl benzylideneacetone (*E*)-**313**/*Z*-**313**,  $\alpha,\beta$ -dimethylbenzylidene acetone (*E*)-**314**/*Z*-**314** derivatives of benzalacetone were prepared as substrates to carry out *N*-oxide catalysed BV reactions (Scheme 131). The configuration of each set of diastereomeric enones (and their synthetic intermediate precursors) was confirmed by comparison of their <sup>1</sup>H NMR spectra to literature precedent (where possible) and from analysis of the <sup>4</sup>*J*<sub>H-H</sub> and <sup>5</sup>*J*<sub>H-H</sub> coupling constants and nOe interactions of their alkene and methyl resonances.



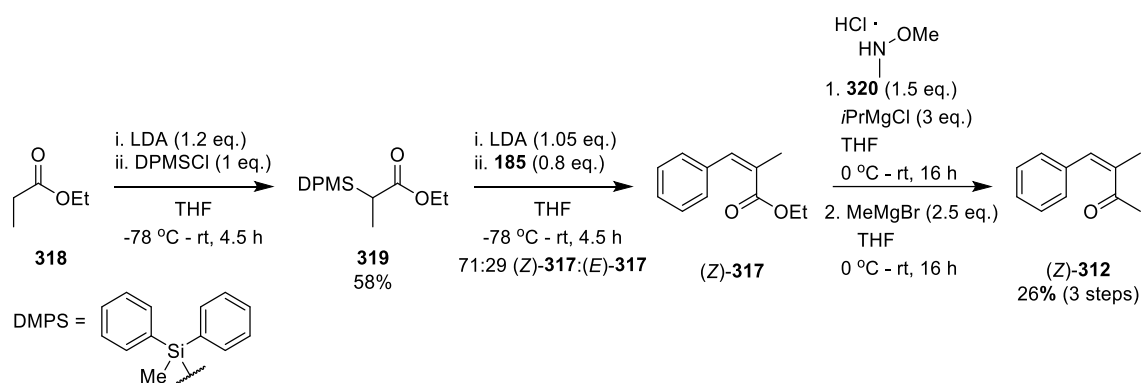
Scheme 131: (*E*)- and (*Z*)-diastereomers of α-methyl benzylidene acetone (*E*)-**312**/(*Z*)-**312**, β-methyl benzylideneacetone (*E*)-**313**/(*Z*)-**313**, and α,β-dimethylbenzylidene acetone (*E*)-**314**/(*Z*)-**314**.

Diastereoselective synthesis of (*E*)-α-methyl benzylidene acetone (*E*)-**312** was achieved in 44% yield using a sulfuric acid-catalysed Claisen-Schmidt condensation reaction between butanone **315** and benzaldehyde **185** in acetic acid under thermodynamic control (Scheme 132a).<sup>469</sup> Attempts to synthesise (*Z*)-**312** using a Horner-Wadsworth-Emmons (HWE) reaction between the anion of α-methyl triethylphosphonoacetate **316** and benzaldehyde **185** produced a disappointing 9:1 ratio of diastereomers (*E*)-**317** and (*Z*)-**317**, which proved to be essentially inseparable by chromatography at this ratio (Scheme 132b).



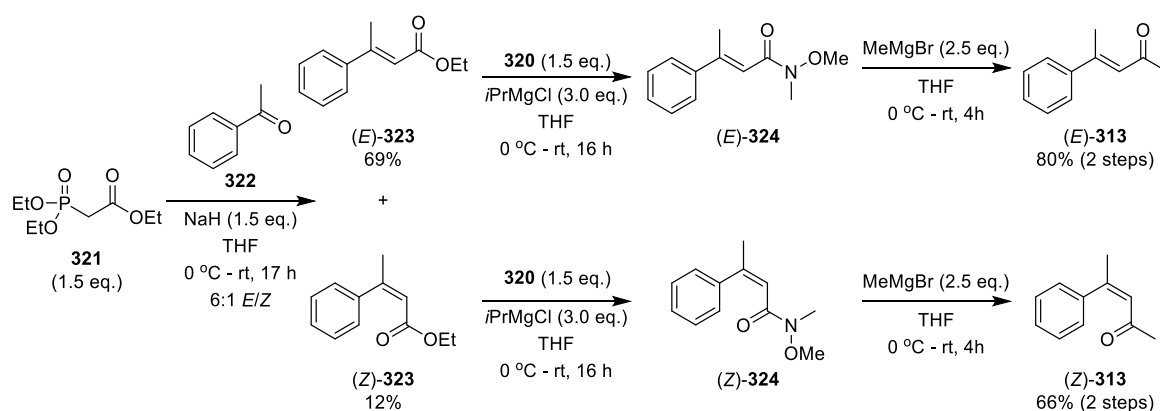
Scheme 132: (a) Aldol condensation reaction for the synthesis of (*E*)-α-methyl benzylidene acetone (*E*)-**312**. (b) (*E*)-selective HWE synthesis of 9:1 mixture of α-methyl benzylidene acetones (*E*)-**317**:(*Z*)-**317**.

Consequently, an alternative four-step synthesis of (*Z*)-α-methyl-α,β-unsaturated ester (*Z*)-**312** was devised based on a Peterson olefination methodology (Scheme 133). Treatment of the lithium enolate of ethyl propionate **318** with diphenylmethylchlorosilane (DPMSCl) resulted in formation of C-α-silyl ester **319** in 58% yield.<sup>470,471</sup> Deprotonation of α-silyl ester **319** with LDA followed by addition of benzaldehyde **185** resulted in a Peterson olefination reaction to produce a 71:29 mixture of the α,β-unsaturated esters (*Z*)-**317** and (*E*)-**317**.<sup>472,473</sup> This inseparable mixture was subsequently converted to a mixture of Weinreb amides using Weinreb's salt **320** and isopropylmagnesium chloride. Finally, treatment with MeMgBr produced a mixture of their corresponding α,β-unsaturated ketones (*Z*)-**312** and (*E*)-**312** (same *dr*), which was separated by chromatography to afford (*Z*)-**312** in 26% yield over three steps ((*E*)-**312** also isolated in 15% yield, 41% combined yield over three steps).



Scheme 133: Four-step synthesis of (Z)- $\alpha$ -methyl benzylidene acetone (Z)-**312**.

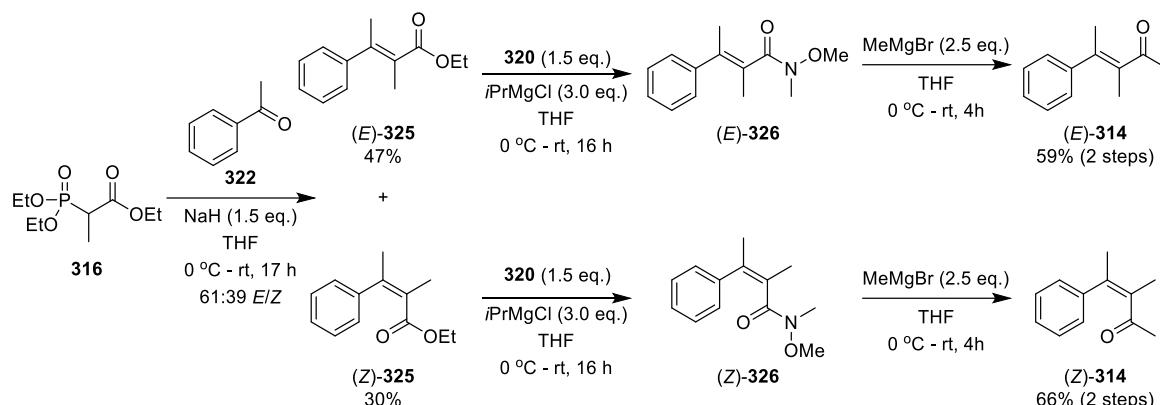
A similar three-step synthetic approach was employed to prepare  $\beta$ -methylated  $\alpha,\beta$ -unsaturated ketones (E)-**313** and (Z)-**313** (Scheme 134). First, HWE reaction of the anion of triethylphosphonate ester **321** with acetophenone **322** was used to prepare a 6:1 diastereomeric mixture of unsaturated esters (E)-**323** and (Z)-**323**, which could be separated by column chromatography to afford (E)-**323** in 69% yield and (Z)-**323** in 12% yield, for a combined 81% yield. Each substrate was then converted into their corresponding Weinreb amides (E)-**324** and (Z)-**324** via separate treatment with Weinreb's salt **320** and isopropylmagnesium chloride. Final addition of MeMgBr to each of the Weinreb amides then gave  $\beta$ -methyl benzylidenacetones (E)-**313** and (Z)-**313** in 80% and 66% yield over two steps, respectively.



Scheme 134: Three-step syntheses of (E)- and (Z)- $\beta$ -methyl benzylidene acetone (E)-**313** and (Z)-**313**.

Synthesis of the  $\alpha,\beta$ -dimethyl- $\alpha,\beta$ -unsaturated ketones (E)-**314** and (Z)-**314** (Scheme 135) commenced with a sodium ethoxide-mediated HWE reaction between  $\alpha$ -methyl triethylphosphonate **316** and acetophenone **322** which gave a 61:39 mixture of  $\alpha,\beta$ -unsaturated esters (E)-**325** and (Z)-**325**. This mixture was then separated by column chromatography to afford (E)-**325** and (Z)-**325** in 47% and 30% yields, respectively. These diastereomerically-pure esters (E)-**325** and (Z)-**325** were then separately converted into their corresponding Weinreb amides (E)-**326** and (Z)-**326** via treatment with Weinreb's salt **320** and isopropylmagnesium chloride as above. Finally, separate reaction of Weinreb amides (E)-**326** and (Z)-**326** with MeMgBr gave the

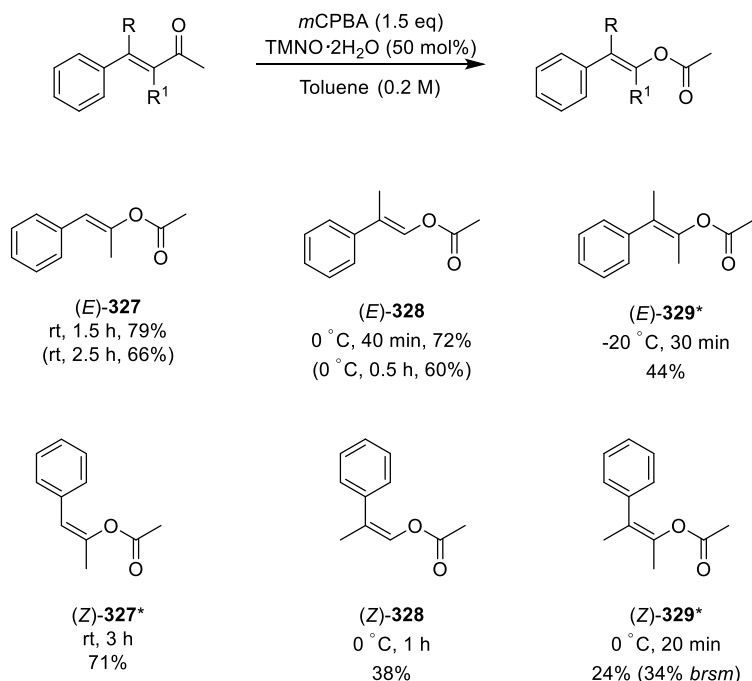
desired (*E*)- $\alpha,\beta$ -dimethyl benzylidene acetone (*E*)-**314** and (*Z*)- $\alpha,\beta$ -methyl benzylidene acetone (*Z*)-**314** in 59% and 66% yields, respectively.



Scheme 135: Three-step syntheses of (*E*)- and (*Z*)- $\alpha,\beta$ -dimethyl benzylidene acetone **314**.

Having synthesised all six possible isomers of methyl-benzalacetone **312-314**, they were subjected to 50 mol% TMNO-catalysed BV oxidation reactions using 1.5 equiv. of *m*CPBA to produce their corresponding vinyl esters. The BV oxidation reactions of  $\alpha$ -methyl (*E*)-**312** and  $\beta$ -methyl (*E*)-**313** proceeded well, affording their desired vinyl esters (*E*)-**327** and (*E*)-**328** in good 79% and 72% yields, an improvement on the corresponding 66% and 60% yields that were obtained using DMAPO as a catalyst. BV oxidation reactions of both  $\alpha$ -methyl (*Z*)-**312** and  $\beta$ -methyl (*Z*)-**313** diastereomers were also successful, affording their corresponding vinyl ester (*Z*)-**327** and (*Z*)-**328** in 71% and 38% yield, respectively. The BV oxidation reactions of both  $\beta$ -substituted substrates were carried out at 0 °C, as carrying out their BV reactions at room temperature resulted in preferential formation of their corresponding epoxides. BV oxidation of these  $\beta$ -methyl benzylidene acetone substrates proceeded faster than the  $\alpha$ -methyl benzylidene acetone substrates, which is likely due to decreased steric hindrance towards nucleophilic attack of *m*CPBA at their carbonyl groups. BV oxidation of both dimethyl benzalacetone (*E*)-**314** and (*Z*)-**314** also required cooling to -20 °C and 0 °C to prevent over-epoxidation pathways from dominating, which allowed dimethyl vinyl esters ((*E*)-**329** and (*Z*)-**329**) to be obtained in modest 44% and 24% yields, respectively. The BV oxidation reactions of the dimethyl benzalacetone analogues were relatively slow, presumably due to significant steric crowding around their ketone groups. Although some of the isolated yields obtained are far from optimal, the successful syntheses of all six ‘methylated styryl acetates’ is a significant achievement, as these type of  $\alpha/\beta$ -substituted vinyl esters have never previously been synthesised using BV oxidation processes (pure  $\alpha$ -methyl (*Z*)-**327** and dimethyl (*E*)-**329** and (*Z*)-**329** are novel compounds), with alternative synthetic approaches more complex and often poorly diastereoselective (for some examples of non-selective syntheses of **312-313** see <sup>474,475</sup>).

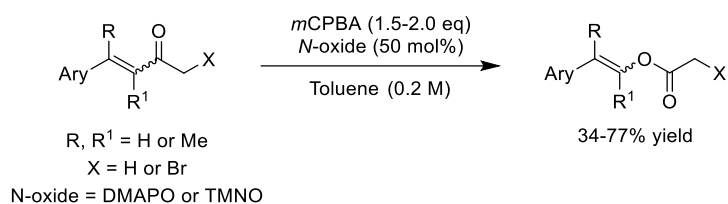




Scheme 136: DMAPO-catalysed BV oxidation of benzalacetone methylated analogues (*E*)- and (*Z*)-**312-314**. Values in brackets are yields from 1<sup>st</sup> generation DMAPO method, 1.8 equiv. *m*CPBA, 50 mol% DMAPO (see Scheme 110). \* Denotes compounds not previously purified or reported in the literature.

## 4.7. Conclusions

This fourth chapter describes the development of novel DMAPO-catalysed BV oxidation methodology for ketones and  $\alpha,\beta$ -unsaturated ketones, that enable good yields of ester and vinyl ester products to be produced, with these investigations also providing important insights into the role of the *N*-oxide catalyst in these BV oxidation reactions. Initial reoptimisation studies identified conditions that enabled DMAPO to be used as a catalyst for the BV reactions of a series of  $\alpha,\beta$ -unsaturated ketones to afford vinyl esters, with this *N*-oxide shown to accelerate the first step of the BV reaction and inhibit competing epoxidation reactions of the vinyl ester products. Catalyst stability studies revealed that the dimethylamino group of DMAPO is oxidised by *m*CPBA to form DMAPO<sub>2</sub> in these BV reactions, whilst it was also found that DMAPO/DMAPO<sub>2</sub> decomposes the *m*CPBA oxidant. These issues could be resolved for the BV reactions of conventional ketones through the inclusion of excess *m*CPBA oxidant to drive reactions to completion. However, competing epoxidation reactions of the alkene bonds of the vinyl esters produced in BV reactions of  $\alpha,\beta$ -unsaturated ketones meant that a new more stable TMNO catalyst was developed that resulted in less *m*CPBA decomposition which gave better yields of vinyl ester products.



Scheme 137: *N*-oxide catalysed Baeyer-Villiger oxidation of arylidene ketones for the synthesis of complex vinyl esters

These results describe robust methodology that should be applicable for catalysing the BV reactions of a wide range of ketones and  $\alpha,\beta$ -unsaturated ketones to provide esters and vinyl esters in improved yields in shorter times. Additionally, investigations into the mechanism of the *N*-oxide catalytic mechanism of DMAPO/TMNO suggest that they may also be useful as proton-transfer catalysts to facilitate other types of synthetic transformation where proton-transfer steps are rate determining (*e.g.* transesterification reactions).

#### 4.8. Future work

Future work will concentrate on trying to identify the optimal stable *N*-oxide catalyst with improved reactivity in these *m*CPBA facilitated BV reactions of ketones and  $\alpha,\beta$ -unsaturated ketones. In this respect, electron-rich pyridine *N*-oxides such as 4-methoxypyridine *N*-oxide ( $pK_{aH}$  for 4-MeOPNOH<sup>+</sup> = 2.04), 4-Hydroxypyridine *N*-oxide ( $pK_{aH}$  for 4-HOPNO = 2.54) or 4-aminopyridine *N*-oxide ( $pK_{aH}$  for 4-APNO = 3.69) will be trialled, whose BV reactivity profiles are also likely to be useful in informing mechanistic understanding of these BV reactions further.<sup>448,476</sup>

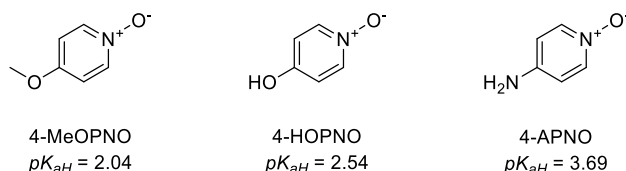
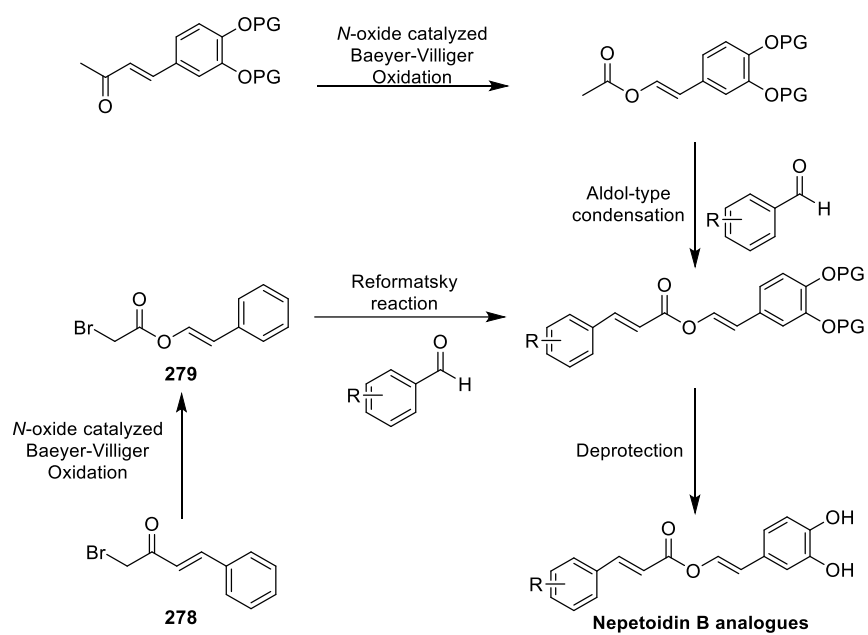


Figure 55: Proposed electron-rich pyridine *N*-oxide catalysts for BV oxidation reactions and associated  $pK_{aH}$ 's.<sup>448,476</sup>

Once a fully optimised *N*-oxide catalysed system has been identified, its utility will be demonstrated for BV oxidation of a wide range of ketones and  $\alpha,\beta$ -unsaturated ketones to fully demonstrate its synthetic utility for medicinal chemistry and natural product applications. For example, the potential of this *N*-oxide-catalysed BV methodology complex vinyl ester building blocks will be explored for the synthesis of analogues of nepetoidin natural products that have been shown to exhibit important anti-oxidant, anti-fungal, anti-bacterial and anti-coagulant activities.<sup>385,477–489</sup>



Scheme 138: Proposed routes for the synthesis of nepetoidin B analogues.

## 5. EXPERIMENTAL

At this point, the author wishes to briefly acknowledge and explain the context of this thesis. Quite clearly, this thesis describes work from two different research projects. This arose due to a variety of circumstances, including that the initial intended project on vinyl esters did not proceed as expected due to incorrect/imprecise precedent, as well as the serious disruption caused by the global Covid-19 pandemic (including 4 months of lost lab time). Therefore, the first three chapters arose from a very successful side-project carried out of the course of the second and third year of the PhD, with the lengthy and detailed literature review of the first chapter being written predominantly during the first national lockdown when access to labs was not allowed. The fourth and final research chapter presents work from the author's original PhD project, focusing on the novel synthesis and applications of vinyl esters. As shown in that chapter, a number of assumptions and prior work were found to be inaccurate/incorrect, and so much of the work carried out at the beginning of this PhD were voided or set in a new context, and so it was decided to exclude them and other related vinyl ester side-projects for this thesis for the sake of brevity and clarity.

### 5.1. General experimental details

Unless preparative details are given, reagents and solvents were obtained from commercial suppliers and used without further purification. Reactions were performed without air exclusion or drying, at room temperature and with magnetic stirring, unless otherwise stated. Anhydrous  $\text{MgSO}_4$  or  $\text{Na}_2\text{SO}_4$  were used as a drying agent for organic solutions. Thin layer chromatography (TLC) was carried out on Macherey-Nagel aluminium-backed plates that were precoated with silica. Compounds were visualised by either quenching of UV fluorescence at 254 nm, or by staining ( $\text{KMnO}_4$ , PMA, Curcumin,<sup>490</sup>  $\text{I}_2$ ) dip followed by gentle heating. Purification by flash column chromatography was performed using high-purity grade silica gel (60 Å pore size, 40-75 µm particle size). In the context of purification, PE refers to Petroleum ether 40-60 °C.

Capillary melting points are reported uncorrected to the nearest °C, and were determined using a Stuart digital SMP10 melting point apparatus. Optical rotations were measured using an Optical Activity Ltd AA-10 Series Automatic Polarimeter, with a path length of 1 dm, and with concentration (c) quoted in g/100 mL.

Nuclear Magnetic Resonance (NMR) spectroscopy experiments were performed in deuterated solvent at 298 K (unless stated otherwise) on either a Bruker Avance, 300, 400 or 500 MHz spectrometer or an Agilent ProPulse 500 MHz spectrometer.  $^1\text{H}$ ,  $^{13}\text{C}$ ,  $^{11}\text{B}$  and  $^{19}\text{F}$  NMR chemical shifts ( $\delta$ ) are quoted in parts per million (ppm) and are referenced to either the residual solvent peak or tetramethylsilane (TMS) when possible. Coupling constants ( $J$ ) are quoted in Hz.

Infrared (IR) spectra were recorded using a PerkinElmer Spectrum 100 FTIR spectrometer fitted with a Universal ATR FTIR accessory, with samples run neat and the most relevant, characteristic absorbances quoted as  $\nu$  in  $\text{cm}^{-1}$ .

High resolution mass spectrometry (HRMS) results were acquired on an externally calibrated Bruker Daltonics maXis HD™ UHR-TOF mass spectrometer coupled to an electrospray source (ESI-TOF), or an Agilent QTOF 6545 with Jetstream ESI. In most cases molecular ions were detected either in positive mode as their protonated, sodiated, or ammonium adduct forms, or in negative mode as the deprotonated of acetate adduct species. Comment and associated references are provided where more complex ionic forms were detected.

All compounds that were synthesised or purified in this thesis are characterised below. Where compounds had been previously characterised in the literature,  $^1\text{H}$  NMR and  $^{13}\text{C}$  NMR spectroscopic analysis was carried out (where possible).  $^{11}\text{B}$  and  $^{19}\text{F}$  NMR spectra were also recorded where possible. Where appropriate, melting point (solid products) and optical rotation (enantiopure chiral compounds) were measured. In the case where compounds were novel (not known in the literature, or where complete and suitable characterisation data could not be found, full characterisation was carried out, including the above methods, as well as FTIR and HRMS. Agreement between experimental data and literature was assessed on a case by case basis, but is usually: within 2-3 degrees for uncorrected melting points; within 0.06 ppm for chemical shifts and 0.2 Hz for coupling constants in  $^1\text{H}$  NMR spectra; within 1.0 ppm for  $^{13}\text{C}$  NMR chemical shifts.

## **5.2. Experimental details for Bull-James assemblies in chapters 1-3**

### *5.2.1 NMR spectroscopy experimental details*

By default, all 1D  $^1\text{H}$  NMR spectra were generated from 8 scans, unless otherwise stated. For low-concentration experiments, the number of scans was increased as follows: 16 scans for 12.5 mM; 32 scans for 5.0 mM; 64 scans for 2.5 mM; and 128 scans for 1.0 mM.

Quantitative fluorine NMR spectroscopy was carried using 16 scan proton-decoupled  $^{19}\text{F}\{^1\text{H}\}$  NMR experiments, with an increased relaxation time  $T_1 = 30$  s.

Diffusion measurements were made on a Bruker advance 500 MHz spectrometer, without sample spinning using the convection-compensated double-stimulated echo (DSTEBPGP3S) sequence<sup>491,492</sup> employing  $\text{sine}^2$  gradient pulses. The gradient strength was incremented linearly in 8 steps from 10% to 90% power (4.491 to 61.75 G/cm); the diffusion delay big delta,  $\Delta$ , was set to 50 ms; little delta,  $\delta$ , to 2 ms; the eddy current delay,  $T_e$ , to 5 ms; the recycle time ( $Aq + d_1$ ) totalled 7.45 s; and the number of scans per gradient increment was 16.

Numerical values for  $D$  were calculated from the imine proton resonance integrations of IBE complexes using Dynamics Centre 2.5.2.  $MW$  and  $R_{hyd}$  were predicted from  $D$  using the Manchester NMR Methodology Group's SEGWE calculator.<sup>327,328</sup>

### 5.2.2 Experimental details for the chiral derivatization of Ellman's sulfinamide **129a** with BINOL **9**

#### General procedure 1 for the three-component assembly of Ellman's sulfinamide **129a**, 2-FPBA **1** and BINOL **9**.

Ellman's sulfinamide **129** (1.0 mL, 0.1 M in CDCl<sub>3</sub> with ~6 mM TMS) of known enantiopurity was added to a mixture of 2-FPBA **1** (15 mg, 0.10 mmol, 1.0 equiv.) and enantiopure (*R*)- or (*S*)-BINOL **9** (34 mg, 0.11 mmol, 1.2 equiv.) and the mixture was left to stir for 1 h at room temperature. After this time, a 600 µL aliquot was removed and its 500 MHz <sup>1</sup>H NMR spectrum was recorded immediately.

Scalemic and racemic samples of Ellman's sulfinamide **129a** were prepared from commercially available enantiopure samples of (*R*)- and (*S*)-*tert*-butyl sulfinamide **129a**. 100 mM solutions of enantiopure **129a** in CDCl<sub>3</sub> were prepared, and then combined to produce scalemic samples of **129a**, the *ee* of which was determined by the ratio of enantiopure stock solutions.

For concentrations screening experiments dilute samples were prepared directly from this stock solution as follows (example illustrated for the preparation of a 25 mM sample): A 150 µL aliquot was removed from the stock solution and transferred to an NMR tube, before being diluted to 600 µL with CDCl<sub>3</sub> (525 µL, no added TMS). A 500 MHz <sup>1</sup>H NMR spectrum was recorded immediately.

### 5.2.3 Experimental details for the stepwise chiral derivatization of Ellman's sulfinamide **129a** with pinanediol **180**

#### General procedure 2 for the three-component assembly of sulfinamides **129a**, FPBA templates and pinanediol **180**.

A formylphenylboronic acid (0.12 mmol, 1.2 equiv.) and anhydrous MgSO<sub>4</sub> (200 mg) were added to a stirred solution of sulfinamide **129a-h** (0.1 mmol, 1.0 equiv.) in CDCl<sub>3</sub> (1.0 mL, ~6 mM TMS internal standard). The reaction was stirred at room temperature for 1 h, before addition of pinanediol **180** (22 mg, 0.13 mmol, 1.3 equiv.). The reaction was then stirred for a further 10 min, before the reaction was filtered and the 500 MHz <sup>1</sup>H NMR spectrum and/or 470 MHz <sup>19</sup>F spectrum of the resultant iminoboronate esters were acquired.

Preparation of scalemic, racemic and dilute samples was carried out following the same procedure as detailed previously.

#### 5.2.4 Procedures for the chiral derivatization of non-sulfinamide analytes

**General procedure 3 for three-component derivatization of 4-methoxy- $\alpha$ -methylbenzylamine **3b**, as used to prepare the spectra for Figure 3, adapted from Pérez-Fuertes *et al.*<sup>116</sup>**

4-Methoxy- $\alpha$ -methylbenzylamine **3b** (1.0 mL, 0.10 M in CDCl<sub>3</sub> with ~6 mM TMS internal standard, variable *ee*) was added to 2-formylphenyl boronic acid **1** (15 mg, 0.10 mmol, 1.0 equiv.) and (*S*)-BINOL **9** (31.5 mg, 0.11 mmol, 1.1 equiv.). The reaction was stirred for 10 min before an aliquot (0.7 mL) was removed and the 500 MHz <sup>1</sup>H NMR spectrum the resultant iminoboronate esters acquired.

Preparation of scalemic, racemic and dilute samples was carried out following the same procedure as detailed previously.

Three-component assemblies of amines, diamines and *O*-silyl amino alcohols with pinanediol (Scheme 87) were carried following the same general procedure with the appropriate reagents. The chiral derivatization of hydroxylamines was carried out with the addition of Cs<sub>2</sub>CO<sub>3</sub> (49 mg, 0.11 mmol) following the published methodology.<sup>143</sup>

Three-component assembly of  $\alpha$ -quaternary amino ester hydrochloride salts **208** and **210** was carried out using K<sub>2</sub>CO<sub>3</sub> (2.0 equiv., 28 mg, 0.20 mmol).

### 5.3. Synthetic and characterization details for chapter 3

Where certain <sup>13</sup>C signals could not be observed by 1D NMR due to low solubility, adjacent quadrupolar <sup>11</sup>B nuclei or lack of adjacent <sup>1</sup>H nuclei (no nOe enhancement), their chemical shift was deduced from 2D HMBC experiments, where possible. This approach was validated by variable temperature (VT) 1D NMR of boronate ester (3a*S*,4*S*,6*S*,7a*R*)-**182** (see Appendix D). Formyl boronic acids were detected by HRMS as their deprotonated methyl hydrogen boronate ions [M+13]<sup>-</sup> (from substitution by methanol and deprotonation), as reported by Wang *et al.*<sup>493</sup>

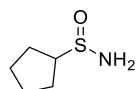
#### 5.3.1 Synthesis of (*rac*)-sulfinamides **129c-h**

**General procedure 4 for the synthesis of (*rac*)-sulfinamides **129c-h** from thiols by the method of Di *et al.*<sup>348</sup>**

*N*-bromosuccinimide (2.0 equiv.) was added to a stirred solution of the thiol (1.0 equiv.) in CH<sub>2</sub>Cl<sub>2</sub>/MeOH (1:1, 0.1 M) at 0 °C. The reaction was allowed to warm to room temperature and reaction progress was monitored by TLC. Upon completion (15 min - 1 h) the reaction mixture was quenched and diluted by half through the addition of saturated Na<sub>2</sub>CO<sub>3</sub>. The layers were separated, and the aqueous phase extracted twice with CH<sub>2</sub>Cl<sub>2</sub>. The combined organics were then washed with brine, dried (MgSO<sub>4</sub>), filtered, and concentrated to dryness *in vacuo* to afford a methyl sulfinates product **189c-h** as a clear oil.

The crude methyl sulfinite (1.0 equiv.) was dissolved in anhydrous THF (0.33 M) and cooled to -78 °C. LiHMDS (1.5 equiv., 1M in THF) was then added dropwise over 5 min and the reaction left to stir at -78 °C for 1.5 h. After this time the reaction was quenched with saturated NH<sub>4</sub>Cl, allowed to warm to room temperature and left to stir. After 30 min, the reaction was diluted with EtOAc, the aqueous phase extracted twice with EtOAc, and the combined organics were washed with brine, dried (MgSO<sub>4</sub>), filtered and concentrated *in vacuo*. The crude product was purified by either recrystallization or column chromatography to afford the desired sulfinamide **129c-h**.

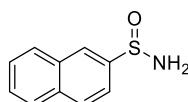
**(rac)-Cyclopentanesulfinamide 129c.**



General procedure 4 was followed using cyclopentanethiol (334 µL, 3.12 mmol). Recrystallisation from 1:10 EtOAc/*n*-hexane afforded the title compound **129c** (299 mg, 2.24 mmol) as a white solid in 72% yield. All characterisation data were consistent with previous literature reports.<sup>344</sup>

m.p.: 86-88 °C (lit.<sup>344</sup> 82-83 °C); IR (neat): 3189, 3089, 2957, 2868, 1450, 1166, 1001, 908, 697 cm<sup>-1</sup>; <sup>1</sup>H NMR (500 MHz, CDCl<sub>3</sub>) δ<sub>H</sub> 3.91 (bs, 2H, -NH<sub>2</sub>), 3.05 (p, 1H, *J* = 7.5, SCH), 2.04 (dt, 2H, *J* = 13.9, 6.9, CH<sub>2</sub>), 1.98-1.88 (m, 2H, CH<sub>2</sub>), 1.83-1.59 (m, 4H, CH<sub>2</sub>); <sup>13</sup>C{<sup>1</sup>H} NMR (126 MHz, CDCl<sub>3</sub>) δ<sub>C</sub> 65.2, 27.7, 26.1, 25.9, 25.6.

**(rac)-Naphthalene-2-sulfinamide 129d.**

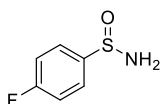


General procedure 4 was followed using naphthalene-2-thiol (500 mg, 3.12 mmol). Recrystallisation from 2:1 EtOAc/*n*-hexane afforded the title compound **129d** (408 mg, 2.13 mmol) as a white solid in 63% yield.

m.p.: 134-138 °C (decomposed); IR (neat): 3292, 3155, 3063, 1589, 1560, 1500, 1344, 1014, 822, 739 cm<sup>-1</sup>; <sup>1</sup>H NMR (500 MHz, CDCl<sub>3</sub>) δ<sub>H</sub> 8.34 (s, 1H, ArH), 7.99-7.89 (m, 3H, ArH), 7.71 (dd, 1H, ArH), 7.65-7.55 (m, 2H, ArH); 4.34 (bs, 2H, -NH<sub>2</sub>); <sup>13</sup>C{<sup>1</sup>H} NMR (126 MHz, CDCl<sub>3</sub>) δ<sub>C</sub> 143.6, 134.6, 132.8, 129.2, 129.0, 128.1, 128.1, 127.3, 125.8, 121.9; HRMS (ESI+): Calculated for [M+Na]<sup>+</sup> C<sub>10</sub>H<sub>9</sub>NOSNa<sup>+</sup>: 214.0297; Found: 214.0288.



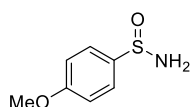
**(rac)-4-Fluorobenzenesulfinamide 129e.**



General procedure 4 was followed using 4-fluorothiophenol (332  $\mu$ L, 3.12 mmol). Recrystallization from 1:1 EtOAc/*n*-hexane afforded the title compound **129e** (268 mg, 1.68 mmol) as a white solid in 54% yield. Characterisation data were generally consistent with previous literature reports, despite some variation.<sup>494,495</sup>

m.p.: 134-139 °C (lit.<sup>494,495</sup> 128, 144.8-146.8 °C); IR (neat): 3269, 3154, 3065, 1587, 1481, 1229, 1211, 1156, 1087, 1005, 887, 834, 667  $\text{cm}^{-1}$ ;  $^1\text{H}$  NMR (500 MHz,  $\text{CDCl}_3$ )  $\delta_{\text{H}}$  7.79-7.71 (dd, 2H,  $J$  = 8.7, 5.1, *ArH*), 7.24-7.15 (app. t, exp. dd, 2H,  $J$  = 8.6 Hz, *ArH*), 4.32 (bs, 2H,  $\text{NH}_2$ );  $^{13}\text{C}\{^1\text{H}\}$  NMR (126 MHz,  $\text{CDCl}_3$ )  $\delta_{\text{C}}$  164.6 (d,  $^1J_{\text{F-C}}$  = 251.7), 142.2, 128.0 (d,  $^3J_{\text{F-C}}$  = 9.0), 116.2 (d,  $^2J_{\text{F-C}}$  = 22.4);  $^{19}\text{F}$  NMR (471 MHz,  $\text{CDCl}_3$ )  $\delta_{\text{F}}$  -113.8 (tt,  $J$  = 8.4, 5.1).

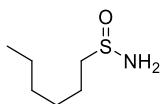
**(rac)-4-Methoxybenzenesulfinamide 129f.**



General procedure 4 was followed using 4-methoxythiophenol (383  $\mu$ L, 3.12 mmol). Recrystallization from 1:2 EtOAc/*n*-hexane afforded the title compound **129f** (262 mg, 1.53 mmol) as a white solid in 49% yield. All characterisation data were consistent with previous literature reports.<sup>283</sup>

m.p.: 127-131 °C (lit.<sup>283</sup> 129-131 °C); IR (neat): 3261, 3067, 2840, 1591, 1490, 1450, 1245, 1025, 1001, 823, 794  $\text{cm}^{-1}$ ;  $^1\text{H}$  NMR (500 MHz,  $\text{CDCl}_3$ )  $\delta_{\text{H}}$  7.68 (d, 2H,  $J$  = 8.8, *ArH*), 7.02 (d, 2H,  $J$  = 8.8, *ArH*), 4.24 (bs, 2H,  $\text{NH}_2$ ), 3.87 (s, 3H,  $\text{OCH}_3$ );  $^{13}\text{C}\{^1\text{H}\}$  NMR (126 MHz,  $\text{CDCl}_3$ )  $\delta_{\text{C}}$  162.1, 138.0, 127.2, 114.4, 55.7.

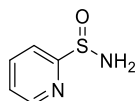
**(rac)-Hexane-1-sulfinamide 129g.**



General procedure 4 was followed using 1-hexanethiol (1.421 mL, 10.0 mmol). Recrystallization from *n*-hexane afforded the title compound **129g** (356 mg, 2.38 mmol) as an off-white solid in 24% yield. *Note: Although crude mass recovery was high, the low melting point of this novel sulfinamide led to significant issues during recrystallisation, leading to a decreased yield.*

m.p.: 41-42 °C; IR (neat): 3282, 3200, 2954, 2924, 2849, 1553, 1464, 1417, 1066, 1035, 1001, 890  $\text{cm}^{-1}$ ;  $^1\text{H}$  NMR (500 MHz,  $\text{CDCl}_3$ )  $\delta_{\text{H}}$  3.99 (bs, 2H,  $\text{NH}_2$ ), 2.73 (2  $\times$  ddd, 2H,  $J = 13.0, 8.5, 6.7$ ,  $\text{SCH}_2$ ), 1.79-1.63 (m, 2H,  $\text{SCH}_2\text{CH}_2$ ), 1.50-1.37 (m, 2H,  $\text{SCH}_2\text{CH}_2\text{CH}_2$ ), 1.36-1.29 (m, 4H,  $\text{MeCH}_2\text{CH}_2$ ), 0.91-0.87 (m, 3H,  $\text{CH}_3$ );  $^{13}\text{C}\{^1\text{H}\}$  NMR (126 MHz,  $\text{CDCl}_3$ )  $\delta_{\text{C}}$  57.9, 31.5, 28.4, 22.9, 22.5, 14.1; HRMS (ESI<sup>+</sup>): Calculated for  $[\text{M}+\text{NH}_4]^+$   $\text{C}_6\text{H}_{19}\text{N}_2\text{OS}^+$ : 167.1213; Found: 167.1215.

#### (rac)-Pyridine-2-sulfonamide **129h**.



General procedure 4 was followed using 2-mercapto pyridine (1.998 g, 18.0 mmol). Recrystallization from  $\text{CH}_2\text{Cl}_2$  afforded the title compound **129h** (128 mg, 0.972 mmol) as a white solid in 5% yield. Characterisation data were generally consistent with previous literature reports, despite some variation.<sup>496</sup> *Note: Although crude mass recovery of the methyl sulfinate and sulfonamide were initially high, significant degradation was observed on standing and during handling, presumed to be undesired reaction/polymerization between the pyridine and the sulfinate/sulfonamide.*

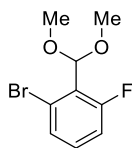
m.p.: 102-104 °C (lit.<sup>496</sup> 98-100 °C); IR (neat): 3306, 3184, 3080, 1573, 1458, 1419, 1024, 991, 775  $\text{cm}^{-1}$ ;  $^1\text{H}$  NMR (500 MHz,  $\text{CDCl}_3$ )  $\delta_{\text{H}}$  8.71 (ddd, 1H,  $J = 4.7, 4.7, 1.5$ , ArH), 7.99-7.89 (m, 2H, ArH), 7.44 (ddd, 1H,  $J = 7.4, 4.7, 1.4$ , ArH), 4.66 (bs, 2H,  $\text{NH}_2$ );  $^{13}\text{C}\{^1\text{H}\}$  NMR (126 MHz,  $\text{CDCl}_3$ )  $\delta_{\text{C}}$  164.5, 150.0, 138.1, 125.6, 120.6; HRMS (ESI<sup>+</sup>): Calculated for  $[\text{M}+\text{Na}]^+$   $\text{C}_5\text{H}_6\text{N}_2\text{OSNa}^+$ : 165.0093; Found: 165.0094.

#### 5.3.2 Synthesis of fluoro-2-FPBA F-1 templates

**General procedure 5 for the synthesis of 1-bromo-2-(dimethoxymethyl)-fluorobenzenes **199a-d** by the method of Kowalska *et al.*<sup>120</sup>**

$\text{H}_2\text{SO}_4$  (0.093 equiv., 0.47 mmol, 25  $\mu\text{L}$ ) and trimethyl orthoformate (1.3 equiv., 6.50 mmol, 711  $\mu\text{L}$ ) were added to a stirred solution of a 2-bromo-fluorobenzaldehyde **198** (1.0 equiv., 5.00 mmol, 1.02 g) in MeOH (2.0 mL). The reaction was heated at reflux for 1.5 h, before cooling to room temperature and quenching with triethylamine (1.00 mL, 7.17 mmol). The volatiles were removed *in vacuo*, and the resulting mixture dissolved in water (30 mL) and extracted with  $\text{Et}_2\text{O}$  (30 mL). The organics were washed with water (3  $\times$  30 mL) and brine (30 mL), dried ( $\text{MgSO}_4$ ), filtered, and concentrated *in vacuo* to afford the desired dimethyl acetals **199a-d** as clear oils.

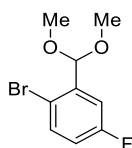
### 2-Bromo-1-(dimethoxymethyl)-6-fluorobenzene **199a**.



General procedure 5 was followed using 2-bromo-6-fluorobenzaldehyde **198a** (5.00 mmol, 1.02 g), affording the title compound **199a** (1.09 g, 4.41 mmol) as a colourless oil in 88% yield.

IR (neat): 2930, 2830, 1602, 1572, 1455, 1376, 1249, 1201, 1102, 1062, 168, 893, 781, 730  $\text{cm}^{-1}$ ;  $^1\text{H}$  NMR (500 MHz,  $\text{CDCl}_3$ )  $\delta_{\text{H}}$  7.73 (dt, 1H,  $J = 8.0, 1.1$ , ArH), 7.17 (td, 1H,  $J = 8.2, 5.6$ , ArH), 7.05 (dd, 1H,  $J = 10.4, 8.3, 1.2$ , ArH), 5.71 (d, 1H,  $J = 1.2$ , MeOCH), 3.49 (s, 6H,  $2 \times \text{OCH}_3$ );  $^{13}\text{C}\{^1\text{H}\}$  NMR (126 MHz,  $\text{CDCl}_3$ )  $\delta_{\text{C}}$  161.5 (d,  $^1J_{\text{F-C}} = 256.3$ ), 131.0 (d,  $J_{\text{F-C}} = 9.9$ ), 129.2 (d,  $J_{\text{F-C}} = 3.4$ ), 125.4 (d,  $J_{\text{F-C}} = 14.4$ ), 123.5 (d,  $J_{\text{F-C}} = 5.3$ ), 116.2 (d,  $J_{\text{F-C}} = 23.0$ ), 104.9, 55.7;  $^{19}\text{F}$  NMR (470 MHz,  $\text{CDCl}_3$ )  $\delta_{\text{F}}$  -111.1 (dd,  $J = 10.6, 5.6$ ); HRMS (ESI<sup>+</sup>): Calculated for  $[\text{M}+\text{Na}]^+$   $\text{C}_9\text{H}_{10}\text{O}_2\text{BrFNa}^+$ : 270.9740; Found: 270.9749.

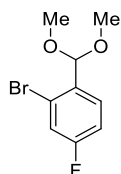
### 2-Bromo-1-(dimethoxymethyl)-5-fluorobenzene **199b**.



General procedure 5 was followed using 2-bromo-5-fluorobenzaldehyde **198b** (5.00 mmol, 1.02 g), affording the title compound **199b** (1.16 g, 4.65 mmol) as a colourless oil in 95% yield.

IR (neat): 2935, 2832, 1581, 1464, 1365, 1264, 1154, 1095, 1055, 972, 880  $\text{cm}^{-1}$ ;  $^1\text{H}$  NMR (300 MHz,  $\text{CDCl}_3$ )  $\delta_{\text{H}}$  7.51 (dd, 1H,  $J = 8.8, 5.1$ , ArH), 7.35 (dd, 1H,  $J = 9.4, 3.1$ , ArH), 6.93, ddd,  $J = 8.8, 7.7, 3.1$ , ArH), 5.50 (d, 1H,  $J = 1.2$ , MeCOCH), 3.38 (s, 6H,  $2 \times \text{OCH}_3$ );  $^{13}\text{C}\{^1\text{H}\}$  NMR (126 MHz,  $\text{CDCl}_3$ )  $\delta_{\text{C}}$  162.1 (d,  $^1J_{\text{F-C}} = 247.2$ ), 139.3 (d,  $J_{\text{F-C}} = 7.0$ ), 134.2 (d,  $J_{\text{F-C}} = 7.7$ ), 117.4 (d,  $J_{\text{F-C}} = 22.7$ ), 116.9 (d,  $J_{\text{F-C}} = 3.2$ ), 115.9 (d,  $J_{\text{F-C}} = 24.3$ ), 102.4, 54.0;  $^{19}\text{F}$  NMR (470 MHz,  $\text{CDCl}_3$ )  $\delta_{\text{F}}$  -114.3; HRMS (ESI<sup>+</sup>): Calculated for  $[\text{M}+\text{Na}]^+$   $\text{C}_9\text{H}_{10}\text{O}_2\text{BrFNa}^+$ : 270.9740; Found: 270.9748.

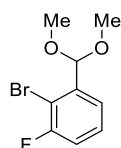
### 2-Bromo-1-(dimethoxymethyl)-4-fluorobenzene **199c**.



General procedure 5 was followed using 2-bromo-4-fluorobenzaldehyde **198c** (5.00 mmol, 1.02 g), affording the title compound **199c** (1.16 g, 4.65 mmol) as a colourless oil in 93% yield.

IR (neat): 2937, 2826, 1599, 1484, 1361, 1226, 1193, 1103, 1054, 982, 857, 812  $\text{cm}^{-1}$ ;  $^1\text{H}$  NMR (500 MHz,  $\text{CDCl}_3$ )  $\delta_{\text{H}}$  7.60 (dd, 1H,  $J = 8.7, 6.2$ , ArH), 7.31 (dd, 1H,  $J = 8.2, 2.6$ , ArH), 7.05 (td,  $J = 8.3, 2.6$ , ArH), 5.52 (s, 1H, MeOCH), 3.37 (s, 6H,  $2 \times \text{OCH}_3$ );  $^{13}\text{C}\{^1\text{H}\}$  NMR (126 MHz,  $\text{CDCl}_3$ )  $\delta_{\text{C}}$  162.5 (d,  $^1J_{\text{F-C}} = 251.8$ ), 133.2 (d,  $J_{\text{F-C}} = 3.6$ ), 129.7 (d,  $J_{\text{F-C}} = 8.5$ ), 123.2 (d,  $J_{\text{F-C}} = 9.4$ ), 120.2 (d,  $J_{\text{F-C}} = 24.8$ ), 114.5 (d,  $J_{\text{F-C}} = 20.9$ ), 102.6, 54.0;  $^{19}\text{F}$  NMR (470 MHz,  $\text{CDCl}_3$ )  $\delta_{\text{F}}$  -111.4; HRMS (ESI+): Calculated for  $[\text{M}+\text{Na}]^+$   $\text{C}_9\text{H}_{10}\text{O}_2\text{BrFNa}^+$ : 270.9740; Found: 270.9747.

## 2-Bromo-1-(dimethoxymethyl)-3-fluorobenzene **199d**.



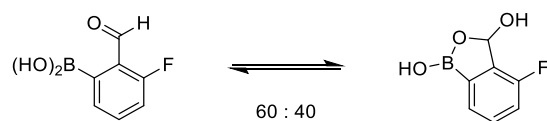
General procedure 5 was followed using 2-bromo-3-fluorobenzaldehyde **198d** (5.00 mmol, 1.02 g), affording the title compound **199d** (1.18 g, 4.75 mmol) as a colourless oil in 95% yield.

IR (neat): 2959, 2835, 1577, 1464, 1436, 1357, 1261, 1115, 1035, 1004, 825, 776  $\text{cm}^{-1}$ ;  $^1\text{H}$  NMR (500 MHz,  $\text{CDCl}_3$ )  $\delta_{\text{H}}$  7.43-7.39 (m, 1H, ArH), 7.34-7.28 (m, 1H, ArH), 7.14-7.09 (m, 1H, ArH), 5.57 (s, 1H, MeOCH), 3.39 (s, 6H,  $2 \times \text{OCH}_3$ );  $^{13}\text{C}\{^1\text{H}\}$  NMR (126 MHz,  $\text{CDCl}_3$ )  $\delta_{\text{C}}$  159.2 (d,  $^1J_{\text{F-C}} = 246.5$ ), 139.4, 128.3 (d,  $J_{\text{F-C}} = 7.9$ ), 123.7 (d,  $J_{\text{F-C}} = 3.3$ ), 116.5 (d,  $J_{\text{F-C}} = 22.6$ ), 110.2 (d,  $J_{\text{F-C}} = 21.3$ ), 102.6 (d,  $J_{\text{F-C}} = 3.6$ ), 54.1;  $^{19}\text{F}$  NMR (470 MHz,  $\text{CDCl}_3$ )  $\delta_{\text{F}}$  -105.5 (dd,  $J = 8.3, 5.1$ ); HRMS (ESI+): Calculated for  $[\text{M}+\text{Na}]^+$   $\text{C}_9\text{H}_{10}\text{O}_2\text{BrFNa}^+$ : 270.9740; Found: 270.9741.

## General procedure 6 for the synthesis of fluoro-2-formylphenyl boronic acids **F-1** by the method of Kowalska *et al.*<sup>120</sup>

*n*-Butyllithium (2.5 M in THF, 1.15 equiv.) was added dropwise (15 min) to a stirred solution of a fluoro-1-bromo-2-(dimethoxymethyl)-fluorobenzene **199** (1.0 equiv.) in anhydrous  $\text{Et}_2\text{O}$ /THF (5:1 mixture, 0.33 M) under an inert  $\text{N}_2$  atmosphere. The resultant solution was then cooled to  $-78^\circ\text{C}$ , and stirred for 1 h, before addition of trimethyl borate (1.15 equiv.). The reaction was warmed to room temperature and allowed to stir for 15 min, before acidifying to pH 3 using HCl (3M, aq.). The reaction was diluted with  $\text{Et}_2\text{O}$ , and the aqueous phase extracted 3 times. The combined organics were washed with brine, dried over  $\text{MgSO}_4$ , and concentrated to dryness, with the resultant crude product recrystallised from  $\text{EtOAc}$ /hexane to afford the desired formyl boronic acid **F-1** (observed in tautomeric equilibrium with the related benzoxaborole minor product by NMR). *Note: Due to the inherent reactivity of 2-FPBA and its derivatives towards nucleophilic attack, therefore fresh spectra should be prepared for NMR analysis in acetone –  $d_6$ , and acetone should not be used as a solvent for handling/transferring/dissolving these compounds, as aldol condensation will occur.*

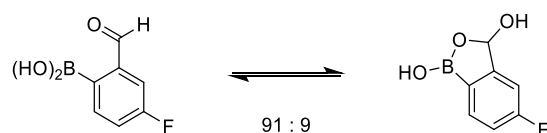
### (3-Fluoro-2-formylphenyl)boronic acid 3-F-1.



General procedure 6 was followed using 1-bromo-2-(dimethoxymethyl)-3-fluorobenzene **199a** (1.09 g, 4.41 mmol), affording the title compound 3-F-1 (444 mg, 2.64 mmol) as a white solid in 60% yield. 40% benzoxaborole tautomer was observed in the NMR spectrum. All characterisation data were consistent with previous literature reports.<sup>119</sup>

m.p.: 125-128 °C (lit.<sup>119</sup> 127-129 °C); IR (neat): 3309, 3071, 2943, 1675, 1561, 1427, 1294, 1235, 1184, 1083, 908, 825, 793, 732 cm<sup>-1</sup>; <sup>1</sup>H NMR (500 MHz, acetone-*d*<sub>6</sub>)  $\delta_H$  10.38 (s, 1H, OCH, major), 8.42 (bs, 1H, BOH, minor), 7.77-7.61 (m, 1H, ArH, major), 7.54-7.41 (m, 2H major + 1H minor, ArH), 7.32 (bs, 2H, BOH, major), 7.26 (ddd, 1H, *J* = 11.2, 8.3, 1.1, ArH, major), 7.21 (ddd, 1H, *J* = 9.8, 7.9, 1.1, ArH, minor), 6.45 (s, 1H, HCO, minor), 6.13 (bs, 1H, COH, minor); <sup>11</sup>B NMR (375.5 MHz, acetone-*d*<sub>6</sub>)  $\delta_B$  31.2 (minor), 29.5 (major); <sup>19</sup>F NMR (470 MHz, acetone-*d*<sub>6</sub>)  $\delta_F$  -120.8 (dd, *J* = 9.9, 4.2, minor), -122.4 (dd, *J* = 121.1, 5.3, major). HRMS (ESI<sup>-</sup>): Calculated for [M-H<sub>2</sub>O+OMe]<sup>-</sup> C<sub>8</sub>H<sub>7</sub>FBO<sub>3</sub><sup>-</sup>: 181.0478; Found: 181.0475. <sup>13</sup>C NMR spectrum is not reported, as the signal intensity was too weak due to the combined effect of tautomerization, <sup>19</sup>F splitting and the adjacent <sup>11</sup>B.

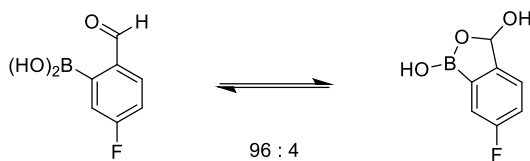
### (4-Fluoro-2-formylphenyl)boronic acid 4-F-1.



General procedure 6 was followed using 1-bromo-2-(dimethoxymethyl)-4-fluorobenzene **199b** (1.18 g, 4.75 mmol), affording the title compound 4-F-1 (410 mg, 2.44 mmol) as a white solid in 55% yield. 9% benzoxaborole tautomer was observed in the NMR spectrum. All characterisation data were consistent with previous literature reports.<sup>162</sup>

m.p.: 123-126 °C (lit.<sup>162</sup> 123-125 °C); IR (neat): 3217, 1670, 1601, 1578, 1428, 1366, 1339, 1273, 1221, 1156, 1088, 1039, 886, 829, 768, 727 cm<sup>-1</sup>; <sup>1</sup>H NMR (500 MHz, acetone-*d*<sub>6</sub>)  $\delta_H$  10.33 (s, 1H, OCH, major), 8.28 (bs, 1H, BOH, minor), 7.93 (dd, 1H, *J* = 8.3, 5.9, ArH, major), 7.74 (bs, 2H, BOH, major), 7.74 (dd, 1H, *J* = 8.0, 5.7, ArH, minor), 7.66 (dd, 1H, *J* = 9.6, 7.2, ArH, major), 7.44 (td, *J* = 8.4, 2.7, ArH, major), 7.21-7.13 (m, 2H, ArH, minor); <sup>11</sup>B NMR (375.5 MHz, acetone-*d*<sub>6</sub>)  $\delta_B$  31.3 (minor), 28.9 (major); <sup>19</sup>F NMR (470 MHz, acetone-*d*<sub>6</sub>)  $\delta_F$  -111.2 (minor), -111.7 (major); HRMS (ESI<sup>-</sup>): Calculated for [M-H<sub>2</sub>O+OMe]<sup>-</sup> C<sub>8</sub>H<sub>7</sub>FBO<sub>3</sub><sup>-</sup>: 181.0478; Found: 181.0471. <sup>13</sup>C NMR spectrum is not reported, as the signal intensity was too weak due to the combined effect of tautomerization, <sup>19</sup>F splitting and the adjacent <sup>11</sup>B.

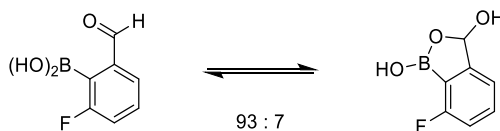
**(5-Fluoro-2-formylphenyl)boronic acid 5-F-1.**



General procedure 6 was followed using 1-bromo-2-(dimethoxymethyl)-5-fluorobenzene **199c** (1.16 g, 4.65 mmol), affording the title compound **5-F-1** (388 mg, 2.31 mmol) as a white solid in 50% yield. 4% benzoxaborole tautomer was observed in the NMR spectrum.

m.p.: 126-131 °C; IR (neat): 3309, 3069, 1669, 1596, 1571, 1419, 1344, 1226, 1167, 1103, 1044, 905, 797, 737, 692  $\text{cm}^{-1}$ ;  $^1\text{H}$  NMR (500 MHz, acetone- $d_6$ )  $\delta_{\text{H}}$  10.17 (s, 1H, OCH, major), 8.06 (m, 1H major + 1H minor, ArH), 7.84 (s, 2H, BOH, major), 7.56 (dd, 1H,  $J = 9.5, 2.7$ , ArH, major), 7.50 (dd, 1H,  $J = 8.3, 4.7$ , ArH, minor), 7.37 (td, 1H,  $J = 8.4, 2.7$ , ArH, major), 7.31-7.22 (m, 1H, ArH, minor), 6.27 (bs, 1H, OCH, minor) (some signals not observed due to low concentration of minor tautomer)<sup>19</sup>;  $^{11}\text{B}$  NMR (375.5 MHz, acetone- $d_6$ )  $\delta_{\text{B}}$  28.9 (major), 20.2 (minor);  $^{19}\text{F}$  NMR (470 MHz, acetone- $d_6$ )  $\delta_{\text{F}}$  -106.7 (dd,  $J = 8.1, 8.1$ , major), -116.1 (minor); HRMS (ESI<sup>-</sup>): Calculated for  $[\text{M}-\text{H}_2\text{O}+\text{OMe}]^-$   $\text{C}_8\text{H}_7\text{FBO}_3^-$ : 181.0478; Found: 181.0473.  $^{13}\text{C}$  NMR spectrum is not reported, as the signal intensity was too weak due to the combined effect of tautomerization,  $^{19}\text{F}$  splitting and the adjacent  $^{11}\text{B}$ .

**(6-Fluoro-2-formylphenyl)boronic acid 6-F-1.**



General procedure 6 was followed using 1-bromo-2-(dimethoxymethyl)-6-fluorobenzene **199d** (1.18 g, 4.75 mmol), affording the title compound **6-F-1** (223 mg, 1.33 mmol) as a white solid in 28% yield. 7% benzoxaborole tautomer was observed in the NMR spectrum.

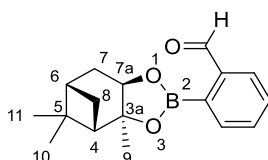
m.p.: 153-156 °C; IR (neat): 3255, 2848, 1674, 1601, 1567, 1451, 1324, 1301, 1231, 1213, 1160, 1040, 786, 730, 681  $\text{cm}^{-1}$ ;  $^1\text{H}$  NMR (500 MHz, acetone- $d_6$ )  $\delta_{\text{H}}$  10.04 (d, 1H,  $J = 2.3$ , OCH, major), 7.75 (d, 1H,  $J = 7.4$ , ArH, major), 7.64-7.54 (m, 1H major + 1H minor, ArH), 7.38-7.24 (m, 1H major + 1H minor, ArH), 7.06 (t, 1H,  $J = 8.1$ , ArH, major), 6.26 (bs, 1H, OCH, minor) (some signals not observed due to low concentration of minor tautomer)<sup>19</sup>;  $^{11}\text{B}$  NMR (375.5 MHz, acetone- $d_6$ )  $\delta_{\text{B}}$  29.3 (major), 20.2 (minor);  $^{19}\text{F}$  NMR (470 MHz, acetone- $d_6$ )  $\delta_{\text{F}}$  -105.6 (minor), -106.1 (t,  $J = 6.7$ , major); HRMS (ESI<sup>-</sup>): Calculated for  $[\text{M}-\text{H}_2\text{O}+\text{OMe}]^-$   $\text{C}_8\text{H}_7\text{FBO}_3^-$ : 181.0478; Found: 181.0473.  $^{13}\text{C}$  NMR spectrum is not reported, as the signal intensity was too weak due to the combined effect of tautomerization,  $^{19}\text{F}$  splitting and the adjacent  $^{11}\text{B}$ .

### 5.3.3 Synthesis and characterization of two-and three-component products

#### General procedure 7 for the synthesis of 2-formyl boronate esters **182** and **3-F-182**.

(1*S*,2*S*,3*R*,5*S*)-Pinanediol **180** (1.0 equiv.) was added to a stirred suspension of a 2-formylbenzene boronic acid **2** (1.1 equiv.) in CHCl<sub>3</sub> (0.10 M). After 15 min, the reaction was diluted with an equivalent amount of CH<sub>2</sub>Cl<sub>2</sub> and passed through a silica plug. The plug was washed with CH<sub>2</sub>Cl<sub>2</sub> until no more product eluted and the solvent removed *in vacuo* to afford the desired boronate ester as a clear oil.

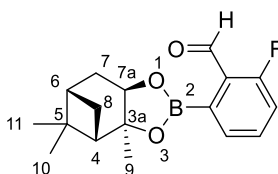
#### 2-((3*aS*,4*S*,6*S*,7*aR*)-3*a*,5,5-Trimethylhexahydro-4,6-methanobenzo[*d*][1,3,2]dioxaborol-2-yl)benzaldehyde **182**.



General procedure 7 was followed using 2-FPBA **1** (83 mg, 0.55 mmol) and (1*S*, 2*S*, 3*R*, 5*S*)-pinanediol **180** (85 mg, 0.5 mmol), affording the title compound (3*aS*,4*S*,6*S*,7*aR*)-**182** (110 mg, 0.39 mmol) as a clear oil in 70% yield.

[ $\alpha$ ]<sub>D</sub><sup>23</sup> = +18 (*c* 1.0, CHCl<sub>3</sub>); IR (neat): 2921, 2870, 1693, 1593, 1488, 1370, 1337, 1236, 1076, 754, 666 cm<sup>-1</sup>; <sup>1</sup>H NMR (500 MHz, CDCl<sub>3</sub>)  $\delta$ <sub>H</sub> 10.55 (s, 1H, OCH), 7.98-7.95 (m, 1H, ArH), 7.90-7.86 (m, 1H, ArH), 7.62-7.53 (m, 2H, ArH), 4.52 (dd, 1H, *J* = 8.8, 1.9, H-7a), 2.48-2.39 (m, 1H, H-7), 2.32-2.23 (m, 1H, H-8), 2.16 (dd, 1H, *J* = 6.0, 4.9, H-4), 2.04-1.94 (m, 2H, H-6 + H-7), 1.53 (s, 3H, H-9), 1.33 (d, 1H, *J* = 10.8, H-8), 1.32 (s, 3H, H-10/11), 0.90 (s, 3H, H-10/11); <sup>13</sup>C{<sup>1</sup>H} NMR (126 MHz, CDCl<sub>3</sub>)  $\delta$ <sub>C</sub> 194.7, 141.4, 135.7, 133.1, 131.9 (deduced from HMBC, confirmed by -15 °C VT NMR), 130.8, 128.0, 86.9, 78.6, 51.5, 39.7, 38.4, 35.5, 28.7, 27.2, 26.6, 24.2; <sup>11</sup>B NMR (375.5 MHz, CDCl<sub>3</sub>)  $\delta$ <sub>B</sub> 30.7; HRMS (ESI<sup>+</sup>): Calculated for [M+Na]<sup>+</sup> C<sub>17</sub>H<sub>21</sub>BO<sub>3</sub>Na<sup>+</sup>: 307.1479<sup>+</sup>; Found: 307.1493.

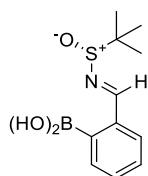
#### 2-fluoro-6-((3*aS*,4*S*,6*S*,7*aR*)-3*a*,5,5-Trimethylhexahydro-4,6-methanobenzo[*d*][1,3,2]dioxaborol-2-yl)benzaldehyde **3-F-182**.



General procedure 7 was followed using 3-fluoro-2-FPBA **3-F-1** (47 mg, 0.28 mmol) and (1*S*,2*S*,3*R*,5*S*)-pinanediol **180** (96 mg, 0.25 mmol), affording the title compound (3*aS*,4*S*,6*S*,7*aR*)-**3-F-182** (73 mg, 0.39 mmol) as a clear oil in 96% yield.

$[\alpha]_D^{23} = +20$  (c 1.0,  $\text{CHCl}_3$ ); IR (neat): 2918, 2869, 1695, 1568, 1480, 1439, 1339, 1238, 1029, 794,  $666\text{ cm}^{-1}$ ;  $^1\text{H}$  NMR (500 MHz,  $\text{CDCl}_3$ )  $\delta_H$  10.43 (d, 1H,  $J = 1.0$ , OCHC), 7.58 (ddd, 1H,  $J = 8.3, 7.2, 5.2$ , ArH), 7.40 (d, 1H,  $J = 7.2$ , ArH), 7.17 (ddd, 1H,  $J = 10.6, 8.3, 1.0$ , ArH), 4.55 (dd, 1H,  $J = 8.8, 2.0$ , H-7a), 2.48-2.38 (m, 1H, H-7), 2.37-2.27 (m, 1H, H-8), 2.17-2.11 (m, 1H, H-4), 2.06-1.96 (m, 2H, H-6 and H-7), 1.58 (s, 3H, H-9), 1.55 (d, 1H,  $J = 10.8$ , H-8), 1.34 (s, 3H, H-10/11), 0.91 (s, 3H, H-10/11);  $^{13}\text{C}\{^1\text{H}\}$  NMR (126 MHz,  $\text{CDCl}_3$ )  $\delta_C$  189.0 (d,  $J_{F-C} = 6.2$ ), 164.3 (d,  $^1J_{F-C} = 259.8$ ), 135.7 (d,  $J_{F-C} = 8.7$ ), 129.1 (d,  $J_{F-C} = 3.8$ ), 127.8 (d,  $J_{F-C} = 6.9$ ), 121.6 (deduced from HMBC), 117.5 (d,  $J_{F-C} = 20.9$ ), 86.6, 78.8, 51.7, 39.7, 38.5, 35.5, 28.4, 27.3, 26.5, 24.2;  $^{11}\text{B}$  NMR (375.5 MHz,  $\text{CDCl}_3$ )  $\delta_B$  30.9;  $^{19}\text{F}$  NMR (470 MHz,  $\text{CDCl}_3$ )  $\delta_F$  -121.0 (dd,  $J = 10.5, 5.3$ ); HRMS (ESI<sup>+</sup>): Calculated for  $[\text{M}+\text{Na}]^+ \text{C}_{17}\text{H}_{20}\text{BO}_3\text{FNa}^+$ : 325.1385; Found: 325.1381.

## 2-(*tert*-Butylsulfinyl)-1*H*-1 $\lambda^4$ ,2 $\lambda^4$ -benzo[*c*][1,2]azaborole-1,1-diol (*S*)-**181**.



(*R*)-Ellman's sulfinamide **129a** (33 mg, 0.27 mmol, 1.35 equiv.) was added to a stirred suspension of 2-formylbenzene boronic acid **2-F-1** (30 mg, 0.20 mmol, 1.0 equiv.) and  $\text{MgSO}_4$  (500 mg) in  $\text{CDCl}_3$  (2.0 mL) and the reaction stirred for 2 h, before filtering through a cottonwool-celite plug. The title compound (*S*)-**181** was formed in solution in 95% yield (5% 2-FPBA **1** and 0.45 equiv. (*S*)-**129a** remaining in solution). The product was analysed and characterised as is in solution and was not isolated.

$^1\text{H}$  NMR (500 MHz,  $\text{CDCl}_3$ )  $\delta_H$  9.12 (s, 1H, NCH), 8.15-8.10 (m, 1H, ArH), 7.96-7.89 (m, 1H, ArH), 7.59-7.53 (m, 2H, ArH), 7.19 (bs, 1H, 2  $\times$  OH), 1.30 (s, 9H, 3  $\times$   $\text{CH}_3$ ), 0.88 (s, 3H, H-10/11);  $^{13}\text{C}$  NMR (126 MHz,  $\text{CDCl}_3$ )  $\delta_C$  167.3, 138.0, 137.2, 134.7 (deduced by HMBC), 132.1, 132.0, 130.8, 58.3, 22.6.  $^{11}\text{B}$  NMR (375.5 MHz,  $\text{CDCl}_3$ )  $\delta_B$  28.6; HRMS (ESI<sup>+</sup>): Calculated for  $[\text{M}-2\text{H}_2\text{O}+2\text{MeOH}+\text{Na}]^+ \text{C}_{13}\text{H}_{20}\text{BNO}_3\text{SNa}^+$ : 304.1149, Found 304.1138. IR and specific rotation data were not acquired due to the presence of significant residual (*R*)-**129a**. Slow evaporation from  $\text{CDCl}_3$ /n-hexane afforded white crystals suitable for X-ray crystallography (see Appendix A).

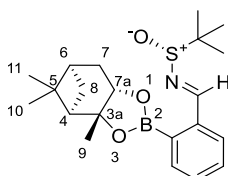
## General procedure 8 for the synthesis of *tert*-butyl sulfiniminoboronates **183a** and **184a**.

Enantiopure *tert*-butyl sulfinamide **129a** (61 mg, 0.50 mmol, 1.0 equiv.) was added to a stirred suspension of 2-formylbenzene boronic acid **1** (90 mg, 0.60 mmol, 1.2 equiv.) and  $\text{MgSO}_4$  (1.00 g) in  $\text{CHCl}_3$  (5.0 mL) and the reaction stirred for 2 h, before (1*R*,2*R*,3*S*,5*R*)-pinanediol **180** (111 mg, 0.65 mmol, 1.3 equiv.) was added. After 10 min, the reaction was filtered and concentrated to dryness *in vacuo* and the residue purified by chromatography (0.5% MeOH in 1:1  $\text{CH}_2\text{Cl}_2$ /n-hexane)



afforded the desired sulfiniminoboronate ester as a clear oil. The low stability of these complexes to the purification conditions employed meant that small amounts of 2-formyl boronate ester **182** remained.

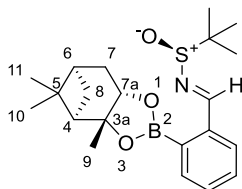
**(*R*)-2-Methyl-*N*-((*E*)-2-((3*aR*,4*R*,6*R*,7*aS*)-3*a*,5,5-trimethylhexahydro-4,6-methanobenzo[*d*][1,3,2]dioxaborol-2-yl)benzylidene)propane-2-sulfinamide **183**.**



General procedure 8 was followed using (*R*)-Ellman's sulfinamide **129a** (61 mg, 0.50 mmol), affording the title compound (*R*<sub>S</sub>,3*aR*,4*R*,6*R*,7*aS*)-**183a** (24 mg, 0.062 mmol) as a clear oil in 12% yield, as a 89:11 mixture with the related formyl boronate ester (3*aR*,4*R*,6*R*,7*aS*)-**182**.

<sup>1</sup>H NMR (500 MHz, CDCl<sub>3</sub>)  $\delta_H$  9.36 (s, 1H, NCH), 8.13-8.06 (m, 1H, ArH), 7.94-7.88 (m, 1H, ArH), 7.54-7.46 (m, 2H, ArH), 4.51 (dd, 1H, *J* = 8.8, 2.0, H-7a), 2.48-2.37 (m, 1H, H-7), 2.29-2.21 (m, 1H, H-8), 2.18 (dd, 1H, *J* = 6.1, 5.1, H-4), 2.02 (ddd, 1H, *J* = 14.7, 3.4, 2.0, H-7), 1.97-1.97 (m, 1H, H-6), 1.51 (s, 3H, H-9), 1.30 (s, 3H, H-10/11), 1.26 (s, 9H, *tert*-butyl), 1.23 (d, 1H, *J* = 10.9, H-8), 0.88 (s, 3H, H-10/11); <sup>11</sup>B NMR (375.5 MHz, CDCl<sub>3</sub>)  $\delta_B$  30.5; HRMS (ESI<sup>+</sup>): Calculated for [M+H]<sup>+</sup> C<sub>21</sub>H<sub>31</sub>BNO<sub>3</sub>S: 388.2116, Found 388.2118; Calculated for [M+Na]<sup>+</sup> C<sub>21</sub>H<sub>30</sub>BNO<sub>3</sub>SN<sup>+</sup>: 410.1936; Found: 410.1940. IR and specific rotation data were not acquired due to the presence of significant residual (3*aR*,4*R*,6*R*,7*aS*)-**182**. <sup>13</sup>C NMR spectra are not reported, as this impurity and the adjacent <sup>11</sup>B nucleus led to unassignable spectra.

**(*S*)-2-Methyl-*N*-((*E*)-2-((3*aR*,4*R*,6*R*,7*aS*)-3*a*,5,5-trimethylhexahydro-4,6-methanobenzo[*d*][1,3,2]dioxaborol-2-yl)benzylidene)propane-2-sulfinamide **184a**.**



General procedure 8 was followed using (*S*)-Ellman's sulfinamide **129a**, affording the title compound (*S*<sub>S</sub>,3*aR*,4*R*,6*R*,7*aS*)-**184a** (37 mg, 0.096 mg) as a clear oil in 19% yield, as a 96:4 mixture with the related formyl boronate ester (3*aR*,4*R*,6*R*,7*aS*)-**182**.

<sup>1</sup>H NMR (500 MHz, CDCl<sub>3</sub>)  $\delta_H$  9.27 (s, 1H, NCH), 8.08-8.03 (m, 1H, ArH), 7.90-7.83 (m, 1H, ArH), 7.54-7.47 (m, 2H, ArH), 4.51 (dd, 1H, *J* = 8.7, 1.9, H-7a), 2.49-2.38 (m, 1H, H-7), 2.32-2.21 (m, 1H, H-8), 2.17 (dd, 1H, *J* = 6.0, 5.0, H-4), 2.09-1.91 (m, 2H H-7 + H-6), 1.51 (s, 3H, H-9), 1.31 (s, 3H, H-

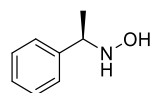
10/11), 1.28-1.22 (m, 12H, tert-butyl + H-8), 0.88 (s, 3H, H10/11);  $^{11}\text{B}$  NMR (375.5 MHz,  $\text{CDCl}_3$ )  $\delta_{\text{B}}$  31.2; HRMS (ESI+): Calculated for  $[\text{M}+\text{H}]^+$   $\text{C}_{21}\text{H}_{31}\text{BNO}_3\text{S}^+$ : 388.2116, Found 388.2112; Calculated for  $[\text{M}+\text{Na}]^+$   $\text{C}_{21}\text{H}_{30}\text{BNO}_3\text{S}$ : 410.1936; Found: 410.1937; IR and specific rotation data were not acquired due to the presence of significant residual (3a*R*,4*R*,6*R*,7a*S*)-**182**.  $^{13}\text{C}$  NMR spectra are not reported, as this impurity and the adjacent  $^{11}\text{B}$  nucleus led to unassignable spectra.

#### 5.3.4 Synthesis and characterization of non-sulfinamide analytes

##### General procedure 9 for the enantioselective synthesis of $\alpha$ -(methylbenzyl)hydroxylamines by the method of Tickell *et al.*<sup>143</sup>

$\text{MgSO}_4$  (2.0 g) and *p*-anisaldehyde (501  $\mu\text{L}$ , 4.12 mmol, 1.0 equiv.) were added to a solution of the enantiopure amine (531  $\mu\text{L}$ , 4.12 mmol, 1.0 equiv.) in MeOH (25 mL). The mixture was stirred for 24 h, filtered and the solvent evaporated under reduced pressure. The residue was then dissolved in anhydrous  $\text{CH}_2\text{Cl}_2$  (5 mL), cooled to 0 °C and a solution of *m*CPBA (75% purity, 1.138 g, 4.94 mmol, 1.2 equiv.) in anhydrous  $\text{CH}_2\text{Cl}_2$  (30 mL) was added dropwise. The reaction was stirred for 1 h at 0 °C, before warming to room temperature and stirring for a further 3 h. The resultant white suspension was filtered, and the filtrate was neutralised with  $\text{NaHCO}_3$  (sat. aq., 20 mL) and washed with brine (20 mL). The organic layer was dried over  $\text{MgSO}_4$  and the solvent evaporated under reduced pressure to yield the oxaziridine intermediate. The crude oxaziridine was subsequently dissolved in anhydrous MeOH (20 mL) and hydroxylamine hydrochloride (573 mg, 8.24 mmol, 2.0 equiv.) was added, and the mixture was stirred for 16 h. After this time,  $\text{CHCl}_3$  (20 mL) was added to precipitate unreacted hydroxylamine hydrochloride, and the solution was filtered and solvent removed *in vacuo*. Water (20 mL) and  $\text{Et}_2\text{O}$  (20 mL) were added to the residue and the aqueous layer extracted repeatedly with  $\text{Et}_2\text{O}$  (10  $\times$  20 mL). The aqueous layer was saturated with  $\text{NaHCO}_3$  and extracted with  $\text{Et}_2\text{O}$  (3  $\times$  20 mL). The combined organic layers were then dried over  $\text{MgSO}_4$  and concentrated to dryness *in vacuo*. The crude product was purified by recrystallization from 1:4  $\text{CHCl}_3$ /hexane.

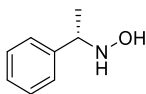
##### (*R*)-*N*-(1-Phenylethyl)hydroxylamine (*R*)-56a.



General procedure 9 was followed using (*R*)- $\alpha$ -methylbenzylamine (*R*)-**3a**, to afford the title compound (*R*)-**56a** (271 mg, 1.98 mmol) as a fluffy white solid in 48% yield. All characterisation data were consistent with previous literature reports.<sup>143</sup>

m.p.: 98-99 °C (lit.<sup>143</sup> 96-99 °C);  $[\alpha]_{\text{D}}^{23} = +32$  (c 1.0,  $\text{CHCl}_3$ ; lit.<sup>143</sup> +37, c 1.0,  $\text{CH}_2\text{Cl}_2$ , 22 °C);  $^1\text{H}$  NMR (500 MHz,  $\text{CDCl}_3$ )  $\delta_{\text{H}}$  7.40-7.27 (m, 5H, ArH), 4.18 (q, 1H,  $J = 6.7$ , ArCH), 1.42 (d, 3H,  $J = 6.7$ ,  $\text{CH}_3$ ).

**(S)-N-(1-Phenylethyl)hydroxylamine (S)-56a.**



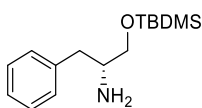
General procedure 9 was followed using (S)- $\alpha$ -methylbenzylamine (S)-**3a**, to afford the title compound (S)-**56a** (288 mg, 2.14 mmol) as a fluffy white solid in 51% yield. All characterisation data were consistent with previous literature reports.<sup>497</sup>

m.p.: 96-97 °C (lit.<sup>497</sup> 97-98 °C);  $[\alpha]_D^{23} = -33$  (c 1.0, CHCl<sub>3</sub>; lit.<sup>497</sup> -34.6, c 1.0, CHCl<sub>3</sub>, 25 °C); <sup>1</sup>H NMR (500 MHz, CDCl<sub>3</sub>)  $\delta_H$  7.40-7.27 (m, 5H, ArH), 4.18 (q, 1H, *J* = 6.7, ArCH), 1.41 (d, 3H, *J* = 6.7, CH<sub>3</sub>).

**General procedure 10 for the synthesis of O-silyl amino alcohols.**

*tert*-Butyldimethylsilylchloride (302 mg, 2.0 mmol, 1.0 equiv.), *N,N*-dimethylaminopyridine (24 mg, 0.4 mmol, 0.2 equiv.), triethylamine (557  $\mu$ L, 4.0 mmol, 2.0 equiv.) and the enantiopure 2-amino-3-phenylpropan-1-ol (302 mg, 2.0 mmol, 1.0 equiv.) were dissolved in CH<sub>2</sub>Cl<sub>2</sub> (5 mL) and left to stir for 16 h. After this time, the reaction was quenched with H<sub>2</sub>O (10 mL), diluted with CH<sub>2</sub>Cl<sub>2</sub> (10 mL) and separated. The aqueous phase was extracted with CH<sub>2</sub>Cl<sub>2</sub> twice more (2  $\times$  10 mL), and the combined organics were washed with brine (20 mL), dried (MgSO<sub>4</sub>), filtered, and concentrated to dryness *in vacuo*. The crude product was purified by flash column chromatography (SiO<sub>2</sub>, 0-10% MeOH in CHCl<sub>3</sub>) to afford the desired product.

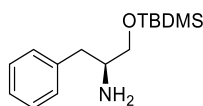
**(R)-1-((*tert*-Butyldimethylsilyl)oxy)-3-phenylpropan-2-amine (R)-55a.**



General procedure 10 was followed using (R)-2-amino-3-phenylpropan-1-ol (R)-**50** to afford the title compound (R)-**55a** (263 mg, 0.99 mmol) as a pale yellow oil in 50% yield. All characterisation data were consistent with previous literature reports.<sup>498</sup>

$[\alpha]_D^{23} = +4$  (c 1.0, CHCl<sub>3</sub>; lit.<sup>498</sup> -3.6 for (S)-**55a**, c 1.0, CHCl<sub>3</sub>, 25 °C); <sup>1</sup>H NMR (300 MHz, CDCl<sub>3</sub>)  $\delta_H$  7.30-7.12 (m, 5H, ArH), 3.53 (dd, 1H, *J* = 9.7, 4.3, OCH<sub>2</sub>), 3.48-3.34 (m, 1H, OCH<sub>2</sub>), 3.11-2.96 (bm, 1H, H<sub>2</sub>NCH), 2.74 (dd, 1H, *J* = 13.3, 5.4, PhCH<sub>2</sub>), 2.47 (dd, 1H, *J* = 13.3, 8.3, PhCH<sub>2</sub>), 0.85 (s, 9H, SiC(CH<sub>3</sub>)<sub>3</sub>), 0.00 (s, 6H, 2  $\times$  SiCH<sub>3</sub>).

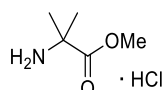
**(S)-1-((*tert*-Butyldimethylsilyl)oxy)-3-phenylpropan-2-amine (S)-55a.**



General procedure 10 was followed using (S)-2-amino-3-phenylpropan-1-ol (S)-50a, to afford the title compound (S)-55a (242 mg, 0.92 mmol) as a pale yellow oil in 46% yield. All characterisation data were consistent with previous literature reports.<sup>498,499</sup>

$[\alpha]_D^{23} = -4$  (*c* 1.0, CHCl<sub>3</sub>; lit.<sup>498</sup> -3.6, *c* 1.0, CHCl<sub>3</sub>, 25 °C); <sup>1</sup>H NMR (500 MHz, CDCl<sub>3</sub>)  $\delta_H$  7.35-7.27 (m, 2H, ArH), 7.27-7.17 (m, 3H, ArH), 3.58 (d, 1H, *J* = 9.7, 4.3, OCH<sub>2</sub>), 3.45 (dd, 1H, *J* = 9.7, 6.5, OCH<sub>2</sub>), 2.80 (dd, 1H, *J* = 13.4, 5.4, PhCH<sub>2</sub>), 2.54 (ddd, 1H, *J* = 13.4, 8.3, 2.0, PhCH<sub>2</sub>), 0.91 (s, 9H, SiC(CH<sub>3</sub>)<sub>3</sub>), 0.06 (s, 6H, 2 × SiCH<sub>3</sub>).

**Methyl 2-amino-2-methylpropanoate hydrochloride 208.**



2-Aminoisobutyric acid (Aib, 1.03 g, 10.0 mmol, 1.0 equiv.) was dissolved in MeOH (20 mL), and the stirred solution was cooled to 0 °C. Thionyl chloride (SOCl<sub>2</sub>, 800  $\mu$ L, 20.0 mmol, 2.0 equiv.) was added dropwise over 5 min. The reaction was heated to reflux for 2 h. After this time, the reaction was cooled to room temperature and concentrated to dryness *in vacuo* to afford the title compound **208** (1.51 g, 9.80 mmol) as a white solid in 98% yield. All characterisation data were consistent with previous literature reports.<sup>500,501</sup>

m.p.: 180-182 °C (lit.<sup>500</sup> 181 °C); <sup>1</sup>H NMR (500 MHz, DMSO-*d*<sub>6</sub>)  $\delta_H$  8.57 (bs, 3H, NH<sub>3</sub>), 3.76 (s, 3H, OCH<sub>3</sub>), 1.47 (s, 6H, 2 × NCCH<sub>3</sub>).

## **5.4. Synthetic and characterization details for chapter 4**

### *5.4.1 General experimental details for screening/sampling experiments*

**General procedure 11 for the screening and optimisation of BV oxidation reactions (representative example for Table 10, entry 7).**

Commercial *m*CPBA (75 wt%, 69 mg, 0.30 mmol) was suspended in toluene (720  $\mu$ L) and stirred until a homogeneously cloudy mixture was formed. DMAP (0.5 M in toluene, 80  $\mu$ L, 0.040 mmol) was added to the mixture, and the reaction was allowed to stir for 15 min. After this time, *p*-methoxyacetophenone **263** (1.0 M in toluene, 200  $\mu$ L, 0.20 mmol) was added, and the reaction was stirred for 30 min. After this time an aliquot (~20  $\mu$ L) was removed and diluted up to 600  $\mu$ L with CDCl<sub>3</sub>. A <sup>1</sup>H NMR spectrum was recorded immediately.

Representative general procedure 11 was used for all screening experiments in chapter 4, with the following modifications:

When precatalysts/catalysts other than DMAP were employed that were not soluble in toluene, a stock solution was not used, and the catalyst was instead added to the reaction as a solid, and 800  $\mu\text{L}$  of toluene were used.

Where benzalacetone (*E*)-**232** or styryl acetate (*E*)-**233** were used as the substrate, they were added as a stock solution in toluene containing TetMB internal standard (200  $\mu\text{L}$ , 1.0 M substrate, 0.25 M TetMB).

For DMAP and DOAP precatalyst screens, the precatalyst was also added as a stock solution (0.5 M in toluene). In all instances the initial volume of toluene added was selected to ensure the reaction concentration was 0.2 M following substrate addition.

#### 5.4.2 General synthetic procedures

##### **General procedure 12 for the synthesis of Weinreb amides from esters.**

The desired ester (1.0 equiv.) and *N,O*-dimethylhydroxylamine hydrochloride **320** (1.5 equiv.) were added to anhydrous THF (0.4 M in ester) under an inert  $\text{N}_2$  atmosphere. The reaction was cooled to 0  $^{\circ}\text{C}$  and isopropylmagnesium chloride (2.0 M in THF, 3.0 equiv.) was added dropwise over 10 min. The reaction was then allowed to warm to room temperature and stirred for 16 h. The reaction was then cooled back to 0  $^{\circ}\text{C}$  and quenched with  $\text{NH}_4\text{Cl}$  and diluted by half with EtOAc. The layers were separated, and the aqueous phase was extracted twice more with EtOAc. The combined organics were washed with brine, dried ( $\text{Na}_2\text{SO}_4$ ) and purified by silica plug (DCM then 10% MeOH/DCM) afforded the desired Weinreb amide in sufficient purity for the subsequent synthetic steps.  $^1\text{H}$  NMR spectroscopic analysis was performed for all Weinreb amides to assess purity exclusively, and so further characterisation as not systematically carried out.

##### **General procedure 13 for the addition of MeMgBr to Weinreb amides.**

The desired Weinreb amide (1.0 equiv.) was dissolved in anhydrous THF (0.2 M) under an inert  $\text{N}_2$  atmosphere and cooled to 0  $^{\circ}\text{C}$ . MeMgBr in THF (2.5 equiv.) was added dropwise over 5 min, and the reaction was stirred for 10 min before warming to room temperature and allowing to stir for 4 h. After this time, the reaction was cooled to 0  $^{\circ}\text{C}$ , quenched with  $\text{NH}_4\text{Cl}$  and diluted by half with EtOAc. The phases were separated, and the aqueous layer was extracted with EtOAc once more. The combined organics were washed with water then brine, dried ( $\text{MgSO}_4$ ), filtered, and concentrated to dryness *in vacuo*. Purification by flash column chromatography ( $\text{SiO}_2$ ) afforded the desired methyl ketone.

**General procedure 14 for the DMAPO-catalysed Baeyer-Villiger oxidation of  $\alpha,\beta$ -unsaturated ketones.**

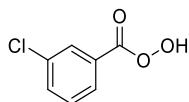
*m*CPBA (2.0 equiv.) was added to a solution of DMAP (0.5 equiv.) in toluene (0.2 M), and the suspension was stirred for 15 min, becoming a pale yellow solution. After this time, the desired  $\alpha,\beta$ -unsaturated ketone was added, and the reaction was monitored by TLC until total consumption of this starting material. The reaction mixture was quenched by diluting by half with EtOAc and sodium metabisulfite ( $\text{Na}_2\text{S}_2\text{O}_5$ , sat. aq.) and stirring for 10 min (until potassium iodide starch test paper showed no colour). The layers were separated, and the aqueous layer was extracted once more with EtOAc. The combined organics were washed three times with  $\text{NaHCO}_3$  (sat. aq.), brine, dried ( $\text{MgSO}_4$ ), filtered, and concentrated to dryness *in vacuo*. Purification by flash column chromatography afforded the desired vinyl ester product.

**General procedure 15 for the TMNO-catalysed Baeyer-Villiger oxidation of  $\alpha,\beta$ -unsaturated ketones.**

TMNO·2H<sub>2</sub>O (0.5 equiv.) was added to a suspension of *m*CPBA (1.5 equiv.) in toluene (0.2 M), and the desired  $\alpha,\beta$ -unsaturated ketone was added, and the reaction was monitored by TLC until total consumption of this starting material. The reaction mixture was quenched by diluting by half with EtOAc and sodium metabisulfite ( $\text{Na}_2\text{S}_2\text{O}_5$ , sat. aq.) and stirring for 10 min (until potassium iodide starch test paper showed no colour). The layers were separated, and the aqueous layer was extracted once more with EtOAc. The combined organics were washed three times with  $\text{NaHCO}_3$  (sat. aq.), brine, dried ( $\text{MgSO}_4$ ), filtered, and concentrated to dryness *in vacuo*. Purification by flash column chromatography afforded the desired vinyl ester product.

**5.4.3 Purification and titration of *m*CPBA**

**Purification of commercial *m*CPBA following the procedure of Aggarwal *et al.*<sup>502</sup>**



Commercial *m*CPBA (~75 wt% purity, 3.35 g; 2.513 active *m*CPBA, 14.6 mmol) was dissolved in Et<sub>2</sub>O (30 mL) and washed with pH 7.5 PBS buffer (0.1 M aq., 3 × 15 mL). The organic layer was dried over  $\text{MgSO}_4$  and concentrated to dryness *in vacuo* in a 0 °C water bath before further drying under high vacuum overnight to afford pure *m*CPBA as a white solid (2.008 g, 11.6 mmol, 80% mass recovery *m*CPBA, > 95% pure by NMR). **Caution:** *m*CPBA is potentially explosive at higher > 85% purity and on exposure to heat. Purified *m*CPBA was stored in a padded cotton wool-lined box at -20 °C in the freezer.

$^1\text{H}$  NMR (400 MHz,  $\text{CDCl}_3$ )  $\delta_{\text{H}}$  11.55 (s, 1H, OOH), 7.99 (t, 1H,  $J = 2.0$ , ArH), 7.89 (ddd, 1H,  $J = 7.9$ , 1.3, 1.3, ArH), 7.63 (ddd, 1H,  $J = 8.0$ , 2.0, 1.1, ArH), 7.46 (t, 1H,  $J = 7.9$ , ArH).  $^{13}\text{C}\{^1\text{H}\}$  NMR (101 MHz,  $\text{CDCl}_3$ )  $\delta_{\text{C}}$  167.1, 135.3, 134.6, 130.4, 129.5, 127.5, 127.0.

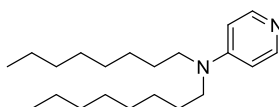
#### Iodometric titration of *m*CPBA purity/content following the procedure of Olofsson *et al.*<sup>421</sup>

Commercial samples of *m*CPBA were titrated on receipt from the supplier and intermittently thereafter. NaI (1.500 g) was dissolved in distilled water (50 mL). A solution of commercial *m*CPBA (300 mg) in chloroform (5.0 mL) and glacial acetic acid (5.0 mL) was added to the solution and the mixture was stirred vigorously. This solution was then titrated with  $\text{Na}_2\text{S}_2\text{O}_3$  (aq., 0.100 M), and end-point was determined when the persistent brown/yellow colour disappeared. 1.0 mL of the  $\text{Na}_2\text{S}_2\text{O}_3$  solution accounts of 8.6 mg of pure *m*CPBA.

In all instances fresh commercial *m*CPBA was found to contain 74-78 wt% *m*CPBA, and so *m*CPBA was presumed to be 75 wt% pure throughout this thesis, unless otherwise stated.

#### 5.4.4 Synthesis of DOAP

##### *N,N*-Dioctylpyridin-4-amine DOAP.



*Note: The reaction was carried out with a dry condenser and behind a blast-shield.*

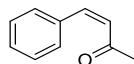
4-Aminopyridine **306** (1.410 g, 15 mmol, 1.0 equiv.) and 1-bromooctane **307** (6.478 mL, 37.5 mmol, 2.5 equiv.) were dissolved in anhydrous THF (15 mL) under an inert  $\text{N}_2$  atmosphere. Sodium hydride (60 wt% in mineral oil, 2.880 g, 36 mmol, 2.4 equiv.) was added in six batches, waiting for effervescence to stop between each batch (approx. every 5 min). After stirring at room temperature for 30 min, the reaction was slowly warmed to 66 °C in 5 °C increments, allowing the reaction to equilibrate at each increment for 10 min. The reaction was refluxed for 6 h, and then allowed to cool to room temperature slowly (left in oil bath). The reaction was cooled to 0 °C and quenched by dropwise addition of  $\text{NH}_4\text{Cl}$  (sat. aq., 10 mL) over 30 min. The mixture was then diluted with DCM (30 mL), and the layers were separated, and the aqueous phase was washed twice more with DCM ( $2 \times 30$  mL). The combined organics were dried ( $\text{Na}_2\text{SO}_4$ ) and concentrated to dryness *in vacuo* and purified by flash column chromatography ( $\text{SiO}_2$ , 2% MeOH/2%  $\text{NEt}_3$  in DCM) to afford the title compound DOAP (1.120 g, 7.05 mmol) as a brown oil in 47% yield. Characterisation data were consistent with previous literature reports.<sup>458</sup>

$R_f$ : 0.42 (5% MeOH/DCM, significant streaking);  $^1\text{H}$  NMR (300 MHz,  $\text{CDCl}_3$ )  $\delta_{\text{H}}$  8.24 – 8.06 (m, 2H, ArH), 6.52 – 6.35 (m, 2H, ArH), 3.33 – 3.21 (t, 4H,  $J = 7.8$ ,  $2 \times \text{NCH}_2$ ), 1.70 – 1.48 (m, 4H,  $2 \times \text{NCH}_2\text{CH}_2$ ),

1.36 – 1.21 (m, 20H, AlkH), 0.94 – 0.83 (m, 6H, 2 × CH<sub>3</sub>); <sup>13</sup>C{<sup>1</sup>H} NMR (101 MHz, CDCl<sub>3</sub>) δ<sub>C</sub> 152.8, 149.4, 106.5, 50.4, 31.94, 29.6, 29.4, 27.2, 27.1, 22.8, 14.2.

#### 5.4.5 Synthesis of monosubstituted α,β-unsaturated ketones

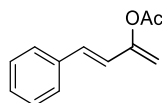
##### (Z)-4-Phenylbut-3-en-2-one (Z)-232.



Following the procedure of Trombini *et al.*:<sup>428</sup> 4-phenylbut-3-yn-2-one **275** (720 μL, 5.0 mmol) was dissolved in *n*-pentane (5.0 mL). Lindlar's catalyst (10 wt% Pd, 70 mg) was added and the solution was degassed thoroughly by N<sub>2</sub> bubbling for 15 min and put under inter N<sub>2</sub> atmosphere. The reaction was then put under H<sub>2</sub> atmosphere by bubbling H<sub>2</sub> for 10 min and leaving under a balloon of 2 gas. After 96 h the reaction was purged by bubbling N<sub>2</sub> and filtered over a pad of celite. The crude product was purified by flash column chromatography (SiO<sub>2</sub>, 10% Et<sub>2</sub>O/PE) to afford the title compounds (Z)-**232** (467 mg, 3.2 mmol) as a yellow oil in 64% yield. Characterisation data were consistent with previous literature reports.<sup>428</sup>

*R*<sub>f</sub>: 0.21 (SiO<sub>2</sub>, 15% Et<sub>2</sub>O/PE); IR (neat) 2928, 1691 (C=O), 1605, 1353, 1182, 1163, 774, 691 cm<sup>-1</sup>; <sup>1</sup>H NMR (500 MHz, DMSO-*d*<sub>6</sub>) δ<sub>H</sub> 7.55 – 7.49 (m, 2H, ArH), 7.39 – 7.33 (m, 3H, ArH), 6.88 (d, 1H, *J* = 12.7, PhCH), 6.28 (d, 1H, *J* = 12.8, PHCHCH), 2.15 (s, 3H, CH<sub>3</sub>), <sup>13</sup>C{<sup>1</sup>H} NMR (126 MHz, DMSO-*d*<sub>6</sub>) δ<sub>C</sub> 200.2, 138.8, 135.1, 129.3, 129.0, 128.6, 128.2, 30.9. Note: NMR spectra of (Z)-**232** were recorded in DMSO-*d*<sub>6</sub> as rapid isomerisation to (E)-**232** was observed in CDCl<sub>3</sub>.

##### (E)-4-Phenylbuta-1,3-dien-2-yl acetate (E)-277.

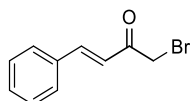


Following the procedure of Isobe *et al.*:<sup>429</sup> Sulfuric acid (3 drops) was added to a stirred solution of (E)-benzalacetone (E)-**232** (620 mg, 4.2 mmol, 1.0 equiv.) in isopropenylacetate **276** (10 mL, 92 mmol, excess/solvent). The reaction was heated to reflux for 2.5 h. After this time the reaction was allowed to cool to rt, diluted with water (10 mL) and Et<sub>2</sub>O (10 mL). The layers were separated and the organic phase was extracted with Et<sub>2</sub>O twice more (2 × 10 mL). The combined organics were washed with brine (20 mL), dried (Na<sub>2</sub>SO<sub>4</sub>) and concentrated *in vacuo* (including isopropenyl acetate). The crude product was purified by column chromatography (SiO<sub>2</sub>, 0-30% EtOAc/PE) to afford the title compound (E)-**277** (524 mg, 2.8 mmol) as a yellow oil in 66% yield. Characterisation data were consistent with previous literature reports.<sup>429</sup>



*R*<sub>f</sub>: 0.24 (SiO<sub>2</sub>, 20% EtOAc/PE); <sup>1</sup>H NMR (500 MHz, CDCl<sub>3</sub>) δ<sub>H</sub> 7.45 – 7.40 (m, 2H, ArH), 7.37 – 7.32 (m, 2H, ArH), 7.29 – 7.24 (m, 1H), 6.67 (d, 1H, *J* = 16.0, PhCH), 6.61 (d, 1H, *J* = 16.0, OCCH), 5.14 (d, 1H, *J* = 1.7, *trans*-OCCH<sub>2</sub>), 4.99 (dd, 1H, *J* = 1.7, 0.5, *cis*-OCCH<sub>2</sub>), 2.32 (s, 3H, CH<sub>3</sub>). <sup>13</sup>C NMR (126 MHz, CDCl<sub>3</sub>) δ<sub>C</sub> 168.9, 152.0, 136.1, 130.0, 128.8, 128.4, 127.0, 122.7, 106.3, 21.1.

**(*E*)-1-Bromo-4-phenylbut-3-en-2-one (*E*)-278.**

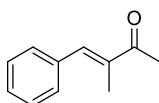


Following the procedure of Isobe *et al.*:<sup>429</sup> Dienolacetate (*E*)-**277** (515 mg, 2.70 mmol, 1.0 equiv.) was dissolved in THF (15 mL) and cooled to 0 °C, and *N*-bromosuccinimide (817 mg, 4.6 mmol, 1.7 equiv.) and water (83 µL) were added. After stirring for 5 min the reaction was warmed to rt, and the reaction was left to stir for 45 min. After this time, the reaction was cooled to 0 °C and quenched with NaHCO<sub>3</sub> (sat. aq., 20 mL) and the aqueous phase was extracted with Et<sub>2</sub>O (3 × 30 mL), and the combined organics were washed with NaHCO<sub>3</sub> (2 × 30 mL), brine, dried (MgSO<sub>4</sub>), filtered, and concentrated *in vacuo*. The crude product was passed through a silica plug (SiO<sub>2</sub>, DCM) and concentrated *in vacuo* to afford the title compound (*E*)-**278** (590 mg, 2.62 mmol) as a brown oil in 97% yield. Characterisation data were consistent with previous literature reports.<sup>429</sup>

*R*<sub>f</sub>: 0.44 (SiO<sub>2</sub>, EtOAc/PE); <sup>1</sup>H NMR (500 MHz, CDCl<sub>3</sub>) δ<sub>H</sub> 7.72 (d, 1H, *J* = 16.0, PhCH), 7.63 – 7.58 (m, 2H, ArH), 7.46 – 7.40 (m, 3H, ArH), 6.97 (d, 1H, *J* = 16.0, PhCHCH), 4.10 (s, 2H, CH<sub>3</sub>); <sup>13</sup>C{<sup>1</sup>H} NMR (126 MHz, CDCl<sub>3</sub>) δ<sub>C</sub> 191.1, 145.6, 134.1, 131.3, 129.2, 128.8, 122.4, 33.2.

**5.4.6 Synthesis of polysubstituted “methylated benzalacetones”**

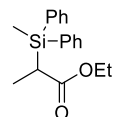
**(*E*)-3-Methyl-4-phenylbut-3-en-2-one (*E*)-312.**



Following the procedure of Clososki *et al.*:<sup>469</sup> 2-butanone **315** (448 µL, 5.0 mmol, 2.0 equiv.) and benzaldehyde **185** (255 µL, 2.5 mmol, 1.0 equiv.) were dissolved in glacial acetic acid (10 mL) and stirred at room temperature. Sulfuric acid (131 µL, 2.4 mmol, 0.96 equiv.) was added dropwise, and the reaction was stirred for 16 h. After this time the reaction was poured onto ice (approx. 5 mL) and neutralised to pH 8 with NaHCO<sub>3</sub> (sat. aq.). The mixture was extracted with EtOAc (3 × 10 mL), and the combined organics were washed with NaHCO<sub>3</sub> (sat. aq., 20 mL), brine (20 mL) and dried (Na<sub>2</sub>SO<sub>4</sub>). Purification by flash column chromatography (SiO<sub>2</sub>, 15% Et<sub>2</sub>O/PE) afforded the title compounds (*E*)-**312** (175 mg, 1.1 mmol) as a yellow oil in 44% yield. Characterization data were consistent with previous literature reports.<sup>469</sup>

$R_f$  = 0.29 (SiO<sub>2</sub>, 15% Et<sub>2</sub>O/PE); <sup>1</sup>H NMR (500 MHz, CDCl<sub>3</sub>)  $\delta_H$  7.53 (q, 1H,  $J$  = 1.4, PhCH), 7.45 – 7.40 (m, 4H, ArH), 7.38 – 7.33 (m, 1H, ArH), 2.48 (s, 3H, C(O)CH<sub>3</sub>), 2.07 (d, 3H,  $J$  = 1.4, C(O)CCH<sub>3</sub>); <sup>13</sup>C{<sup>1</sup>H} NMR (126 MHz, CDCl<sub>3</sub>)  $\delta_C$  200.4, 139.8, 137.9, 136.1, 129.8, 128.7, 128.6, 26.0, 13.1.

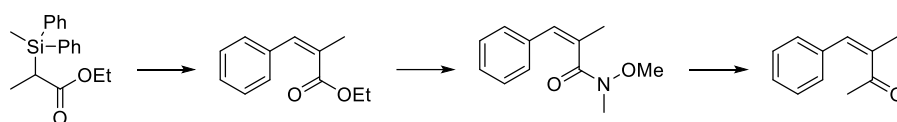
**(rac)-Ethyl 2-(methyldiphenylsilyl)propanoate (rac)-319.**



Following the procedure of Larson *et al.*:<sup>471</sup> Diisopropylamine (1.65 mL, 12 mmol, 1.2 equiv.) was dissolved in anhydrous THF (25 mL) under inert N<sub>2</sub> atmosphere and cooled to -78 °C. *n*-BuLi (2.5 M in THF, 4.8 mL, 12 mmol, 1.2 equiv.) was added dropwise over 20 min, and the reaction was warmed to room temperature, stirred for 5 min and cooled back down to -78 °C. Ethyl propionate **318** (1.16 mL, 10 mmol, 1.0 equiv.) was then added dropwise over 5 min and allowed to stir for 30 min until a persistent bright orange colour developed. DPMSCl (2.103 mL, 10 mmol, 1.0 equiv.) was then added dropwise over 5 min and reaction was stirred for 1 h before warming to room temperature and stirring for a further 2 h. After this time the reaction was cooled to 0 °C and quenched slowly with HCl (1.5 M aq., 10 mL). This mixture was extracted twice with Et<sub>2</sub>O (2 × 30 mL), and the combined organics were washed with brine, dried (MgSO<sub>4</sub>), filtered, and purified by flash column chromatography (SiO<sub>2</sub>, 5-20% Et<sub>2</sub>O/PE) afforded the title compound (*rac*)-**319** (1.727 g, 5.8 mmol) as a colourless oil in 58% yield. Characterization data were consistent with previous literature reports.<sup>503</sup>

$R_f$  = 0.14 (SiO<sub>2</sub>, 12% Et<sub>2</sub>O/PE); <sup>1</sup>H NMR (400 MHz, CDCl<sub>3</sub>)  $\delta_H$  7.60 – 7.52 (m, 4H, ArH), 7.44 – 7.32 (m, 6H, ArH), 3.98 – 3.80 (m, 2H, OCH<sub>2</sub> diastereotopic), 2.65 (q, 1H,  $J$  = 7.2, C(O)CH), 1.25 (d, 3H,  $J$  = 7.2, SiCHCH<sub>3</sub>), 0.96 (t, 3H,  $J$  = 7.1, OCH<sub>2</sub>CH<sub>3</sub>), 0.66 (s, 3H, SiCH<sub>3</sub>); <sup>13</sup>C{<sup>1</sup>H} NMR (126 MHz, CDCl<sub>3</sub>)  $\delta_C$  176.0, 135.0, 134.9, 134.8, 134.5, 129.8, 129.7, 128.0, 127.9, 60.1, 29.1, 14.1, 12.1, -5.4. *Note: Additional peaks in the <sup>13</sup>C aromatic region are due to diastereotopicity of the DPMS phenyl rings.*

**(Z)-3-Methyl-4-phenylbut-3-en-2-one (Z)-312 (telescoped synthesis from (rac)-319 to (Z)-312).**



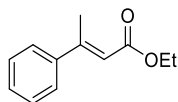
Adapted from the procedure of Larson *et al.*:<sup>470</sup> Diisopropylamine (734  $\mu$ L, 5.2 mmol, 1.30 equiv.) was dissolved in anhydrous THF (6.0 mL) under inert N<sub>2</sub> atmosphere and cooled to -78 °C. *n*-BuLi (2.5 M in THF, 2.08 mL, 5.2 mmol, 1.30 equiv.) was added dropwise over 5 min, and the reaction was warmed to room temperature, stirred for 5 min and cooled back down to -78 °C. A solution of C-silyl ester (*rac*)-**319** (1.492 g, 5.0 mmol, 1.25 equiv.) in anhydrous THF (10 mL) was added

dropwise to this solution over ten minutes before stirring at that temperature for 1 h, before dropwise addition of benzaldehyde (407  $\mu$ L, 4.0 mmol, 1.0 equiv.) over 5 min. The reaction was allowed to warm to room temperature and stirred for 16 h. After this time, the reaction was quenched dropwise with  $\text{NH}_4\text{Cl}$  (sat. aq. 10 mL) and extracted with  $\text{Et}_2\text{O}$  ( $3 \times 10$  mL). The combined organics were washed with brine, dried ( $\text{MgSO}_4$ ), filtered, and purification by flash column chromatography afforded a 71:29 mixture of (Z)-:(E)-**317** (600 mg, 3.16 mmol) as a yellow oil in 61% yield.

General procedure 12 was followed using the 71:29 (E)-/(Z)-**317** (600 mg, 3.16 mmol) mixture obtained, affording the corresponding Weinreb amide intermediate as an (E)/(Z) mixture in quantitative yield. No further purification was carried out. General procedure 13 was followed using this crude material (490 mg, 2.39 mmol). Purification by flash column chromatography ( $\text{SiO}_2$ , 7%  $\text{Et}_2\text{O}/\text{PE}$ ) afforded the title compound (Z)-**312** (160 mg, 1.00 mmol) as a yellow oil in 42% yield over 2 steps, 26% yield over three steps.

$R_f$  = 0.39 ( $\text{SiO}_2$ , 15%  $\text{Et}_2\text{O}/\text{PE}$ ), 0.21 ( $\text{SiO}_2$ , 50%  $\text{DCM}/\text{PE}$ ); IR (neat) 2920, 1686, 1142, 1363, 1202, 1101, 757, 699  $\text{cm}^{-1}$ ;  $^1\text{H}$  NMR (500 MHz,  $\text{CDCl}_3$ )  $\delta_H$  7.34 – 7.27 (m, 3H, ArH), 7.20 – 7.17 (m, 2H, ArH), 6.75 (s, 1H, C(O)CH), 2.03 (d, 3H,  $J$  = 1.6,  $\text{PhCCH}_3$ ), 2.01 (s, 3H, C(O)CH<sub>3</sub>);  $^{13}\text{C}\{^1\text{H}\}$  NMR (126 MHz,  $\text{CDCl}_3$ )  $\delta_C$  207.3, 140.0, 136.7, 132.0, 128.6, 128.6, 128.6, 128.5, 128.47, 128.5, 128.0, 30.1, 21.3; HRMS (ESI-): Calculated for  $[\text{M}+\text{CH}_3\text{CO}_2]^-$   $\text{C}_{13}\text{H}_{15}\text{O}_3^-$  219.1016; Found 219.1015.

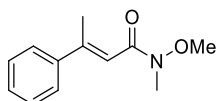
#### Ethyl (E)-3-phenylbut-2-enoate (E)-**323**.



Sodium hydride (60% in mineral oil, 6.00 g, 150 mmol, 1.5 equiv.) was suspended in anhydrous THF (250 mL) at 0 °C under an inert  $\text{N}_2$  atmosphere. Triethyl phosphonoacetate **321** (29.76 mL, 150 mmol, 1.5 equiv.) was added dropwise over 5 min, and the reaction was warmed to room temperature and stirred for 45 min until the mixture had become a clear yellow solution. After cooling again to 0 °C, acetophenone **322** (11.67 mL, 100 mmol, 1.0 equiv.) was added, and the reaction was stirred for 15 min, warmed to room temperature and left to stir for 16 h. After this time, the reaction was quenched by addition of water (50 mL) and the mixture was concentrated down to approx. 100 mL *in vacuo*, before diluting further with  $\text{H}_2\text{O}$  (50 mL) and  $\text{EtOAc}$  (50 mL). The layers were separated, and the aqueous phase was extracted twice more with  $\text{EtOAc}$  (50 mL). The combined organics were washed with water and brine (100 mL each), dried ( $\text{MgSO}_4$ ), filtered, and purified by flash column chromatography ( $\text{SiO}_2$ , 0-10%  $\text{Et}_2\text{O}/\text{PE}$ ) to afford the title compound (E)-**323** (13.05 g, 68.6 mmol) as a colourless oil in 69% yield. Characterization data were consistent with previous literature reports.<sup>504</sup>

$R_f$ : 0.38 (SiO<sub>2</sub>, 15% Et<sub>2</sub>O/PE); <sup>1</sup>H NMR (500 MHz, CDCl<sub>3</sub>)  $\delta_H$  7.55-7.45 (m, 2H, ArH), 7.42-7.30 (m, 3H, ArH), 6.13 (q, 1H,  $J$  = 1.3, C(O)CH), 4.22 (q, 2H,  $J$  = 7.1, OCH<sub>2</sub>), 2.58 (d, 3H,  $J$  = 1.3, PhCCH<sub>3</sub>), 1.32 (t,  $J$  = 7.1, OCH<sub>2</sub>CH<sub>3</sub>); <sup>13</sup>C NMR (126 MHz, CDCl<sub>3</sub>)  $\delta_C$  167.1, 155.7, 142.4, 129.1, 128.7, 126.5, 117.4, 60.0, 18.1, 14.5.

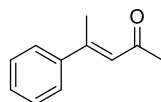
**(*E*)-*N*-Methoxy-*N*-methyl-3-phenylbut-2-enamide (*E*)-324.**



General procedure 12 was followed using (*E*)-**323** (974 mg, 5.12 mmol). Purification by flash column chromatography (SiO<sub>2</sub>, 5-15% EtOAc/PE, 2% NEt<sub>3</sub>) to afford the title compound (*E*)-**324** (1.006 g, 4.97 mmol) as a bright yellow oil in 95% yield. Characterization data were consistent with previous literature reports.<sup>504</sup>

$R_f$ : 0.15 (SiO<sub>2</sub>, 10% EtOAc/PE); <sup>1</sup>H NMR (500 MHz, CDCl<sub>3</sub>)  $\delta_H$  7.51-7.45 (m, 2H, ArH), 7.42-7.33 (m, 3H, ArH), 6.58 (s, 1H, C(O)CH), 3.71 (s, 3H, -OCH<sub>3</sub>), 3.27 (s, 3H, -NCH<sub>3</sub>), 2.53 (d,  $J$  = 1.4, ArCCH<sub>3</sub>); <sup>13</sup>C{<sup>1</sup>H} NMR (126 MHz, CDCl<sub>3</sub>)  $\delta_C$  167.8, 152.2, 143.1, 128.7, 128.6, 126.5, 116.0, 61.8, 32.3, 18.2.

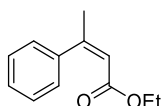
**(*E*)-4-Phenylpent-3-en-2-one (*E*)-313.**



General procedure 13 was followed using (*E*)-**324** (646 mg, 3.15 mmol). Purification by flash column chromatography (SiO<sub>2</sub>, 5% EtOAc/PE) afforded the title compound (*E*)-**313** (425 mg, 2.65 mmol) as a yellow oil in 84% yield. Characterization data were consistent with previous literature reports.<sup>504</sup>

$R_f$ : 0.26 (SiO<sub>2</sub>, 5% EtOAc/PE); <sup>1</sup>H NMR (500 MHz, CDCl<sub>3</sub>)  $\delta_H$  7.55-7.42 (m, 2H, ArH), 7.46-7.30 (m, 3H, ArH), 6.51 (q, 1H,  $J$  = 1.3, ArCCH), 2.54 (d, 3H,  $J$  = 1.3, ArCCH<sub>3</sub>), 2.30 (s, 3H, C(O)CH<sub>3</sub>); <sup>13</sup>C{<sup>1</sup>H} (126 MHz, CDCl<sub>3</sub>)  $\delta_C$  199.1, 154.1, 142.7, 129.3, 128.7, 126.7, 124.7, 32.4, 18.5.

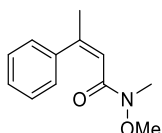
### Ethyl (Z)-2-methyl-3-phenylbut-2-enoate (Z)-323.



From the reaction above, the title compound (Z)-**323** (3.42 g, 18 mmol) was isolated as a major side-product as a colourless oil in 12% yield. Characterization data were consistent with previous literature reports.<sup>504</sup>

$^1\text{H}$  NMR (500 MHz,  $\text{CDCl}_3$ )  $\delta_{\text{H}}$  7.40 – 7.30 (m, 3H, ArH), 7.25 – 7.21 (m, 2H, ArH), 5.93 (q, 1H,  $J = 1.5$ ,  $\text{C}(\text{O})\text{CH}$ ), 4.02 (q, 2H,  $J = 7.1$ ,  $\text{OCH}_2$ ), 2.20 (d,  $J = 1.5$ ,  $\text{PhCCH}_3$ ), 1.10 (t, 3H,  $J = 7.1$ ,  $\text{OCH}_2\text{CH}_3$ );  $^{13}\text{C}\{^1\text{H}\}$  NMR (126 MHz,  $\text{CDCl}_3$ )  $\delta_{\text{C}}$  166.0, 155.4, 140.8, 127.9, 127.7, 167.7, 117.7, 59.7, 72.0, 13.9.

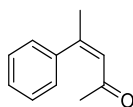
### (Z)-N-Methoxy-N-methyl-3-phenylbut-2-enamide (Z)-324.



General procedure 12 was followed using (Z)-**323** (1.311 g, 6.89 mmol) to afford the title compound (Z)-**324** as a clear oil in 91% crude yield (1.375 g, 6.27 mmol). Characterization data were consistent with previous literature reports.<sup>505</sup>

$^1\text{H}$  NMR (400 MHz,  $\text{CDCl}_3$ )  $\delta_{\text{H}}$  7.40–7.22 (m, 5H, ArH), 6.29 (bs, 1H,  $\text{C}(\text{O})\text{CH}$ ), 3.69 (bs, 3H,  $\text{OCH}_3$ ), 3.11 (bs, 3H,  $\text{NCH}_3$ ), 2.23 (d, 3H,  $J = 1.5$ ,  $\text{PhCCH}_3$ ).

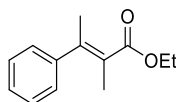
### (Z)-4-Phenylpent-3-en-2-one (Z)-313.



General procedure 13 was employed using (Z)-**324** (1.205 g, 5.87 mmol). Purification by flash column chromatography ( $\text{SiO}_2$ , 5% EtOAc/PE) afforded the title compound (Z)-**313** (672 mg, 4.19 mmol) as a yellow oil in 72% yield, 65% yield over two steps. Characterization data were consistent with previous literature reports.<sup>506</sup>

$R_f = 0.19$  ( $\text{SiO}_2$ , 5% EtOAc/PE);  $^1\text{H}$  NMR (500 MHz,  $\text{CDCl}_3$ )  $\delta_{\text{H}}$  7.41 – 7.31 (m, 3H, ArH), 7.23 – 7.18 (m, 2H, ArH), 6.14 (q, 1H,  $J = 1.4$ ,  $\text{C}(\text{O})\text{CH}$ ), 2.20 (d, 3H,  $J = 1.4$ ,  $\text{PhCCH}_3$ ), 1.81 (s, 3H,  $\text{C}(\text{O})\text{CH}_3$ );  $^{13}\text{C}\{^1\text{H}\}$  NMR (126 MHz,  $\text{CDCl}_3$ )  $\delta_{\text{C}}$  200.4, 153.0, 141.1, 128.7, 128.6, 128.4, 127.3, 30.3, 27.5.

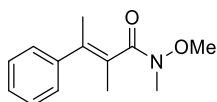
**Ethyl (*E*)-2-methyl-3-phenylbut-2-enoate (*E*)-325:**



Acetophenone **322** (2.336 mL, 20 mmol, 1.0 eq.) and triethyl-2-phosphonopropionate **316** (4.716 mL, 22 mmol, 1.1 eq.) were added to a stirred solution of NaOEt in EtOH (1.4 M, 1.4 eq., prepared fresh from 644 mg sodium metal in 20 mL anhydrous EtOH) under N<sub>2</sub>. The reaction was heated to reflux for 24 h, before being cooled to room temperature and poured into ice water (50 mL). Et<sub>2</sub>O (50 mL) was added to the quenched reaction, the layers were separated, the aqueous phase was extracted thrice more with Et<sub>2</sub>O (3 × 50 mL), and the combined organics were washed with brine (100 mL), dried (MgSO<sub>4</sub>), filtered, and concentrated to dryness *in vacuo*. The crude product was purified by flash column chromatography (SiO<sub>2</sub>, 10% Et<sub>2</sub>O/PE) to afford the title compound (*E*)-**325** (1.920 g, 9.40 mmol) as a pale yellow oil in 47% yield. Characterization data were consistent with previous literature reports.<sup>507</sup>

<sup>1</sup>H NMR (500 MHz, CDCl<sub>3</sub>)  $\delta_H$  7.39 – 7.33 (m, 2H, ArH), 7.31 – 7.23 (m, 1H, ArH), 7.17 – 7.13 (m, 2H, ArH), 4.27 (q, 2H, *J* = 7.1, CH<sub>2</sub>), 2.25 (q, 3H, *J* = 1.5, -CH<sub>2</sub>CH<sub>3</sub>), 1.75 (q, 3H, *J* = 1.6, PhCCH<sub>3</sub>), 1.35 (t, *J* = 7.1, 3H, C(O)CCH<sub>3</sub>); <sup>13</sup>C{<sup>1</sup>H} NMR (126 MHz, CDCl<sub>3</sub>)  $\delta_C$  170.2, 145.5, 143.6, 128.5, 127.4, 127.1, 125.1, 60.5, 23.3, 17.5, 14.5; HRMS (ESI<sup>-</sup>): Calculated for [M+CH<sub>3</sub>COOH-H]<sup>-</sup> C<sub>15</sub>H<sub>19</sub>O<sub>4</sub><sup>-</sup>: 263.1278; Found 263.1294.

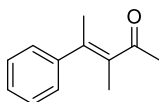
**(*E*)-*N*-Methoxy-*N*,2-dimethyl-3-phenylbut-2-enamide (*E*)-326.**



General procedure 12 was followed using (*E*)-**325** (1.020 g, 5.0 mmol) to afford the title compound (*E*)-**326** as a clear oil in 93% crude yield (1.006 g, 4.60 mmol).

<sup>1</sup>H NMR (500 MHz, CDCl<sub>3</sub>)  $\delta_H$  7.40 – 7.34 (m, 2H, ArH), 7.32 – 7.24 (m, 1H, ArH), 7.21 (m, app. bd, 2H, ArH), 3.74 (bs, 3H, OCH<sub>3</sub>, rotamers), 3.32 (bs, 3H, NCH<sub>3</sub>), 2.03 (q, 3H, *J* = 1.5, PhCCH<sub>3</sub>), 1.79 (q, 3H, *J* = 1.5, C(O)CCH<sub>3</sub>); HRMS (ESI<sup>+</sup>): Calculated for [M+H]<sup>+</sup> C<sub>13</sub>H<sub>13</sub>NO<sub>2</sub><sup>+</sup> 220.1332; Found 220.1331.

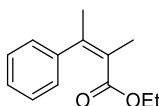
**(E)-3-Methyl-4-phenylpent-3-en-2-one (E)-314.**



General procedure 13 was employed using (E)-**326** (1.000 g, 4.56 mmol). Purification by flash column chromatography (SiO<sub>2</sub>, 0-10% EtOAc/PE) afforded the title compound (E)-**314** (502 mg, 2.92 mmol) as a white solid in 64% yield, 59% yield over two steps. Characterisation data were consistent with previous literature reports.<sup>508</sup>

$R_f$  = 0.30 (SiO<sub>2</sub>, 5%EtOAc/PE); m.p. 35-37 °C; <sup>1</sup>H NMR (500 MHz, CDCl<sub>3</sub>)  $\delta_H$  7.40 – 7.33 (m, 2H, ArH), 7.32 – 7.24 (m, 1H, ArH), 7.19-7.11 (m, 2H, ArH), 2.36 (s, 3H, CH<sub>3</sub>), 2.13 (s, 3H, CH<sub>3</sub>), 1.77 (s, 3H, CH<sub>3</sub>); <sup>13</sup>C{<sup>1</sup>H} NMR (126 MHz, CDCl<sub>3</sub>)  $\delta_C$  206.0, 143.0, 140.4, 133.3, 128.3, 127.4, 127.0, 29.8, 22.6, 17.1; HRMS (ESI+): calculated for [M+H]<sup>+</sup> C<sub>12</sub>H<sub>15</sub>O<sup>+</sup> 175.1117; Found 175.1118.

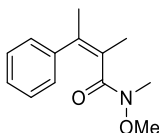
**Ethyl (Z)-2-methyl-3-phenylbut-2-enoate (Z)-325.**



From the reaction above, the title compound (Z)-**325** (1.225 g, 6.00 mmol) was isolated as a major side-product as a colourless oil in 30% yield. Characterization data were consistent with previous literature reports.<sup>507</sup>

<sup>1</sup>H NMR (500 MHz, CDCl<sub>3</sub>)  $\delta_H$  7.32 – 7.20 (m, 3H, ArH), 7.16 – 7.11 (m, 2H, ArH), 3.84 (q,  $J$  = 7.1, 2H, CH<sub>2</sub>), 2.09 (q, 3H,  $J$  = 1.1, C(O)CCH<sub>3</sub>), 2.03 (q, 3H,  $J$  = 1.1, 3H, PhCCH<sub>3</sub>), 0.82 (t,  $J$  = 7.2, 3H, -CH<sub>2</sub>CH<sub>3</sub>). <sup>13</sup>C{<sup>1</sup>H} (126 MHz, CDCl<sub>3</sub>) 170.8, 144.4, 143.0, 128.1, 127.1, 127.0, 126.3, 60.3, 21.8, 16.5, 13.7. HRMS (ESI+): calculated for [M+H]<sup>+</sup> C<sub>13</sub>H<sub>17</sub>O<sub>2</sub><sup>+</sup> 205.1223; Found 205.1226.

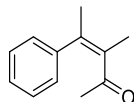
**(Z)-N-Methoxy-N,2-dimethyl-3-phenylbut-2-enamide (Z)-326.**



General procedure 12 was followed using (Z)-**325** (1.400 g, 7.4 mmol) to afford the title compound (Z)-**326** as a clear oil in 91% crude yield (1.375 g, 6.27 mmol).

<sup>1</sup>H NMR (500 MHz, CDCl<sub>3</sub>)  $\delta_H$  7.37 – 7.18 (m, 5H, ArH), 3.38 (bs, 3H, OCH<sub>3</sub>), 2.90 (bs, 3H, NCH<sub>3</sub>), 2.08 (s, 3H, CH<sub>3</sub>), 2.02 (s, 3H, CH<sub>3</sub>); HRMS (ESI+): Calculated for [M+Na]<sup>+</sup> C<sub>13</sub>H<sub>17</sub>NO<sub>2</sub>Na<sup>+</sup> 242.1151; Found 242.1154.

**(Z)-3-Methyl-4-phenylpent-3-en-2-one (Z)-314.**

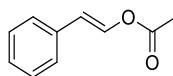


General procedure 13 was employed using (Z)-**326** (438 mg, 2.0 mmol). Purification by flash column chromatography (SiO<sub>2</sub>, 0-10% EtOAc/PE) afforded the title compound (Z)-**314** (254 mg, 1.46 mmol) as a colourless oil in 73% yield, 66% over two steps.

$R_f$  = 0.32 (SiO<sub>2</sub>, 5% EtOAc/PE); IR (neat) 2912, 1672 (C=O), 1442, 1352, 1304, 1234, 766, 702 cm<sup>-1</sup>; <sup>1</sup>H NMR (500 MHz, CDCl<sub>3</sub>)  $\delta_H$  7.35 – 7.27 (m, 3H, ArH), 7.18 – 7.14 (m, 2H, ArH), 2.12 (q, 3H,  $J$  = 1.1, PhCCH<sub>3</sub>), 1.96 (q, 3H,  $J$  = 1.1, C(O)CCH<sub>3</sub>), 1.66 (s, 3H, C(O)CH<sub>3</sub>); <sup>13</sup>C{<sup>1</sup>H} NMR (126 MHz, CDCl<sub>3</sub>)  $\delta_C$  207.4, 143.6, 141.1, 136.1, 128.6, 128.0, 128.0, 127.9, 30.6, 21.9, 16.7; HRMS (ESI<sup>+</sup>): calculated for [M+H]<sup>+</sup> C<sub>12</sub>H<sub>15</sub>O<sup>+</sup> 175.1117; Found 175.1113.

**5.4.7 DMAPO-catalysed BV oxidation of ketones.**

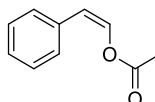
**(E)-Styryl acetate (E)-233.**



General procedure 14 was followed using (E)-**322** (292 mg, 2.0 mmol) for 2.5 h. Purification by flash column chromatography (SiO<sub>2</sub>, 10% EtOAc/PE) afforded the title compound (E)-**323** (235 mg, 152 mmol) as a white solid in 76% yield. Characterisation data were consistent with previous literature reports.<sup>418</sup>

$R_f$  = 0.41 (SiO<sub>2</sub>, 15% Et<sub>2</sub>O/PE); m.p. 46-48 °C, (lit.<sup>509</sup> 46 °C); <sup>1</sup>H NMR (400 MHz, CDCl<sub>3</sub>)  $\delta_H$  7.85 (d, 1H,  $J$  = 12.8, OCH), 7.40 – 7.17 (m, 5H, ArH), 6.40 (d, 1H,  $J$  = 12.8, PhCH), 2.20 (s, 3H, CH<sub>3</sub>); <sup>13</sup>C{<sup>1</sup>H} NMR (126 MHz, CDCl<sub>3</sub>)  $\delta_C$  168.1, 136.4, 134.3, 128.9, 127.6, 126.4, 115.4, 20.9.

**(Z)-Styryl acetate (Z)-233.**

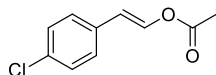


General procedure 14 was followed using (Z)-**322** (145 mg, 1.0 mmol) for 45 min, with purification by flash chromatography (SiO<sub>2</sub>, 8% Et<sub>2</sub>O/*n*-hexane) affording the title compound (Z)-**323** (104 mg, 0.64 mmol) as a colourless oil in 64% yield. Characterisation data were consistent with previous literature reports.<sup>510</sup>



$R_f = 0.37$  (SiO<sub>2</sub>, 15% Et<sub>2</sub>O/PE); <sup>1</sup>H NMR (500 MHz, CDCl<sub>3</sub>)  $\delta_H$  7.61 – 7.58 (m, 2H, ArH), 7.39 – 7.35 (m, 2H, ArH), 7.31 (d, 1H,  $J = 7.3$ , PHCH), 7.29 – 7.24 (m, 1H, ArH), 5.72 (d, 1H,  $J = 7.2$ , OCH), 2.29 (s, 3H, CH<sub>3</sub>); <sup>13</sup>C{<sup>1</sup>H} NMR (126 MHz, CDCl<sub>3</sub>)  $\delta_C$  167.6, 134.2, 134.0, 129.3, 128.6, 127.5, 112.0, 21.1.

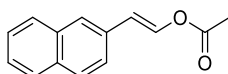
**(*E*)-4-Chlorostyryl acetate (*E*)-217.**



General procedure 14 was followed using (*E*)-*p*-chlorobenzalacetone (360 mg, 2.0 mmol) for 2 h, with purification by flash chromatography (SiO<sub>2</sub>, 8% EtOAc/PE) affording the title compound (*E*)-**271** (284 mg, 1.46 mmol) as a yellow solid in 72% yield. Characterisation data were consistent with previous literature reports.<sup>418</sup>

$R_f = 0.37$  (SiO<sub>2</sub>, 15% Et<sub>2</sub>O/PE); m.p. 64–68 °C, (lit.<sup>418</sup> 66–68 °C); <sup>1</sup>H NMR (400 MHz, CDCl<sub>3</sub>)  $\delta_H$  7.85 (d, 1H,  $J = 12.8$ , OCH), 7.32 – 7.24 (m, 4H, ArH), 6.37 (d,  $J = 12.8$ , ArCH), 2.22 (s, 3H, CH<sub>3</sub>); <sup>13</sup>C{<sup>1</sup>H} NMR (126 MHz, CDCl<sub>3</sub>)  $\delta_C$  168.0, 136.7, 133.2, 132.8, 129.0, 127.5, 114.3, 20.8.

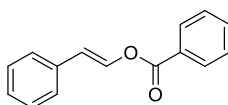
**(*E*)-2-(Naphthalen-2-yl)vinyl acetate 272.**



General procedure 14 was followed using (*E*)-4-(naphthalen-2-yl)but-3-en-2-one (393 mg, 2.0 mmol) for 3 h, with purification by flash chromatography (SiO<sub>2</sub>, 10% EtOAc/PE) affording the title compound (*E*)-**272** (297 mg, 1.40 mmol) as a yellow solid in 70% yield. Characterisation data were consistent with previous literature reports.<sup>418</sup>

$R_f = 0.31$  (SiO<sub>2</sub>, 15% Et<sub>2</sub>O/PE); m.p. 104–108 °C, (lit.<sup>418</sup> 106–108 °C); <sup>1</sup>H NMR (400 MHz, CDCl<sub>3</sub>)  $\delta_H$  7.98 (d, 1H,  $J = 12.8$ , OCH), 7.83 – 7.74 (m, 3H, ArH), 7.70 (s, 1H, ArH), 7.52 (dd, 1H,  $J = 8.5, 1.8$ , ArH), 7.50 – 7.39 (m, 2H, ArH), 6.55 (d, 1H,  $J = 12.8$ , ArCH), 2.23 (s, 3H, CH<sub>3</sub>); <sup>13</sup>C{<sup>1</sup>H} NMR (126 MHz, CDCl<sub>3</sub>)  $\delta_C$  168.2, 136.7, 133.8, 132.9, 131.8, 128.5, 127.9, 127.8, 126.5, 126.1, 126.0, 123.5, 115.6, 20.9.

**(*E*)-Styryl benzoate (*E*)-273.**

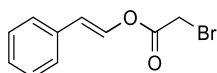


General procedure 14 was followed using (*E*)-chalcone (416 mg, 2.0 mmol) for 24 h, with purification by flash chromatography (SiO<sub>2</sub>, 8% Et<sub>2</sub>O/PE) affording the title compound (*E*)-**273**

(183 mg, 0.82 mmol) as a white solid in 41% yield. Characterisation data were consistent with previous literature reports.<sup>418</sup>

$R_f$  = 0.47 (SiO<sub>2</sub>, 15% Et<sub>2</sub>O/PE); m.p. 53-55 °C, (lit.<sup>416</sup> 52-54 °C); <sup>1</sup>H NMR (400 MHz, CDCl<sub>3</sub>)  $\delta_H$  8.19 – 8.15 (m, 2H, ArH), 8.11 (d, 1H,  $J$  = 12.8, OCH), 7.67 – 7.60 (m, 1H, ArH), 7.55-7.49 (m, 2H, ArH), 7.45 – 7.40 (m, 2H, ArH), 7.38-7.33 (m, 2H, Ar), 7.31-7.25 (m, 1H, ArH), 6.61 (d, 1H,  $J$  = 12.8, PhCH); <sup>13</sup>C{<sup>1</sup>H} NMR (126 MHz, CDCl<sub>3</sub>)  $\delta_C$  163.8, 136.7, 134.3, 133.8, 130.2, 129.1, 128.9, 128.7, 127.6, 126.5, 116.0.

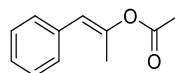
**(*E*)-Styryl 2-bromoacetate (*E*)-279.**



General procedure 14 was followed using (*E*)-**278** (1.00 g, 4.50 mmol) for 1.5 h, with purification by flash chromatography (SiO<sub>2</sub>, 8% EtOAc/PE) affording the title compound (*E*)-**279** (570 mg, 2.39 mmol) as an orange oil in 53% yield.

$R_f$  = 0.44 (SiO<sub>2</sub>, 10% EtOAc/PE); IR (neat): 3087, 2161, 1748 (C=O), 1656, 1260, 1206, 1116, 932, 751, 693 (C-Br) cm<sup>-1</sup>; <sup>1</sup>H NMR (500 MHz, CDCl<sub>3</sub>)  $\delta_H$  7.83 (d, 1H,  $J$  = 12.7, OCH), 7.37 – 7.24 (m, 5H, ArH), 6.51 (d,  $J$  = 12.7, PhCH), 3.96 (s, 2H, CH<sub>2</sub>Br); <sup>13</sup>C{<sup>1</sup>H} NMR (126 MHz, CDCl<sub>3</sub>)  $\delta_C$  164.4, 136.1, 128.8, 127.8, 126.4, 116.9, 77.3, 77.0, 76.8, 25.0. HRMS (ESI+): Calculated for [M+H]<sup>+</sup> C<sub>10</sub>H<sub>10</sub>O<sub>2</sub>Br<sup>+</sup> 240.9859; Found 240.9878.

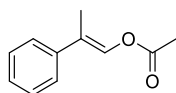
**(*E*)-1-Phenylprop-1-en-2-yl acetate (*E*)-327.**



General procedure 14 was followed using (*E*)-**312** (160 mg, 1.0 mmol) for 6 h. Purification by flash column chromatography (SiO<sub>2</sub>, 10% Et<sub>2</sub>O/PE) afforded the title compound (*E*)-**327** (117 mg, 0.66 mmol) as a colourless oil in 66% yield.

$R_f$  = 0.22 (SiO<sub>2</sub>, 10% Et<sub>2</sub>O/PE); IR (neat) 3057, 3028, 2994, 2914, 1744, 1678, 1436, 1372, 1212, 1126, 1024, 932, 877, 750, 701 cm<sup>-1</sup>; <sup>1</sup>H NMR (500 MHz, CDCl<sub>3</sub>)  $\delta_H$  7.36 – 7.31 (m, 2H, ArH), 7.28 – 7.21 (m, 3H, ArH), 6.26 (s, 1H, PhCH), 2.18 (s, 3H, C(O)CH<sub>3</sub>), 2.11 (d, 3H,  $J$  = 1.1, C(O)CCH<sub>3</sub>); <sup>13</sup>C{<sup>1</sup>H} NMR (126 MHz, CDCl<sub>3</sub>)  $\delta_C$  169.6, 148.0, 135.0, 128.9, 128.5, 127.0, 118.9, 21.3, 17.3; HRMS (ESI+) Calculated for [M+Na]<sup>+</sup> C<sub>11</sub>H<sub>12</sub>O<sub>2</sub>Na<sup>+</sup> 199.0730: Found 199.0732.

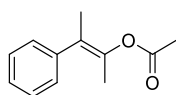
**(E)-2-Phenylprop-1-en-1-yl acetate (E)-328.**



General procedure 14 was followed using (E)-**313** (500 mg, 3.10 mmol). Purification by flash column chromatography (SiO<sub>2</sub>, 8% EtOAc/PE) afforded the title compound (E)-**328** (326 mg, 1.85 mmol) as a colourless oil in 60% yield. Characterisation data were consistent with previous literature reports.<sup>511</sup>

$R_f$  = 0.39 (SiO<sub>2</sub>, 15% Et<sub>2</sub>O/PE); <sup>1</sup>H NMR (500 MHz, CDCl<sub>3</sub>)  $\delta_H$  7.51 (q, 1H,  $J$  = 1.5, OCH), 7.43-7.22 (m, 5H, ArH), 2.22 (s, 3H, C(O)CH<sub>3</sub>), 2.10 (d, 3H,  $J$  = 1.5, PhCCH<sub>3</sub>); <sup>13</sup>C{<sup>1</sup>H} NMR (126 MHz, CDCl<sub>3</sub>)  $\delta_C$  168.2, 139.3, 132.8, 128.6, 127.5, 126.0, 121.8, 21.0, 13.8.

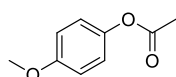
**(E)-3-Phenylbut-2-en-2-yl acetate (E)-329.**



General procedure 14 was followed using (E)-**314** (174 mg, 1.0 mmol) at -10 °C for 3 h. Purification by flash column chromatography (SiO<sub>2</sub>, 20-100% DCM/*n*-hexane) afforded the title compound (E)-**329** (46 mg, 0.24 mmol) as a colourless oil in 24% yield.

$R_f$  = 0.30 (SiO<sub>2</sub>, 15% Et<sub>2</sub>O/PE), 0.23 (SiO<sub>2</sub>, 33% DCM/PE); IR (neat) 2999, 2924, 1746, 1686, 1372, 1222, 1164, 1106, 764, 701 cm<sup>-1</sup>; <sup>1</sup>H NMR (500 MHz, CDCl<sub>3</sub>)  $\delta_H$  7.37 – 7.32 (m, 2H, ArH), 7.29 – 7.23 (m, 3H, ArH), 2.21 (s, 3H, C(O)CH<sub>3</sub>), 1.89 (q, 3H,  $J$  = 1.5, OCCH<sub>3</sub>), 1.84 (q, 3H,  $J$  = 1.5, PhCCH<sub>3</sub>); <sup>13</sup>C{<sup>1</sup>H} NMR (126 MHz, CDCl<sub>3</sub>)  $\delta_C$  169.1, 142.3, 141.1, 128.6, 128.3, 127.0, 124.8, 21.1, 18.0, 17.4, 17.4; HRMS (ESI-) Calculated for [M+CH<sub>3</sub>COO]<sup>-</sup> C<sub>14</sub>H<sub>17</sub>O<sub>4</sub><sup>-</sup> 249.1121; Found 249.1133.

***p*-Acetoxy anisole 259.**



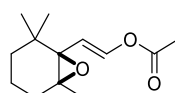
*m*CPBA (1.381 g, 6.0 mmol, 3.0 equiv.) was suspended in toluene (10 mL) and DMAP (49 mg, 0.4 mmol, 0.2 equiv.) was added and the reaction was stirred at rt for 15 min. After this time *p*-methoxyacetophenone **263** (300 mg, 2.0 mmol) was added and the reaction was left to stir for 1 h. At this point the reaction was quenched adding sodium metabisulfite (Na<sub>2</sub>S<sub>2</sub>O<sub>5</sub>, sat. aq., 10 mL) and stirring for 10 min (until potassium iodide starch test paper showed no colour). EtOAc (10 mL) was added and the layers were separated, and the aqueous layer was extracted once more with EtOAc (10 mL). The combined organics were washed three times with NaHCO<sub>3</sub> (sat. aq., 20 mL), brine (20 mL, dried (MgSO<sub>4</sub>), filtered, and concentrated to dryness *in vacuo*. Purification by flash

column (SiO<sub>2</sub>, 8% EtOAc/PE) afforded the title compound **259** (298 mg, 1.80 mmol) as a white solid in 90% yield. Crude product following workup was found to be > 95% pure and would be suitable for further synthetic use. Characterisation data were consistent with previous literature reports.<sup>418</sup>

$R_f$  = 0.24 (SiO<sub>2</sub>, 10% EtOAc/PE); m.p. 32–33 °C, (lit.<sup>418</sup> 33–35 °C); <sup>1</sup>H NMR (400 MHz, CDCl<sub>3</sub>)  $\delta_H$  7.03 – 6.97 (m, 2H, 2 × MeOCCH), 6.92 – 6.86 (m, 2H, 2 × AcOCCH), 3.80 (s, 3H, OCH<sub>3</sub>), 2.28 (s, 3H, O<sub>2</sub>CCH<sub>3</sub>); <sup>13</sup>C{<sup>1</sup>H} NMR (126 MHz, CDCl<sub>3</sub>)  $\delta_C$  170.0, 157.4, 144.3, 122.4, 114.6, 55.7, 21.2.

#### 5.4.8 Oxidation reactions of $\beta$ -ionone **250**

**(rac)-(E)-2-(2,2,6-Trimethyl-7-oxabicyclo[4.1.0]heptan-1-yl)vinyl acetate (rac)-280.**

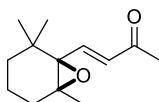


*m*CPBA (1.380 g, 6.0 mmol, 3.0 equiv.) was added to a solution of DMAP (122 mg, 1.0 mmol, 0.5 equiv.) in toluene (10.0 mL), and the suspension was stirred for 15 min, becoming a bright yellow solution. After this time, the reaction was cooled to -20 °C (NaCl/ice bath),  $\beta$ -ionone **250** (407  $\mu$ L, 2.0 mmol, 1.0 equiv.) was added, and the reaction was left to stir for 90 min. After the time the reaction mixture was quenched by diluting by half with EtOAc and Na<sub>2</sub>S<sub>2</sub>O<sub>5</sub> (sat. aq.) and stirring for 10 min (until potassium iodide starch test paper showed no color). The layers were separated, and the aqueous layer was extracted once more with EtOAc (10 mL). The combined organics were washed three times with NaHCO<sub>3</sub> (20 mL, sat. aq.), brine (30 mL), dried (Na<sub>2</sub>SO<sub>4</sub>) and concentrated to dryness *in vacuo*. Purification by flash column chromatography (SiO<sub>2</sub>, 5% Et<sub>2</sub>O in hexanes) afforded the desired product **(rac)-280** (363 mg, 1.62 mmol) as a colourless oil in 81% yield. Characterisation data were consistent with previous literature reports.<sup>432</sup>

This same procedure could also be employed using TMNO·2H<sub>2</sub>O (45 mg, 0.40 mmol, 0.2 equiv.) in the place of DMAP, affording the title compound **(rac)-280** (380 mg, 1.70 mmol) in 85% yield.

$R_f$  = 0.30 (SiO<sub>2</sub>, 10% Et<sub>2</sub>O/*n*-hexane); <sup>1</sup>H NMR (500 MHz, CDCl<sub>3</sub>)  $\delta_H$  7.17 (d, 1H, *J* = 12.3, OCH), 5.62 (d, 1H, *J* = 12.3, OCHCH), 2.13 (s, 3H, O<sub>2</sub>CCH<sub>3</sub>), 1.94–1.84 (m, 1H, AlkH), 1.77 – 1.70 (m, 1H, AlkH), 1.50 – 1.35 (m, 3H, AlkH), 1.21 (s, 3H,  $\delta$ -CH<sub>3</sub>), 1.08 – 1.02 (m, 1H, AlkH), 1.04 (s, 3H, 1 × *gem*-CH<sub>3</sub>), 0.96 (s, 3H, 1 × *gem*-CH<sub>3</sub>); <sup>13</sup>C{<sup>1</sup>H} NMR (126 MHz, CDCl<sub>3</sub>)  $\delta_C$  167.9, 139.3, 110.9, 68.6, 65.3, 35.7, 33.6, 30.1, 25.9, 25.8, 21.2, 20.9, 17.2.

**(E)-4-(2,2,6-Trimethyl-7-oxabicyclo[4.1.0]heptan-1-yl)but-3-en-2-one (rac)-252.**

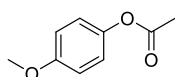


$\beta$ -ionone **250** (407  $\mu$ L, 2.0 mmol, 1.0 equiv.) was added to a vigorously stirred suspension of *m*CPBA (598 mg, 1.3 mmol, 1.30 equiv.) in toluene (10 mL) and stirred at rt for 1 h. After the time the reaction mixture was quenched by diluting by half with EtOAc and Na<sub>2</sub>S<sub>2</sub>O<sub>5</sub> (sat. aq.) and stirring for 10 min (until potassium iodide starch test paper showed no color). The layers were separated, and the aqueous layer was extracted once more with EtOAc (10 mL). The combined organics were washed three times with NaHCO<sub>3</sub> (20 mL, sat. aq.), brine (30 mL), dried (Na<sub>2</sub>SO<sub>4</sub>) and concentrated to dryness *in vacuo*. Purification by flash column chromatography (SiO<sub>2</sub>, 15% Et<sub>2</sub>O in hexanes) afforded the desired product (*rac*)-**252** (342 mg, 1.68 mmol) as a white solid 84% yield. Characterisation data were consistent with previous literature reports.<sup>430,512</sup>

*R*<sub>f</sub>: 0.13 (SiO<sub>2</sub>, 10% Et<sub>2</sub>O/*n*-hexane); m.p.: 45-47 °C (lit.<sup>512</sup> 46 °C); <sup>1</sup>H NMR (500 MHz, CDCl<sub>3</sub>)  $\delta$ <sub>H</sub> 7.03 (d, 1H, *J* = 15.6, C(O)CHCH), 6.30 (d, 1H, *J* = 15.6, C(O)CH), 2.28 (s, 3H, C(O)CH<sub>3</sub>), 1.96 – 1.87 (m, 1H, AlkH), 1.80-1.73 (m, 1H, AlkH), 1.52 – 1.38 (m, 3H, AlkH), 1.15 (s, 6H, 2  $\times$  *gem*-CH<sub>3</sub>), 1.11 – 1.05 (m, 1H, AlkH), 0.94 (s, 3H,  $\delta$ -CH<sub>3</sub>); <sup>13</sup>C{<sup>1</sup>H} NMR (126 MHz, CDCl<sub>3</sub>)  $\delta$ <sub>C</sub> 197.7, 142.8, 132.6, 70.8, 66.0, 35.6, 33.7, 29.9, 28.4, 26.1, 26.0, 21.0, 17.0.

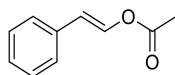
#### 5.4.9 TMNO-catalysed BV oxidation of ketones

***p*-Methoxyphenyl acetate 259.**



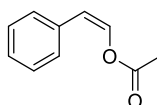
*m*CPBA (75 wt%, 598 mg, 2.60 mmol, 1.3 equiv.) was suspended in toluene (10 mL) and TMNO·2H<sub>2</sub>O (45 mg, 0.40 mmol, 0.2 equiv.) was added and the reaction was stirred at rt for 15 min. After this time *p*-methoxyacetophenone **263** (300 mg, 2.0 mmol) was added and the reaction was left to stir for 5 h. At this point the reaction was quenched adding sodium metabisulfite (Na<sub>2</sub>S<sub>2</sub>O<sub>5</sub>, sat. aq., 10 mL) and stirring for 10 min (until potassium iodide starch test paper showed no colour). EtOAc (10 mL) was added and the layers were separated, and the aqueous layer was extracted once more with EtOAc (10 mL). The combined organics were washed three times with NaHCO<sub>3</sub> (sat. aq., 20 mL), brine (20 mL, dried (MgSO<sub>4</sub>), filtered, and concentrated to dryness *in vacuo*. Purification by flash column (SiO<sub>2</sub>, 8% EtOAc/PE) afforded the title compound *p*-acetoxy anisole **259** (301 mg, 1.82 mmol) as a white solid in 91% yield. Crude product following workup was found to be > 95% pure and would be suitable for further synthetic use. Characterisation data were in consistent with the previous report in this thesis (*vide supra*).

**(E)-Styryl acetate (E)-233.**



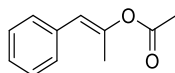
General procedure 15 was followed using (E)-**232** (292 mg, 2.0 mmol) for 2.5 h. Purification by flash column chromatography (SiO<sub>2</sub>, 10% EtOAc/PE) afforded the title compound (E)-**233** (249 mg, 1.54 mmol) as a white solid in 77% yield. Characterisation data were in consistent with the previous report in this thesis (*vide supra*).

**(Z)-Styryl acetate (Z)-233.**



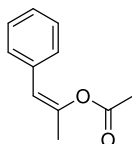
General procedure 15 was followed using (Z)-**232** (73 mg, 0.50 mmol) for 40 min, with purification by flash chromatography (SiO<sub>2</sub>, 8% Et<sub>2</sub>O/*n*-hexane) affording the title compounds (Z)-**233** (58 mg, 0.36 mmol) as a colourless oil in 71 % yield. Characterisation data were in consistent with the previous report in this thesis (*vide supra*).

**(E)-1-Phenylprop-1-en-2-yl acetate (E)-327.**



General procedure 15 was followed using (E)-**312** (160 mg, 1.0 mmol) for 1.5 h. Purification by flash column chromatography (SiO<sub>2</sub>, 10% Et<sub>2</sub>O/PE) afforded the title compound (E)-**327** (139 mg, 0.79 mmol) as a white solid in 79% yield. Characterisation data were in consistent with the previous report in this thesis (*vide supra*).

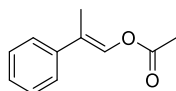
**(Z)-1-Phenylprop-1-en-2-yl acetate (Z)-327.**



General procedure 15 was followed using (Z)-**312** (34 mg, 0.20 mmol) for 3 h. Purification by flash column chromatography (SiO<sub>2</sub>, 20-50% DCM/*n*-pentane) afforded the title compound (Z)-**327** (25 mg, 0.14 mmol) as a clear oil in 71% yield.

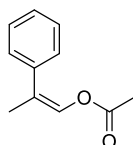
$R_f$  = 0.29 (SiO<sub>2</sub>, 50% DCM/PE); IR (neat) 3026, 2921, 1752, 1680, 1370, 1202, 1147, 1006, 750, 695 cm<sup>-1</sup>; <sup>1</sup>H NMR (500 MHz, CDCl<sub>3</sub>)  $\delta_H$  7.37 – 7.33 (m, 2H, ArH), 7.29 (dd, 2H,  $J$  = 8.5, 6.9, ArH), 7.23 – 7.18 (m, 1H, ArH), 5.96 (s, 1H, PhCH), 2.19 (s, 3H, C(O)CH<sub>3</sub>), 2.09 (d, 3H,  $J$  = 1.1, C(O)CCH<sub>3</sub>); <sup>13</sup>C{<sup>1</sup>H} NMR (126 MHz, CDCl<sub>3</sub>)  $\delta_C$  168.7, 146.4, 134.6, 128.5, 128.3, 127.1, 116.7, 21.3, 20.8; HRMS (ESI+): Calculated for [M+NH<sub>4</sub>]<sup>+</sup> C<sub>11</sub>H<sub>16</sub>O<sub>2</sub>N<sup>+</sup> 194.1176; Found 194.1178.

**(E)-2-Phenylprop-1-en-1-yl acetate (E)-327.**



General procedure 15 was followed using (E)-**313** (156mg, 1.0 mmol). Purification by flash column chromatography (SiO<sub>2</sub>, 8% EtOAc/PE) afforded the title compound (E)-**328** (127 mg, 0.72 mmol) as a colourless oil in 72% yield. Characterisation data were in consistent with the previous report in this thesis (*vide supra*).

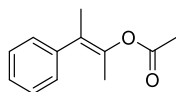
**(Z)-2-Phenylprop-1-en-1-yl acetate (Z)-328.**



General procedure 15 was followed using (Z)-**313** (176 mg, 1.0 mmol) at 0 °C for 1 h. Purification by flash column chromatography (SiO<sub>2</sub>, 5% Et<sub>2</sub>O/*n*-hexane) afforded the title compound (Z)-**328** (65 mg, 0.38 mmol) as a colourless oil in 38% yield.

$R_f$  = 0.24 (SiO<sub>2</sub>, 5% Et<sub>2</sub>O/PE); IR (neat) 3083, 3058, 2972, 1752, 1664, 1371, 1206, 1102, 1074, 905, 826, 754, 694 cm<sup>-1</sup>; <sup>1</sup>H NMR (500 MHz, CDCl<sub>3</sub>)  $\delta_H$  7.48 – 7.45 (m, 2H, ArH), 7.39 – 7.34 (m, 2H, ArH), 7.29 – 7.25 (m, 1H, ArH), 7.20 (q, 1H,  $J$  = 1.5, OCH), 2.12 (s, 3H, C(O)CH<sub>3</sub>), 2.03 (d, 3H,  $J$  = 1.6, PhCCH<sub>3</sub>); <sup>13</sup>C{<sup>1</sup>H} NMR (126 MHz, CDCl<sub>3</sub>)  $\delta_C$  168.2, 137.6, 130.8, 128.2, 128.1, 127.4, 119.8, 21.0, 19.2; HRMS (ESI-): Calculated for [M+CH<sub>3</sub>CO<sub>2</sub>]<sup>-</sup> C<sub>13</sub>H<sub>15</sub>O<sub>4</sub><sup>-</sup> 235.0965; Found 235.0974.

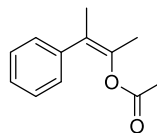
**(E)-3-Phenylbut-2-en-2-yl acetate (E)-329.**



General procedure 15 was followed using (E)-**314** (95 mg, 0.5 mmol). Purification by flash column chromatography (SiO<sub>2</sub>, 20-100% DCM/*n*-pentane) afforded the title compound (E)-**329** (45 mg,

0.22 mmol) as a colourless oil in 44% yield. Characterisation data were in consistent with the previous report in this thesis (*vide supra*).

**(Z)-3-Phenylbut-2-en-2-yl acetate (Z)-329.**



General procedure 15 was followed using (Z)-**314** (87 mg, 0.5 mmol). Purification by flash column chromatography (SiO<sub>2</sub>, 20-50% DCM/*n*-hexane) afforded the title compound (Z)-**329** (23 mg, 0.12 mmol) as a colourless oil in 24% yield. 28% of the (Z)-**314** starting material was recovered (24 mg, 0.14 mmol), and so the yield based on recovered starting material is 34%.

$R_f$  = 0.33 (SiO<sub>2</sub>, 50% DCM/PE); IR (neat) 2921, 1744, 1686, 1366, 1221, 1170, 1111, 903, 764, 700 cm<sup>-1</sup>; <sup>1</sup>H NMR (500 MHz, CDCl<sub>3</sub>)  $\delta_H$  7.32 – 7.27 (m, 2H, ArH), 7.23 – 7.15 (m, 3H, ArH), 2.03 (s, 3H, PhCCH<sub>3</sub>), 2.02 (s, 3H, OCCH<sub>3</sub>), 1.87 (s, 3H, C(O)CH<sub>3</sub>); <sup>13</sup>C{<sup>1</sup>H} NMR (126 MHz, CDCl<sub>3</sub>)  $\delta_C$  169.8, 140.7, 140.6, 128.2, 127.7, 126.8, 123.7, 20.9, 19.3, 17.0.; HRMS (ESI-): Calculated for [M+CH<sub>3</sub>CO<sub>2</sub>]<sup>-</sup> C<sub>14</sub>H<sub>17</sub>O<sub>4</sub><sup>-</sup> 249.1121; Found 249.1132.



## 6. REFERENCES

- 1 A. Ault, *J. Chem. Educ.*, 2002, **79**, 572–577.
- 2 N. M. Maier, P. Franco and W. Lindner, *J. Chromatogr. A*, 2001, **906**, 3–33.
- 3 T. J. Ward and K. D. Ward, *Anal. Chem.*, 2012, **84**, 626–635.
- 4 Y. Okamoto and E. Yashima, *Angew. Chem. Int. Ed.*, 1998, **37**, 1020–1043.
- 5 J. Teixeira, M. E. Tiritan, M. M. M. Pinto and C. Fernandes, *Molecules*, 2019, **24**, 865–902.
- 6 S.-M. Xie and L.-M. Yuan, *J. Sep. Sci.*, 2017, **40**, 124–137.
- 7 Y. Zhang, D. R. Wu, D. B. Wang-Iverson and A. A. Tymiak, *Drug Discov. Today*, 2005, **10**, 571–577.
- 8 Y. Okamoto and T. Ikai, *Chem. Soc. Rev.*, 2008, **37**, 2593–2608.
- 9 I. Ilisz, R. Berkecz and A. Péter, *J. Pharm. Biomed. Anal.*, 2008, **47**, 1–15.
- 10 S. E. Denmark and N. Carson, *Org. Lett.*, 2015, **17**, 5728–5731.
- 11 O. Quinonero, C. Lemaitre, M. Jean, N. Vanthuyne, C. Roussel, D. Bonne, T. Constantieux, C. Bressy, X. Bugaut and J. Rodriguez, *Org. Lett.*, 2021, **23**, 3394–3398.
- 12 J. L. Dores-Sousa, J. De Vos and S. Eeltink, *J. Sep. Sci.*, 2019, **42**, 38–50.
- 13 R. E. Lyle and G. G. Lyle, *J. Chem. Educ.*, 1964, **41**, 308–313.
- 14 B. T. Herrera, S. L. Pilicer, E. V Anslyn, L. A. Joyce and C. Wolf, *J. Am. Chem. Soc.*, 2018, **140**, 10385–10401.
- 15 J. W. Canary, Z. Dai and S. Mortezaei, in *Comprehensive Chirality*, Elsevier, 2012, vol. 8, pp. 600–624.
- 16 H. H. Jo, C.-Y. Lin and E. V Anslyn, *Acc. Chem. Res.*, 2014, **47**, 2212–2221.
- 17 N. Berova, K. Nakanishi and R. W. Woody, *Circular dichroism: principles and applications*, WILEY-VCH, New York, second ed., 2000.
- 18 C. Wolf and K. W. Bentley, *Chem. Soc. Rev.*, 2013, **42**, 5408.
- 19 V. Charbonneau and W. W. Ogilvie, *Mini. Rev. Org. Chem.*, 2005, **2**, 313–332.
- 20 D. Leung, S. O. Kang and E. V. Anslyn, *Chem. Soc. Rev.*, 2012, **41**, 448–479.
- 21 M. G. Finn, *Chirality*, 2002, **14**, 534–540.
- 22 M. T. Reetz, K. M. Kühling, H. Hinrichs and A. Deege, *Chirality*, 2000, **12**, 479–482.
- 23 T. J. Wenzel, in *Top Curr Chem*, Springer, Cham, 2013, vol. 341, pp. 1–68.
- 24 T. J. Wenzel, *Differentiation of Chiral Compounds Using NMR Spectroscopy*, John Wiley & Sons, Inc., Hoboken, sec., 2018.
- 25 F. Balzano, G. Uccello-Barretta and F. Aiello, in *Chiral Analysis: Advances in Spectroscopy, Chromatography and Emerging Methods*, ed. P. L. Polavrapu, Elsevier Inc., second ed., 2018, pp. 367–427.
- 26 W. H. Pirkle, *J. Am. Chem. Soc.*, 1966, **96**, 1837–1837.

- 27 W. H. Pirkle, S. D. Beare and R. L. Muntz, *J. Am. Chem. Soc.*, 1969, **91**, 4575–4575.
- 28 W. H. Pirkle and D. J. Hoover, *Top. Stereochem.*, 1982, **13**, 263–332.
- 29 W. H. Pirkle and S. D. Beare, *Tetrahedron Lett.*, 1968, **9**, 2579–2582.
- 30 T. G. Burlingame and W. H. Pirkle, *J. Am. Chem. Soc.*, 1966, **88**, 4294–4294.
- 31 W. H. Pirkle and T. G. Burlingame, *Tetrahedron Lett.*, 1967, **8**, 4039–4042.
- 32 W. H. Pirkle and S. D. Beare, *Tetrahedron Lett.*, 1967, **89**, 4585–5487.
- 33 W. H. Pirkle, T. G. Burlingame and S. D. Beare, *Tetrahedron Lett.*, 1968, **9**, 5849–5852.
- 34 M. J. Shapiro, A. E. Archinal and M. A. Jarema, *J. Org. Chem.*, 1989, **54**, 5826–5828.
- 35 A. E. Lovely and T. J. Wenzel, *Org. Lett.*, 2006, **8**, 2823–2826.
- 36 S. Bozkurt, M. Durmaz, H. N. Naziroglu, M. Yilmaz and A. Sirit, *Tetrahedron Asymmetry*, 2011, **22**, 541–549.
- 37 I. Pal, S. R. Chaudhari and N. R. Suryaprakash, *Magn. Reson. Chem.*, 2015, **53**, 142–146.
- 38 F. Toda, K. Mori and A. Sato, *Bull. Chem. Soc. Japan*, 1988, **61**, 4167–4169.
- 39 M. Ardej-Jakubisiak and R. Kawecki, *Tetrahedron Asymmetry*, 2008, **19**, 2645–2647.
- 40 T. Ema, D. Tanida and T. Sakai, *J. Am. Chem. Soc.*, 2007, **129**, 10591–10596.
- 41 J. Labuta, S. Ishihara, T. Šikorský, Z. Futera, A. Shundo, L. Hanyková, J. V. Burda, K. Ariga and J. P. Hill, *Nat. Commun.*, 2013, **4**, 2188.
- 42 Z. Chen, H. Fan, S. Yang, G. Bian and L. Song, *Org. Biomol. Chem.*, 2018, **16**, 6933–6939.
- 43 S. K. Mishra, S. R. Chaudhari and N. Suryaprakash, *Org. Biomol. Chem.*, 2014, **12**, 495–502.
- 44 K. D. Klika, S. K. Mishra, S. R. Chaudhari and N. Suryaprakash, *Tetrahedron Asymmetry*, 2014, **25**, 705–708.
- 45 M. K. Meadows, E. K. Roesner, V. M. Lynch, T. D. James and E. V. Anslyn, *Org. Lett.*, 2017, **19**, 3179–3182.
- 46 A. Winkel and R. Wilhelm, *Eur. J. Org. Chem.*, 2010, **2010**, 5817–5824.
- 47 W. D. G. Brittain, B. M. Chapin, W. Zhai, V. M. Lynch, B. R. Buckley, E. V. Anslyn and J. S. Fossey, *Org. Biomol. Chem.*, 2016, **14**, 10778–10782.
- 48 A. Böhm and D. Seebach, *Helv. Chim. Acta*, 2000, **83**, 3262–3278.
- 49 G. Uccello-Barretta, R. Bernardini, F. Balzano and P. Salvadori, *Chirality*, 2002, **14**, 484–489.
- 50 G. M. Whitesides and D. W. Lewis, *J. Am. Chem. Soc.*, 1970, **92**, 6979–6980.
- 51 D. Parker, *Chem. Rev.*, 1991, 1441–1457.
- 52 J. M. Seco, E. Quiñoa and R. Riguera, *Chem. Rev.*, 2012, **112**, 4603–4641.
- 53 M. E. Powell, C. D. Evans, S. D. Bull, T. D. James and P. S. Fordred, *Compr. Chirality*, 2012, **8**, 571–599.
- 54 M. Raban and K. Mislow, *Tetrahedron Lett.*, 1965, **48**, 4249–4253.
- 55 J. A. Dale and H. S. Mosher, *J. Am. Chem. Soc.*, 1973, **95**, 512–519.

- 56 J. A. Dale, D. L. Dull and H. S. Mosher, *J. Org. Chem.*, 1969, **34**, 2543–2549.
- 57 G. R. Sullivan, J. A. Dale and H. S. Mosher, *J. Org. Chem.*, 1973, **38**, 2143–2147.
- 58 J. A. Dale and H. S. Mosher, *J. Am. Chem. Soc.*, 1968, **90**, 3732–3738.
- 59 T. J. Wenzel and C. D. Chisholm, *Chirality*, 2011, **23**, 190–214.
- 60 Y. Takeuchi, M. Segawa, H. Fujisawa, K. Omata, S. N. Lodwig and C. J. Unkefer, *Angew. Chem. Int. Ed.*, 2006, **45**, 4617–4619.
- 61 J. M. Seco, E. Quiñoá and R. Riguera, *J. Org. Chem.*, 1999, **64**, 4669–4675.
- 62 A. Ichikawa, H. Ono and Y. Mikata, *CrystEngComm*, 2013, **15**, 8088–8096.
- 63 A. Ichikawa, H. Ono and Y. Mikata, *Molecules*, 2015, **20**, 12880–12900.
- 64 J. M. Seco, E. Quiñoá and R. Riguera, *Chem. Rev.*, 2004, **104**, 17–117.
- 65 J. M. Seco, S. Latypov, E. Quiñoá and R. Riguera, *Tetrahedron Asymmetry*, 1995, **6**, 107–110.
- 66 T. R. Hoye, C. S. Jeffrey and F. Shao, *Nat. Protoc.*, 2007, **2**, 2451–2458.
- 67 J. M. Seco, E. Quiñoá and R. Riguera, *The Assignment of the Absolute Configuration by NMR Using Chiral Derivatizing Agents: A Practical Guide*, Oxford University Press, New York, 2015.
- 68 O. Thillaye Du Boullay, A. Alba, F. Oukhatar, B. Martin-Vaca and D. Bourissou, *Org. Lett.*, 2008, **10**, 4669–4672.
- 69 A. Alexakis and A. S. Chauvin, *Tetrahedron Asymmetry*, 2001, **12**, 1411–1415.
- 70 A. Meddour and J. Courtieu, *Tetrahedron Asymmetry*, 2000, **11**, 3635–3644.
- 71 M. S. Silva, *Molecules*, 2017, **22**, 247.
- 72 O. N. Gorunova, I. M. Novitskiy, M. V. Livantsov, Y. K. Grishin, K. A. Kochetkov and V. V. Dunina, *J. Organomet. Chem.*, 2015, **783**, 96–104.
- 73 N. B. G. Marques, R. G. Jacob, G. Perin, E. J. Lenardão, D. Alves and M. S. Silva, *Chirality*, 2019, **31**, 41–51.
- 74 N. V. Orlov and V. P. Ananikov, *Chem. Commun.*, 2010, **46**, 3212–3214.
- 75 A. M. Harned, *Tetrahedron*, 2018, **74**, 3797–3841.
- 76 D. A. Tickell, E. V Lampard, J. P. Lowe, T. D. James and S. D. Bull, *J. Org. Chem.*, 2016, **81**, 6795–6799.
- 77 T. Andersson, B. Borhan, N. Berova, K. Nakanishi, J. A. Haugan and S. Liaaen-Jensen, *J. Chem. Soc. Perkin Trans. 1*, 2000, **1**, 2409–2414.
- 78 K. Omata, K. Kotani, K. Kabuto, T. Fujiwara and Y. Takeuchi, *Chem. Commun.*, 2010, **46**, 3610–3612.
- 79 M. Blanco, J. Coello, H. Iturriaga, S. MasPOCH and M. Porcel, *Anal. Chim. Acta*, 2001, **431**, 115–123.
- 80 L. Tang, G. Wei, R. Nandhakumar and Z. Guo, *Bull. Korean Chem. Soc.*, 2011, **32**, 3367–3371.
- 81 Z. Rozwadowski, *Annu. Reports NMR Spectrosc.*, 2011, **74**, 125–180.
- 82 F. Dufrasne, M. Gelbcke and J. Nève, *Spectrochim. Acta Part A*, 2003, **59**, 1239–1245.

- 83 F. Dufrasne, M. Gelbcke and M. Galanski, *Spectrochim. Acta - Part A Mol. Biomol. Spectrosc.*, 2006, **65**, 869–873.
- 84 V. Nardini, V. Palaretti and G. V. J. da Silva, *Microchem. J.*, 2017, **133**, 208–215.
- 85 S. M. Gibson, R. M. Lanigan, L. Benhamou, A. E. Aliev and T. D. Sheppard, *Org. Biomol. Chem.*, 2015, **13**, 9050–9054.
- 86 H. Fukui and Y. Fukushi, *Org. Lett.*, 2010, **12**, 2856–2859.
- 87 V. Nardini, V. Palaretti, L. Dias and G. da Silva, *Molecules*, 2019, **24**, 2830.
- 88 M. K. Kwan, H. Park, H. J. Kim, J. Chin and W. Nam, *Org. Lett.*, 2005, **7**, 3525–3527.
- 89 R. Nandhakumar, J. Ryu, H. Park, L. Tang, S. Choi and K. M. Kim, *Tetrahedron*, 2008, **64**, 7704–7708.
- 90 Y. Chi, T. J. Peelen and S. H. Gellman, *Org. Lett.*, 2005, **7**, 3469–3472.
- 91 S. D. Bull, S. G. Davies, S. W. Epstein and J. V. A. Ouzman, *Chem. Commun.*, 1998, 659–660.
- 92 S. D. Bull, S. G. Davies, S. Delgado-Ballester, P. M. Kelly, L. J. Kotchie, M. Gianotti, M. Laderas and A. D. Smith, *J. Chem. Soc. Perkin 1*, 2001, **1**, 3112–3121.
- 93 S. D. Bull, S. G. Davies, D. J. Fox, M. Gianotti, P. M. Kelly, C. Pierres, E. D. Savory and A. D. Smith, *J. Chem. Soc. Perkin 1*, 2002, **2**, 1858–1868.
- 94 D. J. Aitken, S. D. Bull, I. R. Davies, L. Drouin, J. Ollivier and J. Peed, *Synlett*, 2010, **2010**, 2729–2732.
- 95 C. D. Evans, M. F. Mahon, P. C. Andrews, J. Muir and S. D. Bull, *Org. Lett.*, 2011, **13**, 6276–6279.
- 96 T. Boddaert, J. E. Taylor, S. D. Bull and D. J. Aitken, *Org. Lett.*, 2019, **21**, 100–103.
- 97 E. Galbraith and T. D. James, *Chem. Soc. Rev.*, 2010, **39**, 3831–3842.
- 98 T. D. James, K. R. A. Samankumara Sandanayake and S. Shinkai, *Nature*, 1995, **374**, 345–347.
- 99 T. D. James, K. R. A. Samankumara Sandanayake and S. Shinkai, *Angew. Chem. Int. Ed.*, 1996, **35**, 1910–1922.
- 100 S. D. Bull, M. G. Davidson, J. M. H. Van Den Elsen, J. S. Fossey, A. T. A. Jenkins, Y.-B. Jiang, Y. Kubo, F. Marken, K. Sakurai, J. Zhao and T. D. James, *Acc. Chem. Res.*, 2012, **46**, 312–326.
- 101 D. Wu, A. C. Sedgwick, T. Gunnlaugsson, E. U. Akkaya, J. Yoon and T. D. James, *Chem. Soc. Rev.*, 2017, **46**, 7105–7123.
- 102 T. D. James, K. R. A. S. Sandanayake, R. Iguchi and S. Shinkai, *J. Am. Chem. Soc.*, 1995, **117**, 8982–8987.
- 103 M. Mortellaro and A. DeHennis, *Biosens. Bioelectron.*, 2014, **61**, 227–231.
- 104 B. C. Crane, N. P. Barwell, P. Gopal, M. Gopichand, T. Higgs, T. D. James, C. M. Jones, A. Mackenzie, K. P. Mulavisala and W. Paterson, *J. Diabetes Sci. Technol.*, 2015, **9**, 751–61.
- 105 M. Lauer, H. Böhnke, R. Grotstollen, M. Salehnia and G. Wulff, *Chem. Ber.*, 1985, **118**, 246–260.
- 106 X. Sun, T. D. James and E. V. Anslyn, *J. Am. Chem. Soc.*, 2018, **140**, 2348–2354.

- 107 X. Sun, B. M. Chapin, P. Metola, B. Collins, B. Wang, T. D. James and E. V. Anslyn, *Nat. Chem.*, 2019, **11**, 768–778.
- 108 J. Zhao, T. M. Fyles and T. D. James, *Angew. Chem. Int. Edi.*, 2004, **43**, 3461–3464.
- 109 N. Hiller, N. Silva, T. Tavares, R. Faria, M. Eberlin and D. Martins, *Eur. J. Org. Chem.*, 2020, **2020**, 4841–4877.
- 110 Y. Kanekiyo and S. Shinkai, in *Monographs in Supramolecular Chemistry*, Royal Society of Chemistry, 2016, pp. 1–43.
- 111 Wikipedia, Nomikai, <https://en.wikipedia.org/wiki/Nomikai>, (accessed 31 July 2020).
- 112 T. D. James, *Beilstein J. Org. Chem.*, 2016, **12**, 391–405.
- 113 H. E. Dunn, J. C. Gatlin and H. R. Snyder, *J. Org. Chem.*, 1968, **33**, 4483–4486.
- 114 G. A. Molander and D. L. Sandrock, in *Encyclopedia of Reagents for Organic Synthesis*, John Wiley & Sons, Ltd, 2009.
- 115 Y. Pérez-Fuertes, A. M. Kelly, A. L. Johnson, S. Arimori, S. D. Bull and T. D. James, *Org. Lett.*, 2006, **8**, 609–612.
- 116 Y. Pérez-Fuertes, A. M. Kelly, J. S. Fossey, M. E. Powell, S. D. Bull and T. D. James, *Nat. Protoc.*, 2008, **3**, 210–214.
- 117 Y. Pérez-Fuertes, PhD Thesis, University of Bath, 2005.
- 118 B. M. Chapin, P. Metola, V. M. Lynch, J. F. Stanton, T. D. James and E. V. Anslyn, *J. Org. Chem.*, 2016, **81**, 8319–8330.
- 119 S. L. Lulinski, I. Madura, J. Serwatowski, H. Szatyłowicz and J. Zachara, *New J. Chem.*, 2007, **31**, 144–154.
- 120 K. Kowalska, A. Adamczyk-Woźniak, P. Gajowiec, B. Gierczyk, E. Kaczorowska, Ł. Popena, G. Schroeder, A. Sikorski and A. Sporzyński, *J. Fluor. Chem.*, 2016, **187**, 1–8.
- 121 A. Adamczyk-Woźniak, K. Ejsmont, B. Gierczyk, E. Kaczorowska, A. Matuszewska, G. Schroeder, A. Sporzyński and B. Zarychta, *J. Organomet. Chem.*, 2015, **788**, 36–41.
- 122 A. Adamczyk-Woźniak, I. Madura, A. H. Velders and A. Sporzyński, *Tetrahedron Lett.*, 2010, **51**, 6181–6185.
- 123 A. Adamczyk-Woźniak, M. K. Cyrański, B. T. Frczak, A. Lewandowska, I. D. Madura and A. Sporzyński, *Tetrahedron*, 2012, **68**, 3761–3767.
- 124 N. J. Gutiérrez-Moreno, F. Medrano and A. K. Yatsimirsky, *Org. Biomol. Chem.*, 2012, **10**, 6960–6972.
- 125 P. Schmidt, C. Stress and D. Gillingham, *Chem. Sci.*, 2015, **6**, 3329–3333.
- 126 D. Gillingham, *Org. Biomol. Chem.*, 2016, **14**, 7606–7609.
- 127 C. J. Stress, P. J. Schmidt and D. G. Gillingham, *Org. Biomol. Chem.*, 2016, **14**, 5529–5533.
- 128 S. Nieto, P. Arnau, E. Serrano, R. Navarro, T. Soler, C. Cativiela and E. P. Urriolabeitia, *Inorg. Chem.*, 2009, **48**, 11963–11975.
- 129 Y. Pérez-Fuertes, J. E. Taylor, D. A. Tickell, M. F. Mahon, S. D. Bull and T. D. James, *J. Org. Chem.*, 2011, **76**, 6038–6047.

- 130 P. J. M. Taylor and S. D. Bull, *Tetrahedron Asymmetry*, 2006, **17**, 1170–1178.
- 131 R. M. Archer, M. Hutchby, C. L. Winn, J. S. Fossey and S. D. Bull, *Tetrahedron*, 2015, **71**, 8838–8847.
- 132 P. Axe, S. D. Bull, M. G. Davidson, C. J. Gilfillan, M. D. Jones, D. E. J. E. Robinson, L. E. Turner and W. L. Mitchell, *Org. Lett.*, 2007, **9**, 223–226.
- 133 T. L. March, M. R. Johnston and P. J. Duggan, *Org. Lett.*, 2012, **14**, 182–185.
- 134 C. Shi, T. W. Geders, S. Woong Park, D. J. Wilson, H. I. Boshoff, O. Abayomi, C. E. Barry, D. Schnappinger, B. C. Finzel and C. C. Aldrich, *J. Am. Chem. Soc.*, 2011, **133**, 18194–18201.
- 135 S. Nieto, J. M. Dagna and E. V. Anslyn, *Chem. Eur. J.*, 2010, **16**, 227–232.
- 136 N. Lokesh, S. L. Sachin, L. V. Narendra, K. Arun and N. Suryaprakash, *Org. Biomol. Chem.*, 2015, **13**, 7230–7235.
- 137 J. S. Fossey, E. V Anslyn, W. D. G. Brittain, S. D. Bull, B. M. Chapin, C. Cécile, S. Le Duff, T. D. James, G. Lees, S. Lim, J. A. C. Lloyd, C. V Manville, D. T. Payne and K. A. Roper, *J. Chem. Educ.*, 2017, **94**, 79–84.
- 138 A. M. Kelly, S. D. Bull and T. D. James, *Tetrahedron Asymmetry*, 2008, **19**, 489–494.
- 139 P. Mangeney, A. Alexakis and J. F. Normant, *Tetrahedron Lett.*, 1988, **29**, 2677–2680.
- 140 D. Cuvinot, A. Alexakis, J.-F. Normant and J.-P. Lellouch, *J. Org. Chem.*, 1989, **54**, 2420–2425.
- 141 A. Alexakis, J. C. Frutos and P. Mangeney, *Tetrahedron Asymmetry*, 1993, **4**, 2431–2434.
- 142 M. E. Powell, A. M. Kelly, S. D. Bull and T. D. James, *Tetrahedron Lett.*, 2008, **50**, 876–879.
- 143 D. A. Tickell, M. F. Mahon, S. D. Bull and T. D. James, *Org. Lett.*, 2013, **15**, 860–863.
- 144 W. Kliegel and D. Nanninga, *J. Organomet. Chem.*, 1983, **247**, 247–252.
- 145 A. M. Kelly, Y. Pérez-Fuertes, S. Arimori, S. D. Bull and T. D. James, *Org. Lett.*, 2006, **8**, 1971–1974.
- 146 A. M. Kelly, Y. Pérez-Fuertes, J. S. Fossey, S. Lozano Yeste, S. D. Bull and T. D. James, *Nat. Protoc.*, 2008, **3**, 215–219.
- 147 M. D. Reddy, H. Kobori, T. Mori, J. Wu, H. Kawagishi and E. B. Watkins, *J. Nat. Prod.*, 2017, **80**, 2561–2565.
- 148 D. Urabe, H. Todoroki, K. Masuda and M. Inoue, *Tetrahedron*, 2012, **68**, 3210–3219.
- 149 M. Göhl and K. Seifert, *Eur. J. Org. Chem.*, 2015, **2015**, 6249–6258.
- 150 C. Chopard, R. Azerad and T. Prangé, *J. Mol. Catal. B Enzym.*, 2008, **50**, 53–60.
- 151 S. H. Shabbir, C. J. Regan, E. V Anslyn and J. Rebek, *Proc. Natl. Acad. Sci.*, 2009, **106**, 10487–10492.
- 152 S. H. Shabbir, L. A. Joyce, G. M. Da Cruz, V. M. Lynch, S. Sorey and E. V. Anslyn, *J. Am. Chem. Soc.*, 2009, **131**, 13125–13131.
- 153 P. S. Fordred and S. D. Bull, *Tetrahedron Lett.*, 2013, **54**, 27–31.
- 154 M. Zeng and S. B. Herzon, *J. Org. Chem.*, 2015, **80**, 8604–8618.
- 155 Z. Li, C. Chen, S. Gröger and J. Kressler, *Polymer*, 2012, **53**, 2613–2618.

- 156 S. R. Chaudhari and N. Suryaprakash, *J. Org. Chem.*, 2012, **77**, 648–651.
- 157 S. R. Chaudhari and N. Suryaprakash, *Org. Biomol. Chem.*, 2012, **10**, 6410–6419.
- 158 S. K. Mishra and N. Suryaprakash, *RSC Adv.*, 2015, **5**, 67277–67283.
- 159 S. R. Chaudhari and N. R. Suryaprakash, *New J. Chem.*, 2014, **38**, 790–794.
- 160 S. K. Mishra and N. Suryaprakash, *Tetrahedron Asymmetry*, 2017, **28**, 250–256.
- 161 N. Lokesh, S. R. Chaudhari and N. Suryaprakash, *Org. Biomol. Chem.*, 2014, **12**, 993–997.
- 162 S. L. Yeste, M. E. Powell, S. D. Bull and T. D. James, *J. Org. Chem.*, 2009, **74**, 427–430.
- 163 S. Lozano Yeste, M. E. Powell, S. D. Bull and T. D. James, *J. Org. Chem.*, 2019, **84**, 9395–9396.
- 164 N. Hamaguchi, Y. Okuno, Y. Oe and T. Ohta, *Chirality*, 2019, **31**, 34–40.
- 165 Y. R. Lima, T. J. Peglow, P. C. Nobre, P. T. Campos, G. Perin, E. J. Lenardão and M. S. Silva, *ChemistrySelect*, 2019, **4**, 4797–4803.
- 166 S. S. Oliveira, R. L. O. R. Cunha and M. S. Silva, *Tetrahedron Lett.*, 2016, **57**, 4556–4559.
- 167 P. Metola, E. V Anslyn, T. D. James and S. D. Bull, *Chem. Sci.*, 2012, **3**, 156–161.
- 168 S. Stewart, M. A. Ivy and E. V. Anslyn, *Chem. Soc. Rev.*, 2014, **43**, 70–84.
- 169 K. W. Bentley, Y. G. Nam, J. M. Murphy and C. Wolf, *J. Am. Chem. Soc.*, 2013, **135**, 18052–18055.
- 170 E. G. Shcherbakova, T. Minami, V. Brega, T. D. James and P. Anzenbacher, *Angew. Chem. Int. Ed.*, 2015, **54**, 7130–7133.
- 171 E. G. Shcherbakova, V. Brega, T. Minami, S. Sheykhi, T. D. James and P. Anzenbacher, *Chem. - A Eur. J.*, 2016, **22**, 10074–10080.
- 172 E. G. Shcherbakova, V. Brega, V. M. Lynch, T. D. James and P. Anzenbacher, *Chem. - A Eur. J.*, 2017, **23**, 10222–10229.
- 173 M. Pushina, S. Farshbaf, E. G. Shcherbakova and P. Anzenbacher, *Chem. Commun.*, 2019, **55**, 4495–4498.
- 174 E. G. Shcherbakova, T. D. James and P. Anzenbacher, *Nat. Protoc.*, 2020, **15**, 2203–2229.
- 175 L. Wu, C. Huang, B. P. Emery, A. C. Sedgwick, S. D. Bull, X. P. He, H. Tian, J. Yoon, J. L. Sessler and T. D. James, *Chem. Soc. Rev.*, 2020, **49**, 5110–5139.
- 176 G. Mirri, S. D. Bull, P. N. Horton, T. D. James, L. Male and J. H. R. Tucker, *J. Am. Chem. Soc.*, 2010, **132**, 8903–8905.
- 177 A. Wilson, G. Gasparini and S. Matile, *Chem. Soc. Rev.*, 2014, **43**, 1948–1962.
- 178 J. F. Reuther, S. D. Dahlhauser and E. V Anslyn, *Angew. Chem. Int. Ed.*, 2019, **58**, 74–85.
- 179 H. M. Seifert, K. R. Trejo and E. V Anslyn, *J. Am. Chem. Soc.*, 2016, **138**, 10916–10924.
- 180 V. E. Campbell and J. R. Nitschke, *Synlett*, 2008, **20**, 3077–3090.
- 181 M. Hutin, G. Bernardinelli and J. R. Nitschke, *Chem. - A Eur. J.*, 2008, **14**, 4585–4593.
- 182 R. Nishiyabu, Y. Kubo, T. D. James and J. S. Fossey, *Chem. Commun.*, 2011, **47**, 1124–1150.

- 183 Y. Kubo, R. Nishiyabu and T. D. James, *Chem. Commun.*, 2015, **51**, 2005–2020.
- 184 E. Galbraith, A. M. Kelly, J. S. Fossey, G. Kociok-Köhn, M. G. Davidson, S. D. Bull and T. D. James, *New J. Chem.*, 2009, **33**, 181–185.
- 185 D. W. Norman, J. P. Edwards, C. M. Vogels, A. Decken and S. A. Westcott, *Can. J. Chem.*, 2002, **80**, 31–40.
- 186 F. A. Appoh, S. S. Barnes, M. J. Manning, C. S. Turner, C. M. Vogels, S. A. Westcott and A. Decken, *J. Heterocycl. Chem.*, 2008, **45**, 1415–1418.
- 187 S. N. Fischer and A. Geyer, *Beilstein J. Org. Chem.*, 2015, **11**, 2646–2653.
- 188 A. Wuttke, S. N. Fischer, A. Nebel, M. Marsch and A. Geyer, *Org. Biomol. Chem.*, 2016, **14**, 5032–5048.
- 189 H. Y. Su, D. Gorelik and M. S. Taylor, *Supramol. Chem.*, 2019, **31**, 190–202.
- 190 E. N. Keyzer, A. Sava, T. K. Ronson, J. R. Nitschke and A. J. McConnell, *Chem. - A Eur. J.*, 2018, **24**, 12000–12005.
- 191 E. Amado and J. Rg Kressler, *Macromolecules*, 2016, **49**, 1532–1544.
- 192 D. Ailincăi, L. Marin, S. Morariu, M. Mares, A. C. Bostanaru, M. Pinteala, B. C. Simionescu and M. Barboiu, *Carbohydr. Polym.*, 2016, **152**, 306–316.
- 193 S. S. Delpierre, B. Willocq, G. Manini, V. Lemaure, J. Goole, P. Gerbaux, J. Jérôme Cornil, P. Dubois and J.-M. Raquez, *Chem. Mater.*, 2019, **31**, 3736–3744.
- 194 S. Delpierre, B. Willocq, J. De Winter, P. Dubois, P. Gerbaux and J.-M. Raquez, *Chem. - A Eur. J.*, 2017, **23**, 6730–6735.
- 195 Y. Yang, L. Huang, R. Wu, W. Fan, Q. Dai, J. He and C. Bai, *ACS Appl. Mater. Interfaces*, 2020, **12**, 33305–33314.
- 196 S. Li, C. Zuo, Y. H. Jo, S. Li, K. Jiang, L. Yu, Y. Zhang, J. Wang, L. Li and Z. Xue, *J. Memb. Sci.*, 2020, **608**, 118218.
- 197 X. Zhang, J. Gao, X. Zhao, Z. Liu, Z. Liu, K. Wang, G. Li and J. Jiang, *Chinese Chem. Lett.*, 2020, **31**, 1822–1826.
- 198 C. C. Deng, W. L. A. Brooks, K. A. Abboud and B. S. Sumerlin, *ACS Macro Lett.*, 2015, **4**, 220–224.
- 199 J. Hu, Q. Hu, X. He, C. Liu, Y. Kong, Y. Cheng and Y. Zhang, *Adv. Healthc. Mater.*, 2020, **9**, 1901329.
- 200 Y. Li, Y. Liu, R. Ma, Y. Xu, Y. Zhang, B. Li, Y. An and L. Shi, *ACS Appl. Mater. Interfaces*, 2017, **9**, 13056–13067.
- 201 C. Arnal-Hérault, A. Pasc, M. Michau, D. Cot, E. Petit and M. Barboiu, *Angew. Chem. Int. Ed.*, 2007, **46**, 8409–8413.
- 202 S. Mihai, Y. Le Duc, D. Cot and M. Barboiu, *J. Mater. Chem.*, 2010, **20**, 9443–9448.
- 203 A. Biswas, T. Ghosh, P. K. Gavel and A. K. Das, *ACS Appl. Bio Mater.*, 2020, **3**, 1052–1060.
- 204 A. Sikora, J. Zielonka, M. Lopez, J. Joseph and B. Kalyanaraman, *Free Radic. Biol. Med.*, 2009, **47**, 1401–1407.



- 205 K. Debowska, D. Debski, M. Hardy, M. Jakubowska, B. Kalyanaraman, A. Marcinek, R. Michalski, B. Michalowski, O. Ouari, A. Sikora, R. Smulik and J. Zielonka, *Pharmacol. Reports*, 2015, **67**, 756–764.
- 206 L. Wu, A. C. Sedgwick, X. Sun, S. D. Bull, X. P. He and T. D. James, *Acc. Chem. Res.*, 2019, **52**, 2582–2597.
- 207 J. Yu, H. Chao, G. Li, R. Tang, Z. Liu, Z. Liu and J. Jiang, *Macromol. Chem. Phys.*, 2018, **219**, 1800346.
- 208 Y. Liu, G. Li, J. Chen, Z. Liu, Z. Liu and J. Jiang, *Macromol. Rapid Commun.*, 2017, **38**, 1600805.
- 209 X. Zhang, G. Li, Z. Liu, Z. Liu and J. Jiang, *Macromol. Chem. Phys.*, 2020, **221**, 2000022.
- 210 R. Cheng, G. Li, L. Fan, Z. Liu, Z. Liu and J. Jiang, *J. Mater. Chem. B*, 2018, **6**, 7800–7804.
- 211 R. Cheng, G. Li, L. Fan, J. Jiang and Y. Zhao, *Chem. Commun.*, 2020, **56**, 12246–12249.
- 212 R. Ma, C. Zhang, Y. Liu, C. Li, Y. Xu, B. Li, Y. Zhang, Y. An and L. Shi, *RSC Adv.*, 2017, **7**, 21328–21335.
- 213 B. Akgun and D. G. Hall, *Angew. Chem. Int. Ed.*, 2018, **57**, 13028–13044.
- 214 J. P. M. António, R. Russo, C. P. Carvalho, P. M. S. D. Cal and P. M. P. Gois, *Chem. Soc. Rev.*, 2019, **48**, 3513–3536.
- 215 S. Cambray and J. Gao, *Acc. Chem. Res.*, 2018, **51**, 2198–2206.
- 216 S. Chatterjee, E. V. Anslyn and A. Bandyopadhyay, *Chem. Sci.*, 2021, **23**, 1585–1599.
- 217 A. Bandyopadhyay and J. Gao, *Chem. - A Eur. J.*, 2015, **21**, 14748–14752.
- 218 P. M. S. D. Cal, J. B. Vicente, E. Pires, A. V. Coelho, L. F. Veiros, C. Cordeiro and P. M. P. Gois, *J. Am. Chem. Soc.*, 2012, **134**, 10299–10305.
- 219 X. Liu, Z. Li, H. Xu, Y. Zhan, P. Ma, H. Chen and B. Jiang, *Tetrahedron Lett.*, 2017, **58**, 3101–3106.
- 220 H. Gu, T. I. Chio, Z. Lei, R. J. Staples, J. S. Hirschi and S. Bane, *Org. Biomol. Chem.*, 2017, **15**, 7543–7548.
- 221 O. Dilek, Z. Lei, K. Mukherjee and S. Bane, *Chem. Commun.*, 2015, **51**, 16992–16995.
- 222 H. Gu, S. Ghosh, R. J. Staples and S. L. Bane, *Bioconjug. Chem.*, 2019, **30**, 2604–2613.
- 223 A. Bandyopadhyay, S. Cambray and J. Gao, *J. Am. Chem. Soc.*, 2017, **139**, 871–878.
- 224 H. Faustino, M. J. S. A. Silva, L. F. Veiros, G. J. L. Bernardes and P. M. P. Gois, *Chem. Sci.*, 2016, **7**, 5052–5058.
- 225 T. S. L. Tang, D. Cardella, A. J. Lander, X. Li, J. S. Escudero, Y.-H. Tsai and L. Y. P. Luk, *Chem. Sci.*, 2020, **11**, 5881–5888.
- 226 M. Palucki, P. J. Pospisil and W. Zhang, *J. Am. Chem. Soc.*, 1994, **116**, 9333–9334.
- 227 A. Bandyopadhyay and J. Gao, *J. Am. Chem. Soc.*, 2016, **138**, 2098–2101.
- 228 K. Li and J. Gao, *Synlett*, 2017, **28**, 1913–1916.
- 229 S. Borsley and S. L. Cockroft, *ACS Nano*, 2018, **12**, 786–794.
- 230 P. M. S. D. Cal, R. F. M. Frade, V. Chudasama, C. Cordeiro, S. Caddick and P. M. P. Gois, *Chem.*

- Commun.*, 2014, **50**, 5261–5263.
- 231 P. M. S. D. Cal, R. F. M. Frade, C. Cordeiro and P. M. P. Gois, *Chem. - A Eur. J.*, 2015, **21**, 8182–8187.
  - 232 G. Akçay, M. A. Belmonte, B. Aquila, C. Chuaqui, A. W. Hird, M. L. Lamb, P. B. Rawlins, N. Su, S. Tentarelli, N. P. Grimster and Q. Su, *Nat. Chem. Biol.*, 2016, **12**, 931–936.
  - 233 A. Bandyopadhyay, K. A. McCarthy, M. A. Kelly and J. Gao, *Nat. Commun.*, 2015, **6**, 6561.
  - 234 M. Kelly, S. Cambray, K. A. McCarthy, W. Wang, E. Geisinger, J. Ortiz-Marquez, T. Van Opijnen and J. Gao, *ACS Infect. Dis.*, 2020, **6**, 2410–2418.
  - 235 K. A. McCarthy, M. A. Kelly, K. Li, S. Cambray, A. S. Hosseini, T. Van Opijnen and J. Gao, *J. Am. Chem. Soc.*, 2018, **140**, 6137–6145.
  - 236 A. J. van der Zouwen, A. Jeucken, R. Steneker, K. F. Hohmann, J. Lohse, D. J. Slotboom and M. Witte, *Chem. – A Eur. J.*, 2020, **27**, 3292–3296.
  - 237 S. Palvai, J. Bhangu, B. Akgun, C. T. Moody, D. G. Hall and Y. Brudno, *Bioconjug. Chem.*, 2020, **31**, 2288–2292.
  - 238 B. Akgun, C. Li, Y. Hao, G. Lambkin, R. Derda and D. G. Hall, *J. Am. Chem. Soc.*, 2017, **139**, 14285–14291.
  - 239 R. Russo, R. Padanha, F. Fernandes, L. Veiros, F. Corzana and P. M. P. Gois, *Chem. – A Eur. J.*, 2020, **26**, 15226–15231.
  - 240 R. R. Groleau, T. D. James and S. D. Bull, *Coord. Chem. Rev.*, 2021, **428**, 213599.
  - 241 F. A. Davis, R. E. Reddy, J. M. Szewczyk, G. V. Reddy, P. S. Portonovo, H. Zhang, D. Fanelli, R. T. Reddy, P. Zhou and P. J. Carroll, *J. Org. Chem.*, 1997, **62**, 2555–2563.
  - 242 H.-Q. Dong, M.-H. Xu, C.-G. Feng, X.-W. Sun and G.-Q. Lin, *Org. Chem. Front.*, 2015, **2**, 73–89.
  - 243 F. A. Davis, *J. Org. Chem.*, 2006, **71**, 8993–9003.
  - 244 P. Zhou, B.-C. Chen and F. A. Davis, *Tetrahedron*, 2004, **60**, 8006–8030.
  - 245 C. Achuenu, S. Carret, J. Poisson and F. Berthiol, *Eur. J. Org. Chem.*, 2020, **2020**, 5901–5916.
  - 246 R. Bentley, *Chem. Soc. Rev.*, 2005, **34**, 609–624.
  - 247 M. J. S. Dewar and W. B. Jennings, *J. Am. Chem. Soc.*, 1971, **93**, 401–403.
  - 248 J. J. Petkowski, W. Bains and S. Seager, *J. Nat. Prod.*, 2018, **81**, 423–446.
  - 249 N. Gould, P. T. Doulias, M. Tenopoulou, K. Raju and H. Ischiropoulos, *J. Biol. Chem.*, 2013, **288**, 26473–26479.
  - 250 S. R. Tannenbaum and J. E. Kim, *Nat. Chem. Biol.*, 2005, **1**, 126–127.
  - 251 G. Keceli and J. P. Toscano, *Biochemistry*, 2014, **53**, 3689–3698.
  - 252 G. Keceli and J. P. Toscano, *Biochemistry*, 2012, **51**, 4206–4216.
  - 253 G. Keceli, C. D. Moore, J. W. Labonte and J. P. Toscano, *Biochemistry*, 2013, **52**, 7387–7396.
  - 254 H. Grigoryan, H. Li, A. T. Iavarone, E. R. Williams and S. M. Rappaport, *Chem. Res. Toxicol.*, 2012, **25**, 1633–1642.

- 255 G. M. Johnson, T. J. Chozinski, E. S. Gallagher, C. A. Aspinwall and K. M. Miranda, *Free Radic. Biol. Med.*, 2014, **76**, 299–307.
- 256 V. K. Aggarwal, N. Barbero, E. M. McGarrigle, G. Mickle, R. Navas, J. Ramón Suárez, M. G. Unthank and M. Yar, *Tetrahedron Lett.*, 2009, **50**, 3482–3484.
- 257 M. T. Robak, M. A. Herbage and J. A. Ellman, *Chem. Rev.*, 2010, **110**, 3600–3740.
- 258 M. Wakayama and J. A. Ellman, *J. Org. Chem.*, 2009, **74**, 2646–2650.
- 259 S. Wen, K. L. Carey, Y. Nakao, N. Fusetani, G. Packham and A. Ganesan, *Org. Lett.*, 2007, **9**, 1105–1108.
- 260 J. W. Evans and J. A. Ellman, *J. Org. Chem.*, 2003, **68**, 9948–9957.
- 261 Z.-J. Liu, Y.-Q. Mei and J.-T. Liu, *Tetrahedron*, 2007, **63**, 855–860.
- 262 J. C. Barrow, P. L. Ngo, J. M. Pellicore, H. G. Selnick and P. G. Nantermet, *Tetrahedron Lett.*, 2001, **42**, 2051–2054.
- 263 A. Viso, R. Fernández De La Pradilla, M. L. López-Rodríguez, A. García, A. Flores and M. Alonso, *J. Org. Chem.*, 2004, **69**, 1542–1547.
- 264 K. W. Kells and J. M. Chong, *Org. Lett.*, 2003, **5**, 4215–4218.
- 265 L. P. Jayathilaka, M. Deb and R. F. Standaert, *Org. Lett.*, 2004, **6**, 3659–3662.
- 266 T. P. Tang and J. A. Ellman, *J. Org. Chem.*, 2002, **67**, 7819–7832.
- 267 Z. Han, S. G. Koenig, H. Zhao, X. Su, S. P. Singh and R. P. Bakale, *Org. Process Res. Dev.*, 2007, **11**, 726–730.
- 268 W. Y. Zhang, P. C. Hogan, C. L. Chen, J. Niu, Z. Wang, D. Lafrance, O. Gilicky, N. Dunwoody and M. Ronn, *Org. Process Res. Dev.*, 2015, **19**, 1784–1795.
- 269 D. A. Thaisrivongs, J. R. Naber, N. J. Rogus and G. Spencer, *Org. Process Res. Dev.*, 2018, **22**, 403–408.
- 270 K. Brak and J. A. Ellman, *Org. Lett.*, 2010, **12**, 2004–2007.
- 271 N. J. Oldenhuis, V. M. Dong and Z. Guan, *J. Am. Chem. Soc.*, 2014, **136**, 12548–12551.
- 272 P. Dinér, A. Sadhukhan and B. Blomkvist, *ChemCatChem*, 2014, **6**, 3063–3066.
- 273 K. L. Kimmel, M. A. T. Robak and J. A. Ellman, *J. Am. Chem. Soc.*, 2009, **131**, 8754–8755.
- 274 K. L. Kimmel, M. T. Robak, S. Thomas, M. Lee and J. A. Ellman, *Tetrahedron*, 2012, **68**, 2704–2712.
- 275 K. L. Kimmel, J. D. Weaver and J. A. Ellman, *Chem. Sci.*, 2012, **3**, 121–125.
- 276 M. T. Robak, M. Trincado and J. A. Ellman, *J. Am. Chem. Soc.*, 2007, **129**, 15110–15111.
- 277 L. G. Borrego, R. Recio, E. Álvarez, A. Sánchez-Coronilla, N. Khiar and I. Fernandez, *Org. Lett.*, 2019, **21**, 6513–6518.
- 278 E. Wojaczyńska and J. Wojaczyński, *Chem. Rev.*, 2020, **120**, 4578–4611.
- 279 P. K. T. Lo, G. A. Oliver and M. C. Willis, *J. Org. Chem.*, 2020, **85**, 5753–5760.
- 280 G. R. Revankar, N. B. Hanna, N. Imamura, A. F. Lewis, S. B. Larson, R. A. Finch, T. L. Avery and R. K. Robins, *J. Med. Chem.*, 1990, **33**, 121–128.

- 281 China, CN108440349, 2018.
- 282 J. Liao, X. Sun, X. Cui, K. Yu, J. Zhu and J. Deng, *Chem. - A Eur. J.*, 2003, **9**, 2611–2615.
- 283 C. K. Savile, V. P. Magloire and R. J. Kazlauskas, *J. Am. Chem. Soc.*, 2005, **127**, 2104–2113.
- 284 P. F. Mugford, V. P. Magloire and R. J. Kazlauskas, *J. Am. Chem. Soc.*, 2005, **127**, 6536–6537.
- 285 D. A. Cogan, G. Liu, K. Kim, B. J. Backes and J. A. Ellman, *J. Am. Chem. Soc.*, 1998, **120**, 8011–8019.
- 286 D. J. Weix and J. A. Ellman, *Org. Lett.*, 2003, **5**, 1317–1320.
- 287 Y. Zhang, S. Chitale, N. Goyal, G. Li, Z. S. Han, S. Shen, S. Ma, N. Grinberg, H. Lee, B. Z. Lu and C. H. Senanayake, *J. Org. Chem.*, 2012, **77**, 690–695.
- 288 K. K. Andersen, W. Gaffield, N. E. Papanikolaou, J. W. Foley and R. I. Perkins, *J. Am. Chem. Soc.*, 1964, **86**, 5637–5646.
- 289 R. Annunziata, M. Cinquini and F. Cozzi, *J. Chem. Soc. Perkin Trans. 1*, 1982, 339–343.
- 290 P. Decroos, Z. S. Han, K. Sidhu, J. Lorenz, L. Nummy, D. Byrne, B. Qu, Y. Xu, L. Wu, H. Lee, F. Roschangar, J. J. Song and C. H. Senanayake, *Org. Process Res. Dev.*, 2019, **23**, 263–268.
- 291 Z. S. Han, M. A. Herbage, H. P. R. Mangunuru, Y. Xu, L. Zhang, J. T. Reeves, J. D. Sieber, Z. Li, P. DeCroos, Y. Zhang, G. Li, N. Li, S. Ma, N. Grinberg, X. Wang, N. Goyal, D. Krishnamurthy, B. Lu, J. J. Song, G. Wang and C. H. Senanayake, *Angew. Chem. Int. Ed.*, 2013, **52**, 6713–6717.
- 292 Z. Han, D. Krishnamurthy, P. Grover, Q. K. Fang and C. H. Senanayake, *J. Am. Chem. Soc.*, 2002, **124**, 7880–7881.
- 293 D. J. Weix and J. A. Ellman, *Org. Synth.*, 2005, **82**, 157–165.
- 294 R. R. Groleau, R. S. L. Chapman, H. Ley-Smith, L. Liu, T. D. James and S. D. Bull, *J. Org. Chem.*, 2020, **85**, 1208–1215.
- 295 I. Fernández, A. Alcudia, B. Gori, V. Valdivia, R. Recio, M. V. García and N. Khiar, *Org. Biomol. Chem.*, 2010, **8**, 4388–4393.
- 296 S. Li, L. Zhang, J. Jiang, Y. Meng and M. Liu, *Appl. Mater. Interfaces*, 2017, **9**, 37386–37394.
- 297 V. A. Soloshonok and K. D. Klika, *Helv. Chim. Acta*, 2014, **97**, 1583–1589.
- 298 V. A. Soloshonok, *Angew. Chem. Int. Ed.*, 2006, **45**, 766–769.
- 299 K. C. Cundy and P. A. Crooks, *J. Chromatogr. A*, 1983, **281**, 17–33.
- 300 C. P. Brock, W. B. Schweizer and J. D. Dunitz, *J. Am. Chem. Soc.*, 1991, **113**, 9811–9820.
- 301 K.-H. Ernst, *Chim. Int. J. Chem.*, 2018, **72**, 399–403.
- 302 O. Wallach, *Justus Liebig's Ann. der Chemie*, 1895, **286**, 119–143.
- 303 E. Tokunaga, T. Yamamoto, E. Ito and N. Shibata, *Sci. Rep.*, 2018, **8**, 1–7.
- 304 T. Katagiri, C. Yoda, K. Furuhashi, K. Ueki and T. Kubota, *Chem. Lett.*, 1996, 115–116.
- 305 M. Yasumoto, H. Ueki and V. A. Soloshonok, *J. Fluor. Chem.*, 2010, **131**, 540–544.
- 306 J. Han, D. J. Nelson, A. E. Soroichinsky and V. A. Soloshonok, *Curr. Org. Synth.*, 2011, **8**, 310–317.

- 307 H. Kwart and D. P. Hoster, *J. Org. Chem.*, 1967, **32**, 1867–1870.
- 308 J. Han, O. Kitagawa, A. Wzorek, K. D. Klika and V. A. Soloshonok, *Chem. Sci.*, 2018, **9**, 1718–1739.
- 309 G. Storch, M. Haas and O. Trapp, *Chem. Eur. J.*, 2017, **23**, 5414–5418.
- 310 V. Nieminen, D. Y. Murzin and K. D. Klika, *Org. Biomol. Chem.*, 2009, **7**, 537–542.
- 311 V. A. Soloshonok, C. Roussel, O. Kitagawa and A. E. Sorochinskaya, *Chem. Soc. Rev.*, 2012, **41**, 4180–4188.
- 312 Z. Szakács, Z. Sánta, A. Lomoschitz and C. Szántay, *Trends Anal. Chem.*, 2018, **109**, 180–197.
- 313 A. Baumann, A. Wzorek, V. A. Soloshonok, K. D. Klika and A. K. Miller, *Symmetry*, 2020, **12**, 1106.
- 314 P. Borowiecki, *Tetrahedron Asymmetry*, 2015, **26**, 16–23.
- 315 Z. Xu, Q. Wang and J. Zhu, *J. Am. Chem. Soc.*, 2015, **137**, 6712–6724.
- 316 S. D. Bergman and M. Kol, *Inorg. Chem.*, 2005, **44**, 1647–1654.
- 317 P. Dhanishta, P. Sai Siva Kumar, S. K. Mishra and N. Suryaprakash, *RSC Adv.*, 2018, **8**, 11230–11240.
- 318 C. Guzmán-Afonso, Y. lee Hong, H. Colaux, H. Iijima, A. Saitow, T. Fukumura, Y. Aoyama, S. Motoki, T. Oikawa, T. Yamazaki, K. Yonekura and Y. Nishiyama, *Nat. Commun.*, 2019, **10**, 1–10.
- 319 S. K. Mishra and N. Suryaprakash, *Molecules*, 2017, **22**, 423.
- 320 M. Majumder and N. Sathyamurthy, *Theor. Chem. Acc.*, 2012, **131**, 1–11.
- 321 I. Katsuyama, A. A. Khalil, C. Dunbar and J. K. Zjawiony, *Spectrosc. Lett.*, 2003, **36**, 477–485.
- 322 S. Latypov, M. A. Fakhfakh, J. C. Jullian, X. Franck, R. Hocquemiller and B. Figadère, *Bull. Chem. Soc. Jpn.*, 2005, **78**, 1296–1301.
- 323 A. Mitra, P. J. Seaton, R. A. Assarpour and T. Williamson, *Tetrahedron*, 1998, **54**, 15489–15498.
- 324 J. Song, H. Wang and M. Li, *J. Mol. Struct.*, 2015, **1079**, 250–257.
- 325 A. S. Shetty, J. Zhang and J. S. Moore, *J. Am. Chem. Soc.*, 1996, **118**, 1019–1027.
- 326 Z. Dega-Szafran and E. Dulewicz, *Org. Magn. Reson.*, 1981, **16**, 214–219.
- 327 R. Evans, Z. Deng, A. K. Rogerson, A. S. McLachlan, J. J. Richards, M. Nilsson and G. A. Morris, *Angew. Chem.*, 2013, **125**, 3281–3284.
- 328 R. Evans, G. Dal Poggetto, M. Nilsson and G. A. Morris, *Anal. Chem.*, 2018, **90**, 3987–3994.
- 329 A. S. Virk, A. M. Torres, S. A. Willis and W. S. Price, *J. Mol. Liq.*, 2016, **214**, 157–161.
- 330 A. M. Kelly, PhD Thesis, University of Bath, 2008.
- 331 C. E. Lin, W. C. Chiou and W. C. Lin, *J. Chromatogr. A*, 1996, **723**, 189–195.
- 332 SCRF | Gaussian.com, <https://gaussian.com/scrf/>, (accessed 7 March 2021).
- 333 K. S. Eccles, R. E. Morrison, C. A. Daly, G. E. O’Mahony, A. R. Maguire and S. E. Lawrence,

*CrystEngComm*, 2013, **15**, 7571–7575.

- 334 C. D. Roy and H. C. Brown, *Monatshefte für Chemie*, 2007, **138**, 747–753.
- 335 C. D. Roy and H. C. Brown, *Monatshefte für Chemie*, 2007, **138**, 879–887.
- 336 S. Higashibayashi, H. Tohmiya, T. Mori, K. Hashimoto and M. Nakata, *Synlett*, 2004, 457–460.
- 337 H. Mei, J. Han, S. Fustero, R. Román, R. Ruzziconi and V. A. Soloshonok, *J. Fluor. Chem.*, 2018, **216**, 57–70.
- 338 J. F. Collados, E. Toledano, D. Guijarro and M. Yus, *J. Org. Chem.*, 2012, **77**, 5744–5750.
- 339 W. Li, G. Kagan, R. Hopson and P. G. Williard, *J. Chem. Educ.*, 2011, **88**, 1331–1335.
- 340 J. L. G. Ruano, J. Alemán, A. Parra, B. Cid, K. Oisaki and M. Shibasaki, *Org. Synth.*, 2007, **84**, 129–138.
- 341 M. Das and D. F. O'Shea, *Org. Lett.*, 2016, **18**, 336–339.
- 342 H. Karoui and C. Ritchie, *Dalt. Trans.*, 2016, **45**, 18838–18841.
- 343 S. Garg, D. K. Unruh and C. Krempner, *Dalt. Trans.*, 2021, **50**, 5044–5049.
- 344 J. Di, H. He, F. Wang, F. Xue, X.-Y. Liu and Y. Qin, *Chem. Commun.*, 2018, **54**, 4692–4695.
- 345 J. Wallbaum, L. K. B. Garve, P. G. Jones and D. B. Werz, *Org. Lett.*, 2017, **19**, 98–101.
- 346 C. Ravi, D. Chandra Mohan and S. Adimurthy, *Org. Lett.*, 2014, **16**, 2978–2981.
- 347 H. Ghafari and M. M. Hashemi, *J. Sulfur Chem.*, 2009, **30**, 578–580.
- 348 F. Xue, F. Wang, J. Liu, J. Di, Q. Liao, H. Lu, M. Zhu, L. He, H. He, D. Zhang, H. Song, X. Liu and Y. Qin, *Angew. Chem. Int. Ed.*, 2018, **57**, 6667–6671.
- 349 C. Silva-Cuevas, C. Perez-Arrieta, L. A. Polindara-García and J. A. Lujan-Montelongo, *Tetrahedron Lett.*, 2017, **58**, 2244–2247.
- 350 S. H. Norton, S. M. Bachrach and J. M. Hayes, *J. Org. Chem.*, 2005, **70**, 5896–5902.
- 351 J. G. Tillett, *Chem. Rev.*, 1976, **76**, 747–772.
- 352 K. Kawaoka, A. U. Khan, D. R. Kearns, N. J. Turro, M.-F. Chow and J. Rigaudy, *J. Am. Chem. Soc.*, 1979, **101**, 1302–1303.
- 353 B. Bujnicki, J. Drabowicz and M. Mikołajczyk, *Molecules*, 2015, **20**, 2949–2972.
- 354 S. L. Yeste, PhD Thesis, University of Bath, 2007.
- 355 R. E. Booms and D. J. Cram, *J. Am. Chem. Soc.*, 1972, **94**, 5438–5446.
- 356 A. H. J. Engwerda, N. Koning, P. Tinnemans, H. Meekes, F. M. Bickelhaupt, F. P. J. T. Rutjes and E. Vlieg, *Cryst. Growth Des.*, 2017, **17**, 4454–4457.
- 357 C. Aurisicchio, E. Baciocchi, M. F. Gerini and O. Lanzalunga, *Org. Lett.*, 2007, **9**, 1939–1942.
- 358 H. Marom, P. U. Biedermann and I. Agranat, *Chirality*, 2007, **19**, 559–569.
- 359 D. R. Rayner, E. G. Miller, P. Bickart, A. J. Gordon and K. Mislow, *J. Am. Chem. Soc.*, 1966, **88**, 3138–3139.
- 360 M. Mikołajczyk and J. Drabowicz, *Top. Stereochem.*, 2007, **13**, 333–468.

- 361 V. Reddy Arava, L. Gorentla, P. K. Dubey and V. R. Arava, *Beilstein J. Org. Chem*, 2011, **7**, 9–12.
- 362 P. M. Wovkulich and M. R. Uskoković, *Tetrahedron*, 1985, **41**, 3455–3462.
- 363 L. Byrne, J. Solà, T. Boddaert, T. Marcelli, R. W. Adams, G. A. Morris and J. Clayden, *Angew. Chem. Int. Ed.*, 2014, **53**, 151–155.
- 364 M. Ilies, L. Di Costanzo, D. P. Dowling, K. J. Thorn and D. W. Christianson, *J. Med. Chem.*, 2011, **54**, 5432–5443.
- 365 H. Vogt and S. Bräse, *Org. Biomol. Chem.*, 2007, **5**, 406–430.
- 366 C. Toniolo, G. M. Bonora, A. Bavoso, E. Benedetti, B. di Blasio, V. Pavone and C. Pedone, *Biopolymers*, 1983, **22**, 205–215.
- 367 G. Zhao, S. S. Samanta, J. Michieletto and S. P. Roche, *Org. Lett.*, 2020, **22**, 5822–5827.
- 368 J. E. Hein and D. G. Blackmond, *Acc. Chem. Res.*, 2012, **45**, 2045–2054.
- 369 H. Abas, J. Mas-Roselló, M. M. Amer, D. J. Durand, R. R. Groleau, N. Fey and J. Clayden, *Angew. Chem. Int. Ed.*, 2019, **58**, 2418–2422.
- 370 A. von Baeyer and V. Villiger, *Chem. Ber.*, 1899, **32**, 3625–3633.
- 371 G. R. Krow, in *Organic Reactions*, John Wiley & Sons, Inc., Hoboken, NJ, USA, 1993, pp. 251–798.
- 372 X. Cui and J. Shi, *Sci. China Mater.*, 2016, **59**, 675–700.
- 373 G.-J. ten Brink, I. W. C. E. Arends and R. A. Sheldon, *Chem. Rev.*, 2004, **104**, 4105–4123.
- 374 C. Jiménez-Sanchidrián and J. R. Ruiz, *Tetrahedron*, 2008, **64**, 2011–2026.
- 375 F. E. Ziegler and H. Kim, *Tetrahedron Lett.*, 1993, **34**, 7669–7672.
- 376 R. Llamas, C. Jiménez-Sanchidrián and J. R. Ruiz, *React. Kinet. Catal. Lett.*, 2007, **90**, 309–313.
- 377 W. von. E. Doering and L. Speers, *J. Am. Chem. Soc.*, 1950, **72**, 5515–5518.
- 378 W. Von, E. Doering and E. Dorfman, *J. Am. Chem. Soc.*, 1953, **75**, 5595–5598.
- 379 S. L. Friess, *J. Am. Chem. Soc.*, 1949, **71**, 2571–2575.
- 380 M. Snowden, A. Bermudez, D. R. Kelly and J. L. Radkiewicz-Poutsma, *J. Org. Chem.*, 2004, **69**, 7148–7156.
- 381 J. R. Alvarez-Idaboy, L. Reyes and N. Mora-Diez, *Org. Biomol. Chem.*, 2007, **5**, 3682–3689.
- 382 L. Reyes, M. Castro, J. Cruz and M. Rubio, *J. Phys. Chem. A*, 2005, **109**, 3383–3390.
- 383 J. Clayden, N. Greeves and S. G. Warren, *Organic chemistry*, Oxford University Press, New York, 2nd edn., 2012.
- 384 A. Cutignano, V. Notti, G. d'Ippolito, A. Domenech Coll, G. Cimino and A. Fontana, *Org. Biomol. Chem.*, 2004, **2**, 31671–3171.
- 385 X. Wu, H. Gao, W. Sun, J. Yu, H. Hu, Q. Xu and X. Chen, *Phyther. Res.*, 2017, **31**, 1072–1077.
- 386 Y. Fukuyama, H. Minami, M. Kagawa, M. Kodama and K. Kawazu, *J. Nat. Prod.*, 1999, **62**, 337–339.

- 387 J. Xie and Y. Hsieh, *J. Polym. Sci. Part A Polym. Chem.*, 2001, **39**, 1931–1939.
- 388 H. Yang, E. Henke and U. T. Bornscheuer, *J. Org. Chem.*, 1998, **64**, 1709–1712.
- 389 G. Roscher, in *Ullmann's Encyclopedia of Industrial Chemistry*, Wiley-VCH Verlag GmbH & Co. KGaA, Weinheim, Germany, 2000.
- 390 Z. Zha and P. Deshlahra, *ACS Catal.*, 2021, **11**, 1841–1857.
- 391 M. Rotem and Y. Shvo, *Organometallics*, 1983, **2**, 1689–1691.
- 392 A. Lumbroso, N. R. Vautravers and B. Breit, *Org. Lett.*, 2010, **12**, 5498–5501.
- 393 D. Yang, S. Ding, J. Huang and K. Zhao, *Chem. Commun.*, 2013, **49**, 1211.
- 394 M. S. Chen and M. C. White, *J. Am. Chem. Soc.*, 2004, **126**, 1346–1347.
- 395 Böeseken, J. - CHG, <https://chg.kncv.nl/boeseken>, (accessed 24 March 2021).
- 396 A. F. Holleman, *Recl. des Trav. Chim. des Pays-Bas*, 1938, **57**, 489–491.
- 397 N. Prileschajew, *Oxydation ungesättigter Verbindungen mittels Org. Superoxyde*, 1909, **42**, 4811–4815.
- 398 Z. Wang, in *Comprehensive Organic Name Reactions and Reagents*, John Wiley & Sons, Inc., Hoboken, NJ, USA, 2010, pp. 3976–3979.
- 399 J. Böeseken and A. Kremer, *Recl. des Trav. Chim. des Pays-Bas*, 1931, **50**, 827–832.
- 400 J. Böeseken and A. L. Soesman, *Recl. des Trav. Chim. des Pays-Bas*, 1933, **52**, 874–880.
- 401 Böeseken and J. Jacobs, *Recl. des Trav. Chim. des Pays-Bas*, 1936, **55**, 786–790.
- 402 J. Böeseken and J. S. P. Blumberger, *Recl. des Trav. Chim. des Pays-Bas*, 1925, **44**, 90–95.
- 403 J. Böeseken, *Recl. des Trav. Chim. des Pays-Bas*, 1926, **45**, 838–844.
- 404 Z. Wang, in *Comprehensive Organic Name Reactions and Reagents*, John Wiley & Sons, Inc., Hoboken, NJ, USA, 2010.
- 405 H. M. Walton, *J. Org. Chem.*, 1957, **22**, 1161–1165.
- 406 E. Caspi, Y. W. Chang and R. I. Dorfman, *J. Med. Chem.*, 1962, **5**, 714–719.
- 407 J. Böeseken, W. D. Cohen and C. J. Kip, *Recl. des Trav. Chim. des Pays-Bas*, 1936, **55**, 815–820.
- 408 J. Böeseken and J. Greup, *Recl. des Trav. Chim. des Pays-Bas*, 1939, **58**, 528–537.
- 409 H. D. Dakin, *Am. Chem. J.*, 1909, **42**, 477–498.
- 410 US. Pat., 3058995, 1962.
- 411 US Pat., 3927122, 1975.
- 412 L. Syper, *Tetrahedron*, 1987, **43**, 2853–2871.
- 413 J. A. Guzmán, V. Mendoza, E. García, C. F. Garibay, L. Z. Olivares and L. A. Maldonado, *Synth. Commun.*, 1995, **25**, 2121–2133.
- 414 L. Yu, Y. Wu, H. Cao, X. Zhang, X. Shi, J. Luan, T. Chen, Y. Pan and Q. Xu, *Green Chem.*, 2014, **16**, 287–293.



- 415 L. Yu, Z. Bai, X. Zhang, X. Zhang, Y. Ding and Q. Xu, *Catal. Sci. Technol.*, 2016, **6**, 1804–1809.
- 416 X. Zhang, J. Ye, L. Yu, I. Shi, M. Zhang, Q. Xu and M. Lautens, *Adv. Synth. Catal*, 2015, **357**, 955–960.
- 417 B. Poladura, A. Martinez-Castaneda, H. Rodriguez-Solla, R. Llavona, C. Concellón and V. del Amo, *Org. Lett.*, 2013, **15**, 2810–2813.
- 418 R. Lawrence, PhD Thesis, University of Bath, 2016.
- 419 E. Wenkert and M. Rubin, *Nature*, 1952, **170**, 708–709.
- 420 R. Tank, *Synlett*, 2007, **2007**, 664–665.
- 421 N. Jalalian and B. Olofsson, *Org. Synth.*, 2013, **90**, 1–9.
- 422 A. Horn and U. Kizmaier, *Eur. J. Org. Chem.*, 2018, **2018**, 2531–2536.
- 423 R. S. L. Chapman, R. Lawrence, J. M. J. Williams and S. D. Bull, *Org. Lett.*, 2017, **19**, 4908–4911.
- 424 R. S. L. Chapman, M. Francis, R. Lawrence, J. D. Tibbetts and S. D. Bull, *Tetrahedron*, 2018, **74**, 6442–6452.
- 425 A. D. Adleb, F. R. Longo, J. D. Finarelli, J. Goldmacher, J. Assour, L. Korsakoff, A. D. Adler, F. R. Longo and W. Shergalis, *A second paper on further studies is in preparation*, 1964, vol. 32.
- 426 A. DeBoer and R. E. Ellwanger, *J. Org. Chem.*, 1974, **39**, 77–83.
- 427 P. W. Baures, D. S. Eggleston, J. R. Flisak, K. Gombatz, I. Lantos, W. Mendelson and J. J. Remich, *Tetrahedron Lett.*, 1990, **31**, 6501–6504.
- 428 G. P. Boldrini, M. Bortolotti, F. Mancini, E. Tagliavini, C. Trombini and A. Umani-Ronchi, *J. Org. Chem.*, 1991, **56**, 5820–5826.
- 429 M. Kuse and M. Isobe, *Tetrahedron*, 2000, **56**, 2629–2639.
- 430 S. Bull, W. B. Cunningham, J. D. Tibbetts, M. Hutchby, K. A. Smug, M. G. Davidson, U. Hintermair and P. Plucinski, *Green Chem.*, 2020, **22**, 513–524.
- 431 Y. Fujise, K. Fujiwara and Y. Ito, *Chem. Lett.*, 1988, **9**, 1475–1476.
- 432 G. W. Burton, J. Daroszewski, J. G. Nickerson, J. B. Johnston, T. J. Mogg and G. B. Nikiforov, *Can. J. Chem.*, 2014, **92**, 305–316.
- 433 R. A. Michelin, P. Sgarbossa, A. Scarso and G. Strukul, *Coord. Chem. Rev.*, 2010, **254**, 646–660.
- 434 M. Del Todesco Frisone, F. Pinna and G. Strukul, *Organometallics*, 1993, **12**, 148–156.
- 435 J. K. Whitesell, R. Matthews and A. M. Helbling, *J. Org. Chem.*, 1978, **43**, 784–786.
- 436 Y. Okuno, *Chem. - A Eur. J.*, 1997, **3**, 212–218.
- 437 R. D. Bach, *J. Org. Chem.*, 2012, **77**, 6801–6815.
- 438 S. Yamabe and S. Yamazaki, *J. Org. Chem.*, 2007, **72**, 3031–3041.
- 439 Y. Ogata and Y. Sawaki, *J. Org. Chem.*, 1972, **37**, 2953–2957.
- 440 S. Bhunia, A. Rana, S. Ghosh, A. Ivancich and A. Dey, *Chem. Sci.*, 2020, **11**, 2681–2695.

- 441 R. C. Weast, Ed., *Handbook of Chemistry and Physics*, CRC Press Inc., Boca Raton, Florida, 60th editi., 1979, vol. 17.
- 442 J. R. Alvarez-Idaboy, L. Reyes and J. Cruz, *Org. Lett.*, 2006, **8**, 1763–1765.
- 443 L. Reyes, J. R. Alvarez-Idaboy and N. Mora-Diez, *J. Phys. Org. Chem.*, 2009, **22**, 643–649.
- 444 A. Petrosyan, R. Hauptmann and J. Pospech, *Eur. J. Org. Chem.*, 2018, **2018**, 5237–5252.
- 445 J. Berdys, M. Makowski, M. Makowska, A. Puszko and L. Chmurzyński, *J. Phys. Chem. A*, 2003, **107**, 6293–6300.
- 446 R. C. Wast, Ed., *CRC Handbook of Chemistry and Physics: Student Edition*, CRC Press, Boca Raton, 1st edn., 1988, vol. 17.
- 447 I. Alkorta and J. Elguero, *J. Phys. Chem. A*, 1999, **103**, 272–279.
- 448 P. Mech, M. Bogunia, A. Nowacki and M. Makowski, *J. Phys. Chem. A*, 2020, **124**, 538–551.
- 449 A. J. K. Roth, M. Tretbar and C. B. W. Stark, *Chem. Commun.*, 2015, **51**, 14175–14178.
- 450 A. K. C. Schmidt and C. B. W. Stark, *Org. Lett.*, 2011, **13**, 4164–4167.
- 451 V. Pansevich-Kolyada, *Zhurnal Obs. Khimii*, 1967, **37**, 745–746.
- 452 Eur. Pat., 0168719, 1985.
- 453 C. R. Birnie, D. Malamud and R. L. Schnaare, *Antimicrob. Agents Chemother.*, 2000, **44**, 2514–2517.
- 454 US Pat., 3277003, 1964.
- 455 T. Rosenau, A. Potthast, H. Sixta and P. Kosma, *Prog. Polym. Sci.*, 2001, **26**, 1763–1837.
- 456 Y. Wang, Q. Gao, Z. Liu, S. Bai, X. Tang, H. Yin and Q. Meng, *J. Org. Chem.*, 2018, **83**, 2263–2273.
- 457 Y. Wang, H. Yin, X. Tang, Y. Wu, Q. Meng and Z. Gao, *J. Org. Chem.*, 2016, **81**, 7042–7050.
- 458 R. Tandon, T. A. Nigst and H. Zipse, *Eur. J. Org. Chem.*, 2013, **2013**, 5423–5430.
- 459 T. J. Lang, G. J. Wolber and R. D. Bach, *J. Am. Chem. Soc.*, 1981, **103**, 3275–3282.
- 460 V. G. Dryuk, *Tetrahedron*, 1976, **32**, 2855–2866.
- 461 G. A. Olah, D. G. Parker and N. Yoneda, *Angew. Chem. Int. Ed.*, 1978, **17**, 909–931.
- 462 R. D. Bach, C. Canepa, J. E. Winter and P. E. Blanchette, *J. Org. Chem.*, 1997, **62**, 5191–5197.
- 463 H. Shi, Z. Zhang and Y. Wang, *J. Mol. Catal. A Chem.*, 2005, **238**, 13–25.
- 464 M. Gopiraman, H. Bang, S. G. Babu, K. Wei, R. Karvembu and I. S. Kim, *Catal. Sci. Technol.*, 2014, **4**, 2099–2106.
- 465 K. M. Roberts and J. P. Jones, *Chem. - A Eur. J.*, 2010, **16**, 8096–8107.
- 466 Z. Yuan, Y. Ni and A. R. P. Van Heiningen, *Can. J. Chem. Eng.*, 1997, **75**, 37–41.
- 467 X. Zhao, T. Zhang, Y. Zhou and D. Liu, *J. Mol. Catal. A Chem.*, 2007, **271**, 246–252.
- 468 Y. Qu and D. W. Bolen, *Biochemistry*, 2003, **42**, 5837–5849.
- 469 R. M. Silva, L. T. Okano, J. A. R. Rodrigues and G. C. Clososki, *Tetrahedron Asymmetry*, 2017,

**28**, 939–944.

- 470 G. L. Larson, C. F. de Kaifer, R. Seda, L. E. Torres and J. Roberto Ramirez, *J. Org. Chem.*, 1984, **49**, 3385–3386.
- 471 G. L. Larson and L. M. Fuentes, *J. te Am. Chem. Soc.*, 1981, **103**, 2418–2419.
- 472 J. Nagy and J. Réffy, *J. Organomet. Chem.*, 1970, **23**, 71–78.
- 473 J. M. Angelelli, J. C. Maire and Y. Vignollet, *J. Organomet. Chem.*, 1970, **22**, 313–319.
- 474 R. Gronheid, G. Lodder, M. Ochiai, T. Sueda and T. Okuyama, *J. Am. Chem. Soc.*, 2001, **123**, 8760–8765.
- 475 J. S. Sharley, A. María, C. P. Erez, E. E. Ferri, A. Fernandez Miranda and I. R. Baxendale, *Tetrahedron*, 2016, **72**, 2947–2954.
- 476 B. J. N Gardner and A. R. Katritzky, *J. Chem. Soc.*, 1957, 4375–4385.
- 477 S. F. Tsai and S. S. Lee, *Phytochemistry*, 2014, **101**, 121–127.
- 478 T. Murata, T. Miyase and F. Yoshizaki, *J. Nat. Med.*, 2011, **65**, 385–390.
- 479 G. C. Wang, T. Li, F. Y. Deng, Y. L. Li and W. C. Ye, *Bioorg. Med. Chem. Lett.*, 2013, **23**, 1379–1382.
- 480 W. Zhou, H. Xie, X. Xu, Y. Liang and X. Wei, *J. Funct. Foods*, 2014, **6**, 492–498.
- 481 R. Kubínová, E. Švajdlenka, K. Schneiderová, Z. Hanáková, S. Dall’Acqua and O. Farsa, *Biochem. Syst. Ecol.*, 2013, **49**, 39–42.
- 482 S. L. Ho, S. Tsai, C. Lin, H. Kim and S. Lee, *J. Drug Des. Med. Chem.*, 2020, **6**, 1–6.
- 483 S. Arihara, P. Rüedi and C. H. Eugster, *Helv. Chim. Acta*, 1975, **58**, 447–453.
- 484 J. D. Zhong, Y. Feng, H. M. Li, X. S. Xia and R. T. Li, *Nat. Prod. Res.*, 2016, **30**, 2278–2284.
- 485 B. M. Fraga, A. González-Coloma, S. Alegre-Gómez, M. López-Rodríguez, L. J. Amador and C. E. Díaz, *Phytochemistry*, 2017, **133**, 59–68.
- 486 D. V. Banthorpe, H. J. Bilyard and D. G. Watson, *Phytochemistry*, 1985, **24**, 2677–2680.
- 487 R. J. Grayer, M. R. Eckert, N. C. Veitch, G. C. Kite, P. D. Marin, T. Kokubun, M. S. J. Simmonds and A. J. Paton, *Phytochemistry*, 2003, **64**, 519–528.
- 488 Z. Y. Huang, B. Huang, C. J. Xiao, X. Dong and B. Jiang, *Nat. Prod. Res.*, 2015, **29**, 628–632.
- 489 D. V. Banthorpe, H. J. Bilyard and G. D. Brown, *Phytochemistry*, 1989, **28**, 2109–2113.
- 490 K. Lawrence, S. E. Flower, G. Kociok-Kohn, C. G. Frost and T. D. James, *Anal. Methods*, 2012, **4**, 2215–2217.
- 491 A. Jerschow and N. Müller, *J. Magn. Reson.*, 1997, **125**, 372–375.
- 492 A. Jerschow and N. Müller, *J. Magn. Reson. - Ser. A*, 1996, **123**, 222–225.
- 493 L. Wang, C. Dai, S. K. Burroughs, S. L. Wang and B. Wang, *Chem. Eur. J.*, 2013, **19**, 7587–7594.
- 494 L. Ma, G. Li, J. Huang, J. Zhu and Z. Tang, *Tetrahedron Lett.*, 2018, **59**, 4255–4258.
- 495 R. Kowalczyk, A. J. F. Edmunds, R. G. Hall and C. Bolm, *Org. Lett.*, 2011, **13**, 768–771.

- 496 B. Wang, T. Xu, L. Zhu, Y. Lan, J. Wang, N. Lu, Z. Wei, Y. Lin and H. Duan, *Org. Chem. Front.*, 2017, **4**, 1266–1271.
- 497 Z. Y. Chang and R. M. Coates, *J. Org. Chem.*, 1990, **55**, 3464–3474.
- 498 T. Isobe, K. Fukuda, K. Yamaguchi, H. Seki, T. Tokunaga and T. Ishikawa, *J. Org. Chem.*, 2000, **65**, 7779–7785.
- 499 X. Zhao, L. Shi, W. He, F. Yang and J. Li, *Arkivoc*, 2020, **2020**, 94–104.
- 500 J. W. Tsang, B. Schmied, R. Nyfeler and M. Goodman, *J. Med. Chem.*, 1984, **27**, 1663–1668.
- 501 Ø. Jacobsen, H. Maekawa, N. H. Ge, C. H. Görbitz, P. Rongved, O. P. Ottersen, M. Amiry-Moghaddam and J. Klaveness, *J. Org. Chem.*, 2011, **76**, 1228–1238.
- 502 V. K. Aggarwal, Z. Gültekin, R. S. Grainger, H. Adams and P. L. Spargo, *J. Chem. Soc., Perkin Trans. 1*, 1998, 2771–2782.
- 503 H. Keipour and T. Ollevier, *Org. Lett.*, 2017, **19**, 5736–5739.
- 504 F. Chen, Y. Zhang, L. Yu and S. Zhu, *Angew. Chem. Int. Ed.*, 2017, **56**, 2022–2025.
- 505 S. Mimura, S. Mizushima, Y. Shimizu and M. Sawamura, *Beilstein J. Org. Chem.*, 2020, **16**, 537–543.
- 506 Y. Kanazawa, Y. Tsuchiya, K. Kobayashi, T. Shiomi, J. Itoh, M. Kikuchi, Y. Yamamoto and H. Nishiyama, *Chem. - A Eur. J.*, 2006, **12**, 63–71.
- 507 H. Nakatsuji, Y. Ashida, H. Hori, Y. Sato, A. Honda, M. Taira and Y. Tanabe, *Org. Biomol. Chem.*, 2015, **13**, 8205–8210.
- 508 Q.-Q. Zhang, J.-H. Xie, X.-H. Yang, J.-B. Xie and Q.-L. Zhou, *Org. Lett.*, 2012, **14**, 6158–6161.
- 509 D. Dodd, M. D. Johnson and B. L. Lockman, *J. Am. Chem. Soc.*, 1977, **99**, 3664–3673.
- 510 D. Gärtner, A. L. Stein, S. Grupe, J. Arp and A. J. von Wangelin, *Angew. Chem. Int. Ed.*, 2015, **54**, 10545–10549.
- 511 C. Liu, J. Yuan, J. Zhang, Z. Wang, Z. Zhang and W. Zhang, *Org. Lett.*, 2018, **20**, 108–111.
- 512 B. R. von Wartburg, H. R. Wolf and O. Jeger, *Helv. Chim. Acta*, 1973, **56**, 1948–1955.

## 7. APPENDIX A – X-RAY CRYSTALLOGRAPHIC DATA

### (*E*)-((2-Boronobenzylidene)amino)(*tert*-butyl)- $\lambda^3$ -(*S*)-sulfanolate (*S*)-181.

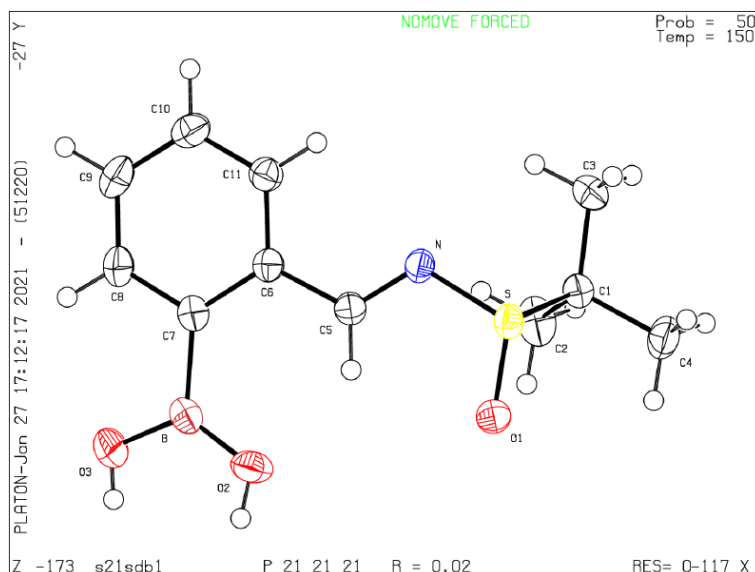


Table 20: Crystal data and structure refinement for (*S*)-181.

Identification code	s21sdb1
Empirical formula	C <sub>11</sub> H <sub>16</sub> B N O <sub>3</sub> S
Formula weight	253.12
Temperature	150.00(10) K
Wavelength	1.54184 Å
Crystal system	Orthorhombic
Space group	P2 <sub>1</sub> 2 <sub>1</sub> 2 <sub>1</sub>
Unit cell dimensions	a = 9.60006(9) Å b = 11.60553(15) Å c = 11.64615(12) Å
Volume	1297.54(2) Å <sup>3</sup>
Z	4
Density (calculated)	1.296 Mg/m <sup>3</sup>
Absorption coefficient	2.187 mm <sup>-1</sup>
F(000)	536
Crystal size	0.389 × 0.236 × 0.119 mm <sup>3</sup>
Theta range for data collection	5.381 to 73.698°.
Index ranges	-11 ≤ h ≤ 11, -14 ≤ k ≤ 11, -14 ≤ l ≤ 14
Reflections collected	24769
Independent reflections	2623 [R(int) = 0.0286]
Completeness to theta = 67.684°	100.0 %
Absorption correction	Gaussian
Max. and min. transmission	1.000 and 0.284
Refinement method	Full-matrix least-squares on F <sup>2</sup>
Data / restraints / parameters	2623 / 0 / 165
Goodness-of-fit on F <sup>2</sup>	1.066
Final R indices [I > 2σ(I)]	R1 = 0.0230, wR2 = 0.0615
R indices (all data)	R1 = 0.0232, wR2 = 0.0617
Absolute structure parameter	-0.002(5)
Extinction coefficient	n/a
Largest diff. peak and hole	0.226 and -0.230 e.Å <sup>-3</sup>

Table 21: Atomic coordinates ( $\times 10^4$ ) and equivalent isotropic displacement parameters ( $\text{\AA}^2 \times 10^3$ ) for (S)-**181**. U(eq) is defined as one third of the trace of the orthogonalized  $U^{ij}$  tensor.

Atom	x	y	z	U(eq)
C(1)	4491(2)	2551(2)	3772(2)	28(1)
C(2)	5651(2)	1662(2)	3703(2)	43(1)
C(3)	4459(2)	3181(2)	4918(2)	42(1)
C(4)	3074(2)	2021(2)	3501(2)	40(1)
S	4746(1)	3640(1)	2643(1)	27(1)
O(1)	4864(2)	2991(1)	1542(1)	41(1)
N	6323(2)	4113(1)	3065(1)	27(1)
C(5)	7313(2)	4047(1)	2344(2)	26(1)
C(6)	8712(2)	4489(1)	2616(2)	24(1)
C(7)	9849(2)	4303(1)	1868(2)	26(1)
B	9805(2)	3613(2)	693(2)	30(1)
O(2)	8588(2)	3250(1)	242(1)	38(1)
O(3)	11054(2)	3421(2)	183(2)	53(1)
C(8)	11141(2)	4750(2)	2202(2)	32(1)
C(9)	11311(2)	5358(2)	3211(2)	37(1)
C(10)	10187(2)	5538(2)	3934(2)	34(1)
C(11)	8894(2)	5109(2)	3638(2)	29(1)

Table 22: Bond lengths [ $\text{\AA}$ ] for (S)-**181**.

C(1)-C(2)	1.520(3)	C(5)-H(5)	0.9500
C(1)-C(3)	1.522(3)	C(6)-C(11)	1.402(3)
C(1)-C(4)	1.526(3)	C(6)-C(7)	1.413(2)
C(1)-S	1.8398(18)	C(7)-C(8)	1.399(3)
C(2)-H(2A)	0.9800	C(7)-B	1.586(3)
C(2)-H(2B)	0.9800	B-O(2)	1.349(3)
C(2)-H(2C)	0.9800	B-O(3)	1.357(2)
C(3)-H(3A)	0.9800	O(2)-H(2)	0.82(3)
C(3)-H(3B)	0.9800	O(3)-H(3)	0.79(4)
C(3)-H(3C)	0.9800	C(8)-C(9)	1.380(3)
C(4)-H(4A)	0.9800	C(8)-H(8)	0.9500
C(4)-H(4B)	0.9800	C(9)-C(10)	1.385(3)
C(4)-H(4C)	0.9800	C(9)-H(9)	0.9500
S-O(1)	1.4912(14)	C(10)-C(11)	1.380(3)
S-N	1.6837(15)	C(10)-H(10)	0.9500
N-C(5)	1.271(2)	C(11)-H(11)	0.9500
C(5)-C(6)	1.472(2)	C(5)-H(5)	0.9500

Table 23: Bond angles [°] for (S)-181.

C(2)-C(1)-C(3)	112.77(17)	C(5)-N-S	117.38(13)
C(2)-C(1)-C(4)	111.63(17)	N-C(5)-C(6)	121.27(16)
C(3)-C(1)-C(4)	110.92(16)	N-C(5)-H(5)	119.4
C(2)-C(1)-S	109.31(13)	C(6)-C(5)-H(5)	119.4
C(3)-C(1)-S	107.45(14)	C(11)-C(6)-C(7)	120.39(16)
C(4)-C(1)-S	104.32(13)	C(11)-C(6)-C(5)	118.39(15)
C(1)-C(2)-H(2A)	109.5	C(7)-C(6)-C(5)	121.23(16)
C(1)-C(2)-H(2B)	109.5	C(8)-C(7)-C(6)	117.15(17)
H(2A)-C(2)-H(2B)	109.5	C(8)-C(7)-B	116.78(16)
C(1)-C(2)-H(2C)	109.5	C(6)-C(7)-B	126.06(16)
H(2A)-C(2)-H(2C)	109.5	O(2)-B-O(3)	122.92(18)
H(2B)-C(2)-H(2C)	109.5	O(2)-B-C(7)	121.16(16)
C(1)-C(3)-H(3A)	109.5	O(3)-B-C(7)	115.92(17)
C(1)-C(3)-H(3B)	109.5	B-O(2)-H(2)	112(2)
H(3A)-C(3)-H(3B)	109.5	B-O(3)-H(3)	109(3)
C(1)-C(3)-H(3C)	109.5	C(9)-C(8)-C(7)	122.08(18)
H(3A)-C(3)-H(3C)	109.5	C(9)-C(8)-H(8)	119.0
H(3B)-C(3)-H(3C)	109.5	C(7)-C(8)-H(8)	119.0
C(1)-C(4)-H(4A)	109.5	C(8)-C(9)-C(10)	120.16(18)
C(1)-C(4)-H(4B)	109.5	C(8)-C(9)-H(9)	119.9
H(4A)-C(4)-H(4B)	109.5	C(10)-C(9)-H(9)	119.9
C(1)-C(4)-H(4C)	109.5	C(11)-C(10)-C(9)	119.65(17)
H(4A)-C(4)-H(4C)	109.5	C(11)-C(10)-H(10)	120.2
H(4B)-C(4)-H(4C)	109.5	C(9)-C(10)-H(10)	120.2
O(1)-S-N	110.36(8)	C(10)-C(11)-C(6)	120.58(17)
O(1)-S-C(1)	106.15(9)	C(10)-C(11)-H(11)	119.7
N-S-C(1)	97.76(8)	C(6)-C(11)-H(11)	119.7

Table 24: Anisotropic displacement parameters ( $\text{\AA}^2 \times 10^3$ ) for (S)-181. The anisotropic displacement factor exponent takes the form:  $-2\pi^2 [h^2 a^{*2} U^{11} + \dots + 2 h k a^* b^* U^{12}]$ .

	$U^{11}$	$U^{22}$	$U^{33}$	$U^{23}$	$U^{13}$	$U^{12}$
C(1)	27(1)	29(1)	28(1)	0(1)	3(1)	-2(1)
C(2)	38(1)	35(1)	55(1)	13(1)	7(1)	7(1)
C(3)	39(1)	62(1)	27(1)	-6(1)	7(1)	-9(1)
C(4)	32(1)	39(1)	49(1)	1(1)	3(1)	-12(1)
S	21(1)	31(1)	29(1)	2(1)	0(1)	-1(1)
O(1)	33(1)	64(1)	25(1)	-5(1)	-2(1)	-13(1)
N	23(1)	27(1)	32(1)	-2(1)	2(1)	-3(1)
C(5)	25(1)	28(1)	25(1)	1(1)	0(1)	0(1)
C(6)	25(1)	22(1)	27(1)	3(1)	0(1)	0(1)
C(7)	25(1)	24(1)	29(1)	4(1)	2(1)	2(1)
B	31(1)	28(1)	30(1)	2(1)	6(1)	2(1)
O(2)	33(1)	51(1)	30(1)	-12(1)	-2(1)	9(1)
O(3)	37(1)	65(1)	56(1)	-25(1)	21(1)	-11(1)
C(8)	23(1)	36(1)	38(1)	5(1)	2(1)	-1(1)
C(9)	29(1)	38(1)	45(1)	4(1)	-9(1)	-9(1)
C(10)	41(1)	30(1)	32(1)	-1(1)	-5(1)	-6(1)
C(11)	31(1)	27(1)	29(1)	0(1)	2(1)	-1(1)

Table 25: Hydrogen coordinates ( $\times 10^4$ ) and isotropic displacement parameters ( $\text{\AA}^2 \times 10^{-3}$ ) for (S)-**181**.

	x	y	z	U(eq)
H(2A)	5666	1321	2934	64
H(2B)	5488	1057	4275	64
H(2C)	6547	2036	3857	64
H(3A)	5373	3525	5068	64
H(3B)	4231	2635	5532	64
H(3C)	3751	3789	4893	64
H(4A)	2362	2626	3500	60
H(4B)	2843	1444	4084	60
H(4C)	3106	1654	2744	60
H(5)	7148	3705	1616	31
H(2)	8700(30)	2900(30)	-360(30)	69(10)
H(3)	10940(40)	3050(30)	-380(30)	83(12)
H(8)	11925	4632	1719	39
H(9)	12201	5654	3410	45
H(10)	10304	5953	4630	41
H(11)	8121	5236	4131	35

Table 26: Torsion angles [ $^\circ$ ] for (S)-**181**.

C(2)-C(1)-S-O(1)	53.80(16)	C(11)-C(6)-C(7)-B	179.52(16)
C(3)-C(1)-S-O(1)	176.49(13)	C(5)-C(6)-C(7)-B	-0.8(3)
C(4)-C(1)-S-O(1)	-65.70(14)	C(8)-C(7)-B-O(2)	-173.26(18)
C(2)-C(1)-S-N	-60.09(15)	C(6)-C(7)-B-O(2)	7.9(3)
C(3)-C(1)-S-N	62.60(14)	C(8)-C(7)-B-O(3)	6.6(3)
C(4)-C(1)-S-N	-179.60(13)	C(6)-C(7)-B-O(3)	-172.26(18)
O(1)-S-N-C(5)	11.65(17)	C(6)-C(7)-C(8)-C(9)	-0.6(3)
C(1)-S-N-C(5)	122.14(15)	B-C(7)-C(8)-C(9)	-179.52(17)
S-N-C(5)-C(6)	177.10(12)	C(7)-C(8)-C(9)-C(10)	0.4(3)
N-C(5)-C(6)-C(11)	-7.4(2)	C(8)-C(9)-C(10)-C(11)	-0.3(3)
N-C(5)-C(6)-C(7)	172.95(16)	C(9)-C(10)-C(11)-C(6)	0.4(3)
C(11)-C(6)-C(7)-C(8)	0.7(3)	C(7)-C(6)-C(11)-C(10)	-0.6(3)
C(5)-C(6)-C(7)-C(8)	-179.66(15)	C(5)-C(6)-C(11)-C(10)	179.72(17)

Table 27: Hydrogen bonds for (S)-**181** [ $\text{\AA}$  and  $^\circ$ ].

D-H...A	d(D-H)	d(H...A)	d(D...A)	$\angle(\text{DHA})$
O(2)-H(2)...O(1)#1	0.82(3)	2.05(3)	2.808(2)	154(3)
O(3)-H(3)...O(1)#1	0.79(4)	2.09(4)	2.834(2)	157(4)

Symmetry transformations used to generate equivalent atoms:

#1  $x+1/2, -y+1/2, -z$



**(*E*)-((2-Boronobenzylidene)amino)(*tert*-butyl)- $\lambda^3$ -(*R*)-sulfanolate (*R*)-181.**

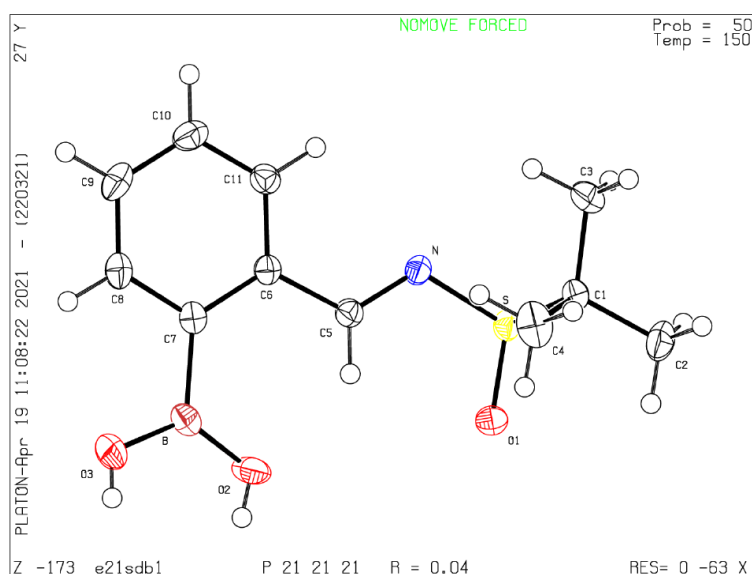


Table 28: Crystal data and structure refinement for (*R*)-**181**.

Identification code	e21sdb1
Empirical formula	C11 H16 B N O3 S
Formula weight	253.12
Temperature	150.01(10) K
Wavelength	0.71073 Å
Crystal system	Orthorhombic
Space group	P2 <sub>1</sub> 2 <sub>1</sub> 2 <sub>1</sub>
Unit cell dimensions	a = 9.6026(2) Å b = 11.6066(3) Å c = 11.6791(4) Å
Volume	1301.68(6) Å <sup>3</sup>
Z	4
Density (calculated)	1.292 Mg/m <sup>3</sup>
Absorption coefficient	0.243 mm <sup>-1</sup>
F(000)	536
Crystal size	0.453 × 0.375 × 0.342 mm <sup>3</sup>
Theta range for data collection	3.259 to 30.204°.
Index ranges	-13 ≤ h ≤ 13, -16 ≤ k ≤ 16, -16 ≤ l ≤ 16
Reflections collected	22081
Independent reflections	3612 [R(int) = 0.0321]
Completeness to theta = 25.242°	99.8 %
Absorption correction	Semi-empirical from equivalents
Max. and min. transmission	1.00000 and 0.93594
Refinement method	Full-matrix least-squares on F <sup>2</sup>
Data / restraints / parameters	3612 / 0 / 165
Goodness-of-fit on F <sup>2</sup>	1.079
Final R indices [I > 2σ(I)]	R1 = 0.0361, wR2 = 0.0796
R indices (all data)	R1 = 0.0405, wR2 = 0.0812
Absolute structure parameter	-0.01(2)
Extinction coefficient	n/a
Largest diff. peak and hole	0.327 and -0.228 e.Å <sup>-3</sup>

Table 29: Atomic coordinates ( $\times 10^4$ ) and equivalent isotropic displacement parameters ( $\text{\AA}^2 \times 10^3$ ) for (*R*)-**181**.  $U(\text{eq})$  is defined as one third of the trace of the orthogonalized  $U^{ij}$  tensor.

Atom	x	y	z	U(eq)
S	-256(1)	6360(1)	7639(1)	21(1)
O(1)	-136(2)	7014(2)	6540(1)	35(1)
N	1321(2)	5885(1)	8063(2)	22(1)
C(1)	-514(2)	7447(2)	8768(2)	22(1)
C(2)	-1933(2)	7976(2)	8499(2)	34(1)
C(3)	-548(2)	6813(2)	9911(2)	37(1)
C(4)	645(3)	8335(2)	8703(2)	37(1)
C(5)	2313(2)	5955(2)	7345(2)	21(1)
C(6)	3713(2)	5513(2)	7616(2)	19(1)
C(7)	4851(2)	5697(2)	6868(2)	21(1)
C(8)	6141(2)	5247(2)	7203(2)	26(1)
C(9)	6313(2)	4641(2)	8212(2)	31(1)
C(10)	5189(2)	4463(2)	8932(2)	28(1)
C(11)	3897(2)	4894(2)	8639(2)	23(1)
B	4807(3)	6383(2)	5695(2)	25(1)
O(2)	3587(2)	6745(2)	5242(1)	32(1)
O(3)	6058(2)	6578(2)	5189(2)	47(1)

Table 30: Bond lengths [ $\text{\AA}$ ] for (*R*)-**181**.

S-O(1)	1.4956(15)	C(5)-H(5)	0.9500
S-N	1.6869(17)	C(6)-C(11)	1.406(3)
S-C(1)	1.841(2)	C(6)-C(7)	1.415(3)
N-C(5)	1.272(2)	C(7)-C(8)	1.400(3)
C(1)-C(4)	1.520(3)	C(7)-B	1.585(3)
C(1)-C(3)	1.524(3)	C(8)-C(9)	1.382(3)
C(1)-C(2)	1.527(3)	C(8)-H(8)	0.9500
C(2)-H(2A)	0.9800	C(9)-C(10)	1.385(3)
C(2)-H(2B)	0.9800	C(9)-H(9)	0.9500
C(2)-H(2C)	0.9800	C(10)-C(11)	1.381(3)
C(3)-H(3A)	0.9800	C(10)-H(10)	0.9500
C(3)-H(3B)	0.9800	C(11)-H(11)	0.9500
C(3)-H(3C)	0.9800	B-O(2)	1.352(3)
C(4)-H(4A)	0.9800	B-O(3)	1.357(3)
C(4)-H(4B)	0.9800	O(2)-H(2)	0.75(3)
C(4)-H(4C)	0.9800	O(3)-H(3)	0.71(3)
C(5)-C(6)	1.474(2)		

Table 31: Bond angles [°] for (*R*)-**181**.

O(1)-S-N	110.42(9)	H(4B)-C(4)-H(4C)	109.5
O(1)-S-C(1)	106.10(9)	N-C(5)-C(6)	121.27(19)
N-S-C(1)	97.76(9)	N-C(5)-H(5)	119.4
C(5)-N-S	117.23(15)	C(6)-C(5)-H(5)	119.4
C(4)-C(1)-C(3)	112.75(19)	C(11)-C(6)-C(7)	120.33(17)
C(4)-C(1)-C(2)	111.74(19)	C(11)-C(6)-C(5)	118.35(17)
C(3)-C(1)-C(2)	110.82(18)	C(7)-C(6)-C(5)	121.32(18)
C(4)-C(1)-S	109.29(14)	C(8)-C(7)-C(6)	117.04(19)
C(3)-C(1)-S	107.42(15)	C(8)-C(7)-B	116.90(18)
C(2)-C(1)-S	104.38(15)	C(6)-C(7)-B	126.05(17)
C(1)-C(2)-H(2A)	109.5	C(9)-C(8)-C(7)	122.3(2)
C(1)-C(2)-H(2B)	109.5	C(9)-C(8)-H(8)	118.9
H(2A)-C(2)-H(2B)	109.5	C(7)-C(8)-H(8)	118.9
C(1)-C(2)-H(2C)	109.5	C(8)-C(9)-C(10)	120.1(2)
H(2A)-C(2)-H(2C)	109.5	C(8)-C(9)-H(9)	120.0
H(2B)-C(2)-H(2C)	109.5	C(10)-C(9)-H(9)	120.0
C(1)-C(3)-H(3A)	109.5	C(11)-C(10)-C(9)	119.73(19)
C(1)-C(3)-H(3B)	109.5	C(11)-C(10)-H(10)	120.1
H(3A)-C(3)-H(3B)	109.5	C(9)-C(10)-H(10)	120.1
C(1)-C(3)-H(3C)	109.5	C(10)-C(11)-C(6)	120.57(19)
H(3A)-C(3)-H(3C)	109.5	C(10)-C(11)-H(11)	119.7
H(3B)-C(3)-H(3C)	109.5	C(6)-C(11)-H(11)	119.7
C(1)-C(4)-H(4A)	109.5	O(2)-B-O(3)	123.0(2)
C(1)-C(4)-H(4B)	109.5	O(2)-B-C(7)	121.14(18)
H(4A)-C(4)-H(4B)	109.5	O(3)-B-C(7)	115.86(19)
C(1)-C(4)-H(4C)	109.5	B-O(2)-H(2)	112(3)
H(4A)-C(4)-H(4C)	109.5	B-O(3)-H(3)	110(3)

Table 32: Anisotropic displacement parameters ( $\text{\AA}^2 \times 10^3$ ) for (*R*)-**181**. The anisotropic displacement factor exponent takes the form:  $-2\pi^2 [h^2 a^{*2} U^{11} + \dots + 2 h k a^* b^* U^{12}]$ .

	$U^{11}$	$U^{22}$	$U^{33}$	$U^{23}$	$U^{13}$	$U^{12}$
S	17(1)	25(1)	22(1)	-2(1)	0(1)	1(1)
O(1)	29(1)	56(1)	19(1)	6(1)	-2(1)	12(1)
N	18(1)	22(1)	26(1)	3(1)	1(1)	3(1)
C(1)	22(1)	24(1)	21(1)	-2(1)	4(1)	3(1)
C(2)	28(1)	33(1)	42(1)	-1(1)	3(1)	11(1)
C(3)	34(1)	54(2)	22(1)	6(1)	6(1)	7(1)
C(4)	34(1)	30(1)	47(1)	-12(1)	6(1)	-7(1)
C(5)	20(1)	22(1)	20(1)	0(1)	0(1)	0(1)
C(6)	20(1)	17(1)	21(1)	-2(1)	1(1)	0(1)
C(7)	19(1)	18(1)	24(1)	-4(1)	2(1)	-2(1)
C(8)	18(1)	30(1)	31(1)	-3(1)	2(1)	1(1)
C(9)	24(1)	32(1)	37(1)	-3(1)	-8(1)	7(1)
C(10)	35(1)	24(1)	27(1)	2(1)	-4(1)	6(1)
C(11)	26(1)	22(1)	22(1)	0(1)	2(1)	0(1)
B	27(1)	23(1)	23(1)	-2(1)	6(1)	-2(1)
O(2)	28(1)	46(1)	23(1)	13(1)	-2(1)	-9(1)
O(3)	34(1)	57(1)	50(1)	25(1)	21(1)	12(1)

Table 33: Hydrogen coordinates ( $\times 10^4$ ) and isotropic displacement parameters ( $\text{\AA}^2 \times 10^{-3}$ ) for (*R*)-**181**.

	x	y	z	U(eq)
H(2A)	-2165	8551	9083	52
H(2B)	-2643	7370	8495	52
H(2C)	-1901	8347	7746	52
H(3A)	-770	7359	10525	55
H(3B)	365	6465	10058	55
H(3C)	-1259	6209	9885	55
H(4A)	480	8940	9272	56
H(4B)	663	8677	7936	56
H(4C)	1541	7962	8858	56
H(5)	2147	6300	6620	25
H(8)	6925	5363	6720	32
H(9)	7204	4346	8410	37
H(10)	5306	4047	9626	34
H(11)	3125	4770	9133	28
H(2)	3690(30)	7080(30)	4700(30)	51(10)
H(3)	5960(40)	6880(30)	4660(30)	57(11)

Table 34: Torsion angles [ $^\circ$ ] for (*S*)-**181**.

O(1)-S-N-C(5)	-11.58(19)	C(11)-C(6)-C(7)-B	-179.51(18)
C(1)-S-N-C(5)	-122.03(16)	C(5)-C(6)-C(7)-B	0.8(3)
O(1)-S-C(1)-C(4)	-53.81(18)	C(6)-C(7)-C(8)-C(9)	0.4(3)
N-S-C(1)-C(4)	60.13(17)	B-C(7)-C(8)-C(9)	179.50(19)
O(1)-S-C(1)-C(3)	-176.44(14)	C(7)-C(8)-C(9)-C(10)	-0.2(3)
N-S-C(1)-C(3)	-62.50(15)	C(8)-C(9)-C(10)-C(11)	0.0(3)
O(1)-S-C(1)-C(2)	65.85(16)	C(9)-C(10)-C(11)-C(6)	-0.1(3)
N-S-C(1)-C(2)	179.79(14)	C(7)-C(6)-C(11)-C(10)	0.4(3)
S-N-C(5)-C(6)	-177.15(13)	C(5)-C(6)-C(11)-C(10)	-179.90(19)
N-C(5)-C(6)-C(11)	7.0(3)	C(8)-C(7)-B-O(2)	173.0(2)
N-C(5)-C(6)-C(7)	-173.33(18)	C(6)-C(7)-B-O(2)	-8.0(3)
C(11)-C(6)-C(7)-C(8)	-0.5(3)	C(8)-C(7)-B-O(3)	-7.0(3)
C(5)-C(6)-C(7)-C(8)	179.77(17)	C(6)-C(7)-B-O(3)	171.9(2)

Table 35: Hydrogen bonds for (*S*)-**181** [ $\text{\AA}$  and  $^\circ$ ].

D-H...A	d(D-H)	d(H...A)	d(D...A)	$\angle(\text{DHA})$
O(2)-H(2)...O(1)#1	0.75(3)	2.11(3)	2.813(2)	155(3)
O(3)-H(3)...O(1)#1	0.71(3)	2.18(3)	2.840(3)	155(4)

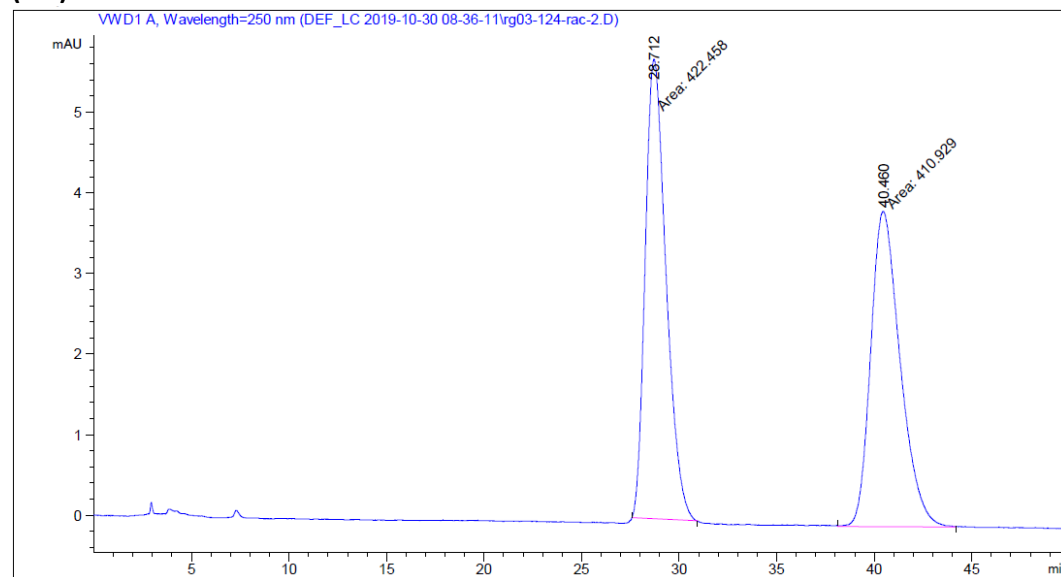
Symmetry transformations used to generate equivalent atoms:

#1  $x+1/2, -y+3/2, -z$

## 8. APPENDIX B – HPLC ANALYSIS OF COMMERCIAL SAMPLES OF (R)-129B

HPLC analysis of a samples of Davis' sulfinamide **129b** purchased from Sigma-Aldrich, using a Daicel Chiracel OD column, flow rate 1 mL/min, Hexane/*i*-PrOH 95:5, (*R*)-**129b**  $t_R$  = 28.7 min, (*S*)-**129b**  $t_R$  = 40.5 min, HPLC conditions taken from the literature.<sup>295</sup>

### (rac)-129b:

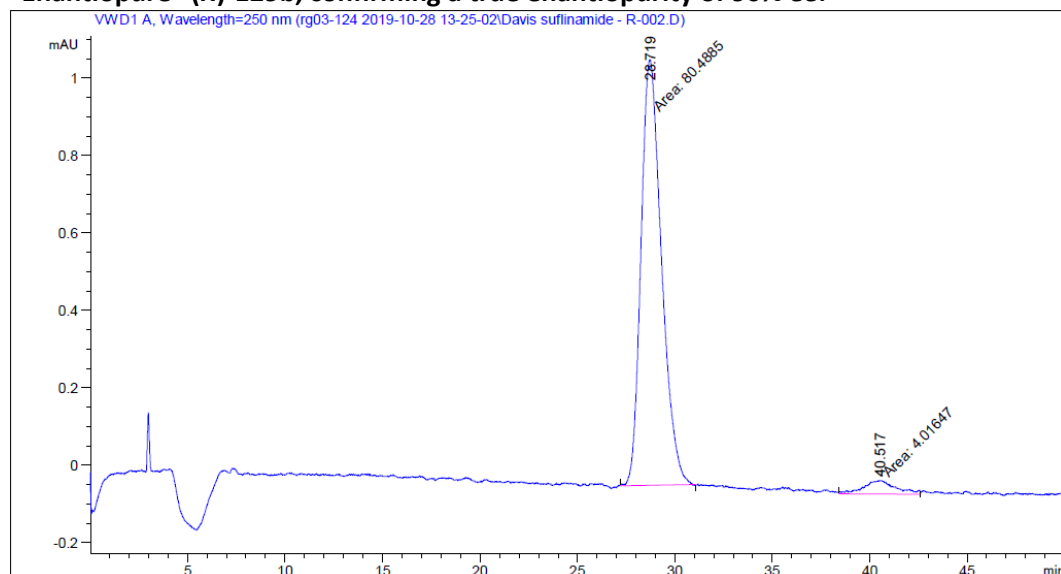


Signal 1: VWD1 A, Wavelength=250 nm

Peak #	RetTime [min]	Type	Width [min]	Area [mAU*s]	Height [mAU]	Area %
1	28.712	MM	1.2361	422.45792	5.69616	50.6917
2	40.460	MM	1.7521	410.92896	3.90890	49.3083

Totals : 833.38687 9.60507

**“Enantiopure” (R)-129b, confirming a true enantiopurity of 90% ee.**

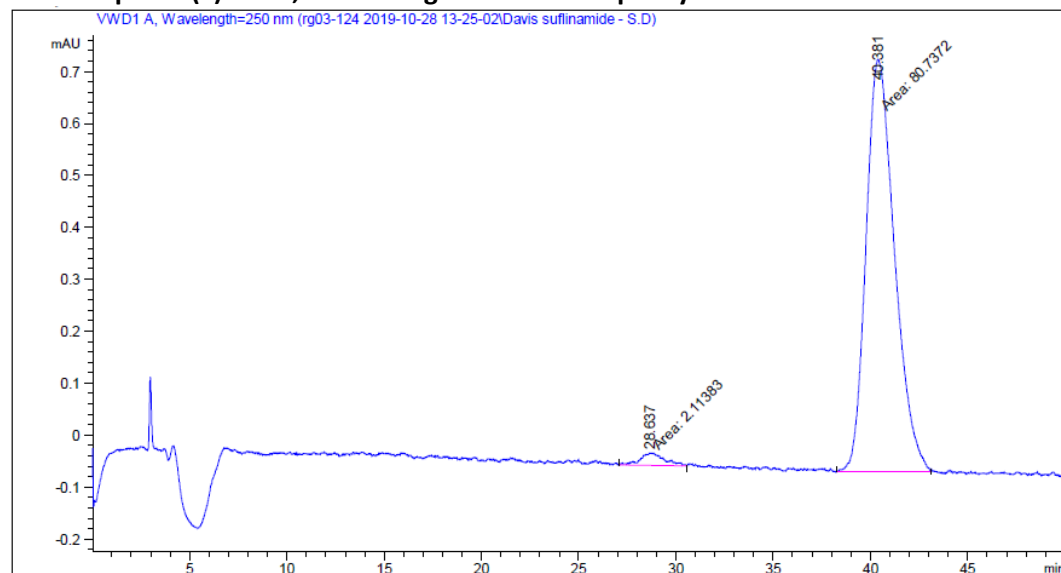


Signal 1: VWD1 A, Wavelength=250 nm

Peak #	RetTime [min]	Sig	Type	Area [mAU*s]	Height [mAU]	Area %
1	28.719	1	MM	80.48846	1.09996	95.2471
2	40.517	1	MM	4.01647	3.54244e-2	4.7529

Totals : 84.50493 1.13539

**“Enantiopure” (S)-129b, confirming a true enantiopurity of 94% ee.**

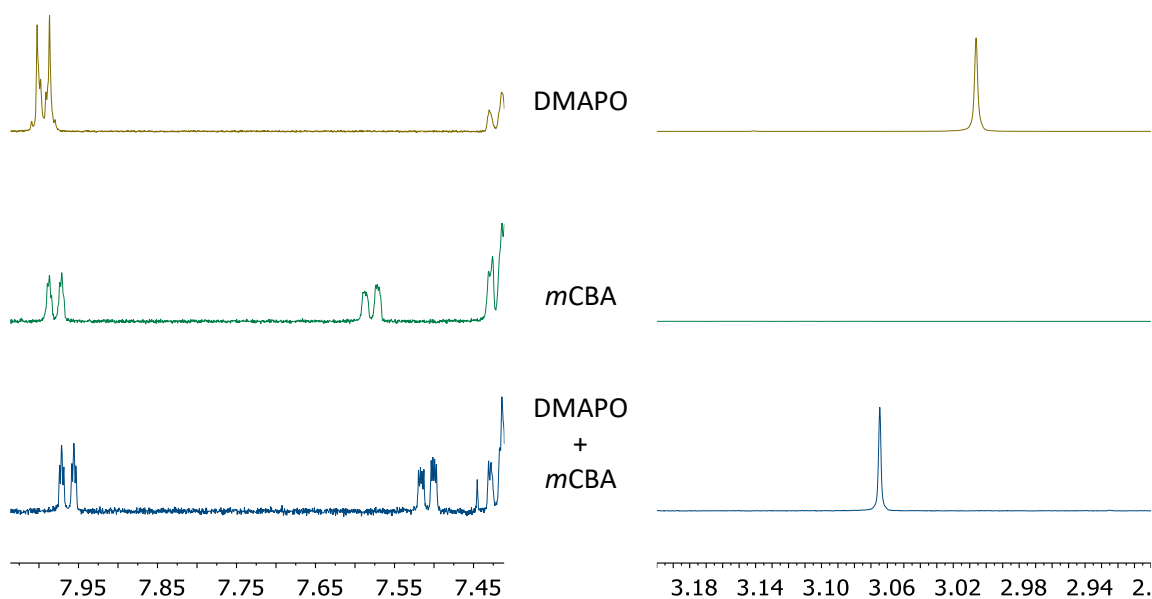


Signal 1: VWD1 A, Wavelength=250 nm

Peak #	RetTime [min]	Sig	Type	Area [mAU*s]	Height [mAU]	Area %
1	28.637	1	MM	2.11383	2.42195e-2	2.5514
2	40.381	1	MM	80.73721	7.93269e-1	97.4486

Totals : 82.85104 8.17488e-1

## 9. APPENDIX C – $^1\text{H}$ NMR SPECTRA OF DMAPO + *m*CBA

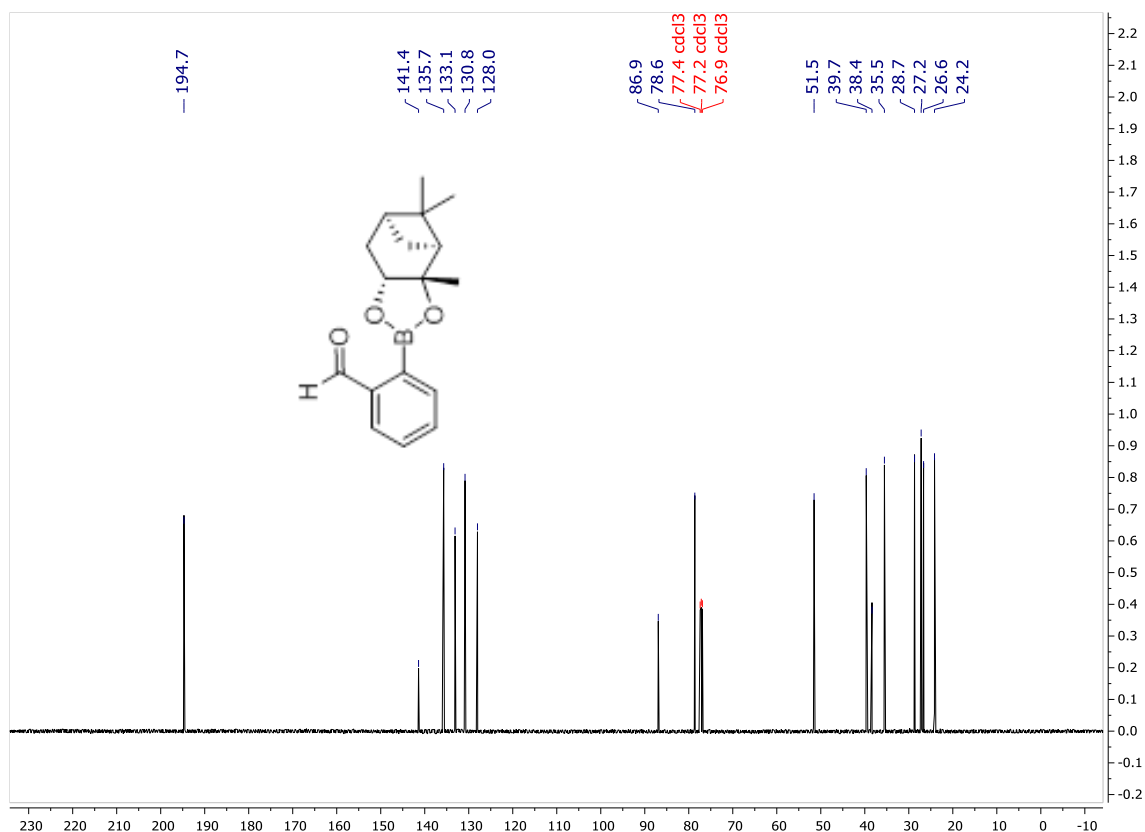


Procedure for the production of the spectra in Appendix C:

DMAPO (6.2 mg, 0.04 mmol) or DMAPO (6.2 mg, 0.04 mmol), or both, were added to toluene (1.0 mL) and stirred for 5 min. After this time, an aliquot ( $\sim 20\ \mu\text{L}$ ) was removed and diluted up to  $600\ \mu\text{L}$  in  $\text{CDCl}_3$ , and a  $^1\text{H}$  NMR (500 MHz) spectrum was acquired.

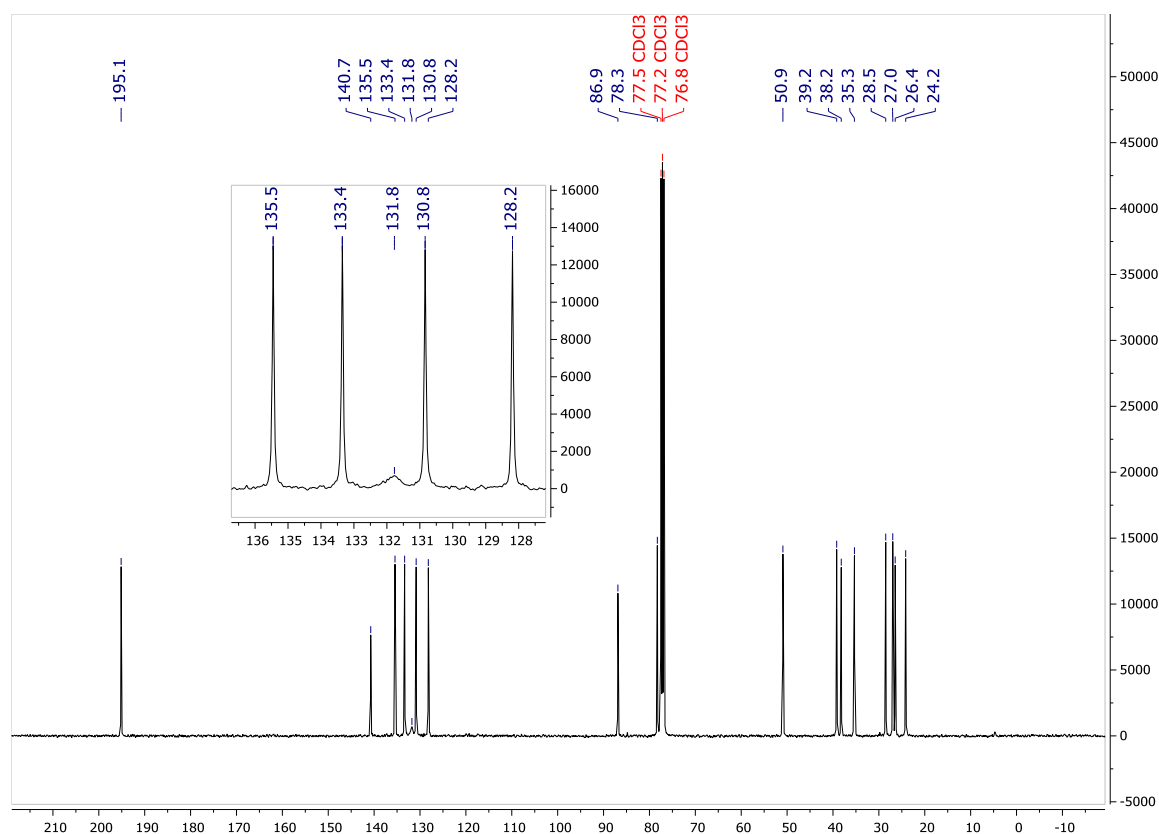
## 10. APPENDIX D – REPRESENTATIVE NMR SPECTRA FOR DETERMINING C-B <sup>13</sup>C NMR CHEMICAL SHIFTS

2-((3a*S*,4*S*,6*S*,7a*R*)-3a,5,5-Trimethylhexahydro-4,6-methanobenzo[*d*][1,3,2]dioxaborol-2-yl)benzaldehyde **182** - <sup>13</sup>C{<sup>1</sup>H} NMR (126 MHz, CDCl<sub>3</sub>)

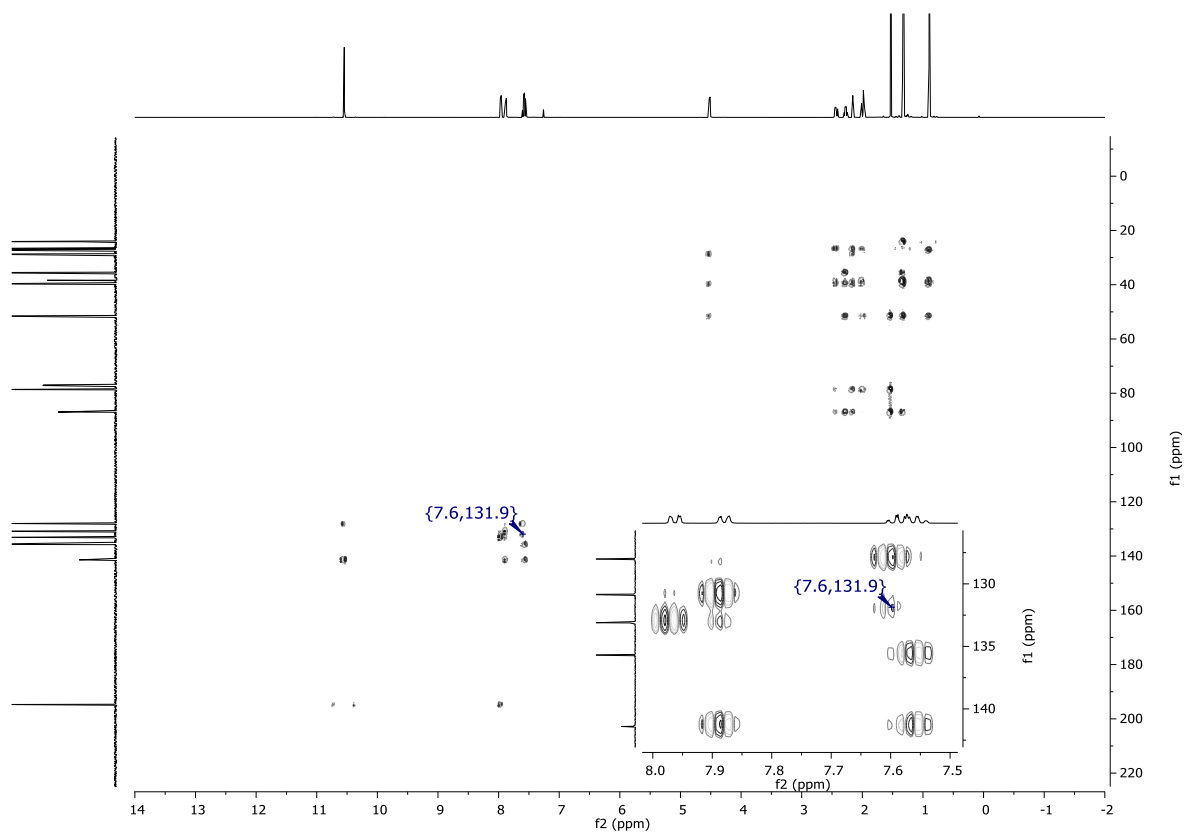




$^{13}\text{C}\{^1\text{H}\}$  NMR (126 MHz,  $\text{CDCl}_3$ ,  $-15^\circ\text{C}$ ) – BC peak visible (131.8 ppm)



HMBC (500 MHz,  $\text{CDCl}_3$ ) - ArH-C(B) correlations shown



## 11. APPENDIX E –PHD PUBLICATIONS

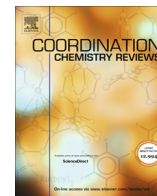
The two publications listed below are composed in most part of content presented in this PhD Thesis, and so have been appended to this work in the current appendix. Both articles are reproduced here in full and unaltered from their published form.

<sup>240</sup> R. R. Groleau, T. D. James and S. D. Bull, *Coord. Chem. Rev.*, 2021, **428**, 213599.

Reproduced with permission from *Coord. Chem. Rev.*, 2021, **428**, 213599. Copyright 2021 Elsevier.

<sup>294</sup> R. R. Groleau, R. S. L. Chapman, H. Ley-Smith, L. Liu, T. D. James and S. D. Bull, *J. Org. Chem.*, 2020, **85**, 1208–1215.

Reproduced with permission from *J. Org. Chem.*, 2020, **85**, 1208. Copyright 2020 American Chemical Society.



## Review

## The Bull-James assembly: Efficient iminoboronate complex formation for chiral derivatization and supramolecular assembly



Robin R. Groleau, Tony D. James\*, Steven D. Bull\*

Department of Chemistry, University of Bath, Claverton Down, Bath BA2 7AY, UK

## ARTICLE INFO

## Article history:

Received 3 August 2020

Received in revised form 6 September 2020

Accepted 6 September 2020

## ABSTRACT

Chiral molecules are widely used in many fields of research and so practically simple, accurate methods to measure their enantiopurities are required. This review's initial focus is on one such method, the Bull-James assembly, which employs a three-component protocol combining 2-formylphenyl boronic acid, an amine, and a diol to self-assemble diastereomeric iminoboronate ester (IBE) complexes whose ratio can be used to measure the *ee*'s of amine and diol analytes using  $^1\text{H}$  and  $^{19}\text{F}$  NMR spectroscopic analysis. Examples where this supramolecular IBE assembly approach has been adapted to determine the *ee* of a range of analytes using other analytical techniques such as circular dichroism, fluorescence, and electrochemistry that are potentially applicable to high-throughput *ee* analysis are also discussed. Selected examples where this orthogonal self-assembly process has been used as a platform technology to construct boracycles, chiral auxiliaries/ligands, synthesise intelligent polymers/hydrogels, and prepare labelled peptides/proteins/biomolecules are also discussed.

© 2020 Elsevier B.V. All rights reserved.

## Contents

1. Introduction	2
2. Discovery and structural features of the Bull-James assembly	3
2.1. Discovery of the Bull-James assembly CDA for determining the <i>ee</i> of amines	3
2.2. Structural and mechanistic features of IBE complex formation	3
3. Three-component assembly for determining <i>ee</i> by NMR spectroscopic analysis	6
3.1. Primary amines	6
3.2. Diamines	8
3.3. Amino alcohols	9
3.4. Hydroxylamines	10
3.5. Sulfinamides	10
3.6. Diols	10
3.7. Hydroxyacids and diacids	14
3.8. $^{19}\text{F}$ NMR spectroscopic analysis	15
3.9. Chalcogen NMR spectroscopic analysis	16
4. Three-component assembly for determining <i>ee</i> by optical methods	17
4.1. Determining the <i>ee</i> of amines and diols using circular dichroism	17
4.2. Determining the <i>ee</i> of amines, amino-alcohols and diols using fluorescence	19
5. Three-component assembly for electrochemical determination of the <i>ee</i> of BINOL	22
6. IBE assemblies as synthetic tools	22
6.1. Self-assembled synthesis of polyheteroatomic boracycles	23
6.2. Chiral IBE ligands for asymmetric catalysis	23
6.3. IBE-derived chiral auxiliaries in CuAAC click reactions	23

Abbreviations: 2-FPBA, 2-formylphenyl boronic acid; IBE, iminoboronate ester; IB, iminoboronate; CDA, chiral derivatizing agent; 2-APBA, 2-acetylphenylboronic acid.

\* Corresponding authors.

E-mail addresses: [T.D.James@bath.ac.uk](mailto:T.D.James@bath.ac.uk) (T.D. James), [S.D.Bull@bath.ac.uk](mailto:S.D.Bull@bath.ac.uk) (S.D. Bull).

6.4. Reversible radical coupling of iminoboronates .....	23
7. Iminoboronate complexes for the formation of polymers and hydrogels. ....	24
7.1. Iminoboronate polymers and hydrogels .....	24
7.2. Dynamic, self-healing and stimuli-responsive polymers and hydrogels .....	25
7.3. Stimuli-responsive aggregates and micelles .....	28
8. Iminoboronate derivatives for biological targeting and tagging .....	28
9. Conclusions and outlook .....	31
Declaration of Competing Interest .....	32
Acknowledgments .....	32
References .....	32

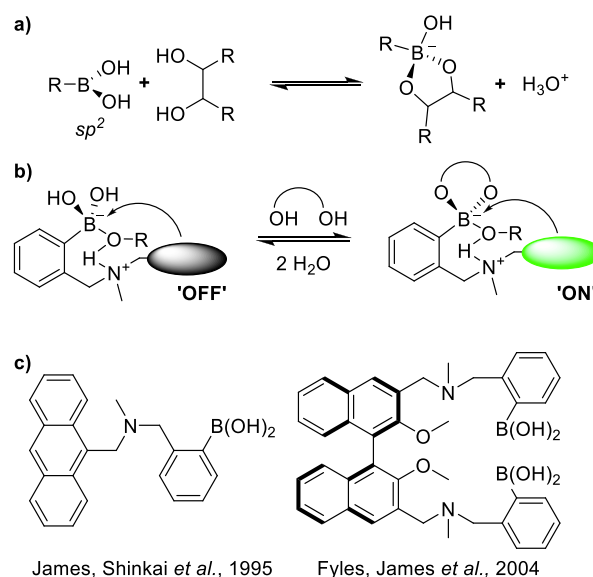
## 1. Introduction

This review describes the many applications of a three-component self-assembly reaction that occurs when an amine, a diol, and a 2-formyl-phenyl boronic acid (2-FPBA) template are mixed together to afford stable iminoboronate ester (IBE) complexes. Development of this versatile supramolecular methodology has been pioneered in the Bull and James groups at the University of Bath (UK) over the last two decades, with its widespread use by numerous research groups for different supramolecular applications resulting in this type of reaction now being termed the “Bull-James assembly”. To date, this self-assembly methodology has found a wide range of applications, including: use as chiral derivatization agents (CDAs) for determining the enantiomeric excess (*ee*) of a range of chiral analytes using NMR, optical and electrochemical techniques; as a supramolecular self-assembly reaction to produce boracycles, chiral auxiliaries and ligands for stereoselective synthesis, and new types of polymers and stimuli-responsive materials; and as the basis of “click” chemistry methodology for modifying/functionalising peptides and proteins.

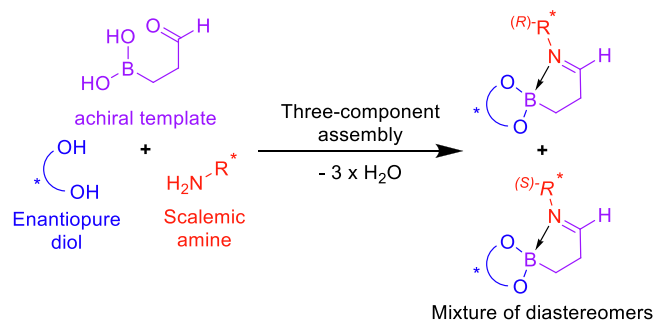
The Bull group have had an interest in the development of asymmetric methodologies for the synthesis of chiral amines for many years, and have often needed to determine the *ee* of new types of chiral amines containing single stereocenters [1–6]. One approach that they have commonly employed involves reaction of a scalemic amine with a CDA such as Mosher's acid chloride (expensive, moisture sensitive, multiple steps) to afford diastereomeric amide derivatives whose diastereomeric ratio (*dr*) can then be determined by NMR spectroscopic analysis [7,8]. Alternatively, the *ee*'s of these chiral amines (or their derivatives) have been determined using chiral HPLC analysis. The range of structures and functional groups present in the chiral amines meant that different CDAs or multiple expensive chiral HPLC columns often needed to be screened before a suitable system was identified for each different class of amine [9,10]. Therefore, the Bull group were interested in identifying a practically simple, cheap, and rapid CDA approach that could be used to rapidly analyse the *ee* values of a wide range of chiral amines using NMR spectroscopic analysis.

The James group have been interested in chemical sensing and supramolecular chemistry for many years, having developed a wide range of self-assembled fluorescent sensors that employ reversible binding of boronic acids (planar  $sp^2$  boron) to diol fragments to produce boronate ester complexes (tetrahedral  $sp^3$  boron) to induce a change in fluorescence (Scheme 1a) [11–16]. They have described that *ortho*-aminomethylphenylboronic acid sensors are particularly effective for the fluorescence, optical, and electrochemical sensing of sugars, with this class of sensors finding recent commercial application for continuous monitoring of glucose levels in critical care patients [17,18]. Diol complexation in

this class of sensors is favoured by the presence of the proximal Lewis-basic tertiary amino group [19], which binds to the boron centre to produce stable intramolecular amino-boronate ester complexes. Orthogonal binding of both the diol analyte and the amine to the boron centre occurs in a cooperative manner, with complexation of the diol producing a boronate ester with a more Lewis acidic  $sp^2$  boron centre, and the intramolecular N→B interaction increasing the overall stability of the complex. Complexation of these types of aminoboronic acid sensors to diols in aqueous/alcoholic media has been shown to produce solvent-inserted amino-boronate complexes, whose formation results in fluorescence “turn-on” through elimination of “loose-bolt” internal conversion quenching of the fluorescence of the parent boronic acid probe (Scheme 1b) [20,21]. The versatility and strength of this type of aminoboronic acid complexation process has been exploited to produce many sensors for the fluorescence detection of a wide range of diols and sugars, as well as sensors for pH, anion, and reactive oxygen species sensing (Scheme 1c) [11]. The added stability of this type of aminoboronate ester complexes has also been used as the basis of supramolecular assemblies for the generation of a



**Scheme 1.** (a) Rapid complexation of a boronic acid with a vicinal diol reversibly affords a cyclic boronate ester. (b) Complexation of a diol to a non-fluorescent *o*-aminomethylphenylboronic acid sensor in water or an alcohol solvent results in formation of a solvent-inserted fluorescent boronate ester complex. Diol binding results in fluorescence “turn-on” due to elimination of a “loose-bolt” effect that causes internal conversion quenching of the fluorescence of the uncomplexed boronic acid probe. (c) Representative *o*-aminomethylphenylboronic acid glucose/diol sensors developed by the James group.



**Scheme 2.** Design principles for a three-component derivatisation protocol to produce an IBE-based CDA for determining the *ee* of a scalemic amine.

wide range of hydrogels, boronic acid appended porphyrins, amphiphiles, polymers and covalent organic frameworks [14,22,23].

Nomikai-inspired [24] conversations during a research trip to Japan in 2002 [25] led James and Bull (and Arimori – PDRA in the groups) to realise that this type of boronate ester complexation chemistry could be exploited to develop a simple three-component protocol for determining the enantiopurity of chiral amines (and diols). Our simple idea was to react an achiral bifunctional template that contained a boronic acid and a proximal aldehyde group (purple) with a chiral 1,2-diol (blue) and a scalemic amine (red) to selectively afford a pair of diastereomeric IBE complexes, whose *dr* could then be determined through integration of pairs of diastereomeric signals in their  $^1\text{H}$  NMR spectrum. So long as no kinetic resolution occurred during the derivatisation process, this *dr* value would be an accurate reflection of the *ee* of the parent scalemic amine. Moreover, the orthogonal three-component nature of the protocol meant that it would be easy to adapt this derivatisation approach to determine the *ee* of chiral diols (and other chiral analytes) (Scheme 2).

## 2. Discovery and structural features of the Bull-James assembly

### 2.1. Discovery of the Bull-James assembly CDA for determining the *ee* of amines

A review of the literature revealed a promising report by Dunn *et al.* [26], who had described the stepwise synthesis of stable IBEs based on imine condensation of 2-FPBA **1** [27] with aniline **2** to afford an iminoboronic acid **3** intermediate that was then reacted with catechol to afford iminoboronate ester **4** (Scheme 3). This precedent indicated that reaction of 2-FPBA **1** with a chiral diol and a scalemic amine could be used as the basis of a three-component derivatisation protocol for determining the *ee* of chiral amines, as outlined in Scheme 2.

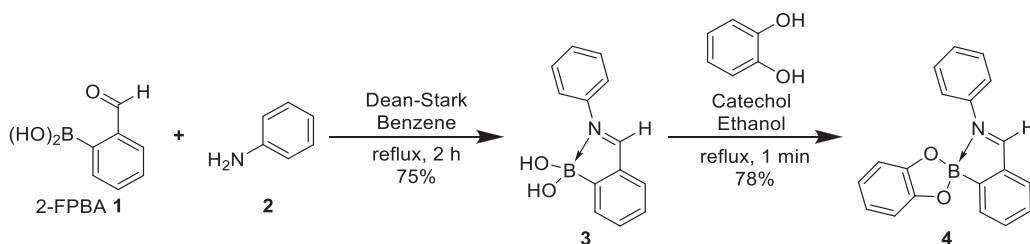
This three-component assembly concept was initially investigated by mixing 2-FPBA **1**, (*S*)-BINOL **5** and (*rac*)-4-methoxy- $\alpha$ -methylbenzylamine **6a** in  $\text{CDCl}_3$  with 4 Å molecular sieves to drive the condensation reactions to completion. To our delight, this reac-

tion led to quantitative formation of a 50:50 mixture of the diastereomeric IBE complexes ( $\alpha$ -*S,S*)-**7aa** and ( $\alpha$ -*R,S*)-**7ba** within 5 min (Fig. 1a) [28], with complexation reactions of scalemic 4-methoxy- $\alpha$ -methylbenzylamine **6a** of known *ee* indicating that no kinetic resolution was occurring. Examination of the  $^1\text{H}$  NMR spectra revealed that the *ee*'s of scalemic amines could be easily determined by integration of corresponding pairs of  $^1\text{H}$  NMR resonances originating from each of the IBE diastereomers that were formed. Resonances for the imine (black),  $\alpha$ -methine (red), *p*-methoxy (green), and  $\alpha$ -methyl (blue) proton resonances of each diastereomer were fully baseline-resolved, exhibiting relatively large chemical shift differences  $\Delta\delta_{\text{H}}$  values of 0.11–0.21 ppm (Fig. 1b). The presence of multiple well-resolved diastereomeric peaks in these  $^1\text{H}$  NMR spectra enabled the integral ratios of multiple pairs of diastereomeric resonances to be used to accurately measure high *ee* values (>95% *ee*), thus minimising any risk of inaccuracy caused by baseline noise or the presence of impurities (Fig. 1b).

This three-component derivatisation reaction was attractive from a practical standpoint, as it was moisture tolerant, employed cheap, commercially available, bench-stable reagents, and proceeded rapidly at room temperature (5 min) in an NMR solvent with no need for reaction workup or purification. Moreover, it produced diastereomeric IBEs whose  $^1\text{H}$  NMR spectra exhibited multiple pairs of baseline-resolved diastereomeric proton resonances with a large  $\Delta\delta_{\text{H}}$ , which meant that their *dr* could be analysed using lowfield NMR spectrometers (e.g. 250 MHz). Furthermore, the imine signals appeared in a region of the  $^1\text{H}$  NMR spectrum that was well removed from any other resonances, thus limiting the risk of overlapping peaks resulting in inaccurate integration values. These initial results indicated that this self-assembling CDA stood a strong chance of being applicable for determining the *ee* of a wide range of chiral amines, with its combinatorial three-component nature affording the opportunity to change the chiral diol component used for derivatisation to maximise the signal resolution of pairs of diastereomeric peaks as required (*vide infra*). The modular nature of this CDA also afforded the opportunity to use an enantiopure amine as a chiral reporter to analyse the *ee* of chiral diols or any other chiral analyte that might show orthogonal reactivity for either the boronic acid or formyl groups of the 2-FPBA template [22].

### 2.2. Structural and mechanistic features of IBE complex formation

Since our initial report describing the use of this three-component method to determine the *ee*'s of amines, significant structural and mechanistic work has been carried out to understand the efficiency of the self-assembling pathways leading to formation of these stable IBE complexes. X-ray crystallographic analysis of the diastereomeric IBEs ( $\alpha$ -*S,S*)-**7ab** and ( $\alpha$ -*R,S*)-**7bb** [29] produced in the three-component assembly reaction of (*S*)-BINOL **5**, 2-FPBA **1** and enantiopure  $\alpha$ -methylbenzylamine **6b** (Fig. 2) revealed N–B distances of 1.656 Å and 1.642 Å respectively, clearly indicating the presence of strong N→B coordination bonds



**Scheme 3.** Stepwise three-component self-assembly of an achiral IBE complex **4** by Dunn *et al.*

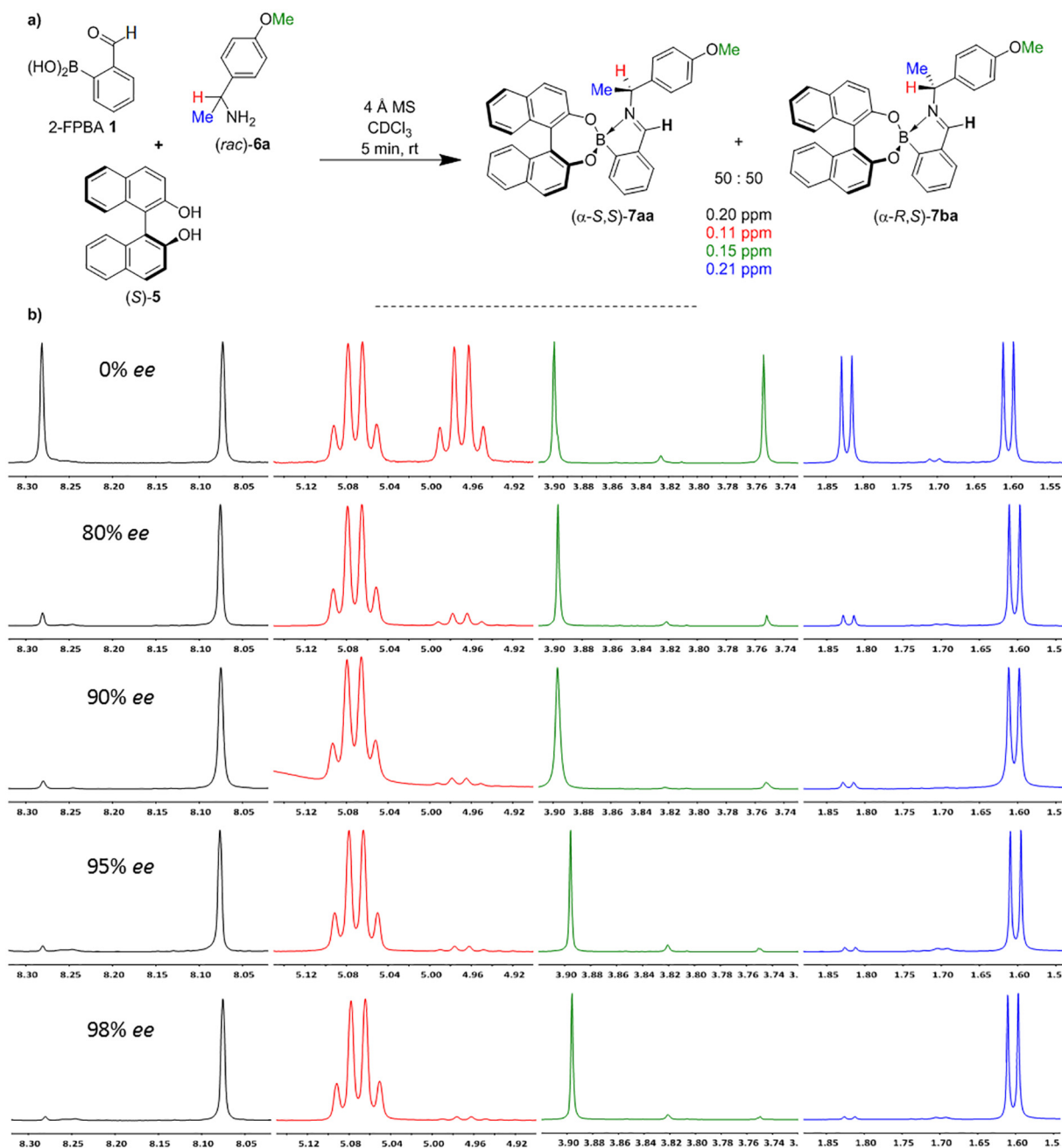


**Fig. 1.** (a) Three-component assembly of 2-FPBA **1**, (S)-BINOL **5** and (rac)-4-methoxy- $\alpha$ -methylbenzylamine **6a** and observed  $\Delta\delta_H$ 's. (b) Expanded  $^1\text{H}$  NMR (500 MHz,  $\text{CDCl}_3$ ) spectra of diastereomeric complexes produced from reaction of 2-FPBA **1** with (S)-BINOL **5** and (S)-**6a** of 0, 80, 90, 95 and 98% ee.

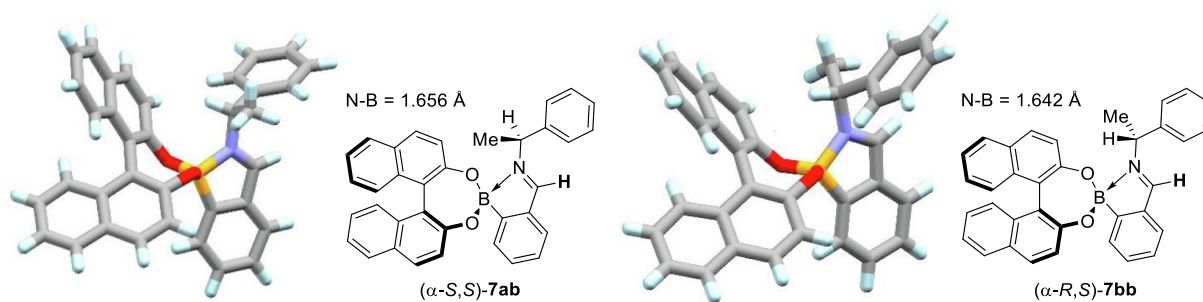
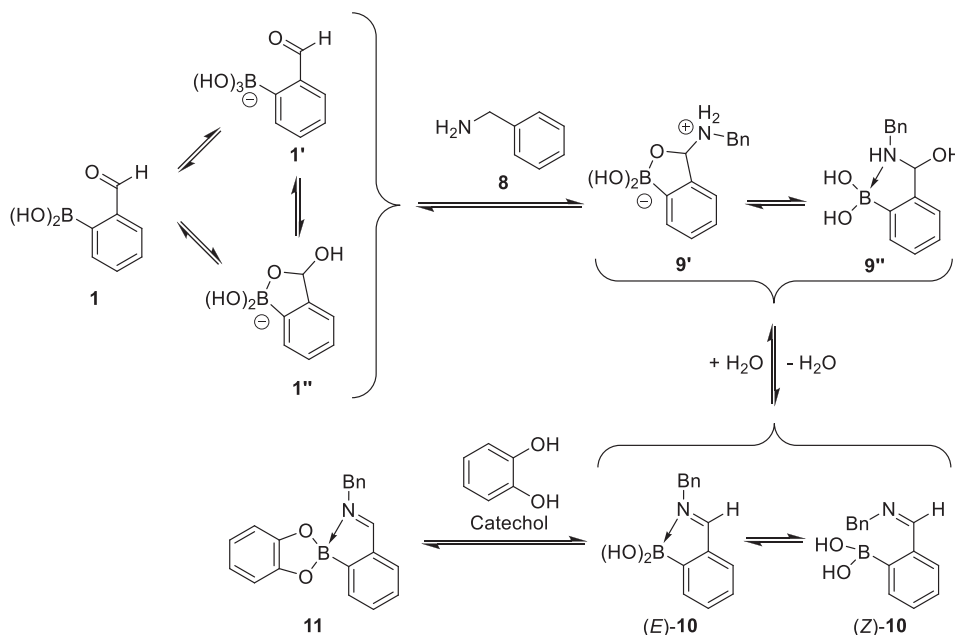


**Fig. 2.** X-ray crystal structures of IBEs (α-S,S)-**7ab** and (α-R,S)-**7bb**.



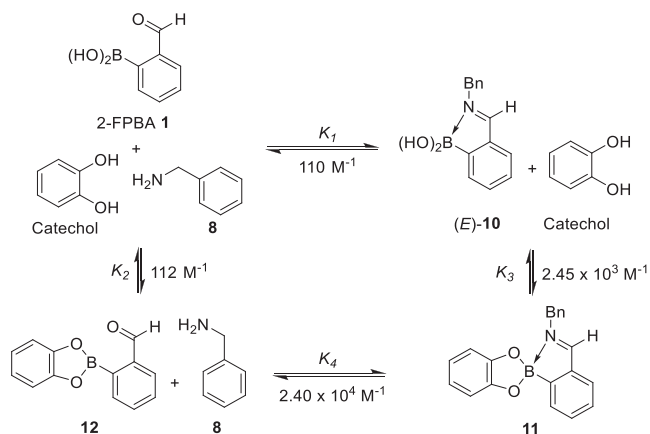
**Scheme 4.** Stepwise mechanism of the three-component assembly of 2-FPBA **1**, benzylamine **8** and catechol in  $\text{CD}_3\text{CN}$ .

that confer structural rigidity. This was further confirmed by  $^{11}\text{B}$  NMR spectroscopy which revealed upfield 'tetrahedral boron' signals for both complexes. This rigidity leads to the benzylic C–H bonds being positioned directly above the boronate centres to minimise steric interaction with the BINOL ligand. Differences in the  $^1\text{H}$  NMR chemical shifts of the  $\alpha$ -methyl protons of the diastereomers can be explained by the homochiral complex ( $\alpha$ -S,S)-**7ab** experiencing anisotropic shielding effects from the BINOL naphthyl moiety that are not present in the heterochiral ( $\alpha$ -S,R)-**7bb** complex. Similar variations in local anisotropic shielding effects between diastereomeric complexes are responsible for the different chemical shifts of multiple pairs of diastereomeric proton resonances observed in the  $^1\text{H}$  NMR spectra. The ease of crystallisation of Bull-James-assembled IBEs also provides the opportunity to determine the absolute configuration of a chiral amine (or diol) analyte through X-ray crystal analysis of a diastereomerically pure IBE complex prepared from a chiral diol (or amine) of known absolute configuration.

A simplified achiral three-component system using 2-FPBA **1**, catechol, and benzylamine **8** was used to explore the mechanism and kinetics of the stepwise formation of these self-assembled IBE complexes [30].  $^1\text{H}$  and  $^{11}\text{B}$  NMR spectroscopic analysis of two- and three-component reactions in acetonitrile- $d_3$  (improved solubility of reagents/products) revealed the presence of a multi-step reaction pathway leading to complex formation (Scheme 4). These studies revealed that the 2-FPBA **1** template exists in equilibrium with its corresponding borate **1'** and benzoxaborole **1''** species, with strong intramolecular binding of a lone-pair of its aldehyde group to the boron centre, activating the aldehyde towards nucleophilic attack [31,32]. Reaction of the aldehyde with an amine produces hemi-aminals **9'** and **9''** that then eliminate water to produce iminoboronic acid **10**. Subsequent addition of catechol then leads to formation of the desired achiral iminoboronate complex **11**. Interestingly, a small amount of the (*Z*)-imine (*Z*)-**10** (no intramolecular N→B coordination) was observed in the two-component complexation reaction, which is consumed through equilibration to (*E*)-IBE **10** upon addition of catechol. Similar reaction pathways and intermediates have been suggested and

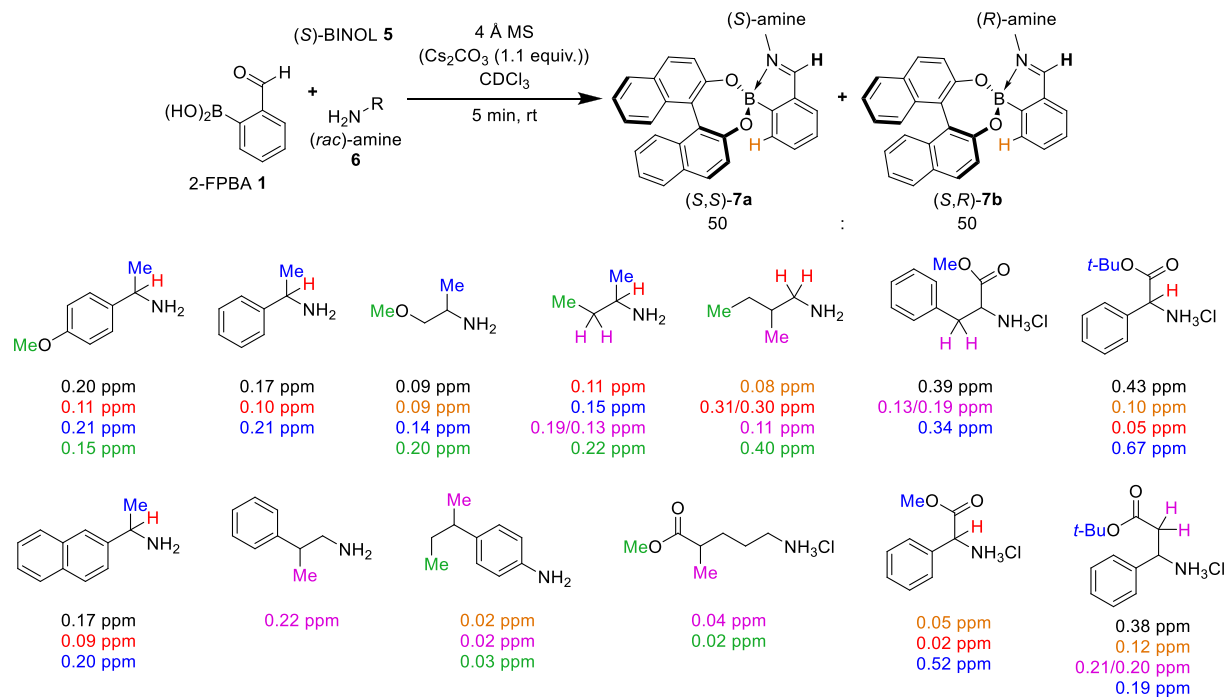
observed by others, including important works by Sporyński and Yatsimirsky [33–35].

In order to further evaluate the nature of the self-assembly processes operating in these complexation reactions, the observed binding constants for each individual two- and three-component assembly step in methanol were calculated (Scheme 5). These data clearly revealed that guest binding of the diol and amine to the 2-FPBA host is a cooperative process, as demonstrated by the dramatic increase in binding affinities when moving from two- to three-component assemblies. This difference in reactivity was observed when catechol binds to the boron centre, as equimolar mixtures of the diol and 2-FPBA **1** did not lead to quantitative formation of formyl boronate ester **12** ( $K_2 = 112 \text{ M}^{-1}$ ), whereas addition of catechol to iminoboronic acid **10** strongly favoured formation of iminoboronate ester **11** ( $K_3 = 2.45 \times 10^3 \text{ M}^{-1}$ ). Similarly, addition of benzylamine to boronate ester **12** to give iminoboronate ester **11** ( $K_4 = 2.40 \times 10^4 \text{ M}^{-1}$ ) was more favoured than addition of benzylamine to 2-FPBA **1** to afford imine **10**

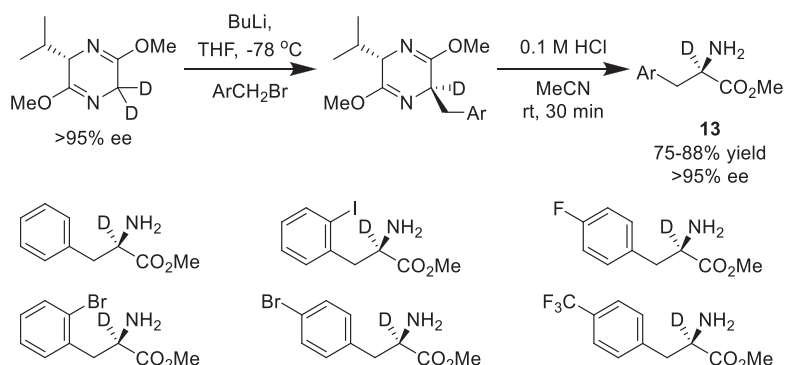


**Scheme 5.** Observed binding constants for intermediates generated in the three-component assembly reaction of 2-FPBA **1**, benzylamine **8** and catechol in  $\text{CD}_3\text{OD}$ .





**Scheme 6.** Three-component assembly reaction of 2-FPBA **1**, (S)-BINOL **5** and (rac)-amines **6** to afford diastereomeric IBEs with  $^1\text{H}$  NMR ( $300\text{ MHz}$ ,  $\text{CDCl}_3$ )  $\Delta\delta_{\text{H}}$  values quoted for selected pairs of diastereomeric resonances.



**Scheme 7.** Three-component CDA method (using enantiopure (R)-BINOL) used to determine the *ee*'s of  $\alpha$ -deuterated- $\alpha$ -amino esters **13** produced in asymmetric enolate alkylation reactions.

( $K_1 = 1100\text{ M}^{-1}$ ) by an order of magnitude. This further confirms that the strength of binding of the diol to the boron centre to produce a boronate ester complex is increased by the presence of a proximal imine functionality (and *vice versa*). These complexation results are consistent with results reported by Gillingham *et al.* to explain the efficiency of bioorthogonal iminoboronate complexation reactions (*vide infra*), as well as explanations provided to explain the reaction pathways present in analogues of *o*-aminomethylphenylboronic acid complexes [36–38].

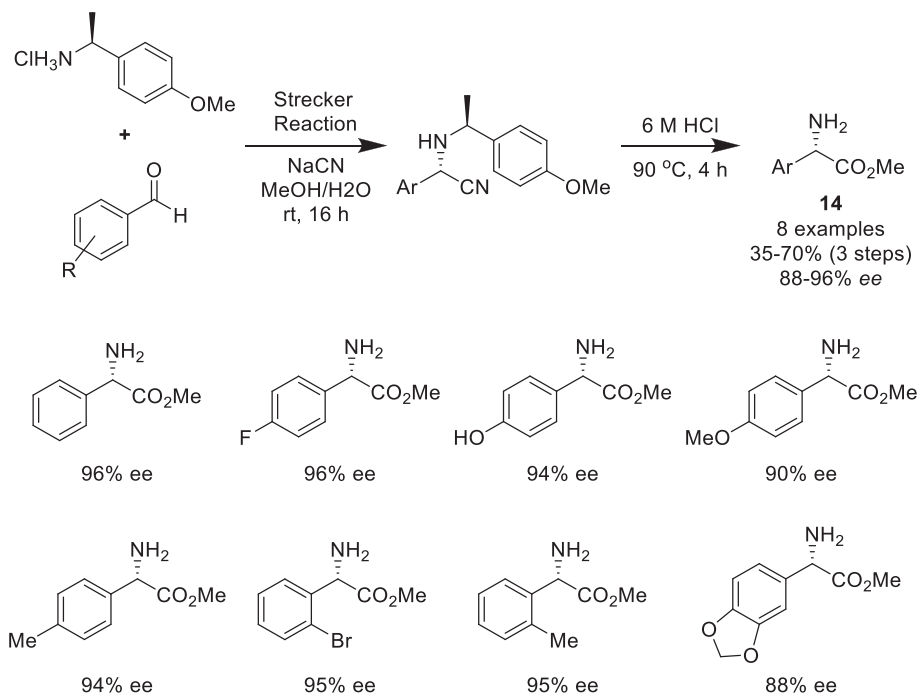
### 3. Three-component assembly for determining *ee* by NMR spectroscopic analysis

#### 3.1. Primary amines

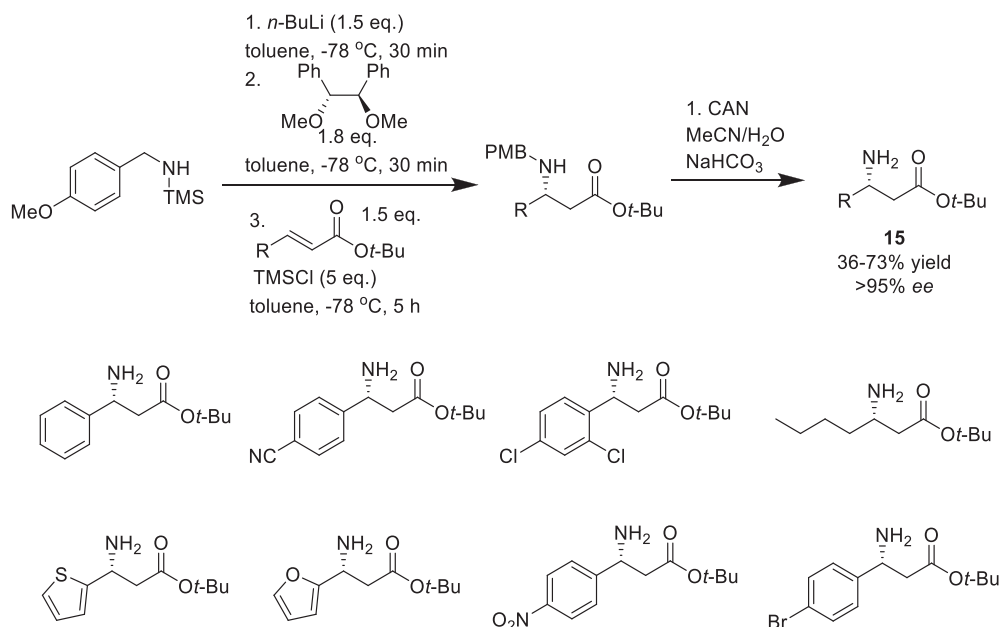
The optimal conditions (enantiopure BINOL,  $\text{CDCl}_3$ , 4 Å molecular sieves, 5 min) that were established to determine the *ee* of 4-

methoxy- $\alpha$ -methylbenzene **6a** have been applied to determine the enantiopurities of a wide array of primary chiral amine analytes (Scheme 6) [28]. This derivatisation approach shows good scope, affording a series of diastereomeric IBEs **7** whose  $^1\text{H}$  NMR spectra all exhibited at least one pair of well-resolved diastereomeric signals that could be integrated to determine their *dr*'s. Complexation using scalemic samples confirmed that none of these chiral amines underwent any kinetic resolution (or epimerisation) during the derivatisation process, thus allowing this new CDA to be used to accurately measure the *ee*'s of a wide range of chiral amine analytes. Interestingly, this derivatisation method was found to be effective for analysing the *ee* of primary amines containing remote stereocenters up to 5 carbon atoms removed from the complexed amino group, whilst direct analysis of chiral ammonium salts could be achieved through incorporation of  $\text{Cs}_2\text{CO}_3$  (1.1 equiv.) as a base for neutralisation. A subsequent report by Urriolabeitia and co-workers described that derivatisation of enantiopure phenyl-





**Scheme 8.** Three-component CDA (using enantiopure (*S*)-BINOL) used to determine the *ee*'s of  $\alpha$ -arylglycines **14** produced in asymmetric Strecker reactions.

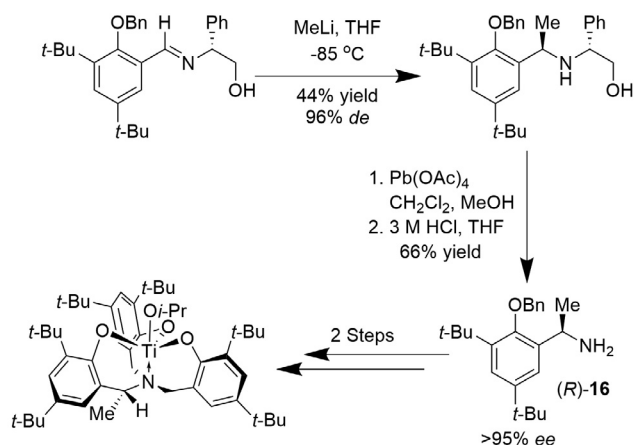


**Scheme 9.** Three-component CDA (using enantiopure (*R*)-BINOL) used to determine the *ee*'s of *tert*-butyl  $\beta$ -amino esters **15** produced in enantioselective *aza*-conjugate addition reactions.

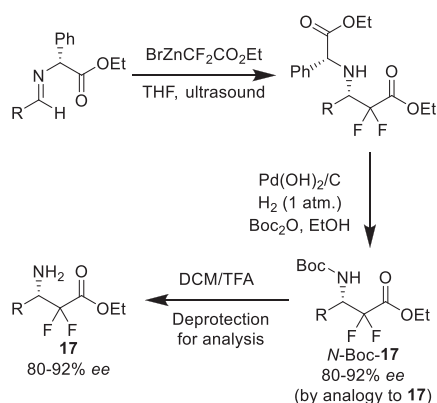
glycine methyl ester salts (more labile  $\alpha$ -stereocenter) resulted in formation of mixtures of diastereoisomeric IBEs when derivatisation reactions were left for extended periods of time ( $> 1$  h) [39]. We subsequently solved this racemisation issue by switching the base used for amine salt neutralisation from  $\text{Cs}_2\text{CO}_3$  to less-soluble  $\text{K}_2\text{CO}_3$ , which allowed racemisation-free derivatisation of chiral amine salts containing potentially labile stereocenters to be carried out [40].

Since our initial report, this CDA method has been published as a general procedure in *Nature Protocols* [41], and been used by the Bull group to validate the enantioselectivities of a number of new asymmetric methods for the production of chiral amines.

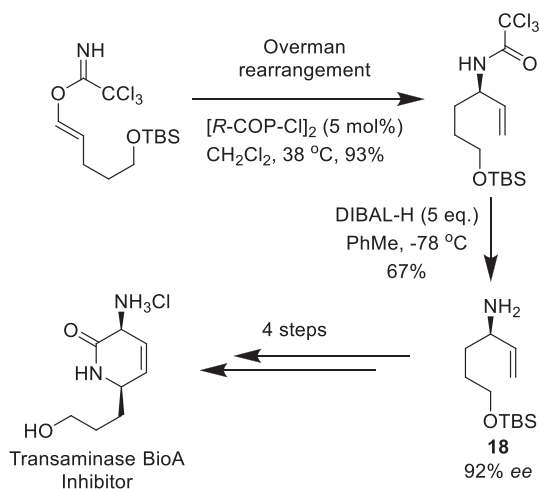
Their first application was to confirm the enantiopurities of (*R*)-[ $\alpha$ - $^2\text{H}$ ]-phenylalanine methyl esters generated by alkylation of the *aza*-enolate of deuterated Schöllkopf's *bis*-lactim ether **13** (Scheme 7) [42]. This CDA method has also been used to confirm the enantiopurities of  $\alpha$ - and  $\beta$ -amino esters **14** and **15** prepared using asymmetric Strecker (Scheme 8) and enantioselective *aza*-conjugate addition reactions, respectively (Scheme 9) [40,43]. It has also been used to confirm the enantiopurity of a chiral  $\alpha$ -methylbenzyl-amine intermediate (*R*)-**16** that was used for the synthesis of a chiral ligand for the preparation of a pseudo- $\text{C}_3$ -symmetric titanium alkoxide propeller-like complex (Scheme 10) [44].



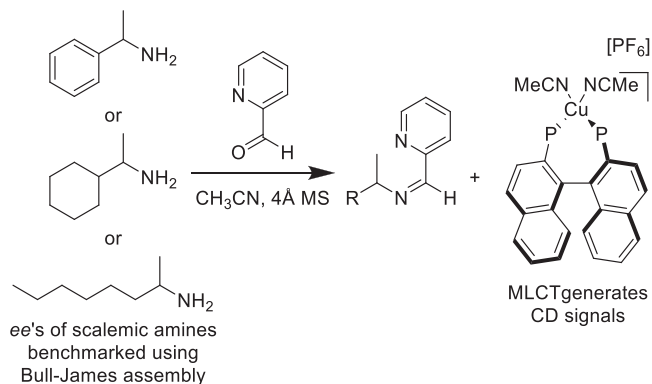
**Scheme 10.** Three-component CDA (using enantiopure BINOL) used to determine the *ee* of a tetradentate amine ligand (*R*)-**16** used to prepare an enantiopure 'propeller-like' pseudo- $C_3$ -symmetric titanium alkoxide.



**Scheme 11.** Three-component CDA method (using enantiopure (*S*)-BINOL) used to determine the *ee* of an  $\alpha,\alpha$ -difluoro- $\beta^3$ -amino ester **17** prepared using a sonocatalyzed Reformatsky reactions.



**Scheme 12.** Three-component CDA method (using enantiopure BINOL) used to determine the *ee* of a chiral allylamine **18** produced in an enantioselective Overman rearrangement reaction.



**Scheme 13.** Three-component analysis used to benchmark the *ee*'s of chiral amines used to develop a MLCT CD assay for high-throughput determination of the *ee*'s of primary amines (using (*S*)-BINOL).

Other research groups have also used the Bull-James assembly to determine the *ee* of amines produced in various stereoselective protocols. Duggan *et al.*, for instance, reported a novel synthesis of aliphatic  $\alpha,\alpha$ -difluoro- $\beta^3$ -amino esters **17** through addition of zinc enolates to chiral phenylglycine-derived imines (Scheme 11) [45], with the three-component CDA approach then used to demonstrate that the *N*-Boc-deprotected amine products had *ee*'s of 80–92%. The *ee* of a chiral allyl amine intermediate **18**, produced in an enantioselective Overman-rearrangement that was used to synthesise a transaminase BioA inhibitor (potential antitubercular agent), was also measured in this manner (Scheme 12) [46].

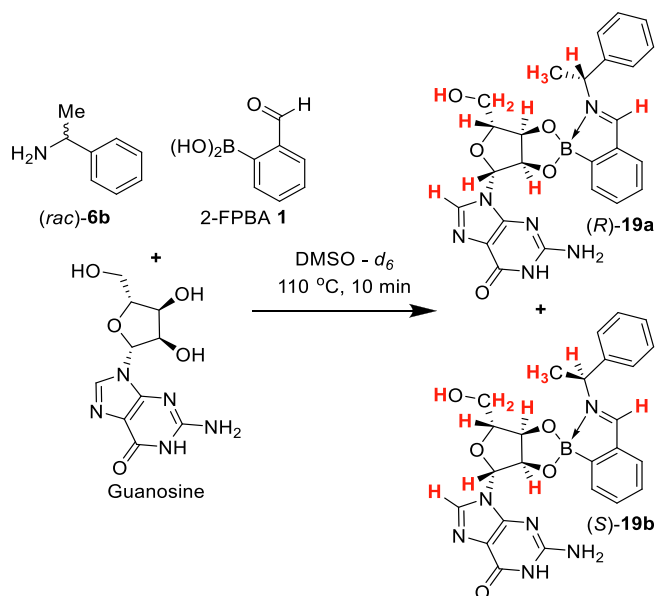
The Anslyn group have also employed NMR spectroscopic analysis of three-component IBE assemblies to benchmark the *ee*'s of amine analytes. These amines were subsequently used to develop a new CD method for high-throughput *ee* determination based on formation of diastereomeric chiral copper complexes that produce different metal-to-ligand charge transfer (MLCT) bands in the visible region of the CD spectrum (Scheme 13) [47].

Suryaprakash *et al.* have reported the use of the chiral diol fragments of RNA nucleosides as chiral selectors for determining the *ee* of a small range of amines [48], as shown for the complexation reaction of guanosine, 2-FPBA **1** and  $\alpha$ -methyl-benzylamine **6b** to produce the diastereomeric complexes **19a** and **19b** shown in Scheme 14. These complexation reactions required more forcing reaction conditions (DMSO, 110 °C) to proceed to completion, and whilst the structural complexity of these diastereomeric IBEs afforded multiple resolved resonance pairs, 800 MHz  $^1\text{H}$  NMR spectra were required to fully resolve them all.

Fossey and co-workers have exemplified the experimental simplicity and reproducibility of this NMR derivatisation protocol by successfully using it as the basis of a research-informed undergraduate teaching class that was used to train a cohort of >100 2<sup>nd</sup> year undergraduate students at the University of Birmingham (UK) [49]. An optimised iminoboronate protocol using 2-FPBA **1**, (*R*)-BINOL **5**, and  $\alpha$ -methylbenzylamine **6b** was used as an educational tool to introduce the students to the principles of dynamic covalent supramolecular chemistry and methods of determining the enantiopurities of chiral molecules, whilst reinforcing their knowledge of carbonyl condensation chemistry and fundamental Lewis acid/base coordination processes.

### 3.2. Diamines

The Bull-James CDA protocol was then applied to determine the *ee*'s of two widely used *trans*-diamines: 1,2-diphenylethane-1,2-diamine **20** and *trans*-cyclohexane-1,2-diamine **21** [50]. Reaction of diamine (*rac*)-**20** with (*R*)-BINOL **5** and 2-FPBA **1** resulted in the formation of a pair of diastereomeric imidazolidines (*R,R,R*)-



**Scheme 14.** Three-component assembly of 2-FPBA **1**, guanosine, and (*rac*)- $\alpha$ -methylbenzylamine **6b**. Pairs of diastereomeric protons that exhibited resolved resonances in a 800 MHz  $^1\text{H}$  NMR spectrum are shown in red.

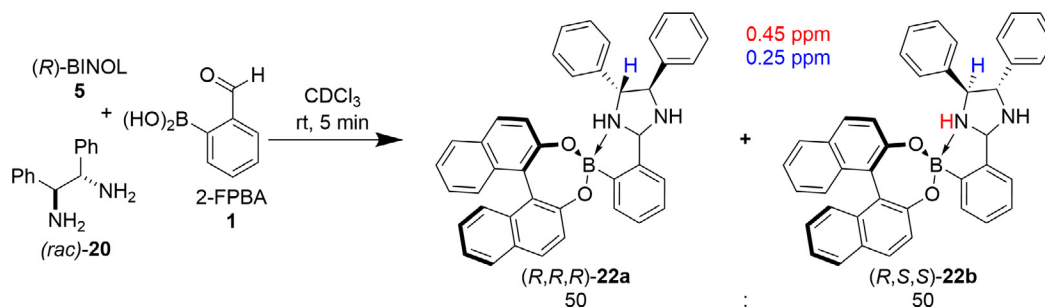
**22a** and (*R,S,S*)-**22b** [51–53], which exhibited well-resolved pairs of diastereomeric signals for the amino (red) and benzylic (blue) protons proximal to their BINOL fragments being observed in their  $^1\text{H}$

NMR spectra (Scheme 15) [50]. Furthermore, these diastereomeric IBE complexes were found to be stable enough for N–H deuteration by addition of  $\text{D}_2\text{O}$ , which resulted in simplified  $^1\text{H}$  NMR spectra that enabled more accurate determination of *dr*'s.

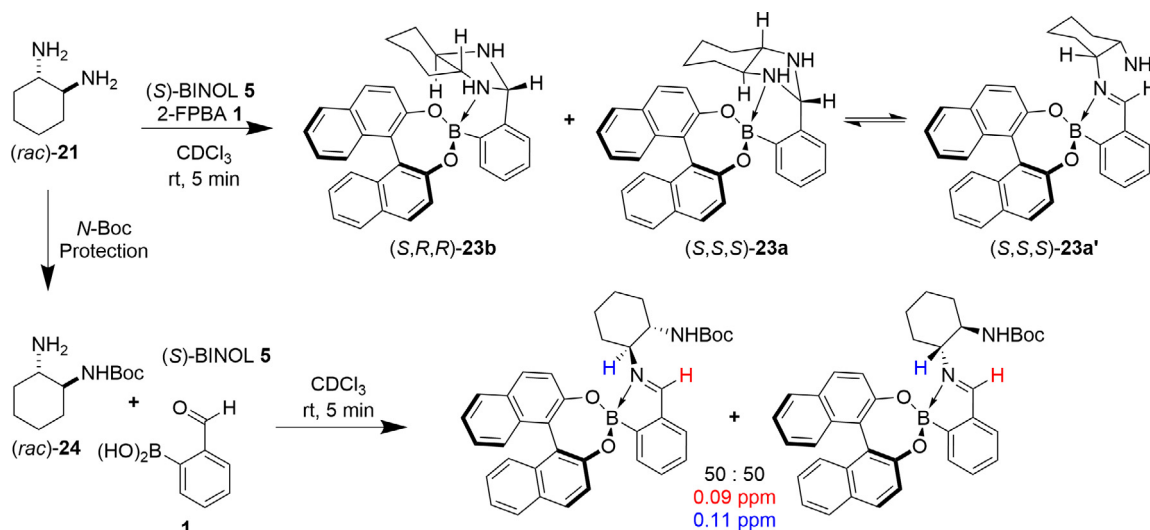
Unfortunately, applying this CDA approach to *trans*-cyclohexane-1,2-diamine **21** proved unsuccessful, with its derivatisation with (*S*)-BINOL **5** and 2-FPBA **1** producing a mixture of products (Scheme 16). Although the heterochiral imidazolidine complex (*S,R,R*)-**23b** proved stable, increased steric demands within the homochiral complex resulted in formation of a dynamically equilibrating mixture of imidazolidine (*S,S,S*)-**23a** and its corresponding imine (*S,S,S*)-**23a'**. A simple solution to this problem was achieved, through *N*-Boc-protection of the parent diamine **21** to afford mono-*N*-Boc-diamine **24**, which then underwent IBE derivatisation to afford the desired mixture of IBE diastereomers in the usual manner.

### 3.3. Amino alcohols

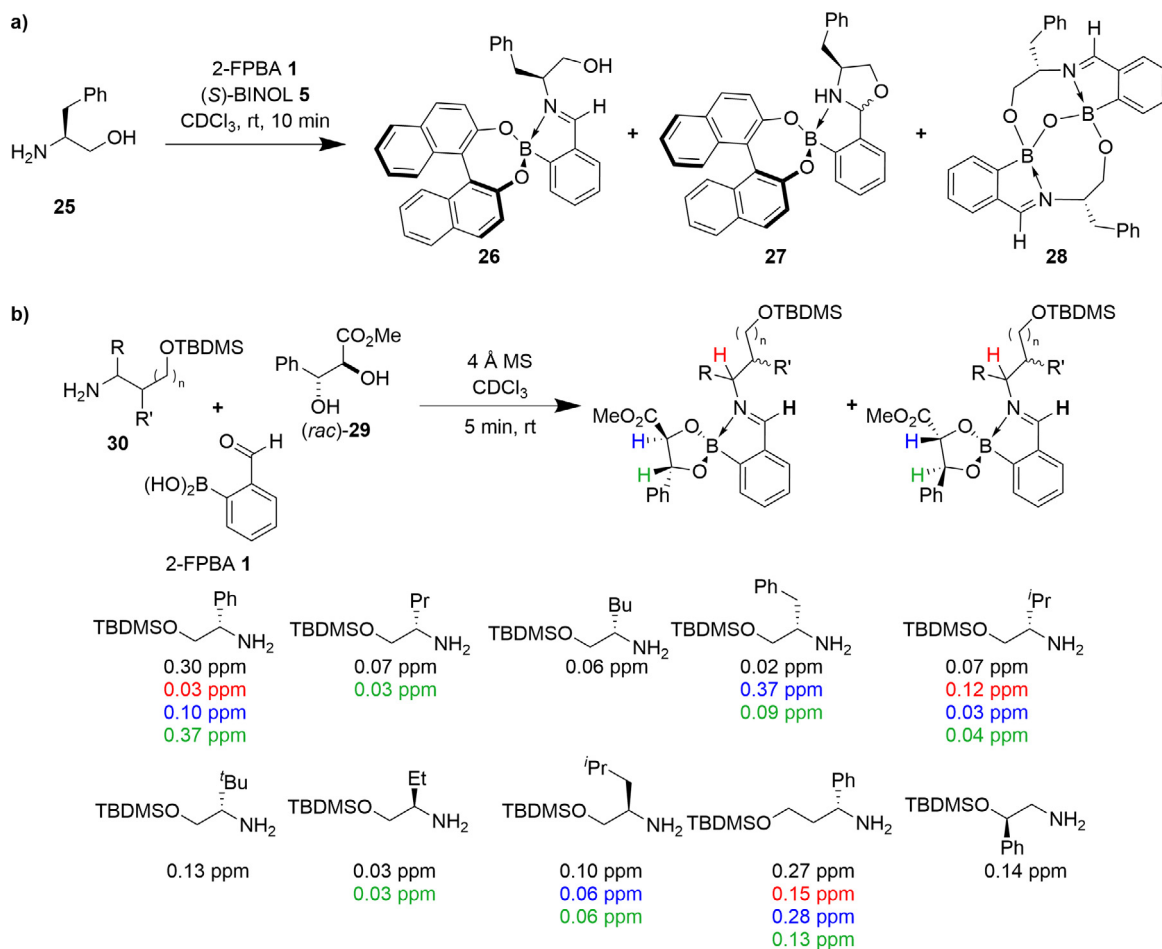
Attempts to apply the CDA methodology to 1,2-amino-alcohols proved similarly problematic, with assembly of (*S*)-phenylglycinol **25**, 2-FPBA **1** and (*S*)-BINOL **5** producing complex equilibrating mixtures of products (Scheme 17), including the desired IBE **26**, oxazolidine boronate ester **27** and a larger polyboracycle **28** [54]. Once again, the problems caused by these competing complexations could be solved using a protection strategy, with *O*-silylation of the problematic alcohol functionality prior to assembly resulting in the three-component complexation proceeding smoothly to give the desired diastereomeric IBEs. A simple diol



**Scheme 15.** Three-component assembly of 2-FPBA **1**, (*R*)-BINOL **5** and (*rac*)-*trans*-diphenylethylenediamine **20** to produce a pair of diastereomeric imidazolidine boronate esters **22** with  $^1\text{H}$  NMR (500 MHz,  $\text{CDCl}_3$ )  $\Delta\delta_{\text{H}}$  of selected resonances.



**Scheme 16.** Three-component derivatisation of 2-FPBA **1**, (*S*)-BINOL **5** with (*rac*)-*trans*-cyclohexane-1,2-diamine **21** and (*rac*)-*N*-Boc-*trans*-cyclohexane-1,2-diamine **24** with  $^1\text{H}$  NMR (400 MHz,  $\text{CDCl}_3$ )  $\Delta\delta_{\text{H}}$  of selected resonances.



**Scheme 17.** (a) Problematic three-component assembly of (S)-phenylglycinol **25**, 2-FPBA **1** and (S)-BINOL **5**. (b) Three-component derivatisation of 2-FPBA **1**, (rac)-**29** and O-silylated 1,2-amino alcohols **30** with <sup>1</sup>H NMR (400 MHz, CDCl<sub>3</sub>)  $\Delta\delta_H$  of selected resonances.

screen revealed that the best results were obtained when BINOL was substituted by (rac)-(syn)-methyl 2,3-dihydroxy-3-phenylpropionate **29**, which was subsequently employed for the successful three-component derivatization of ten enantiopure O-silyl amino alcohol analytes **30**.

### 3.4. Hydroxylamines

Bull-James assembly of hydroxylamines **31** with 2-FPBA **1** and (rac)-BINOL **5** in the presence of Cs<sub>2</sub>CO<sub>3</sub> as base gave mixtures of diastereomeric nitrono-boronate esters **32** (Scheme 18) [55]. Unlike amines, which form five-membered IBEs containing a relatively labile intramolecular N→B bond, hydroxylamines gave more stable diastereomeric six-membered nitrono-boronate ester complexes whose formation was favoured by both strong N-O and O-B bonds [26,56]. These structures were confirmed by X-ray crystallography of (α-S, R)-**32bf**, which revealed a bicyclic assembly containing a coplanar zwitterionic -C=N<sup>+</sup>-O-B<sup>-</sup> arrangement (Fig. 3). This produces a rigid ring system that produces relatively large chemical shift differences for selected pairs of diastereomer resonances (up to 0.242 ppm) in their <sup>1</sup>H NMR spectra.

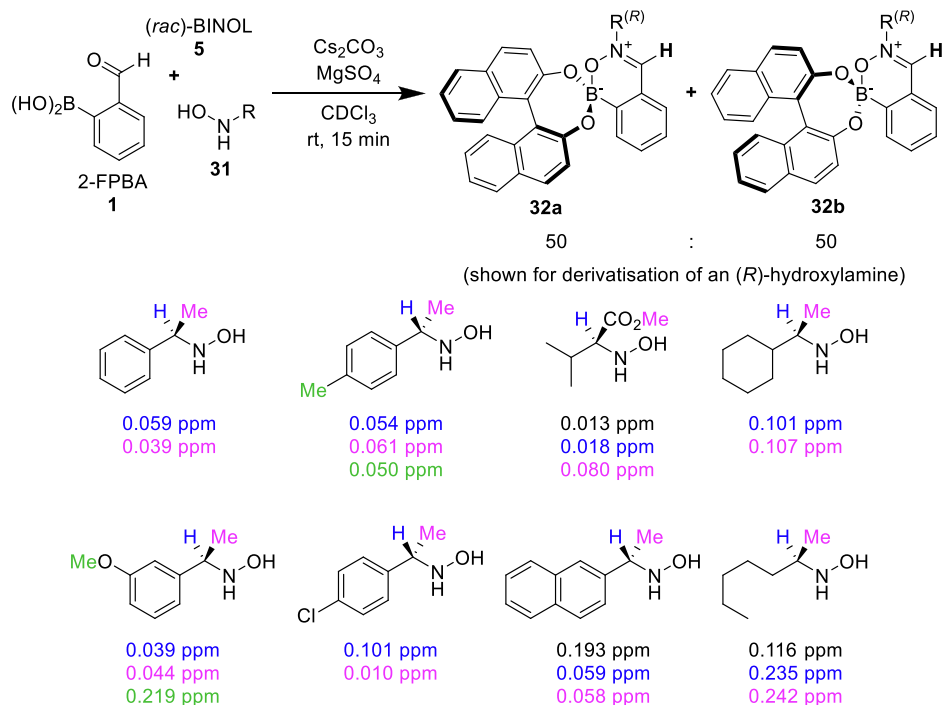
### 3.5. Sulfinamides

Chiral sulfinamides (primarily Ellman's and Davis') are widely used as chiral auxiliaries and ligands to control stereoselectivities in a wide range of asymmetric reactions. These sulfinamides are normally prepared in enantiopure form via either classical resolu-

tion of their corresponding racemates or stereoselective synthesis, which means that robust methods are required to accurately determine their enantiopurities. Application of standard Bull-James complexation conditions to these sulfinamides proved unsuccessful, with their less nucleophilic nitrogen atoms only affording small amounts of the desired sulfiniminoboronates, regardless of reaction conditions or additives employed. Consequently, a stepwise 'one-pot' two-component protocol was developed based on initial reaction of 2-FPBA **1** with a sulfinamide **34** to afford a sulfiniminoboronic acid intermediate **35**, whose boronic acid fragment was then reacted with pinanediol **36** to afford the desired sulfiniminoboronate ester complexes **37** (Scheme 19) [57]. This stepwise protocol was successfully applied to 8 racemic sulfinamides, which resulted in baseline-resolved imine signals for their diastereomeric IBEs in their <sup>1</sup>H NMR spectra in all instances, with no evidence of kinetic resolution.

### 3.6. Diols

The role of analyte and chiral reporter in the three-component CDA are broadly interchangeable, and so the Bull-James assembly has also been adapted to determine the ee's of chiral 1,2- and 1,3-diol analytes through use of an enantiopure amine chiral reporter (Scheme 20) [58]. α-Methylbenzylamine (S)-**6b** was chosen as a cheap readily available chiral amine reporter for reaction with 2-FPBA **1** and a range of racemic chiral diols **38**, which produced diastereomeric complexes (α-S,S,S)-**39a** and (α-S,R,R)-**39b**,



**Scheme 18.** Three-component assembly of 2-FPBA **1**, (*rac*)-BINOL **5**, and chiral hydroxylamine **31** to form diastereomeric nitrono-boronate ester complexes **32a** and **32b** with  $^1\text{H}$  NMR (500 MHz,  $\text{CDCl}_3$ )  $\Delta\delta_H$  of selected resonances.

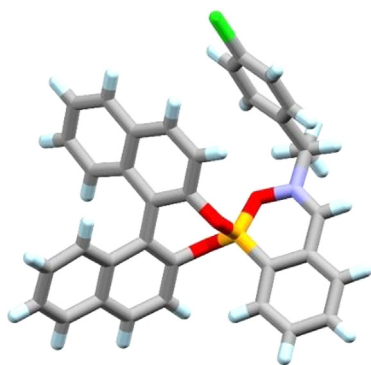
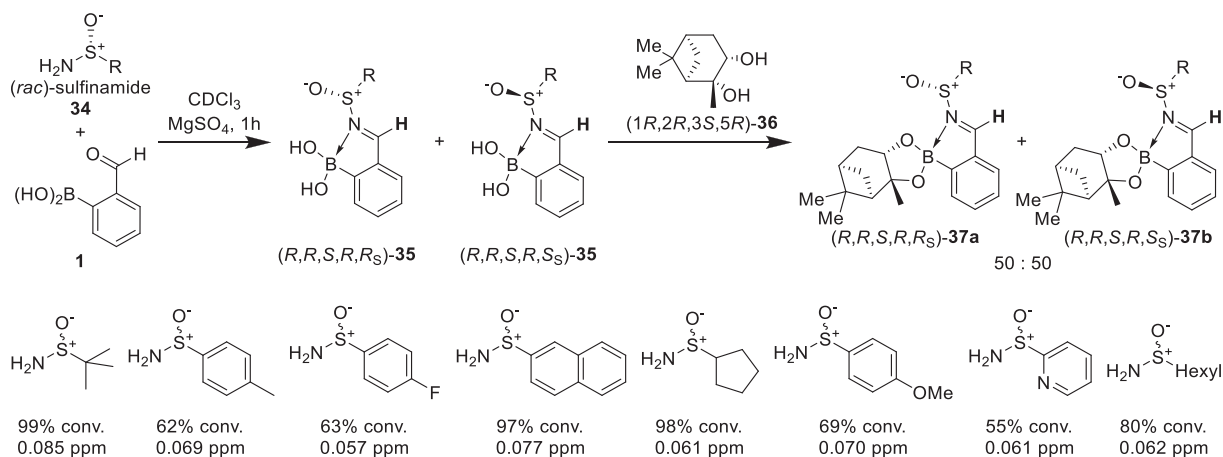


**Fig. 3.** X-ray crystal structure of ( $\alpha$ -*S*, *R*)-**32bf**, from (*S*)-4-chloro- $\alpha$ -methylbenzylamine **31f**.

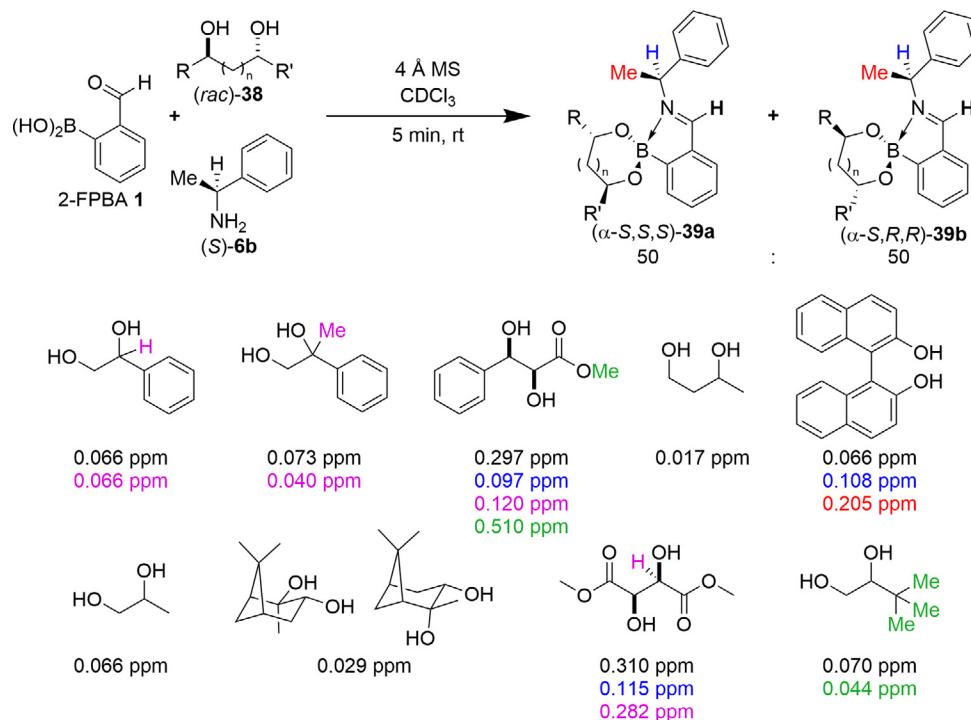
which exhibited one or more baseline-resolved pairs of signals for their IBE diastereomers in their  $^1\text{H}$  NMR spectra.

This method has also been published as a detailed general procedure in *Nature Protocols* [59], and has subsequently been applied to determine the *ee* of a range of chiral 1,2-diols by a number of research groups. One elegant example is the work by Watkins *et al.*, who employed the CDA (using (*S*)- $\alpha$ -methylbenzylamine **6b**) to determine the *ee*'s of a range of chiral furan and thiophene diols (**40** and **41**, respectively) prepared using Sharpless enantioselective ADmix dihydroxylation methodology, that were used for the first stereoselective synthesis of (+)-armillariol C **40a** (Scheme 21) [60]. Inoue *et al.* used enantioselective dihydroxylation reactions of  $\alpha,\beta$ -unsaturated esters to prepare both enantiomers of syn-diol **42** (shown for ADmix- $\alpha$ ), whose  $\beta$ -stereocenters were then inverted in two steps via cyclic organosulfate intermediates to afford their corresponding

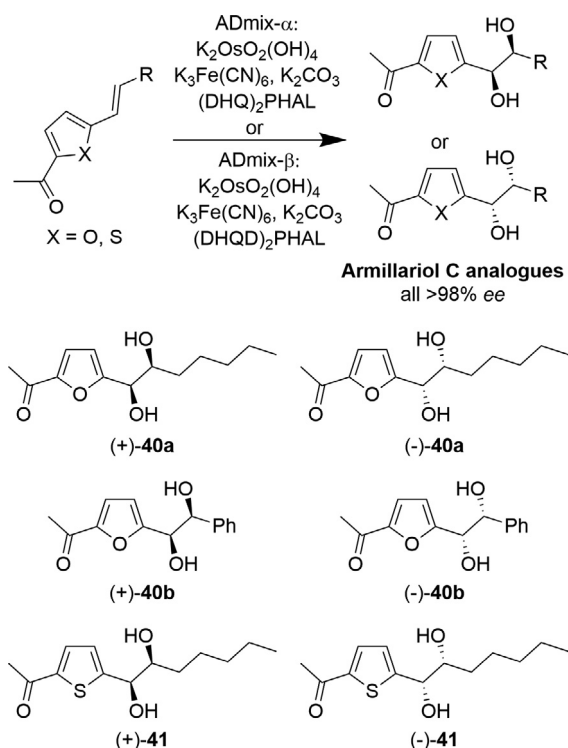


**Scheme 19.** Stepwise three-component assembly of 2-FPBA **1**, (1*R*,2*R*,3*S*,5*R*)-pinanediol **36** and (*rac*)-sulfonamides **34** with  $^1\text{H}$  NMR (500 MHz,  $\text{CDCl}_3$ )  $\Delta\delta_H$  of selected resonances.





**Scheme 20.** Three-component assembly using **2-FPBA 1**, **(S)- $\alpha$ -methyl benzylamine 6b** and **(rac)-diols 38** with  $^1\text{H}$  NMR (300 MHz,  $\text{CDCl}_3$ )  $\Delta\delta_{\text{H}}$  of selected resonances.



**Scheme 21.** Three-component CDA method (using enantiopure **(S)- $\alpha$ -methylbenzylamine**) used to determine the *ee* of both enantiomers of **Armillariol C** and analogues **41** that were produced using a Sharpless asymmetric dihydroxylation reaction.

*anti*-diols. The enantiopurities of all four diol stereoisomers were determined as 96–99% *ee* using three-component chiral derivatization (using  $\alpha$ -methylbenzylamine **6b**), with these stereoisomers then transformed into the four corresponding stereoisomers of

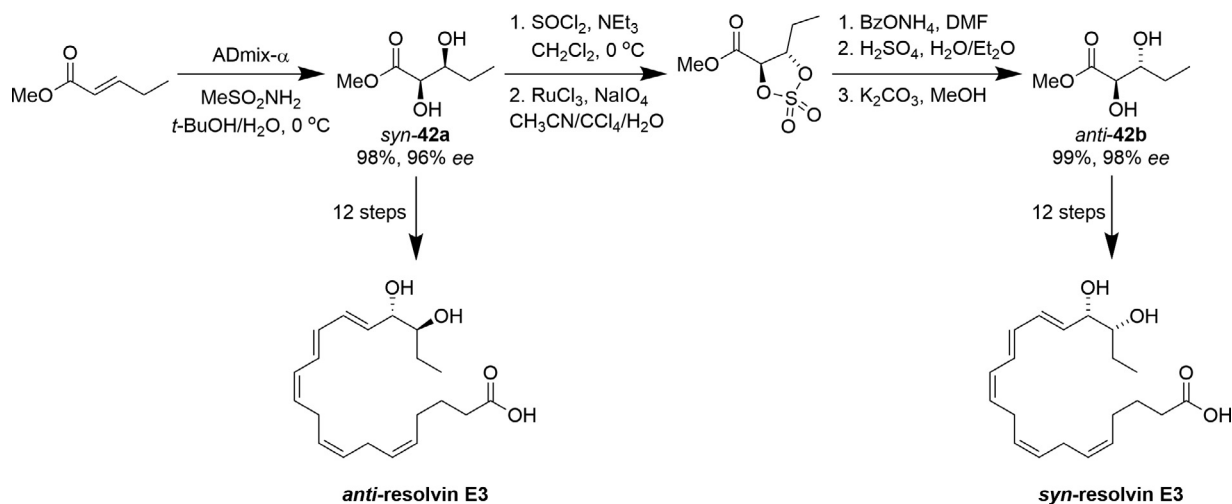
resolvin E3 (**Scheme 22**) [61]. Similarly, this CDA approach has been used to determine the enantiopurity of diol **43** (90% *ee*, single stereocenter, using both **(R)**- and **(S)-6b**) that was also produced in an enantioselective dihydroxylation reaction and subsequently used to prepare 3-oxo and 3 $\beta$ -hydroxytauranin (**Scheme 23**) [62].

Chopard *et al.* have used the three-component CDA to determine the enantiopurities of *cis*-diols **44** and **45**, produced from the microbial *cis*-dihydroxylation of naphthalenes and pyridinones. In this instance, the chiral amine reporter used for derivatization was optimised, which identified phenylglycine *tert*-butyl ester **46** as the chiral reporter that gave diastereomeric IBEs with the best  $\Delta\delta_{\text{H}}$  values (**Scheme 24**) [63].

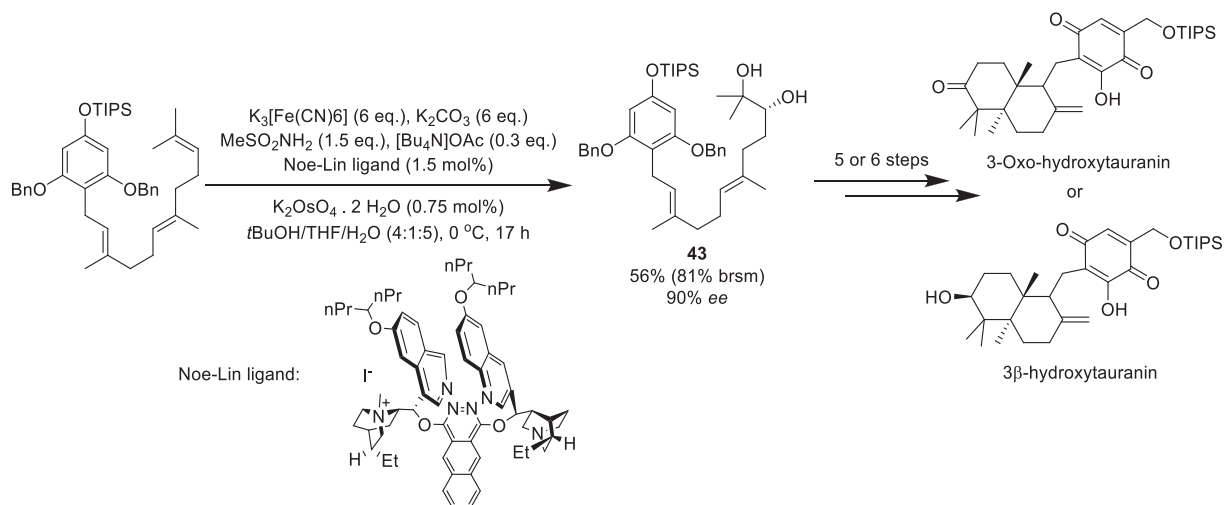
The three-component CDA was also used to measure the *ee*'s of *cis*-diols **47** and **48** produced in Sharpless dihydroxylation reactions by Anslyn *et al.* (**Scheme 25**). The *ee*'s of these diols were then used to benchmark indicator displacement UV–Vis assays for the high-throughput determination of yields and enantioselectivities of Sharpless dihydroxylation reactions. This approach employed reversible host/guest assemblies of an *o*-aminomethylphenylboronic acid sensor, in which the UV–Vis signal intensity is directly determined by the *ee* and concentration of the analyte [64,65].

The Bull group have applied the CDA method to determine the *ee* of a range of chiral 1,3-diols **49** synthesised in moderate to good *ee* by tandem hydroboration/reduction of  $\beta,\gamma$ -unsaturated esters (**Scheme 26**) [66]. The three-component assembly CDA has also been used by Herzon *et al.* to determine the *ee* of 1,3-diol **50** (92%) that was synthesised by catalytic reductive hydration of a chiral alkynylsilane by sequential hydration/hydrogenation using a novel half-sandwich ruthenium complex and formic acid (**Scheme 27**) [67].

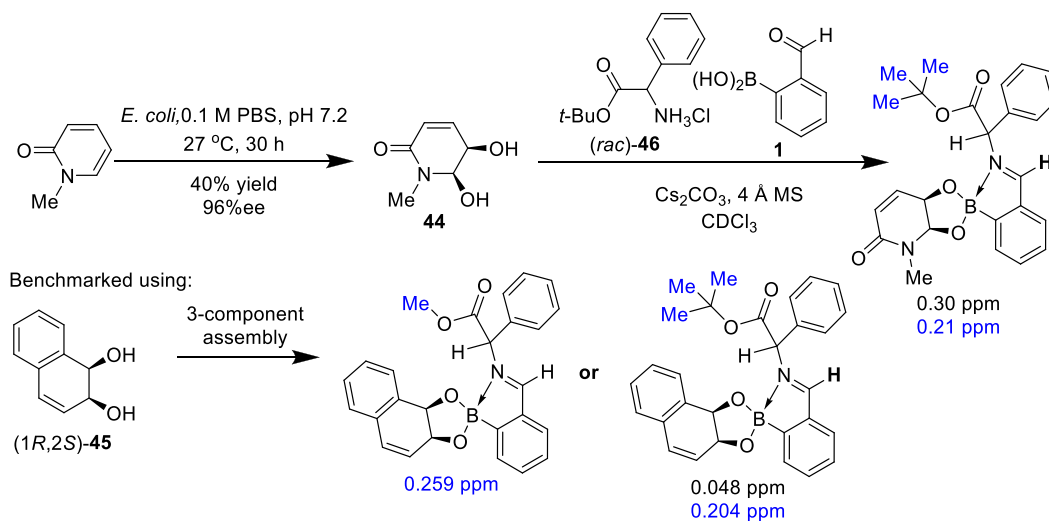
The three-component CDA has also been used to assess the enantiopurity of polymers containing diol fragments, with Kressler *et al.* reporting its application to determine the enantiopurities of poly(glycerol methacrylate)s (PGMA)s (**51**) that were prepared from enantiopure solketal methacrylate monomers using atom transfer



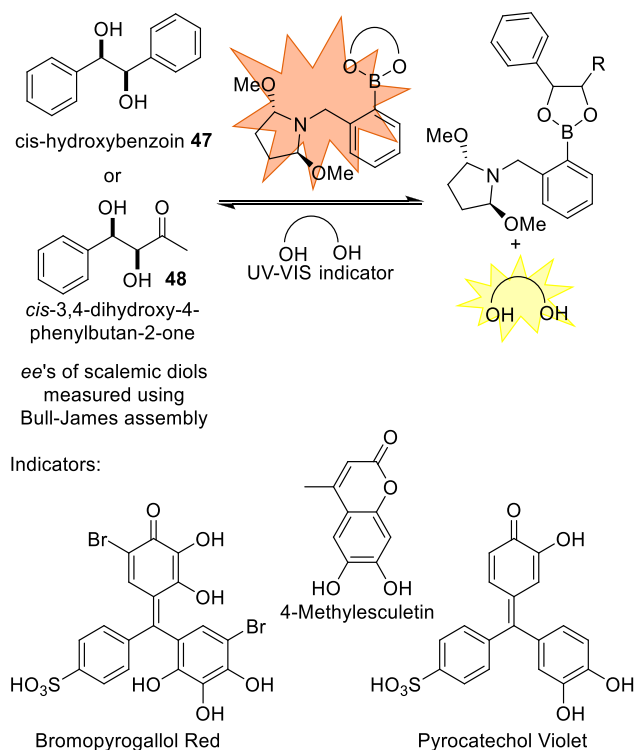
**Scheme 22.** Three-component CDA method (using enantiopure  $\alpha$ -methylbenzylamine) used to determine the *ee*'s of *syn*- and *anti*- diols **42a** & **42b** that were subsequently used to synthesis all four possible stereoisomers of resolvin E3 (shown for ADMix- $\alpha$ ).



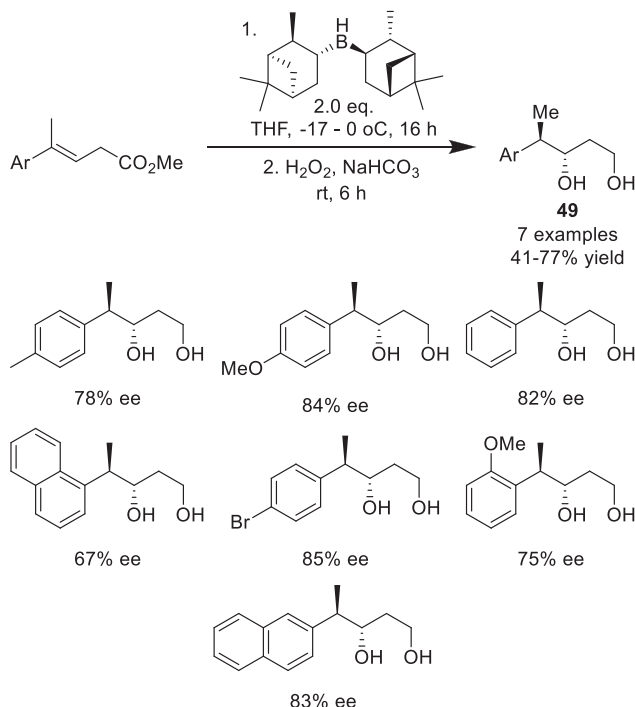
**Scheme 23.** Three-component CDA method (using enantiopure (*R*)- and (*S*)- $\alpha$ -methylbenzylamine) used to determine the *ee* of diol **43** that was subsequently used for total syntheses of 3-oxo- and 3β-hydroxytauranin.



**Scheme 24.** Three-component assembly for determining the enantiopurity of a *cis*-diol arene phenylglycine *tert*-butyl ester **46** and 2-FPBA **1** with  $^1\text{H}$  NMR (250 MHz,  $\text{CDCl}_3$ )  $\Delta\delta_{\text{H}}$  of selected resonances.

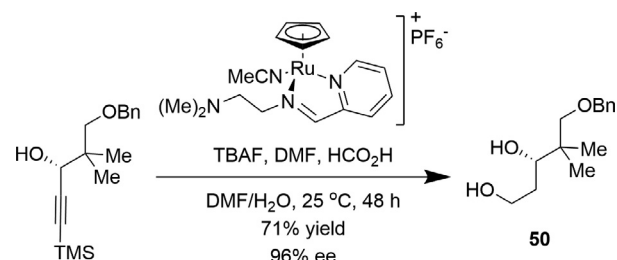


**Scheme 25.** Indicator displacement assay used for UV-Vis and colorimetric determination of enantioselectivity and yield of *cis*-diols **47** and **48** produced in Sharpless dihydroxylation reactions.



**Scheme 26.** Three-component CDA method (using enantiopure (*S*)- $\alpha$ -methylbenzylamine) used to measure the *ee*'s of chiral 1,3-diols **49** formed in tandem chiral borane-mediated asymmetric hydroboration/reduction reactions of  $\beta,\gamma$ -unsaturated esters.

radical polymerization (ATRP) reactions [68]. Enantiopure and racemic polymer chains were derivatised with  $\alpha$ -methylbenzylamine **6b** and 2-FPBA **1** in DMSO-*d*<sub>6</sub>, to afford



**Scheme 27.** Three-component CDA (using enantiopure  $\alpha$ -methylbenzylamine) to measure the *ee* of a 1,3-diol **50** formed in a stereoselective reductive hydration reaction of an alkynyl alcohol catalysed by a half-sandwich ruthenium complex.

mixtures of iminoboronates ( $\alpha$ -*S,S*)-**52a** and ( $\alpha$ -*S,R*)-**52b** that exhibited several pairs of distinct diastereomeric resonances in their <sup>1</sup>H NMR spectra (Fig. 4). Peak broadening caused by the polymeric backbone meant that baseline resolution was not observed, however the  $\Delta\delta_H$ 's of the polymer's methine, *exo* methylene and *endo* methylene proton signals (*aH*, *bH*, *cH*, respectively) were sufficiently different to enable qualitative assessment of the enantiopurity and absolute configurations of the PGMA side-chains of these polymers.

### 3.7. Hydroxyacids and diacids

The groups of Chaudhari and Suryaprakash have also expanded the scope of the Bull-James assembly CDA by demonstrating that it could be used to determine the enantiopurities of hydroxyacids **53/54** and 1,4-diacids **55** [69–71]. Treatment of (*rac*)- $\alpha$ -hydroxyacids (Scheme 28a) and (*rac*)- $\beta$ -hydroxyacids (Scheme 28b) with 2-FPBA **1** and  $\alpha$ -methylbenzylamine **6b** in MeOD-*d*<sub>4</sub> resulted in mixtures of diastereomeric iminoboronate esters which showed modest to excellent  $\Delta\delta_H$  (0.04–0.65 ppm) values in their <sup>1</sup>H NMR spectra. As in previous reports, the role of analyte and reporter in these IBE complexes was found to be interchangeable, and so corresponding use of an enantiopure hydroxyacid could be used to determine the *ee* of scalemic amines.

This methodology was optimised further to improve resolution and sensitivity, with the chiral amine reporter used for IBE complex formation changed from  $\alpha$ -methylbenzylamine **6b** to axially chiral diamine BINAM **56** [71]. Three-component assembly of  $\alpha$ -hydroxyacids **53**, 2-FPBA **1** and BINAM **56** produced diastereomeric IBEs which exhibited excellent chemical shift differences for pairs of diastereomeric resonances in their <sup>1</sup>H, <sup>13</sup>C{<sup>1</sup>H} and <sup>11</sup>B NMR spectra (Scheme 29). Interestingly, the excellent chiral discrimination produced in this self-assembled system resulted in chemical shift differences being observed in an IBE complex derived from achiral substrate glyconic acid, which exhibited a  $\Delta\delta_H$  = 0.04 ppm value for the prochiral  $\alpha$ -protons of its IBE complex.

Simple conformational models of the IBE complexes formed in these systems were developed, allowing the absolute configuration of hydroxyacids to be predicted using either BINAM **56** or  $\alpha$ -methylbenzylamine **53** as a chiral reporter [72,73]. Following benchmarking, analysis of the relative signs of the  $\Delta\delta_H$  values, broadness of signals and 2D nOe interactions enabled the absolute configuration of a range of hydroxyacids and primary amines to be assigned using BINAM **56** as a chiral reporter. In those cases where assignment was hampered by significant signal overlap in the <sup>1</sup>H NMR spectra, these resonances could be successfully deconvoluted using simple 2D RES-TOCSY <sup>1</sup>H NMR experiments [74].

These three-component assembly protocols were also used to determine the *ee*'s of chiral 1,4-diacids **55** (Scheme 30), resulting



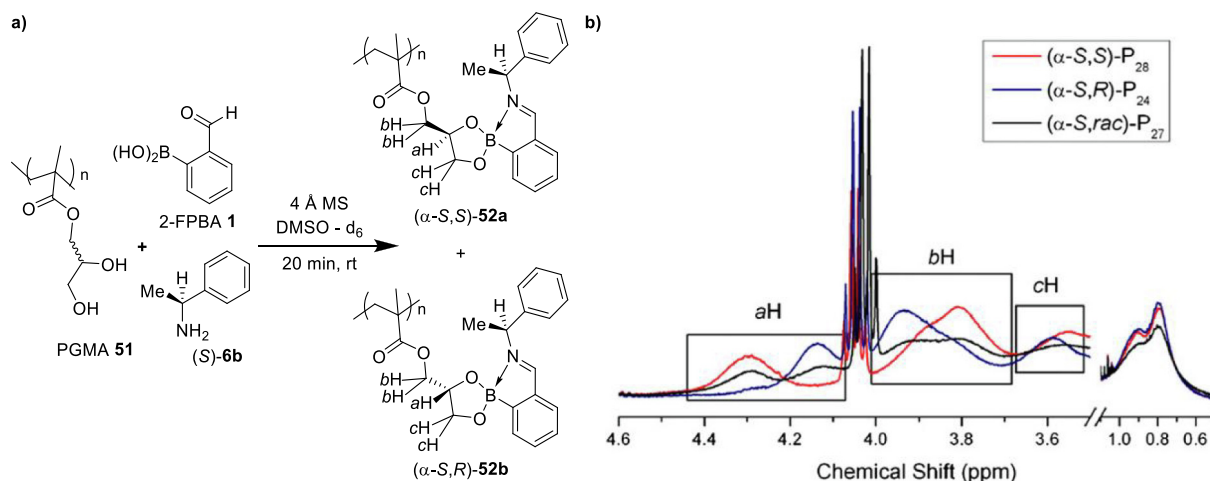
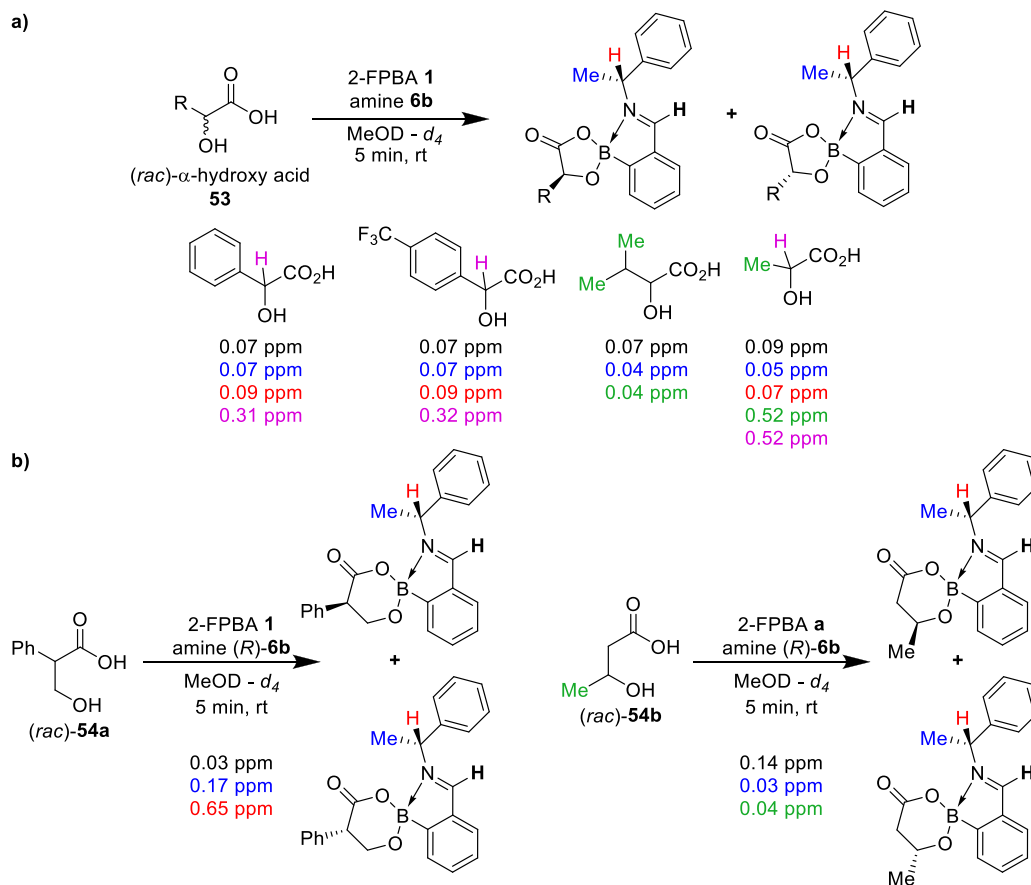


**Fig. 4.** (a) Bull-James assembly used for derivatisation of the diol side-chain of poly(glycerol methacrylate)s **51**. (b) Inset of <sup>1</sup>H NMR (400 MHz, DMSO-*d*<sub>6</sub>) spectra showing chemical shift variation of aH, bH and cH resonances of complexes of (S)-PGMA (red), (R)-PGMA (blue) and (rac)-PGMA (black). Reproduced from ref. [68] with permission from Elsevier.

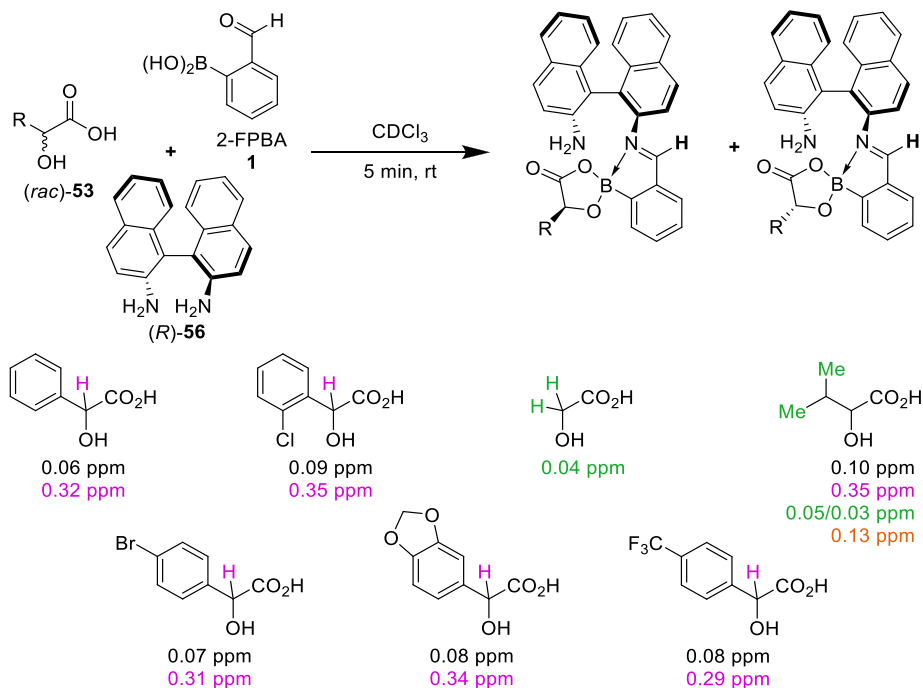


**Scheme 28.** Three-component CDA for determining the enantiopurities of (a) α-hydroxyacids **53**; and (b) β-hydroxyacids **54** with <sup>1</sup>H NMR (400 MHz, MeOD-*d*<sub>4</sub>) Δδ<sub>H</sub> of selected resonances.

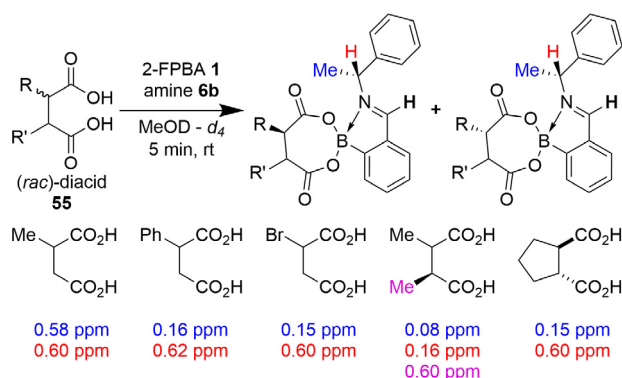
in moderate to excellent chemical shift differences ( $\Delta\delta_H = 0.08$ – $0.62$  ppm) in the <sup>1</sup>H NMR spectra of the diastereomeric IBEs of five diacid analytes [70]. Once again, the components of this assembly could be switched, enabling chiral diacids to be used to produce diastereomeric IBE complexes to determine the *ee*'s of chiral primary amines. In some instances, the large chemical shift differences observed in these diacid/amine-derived IBE complexes even led to full resolution of certain <sup>13</sup>C{<sup>1</sup>H} NMR signals.

### 3.8. <sup>19</sup>F NMR spectroscopic analysis

Fluorine was the first NMR-active heteronucleus to be studied for compatibility with the Bull-James assembly, due to the strength of its signal, its broad range of chemical shifts and the simplicity of <sup>19</sup>F NMR spectra, making it an excellent and widely-used NMR-active reporter. Bull and James first demonstrated incorporation of fluorine into their three-component assembly in 2009 [75,76],



**Scheme 29.** Three-component CDA for determining the enantiopurities of hydroxyacids **53** using 2-FPBA **1** and BINAM **56** with selected  $^1\text{H}$  NMR (400 MHz,  $\text{CDCl}_3$ )  $\Delta\delta_{\text{H}}$  of selected resonances.



**Scheme 30.** Three-component CDA for determining the enantiopurity of 1,4-diacids **55** with  $^1\text{H}$  NMR (400 MHz,  $\text{MeOD}-d_4$ )  $\Delta\delta_{\text{H}}$  of selected resonances.

with initial work focusing on using a fluorinated chiral amine reporter in the three-component protocol (Scheme 31). A range of diols **57**, 4-fluoro- $\alpha$ -methylbenzylamine 4-F-**6b** and 2-FPBA **1** were derivatized to form  $^{19}\text{F}$  NMR-active diastereomeric complexes ( $(\alpha\text{-S,S,S})$ -**58a** and ( $\alpha\text{-R,S,S})$ -**58b**, which exhibited a  $\Delta\delta_{\text{F}}$  range of 0.05–0.75 ppm. A similar approach was subsequently employed by Suryaprakash *et al.* for analysis of hydroxyacid and diacid protocols, with  $\text{CF}_3$ -appended chiral reporters and analytes affording diastereomeric complexes with non-equivalent  $^{19}\text{F}$  NMR signals that could be integrated to determine their *dr* [69,70].

A significant improvement to this fluorine approach was achieved by incorporating the fluorine reporter atom into the achiral 2-FPBA template to produce a generally applicable method for determining the *ee* of different classes of chiral analytes. 4-fluoro-2-formylphenylboronic acid (4-F-2-FPBA, 4-F-**1**) was synthesised and used in the three-component assembly protocol, producing fluorinated diastereomeric complexes **60** which afforded baseline-resolved signals in their  $^{19}\text{F}$  NMR spectra, allowing for

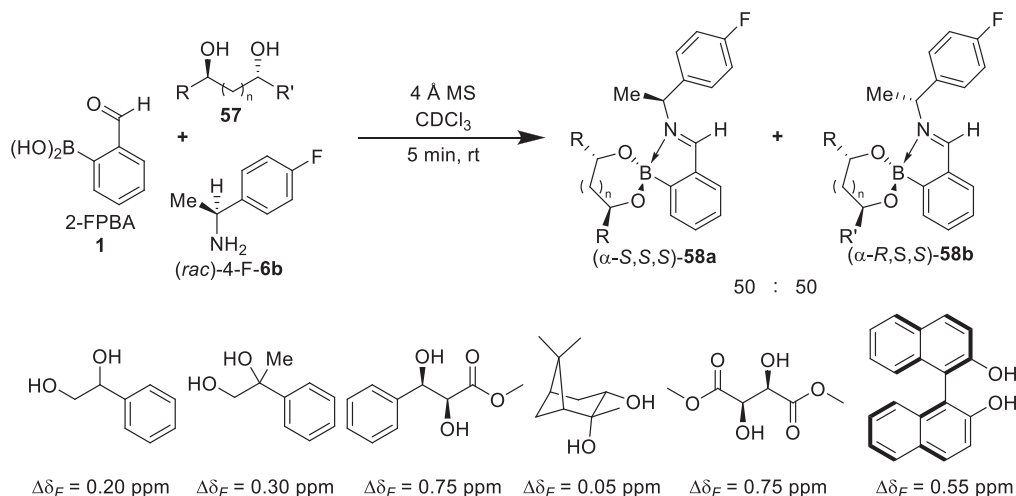
*ee* determination of diols by both  $^{19}\text{F}$  and  $^1\text{H}$  NMR spectroscopic analysis (Fig. 5). Similar results were reported by Suryaprakash *et al.* during their later work on applying this CDA to determine the enantiopurity of diacids [70].

Recently, Oe *et al.* have also reported the three-component assemblies of fluorinated 2-FPBA derivatives 3-F-**1**, 4-F-**1** and 5-F-**1** with (*S*)-BINOL **5** and  $\alpha$ -methylbenzylamine **6b** with the aim of identifying diastereomeric IBEs with the greatest  $\Delta\delta_{\text{F}}$  values (Scheme 32) [77]. After establishing that 5-F-**1** was the best fluorinated template (93% conversion,  $\Delta\delta_{\text{F}} = 0.10$  ppm for their model system), this system was optimised using excess BINOL and triethylamine (1.5 equiv. each) to minimize kinetic resolution and/or epimerisation of  $\alpha$ -amino ester salts **61**.

Finally, a recent study on all four regioisomers of fluoro-2-FPBA as bifunctional templates for analysis of the *ee*'s of sulfinamides revealed that 3-fluoro-2-FPBA 3-F-**1** was the optimal template (Fig. 6) [57], producing an impressive chemical shift difference of  $\Delta\delta_{\text{F}} = -2.328$  ppm between the IBE diastereomers produced from Ellman's sulfinamide (Fig. 6b). A stepwise approach was used to derivatise a small range of sulfinamides **34**, 3-F-**1** and (1*R*,2*R*,3*S*,5*R*)-pinanediol **36** which gave large chemical shift differences and full baseline resolution of the imine and fluorine peaks of their diastereomeric IBE complexes.

### 3.9. Chalcogen NMR spectroscopic analysis

Silva *et al.* have shown that incorporation of NMR-active chalcogens  $^{77}\text{Se}$  and  $^{125}\text{Te}$  into the analyte or chiral reporting unit can also be used to determine *ee* using three-component assembly protocols [78,79]. Their initial report focused on derivatising racemic chalcogen-containing amines **62** (Scheme 33) with 2-FPBA **1** and (*S*)-BINOL **5** to afford pairs of iminoboronate complexes.  $^{77}\text{Se}\{^1\text{H}\}$  and  $^{125}\text{Te}\{^1\text{H}\}$  NMR spectroscopy of these complexes showed excellent chemical shift anisochrony for the diastereomeric IBE complexes formed, with  $\Delta\delta_{\text{Se}}$  values ranging from 26.2 to 34.4 ppm and  $\Delta\delta_{\text{Te}}$  values ranging from 75.6 to 85.7 ppm. Although only racemic samples were employed in this work, the magnitude



**Scheme 31.** Three-component protocol using 2-FPBA **1**, 4-fluoro- $\alpha$ -methylbenzylamine **4-F-6b** and chiral diols **57** to produce fluorinated diastereomeric complexes with good  $^{19}\text{F}$  NMR (400 MHz,  $\text{CDCl}_3$ )  $\Delta\delta_F$  values.

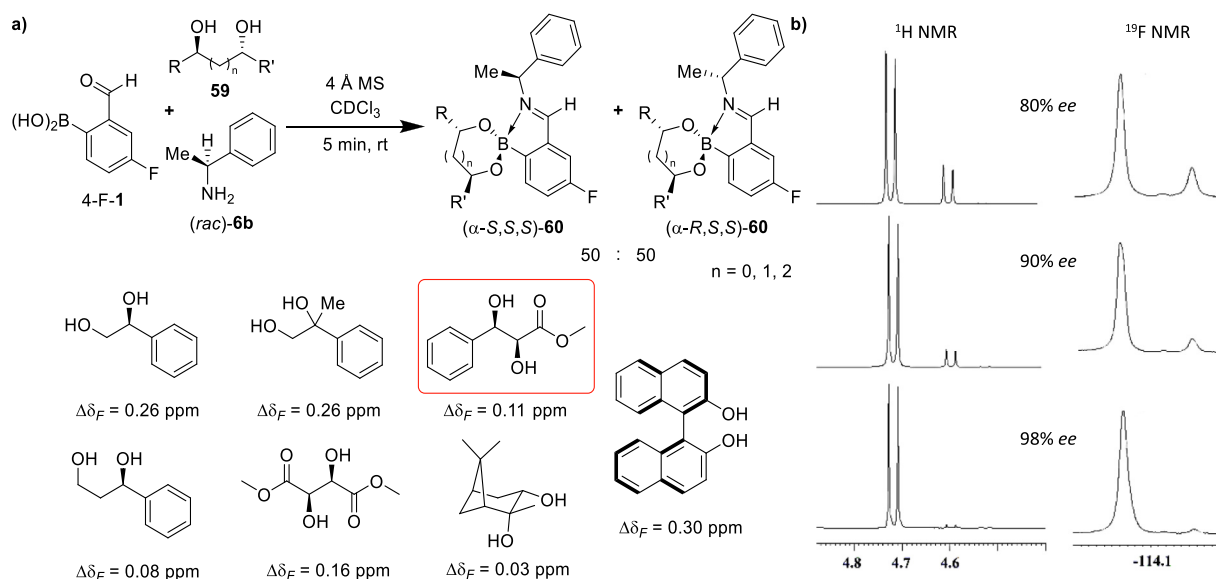


**Fig. 5.** (a) Three-component protocol using 4-F-2-FPBA **4-F-1**, (*rac*)- $\alpha$ -methylbenzylamine **6b** and chiral diols **59**. (b) Expansion of  $^1\text{H}$  (500 MHz,  $\text{CDCl}_3$ ) and  $^{19}\text{F}$  (470 MHz,  $\text{CDCl}_3$ ) NMR spectra of three-component assembly of **4-F-1**, (*R*)-**6b** and a scalemic diol (red) at 80%, 90% and 98% *ee*. Adapted from ref. [75] with permission from the American Chemical Society.

of chemical shift differences observed indicates that these systems would be useful for determining the *ee* of diol analytes.

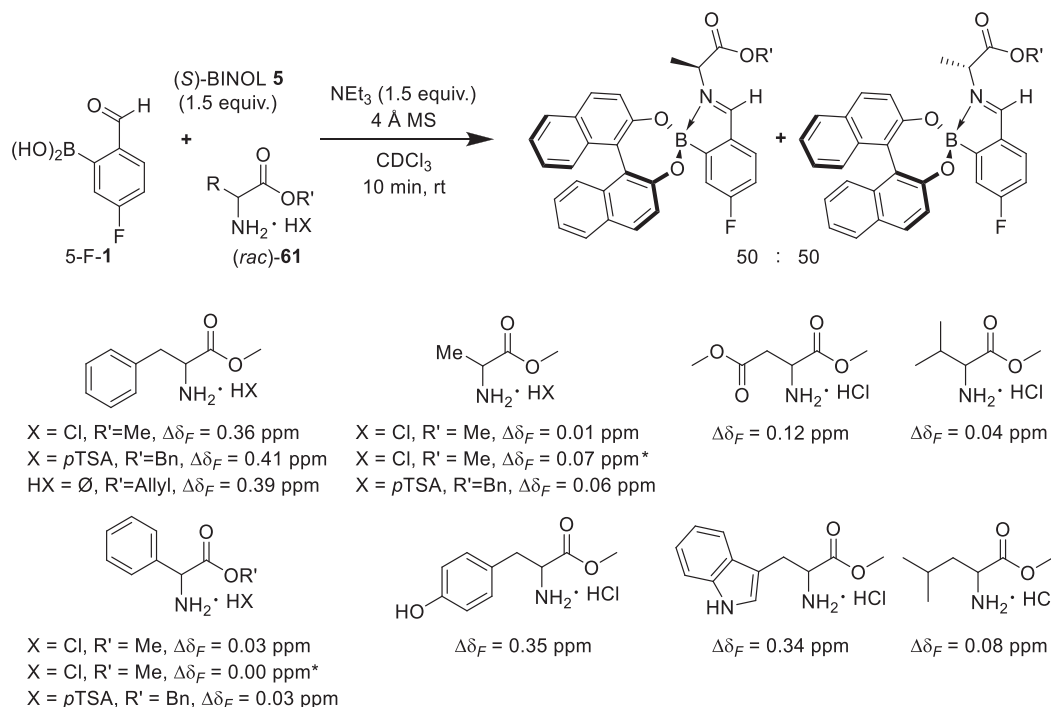
Subsequently, Silva *et al.* synthesised selenium-containing 3-phenylchalcogen-1,2-propanediol **63** for use as a chiral reporter with 2-FPBA **1** and chiral amines **64** which gave pairs of diastereomeric IBEs, the majority of which exhibited baseline-resolved diastereomeric signals in their NMR spectra with chemical shift differences for  $\Delta\delta_{Se}$  and  $\Delta\delta_{Te}$  of 0–1.144 ppm and 0.43 ppm, respectively (Scheme 34) [78]. Interestingly, the chemical shift differences observed in this instance were 100-fold smaller than for their previous examples, implying that the chalcogen atoms occupy positions in space that are relatively remote from the amine stereocenters and so only experience small anisotropic shielding effects. Nevertheless, integration of diastereomeric  $^{77}\text{Se}$  NMR signals could be used to produce accurate measurements of the *ee*'s of scalemic samples of known enantiopurities ( $\pm 4\%$ ).

#### 4. Three-component assembly for determining *ee* by optical methods

The Bull-James assembly has also been applied to the optical sensing of *ee* using methods that rely on CD, UV-Vis, or fluorescence spectroscopic analysis, with the aim of developing methods potentially applicable for high-throughput analysis [80,81]. All of these approaches rely on exploiting differences in the spectroscopic response of diastereomeric IBE complexes, whose *dr*'s correspond to the *ee* of the parent chiral analyte used for the IBE complexation.

##### 4.1. Determining the *ee* of amines and diols using circular dichroism

A collaboration between the Anslyn, Bull and James groups in 2012 reported the use of circular dichroism spectroscopy to anal-



**Scheme 32.** Modified Bull-James assembly of amino ester salts **61** with **5-F-1** and (S)-BINOL **5** with  $^{19}\text{F}$  NMR (376 MHz,  $\text{CDCl}_3$ )  $\Delta\delta_F$  of selected resonances. \*  $\text{CD}_2\text{Cl}_2$  used as solvent.

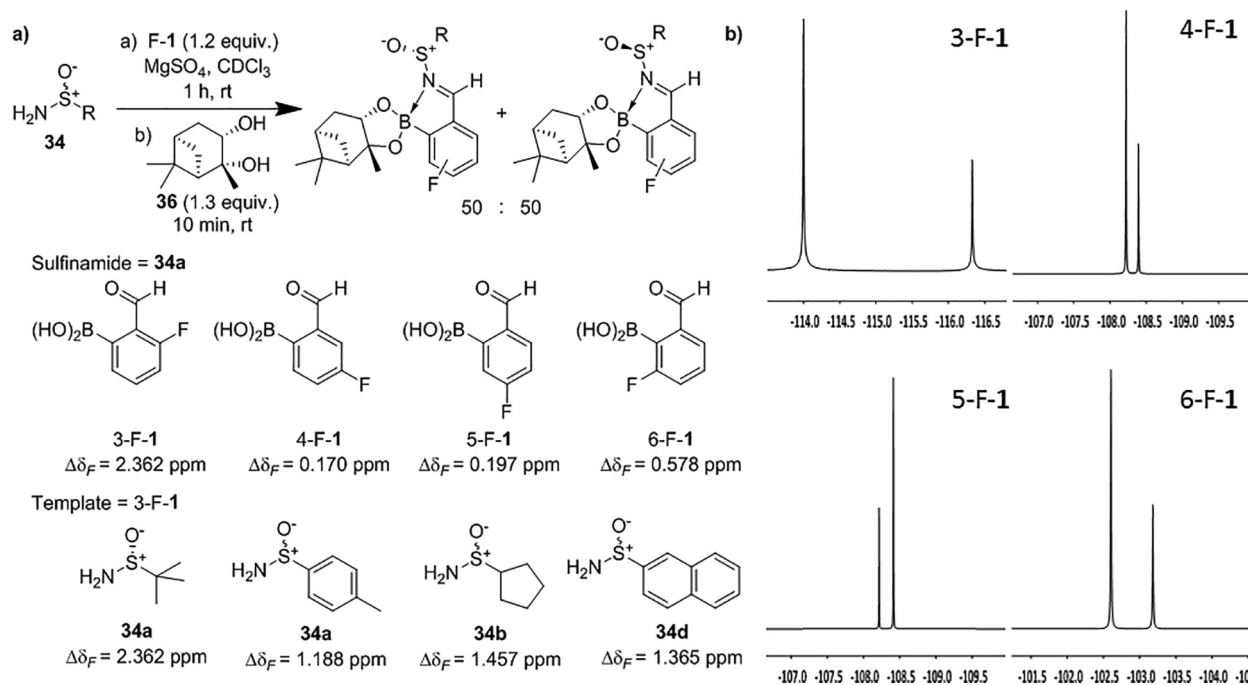
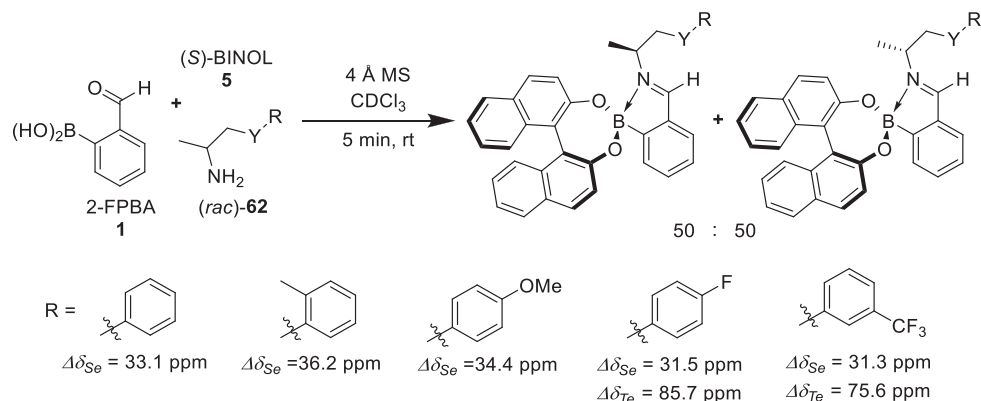


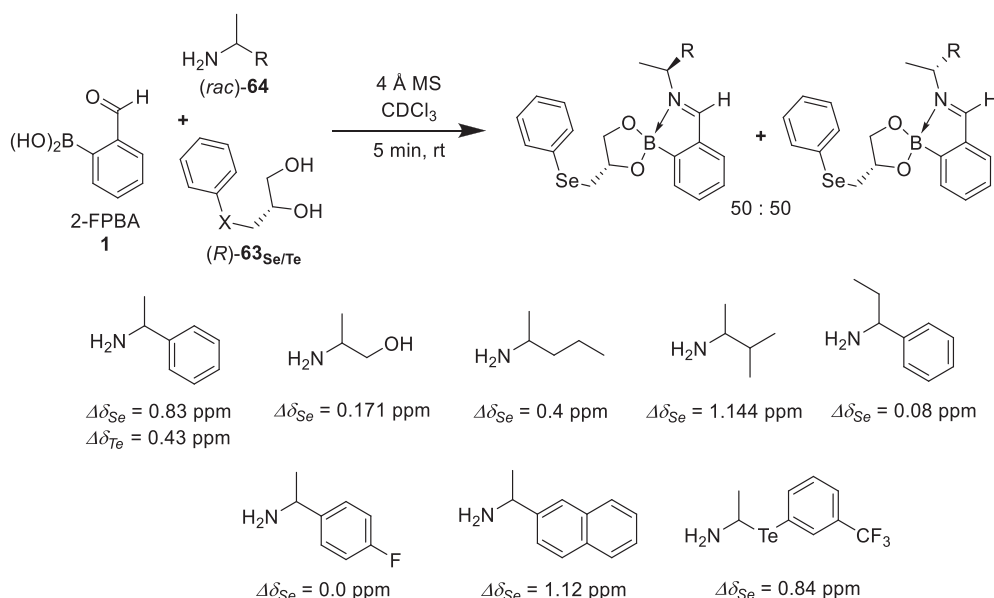
**Fig. 6.** (a) Stepwise three-component assembly of fluorinated 2-FPBA templates, (1R,2R,3S,5R)-pinanediol **36** and sulfinamides **34**. (b) Chemical shift differences in the  $^{19}\text{F}$  NMR (470 MHz,  $\text{CDCl}_3$ ) spectra of IBEs of the three-component assembly of Ellman's sulfinamide (R)-**34a** (33%), (1R,2R,3S,5R)-pinanediol **36** and four fluorinated 2-FPBA isomers (same scale).

ylse diastereomeric IBE complexes formed from the three-component self-assembly of chiral amines **66**, chiral BINOL derivatives **67/68**, and 2-FPBA **1** (Fig. 7a) [82]. As with many multicomponent host-guest assemblies, a strong CD signal was observed between 250 and 270 nm (Fig. 7b), with a maximum difference in signal response between diastereomeric complexes produced from the enantiomers of  $\alpha$ -methylbenzylamine **6b** observed at

253 nm (98,941 deg.cm<sup>2</sup>/dmol). This enabled BINOL and two brominated derivatives to be employed as chiral reporters in an array of sensing ensembles, whose CD signals were processed using Principal Component Analysis (PCA) and Linear Discriminant Analysis (LDA) to produce chemometric statistical models that were capable of differentiating between different  $\alpha$ -chiral amine analytes and determining their *ee*'s with an average error of



**Scheme 33.** Three-component assembly of 2-FPBA **1**, (S)-BINOL **5** and chalcogen containing amines **62**, and the  $\Delta\delta_{\text{Se}}$  (99 MHz,  $\text{CDCl}_3$ ) and  $\Delta\delta_{\text{Te}}$  (132 MHz,  $\text{CDCl}_3$ ) values of their diastereomeric IBE complexes.



**Scheme 34.** Three-component assembly of 2-FPBA **1**, chalcogen containing diols (R)-**63**<sub>Se/Te</sub> and racemic amines **64** with  $\Delta\delta_{\text{Se}}$  (99 MHz,  $\text{CDCl}_3$ ) and  $\Delta\delta_{\text{Te}}$  (132 MHz,  $\text{CDCl}_3$ ).

$\pm 5.8\%$  (Fig. 7c, d). The use of PCA and LDA is widespread in the field of differential sensing as multivariate statistical tools which recognise and amplify patterns from large datasets [83].

Subsequent to this report, Wolf *et al.* described a self-assembling system based on host complexes derived from 4-methoxy-2-FPBA (4-OMe-**1**) and non-chiral 2,2'-binaphthol **69** (Fig. 8a) [84]. Two-component assembly of chiral amines (1-cyclohexylethylamine **70** and 1-aminoindane **71**) with 4-OMe-**1** gave iminoboronic acid complexes with only weak CD signals (dashed lines). However, addition of achiral BINOL-derivative **69** resulted in a large increase in the Cotton signals of the resultant IBEs, consistent with the self-assembly process controlling the helicity of its BINOL fragment (solid lines, Fig. 8b). Although this system was not used for *ee* determination, the amplitude of signal change indicates this type of assembly is likely to be suitable for this purpose.

#### 4.2. Determining the *ee* of amines, amino-alcohols and diols using fluorescence

Collaborations with Anzenbacher have led to the development of multiple Bull-James assembly-derived fluorescence assays [85–88], with the practicality and versatility of this methodology lead-

ing to a *Nature Protocols*, validating its use as an effective method for the high-throughput analysis of the *ee* of chiral diols, amino alcohols and amines produced in stereoselective reactions [89]. Initial reports focused on the development of “turn-off” fluorescence based assemblies using fluorescent host systems comprised of 2-FPBA **1** and 3,3'-diphenyl-2,2'-bi-1-naphthol (VANOL) or 2,2'-diphenyl-(4-biphenanthrol) (VAPOL) as chiral reporter diols for determining the *ee*'s of scalemic amines (Fig. 9a) [85–87]. Interestingly, these extended aryl systems exhibited the same NMR chiral shift behaviour as seen in previous BINOL-based systems, with several sets of baseline-resolved signals observed for each pair of diastereomeric complexes in their  $^1\text{H}$  NMR spectra. This host system (2-FPBA + chiral fluorescent diol) was found to be suitable for *ee* determination of both amines and amino alcohols. In the case of amines (and amino acids/esters), IBE formation resulted in PeT quenching, leading to a “turn-off” fluorescence response (Fig. 9b). As shown in Fig. 9c, fluorescence intensity (FI) was dependent on the chirality of the amine analyte, which enabled *ee* values of amine samples to be correlated to changes in fluorescence intensity with good levels of accuracy ( $\pm 1\text{--}2\%$ ) (Fig. 9d).

This type of fluorescence based three-component self-assembly platform was also applied to the analysis of the *ee*'s of amino alcohols, with formation of oxazolidine intermediates resulting in a



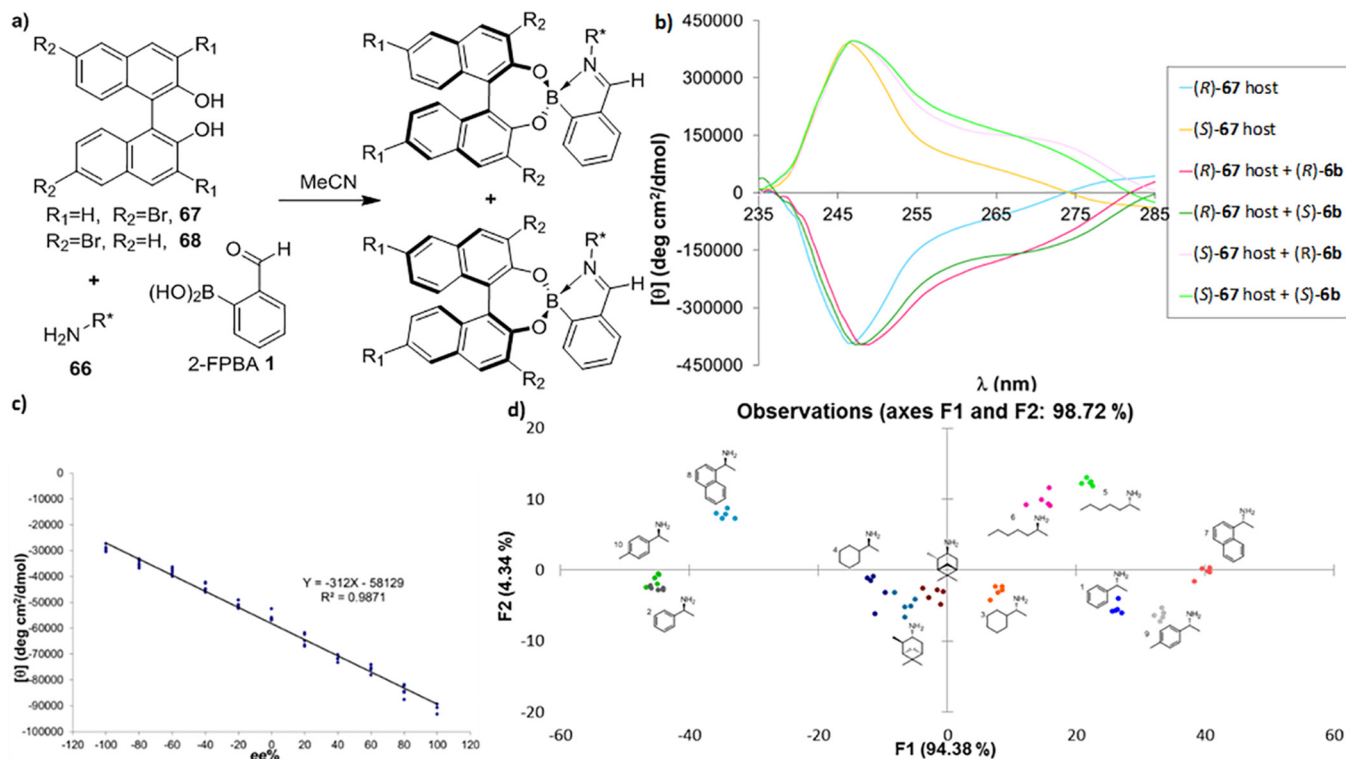


**Fig. 7.** (a) Three-component assembly of 2-FPBA **1**, BINOL-derivatives and a chiral amine. (b) CD spectra of diastereomeric IBE complexes obtained from 2-FPBA **1**, 6,6-dibromobINOL **68** and  $\alpha$ -methylbenzylamine **6b**. (c) Calibration curve for CD outputs of complexes produced from mixing (*R*)-BINOL **5**, 2-FPBA **1** and scalemic **6b** of known *ee*. (d) LDA plot of chiral amine analytes. b, c, d Adapted from ref. [82] with permission from the Royal Society of Chemistry.

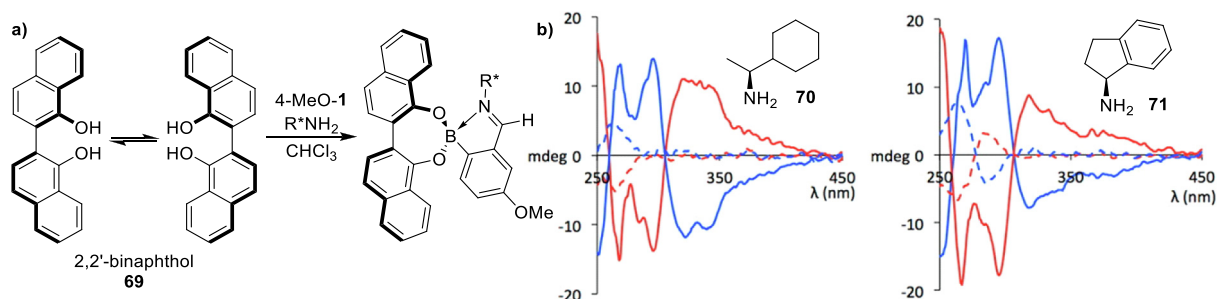


**Fig. 8.** (a) Three-component assembly of 2,2'-binaphthol **69**, 4-OMe-**1** and a chiral amine to afford complexes for CD spectroscopic analysis. (b) CDA spectra produced from complexes derived from amines **70** (left) or **71** (right). Blue and red lines correspond to complexes produced from the (*R*)- or (*S*)- enantiomers of the amines, respectively. Dashed lines correspond to two-component complexes formed from 4-MeO-**1** and the enantiomers of the amines **70** and **71**. C = 37.5  $\mu$ M. Adapted from ref. [81] with permission from the American Chemical Society.

red-shift of the fluorescence signal rather than PeT quenching (Fig. 10a). Differential changes in fluorescence intensities were once again observed between the diastereomeric oxazolidine products produced (*vide supra*), thus allowing for the measurement of the enantiopurity of the parent amino-alcohol analyte. This enabled ratiometric changes in fluorescence to be used to determine the *ee*'s of amino alcohols, as well as providing the ability to distinguish between amino-alcohol and amine analytes. This is seen clearly in Fig. 10b, with LDA revealing large distances between clusters of enantiomers and functional groups of the parent analytes. Interestingly, these studies found that addition of polar/protic additives (water, citric acid, ethylene glycol, sucrose, glycerol) had a more pronounced effect on the equilibrium constants for formation of the heterochiral complexes over the homochiral complexes, thus indicating that the heterochiral complexes were less stable. This led to the discovery that these types of additives could be used to further discriminate between analyte enantiomers in these complexation reactions.

Use of enantiopure L-tryptophan derivatives as fluorescent reporters for three-component complexation meant that these types of fluorescence assays could be adapted to determine the *ee*'s of scalemic diols (Fig. 11) [87] to within a 2% error limit. As for amines and amino-alcohols, the fluorescence profiles of the diastereomeric homochiral and heterochiral complexes produced from various classes of diols were sufficiently different to enable LDA to be used to accurately determine both their structures and *ee* values (Fig. 11).

The practicality of this fluorescence methodology for high-throughput screening was demonstrated by measuring the enantiopurities of 14 samples of Atorvastatin (a hypercholesterolemia drug) of unknown *ee*'s using a high-throughput assay (Fig. 12a), with quantitative linear regression analysis revealing accurate enantiopurity determination in all cases ( $R^2 = 0.999$ ). This type of fluorescence assay was also employed to analyse the *ee* of diols produced in Noyori asymmetric transfer hydrogenation reactions of benzil to hydrobenzoin (diol). In this case, an artificial neural

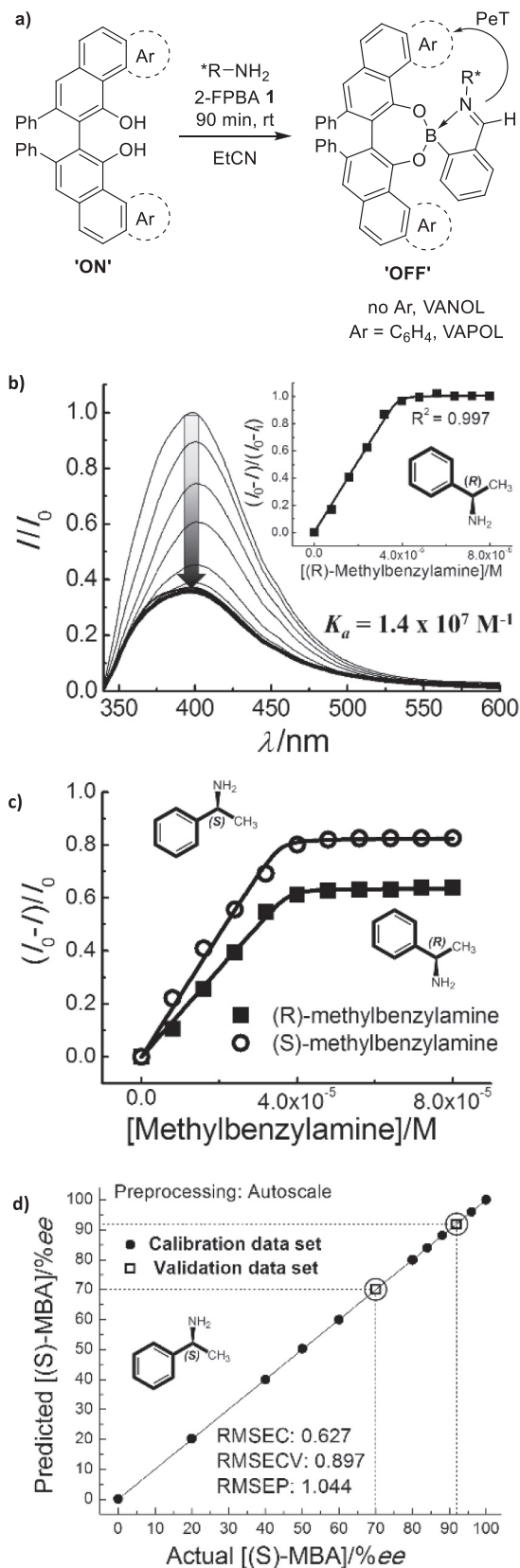


**Fig. 9.** (a) Three-component assembly of 2-FPBA **1**, a chiral primary amine and a fluorescent diol. (b) Fluorescence ( $\lambda_{ex} = 335$  nm) of a mixture of (S)-VANOL (40  $\mu M$ ) and 2-FPBA **1** (40  $\mu M$ ) in dry EtCN decreases on addition of (R)- $\alpha$ -methylbenzylamine **6b** (0–80  $\mu M$ ). (c) Binding isotherms of (S)- and (R)- $\alpha$ -methylbenzylamine **6b** to (S)-VANOL-2-FPBA host. (d) Qualitative LDA of amine, amino alcohol and amino acid enantiomers in EtCN. b, c, d reproduced from ref. [85] with permission from John Wiley and Sons.

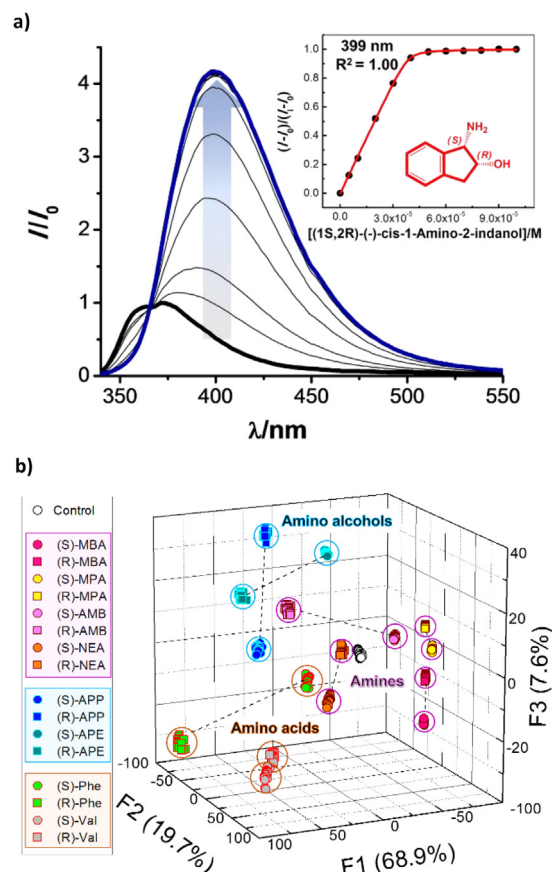


**Fig. 10.** (a) Fluorescence spectra of the three-component assembly of 2-FPBA **1**, (S)-VANOL and [(1S,2R)-(-)-cis-1-amino-2-indanol] (0–100  $\mu M$ ). (b) Qualitative LDA of chiral amine, amino-alcohol and amino acid analytes. Reproduced from refs. [85,86] with permission from John Wiley and Sons.

network was developed that was used to correctly determine the absolute configuration, *ee* and concentration of hydrobenzoin products (both crude and recrystallized) with high levels of accuracy (Fig. 12b, c).

Most recently, Anzenbacher *et al.* have reported a dual chromophore indicator displacement assay which proved to be more sensitive for determining *ee* than their previously developed “turn-off” systems [88]. This approach employed a combination of two fluorescent dyes capable of orthogonal binding to the aldehyde and boronic acid fragments of the 2-FPBA template (Scheme 35). Initial assembly of L-tryptophanol and 6,7-dihydroxycoumarin produced a bichromophoric oxazolidine-boronate complex, with intramolecular fluorescence resonance energy transfer (FRET) processes leading to weak fluorescence of its tryptophanol moiety and enhanced fluorescence of its coumarin fragment. Addition of a scalemic diol (or hydroxyacid) analyte results in displacement of the coumarin dye and separation of the FRET pair, which leads to fluorescence “turn on” of the tryptophanol fluorophore, and “turn off” of the dihydroxycoumarin (Scheme 35a). Since assembly of each enantiomer of the parent analyte proceeds diastereoselectively, each enantiomer leads to a different fluorescence response which can be used to determine the *ee*'s of a scalemic analyte.

Alternatively, use of (S)-VAPOL as a chiral reporter produced an IBE system suitable for determining the enantiopurity of amines and amino alcohols (Scheme 35b). In this case, the fluorescence of both fragments of the enantiopure oxazolidine sensor is likely to be quenched through PeT donation of the nitrogen lone-pair of the oxazolidine fragment to the VAPOL fragment, although the exact mechanism of fluorescence and quenching was not deter-

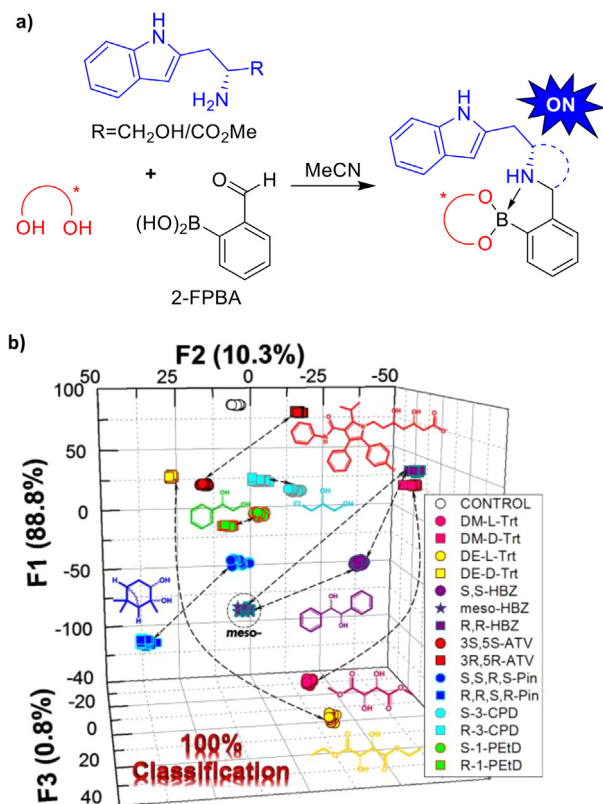


**Fig. 11.** (a) Three-component assembly of 2-FPBA **1**, a chiral diol and a fluorescent tryptophan derivative. (b) Qualitative LDA of 16 chiral diols showing 100% correct structural classification. Reproduced from ref. [87] with permission from John Wiley and Sons.

mined. Addition of a scalemic amine analyte results in displacement of the L-tryptophan unit producing an IBE complex that results in a fluorescence “turn-on” response, with the fluorescence of the VAPOL remaining “turned off”. Use of an amino-alcohol analyte to afford an imidazoline-boronate ester complex also results in displacement and “turn-on” of tryptophan, however the ensuing PeT process leads to amplification of the (S)-VAPOL fluorescence signal which is also “turned-on”. Since addition of the enantiomers of amine, amino ester, diol and hydroxyacid analytes to these chiral indicator displacement sensors result in different fluorescence responses, this bichromophoric Bull-James sensing system could be used to successfully classify the structures of 26 different analytes and accurately determine their absolute configurations and enantiopurities (Fig. 13).

## 5. Three-component assembly for electrochemical determination of the ee of BINOL

Finally, a collaboration with the Tucker group demonstrated that the ee of BINOL could be measured electrochemically through derivatisation with a redox-active two-component iminoboronic acid complex derived from a ferrocene amine and 2-FPBA **1** (Fig. 14a) [90]. It was found that the resultant diastereomeric complexes ( $\alpha$ -R,R)-**72a** and ( $\alpha$ -R,S)-**72b** exhibited significantly different electropotentials of 614 mV and 665 mV, respectively (Fig. 14b). This difference allowed the ee of BINOL **5** to be determined with an error of  $\pm 3\%$ , thus enabling minor enantiomers (<5%) to be detected, even at low concentrations. Crystallographic and <sup>1</sup>H and <sup>11</sup>B NMR spectroscopic analysis showed that whilst the homochiral diastereomeric complex ( $\alpha$ -R,R)-**72a** formed an intramolecular iminoboronate N→B bond, the more sterically hindered heterochiral complex ( $\alpha$ -R,S)-**72b** did not, once again indicating that heterochiral IBE complexes are generally less stable (*vide supra*) [86]. This structural difference is responsible for the differences in their electrochemical behaviour, with the N→B bond of the homochiral complex resulting in (R)-BINOL **5** being more tightly bound, with a ratio of binding strengths  $K_{(\alpha-R,R)}/K_{(\alpha-R,S)}$  of  $\approx 19$ . Electrochemical oxidation of these IBEs results in the binding strength ratio  $K_{(\alpha-R,R)}/K_{(\alpha-R,S)}$  dropping to only 2.5, thus indicating a much larger decrease in stability of the homochiral complex ( $\alpha$ -R,R)-**72a**. This difference is proposed to be due to weakening of the N→B coordination bond of complex ( $\alpha$ -R,R)-**72a** caused by the proximal positive charge of its oxidised ferrocene fragment. Evidence for weakening of the N→B coordination bond of the homochiral ( $\alpha$ -R,R)-**72a** complex was also provided by the larger positive shift in redox potential upon addition of (R)- or (S)-BINOL **5** to iminoboronic acid (R)-**73** (+95 mV for ( $\alpha$ -R,R)-**72a** vs. +44 mV for ( $\alpha$ -R,S)-**72b**). This indicates that the ferrocene unit of complex ( $\alpha$ -R,R)-**72a** is harder to oxidise than ( $\alpha$ -R,S)-**72b**, in line with its imine-boron coordination bond withdrawing electron density from the ferrocene redox system.

## 6. IBE assemblies as synthetic tools

The use of the Bull-James three-component assembly for determining enantiopurity is often credited as one of the first examples where orthogonal dynamic covalent bond formation was used to construct functional supramolecular assemblies [14,91–93]. The power of these chiral iminoboronate systems for self-assembly has led to supramolecular constructs of this type being used to prepare new types of boron-containing materials and as a mechanism to control reactivity and stereoselectivity [94–97].

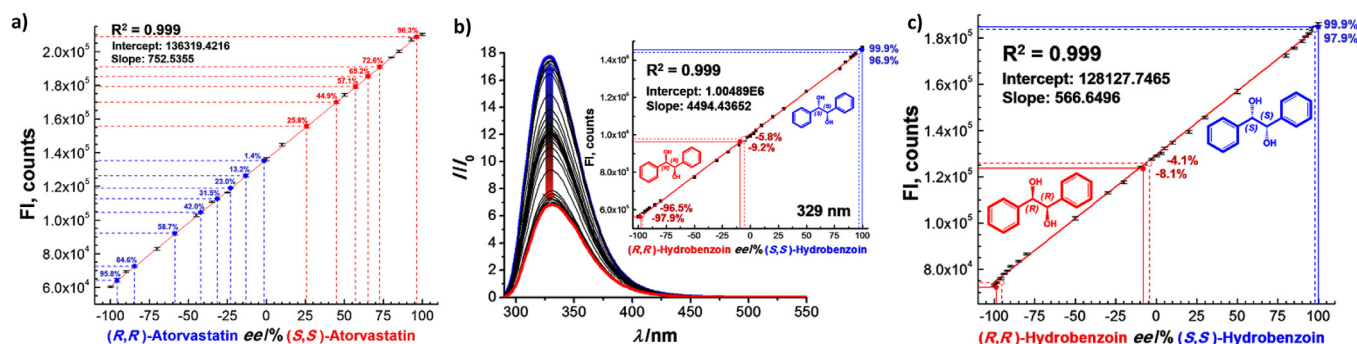
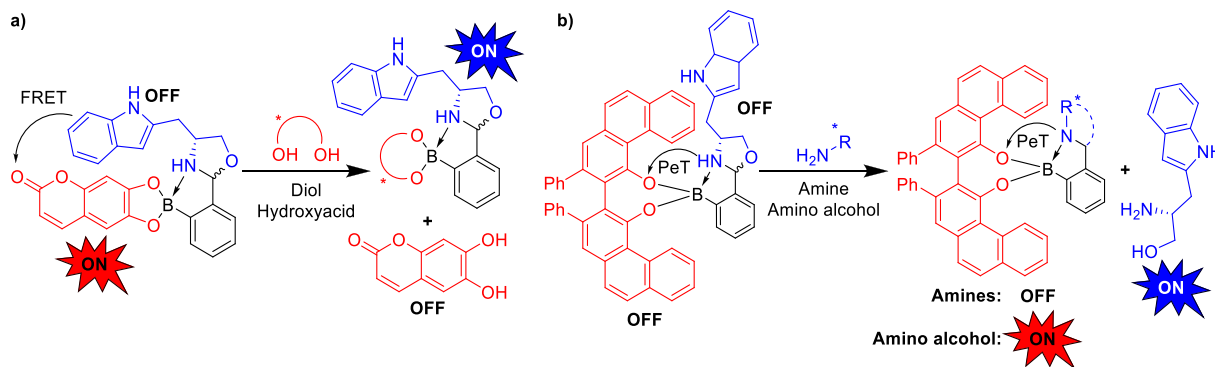


**Fig. 12.** (a) Standard graph of FI vs. ee of L-tryptophan and 2-FPBA **1** assemblies (1:1, 40 mm) of atorvastatin of known (black) and unknown (blue and red) ee values. (b) Fluorescence titration profile of L-tryptophan–2-FPBA (1:1, 40 mm) complexes with hydrobenzoin standards (inset: Standard curve of FI vs. ee). (c) HT fluorescence assay standard curves for FI readings from mixtures of hydrobenzoin of known ee in comparison with six hydrobenzoin samples of unknown ee (red, blue circles). Reproduced from ref. [87] with permission from John Wiley and Sons.





**Scheme 35.** Displacement assays using bichromophoric three-component assemblies for determining the enantiopurities of a range of scalemic analytes: (a) Use of 2-FPBA, L-tryptophan and 6,7-dihydroxycoumarin for the detection and *ee* analysis of diols and hydroxyacids. (b) Use of 2-FPBA, L-tryptophan and (S)-VAPOL for the detection and *ee* analysis of amines and amino alcohols.

### 6.1. Self-assembled synthesis of polyheteroatomic boracycles

The three-component assembly reaction of 2-FPBA **1** with (S)-BINOL **5** and (S)-leucinol **74** resulted in a mixture of imine and oxazolidine boronate products (*vide supra*) [54], however oxazolidine boronate ester (S, 2R, 4S)-**75** fractionally crystallized out of solution after the crude reaction mixture was allowed to stand overnight (Fig. 15a) [98]. Carrying out a two-component assembly using (R)-valinol **74b** and 2-FPBA **1** produced bridged iminoboronate (R,R)-**76b**, comprised of two fused boracycle rings containing two tetrahedral boron centres and a bridging oxygen atom linker (Fig. 15b), in the same manner as related systems reported by Westcott *et al.* [99,100]. Five additional chiral amino alcohols **74a-f** were used as substrates in this two-component self-assembly reaction in combination with either 2-FPBA **1** or 2-formyl furanylborationic acid **77**, which gave their respective boracycles in excellent 84–96% isolated yields. Achiral aromatic amino alcohols **74g** and **74h** were also shown to form boracycles in quantitative yields, although their decreased reactivity required heating under Dean-Stark conditions for complexation reactions to proceed to completion.

Both types of fused bridged bicycles were characterised using X-Ray crystallography (Fig. 15c), which revealed interesting structural variation between the two-component products produced from chiral or achiral amino alcohols. In the case of (R,R)-**76b**, the B–O–B linkage is positioned on the opposite face to the two non-bridging oxo-substituents, which creates a binding pocket walled by the non-bridging oxygens and side-chains, that is capped by a bridging B–O–B bond. Alternatively, all of the atoms of the O–B–O–B–O motif are present in the same plane for complex **76h**, with all three oxygen atoms sitting on the same side of the complex. These structural differences result in the pocket of the chiral complexes containing two potentially coordinating oxygen atoms, whilst the pocket of the achiral complexes are purely hydrophobic in nature.

### 6.2. Chiral IBE ligands for asymmetric catalysis

Three-component assemblies have also been used by the Taylor group, who employed IBE bond forming reactions for combinatorial synthesis of a library of chiral phosphine ligands for enantioselective palladium-catalysed allylic acetate substitution reactions [101]. They performed three achiral formyl boronic acid templates **78a-c**, eleven diol ligands **79a-k** (both chiral and achiral), and four chiral aminophosphines **80a-d** to create a library of 100 phosphinoiminoboronate ligands **81** (Scheme 36) that were individually screened as chiral ligands in palladium-catalysed allylic substitu-

tion reactions of (rac)-**82** with diethyl malonate **83** (Scheme 37). A wide range of enantioselectivities were observed, with the best results obtained for ligands **81aaa** and **81abc** which respectively produced (R)-**84** in 90% *ee* and (S)-**84** in 93% *ee*, which was a significant improvement on the 67% and 69% *ee* values obtained using non-iminoboronate aminophosphine ligands **85**. The sheer volume of data acquired using this combinatorial approach enabled Taylor and co-workers to rapidly assign trends that would not have been evident from a conventional stepwise ligand optimisation strategy. For instance, they were able to show that aliphatic diol ligands gave better stereocontrol as they decreased the Lewis acidity of the boron centre, which weakened the intramolecular N→B bond, thus facilitating stronger bidentate P,N-coordination of the ligand to the metal.

### 6.3. IBE-derived chiral auxiliaries in CuAAC click reactions

Fossey and co-workers have reported use of the Bull-James assembly for asymmetric synthesis, employing it to construct a chiral auxiliary for the kinetic resolution of alkyne amines using a copper(I)-catalysed azide-alkyne cycloaddition (CuAAC) reaction (Scheme 38) [102]. In this system, a racemic alkyne-containing primary amine **86** was self-assembled with 2-FPBA **1** and (R)-BINOL **5** to form a mixture of diastereomeric iminoboronate complexes **87** that were subjected to CuAAC conditions using 0.5 equivalents of benzyl azide. This resulted in the alkyne fragment of the (α,R,R)-**87** diastereomer preferentially undergoing a stereoselective click reaction with a selectivity value of *S* = 4.1. Subsequent acid-catalysed hydrolysis of the IBE ester complexes then afforded amino-azide (R)-**88** in 39% *ee* and recovered amine (S)-**86** in 29% *ee*. Although only moderate stereocontrol was achieved in this unoptimized 'one-pot' kinetic resolution reaction, the simplicity of installing and removing the chiral auxiliary (e.g. BINOL) in this type of system is noteworthy, particularly if more stereoselective transformations of these types of IBE complexes can be identified.

### 6.4. Reversible radical coupling of iminoboronates

McConnell *et al.* found that treatment of a pre-assembled N-aryl iminoboronate catechol ester **89** with the single electron reductant Cp<sub>2</sub>Co resulted in radical homocoupling of its imino benzylic groups to afford amido-boronates (rac<sub>5</sub>)-**90**, (meso<sub>5</sub>)-**90** and (rac<sub>6</sub>)-**90** (Scheme 39) [103]. Kinetic analyses and structural studies revealed that 5-membered (rac<sub>5</sub>)-**90** and (meso<sub>5</sub>)-**90** were formed as kinetic products which then rearranged to 6-membered (rac<sub>6</sub>)-**90** under thermodynamic control, leading to

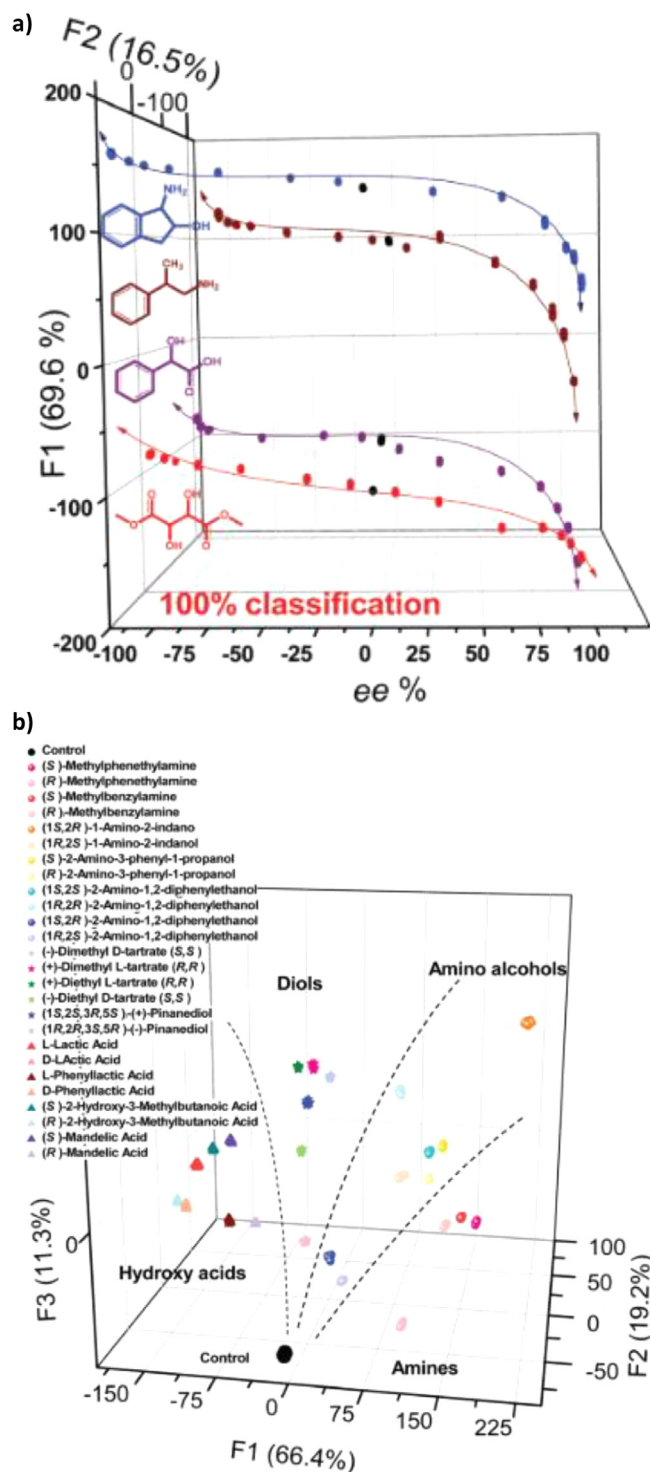


**Fig. 13.** (a) Semi-quantitative LDA of fluorescence response data from displacement assays enable simultaneous determination of the *ee* values of four different types of amine, amino alcohol,  $\alpha$ -hydroxy acid and diol analytes. (b) Qualitative LDA of the fluorescence response of 26 chiral amines, amino alcohols, diols and hydroxyacids (+ controls) in the displacement assay enabled their structures to be predicted with a 100% success rate. Reproduced from ref. [88] with permission from the Royal Society of Chemistry.

mixed time-, temperature- and substrate-dependent ratios of product **90**. These dimeric homo-coupled products were found to be significantly less stable than their IBE precursors, with their treatment with trityl cation ( $\text{Ph}_3\text{C}^+$ ) as an electron acceptor resulting in regeneration of the original IBE monomers.

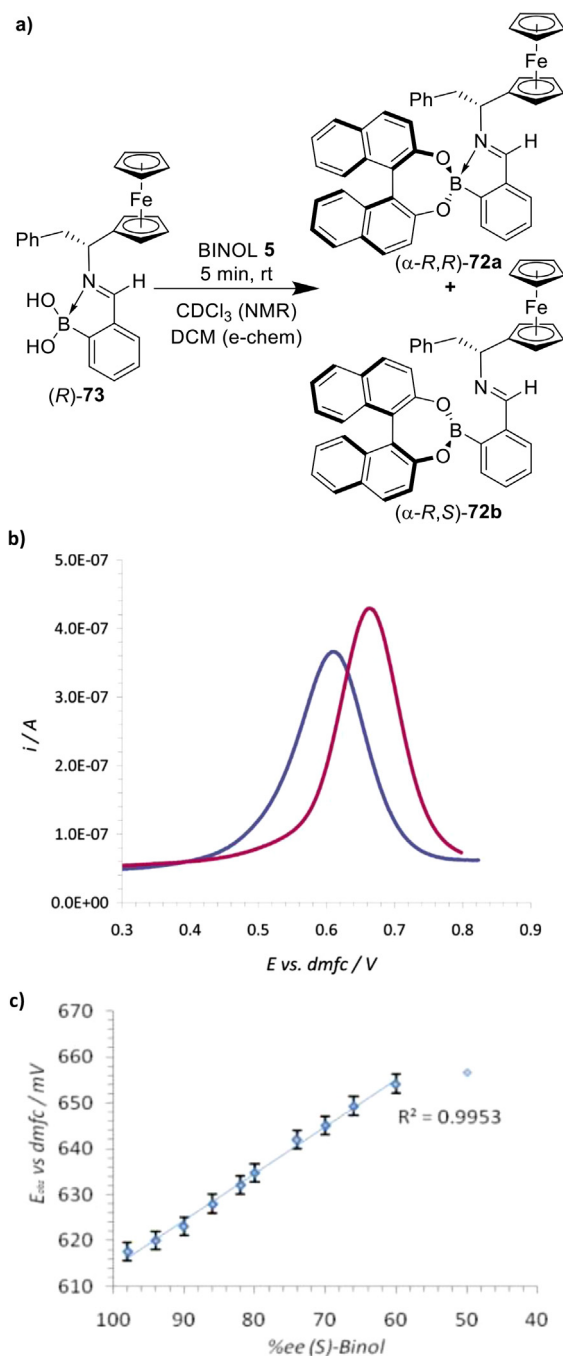


**Fig. 14.** (a) Three-component assembly of 2-FPBA **1**, redox-active ferrocene amine (*R*)-**73** (pre-assembled) and BINOL **5**. (b) Square wave voltammograms of three-component ferrocene IBEs acquired in  $\text{CH}_2\text{Cl}_2$  (0.1 M TBA ·  $\text{PF}_6$ ); (( $\alpha$ -*R,S*)-**72b** shown in blue) and (( $\alpha$ -*R,R*)-**72a** shown in purple). (c) Plot of  $E_{\text{obs}}$  against % *ee* for IBE complexes produced from (*S*)-BINOL **5** showing a linear dependence between 60% and 98% *ee*. b, c Reproduced from ref. [90] with permission from the American Chemical Society.

## 7. Iminoboronate complexes for the formation of polymers and hydrogels

### 7.1. Iminoboronate polymers and hydrogels

Following their demonstration that the Bull-James assembly could be used to assess the chirality of polymers (*vide supra*), Kressler and co-workers have reported that derivatisation of

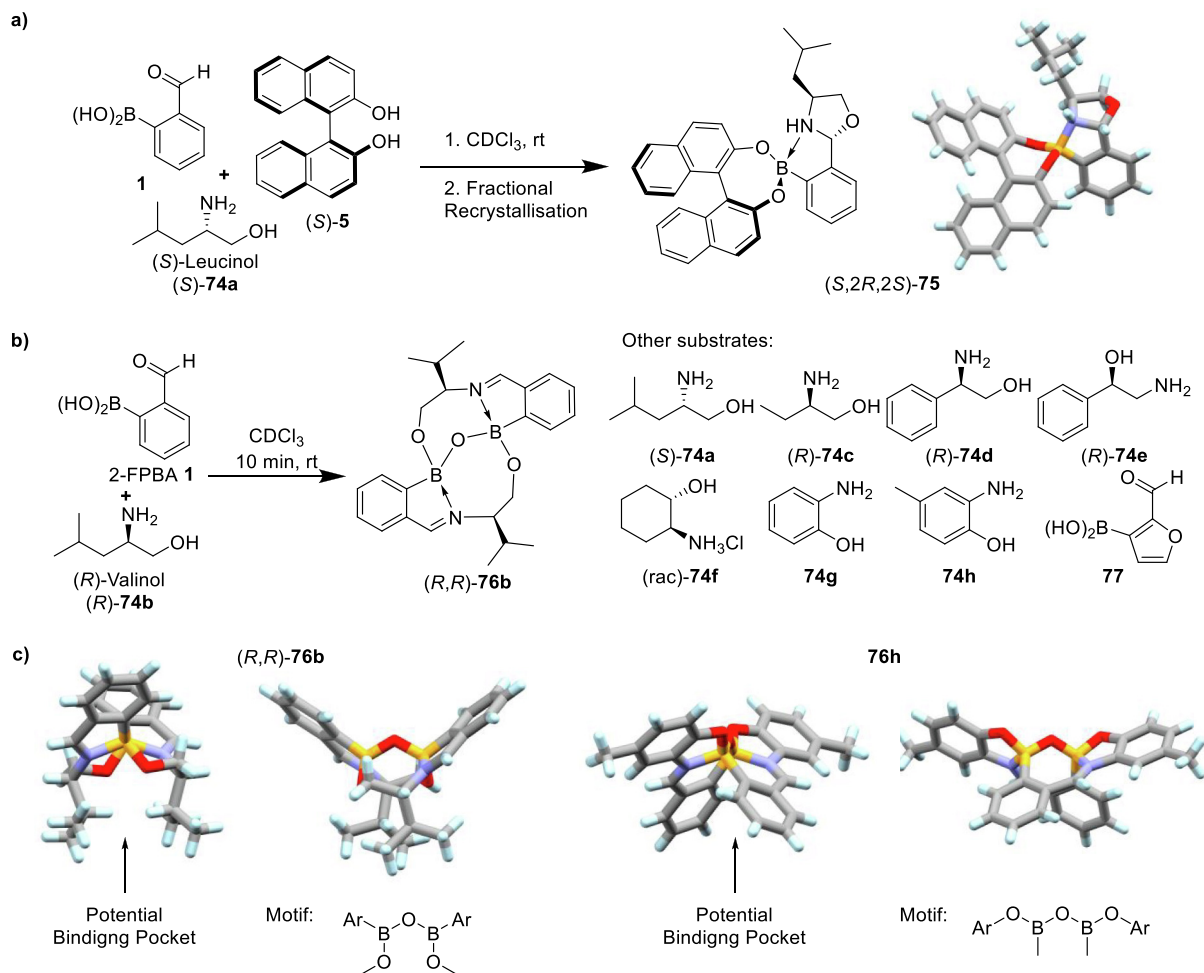
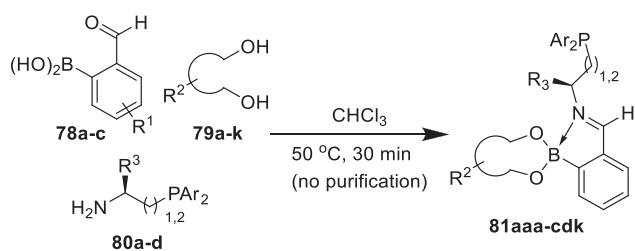
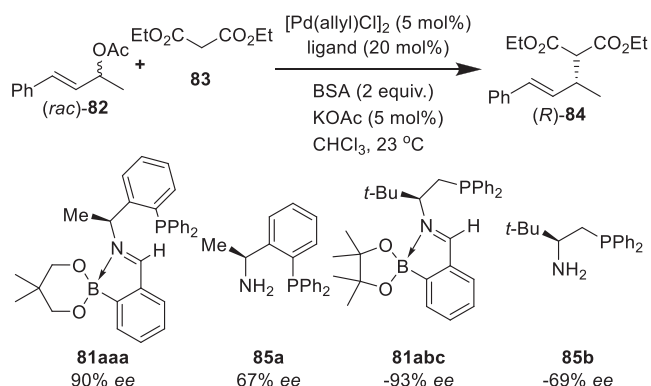


**Fig. 15.** (a) X-ray crystal structure of three-component assembly of (S,2R,2S)-**75** formed from reaction of (S)-leucinol **74a**, BINOL **5** and 2-FPBA **1**. (b) Two-component assembly of formyl aryl boronic acids and 1,2-amino alcohols **74**. (c) X-ray crystal structures of (R,R)-**76b** and **76h** viewed along and perpendicular to the boron-boron axis (left and right respectively).



**Scheme 36.** Combinatorial IBE reactions used for the combinatorial synthesis of 100 chiral phosphine ligands.

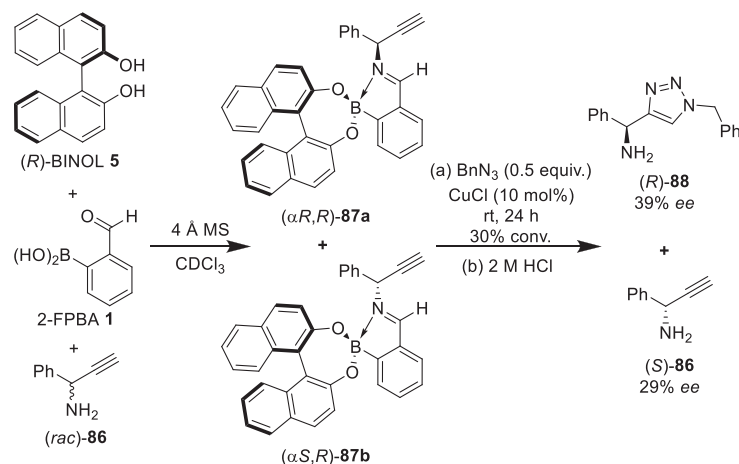


**Scheme 37.** Chiral phosphine-iminoboronate ligands afford enhanced enantioselectivities in palladium-catalysed allylic alkylation reactions.

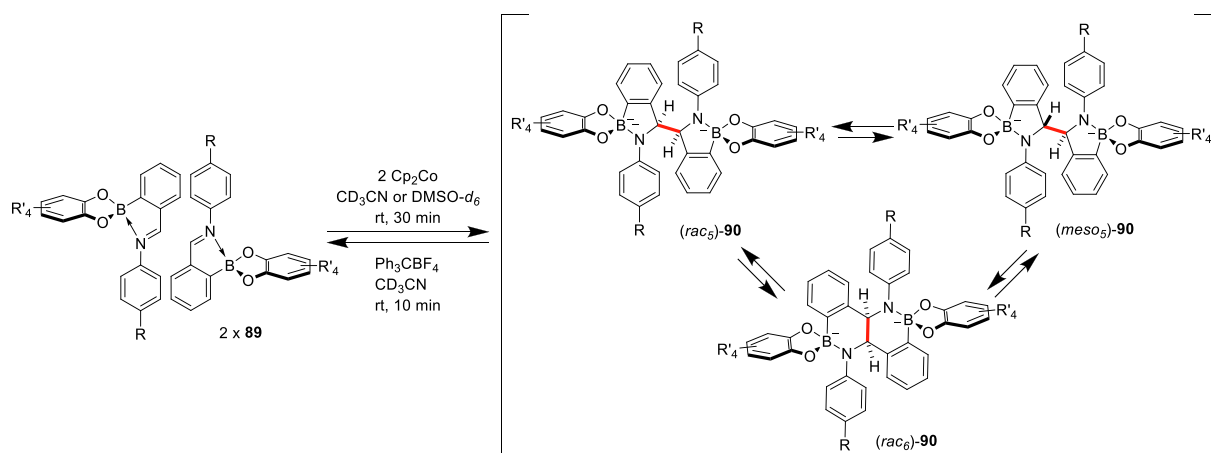
GMA monomers with 2-FPBA **1** and (S)- $\alpha$ -methylbenzylamine **6b** gave iminoboronate GMA-IPB monomers that underwent radical or UV-initiated low-temperature ATRP polymerisation to afford iminoboronate ester polymers in one pot (Scheme 40) [104]. These polymers could then be decomplexed via treatment with a large excess of catechol to afford simple p(GMA)s containing free diol units caused by elimination of catechol-iminoboronate (S)-**91**. A similar process could also be used to polymerise iminoboronate ester monomers containing two equivalents of 2-hydroxyethyl-methacrylate (HEMA), affording highly syndiotactic polymers ( $rr = 70.7\text{--}75.5\%$  for pGMAs and  $74.9\text{--}79.7\%$  for pHEMAs).

## 7.2. Dynamic, self-healing and stimuli-responsive polymers and hydrogels

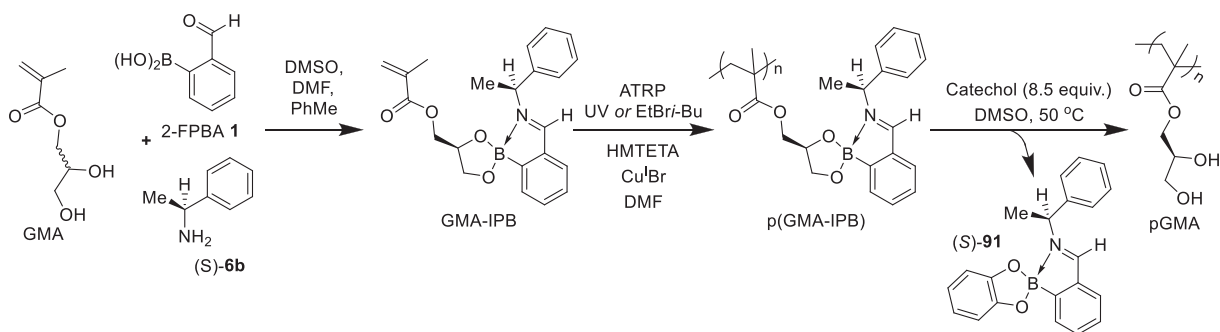
Iminoboronates have also been incorporated into polymeric systems as a structural element to facilitate cross-linking of polymer and hydrogel materials [105]. For example, Raquez *et al.* have developed self-assembled imine-coordinated boroxine polymeric systems that are produced from reaction of a diamine, a



**Scheme 38.** Formation of diastereomeric IBE complexes from alkyne (*rac*)-**86** enables a CuAAC-catalysed click reaction to be used for their kinetic resolution.



**Scheme 39.** Reversible radical coupling of iminoboronates **89** to afford amidoboronates **90** (radical-coupled bond in red) under thermodynamic control.



**Scheme 40.** One-pot complexation and polymerisation of 2-FPBA **1**, (*S*)-**6b**, and GMA to afford iminoboronate ester functionalised polymers that could be decomplexed by treatment with catechol to afford pGMAs.

polyether-containing terminal bis-cyclic carbonate unit and a 2-FPBA boroxine trimer **92** (Fig. 16a). Ring opening of the terminal cyclic anhydride groups by one of the diamine amines results in a urethane bond, with the other amino group then reacting to form a highly cross-linked iminoboroxine complex [106–108]. This self-assembly approach produces polymers with a high degree of stiff-

ness (Young's modulus = 551 MPa) and tensile strength (11 MPa) despite the labile nature of iminoboronates. These dynamic iminoboronate covalent bonds were found to confer self-healing properties to these materials, with heating/cooling and wetting/drying enabling broken imine or boroxine bonds to be reformed (Fig. 16b). Similarly, changes in temperature and humidity can be used as



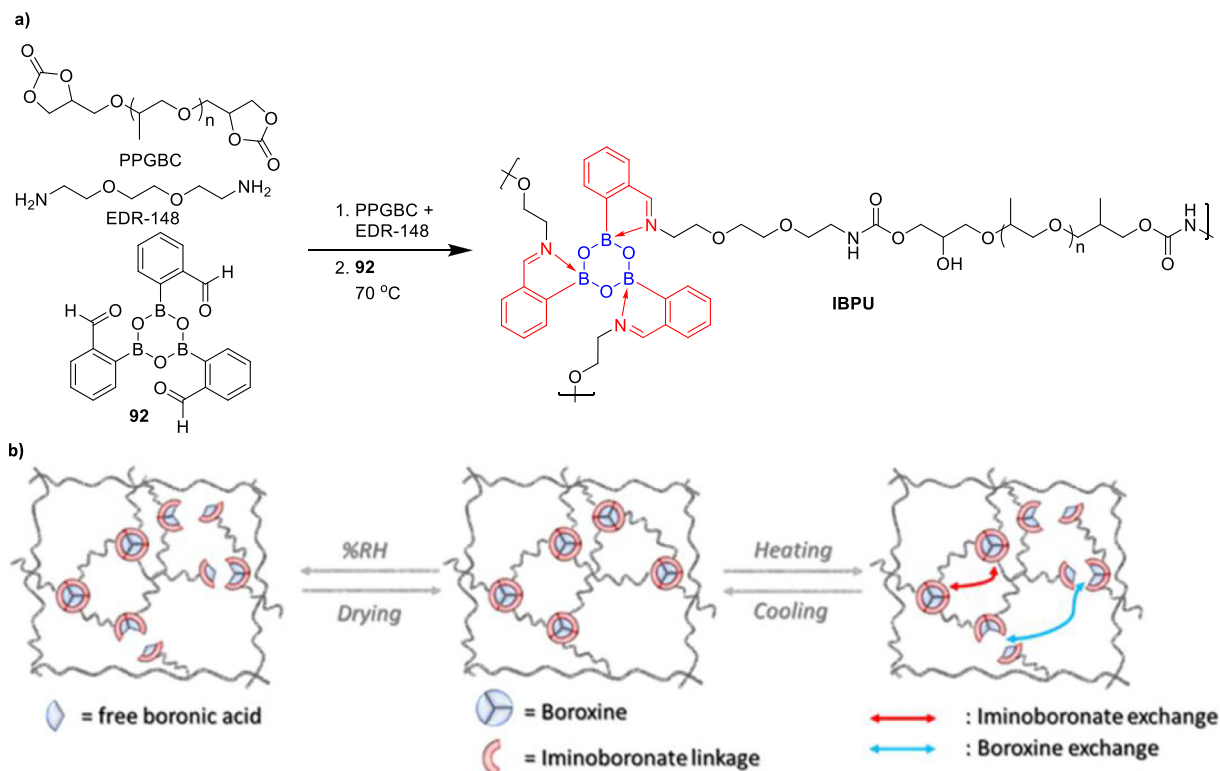


**Fig. 16.** Three-component self-assembly of iminoboroxine-containing self-healing polymers and hydrogels. (a) Synthesis of an iminoboroxine polyurethane network polymer. (b) Self-healing and modular behaviour of iminoboroxine-polyurethane polymers. Reproduced from ref. [106] with permission from the American Chemical Society.

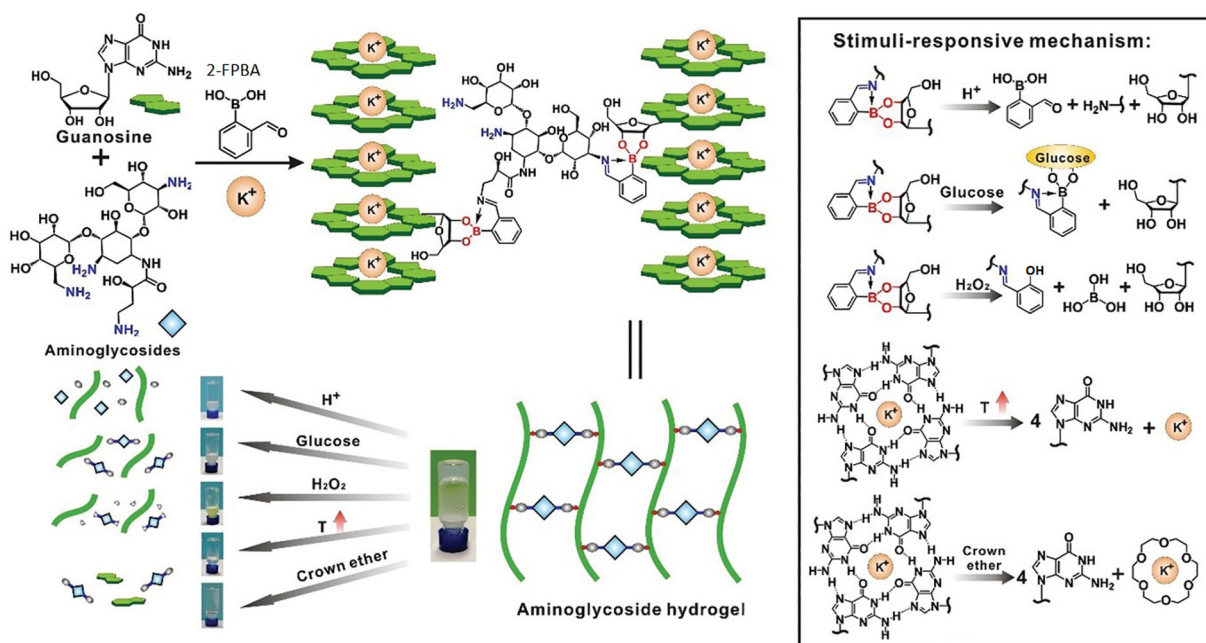


**Fig. 17.** An aminoglycoside iminoboroxine hydrogel assembled from guanosine,  $K^+$ , an aminoglycoside and 2-FPBA. These materials are responsive to multiple external stimuli such as acids, glucose,  $H_2O_2$ , heat and crown ethers, all of which act on different structural elements of the hydrogel network. Reproduced from ref. [112] with permission from John Wiley and Sons.

stimuli to make or break the bonds used to construct the iminoboroxine-boroxine hubs, thus creating stimuli-responsive materials which are remoldable under mild treatment conditions. This provides a simple alternative to common isocyanate-derived polyurethane self-healing and stimuli-responsive polymers, which have been shown to have potential applications as solid polymer

electrolytes [109]. Following these initial reports, functional variants of this core motif have been developed, based on substitution of the iminoboroxine moieties with similar amino- and acrylamido-boroxine motifs [110,111].

This concept has been expanded further for the design of self-assembled IBE-containing polymers that are prepared from

supramolecular assembly of 2-FPBA, guanosine (G), aminoglycosides and potassium chloride (Fig. 17). These stimuli-responsive hydrogels contain a large network of hydrogen-bonded  $K^+$ -centred guanosine tetramers, whose diol units are crosslinked through formation of iminoboronate ester groups with the amino groups of aminoglycoside units [112–116]. These hydrogels were found to be responsive to multiple stimuli, with an increase in temperature or addition of potassium-chelating crown ethers resulting in disruption of the G-quadruplex arrays and release of the aminoglycoside di-iminoboronate guanosine units. The iminoboronate bonds of these complexes are also responsive to disruption by other stimuli, with addition of aqueous acid leading to their hydrolysis to afford 2-FPBA, amine and diol components. Alternatively, the addition of glucose results in transesterification of the boronate ester, releasing a guanosine fragment and the production of new glucose-iminoboronate-aminoglycoside species. Finally, the reactivity of boronates towards reactive oxygen and nitrogen species (ROS/RNS) [117–119] may be exploited, with addition of hydrogen peroxide triggering oxidative deborylation to produce boric acid and release of the guanosine fragment. This multi-responsive behaviour has been exploited for drug delivery for selective release of antibacterial aminoglycosides and the anti-cancer drug Doxorubicin [112,116].  $CO_2$ -responsive iminoboronate poly(oligo(ethylene glycol)) polymers have also been reported by Jiang and co-workers, with bubbling of  $CO_2$  reversibly producing carbonic acid that triggers IBE bond hydrolysis to trigger depolymerisation processes that can be reversed by purging with  $N_2$  gas [120]. This  $CO_2$ -dependent behaviour has been demonstrated in multiple systems (*vide infra*) using both  $^1H$  NMR and fluorescence assays to measure the fragmentation/re-complexation of IBE systems upon sequential  $CO_2/N_2$  bubbling.

### 7.3. Stimuli-responsive aggregates and micelles

The Bull-James multicomponent approach has also been used to produce stimuli-responsive iminoboronate-containing nano-aggregates, micellar assemblies and polymersomes that are stable in aqueous systems. Jiang and co-workers, for example, have reported the three-component assembly of poly(ethylene glycol) amine with 2-FPBA **1** and a nitrophenyl ethanediol (PEG-INEC) to produce amphipathic IBE complexes that self-assemble into nano-aggregates in aqueous systems (Fig. 18) [121]. These nano-aggregates were found to be responsive to three common stimuli: light - which results in release of a nitrosoaryl  $\alpha$ -hydroxy-ketone and an iminoboronic acid fragment; acid - which hydrolyses both the boronate ester and imine bonds to regenerate the original three components; and hydrogen peroxide which oxidatively cleaves the boronate ester to give boric acid, o-hydroxy-benzaldehyde and nitrophenyl ethanediol. Therefore, different external stimuli can

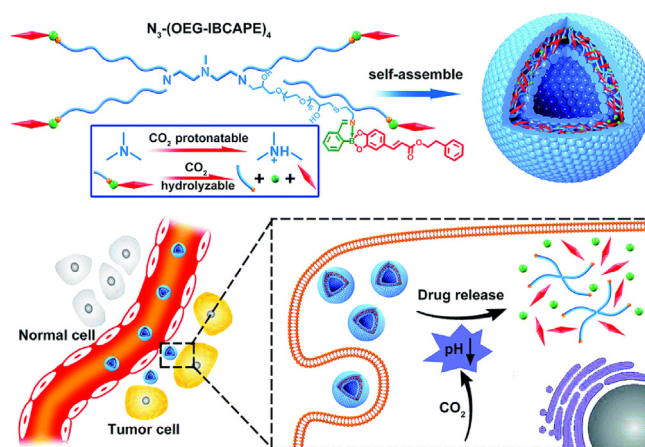


**Fig. 19.** Self assembled prodrug  $N_3$ -(OEG-IBCAPE) $_4$  polymersomes and the stimuli-responsive  $CO_2$ -triggered release of CAPE in cancer cells. Reproduced from ref. [123] with permission from the Royal Society of Chemistry.

be used to trigger controlled decomposition of these aggregates, which is potentially useful for the selective release of encapsulated hydrophobic guest molecules.

The same group have also reported the development of different iminoboronate aggregate systems, whose disassembly is triggered by the action of nucleophilic ROS or  $CO_2$ -induced solvent acidification [122,123]. For example,  $CO_2$  responsive  $N_3$ -(OEG-IBCAPE) $_4$  polymersomes are stable at physiological pH 7.4, however protonation of their tris-amine cores results in nano-aggregate disassembly at mildly acidic pH levels. This enabled iminoboronate ester linkers to be used to generate polymersomes attached to the diol unit of caffeic acid phenethyl ester (CAPE, anti-cancer drug, red) as a  $CO_2$ -responsive drug delivery system (Fig. 19). These polymersomes exhibited improved transport properties that enabled their delivery to  $CO_2$ -rich HL-60 leukaemia cells that exhibit a mildly acidic environment. This acidity results in intracellular hydrolysis of the iminoboronate bonds of the polymersome aggregates, which leads to their disassembly and release of CAPE as a cytotoxic agent within the target cancer cells. The same transport principles have also been employed by Shi and co-workers for pH/GSH-responsive delivery of encapsulated capecitabine to HepG2 liver cancer cells [124].

## 8. Iminoboronate derivatives for biological targeting and tagging

IB-type assemblies have also been employed for the functionalisation and tagging of the amino groups of peptides and proteins,

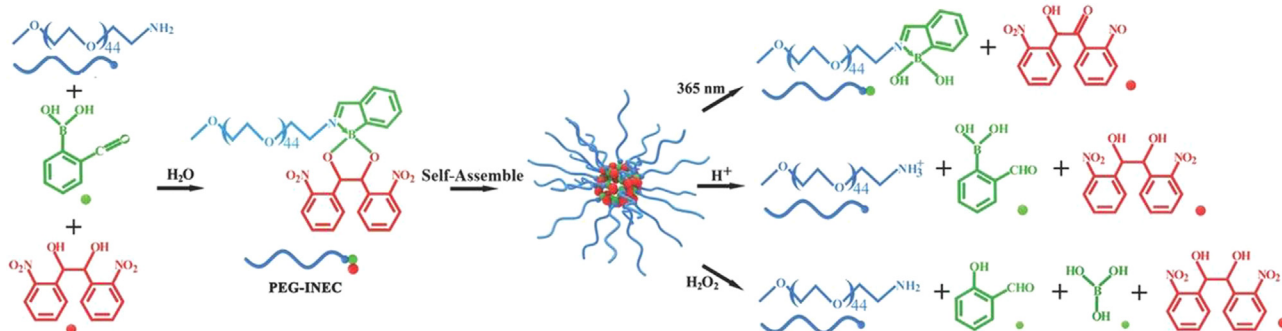
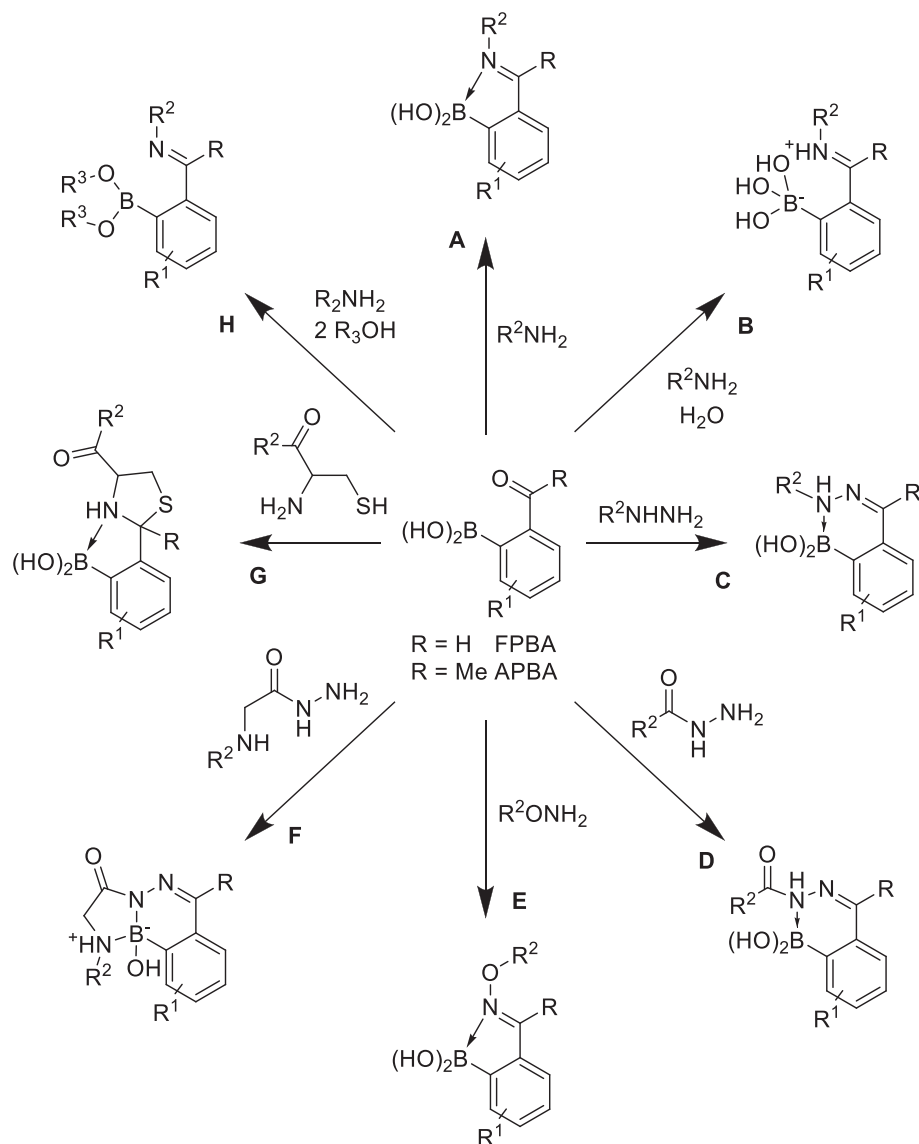


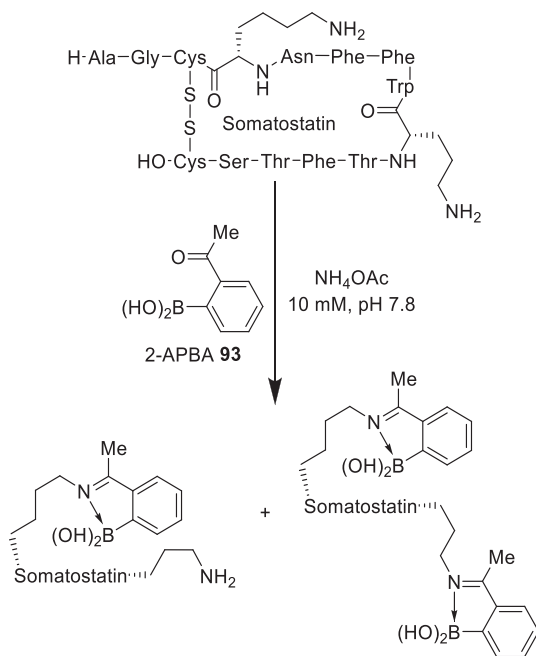
**Fig. 18.** Self-assembled PEG-iminoboronate polymeric nano-aggregates and their stimuli-responsive degradation by light, acid and  $H_2O_2$ . Reproduced from ref. [121] with permission from John Wiley and Sons.



**Scheme 41.** Diverse bioorthogonal IB conjugation chemistries of 2-FPBA- and 2-APBA-derived linkers.

with several recent specialised reviews having covered this topic in detail [125–127], with only a general overview of this area provided herein. The majority of bioorthogonal labelling reactions that have been reported to date are two-component in nature, involving reaction of 2-FPBA (or 2-acetylphenylformyl boronic acid, 2-APBA) with amine or aminothiol residues of peptides or proteins to form imine/thioxazolidine bonds that are stabilised by the presence of a proximal boron centre (Scheme 41). These condensation reactions have been found to proceed with rate constants of over  $10^2$ – $10^3$   $M^{-1} s^{-1}$  [128], which is orders of magnitude faster than traditional alkyne-azide ‘click’ coupling reactions. Gois, Gillingham and Anslyn have carried out binding studies that clearly demonstrate that the proximal boron centre accelerates imine condensation reactions and stabilises imine complex formation, with additives or external stimuli (e.g. changes in pH, ROS, nucleophiles...) normally required to achieve hydrolysis, degradation, or decomplexation [36,37,129,130]. For example, computational studies on the condensation of *n*-butylamine and 2-APBA **93** have shown that the adjacent boronic acid reduces the activation enthalpy for imine condensation drastically by 35–36 kcal/mol [129].

The most commonly employed amine tagging systems involve generation of the two component iminoboronic acid assemblies **A** and **B** (pH interconvertible), both of which have been widely used to label the free  $\epsilon$ -amine groups of lysine residues in peptides and proteins. This approach was first pioneered in 2012 by Gois *et al.* who reported formation of an iminoboronic acid complex between the hormonal neuropeptide Somatostatin and 2-APBA **93** in ammonium acetate buffer (20 mM, pH 5.0–7.0) (Scheme 42) [129]. Following this success, they demonstrated that 2-APBA could be used to successfully tag lysine groups present in lysozyme, cytochrome C, ribonuclease A and myoglobin with a range of 2-formylaryl boronic acids. Improvements to this tagging approach have subsequently been reported based on the use of peptides/proteins containing  $\alpha$ -nucleophiles such as hydrazides, acylhydrazides and alkoxyamines which react more rapidly to afford hydrazone and oxime linkers (**C**, **D**, **E**, Scheme 41) that are more hydrolytically stable [128,131–134]. Similarly, multidentate coordination of bifunctional nucleophiles such as  $\alpha$ -amino hydrazides or 1,2-aminothiols to 2-FPBA/2-APBA templates have proved popular for producing stable bioconjugates containing tricyclic



**Scheme 42.** Reaction of lysine groups in Somatostatin with 2-APBA **93**.

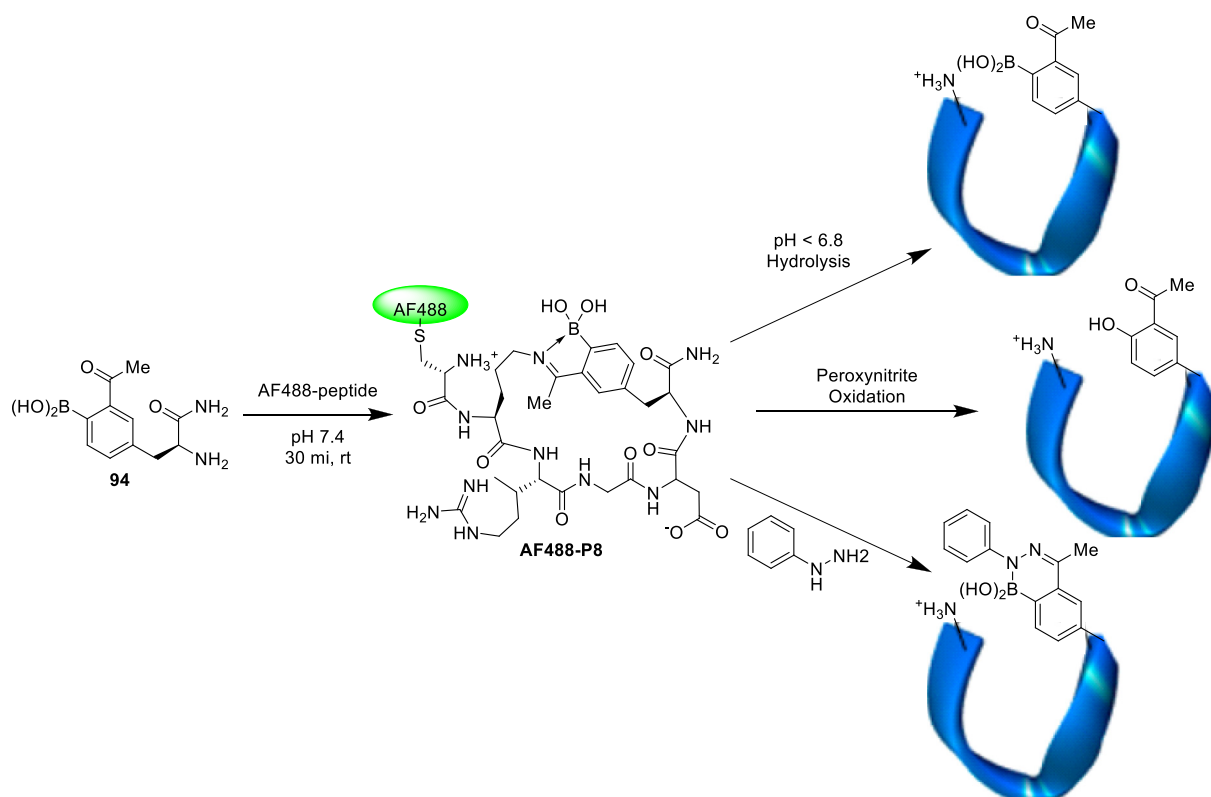
azadiborolidine boracycles (**F**, Scheme 41) and stabilised thioxazolidine linkers (**G**, Scheme 41) [131,133,135–137].

Proof of concept studies have shown that stimulus-triggered decomplexation of this type of protein-boracycle conjugates can be achieved through treatment with fructose, dopamine, glutathione, aqueous acid, ROS/RNS, *etc.*, with this reversibility exploited to induce partial or complete hydrolysis of intramolecu-

lar imine bonds to control ring-opening of cyclic peptides (Scheme 43). Since their inception, these types of stimuli-responsive two-component IB assemblies have been used to derivatise peptides, proteins, aminoglycosides, biological polyamines and amine-rich membrane lipids for fluorescent tagging, targeted fluorophore, biomolecule and therapeutic delivery, covalent protein inhibition, and reversible biomolecule functionalization [138–144].

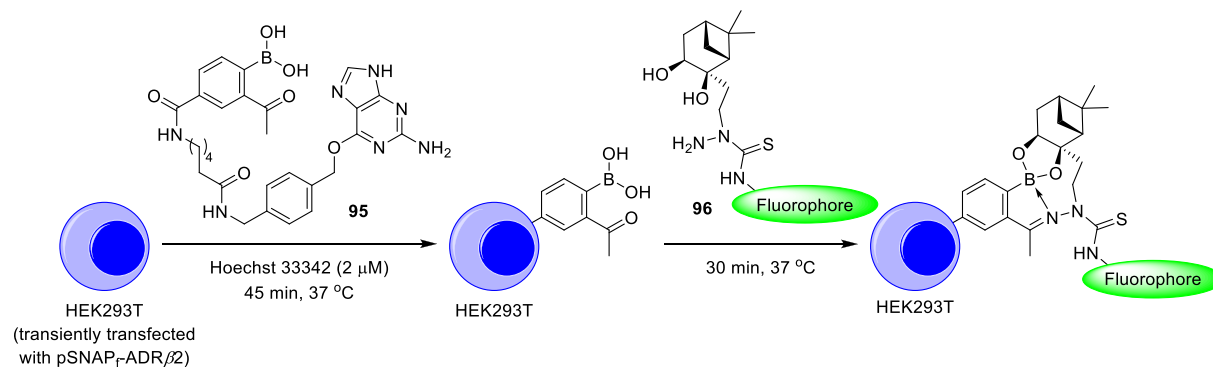
The use of three-component strategies for tagging the amino groups of biomolecules has been less well explored (e.g. **H**, Scheme 42), although three recent reports demonstrate the potential of this approach for producing stable bioconjugates. In 2017, Hall and co-workers reported the bioorthogonal tagging of live cells using a fluorescein fluorophore attached to a “click” boronate/thiosemicarbazone warhead, where the thiosemicarbazide unit underwent rapid imine condensation to afford a complex that was stabilised by the presence of a pendant pinanediol that formed an intramolecular boronate ester bond. This system was employed for live cell imaging using fluorescence microscopy using a SNAP-tag approach, in which HEK293T cancer cells were transiently transfected with the pSNAP<sub>+</sub>-ADR $\beta$ 2 plasmid, allowing 2-APBA-derivative **95** to be secured on the cell membrane, enabling ‘click’ fluorescent tagging of these cells with **96** for visualisation using fluorescence microscopy at concentrations as low as 10  $\mu$ M (Scheme 44) [145].

Most recently, Gois *et al.* have reported a “boron hot spot” (BHS) approach to selectively target the amino groups of *N*-terminal cysteine residues, which was developed to address some of the promiscuity and reversibility issues that are often observed when two-component iminoboronic acid complexation reactions are used to functionalise biomolecules (Scheme 45) [146]. They found that attachment of 3-hydroxyquinolin-2(1H)-one (3HQ)/succinimide groups to the thiol units of *N*-terminal cysteine residues resulted in selective imine condensation of the *N*-terminal amino

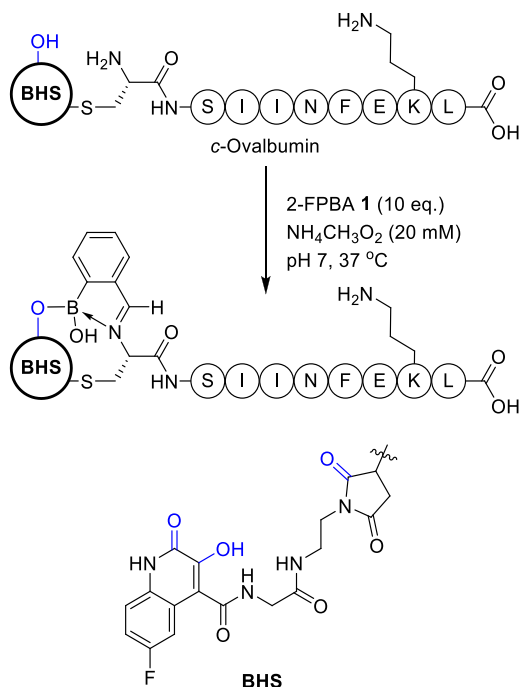


**Scheme 43.** A stimuli-responsive intramolecular iminoboronic acid bond can be used to control the cyclisation of an AF488 fluorophore-appended peptide.





**Scheme 44.** 2-APBA modification of HEK293T cancer cells and subsequent three-component “click” boronate/thiosemicarbazone fluorescent labelling.



**Scheme 45.** Site-selective iminoboronate complexation of an N-terminal boron hot spot-modified c-ovalbumin.

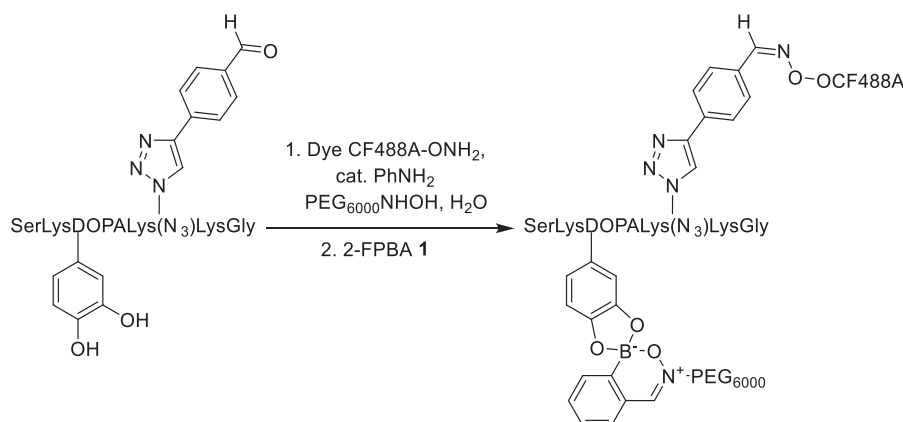
group with 2-FPBA **1**. This was proposed to be due to the IB complex being stabilised by formation of an intramolecular B–O bond between the boronic acid and the α-hydroxy-amide fragment of

the S-appended 3HQ fragment, with further hydrogen bonding stabilisation from the succinimide (blue, [Scheme 45](#)). This boron hot spot approach was used to selectively tag 2-FPBA-modified c-ovalbumin with an impressive  $K_d$  value of  $58,128 \pm 2 \text{ M}^{-1}$ , thus allowing for site-selective labelling of its free N-terminal amino groups in the presence of other lysine residues despite a large excess of 2-FPBA **1**. This tagging approach was used to prepare glutathione-labile boron hot spot fluorescently-labelled protein conjugates that were capable of delivering their fluorescent payloads to HT29 cancer cells.

Finally, a collaboration with Anslyn has reported the use of 2-FPBA **1** and hydroxylamine to irreversibly functionalise the catechol fragment of an L-Dopa-containing peptide derivative. Fluorescent tagging of the peptide containing a Cu(I) Sharpless-Huisgen ‘click’ appended benzaldehyde group was achieved through imine bond formation with the O-functionalized hydroxylamine residue of the CF488A dye. Subsequent addition of 2-FPBA **1** then templated irreversible three-component formation of a highly stable nitrono-boronate linker (*vide supra*) that was formed from incorporation of the catechol unit of the L-Dopa residue and the N-functionalised hydroxylamine group of the solubilising PEG side-chain ([Scheme 46](#)) [147].

## 9. Conclusions and outlook

The body of work presented in this review clearly highlights the versatility and practicality of iminoboronate assemblies, with potential applications across many fields of chemistry and chemical biology. From its initial discovery as a CDA for determining the *ee*'s of chiral amines and diols, the Bull-James three-component



**Scheme 46.** Dual one-pot labelling of L-Dopa-containing peptide with a fluorescent dye and a solubilising PEG side-chain.

assembly has now been developed into a wide-ranging method for the chiral analysis of other analytes using NMR, CD, fluorescence, and electrochemical methods. Beyond analytical applications, iminoboronate assemblies have also proven popular as an orthogonal self-assembly tool for preparing boracycles, polymers, hydrogels and aggregates that exhibit stimuli-responsive properties. Similarly, bioconjugation applications have also been demonstrated, with ongoing development of two- and three-component dynamic labelling methodologies showing great promise as a versatile tool for “click” modification of the free amino groups (or diols) of biomolecules. Although the original application of these IBE assemblies as analytical tools for determining enantiopurities continues to grow both in scope and popularity, the potential applications of these IB systems are far wider ranging than was originally anticipated. Although we expect additional analytical IBE methods to be developed, it is clear that the future of these three-component iminoboronate ester assemblies lies in their innate ability to act as reversible yet highly rigidified linkers. The prospect of expanding the use of these IBEs as chiral auxiliaries for asymmetric synthesis is also an exciting one, and should lead to highly versatile and practically simple methodologies. We also anticipate that the “click” and stimuli-responsive capabilities of these boron-coordination complexes will lead to further development of wide-ranging bioorthogonal and materials-based systems, with increasingly wide-ranging sensing, tagging, theranostic, and logic-based applications.

### Declaration of Competing Interest

The authors declare that they have no known competing financial interests or personal relationships that could have appeared to influence the work reported in this paper.

### Acknowledgments

We would like to thank the many past members of the Bull and James groups who have contributed to the development of the Bull-James assembly (including Drs. Susumu Arimori, Andrew Kelly, Yolanda Perez-Fuertes, Sonia Lozano-Yeste, Magdalena Powell, Ewan Galbraith, David Tickell and Prof. John Fossey), as well as the many local and international collaborators who have also worked on this project. The contributions of the Material and Chemical Characterisation (MC<sup>2</sup>) facility at the University of Bath must also be acknowledged, with particular mention of our crystallographers Drs Gabriel Kociok-Köhn and Mary Mahon.

We would like to thank the University of Bath, the Royal Society and EPSRC for their generous support over the past 20 years (EPSRC Grants: EP/D075351/1, GR/S70289/01). RRG would like to thank the EPSRC Centre for Doctoral Training in Catalysis for funding and support (EP/L016443/1). TDJ would like to thank the Royal Society for a Wolfson Research Merit Award. SDB would like to thank the Royal Society for an International Travel Award (IEC \R3\183068) that provided much needed time to write this review.

### References

- [1] S.D. Bull, S.G. Davies, S.W. Epstein, J.V.A. Ouzman, Chiral relay auxiliary for the synthesis of enantiomerically pure  $\alpha$ -amino acids, *Chem. Commun.* (1998) 659–660, <https://doi.org/10.1039/a800407b>.
- [2] S.D. Bull, S.G. Davies, S. Delgado-Ballester, P.M. Kelly, L.J. Kitchie, M. Gianotti, M. Laderas, A.D. Smith, Asymmetric synthesis of  $\beta$ -haloaryl  $\beta$ -amino acid derivatives, *J. Chem. Soc. Perkin 1* (1) (2001) 3112–3121, <https://doi.org/10.1039/b108573p>.
- [3] S.D. Bull, S.G. Davies, D.J. Fox, M. Gianotti, P.M. Kelly, C. Pierres, E.D. Savory, A. D. Smith, Asymmetric synthesis of  $\beta$ -pyridyl- $\beta$ -amino acid derivatives, *J. Chem. Soc. Perkin 1* (2) (2002) 1858–1868, <https://doi.org/10.1039/b204653a>.
- [4] D. Aitken, S. Bull, I. Davies, L. Drouin, J. Ollivier, J. Peed, An expedient asymmetric synthesis of N-protected (S,S)-2-aminomethyl-1-cyclopropanecarboxylic acid, *Synlett* 2010 (18) (2010) 2729–2732, <https://doi.org/10.1055/s-0030-1258814>.
- [5] C.D. Evans, M.F. Mahon, P.C. Andrews, J. Muir, S.D. Bull, Intramolecular ester enolate-imine cyclization reactions for the asymmetric synthesis of polycyclic  $\beta$ -lactams and cyclic  $\beta$ -amino acid derivatives, *Org. Lett.* 13 (23) (2011) 6276–6279, <https://doi.org/10.1021/ol202750u>.
- [6] T. Boddaert, J.E. Taylor, S.D. Bull, D.J. Aitken, A Selective deprotection strategy for the construction of *trans*-2-aminocyclopropanecarboxylic acid derived peptides, *Org. Lett.* 21 (1) (2019) 100–103, <https://doi.org/10.1021/acs.orglett.8b03533>.
- [7] M. Raban, K. Mislow, The determination of optical purity by nuclear magnetic resonance spectroscopy, *Tetrahedron Lett.* 6 (48) (1965) 4249–4253, [https://doi.org/10.1016/S0040-4039\(00\)71080-X](https://doi.org/10.1016/S0040-4039(00)71080-X).
- [8] J.A. Dale, D.L. Dull, H.S. Mosher,  $\alpha$ -Methoxy- $\alpha$ -trifluoromethylphenylacetic acid, a versatile reagent for the determination of enantiomeric composition of alcohols and amines, *J. Org. Chem.* 34 (1969) 2543–2549, <https://doi.org/10.1021/jo01261a013>.
- [9] T.J. Ward, K.D. Ward, Chiral separations: a review of current topics and trends, *Anal. Chem.* 84 (2) (2012) 626–635, <https://doi.org/10.1021/ac202892w>.
- [10] Y. Zhang, D.-R. Wu, D.B. Wang-Iverson, A.A. Tymiak, Enantioselective chromatography in drug discovery, *Drug Discovery Today* 10 (8) (2005) 571–577, [https://doi.org/10.1016/S1359-6446\(05\)03407-0](https://doi.org/10.1016/S1359-6446(05)03407-0).
- [11] E. Galbraith, T.D. James, Boron based anion receptors as sensors, *Chem. Soc. Rev.* 39 (10) (2010) 3831, <https://doi.org/10.1039/b926165f>.
- [12] T.D. James, K.R.A. Samankumara Sandanayake, S. Shinkai, Chiral discrimination of monosaccharides using a fluorescent molecular sensor, *Nature* 374 (6520) (1995) 345–347, <https://doi.org/10.1038/374345a0>.
- [13] T.D. James, K.R.A.S. Sandanayake, S. Shinkai, Saccharide sensing with molecular receptors based on boronic acid, *Angew. Chem. Int. Ed. Engl.* 35 (17) (1996) 1910–1922, <https://doi.org/10.1002/anie.199619101>.
- [14] S.D. Bull, M.G. Davidson, J.M.H. van den Elsen, J.S. Fossey, A.T.A. Jenkins, Y.-B. Jiang, Y. Kubo, F. Marken, K. Sakurai, J. Zhao, T.D. James, Exploiting the reversible covalent bonding of boronic acids: recognition, sensing, and assembly, *Acc. Chem. Res.* 46 (2) (2013) 312–326, <https://doi.org/10.1021/ar300130w>.
- [15] D.I. Wu, A.C. Sedgwick, T. Gunnlaugsson, E.U. Akkaya, J. Yoon, T.D. James, Fluorescent chemosensors: the past, present and future, *Chem. Soc. Rev.* 46 (23) (2017) 7105–7123, <https://doi.org/10.1039/c7cs00240h>.
- [16] T.D. James, K.R.A.S. Sandanayake, R. Iguchi, S. Shinkai, Novel saccharide-photoinduced electron transfer sensors based on the interaction of boronic acid and amine, *J. Am. Chem. Soc.* 117 (35) (1995) 8982–8987, <https://doi.org/10.1021/ja00140a013>.
- [17] M. Mortellaro, A. DeHennis, Performance characterization of an abiotic and fluorescent-based continuous glucose monitoring system in patients with type 1 diabetes, *Biosens. Bioelectron.* 61 (2014) 227–231, <https://doi.org/10.1016/j.bios.2014.05.022>.
- [18] B.C. Crane, N.P. Barwell, P. Gopal, M. Gopichand, T. Higgs, T.D. James, C.M. Jones, A. Mackenzie, K.P. Mulavilasa, W. Paterson, The development of a continuous intravascular glucose monitoring sensor, *J. Diabetes Sci. Technol.* 9 (4) (2015) 751–761, <https://doi.org/10.1177/1932296815587937>.
- [19] M. Lauer, H. Böhnke, R. Grotstollen, M. Salehnia, G. Wulff, Zur Chemie von Haftgruppen, IV. Über eine außerordentliche Erhöhung der Reaktivität von Arylboronsäuren durch Nachbargruppen, *Chem. Ber.* 118 (1) (1985) 246–260, <https://doi.org/10.1002/cber.19851180124>.
- [20] X. Sun, T.D. James, E.V. Anslyn, Arresting “loose bolt” internal conversion from  $-B(OH)_2$  groups is the mechanism for emission turn-on in ortho-aminomethylphenylboronic acid-based saccharide sensors, *J. Am. Chem. Soc.* 140 (6) (2018) 2348–2354, <https://doi.org/10.1021/jacs.7b12877>.
- [21] X. Sun, B.M. Chapin, P. Metola, B. Collins, B. Wang, T.D. James, E.V. Anslyn, The mechanisms of boronate ester formation and fluorescent turn-on in ortho-aminomethylphenylboronic acids, *Nat. Chem.* 11 (9) (2019) 768–778, <https://doi.org/10.1038/s41557-019-0314-x>.
- [22] N. Hiller, N. Silva, T. Tavares, R. Faria, M. Eberlin, D. Martins, Arylboronic acids and their myriad of applications beyond organic synthesis, *European J. Org. Chem.* 2020 (31) (2020) 4841–4877, <https://doi.org/10.1002/ejoc.202000396>.
- [23] Y. Kanekiyo, S. Shinkai, Chapter 1: supramolecular chemistry of boronic acids, in: *Monogr. Supramol. Chem., Royal Society of Chemistry*, 2016, pp. 1–43, <https://doi.org/10.1039/9781782622123-00001>.
- [24] Wikipedia, Nomikai, (accessed July 31, 2020), <<https://en.wikipedia.org/wiki/Nomikai>> n.d.
- [25] T.D. James, Self and directed assembly: people and molecules, *Beilstein J. Org. Chem.* 12 (2016) 391–405, <https://doi.org/10.3762/bjoc.12.42>.
- [26] H.E. Dunn, J.C. Catlin, H.R. Snyder, Arylboronic acids. Imino derivatives from O-formylbenzeneboronic acid, *J. Org. Chem.* 33 (12) (1968) 4483–4486, <https://doi.org/10.1021/jo01276a040>.
- [27] G.A. Molander, D.L. Sandrock, 2-Formylphenylboronic acid, in: *Encycl. Reagents Org. Synth., John Wiley & Sons, Ltd*, 2009, <https://doi.org/10.1002/047084289x.rm00931>.
- [28] Y. Pérez-Fuertes, A.M. Kelly, A.L. Johnson, S. Arimori, S.D. Bull, T.D. James, Simple protocol for NMR analysis of the enantiomeric purity of primary amines, *Org. Lett.* 8 (4) (2006) 609–612, <https://doi.org/10.1021/ol052776g>.
- [29] Y. Pérez-Fuertes, *New Strategies using BINOL-Boron Compounds for Organic Synthesis*, University of Bath, 2005.
- [30] B.M. Chapin, P. Metola, V.M. Lynch, J.F. Stanton, T.D. James, E.V. Anslyn, Structural and thermodynamic analysis of a three-component assembly

- forming *ortho*-iminophenylboronate esters, *J. Org. Chem.* 81 (18) (2016) 8319–8330, <https://doi.org/10.1021/acs.joc.6b01495>.
- [31] S. Luliński, I. Madura, J. Serwatowski, H. Szatyłowicz, J. Zachara, A tautomeric equilibrium between functionalized 2-formylphenylboronic acids and corresponding 1,3-dihydro-1,3-dihydroxybenzo[c][2,1]oxaboroles, *New J. Chem.* 31 (1) (2007) 144–154, <https://doi.org/10.1039/b611195e>.
  - [32] K. Kowalska, A. Adamczyk-Woźniak, P. Gajowiec, B. Gierczyk, E. Kaczorowska, Ł. Popena, G. Schroeder, A. Sikorski, A. Sporzyński, Fluoro-substituted 2-formylphenylboronic acids: structures, properties and tautomeric equilibria, *J. Fluorine Chem.* 187 (2016) 1–8, <https://doi.org/10.1016/j.jfluchem.2016.05.001>.
  - [33] A. Adamczyk-Woźniak, I. Madura, A.H. Velders, A. Sporzyński, Diverse reactivity of 2-formylphenylboronic acid with secondary amines: synthesis of 3-amino-substituted benzoxaboroles, *Tetrahedron Lett.* 51 (47) (2010) 6181–6185, <https://doi.org/10.1016/j.tetlet.2010.09.091>.
  - [34] A. Adamczyk-Woźniak, M.K. Cyrański, B.T. Frączak, A. Lewandowska, I.D. Madura, A. Sporzyński, Imino- and aminomethylphenylboronic acids: stabilizing effect of hydrogen bonds, *Tetrahedron* 68 (19) (2012) 3761–3767, <https://doi.org/10.1016/j.tet.2012.02.072>.
  - [35] N.J. Gutiérrez-Moreno, F. Medrano, A.K. Yatsimirsky, Schiff base formation and recognition of amino sugars, aminoglycosides and biological polyamines by 2-formyl phenylboronic acid in aqueous solution, *Org. Biomol. Chem.* 10 (34) (2012) 6960, <https://doi.org/10.1039/c2ob26290h>.
  - [36] P. Schmidt, C. Stress, D. Gillingham, Boronic acids facilitate rapid oxime condensations at neutral pH, *Chem. Sci.* 6 (6) (2015) 3329–3333, <https://doi.org/10.1039/c5sc00921a>.
  - [37] D. Gillingham, The role of boronic acids in accelerating condensation reactions of  $\alpha$ -effect amines with carbonyls, *Org. Biomol. Chem.* 14 (32) (2016) 7606–7609, <https://doi.org/10.1039/c6ob01193d>.
  - [38] C.J. Stress, P.J. Schmidt, D.G. Gillingham, Comparison of boron-assisted oxime and hydrazone formations leads to the discovery of a fluorogenic variant, *Org. Biomol. Chem.* 14 (24) (2016) 5529–5533, <https://doi.org/10.1039/c6ob00168h>.
  - [39] S. Nieto, P. Arnau, E. Serrano, R. Navarro, T. Soler, C. Cativiela, E.P. Urriolabeitia, Functionalization of methyl (R)-phenylglycinate through orthopalladation: C–hal, C–O, C–N, and C–C bond coupling, *Inorg. Chem.* 48 (24) (2009) 11963–11975, <https://doi.org/10.1021/jc901941s>.
  - [40] Y. Pérez-Fuertes, J.E. Taylor, D.A. Tickell, M.F. Mahon, S.D. Bull, T.D. James, Asymmetric strecker synthesis of  $\alpha$ -aryl glycines, *J. Org. Chem.* 76 (15) (2011) 6038–6047, <https://doi.org/10.1021/jo200528s>.
  - [41] Y. Pérez-Fuertes, A.M. Kelly, J.S. Fossey, M.E. Powell, S.D. Bull, T.D. James, Simple protocols for NMR analysis of the enantiomeric purity of chiral primary amines, *Nat. Protoc.* 3 (2) (2008) 210–214, <https://doi.org/10.1038/nprot.2007.524>.
  - [42] P.J.M. Taylor, S.D. Bull, An improved synthesis of deuterated Schöllkopf's bis-lactim ether and its use for the asymmetric synthesis of (R)-[ $\alpha$ - $^2$ H]-phenylalanine methyl esters, *Tetrahedron Asymmetry* 17 (8) (2006) 1170–1178, <https://doi.org/10.1016/j.tetasy.2006.04.005>.
  - [43] R.M. Archer, M. Hutchby, C.L. Winn, J.S. Fossey, S.D. Bull, A chiral ligand mediated *aza*-conjugate addition strategy for the enantioselective synthesis of  $\beta$ -amino esters that contain hydroxylolytically sensitive functionality, *Tetrahedron* 71 (46) (2015) 8838–8847, <https://doi.org/10.1016/j.tet.2015.08.018>.
  - [44] P. Axe, S.D. Bull, M.G. Davidson, C.J. Gilfillan, M.D. Jones, D.E.J.E. Robinson, L.E. Turner, W.L. Mitchell, Enantiopure pseudo-C3-symmetric titanium alkoxide with propeller-like Chirality, *Org. Lett.* 9 (2) (2007) 223–226, <https://doi.org/10.1021/ol062655w>.
  - [45] T.L. March, M.R. Johnston, P.J. Duggan, Diastereoselective synthesis of aliphatic  $\alpha,\alpha$ -difluoro- $\beta$ -amino esters via a sonocatalyzed reformatzky reaction, *Org. Lett.* 14 (1) (2012) 182–185, <https://doi.org/10.1021/ol202969w>.
  - [46] C.e. Shi, T.W. Geders, S.W. Park, D.J. Wilson, H.I. Boshoff, O. Abayomi, C.E. Barry III, D. Schnappinger, B.C. Finzel, C.C. Aldrich, Mechanism-based inactivation by aromatization of the transaminase BioA involved in biotin biosynthesis in *Mycobacterium tuberculosis*, *J. Am. Chem. Soc.* 133 (45) (2011) 18194–18201, <https://doi.org/10.1021/ja204036t>.
  - [47] S. Nieto, J.M. Dragna, E.V. Anslyn, A facile circular dichroism protocol for rapid determination of enantiomeric excess and concentration of chiral primary amines, *Chem. Eur. J.* 16 (2010) 227–232, <https://doi.org/10.1002/chem.200902650>.
  - [48] N. Lokesh, S.L. Sachin, L.V. Narendra, K. Arun, N. Suryaprakash, RNA nucleosides as chiral sensing agents in NMR spectroscopy, *Org. Biomol. Chem.* 13 (26) (2015) 7230–7235, <https://doi.org/10.1039/c5ob00513b>.
  - [49] J.S. Fossey, E.V. Anslyn, W.D.G. Brittain, S.D. Bull, B.M. Chapin, C. Cécile, S. Le Duff, T.D. James, G. Lees, S. Lim, J.A.C. Lloyd, C.V. Manville, D.T. Payne, K.A. Roper, Rapid determination of enantiomeric excess via NMR spectroscopy: a research-informed experiment, *J. Chem. Educ.* 94 (2017) 79–84, <https://doi.org/10.1021/acs.jchemed.6b00355>.
  - [50] A.M. Kelly, S.D. Bull, T.D. James, Simple chiral derivatization protocols for NMR analysis of the enantiopurity of 1,2-diphenylethane-1,2-diamine and *N*-Boc-cyclohexane-1,2-diamine, *Tetrahedron Asymmetry* 19 (4) (2008) 489–494, <https://doi.org/10.1016/j.tetasy.2008.01.026>.
  - [51] P. Mangeney, A. Alexakis, J.F. Normant, Resolution and determination of enantiomeric excesses of chiral aldehydes via chiral imidazolidines, *Tetrahedron Lett.* 29 (22) (1988) 2677–2680, [https://doi.org/10.1016/0040-4039\(88\)85258-4](https://doi.org/10.1016/0040-4039(88)85258-4).
  - [52] D. Cuvilot, A. Alexakis, J.-F. Normant, J.-P. Lellouch, Chiral Trifluoro diamines as convenient reagents for determining the enantiomeric purity of aldehydes by use of  $^{19}\text{F}$  NMR spectroscopy, *J. Org. Chem.* 54 (1989) 2420–2425, <https://doi.org/10.1021/jo00271a034>.
  - [53] A. Alexakis, J.C. Frutos, P. Mangeney, An easy and fast way to determine the enantiomeric purity of substituted cyclanones, *Tetrahedron Asymmetry* 4 (12) (1993) 2431–2434, [https://doi.org/10.1016/S0957-4166\(00\)82217-X](https://doi.org/10.1016/S0957-4166(00)82217-X).
  - [54] M.E. Powell, A.M. Kelly, S.D. Bull, T.D. James, A simple chiral derivatization protocol for  $^1\text{H}$  NMR spectroscopic analysis of the enantiopurity of *O*-silyl-1,2-amino alcohols, *Tetrahedron Lett.* 50 (8) (2009) 876–879, <https://doi.org/10.1016/j.tetlet.2008.12.013>.
  - [55] D.A. Tickell, M.F. Mahon, S.D. Bull, T.D. James, A simple protocol for NMR analysis of the enantiomeric purity of chiral hydroxylamines, *Org. Lett.* 15 (2013) 860–863, <https://doi.org/10.1021/ol303566k>.
  - [56] W. Kligel, R. Nanninga, Nitron von 2-formylphenylboronsäureestern, *J. Organomet. Chem.* 247 (3) (1983) 247–252, [https://doi.org/10.1016/0022-328X\(83\)85166-3](https://doi.org/10.1016/0022-328X(83)85166-3).
  - [57] R.R. Groleau, R.S.L. Chapman, H. Ley-Smith, L. Liu, T.D. James, S.D. Bull, A three-component derivatization protocol for determining the enantiopurity of sulfonamides by  $^1\text{H}$  and  $^{19}\text{F}$  NMR spectroscopy, *J. Org. Chem.* 85 (2) (2020) 1208–1215, <https://doi.org/10.1021/acs.joc.9b02473>.
  - [58] A.M. Kelly, Y. Pérez-Fuertes, S. Arimori, S.D. Bull, T.D. James, Simple protocol for NMR analysis of the enantiomeric purity of diols, *Org. Lett.* 8 (10) (2006) 1971–1974, <https://doi.org/10.1021/ol0602351>.
  - [59] A.M. Kelly, Y. Pérez-Fuertes, J.S. Fossey, S.L. Yeste, S.D. Bull, T.D. James, Simple protocols for NMR analysis of the enantiomeric purity of chiral diols, *Nat. Protoc.* 3 (2) (2008) 215–219, <https://doi.org/10.1038/nprot.2007.523>.
  - [60] M.D. Reddy, H. Kobori, T. Mori, J. Wu, H. Kawagishi, E.B. Watkins, Gram-Scale, stereoselective synthesis and biological evaluation of (+)-armillariol C, *J. Nat. Prod.* 80 (9) (2017) 2561–2565, <https://doi.org/10.1021/acs.jnatprod.7b00484>.
  - [61] D. Urabe, H. Todoroki, K. Masuda, M. Inoue, Total syntheses of four possible stereoisomers of resolin E3, *Tetrahedron* 68 (15) (2012) 3210–3219, <https://doi.org/10.1016/j.tet.2012.02.045>.
  - [62] M. Göhl, K. Seifert, Total synthesis of 3-oxo- and 3- $\beta$ -hydroxytauranin via Negishi coupling of a bis(ortho-oxy)-functionalized benzyl chloride, *Eur. J. Org. Chem.* 2015 (28) (2015) 6249–6258, <https://doi.org/10.1002/ejoc.201500815>.
  - [63] C. Chopard, R. Azerad, T. Prangé, Naphthalene-dioxygenase-catalysed *cis*-dihydroxylation of azaarene derivatives, *J. Mol. Catal. B Enzym.* 50 (2–4) (2008) 53–60, <https://doi.org/10.1016/j.molcatb.2007.09.013>.
  - [64] S.H. Shabbir, C.J. Regan, E.V. Anslyn, J. Rebek, A general protocol for creating high-throughput screening assays for reaction yield and enantiomeric excess applied to hydrobenzoin, *Proc. Natl. Acad. Sci.* 106 (2009) 10487–10492, <https://doi.org/10.1073/pnas.0809530106>.
  - [65] S.H. Shabbir, L.A. Joyce, G.M. da Cruz, V.M. Lynch, S. Sorey, E.V. Anslyn, Pattern-based recognition for the rapid determination of identity, concentration, and enantiomeric excess of subtly different three diols, *J. Am. Chem. Soc.* 131 (36) (2009) 13125–13131, <https://doi.org/10.1021/ja904545d>.
  - [66] P.S. Fordred, S.D. Bull, Tandem hydroboration/reduction of trisubstituted  $\beta,\gamma$ -unsaturated esters for the asymmetric synthesis of chiral 1,3-diols, *Tetrahedron Lett.* 54 (1) (2013) 27–31, <https://doi.org/10.1016/j.tetlet.2012.10.047>.
  - [67] M. Zeng, S.B. Herzon, Synthesis of 1,3-amino alcohols, 1,3-diols, amines, and carboxylic acids from terminal alkynes, *J. Org. Chem.* 80 (17) (2015) 8604–8618, <https://doi.org/10.1021/acs.joc.5b01220>.
  - [68] Z. Li, C. Chen, S. Gröger, J. Kressler, Detection of chirality of poly(glycerol methacrylate)s after derivatization by  $^1\text{H}$  NMR spectroscopy, *Polymer* 53 (13) (2012) 2613–2618, <https://doi.org/10.1016/j.polymer.2012.04.019>.
  - [69] S.R. Chaudhari, N. Suryaprakash, Three-component chiral derivatizing protocols for NMR spectroscopic enantiodiscrimination of hydroxy acids and primary amines, *J. Org. Chem.* 77 (1) (2012) 648–651, <https://doi.org/10.1021/jo202334d>.
  - [70] S.R. Chaudhari, N. Suryaprakash, Simple and efficient methods for discrimination of chiral diacids and chiral  $\alpha$ -methyl amines, *Org. Biomol. Chem.* 10 (31) (2012) 6410, <https://doi.org/10.1039/c2ob25599e>.
  - [71] S.K. Mishra, N. Suryaprakash, A simple and rapid approach for testing enantiopurity of hydroxy acids and their derivatives using  $^1\text{H}$  NMR spectroscopy, *RSC Adv.* 5 (82) (2015) 67277–67283, <https://doi.org/10.1039/c5ra11919g>.
  - [72] S.R. Chaudhari, N.R. Suryaprakash, Facile protocols for the configurational assignment of primary amines and hydroxy acids by NMR, *New J. Chem.* 38 (2) (2014) 790, <https://doi.org/10.1039/c3nj01273e>.
  - [73] S.K. Mishra, N. Suryaprakash, Assignment of the absolute configuration of hydroxy acids using  $^1\text{H}$  NMR spectroscopy: a simple and rapid approach, *Tetrahedron Asymmetry* 28 (2) (2017) 250–256, <https://doi.org/10.1016/j.tetasy.2017.01.004>.
  - [74] N. Lokesh, S.R. Chaudhari, N. Suryaprakash, RES-TOCSY: a simple approach to resolve overlapped  $^1\text{H}$  NMR spectra of enantiomers, *Org. Biomol. Chem.* 12 (2014) 993–997, <https://doi.org/10.1039/c3ob42087f>.
  - [75] S.L. Yeste, M.E. Powell, S.D. Bull, T.D. James, Simple chiral derivatization protocols for  $^1\text{H}$  NMR and  $^{19}\text{F}$  NMR spectroscopic analysis of the enantiopurity of chiral diols, *J. Org. Chem.* 74 (1) (2009) 427–430, <https://doi.org/10.1021/jo8019187>.



- [76] S. Lozano Yeste, M.E. Powell, S.D. Bull, T.D. James, Correction: simple chiral derivatization protocols for  $^1\text{H}$  NMR and  $^{19}\text{F}$  NMR spectroscopic analysis of the enantiopurity of chiral diols, *J. Org. Chem.* 84 (2019) 9395–9396, <https://doi.org/10.1021/acs.joc.9b01735>.
- [77] N. Hamaguchi, Y. Okuno, Y. Oe, T. Ohta, A simple quantitative chiral analysis of amino acid esters by fluorine-19 nuclear magnetic resonance using the modified James-Bull method, *Chirality* 31 (1) (2019) 34–40, <https://doi.org/10.1002/chir.23028>.
- [78] Y.R. Lima, T.J. Peglow, P.C. Nobre, P.T. Campos, G. Perin, E.J. Lenardão, M.S. Silva, Chalcogen-containing diols: a novel chiral derivatizing agent for  $^{77}\text{Se}$  and  $^{125}\text{Te}$  NMR chiral recognition of primary amines, *ChemistrySelect* 4 (16) (2019) 4797–4803, <https://doi.org/10.1002/slct.201900097>.
- [79] S.S. Oliveira, R.L.O.R. Cunha, M.S. Silva,  $^{77}\text{Se}$  and  $^{125}\text{Te}$  NMR spectroscopy for enantiopurity determination of chalcogen amines, *Tetrahedron Lett.* 57 (41) (2016) 4556–4559, <https://doi.org/10.1016/j.tetlet.2016.08.091>.
- [80] D. Leung, S.O. Kang, E.V. Anslyn, Rapid determination of enantiomeric excess: a focus on optical approaches, *Chem. Soc. Rev.* 41 (1) (2012) 448–479, <https://doi.org/10.1039/c1cs15135e>.
- [81] B.T. Herrera, S.L. Pilicer, E.V. Anslyn, L.A. Joyce, C. Wolf, Optical analysis of reaction yield and enantiomeric excess: a new paradigm ready for prime time, *J. Am. Chem. Soc.* 140 (33) (2018) 10385–10401, <https://doi.org/10.1021/jacs.8b06607>.
- [82] P. Metola, E.V. Anslyn, T.D. James, S.D. Bull, Circular dichroism of multi-component assemblies for chiral amine recognition and rapid ee determination, *Chem. Sci.* 3 (1) (2012) 156–161, <https://doi.org/10.1039/c1sc00496d>.
- [83] S. Stewart, M.A. Ivy, E.V. Anslyn, The use of principal component analysis and discriminant analysis in differential sensing routines, *Chem. Soc. Rev.* 43 (1) (2014) 70–84, <https://doi.org/10.1039/c3cs60183h>.
- [84] K.W. Bentley, Y.G. Nam, J.M. Murphy, C. Wolf, Chirality sensing of amines, diamines, amino acids, amino alcohols, and  $\alpha$ -hydroxy acids with a single probe, *J. Am. Chem. Soc.* 135 (48) (2013) 18052–18055, <https://doi.org/10.1021/ja410428b>.
- [85] E.G. Shcherbakova, T. Minami, V. Brega, T.D. James, P. Anzenbacher Jr., Determination of enantiomeric excess in amine derivatives with molecular self-assemblies, *Angew. Chem. Int. Ed.* 54 (24) (2015) 7130–7133, <https://doi.org/10.1002/anie.201501736>.
- [86] E.G. Shcherbakova, V. Brega, T. Minami, S. Sheykhi, T.D. James, P. Anzenbacher Jr., Toward fluorescence-based high-throughput screening for enantiomeric excess in amines and amino acid derivatives, *Chem. Eur. J.* 22 (29) (2016) 10074–10080, <https://doi.org/10.1002/chem.201601614>.
- [87] E.G. Shcherbakova, V. Brega, V.M. Lynch, T.D. James, P. Anzenbacher Jr., High-throughput assay for enantiomeric excess determination in 1,2- and 1,3-diols and direct asymmetric reaction screening, *Chem. Eur. J.* 23 (42) (2017) 10222–10229, <https://doi.org/10.1002/chem.201701923>.
- [88] M. Pushina, S. Farshbaf, E.G. Shcherbakova, P. Anzenbacher, A dual chromophore sensor for the detection of amines, diols, hydroxy acids, and amino alcohols, *Chem. Commun.* 55 (31) (2019) 4495–4498, <https://doi.org/10.1039/c9cc01051c>.
- [89] E.G. Shcherbakova, T.D. James, P. Anzenbacher Jr., High-throughput assay for determining enantiomeric excess of chiral diols, amino alcohols, and amines and for direct asymmetric reaction screening, *Nat. Protoc.* 15 (7) (2020) 2203–2229, <https://doi.org/10.1038/s41596-020-0329-1>.
- [90] G. Mirri, S.D. Bull, P.N. Horton, T.D. James, L. Male, J.H.R. Tucker, Electrochemical method for the determination of enantiomeric excess of binol using redox-active boronic acids as chiral sensors, *J. Am. Chem. Soc.* 132 (26) (2010) 8903–8905, <https://doi.org/10.1021/ja103462x>.
- [91] Adam Wilson, Giulio Gasparini, Stefan Matile, Functional systems with orthogonal dynamic covalent bonds, *Chem. Soc. Rev.* 43 (6) (2014) 1948–1962, <https://doi.org/10.1039/c3cs60342c>.
- [92] J.F. Reuther, S.D. Dahlhauser, E.V. Anslyn, Tunable Orthogonal Reversible Covalent (TORC) bonds: dynamic chemical control over molecular assembly, *Angew. Chem. Int. Ed.* 58 (2019) 74–85, <https://doi.org/10.1002/ange.201808371>.
- [93] H.M. Seifert, K. Ramirez Trejo, E.V. Anslyn, Four simultaneously dynamic covalent reactions. experimental proof of orthogonality, *J. Am. Chem. Soc.* 138 (34) (2016) 10916–10924, <https://doi.org/10.1021/jacs.6b04532>.
- [94] V. Campbell, J. Nitschke, Complex systems from simple building blocks via subcomponent self-assembly, *Synlett* 2008 (20) (2008) 3077–3090, <https://doi.org/10.1055/s-00028-1087361>.
- [95] M. Hutin, G. Bernardinelli, J.R. Nitschke, An iminoboronate construction set for subcomponent self-assembly, *Chem. Eur. J.* 14 (15) (2008) 4585–4593, <https://doi.org/10.1002/chem.200800074>.
- [96] R. Nishiyabu, Y. Kubo, T.D. James, J.S. Fossey, Boronic acid building blocks: tools for self assembly, *Chem. Commun.* 47 (4) (2011) 1124–1150, <https://doi.org/10.1039/c0cc02921a>.
- [97] Y. Kubo, R. Nishiyabu, T.D. James, Hierarchical supramolecules and organization using boronic acid building blocks, *Chem. Commun.* 51 (11) (2015) 2005–2020, <https://doi.org/10.1039/c4cc07712a>.
- [98] E. Galbraith, A.M. Kelly, J.S. Fossey, G. Kociok-Köhn, M.G. Davidson, S.D. Bull, T.D. James, Dynamic covalent self-assembled macrocycles prepared from 2-formyl-aryl-boronic acids and 1,2-amino alcohols, *New J. Chem.* 33 (1) (2009) 181–185, <https://doi.org/10.1039/b815138e>.
- [99] D.W. Norman, J.P. Edwards, C.M. Vogels, A. Decken, S.A. Westcott, Synthesis and reactivity of novel Schiff bases containing boronate esters, *Can. J. Chem.* 80 (1) (2002) 31–40, <https://doi.org/10.1139/v01-188>.
- [100] F.A. Appoh, S.S. Barnes, M.J. Manning, C.S. Turner, C.M. Vogels, S.A. Westcott, A. Decken, Synthesis of boron macrocycles from 1,2-aminoalcohols and 2-formylphenylboronic acid, *J. Heterocycl. Chem.* 45 (2008) 1415–1418, <https://doi.org/10.1002/jhet.5570450526>.
- [101] H.Y. Su, D. Gorelik, M.S. Taylor, Chiral phosphine ligand libraries based on the Bull–James three-component supramolecular assembly, *Supramol. Chem.* 31 (3) (2019) 190–202, <https://doi.org/10.1080/10610278.2018.1564829>.
- [102] W.D.G. Brittain, B.M. Chapin, W. Zhai, V.M. Lynch, B.R. Buckley, E.V. Anslyn, J. S. Fossey, The Bull–James assembly as a chiral auxiliary and shift reagent in kinetic resolution of alkyne amines by the CuAAC reaction, *Org. Biomol. Chem.* 14 (46) (2016) 10778–10782, <https://doi.org/10.1039/c6ob01623e>.
- [103] E.N. Keyzer, A. Sava, T.K. Ronson, J.R. Nitschke, A.J. McConnell, Post-assembly reactivity of N-Aryl iminoboronates: reversible radical coupling and unusual B–N dynamic covalent chemistry, *Chem. Eur. J.* 24 (46) (2018) 12000–12005, <https://doi.org/10.1002/chem.201802790>.
- [104] E. Amado, J. Rg Kressler, Reversible complexation of iminophenylboronates with mono- and dihydroxy methacrylate monomers and their polymerization at low temperature by photoinduced ATRP in one pot, *Macromolecules* 49 (5) (2016) 1532–1544, <https://doi.org/10.1021/acs.macromol.5b02771>.
- [105] D. Alilincăi, L. Marin, S. Morariu, M. Mares, A.C. Bostanaru, M. Pinteala, B.C. Simionescu, M. Barboiu, Dual crosslinked iminoboronate-chitosan hydrogels with strong antifungal activity against *Candida* planktonic yeasts and biofilms, *Carbohydr. Polym.* 152 (2016) 306–316, <https://doi.org/10.1016/j.carbpol.2016.07.007>.
- [106] S.S. Delpierre, B. Willocq, G. Manini, V. Lemaure, J. Goole, P. Gerbaux, J. Jérôme Cornil, P. Dubois, J.-M. Raquez, Simple approach for a self-healable and stiff polymer network from iminoboronate-based boroxine chemistry, *Chem. Mater.* 31 (10) (2019) 3736–3744, <https://doi.org/10.1021/acs.chemmater.9b00750>.
- [107] S. Delpierre, B. Willocq, J. De Winter, P. Dubois, P. Gerbaux, J.-M. Raquez, Dynamic iminoboronate-based boroxine chemistry for the design of ambient humidity-sensitive self-healing polymers, *Chem. Eur. J.* 23 (28) (2017) 6730–6735, <https://doi.org/10.1002/chem.201700333>.
- [108] Y. Yang, L. Huang, R. Wu, W. Fan, Q. Dai, J. He, C. Bai, Assembling of reprocessable polybutadiene-based vitrimers with high strength and shape memory via catalyst-free imine-coordinated boroxine, *ACS Appl. Mater. Interfaces* 12 (29) (2020) 33305–33314, <https://doi.org/10.1021/acsami.0c09712>.
- [109] S. Li, C. Zuo, Y.H. Jo, S. Li, K. Jiang, L. Yu, Y. Zhang, J. Wang, L. Li, Z. Xue, Enhanced ionic conductivity and mechanical properties via dynamic-covalent imine boroxine bonds in solid polymer electrolytes, *J. Membr. Sci.* 608 (2020) 118218, <https://doi.org/10.1016/j.memsci.2020.118218>.
- [110] X. Zhang, J. Gao, X. Zhao, Z. Liu, Z. Liu, K. Wang, G. Li, J. Jiang, Hyperbranched polymer micelles with triple-stimuli backbone-breakable iminoboronate ester linkages, *Chin. Chem. Lett.* 31 (7) (2020) 1822–1826, <https://doi.org/10.1016/j.cclet.2020.03.018>.
- [111] C.C. Deng, W.L.A. Brooks, K.A. Abboud, B.S. Sumerlin, Boronic acid-based hydrogels undergo self-healing at neutral and acidic pH, *ACS Macro Lett.* 4 (2) (2015) 220–224, <https://doi.org/10.1021/acsmacrolett.5b00018>.
- [112] J. Hu, Q. Hu, X. He, C. Liu, Y. Kong, Y. Cheng, Y. Zhang, Stimuli-responsive hydrogels with antibacterial activity assembled from guanosine, aminoglycoside, and a bifunctional anchor, *Adv. Healthcare Mater.* 9 (2) (2020) 1901329, <https://doi.org/10.1002/adhm.201901329>.
- [113] Y. Li, Y. Liu, R. Ma, Y. Xu, Y. Zhang, B. Li, Y. An, L. Shi, A G-quadruplex hydrogel via multicompartment self-assembly: formation and zero-order controlled release, *ACS Appl. Mater. Interfaces* 9 (15) (2017) 13056–13067, <https://doi.org/10.1021/acsami.7b00957>.
- [114] C. Arnal-Hérault, A. Pasc, M. Michau, D. Cot, E. Petit, M. Barboiu, Functional G-quartet macroscopic membrane films, *Angew. Chem. Int. Ed.* 46 (44) (2007) 8409–8413, <https://doi.org/10.1002/anie.200702605>.
- [115] S. Mihai, Y. Le Duc, D. Cot, M. Barboiu, Sol-gel selection of hybrid G-quadruplex architectures from dynamic supramolecular guanosine libraries, *J. Mater. Chem.* 20 (42) (2010) 9443–9448, <https://doi.org/10.1039/c0jm01248c>.
- [116] A. Biswas, T. Ghosh, P.K. Gavel, A.K. Das, PEG functionalized stimuli responsive self-healable injectable dynamic imino-boronate G-quadruplex hydrogel for the delivery of doxorubicin, *ACS Appl. Bio Mater.* 3 (2) (2020) 1052–1060, <https://doi.org/10.1021/acsabm.9b01034>.
- [117] A. Sikora, J. Zielonka, M. Lopez, J. Joseph, B. Kalyanaraman, Direct oxidation of boronates by peroxynitrite: mechanism and implications in fluorescence imaging of peroxynitrite, *Free Radical Biol. Med.* 47 (10) (2009) 1401–1407, <https://doi.org/10.1016/j.freeradbiomed.2009.08.006>.
- [118] K. Debowska, D. Debski, M. Hardy, M. Jakubowska, B. Kalyanaraman, A. Marcinek, R. Michalski, B. Michalowski, O. Ouari, A. Sikora, R. Smulik, J. Zielonka, Toward selective detection of reactive oxygen and nitrogen species with the use of fluorogenic probes – limitations, progress, and perspectives, *Pharmacol. Rep.* 67 (4) (2015) 756–764, <https://doi.org/10.1016/j.pharep.2015.03.016>.
- [119] L. Wu, A.C. Sedgwick, X. Sun, S.D. Bull, X.P. He, T.D. James, Reaction-based fluorescent probes for the detection and imaging of reactive oxygen, nitrogen, and sulfur species, *Acc. Chem. Res.* 52 (9) (2019) 2582–2597, <https://doi.org/10.1021/acs.accounts.9b00302>.
- [120] J. Yu, H. Chao, G. Li, R. Tang, Z. Liu, Z. Liu, J. Jiang, Backbone-based LCST-type hyperbranched poly(oligo(ethylene glycol)) with  $\text{CO}_2$ -reversible

- iminoboronate linkers, *Macromol. Chem. Phys.* 219 (24) (2018) 1800346, <https://doi.org/10.1002/macp.201800346>.
- [121] Y. Liu, G. Li, J. Chen, Z. Liu, Z. Liu, J. Jiang, Fabricating triple-sensitive polymer nano-aggregates via an aqueous iminoboronate multicomponent reaction, *Macromol. Rapid Commun.* 38 (8) (2017) 1600805, <https://doi.org/10.1002/marc.201600805>.
- [122] X. Zhang, G. Li, Z. Liu, Z. Liu, J. Jiang, Iminoboronate backbone-based hyperbranched polymeric micelles with Fenton-like enhanced ROS response, *Macromol. Chem. Phys.* 221 (9) (2020) 2000022, <https://doi.org/10.1002/macp.202000022>.
- [123] R. Cheng, G. Li, L. Fan, Z. Liu, Z. Liu, J. Jiang, CO<sub>2</sub>-Acidolysis of iminoboronate ester based polymersomes, *J. Mater. Chem. B* 6 (47) (2018) 7800–7804, <https://doi.org/10.1039/c8tb02496k>.
- [124] R. Ma, C. Zhang, Y. Liu, C. Li, Y. Xu, B. Li, Y. Zhang, Y. An, L. Shi, Iminoboronate-based dual-responsive micelles via subcomponent self-assembly for hydrophilic 1,2-diol-containing drug delivery, *RSC Adv.* 7 (34) (2017) 21328–21335, <https://doi.org/10.1039/C7RA01742A>.
- [125] B. Akgun, D.G. Hall, Boronic acids as bioorthogonal probes for site-selective labeling of proteins, *Angew. Chem. Int. Ed.* 57 (40) (2018) 13028–13044, <https://doi.org/10.1002/anie.201712611>.
- [126] J.P.M. António, R. Russo, C.P. Carvalho, P.M.S.D. Cal, P.M.P. Gois, Boronic acids as building blocks for the construction of therapeutically useful bioconjugates, *Chem. Soc. Rev.* 48 (13) (2019) 3513–3536, <https://doi.org/10.1039/C9CS00184K>.
- [127] S. Cambray, J. Gao, Versatile bioconjugation chemistries of *ortho*-Boronaryl ketones and aldehydes, *Acc. Chem. Res.* 51 (9) (2018) 2198–2206, <https://doi.org/10.1021/acs.accounts.8b00154>.
- [128] A. Bandyopadhyay, J. Gao, Iminoboronate formation leads to fast and reversible conjugation chemistry of  $\alpha$ -nucleophiles at neutral pH, *Chem. Eur. J.* 21 (42) (2015) 14748–14752, <https://doi.org/10.1002/chem.201502077>.
- [129] P.M.S.D. Cal, J.B. Vicente, E. Pires, A.V. Coelho, L.F. Veiros, C. Cordeiro, P.M.P. Gois, Iminoboronates: a new strategy for reversible protein modification, *J. Am. Chem. Soc.* 134 (24) (2012) 10299–10305, <https://doi.org/10.1021/ja303436y>.
- [130] X. Liu, Z. Li, H. Xu, Y. Zhan, P. Ma, H. Chen, B. Jiang, Tris(2-carboxyethyl) phosphine promotes hydrolysis of iminoboronates, *Tetrahedron Lett.* 58 (32) (2017) 3101–3106, <https://doi.org/10.1016/j.tetlet.2017.06.069>.
- [131] H. Gu, T.I. Chio, Z. Lei, R.J. Staples, J.S. Hirschi, S. Bane, Formation of hydrazones and stabilized boron–nitrogen heterocycles in aqueous solution from carbonylhydrazides and *ortho*-formylphenylboronic acids, *Org. Biomol. Chem.* 15 (36) (2017) 7543–7548, <https://doi.org/10.1039/c7ob01708a>.
- [132] O. Dilek, Z. Lei, K. Mukherjee, S. Bane, Rapid formation of a stable boron–nitrogen heterocycle in dilute, neutral aqueous solution for bioorthogonal coupling reactions, *Chem. Commun.* 51 (95) (2015) 16992–16995, <https://doi.org/10.1039/c5cc07453c>.
- [133] H. Gu, S. Ghosh, R.J. Staples, S.L. Bane,  $\beta$ -hydroxy-stabilized boron–nitrogen heterocycles enable rapid and efficient C-terminal protein modification, *Bioconjug. Chem.* 30 (10) (2019) 2604–2613, <https://doi.org/10.1021/acs.bioconjchem.9b00534>.
- [134] A. Bandyopadhyay, S. Cambray, J. Gao, Fast diazaborine formation of semicarbazide enables facile labeling of bacterial pathogens, *J. Am. Chem. Soc.* 139 (2) (2017) 871–878, <https://doi.org/10.1021/jacs.6b11115>.
- [135] H. Faustino, M.J.S.A. Silva, L.F. Veiros, G.J.L. Bernardes, P.M.P. Gois, Iminoboronates are efficient intermediates for selective, rapid and reversible *N*-terminal cysteine functionalisation, *Chem. Sci.* 7 (8) (2016) 5052–5058, <https://doi.org/10.1039/c6sc01520d>.
- [136] T.S.L. Tang, D. Cardella, A.J. Lander, X. Li, J.S. Escudero, Y.-H. Tsai, L.Y.P. Luk, Use of an asparaginyl endopeptidase for chemo-enzymatic peptide and protein labeling, *Chem. Sci.* 11 (23) (2020) 5881–5888, <https://doi.org/10.1039/D0SC02023K>.
- [137] T.I. Chio, H. Gu, K. Mukherjee, L.N. Tumey, S.L. Bane, Site-specific bioconjugation and multi-bioorthogonal labeling via rapid formation of a boron–nitrogen heterocycle, *Bioconjug. Chem.* 30 (5) (2019) 1554–1564, <https://doi.org/10.1021/acs.bioconjchem.9b00246>.
- [138] A. Bandyopadhyay, J. Gao, Iminoboronate-based peptide cyclization that responds to pH, oxidation, and small molecule modulators, *J. Am. Chem. Soc.* 138 (7) (2016) 2098–2101, <https://doi.org/10.1021/jacs.5b12301>.
- [139] K. Li, J. Gao, Iminoboronate-mediated peptide cyclization with lysine homologues, *Synlett* 28 (15) (2017) 1913–1916, <https://doi.org/10.1055/s-0036-1590795>.
- [140] S. Borsley, S.L. Cockcroft, *In situ* synthetic functionalization of a transmembrane protein nanopore, *ACS Nano* 12 (1) (2018) 786–794, <https://doi.org/10.1021/acsnano.7b08105>.
- [141] P.M.S.D. Cal, R.F.M. Frade, V. Chudasama, C. Cordeiro, S. Caddick, P.M.P. Gois, Targeting cancer cells with folic acid–iminoboronate fluorescent conjugates, *Chem. Commun.* 50 (40) (2014) 5261–5263, <https://doi.org/10.1039/c3cc47534d>.
- [142] P.M.S.D. Cal, R.F.M. Frade, C. Cordeiro, P.M.P. Gois, Reversible lysine modification on proteins by using functionalized boronic acids, *Chem. Eur. J.* 21 (22) (2015) 8182–8187, <https://doi.org/10.1002/chem.201500127>.
- [143] G. Akçay, M.A. Belmonte, B. Aquila, C. Chuaqui, A.W. Hird, M.L. Lamb, P.B. Rawlins, N. Su, S. Tentarelli, N.P. Grimster, Q. Su, Inhibition of Mcl-1 through covalent modification of a noncatalytic lysine side chain, *Nat. Chem. Biol.* 12 (11) (2016) 931–936, <https://doi.org/10.1038/nChemBio.2174>.
- [144] A. Bandyopadhyay, K.A. McCarthy, M.A. Kelly, J. Gao, Targeting bacteria via iminoboronate chemistry of amine-presenting lipids, *Nat. Commun.* 6 (1) (2015), <https://doi.org/10.1038/ncomms7561>.
- [145] B. Akgun, C. Li, Y. Hao, G. Lambkin, R. Derda, D.G. Hall, Synergic “Click” boronate/thiosemicarbazone system for fast and irreversible bioorthogonal conjugation in live cells, *J. Am. Chem. Soc.* 139 (40) (2017) 14285–14291, <https://doi.org/10.1021/jacs.7b08693>.
- [146] R. Russo, R. Padanha, F. Fernandes, L. Veiros, F. Corzana, P.M. pimenta Gois, Engineering boron hot spots for the site-selective installation of iminoboronates on peptide chains, *Chem. – A Eur. J.* (2020), <https://doi.org/10.1002/chem.202002675>.
- [147] M.K. Meadows, E.K. Roesner, V.M. Lynch, T.D. James, E.V. Anslyn, Boronic acid mediated coupling of catechols and *N*-hydroxylamines: a bioorthogonal reaction to label peptides, *Org. Lett.* 19 (12) (2017) 3179–3182, <https://doi.org/10.1021/acs.orglett.7b01198>.

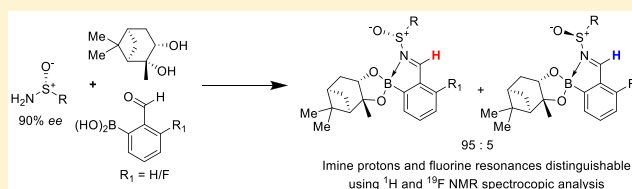
# A Three-Component Derivatization Protocol for Determining the Enantiopurity of Sulfinamides by $^1\text{H}$ and $^{19}\text{F}$ NMR Spectroscopy

Robin R. Groleau,<sup>ID</sup> Robert S. L. Chapman, Harry Ley-Smith, Liyuan Liu, Tony D. James,<sup>\*ID</sup> and Steven D. Bull<sup>\*ID</sup>

Department of Chemistry, University of Bath, Claverton Down, Bath, BA2 7AY, U.K.

## Supporting Information

**ABSTRACT:** A practically simple three-component chiral derivatization protocol has been developed to determine the enantiopurity of eight *S*-chiral sulfinamides by  $^1\text{H}$  and  $^{19}\text{F}$  NMR spectroscopic analysis, based on their treatment with a 2-formylphenylboronic acid template and enantiopure pinanediol to afford a mixture of diastereomeric sulfiniminoboronate esters whose diastereomeric ratio is an accurate reflection of the enantiopurity of the parent sulfinamide.



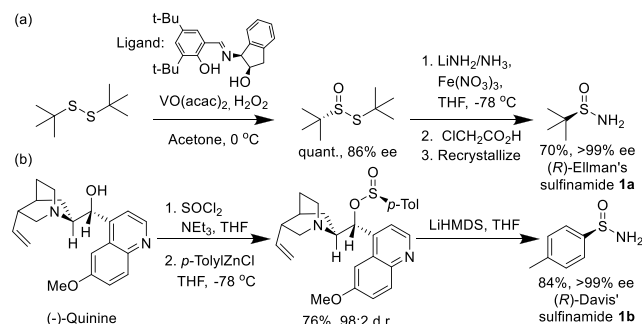
Enantiopure *N*-sulfinyl imines (sulfinimines) are widely used for asymmetric synthesis,<sup>1</sup> with Ellman's and Davis' sulfinamides (**1a** and **1b**) widely used to prepare these chiral sulfinimine intermediates for the stereoselective functionalization of ketones and aldehydes.<sup>2</sup> These chiral auxiliaries have been employed for the asymmetric synthesis of chiral amines, alcohols, diamines, amino-alcohols,  $\alpha$ -organometallic amines, and  $\alpha$ - and  $\beta$ -amino acid derivatives in high enantiomeric excess (*ee*).<sup>3</sup> They have also found applications as chiral organocatalysts, as additives/ligands in enantioselective catalytic systems,<sup>4</sup> and as peptidic/transition state isosteres for medicinal chemistry applications.<sup>5</sup> Sulfinamides are also produced naturally by the action of nitroxyl (HNO) on peptidic cysteine residues in cells.<sup>6</sup>

Several approaches have been developed to synthesize enantiopure sulfinamides (Scheme 1). Treatment of symmetric disulfides with chiral catalysts and stoichiometric oxidants (e.g.,  $\text{H}_2\text{O}_2$ ) is used to afford chiral thiosulfinate intermediates, which are then reacted with nucleophilic ammonia sources (with clean  $\text{S}_\text{N}2$  inversion), affording chiral sulfinamides in high *ee* (Scheme 1a).<sup>7</sup> Chiral auxiliaries are also used to

prepare sulfinate esters with high levels of diastereocontrol, which can then be reacted with amines to afford enantiopure sulfinamides (Scheme 1b).<sup>2a</sup> Classical resolution processes have also been used to separate the enantiomers of (*rac*)-thiosulfinate precursors,<sup>8</sup> and subtilisin has been used for enzymatic kinetic resolution of (*rac*)-*N*-acyl-arylsulfinamides,<sup>9</sup> while direct separation of their enantiomers can be achieved by preparative chiral HPLC.<sup>10</sup> To date, two chiral solvation methods for determining the *ee*'s of sulfinamides have been reported in the literature, using either Pirkle's alcohol<sup>11a</sup> or bifunctional macrocycles.<sup>11b</sup> Unfortunately, these methods lack simplicity and substrate scope, and so the *ee*'s of *S*-chiral sulfinamides are normally determined through chiral HPLC analysis.<sup>7b</sup> This approach, however, requires access to expensive HPLC equipment/chiral columns and often requires significant development time to identify a suitable system to resolve the enantiomers of a target sulfinamide.

Therefore, a practically simple, rapid, and inexpensive chiral derivatization protocol that would enable the rapid determination of the *ee*'s of a wide range of chiral sulfinamides by NMR spectroscopic analysis would be of use to the wider synthetic community. We have previously reported the development of three-component chiral derivatization protocols for determining the *ee*'s of chiral primary amines, diamines, amino alcohols, hydroxylamines, and diols by  $^1\text{H}$  NMR spectroscopic analysis. These protocols involve treatment of a scalemic chiral analyte with 2-formylbenzeneboronic acid **2** (2-FPBA) and an enantiopure chiral selector (amine or diol) to afford pairs of diastereomeric iminoboronate esters. The diastereomeric ratio (*dr*) of these iminoboronate esters can then be measured by comparing the relative intensities of the integrals of their well-resolved imine proton singlets in their  $^1\text{H}$  NMR spectra (see Scheme 2 for how this method is

**Scheme 1. Stereoselective Syntheses of Ellman's Sulfinamide 1a and Davis' Sulfinamide 1b**

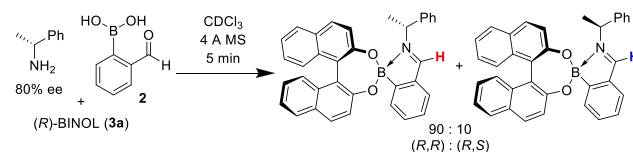


Received: September 11, 2019

Published: November 27, 2019



### Scheme 2. Three-Component Chiral Derivatization Protocol for Determining the Enantiopurity of $\alpha$ -Methylbenzylamine<sup>12a</sup>



used to determine the *ee* of  $\alpha$ -methylbenzylamine).<sup>12</sup> Given its proven utility, we decided to investigate whether this type of three-component <sup>1</sup>H NMR chiral derivatization protocol, often referred to as the Bull–James assembly,<sup>13</sup> could be applied to determine the *ee* of scalemic samples of *S*-chiral sulfinamides.

Treatment of a mixture of scalemic Ellman's sulfinamide (*S*)-**1a** (50% *ee*) with 2-FPBA **2** and (*R*)-BINOL **3a** in CDCl<sub>3</sub> for 1 h led to incomplete formation of a mixture of diastereomeric sulfiniminoboronate ester complexes **4a** and **5a** (85% conversion from 2-FPBA **2**), whose imine proton resonances were only partially resolved in their <sup>1</sup>H NMR spectrum (Table 1, entry 1). The poor yield of this reaction is presumably due to the decreased nucleophilicity of the sulfinamide nitrogen lone pair. This is consistent with previous reports that drying agents, Lewis acid catalysts, and forcing conditions are often required for this type of imine condensation reaction to proceed to completion.<sup>14</sup> Nevertheless, the approximate 3:1 ratio of the partially resolved imine proton signals of the diastereomeric sulfiniminoboronate ester complexes **4a/5a** in the <sup>1</sup>H NMR spectrum was consistent with the 50% *ee* of the parent sulfinamide **1a**, indicating that no kinetic resolution had occurred.

This prompted us to react Ellman's sulfinamide **1a** (50% *ee*) with 2-FPBA **2** and a range of commercially available chiral diols **3b–h** to identify pairs of diastereomeric sulfiniminoboronate esters **4/5** whose imine protons would be baseline-resolved in their <sup>1</sup>H NMR spectra. This screening study revealed that (*S*)-2-phenylethanediol **3f**, (*R*)-1-phenylpropane-1,3-diol **3g**, and (1*R*,2*R*,3*S*,5*R*)-pinanediol **3h** gave pairs of diastereomeric sulfiniminoboronate esters whose imine proton resonances were fully resolved (Table 1, entries 6–8). Derivatization with chiral pinanediol **3h** gave diastereomeric sulfiniminoboronate esters **4h/5h** that exhibited sharp imine peaks with the greatest chemical shift difference ( $\Delta\delta_{\text{H}} = -0.085$  ppm), and it was therefore chosen as the chiral diol for all subsequent sulfinamide derivatization reactions.

A series of experiments were then carried out to try and identify conditions that would result in the three-component reaction of scalemic Ellman's sulfinamide **1a** (33% *ee*), 2-FPBA **2**, and pinanediol **3h** being driven to completion. Reaction of these three components in CDCl<sub>3</sub> for 1 h gave a 70:30 mixture of the two-component formyl boronate ester **6** and the three-component sulfiniminoboronate esters **4h/5h** (Table 2, entry 1). Addition of MgSO<sub>4</sub> as a drying agent only marginally increased the amount of **4h/5h** formed to 40% (Table 2, entry 2). Two-component reaction of 2-FPBA **2** with pinanediol **3h** was found to give boronate ester **6** in 100% conversion after 10 min (Table 2, entry 3). However, no reaction was observed when sulfinamide **1a** was added to a solution of preformed boronate ester **6** in CDCl<sub>3</sub>, indicating that boronate ester **6** is unreactive toward imine bond formation under these conditions (Table 2, entry 4). Two-component reaction of Ellman's sulfinamide **1a** and 2-FPBA **2** proceeded more slowly,

Table 1. Chemical Shift Differences ( $\Delta\delta_{\text{H}}$ ) in the 500 MHz <sup>1</sup>H NMR Spectra of Diastereomeric Iminoboronate Complexes of Ellman's Sulfinamide **1a** (50% *ee*), 2-FPBA **2**, and a Range of Enantiopure Diols **3a–h**

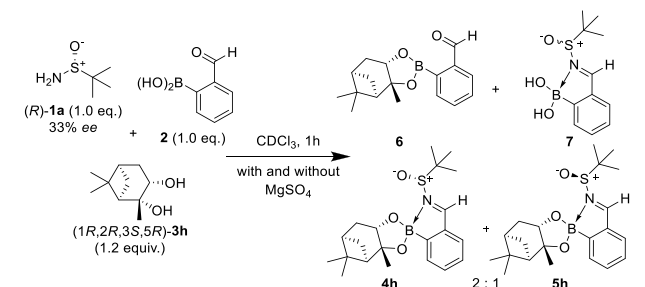
Entry	Diol	$\Delta\delta_{\text{H}}$ (ppm) <sup>a,b</sup>
1	( <i>R</i> )- <b>3a</b>	+0.011
2	( <i>S</i> )- <b>3b</b>	+0.006
3	( <i>R,R</i> )- <b>3c</b>	+0.027
4	( <i>S</i> )- <b>3d</b>	+0.010
5	( <i>S</i> )- <b>3e</b>	+0.014
6 <sup>c</sup>	( <i>S</i> )- <b>3f</b>	+0.037
7 <sup>c</sup>	( <i>R</i> )- <b>3g</b>	+0.047
8 <sup>c</sup>	(1 <i>R</i> ,2 <i>R</i> ,3 <i>S</i> ,5 <i>R</i> )- <b>3h</b>	-0.085

<sup>a</sup> $\Delta\delta_{\text{H}}$  is the chemical shift difference between the imine protons of diastereomeric iminoboronate ester complexes **4/5**. <sup>b</sup>A negative value indicates that the homochiral complex was most deshielded. <sup>c</sup>Full baseline resolution observed for the imine resonances of **4/5**.

affording sulfiniminoboronic acid **7** in 89% yield after 1 h, increasing to 94% in the presence of MgSO<sub>4</sub> (Table 2, entries 5 and 6). Finally, premixing sulfinamide **1a**, 2-FPBA **2**, and MgSO<sub>4</sub> in CDCl<sub>3</sub> for 1 h, followed by addition of pinanediol **3h**, gave a 93% conversion to afford the desired three-component sulfiniminoboronate esters **4h/5h** and the two-component boronate ester **6** in 7% yield (Table 2, entry 7). Therefore, these results suggest that irreversible formation of boronate ester **6** is faster than reversible formation of imine **7**, with only imine **7** competent to react further to afford the desired sulfiniminoboronate esters **4h/5h** in the three-component derivatization reaction.<sup>15</sup>

These results prompted us to develop a new "stepwise" three-component derivatization procedure, involving reaction of (*rac*)-Ellman's sulfinamide **1a**, 1.2 equiv of 2-FPBA **2**, and MgSO<sub>4</sub> in CDCl<sub>3</sub> at rt for 1 h to maximize the amount of reactive imine **7** formed. This was followed by addition of 1.3 equiv of (1*R*,2*R*,3*S*,5*R*)-pinanediol **3h** which gave a 50:50 mixture of diastereomeric sulfiniminoboronate esters **4h/5h** in 99% conversion (Table 3, entry 1). This one-pot stepwise protocol was then applied to the derivatization of seven additional racemic aryl, heteroaryl, cyclic and acyclic

**Table 2. Optimization Study of the Three-Component Assembly Reaction of Ellman's Sulfonamide **1a** with 2-FPBA **2** and Pinanediol **3h****



Entry	Reagents	$\text{MgSO}_4$	Product Ratios <sup>a</sup>		
			6	7	4h/5h
1	<b>1a</b> + <b>2</b> + <b>3h</b>	—	70%	0%	30%
2	<b>1a</b> + <b>2</b> + <b>3h</b>	+	60%	0%	40%
3	<b>2</b> + <b>3h</b>	—	100%	—	—
4 <sup>b</sup>	Premix <b>2</b> + <b>3h</b> then add <b>1a</b>	—	100%	0%	0%
5 <sup>c</sup>	<b>1a</b> + <b>2</b>	—	—	89%	—
6 <sup>c</sup>	<b>1a</b> + <b>2</b>	+	—	94%	—
7 <sup>d</sup>	Premix <b>1a</b> + <b>2</b> then add <b>3h</b>	+	7%	0%	93%

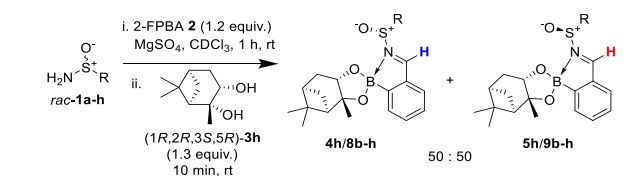
<sup>a</sup>Determined by  $^1\text{H}$  NMR spectroscopic analysis. <sup>b</sup>**2** and **3h** premixed for 10 min. <sup>c</sup>Remaining mass balance comprised of unreacted 2-FPBA **2**. <sup>d</sup>**1a** and **2** premixed for 1 h.

sulfonamides **1b–h**,<sup>16</sup> affording mixtures of their corresponding diastereomeric sulfiniminoboronate esters **8b–h/9b–h** in 55–99% conversions (Table 3, entries 2–8). Analysis of the  $^1\text{H}$  NMR spectra of these mixtures revealed that the imine signals of all pairs of diastereomeric sulfiniminoboronate esters were all baseline-resolved, with their 49:51 to 51:49 *dr* values indicating that no kinetic resolution had occurred in each derivatization reaction.

We,<sup>17</sup> and others,<sup>18</sup> have previously reported the use of fluoro-2-FPBA as an alternative template for the Bull–James three-component protocol, which enables the *dr*'s of their derived iminoboronate esters to be accurately determined using both  $^1\text{H}$  and  $^{19}\text{F}$  NMR spectroscopic analysis. Consequently, we decided to repeat our stepwise three-component reaction using Ellman's sulfonamide **1a** and pinanediol **3h** with 3-fluoro-2-FPBA **10a**, 4-fluoro-2-FPBA **10b**, 3-fluoro-2-FPBA **10c**, and 3-fluoro-2-FPBA **10d** (Table 4).<sup>19</sup> These derivatization reactions gave mixtures of diastereomeric sulfiniminoboronate esters whose imine proton resonances were all well-resolved in their  $^1\text{H}$  NMR spectra, as were the fluorine resonances in their  $^{19}\text{F}$  NMR spectra. 3-Fluoro-2-FPBA **10a** gave the best difference for the fluorine resonances ( $\Delta\delta_{\text{F}} = -2.328$  ppm), and so it was chosen as the template to derivatize three further (*rac*)-sulfonamides **1b–d**, all of which gave a pair of diastereomeric sulfiniminoboronate esters whose  $^1\text{H}$  NMR (imine protons) and  $^{19}\text{F}$  NMR resonances were well resolved.

The detection limits of this new derivatization method using 3-fluoro-2-FPBA **10a** and pinanediol **3h** were then determined using scalemic samples of Ellman's sulfonamide **1a** of 75%, 90%, and 96% *ee* respectively, prepared from enantiopure samples of the sulfonamide (Figures 1a and 1b). Analysis of the resultant mixtures of sulfiniminoboronate esters revealed diastereomeric excesses (*de*) of 75%, 91%, and 95% ( $^1\text{H}$  NMR) and 73%, 89%, and 95% ( $^{19}\text{F}$  NMR), respectively, all of

**Table 3. Chemical Shift Differences ( $\Delta\delta_{\text{H}}$ ) of the Imine Proton Resonances of Pairs of Diastereomeric Sulfiniminoboronate Esters in the  $^1\text{H}$  NMR Spectra from Reaction of Sulfonamides **1a–h** with 2-FPBA **2** and diol **3h****



Entry	( <i>rac</i> )-Sulfonamide	Conv. (%) <sup>a</sup>	<i>dr</i> <sup>a</sup>	$\Delta\delta_{\text{H}}$ (ppm) <sup>b</sup>
1	<b>1a</b>	99	50:50	0.085
2	<b>1b</b>	62	49:51	0.069
3	<b>1c</b>	98	50:50	0.061
4	<b>1d</b>	97	51:49	0.077
5	<b>1e</b>	63	50:50	0.057
6	<b>1f</b>	69	50:50	0.070
7	<b>1g</b>	80	50:50	0.062
8	<b>1h</b>	55	50:50	0.061

<sup>a</sup>Conversion and *dr* determined by  $^1\text{H}$  NMR spectroscopic analysis. <sup>b</sup> $\Delta\delta_{\text{H}}$  is the chemical shift difference between the imine protons of diastereomeric iminoboronate ester complexes **4h/5h** and **8/9**.

which were within the accepted 5% error limit when using chiral derivatizing agents to determine *ee* values by NMR spectroscopy. Having established its applicability, our new stepwise three-component chiral derivatization protocol was then used to assess the enantiomeric excess of commercial samples of enantiopure (*R*)- and (*S*)-Davis' sulfonamide **1b** (purchased from Sigma-Aldrich, Figure 1c for (*R*)-**1b**). Both  $^1\text{H}$  and  $^{19}\text{F}$  NMR analysis revealed that these "enantiopure" reagents were scalemic, with both NMR analyses returning *ee* values of 90% and 94% for (*R*)- and (*S*)-**1b**, respectively, as confirmed subsequently by chiral HPLC analysis (see Supporting Information).

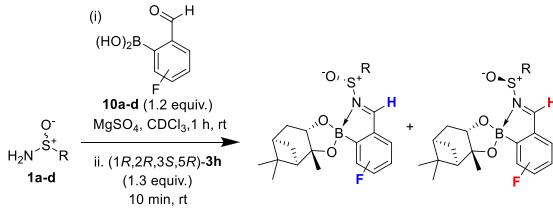
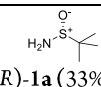
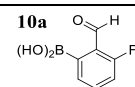
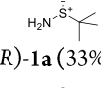
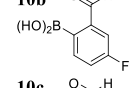
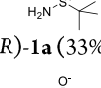
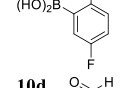
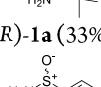
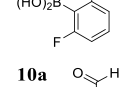
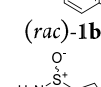
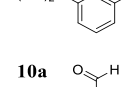
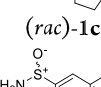
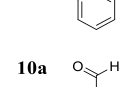
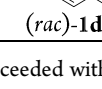
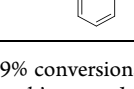
In conclusion, this report describes the first chiral derivatization protocol for determining the enantiopurity of a range of *S*-chiral sulfonamides using both  $^1\text{H}$  and  $^{19}\text{F}$  NMR spectroscopic analysis, including Ellman's and Davis' chiral sulfonamides that are widely used as chiral auxiliaries for asymmetric synthesis.

## EXPERIMENTAL SECTION

Unless preparative details are given, reagents and solvents were obtained from commercial suppliers. All reactions were performed without air exclusion, at room temperature and with magnetic stirring unless otherwise stated. Anhydrous  $\text{MgSO}_4$  was used as a drying agent for organic solutions. Thin layer chromatography (TLC) was carried out on Macherey-Nagel aluminum-backed plates that were precoated



**Table 4. Chemical Shift Differences ( $\Delta\delta_{\text{H/F}}$ ) in the  $^1\text{H}/^{19}\text{F}$  NMR Spectra of Diastereomeric Sulfiniminoboronate Esters Formed from Reaction of Sulfinamides **1a–d** with Fluorinated FPBA Derivatives **10a–d** and Pinanediol **3h****

(i) 			
Entry <sup>a</sup>	( <i>rac</i> )-Sulfinamide	2-FPBA	$\Delta\delta_{\text{H}}^b / \Delta\delta_{\text{F}}^{\text{cd}}$ (ppm) <sup>e</sup>
1	 ( <i>R</i> )- <b>1a</b> (33% <i>ee</i> )		$\Delta\delta_{\text{H}} = -0.064$ $\Delta\delta_{\text{F}} = -2.328$
2	 ( <i>R</i> )- <b>1a</b> (33% <i>ee</i> )		$\Delta\delta_{\text{H}} = -0.029$ $\Delta\delta_{\text{F}} = -0.170$
3	 ( <i>R</i> )- <b>1a</b> (33% <i>ee</i> )		$\Delta\delta_{\text{H}} = -0.079$ $\Delta\delta_{\text{F}} = +0.197$
4	 ( <i>R</i> )- <b>1a</b> (33% <i>ee</i> )		$\Delta\delta_{\text{H}} = -0.201$ $\Delta\delta_{\text{F}} = -0.578$
5	 ( <i>rac</i> )- <b>1b</b>		$\Delta\delta_{\text{H}} = -0.063$ $\Delta\delta_{\text{F}} = -1.188$
6	 ( <i>rac</i> )- <b>1c</b>		$\Delta\delta_{\text{H}} = 0.042$ $\Delta\delta_{\text{F}} = 1.457$
7	 ( <i>rac</i> )- <b>1d</b>		$\Delta\delta_{\text{H}} = 0.070$ $\Delta\delta_{\text{F}} = 1.365$

<sup>a</sup>Reactions proceeded with 37–99% conversions to afford mixtures of sulfiniminoboronate esters whose *dr*'s ranged from 65:35 to 69:31 (entries 1–4) and from 49:51 to 51:49 (entries 5–7), indicating that no kinetic resolution had occurred. <sup>b</sup> $\Delta\delta_{\text{H}}$  is the chemical shift difference between the imine protons of the diastereomeric sulfiniminoboronate esters in their  $^1\text{H}$  NMR spectra. <sup>c</sup> $\Delta\delta_{\text{F}}$  is the chemical shift difference between the fluorine resonances of the diastereomeric sulfiniminoboronate esters. <sup>d</sup>Quantitative  $^{19}\text{F}\{^1\text{H}\}$  NMR experiments carried out using a *T*<sub>1</sub> relaxation time of 30 s. <sup>e</sup>A negative value indicates that the homochiral complex was most deshielded.

with silica. Compounds were visualized by either quenching of UV fluorescence at 254 nm or by staining with potassium permanganate dip followed by gentle heating. Purification by flash column chromatography was performed using high-purity grade silica gel (60 Å pore size, 40–75  $\mu\text{m}$  particle size). Capillary melting points are reported uncorrected to the nearest  $^{\circ}\text{C}$ , and were determined using a Stuart digital SMP10 melting point apparatus. Optical rotations were measured using an Optical Activity Ltd. AA-10 Series Automatic Polarimeter, with a path length of 1 dm, and with concentration (*c*) quoted in g/100 mL. Nuclear Magnetic Resonance (NMR) spectroscopy experiments were performed in deuterated solvent at 298 K (unless stated otherwise) on a Bruker Avance, 300, 400, or 500 MHz spectrometer or an Agilent ProPulse 500 MHz spectrometer, with proton decoupling used for all  $^{13}\text{C}$  NMR spectra.  $^1\text{H}$ ,  $^{13}\text{C}$ ,  $^{11}\text{B}$ ,

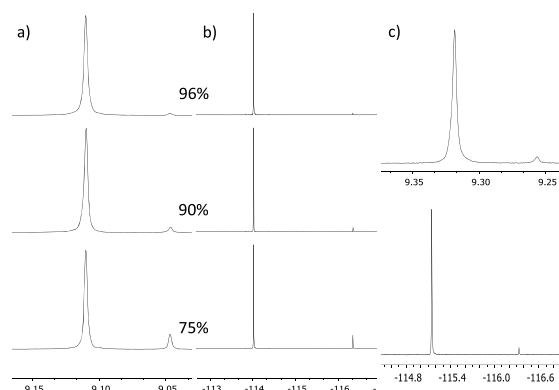


**Figure 1.** (a) Expanded  $^1\text{H}$  NMR spectra of complexes formed from reaction of **10a**, (*1R,2R,3S,5R*)-**3h**, and (*R*)-**1a** (75%, 90%, and 96% *ee*). (b) Expanded  $^{19}\text{F}$  NMR spectra of diastereomeric complexes formed from reaction of **10a**, (*1R,2R,3S,5R*)-**3h**, and (*R*)-**1a** (75%, 90%, and 96% *ee*). (c) Expanded  $^1\text{H}$  and  $^{19}\text{F}\{^1\text{H}\}$  NMR spectra of diastereomeric complexes formed from reaction of **10a**, (*1R,2R,3S,5R*)-**3h**, and a commercial “enantiopure” sample of (*R*)-Davis’ sulfonamide **1b**, revealing its “true” enantiopurity as 90% *ee*.

and  $^{19}\text{F}$  NMR chemical shifts ( $\delta$ ) are quoted in parts per million (ppm) and are referenced to either the residual solvent peak or tetramethylsilane (TMS) when possible. Coupling constants (*J*) are quoted in Hz. Where  $^{13}\text{C}$  signals could not be observed by 1D NMR due to low solubility, adjacent quadrupolar nuclei, or lack of adjacent  $^1\text{H}$  nuclei, their chemical shift was deduced from 2D HMBC experiments, where possible. This approach was validated by variable temperature (VT) 1D NMR of boronate ester **6**. Infrared (IR) spectra were recorded using a PerkinElmer Spectrum 100 FTIR spectrometer fitted with a Universal ATR FTIR accessory, with samples run neat and the most relevant, characteristic absorbances quoted as  $\nu$  in  $\text{cm}^{-1}$ . High resolution mass spectrometry (HRMS) results were acquired on an externally calibrated Bruker Daltonics maXis HD UHR-TOF mass spectrometer coupled to an electrospray source (ESI-TOF). Molecular ions were detected either in positive mode, as their protonated, sodiated, or ammonium adduct forms, or in negative mode as deprotonated species. Aryl boronic acids were detected as their deprotonated methyl hydrogen boronate ions  $[\text{M} + 13]^-$ , as reported by Wang et al.<sup>20</sup> Bruker Daltonics software DataAnalysis 4.3 was used to process NMR data.

**General Procedure 1 for the Synthesis of (*rac*)-Sulfinamides **1c–h** from Thiols by the Method of Di et al.<sup>16</sup>** *N*-Bromo succinimide (2.0 equiv) was added to a stirred solution of the thiol (1.0 equiv) in  $\text{CH}_2\text{Cl}_2/\text{MeOH}$  (1:1, 0.1 M) at  $0^{\circ}\text{C}$ . The reaction was allowed to warm to room temperature, and reaction progress was monitored by TLC. Upon completion (15 min–1 h) the reaction mixture was quenched and diluted by half through the addition of saturated  $\text{Na}_2\text{CO}_3$ . The layers were separated, and the aqueous phase was extracted twice with  $\text{CH}_2\text{Cl}_2$ . The combined organics were then washed with brine, dried ( $\text{MgSO}_4$ ), and concentrated to dryness *in vacuo* to afford a methylsulfonate product as a clear oil.

The methylsulfonate (1.0 equiv) was dissolved in anhydrous THF (0.33 M) and cooled to  $-78^{\circ}\text{C}$ . LiHMDS (1.5 equiv, 1 M in THF) was then added dropwise over 5 min, and the reaction was stirred at  $-78^{\circ}\text{C}$  for 1.5 h. After this time the reaction was quenched with saturated  $\text{NH}_4\text{Cl}$ , allowed to warm to room temperature, and stirred. After 30 min, the reaction was diluted with EtOAc, the aqueous phase was extracted twice with EtOAc, and the combined organics were washed with brine, dried ( $\text{MgSO}_4$ ), and concentrated *in vacuo*. The crude product was purified by either recrystallization or column chromatography to afford the desired sulfinamide **1c–h**.

**(*rac*)-Cyclopentanesulfinamide **1c**.** General procedure 1 was followed using cyclopentanethiol (334  $\mu\text{L}$ , 3.12 mmol). Recrystallization from 1:10 EtOAc/*n*-hexane afforded the title compound **1c** (299 mg, 2.24 mmol) as a white solid in 72% yield. All characterization data

were consistent with previous literature reports.<sup>16</sup> Mp: 86–88 °C (lit.<sup>16</sup> 82–83 °C); IR (neat): 3189, 3089, 2957, 2868, 1450, 1166, 1001, 908, 697 cm<sup>-1</sup>; <sup>1</sup>H NMR (500 MHz, CDCl<sub>3</sub>)  $\delta_H$  3.91 (bs, 2H, –NH<sub>2</sub>), 3.05 (p, 1H, *J* = 7.5, SCH), 2.04 (dt, 2H, *J* = 13.9, 6.9, CH<sub>2</sub>), 1.98–1.88 (m, 2H, CH<sub>2</sub>), 1.83–1.59 (m, 4H, CH<sub>2</sub>); <sup>13</sup>C{<sup>1</sup>H} NMR (126 MHz, CDCl<sub>3</sub>)  $\delta_C$  65.2, 27.7, 26.1, 25.9, 25.6.

**(rac)-Naphthalene-2-sulfonamide 1d.** General procedure 1 was followed using naphthalene-2-thiol (500 mg, 3.12 mmol). Recrystallization from 2:1 EtOAc/*n*-hexane afforded the title compound **1d** (408 mg, 2.13 mmol) as a white solid in 63% yield. Mp: 134–138 °C (decomposed); IR (neat): 3292, 3155, 3063, 1589, 1560, 1500, 1344, 1014, 822, 739 cm<sup>-1</sup>; <sup>1</sup>H NMR (500 MHz, CDCl<sub>3</sub>)  $\delta_H$  8.34 (s, 1H, ArH), 7.99–7.89 (m, 3H, ArH), 7.71 (dd, 1H, ArH), 7.65–7.55 (m, 2H, ArH), 4.34 (bs, 2H, –NH<sub>2</sub>); <sup>13</sup>C{<sup>1</sup>H} NMR (126 MHz, CDCl<sub>3</sub>)  $\delta_C$  143.6, 134.6, 132.8, 129.2, 129.0, 128.1, 128.1, 127.3, 125.8, 121.9; HRMS (ESI<sup>+</sup>): calculated for [M + Na]<sup>+</sup> C<sub>10</sub>H<sub>9</sub>NOSNa, 214.0297; found, 214.0288.

**(rac)-4-Fluorobenzenesulfonamide 1e.** General procedure 1 was followed using 4-fluorothiophenol (332  $\mu$ L, 3.12 mmol). Recrystallization from 1:1 EtOAc/*n*-hexane afforded the title compound **1e** (268 mg, 1.68 mmol) as a white solid in 54% yield. All characterization data were consistent with previous literature reports.<sup>21,22</sup> Mp: 134–139 °C (lit.<sup>21</sup> 144.8–146.8<sup>22</sup> °C); IR (neat): 3269, 3154, 3065, 1587, 1481, 1229, 1211, 1156, 1087, 1005, 887, 834, 667 cm<sup>-1</sup>; <sup>1</sup>H NMR (500 MHz, CDCl<sub>3</sub>)  $\delta_H$  7.79–7.71 (m, 2H, ArH), 7.24–7.15 (m, 2H, ArH), 4.32 (bs, 2H, NH<sub>2</sub>); <sup>13</sup>C{<sup>1</sup>H} NMR (126 MHz, CDCl<sub>3</sub>)  $\delta_C$  164.6 (d, *J*<sub>F-C</sub> = 251.7), 142.2, 128.0 (d, *J*<sub>F-C</sub> = 9.0), 116.2 (d, *J*<sub>F-C</sub> = 22.4); <sup>19</sup>F NMR (471 MHz, CDCl<sub>3</sub>)  $\delta_F$  –109.0 (tt, *J* = 8.4, 5.1).

**(rac)-4-Methoxybenzenesulfonamide 1f.** General procedure 1 was followed using 4-fluorothiophenol (383  $\mu$ L, 3.12 mmol). Recrystallization from 1:2 EtOAc/*n*-hexane afforded the title compound **1f** (262 mg, 1.53 mmol) as a white solid in 49% yield. All characterization data were consistent with previous literature reports.<sup>9</sup> Mp: 127–131 °C (lit.<sup>9</sup> 129–131 °C); IR (neat): 3261, 3067, 2840, 1591, 1490, 1450, 1245, 1025, 1001, 823, 794 cm<sup>-1</sup>; <sup>1</sup>H NMR (500 MHz, CDCl<sub>3</sub>)  $\delta_H$  7.68 (d, 2H, *J* = 8.8, ArH), 7.02 (d, 2H, *J* = 8.8, ArH), 4.24 (bs, 2H, NH<sub>2</sub>), 3.87 (s, 3H, OCH<sub>3</sub>); <sup>13</sup>C{<sup>1</sup>H} NMR (126 MHz, CDCl<sub>3</sub>)  $\delta_C$  162.1, 138.0, 127.2, 114.4, 55.7.

**(rac)-Hexane-1-sulfonamide 1g.** General procedure 1 was followed using 1-hexanethiol (1.421 mL, 10.0 mmol). Recrystallization from *n*-hexane afforded the title compound **1g** (356 mg, 2.38 mmol) as an off-white solid in 24% yield. Mp: 41–42 °C; IR (neat): 3282, 3200, 2954, 2924, 2849, 1553, 1464, 1417, 1066, 1035, 1001, 890 cm<sup>-1</sup>; <sup>1</sup>H NMR (500 MHz, CDCl<sub>3</sub>)  $\delta_H$  3.99 (bs, 2H, NH<sub>2</sub>), 2.73 (2  $\times$  ddd, 2H, *J* = 13.0, 8.5, 6.7, SCH<sub>2</sub>), 1.79–1.63 (m, 2H, SCH<sub>2</sub>CH<sub>2</sub>), 1.50–1.37 (m, 2H, SCH<sub>2</sub>CH<sub>2</sub>CH<sub>2</sub>), 1.36–1.29 (m, 4H, MeCH<sub>2</sub>CH<sub>2</sub>), 0.91–0.87 (m, 3H, CH<sub>3</sub>); <sup>13</sup>C{<sup>1</sup>H} NMR (126 MHz, CDCl<sub>3</sub>)  $\delta_C$  57.9, 31.5, 28.4, 22.9, 22.5, 14.1; HRMS (ESI<sup>+</sup>): calculated for [M + NH<sub>4</sub>]<sup>+</sup> C<sub>6</sub>H<sub>19</sub>N<sub>2</sub>OS, 167.1213; found, 167.1215.

**(rac)-Pyridine-2-sulfonamide 1h.** General procedure 1 was followed using 2-mercapto pyridine (1.998 g, 18.0 mmol). Recrystallization from CH<sub>2</sub>Cl<sub>2</sub> afforded the title compound **1h** (128 mg, 0.972 mmol) as a white solid in 5% yield. All characterization data were consistent with previous literature reports.<sup>23</sup> Mp: 102–104 °C (lit.<sup>23</sup> 98–100 °C); <sup>1</sup>H NMR (500 MHz, CDCl<sub>3</sub>)  $\delta_H$  8.71 (ddd, 1H, *J* = 4.7, 4.7, 1.5, ArH), 7.99–7.89 (m, 2H, ArH), 7.44 (ddd, 1H, *J* = 7.4, 4.7, 1.4, ArH), 4.66 (bs, 2H, NH<sub>2</sub>); <sup>13</sup>C{<sup>1</sup>H} NMR (126 MHz, CDCl<sub>3</sub>)  $\delta_C$  164.5, 150.0, 138.1, 125.6, 120.6.

**General Procedure 2 for the Synthesis of 1-Bromo-2-(dimethoxymethyl)-fluorobenzenes 11a–d by the Method of Kowalska et al.**<sup>19</sup> H<sub>2</sub>SO<sub>4</sub> (0.093 equiv, 0.47 mmol, 25  $\mu$ L) and trimethyl orthoformate (1.3 equiv, 6.50 mmol, 711  $\mu$ L) were added to a stirred solution of a 2-bromo-fluorobenzaldehyde (1.0 equiv, 5.00 mmol, 1.02 g) in MeOH (2.0 mL). The reaction was heated at reflux for 1.5 h, before cooling to room temperature and quenching with triethylamine (1.00 mL, 7.17 mmol). The volatiles were removed *in vacuo*, and the resulting mixture was dissolved in water (30 mL) and extracted with Et<sub>2</sub>O (30 mL). The organics were washed with water

(3  $\times$  30 mL) and brine (30 mL), dried (MgSO<sub>4</sub>), and concentrated *in vacuo* to afford the desired dimethyl acetals **11a–d** as clear oils.

**2-Bromo-1-(dimethoxymethyl)-6-fluorobenzene 11a.** General procedure 2 was followed using 2-bromo-6-fluorobenzaldehyde (5.00 mmol, 1.02 g), affording the title compound **11a** (1.09 g, 4.41 mmol) as a colorless oil in 88% yield. IR (neat): 2930, 2830, 1602, 1572, 1455, 1376, 1249, 1201, 1102, 1062, 168, 893, 781, 730 cm<sup>-1</sup>; <sup>1</sup>H NMR (500 MHz, CDCl<sub>3</sub>)  $\delta_H$  7.73 (dt, 1H, *J* = 8.0, 1.1, ArH), 7.17 (td, 1H, *J* = 8.2, 5.6, ArH), 7.05 (dd, 1H, *J* = 10.4, 8.3, 1.2, ArH), 5.71 (d, 1H, *J* = 1.2, MeOCH), 3.49 (s, 6H, 2  $\times$  OCH<sub>3</sub>); <sup>13</sup>C{<sup>1</sup>H} NMR (126 MHz, CDCl<sub>3</sub>)  $\delta_C$  161.5 (d, *J*<sub>F-C</sub> = 256.3), 131.0 (d, *J*<sub>F-C</sub> = 9.9), 129.2 (d, *J*<sub>F-C</sub> = 3.4), 125.4 (d, *J*<sub>F-C</sub> = 14.4), 123.5 (d, *J*<sub>F-C</sub> = 5.3), 116.2 (d, *J*<sub>F-C</sub> = 23.0), 104.9, 55.7; <sup>19</sup>F NMR (470 MHz, CDCl<sub>3</sub>)  $\delta_F$  –111.1 (dd, *J* = 10.6, 5.6); HRMS (ESI<sup>+</sup>): calculated for [M + Na]<sup>+</sup> C<sub>9</sub>H<sub>10</sub>O<sub>2</sub>BrFNa, 270.9740; found, 270.9749.

**2-Bromo-1-(dimethoxymethyl)-5-fluorobenzene 11b.** General procedure 2 was followed using 2-bromo-5-fluorobenzaldehyde (5.00 mmol, 1.02 g), affording the title compound **11b** (1.16 g, 4.65 mmol) as a colorless oil in 95% yield. IR (neat): 2935, 2832, 1581, 1464, 1365, 1264, 1154, 1095, 1055, 972, 880 cm<sup>-1</sup>; <sup>1</sup>H NMR (300 MHz, CDCl<sub>3</sub>)  $\delta_H$  7.51 (dd, 1H, *J* = 8.8, 5.1, ArH), 7.35 (dd, 1H, *J* = 9.4, 3.1, ArH), 6.93 (ddd, *J* = 8.8, 7.7, 3.1, ArH), 5.50 (d, 1H, *J* = 1.2, MeCOCH), 3.38 (s, 6H, 2  $\times$  OCH<sub>3</sub>); <sup>13</sup>C{<sup>1</sup>H} NMR (126 MHz, CDCl<sub>3</sub>)  $\delta_C$  162.1 (d, *J*<sub>F-C</sub> = 247.2), 139.3 (d, *J*<sub>F-C</sub> = 7.0), 134.2 (d, *J*<sub>F-C</sub> = 7.7), 117.4 (d, *J*<sub>F-C</sub> = 22.7), 116.9 (d, *J*<sub>F-C</sub> = 3.2), 115.9 (d, *J*<sub>F-C</sub> = 24.3), 102.4, 54.0; <sup>19</sup>F NMR (470 MHz, CDCl<sub>3</sub>)  $\delta_F$  –114.3; HRMS (ESI<sup>+</sup>): calculated for [M + Na]<sup>+</sup> C<sub>9</sub>H<sub>10</sub>O<sub>2</sub>BrFNa, 270.9740; found, 270.9748.

**2-Bromo-1-(dimethoxymethyl)-4-fluorobenzene 11c.** General procedure 2 was followed using 2-bromo-4-fluorobenzaldehyde (5.00 mmol, 1.02 g), affording the title compound **11c** (1.16 g, 4.65 mmol) as a colorless oil in 93% yield. IR (neat): 2937, 2826, 1599, 1485, 1361, 1226, 1193, 1103, 1054, 982, 857, 812 cm<sup>-1</sup>; <sup>1</sup>H NMR (500 MHz, CDCl<sub>3</sub>)  $\delta_H$  7.60 (dd, 1H, *J* = 8.7, 6.2, ArH), 7.31 (dd, 1H, *J* = 8.2, 2.6, ArH), 7.05 (td, 8.3, 2.6, ArH), 5.52 (s, 1H, MeOCH), 3.37 (s, 6H, 2  $\times$  OCH<sub>3</sub>); <sup>13</sup>C{<sup>1</sup>H} NMR (126 MHz, CDCl<sub>3</sub>)  $\delta_C$  162.5 (d, *J*<sub>F-C</sub> = 251.8), 133.2 (d, *J*<sub>F-C</sub> = 3.6), 129.7 (d, *J*<sub>F-C</sub> = 8.5), 123.2 (d, *J*<sub>F-C</sub> = 9.4), 120.2 (d, *J*<sub>F-C</sub> = 24.8), 114.5 (d, *J*<sub>F-C</sub> = 20.9), 102.6, 54.0; <sup>19</sup>F NMR (470 MHz, CDCl<sub>3</sub>)  $\delta_F$  –111.4; HRMS (ESI<sup>+</sup>): calculated for [M + Na]<sup>+</sup> C<sub>9</sub>H<sub>10</sub>O<sub>2</sub>BrFNa, 270.9740; found, 270.9747.

**2-Bromo-1-(dimethoxymethyl)-3-fluorobenzene 11d.** General procedure 2 was followed using 2-bromo-3-fluorobenzaldehyde (5.00 mmol, 1.02 g), affording the title compound **11d** (1.18 g, 4.75 mmol) as a colorless oil in 95% yield. IR (neat): 2959, 2835, 1577, 1464, 1436, 1357, 1261, 1115, 1035, 1004, 825, 776 cm<sup>-1</sup>; <sup>1</sup>H NMR (500 MHz, CDCl<sub>3</sub>)  $\delta_H$  7.43–7.39 (m, 1H, ArH), 7.34–7.28 (m, 1H, ArH), 7.14–7.09 (m, 1H, ArH), 5.57 (s, 1H, MeOCH), 3.39 (s, 6H, 2  $\times$  OCH<sub>3</sub>); <sup>13</sup>C{<sup>1</sup>H} NMR (126 MHz, CDCl<sub>3</sub>)  $\delta_C$  159.2 (d, *J*<sub>F-C</sub> = 246.5), 139.4, 128.3 (d, *J*<sub>F-C</sub> = 7.9), 123.7 (d, *J*<sub>F-C</sub> = 3.3), 116.5 (d, *J*<sub>F-C</sub> = 22.6), 110.2 (d, *J*<sub>F-C</sub> = 21.3), 102.6 (d, *J*<sub>F-C</sub> = 3.6), 54.1; <sup>19</sup>F NMR (470 MHz, CDCl<sub>3</sub>)  $\delta_F$  –105.5 (dd, *J* = 8.3, 5.1); HRMS (ESI<sup>+</sup>): calculated for [M + Na]<sup>+</sup> C<sub>9</sub>H<sub>10</sub>O<sub>2</sub>BrFNa, 270.9740; found, 270.9741.

**General Procedure 3 for the Synthesis of Fluoro-2-formylphenyl Boronic Acids 10a–d by the Method of Kowalska et al.**<sup>19</sup> *n*-Butyllithium (2.5 M in THF, 1.15 equiv) was added dropwise (15 min) to a stirred solution of a fluoro-1-bromo-2-(dimethoxymethyl)-fluorobenzene **11a–d** (1.0 equiv) in anhydrous Et<sub>2</sub>O/THF (5:1 mixture, 0.33 M) under an inert N<sub>2</sub> atmosphere. The resultant solution was then cooled to –78 °C and stirred for 1 h, before addition of trimethyl borate (1.15 equiv). The reaction was warmed to room temperature and allowed to stir for 15 min, before acidifying to pH 3 using HCl (3 M, aq.). The reaction was diluted with Et<sub>2</sub>O, and the aqueous phase was extracted 3 times. The combined organics were washed with brine, dried over MgSO<sub>4</sub>, and concentrated to dryness, with the resultant crude product recrystallized from EtOAc/hexane to afford the desired formyl boronic acid **10a–d** (observed by NMR in tautomeric equilibrium with the related benzoxaborole minor product; see [Supporting Information](#)).

**(3-Fluoro-2-formylphenyl)boronic Acid 10a.** General procedure 3 was followed using 1-bromo-2-(dimethoxymethyl)-3-fluorobenzene **11a** (1.09 g, 4.41 mmol), affording the title compound **10a** (444 mg, 2.64 mmol) as a white solid in 60% yield. All characterization data were consistent with previous literature reports.<sup>24</sup> Mp: 125–128 °C (lit.<sup>24</sup> 127–129 °C); IR (neat): 3309, 3071, 2943, 1675, 1561, 1427, 1294, 1235, 1184, 1083, 908, 825, 793, 732 cm<sup>-1</sup>; <sup>1</sup>H NMR (500 MHz, acetone-*d*<sub>6</sub>)  $\delta$ <sub>H</sub> 10.38 (s, 1H, OCH, major), 8.42 (bs, 1H, BOH, minor), 7.77–7.61 (m, 1H, ArH, major), 7.54–7.41 (m, 2H major + 1H minor, ArH), 7.32 (bs, 2H, BOH, major), 7.26 (ddd, 1H, *J* = 11.2, 8.3, 1.1, ArH, major), 7.21 (ddd, 1H, *J* = 9.8, 7.9, 1.1, ArH, minor), 6.45 (s, 1H, HCO, minor), 6.13 (bs, 1H, COH, minor); <sup>11</sup>B NMR (375.5 MHz, acetone-*d*<sub>6</sub>)  $\delta$ <sub>B</sub> 31.2 (minor), 29.5 (major); <sup>19</sup>F NMR (470 MHz, acetone-*d*<sub>6</sub>)  $\delta$ <sub>F</sub> –120.8 (dd, *J* = 9.9, 4.2, minor), –122.4 (dd, *J* = 121.1, 5.3, major). HRMS (ESI<sup>–</sup>): calculated for [M – H<sub>2</sub>O + OMe]<sup>–</sup> C<sub>8</sub>H<sub>7</sub>FBO<sub>3</sub>, 181.0478; found, 181.0475. The <sup>13</sup>C NMR spectrum is not reported, as the signal intensity was too weak due to the combined effect of tautomerization, <sup>19</sup>F splitting, and the adjacent <sup>11</sup>B.

**(4-Fluoro-2-formylphenyl)boronic Acid 10b.** General procedure 3 was followed using 1-bromo-2-(dimethoxymethyl)-4-fluorobenzene **11b** (1.18 g, 4.75 mmol), affording the title compound **10b** (410 mg, 2.44 mmol) as a white solid in 55% yield. All characterization data were consistent with previous literature reports.<sup>17</sup> Mp: 123–126 °C (lit.<sup>17</sup> 123–125 °C); IR (neat): 3217, 1670, 1601, 1578, 1428, 1366, 1339, 1273, 1221, 1156, 1088, 1039, 886, 829, 768, 727 cm<sup>-1</sup>; <sup>1</sup>H NMR (500 MHz, acetone-*d*<sub>6</sub>)  $\delta$ <sub>H</sub> 10.33 (s, 1H, OCH, major), 8.28 (bs, 1H, BOH, minor), 7.93 (dd, 1H, *J* = 8.3, 5.9, ArH, major), 7.74 (bs, 2H, BOH, major), 7.74 (dd, 1H, *J* = 8.0, 5.7, ArH, minor), 7.66 (dd, 1H, *J* = 9.6, 7.2, ArH, major), 7.44 (td, *J* = 8.4, 2.7, ArH, major), 7.21–7.13 (m, 2H, ArH, minor); <sup>11</sup>B NMR (375.5 MHz, acetone-*d*<sub>6</sub>)  $\delta$ <sub>B</sub> 31.3 (minor), 28.9 (major); <sup>19</sup>F NMR (470 MHz, acetone-*d*<sub>6</sub>)  $\delta$ <sub>F</sub> –111.2 (minor), –111.7 (major); HRMS (ESI<sup>–</sup>): calculated for [M – H<sub>2</sub>O + OMe]<sup>–</sup> C<sub>8</sub>H<sub>7</sub>FBO<sub>3</sub>, 181.0478; found, 181.0471. The <sup>13</sup>C NMR spectrum is not reported, as the signal intensity was too weak due to the combined effect of tautomerization, <sup>19</sup>F splitting, and the adjacent <sup>11</sup>B.

**(5-Fluoro-2-formylphenyl)boronic Acid 10c.** General procedure 3 was followed using 1-bromo-2-(dimethoxymethyl)-5-fluorobenzene **11c** (1.16 g, 4.65 mmol), affording the title compound **10c** (388 mg, 2.31 mmol) as a white solid in 50% yield. Mp: 126–131 °C; IR (neat): 3309, 3069, 1669, 1596, 1571, 1419, 1344, 1226, 1167, 1103, 1044, 905, 797, 737, 692 cm<sup>-1</sup>; <sup>1</sup>H NMR (500 MHz, acetone-*d*<sub>6</sub>)  $\delta$ <sub>H</sub> 10.17 (s, 1H, OCH, major), 8.06 (m, 1H major + 1H minor, ArH), 7.84 (s, 2H, BOH, major), 7.56 (dd, 1H, *J* = 9.5, 2.7, ArH, major), 7.50 (dd, 1H, *J* = 8.3, 4.7, ArH, minor), 7.37 (td, 1H, *J* = 8.4, 2.7, ArH, major), 7.31–7.22 (m, 1H, ArH, minor), 6.27 (bs, 1H, OCH, minor) (some signals not observed due to low concentration of minor tautomer); <sup>19</sup>F NMR (375.5 MHz, acetone-*d*<sub>6</sub>)  $\delta$ <sub>B</sub> 28.9 (major), 20.2 (minor); <sup>19</sup>F NMR (470 MHz, acetone-*d*<sub>6</sub>)  $\delta$ <sub>F</sub> –106.7 (dd, *J* = 8.1, 8.1, major), –116.1 (minor); HRMS (ESI<sup>–</sup>): calculated for [M – H<sub>2</sub>O + OMe]<sup>–</sup> C<sub>8</sub>H<sub>7</sub>FBO<sub>3</sub>, 181.0478; found, 181.0473. The <sup>13</sup>C NMR spectrum is not reported, as the signal intensity was too weak due to the combined effect of tautomerization, <sup>19</sup>F splitting, and the adjacent <sup>11</sup>B.

**(6-Fluoro-2-formylphenyl)boronic Acid 10d.** General procedure 3 was followed using 1-bromo-2-(dimethoxymethyl)-6-fluorobenzene **11d** (1.18 g, 4.75 mmol), affording the title compound **10d** (223 mg, 1.33 mmol) as a white solid in 28% yield. Mp: 153–156 °C; IR (neat): 3255, 2848, 1674, 1601, 1567, 1451, 1324, 1301, 1231, 1213, 1160, 1040, 786, 730, 681 cm<sup>-1</sup>; <sup>1</sup>H NMR (500 MHz, acetone-*d*<sub>6</sub>)  $\delta$ <sub>H</sub> 10.04 (d, 1H, *J* = 2.3, OCH, major), 7.75 (d, 1H, *J* = 7.4, ArH, major), 7.64–7.54 (m, 1H major + 1H minor, ArH), 7.38–7.24 (m, 1H major + 1H minor, ArH), 7.06 (t, 1H, *J* = 8.1, ArH, major), 6.26 (bs, 1H, OCH, minor) (some signals not observed due to low concentration of minor tautomer); <sup>11</sup>B NMR (375.5 MHz, acetone-*d*<sub>6</sub>)  $\delta$ <sub>B</sub> 29.3 (major), 20.2 (minor); <sup>19</sup>F NMR (470 MHz, acetone-*d*<sub>6</sub>)  $\delta$ <sub>F</sub> –105.6 (minor), –106.1 (t, *J* = 6.7, major); HRMS (ESI<sup>–</sup>): calculated for [M – H<sub>2</sub>O + OMe]<sup>–</sup> C<sub>8</sub>H<sub>7</sub>FBO<sub>3</sub>, 181.0478; found, 181.0473. The <sup>13</sup>C NMR spectrum is not reported, as the signal

intensity was too weak due to the combined effect of tautomerization, <sup>19</sup>F splitting, and the adjacent <sup>11</sup>B.

**General Procedure 4 for the Synthesis of 2-Formyl Boronate Esters 6 and 3-F-6.** (1*S*,2*S*,3*R*,5*S*)-Pinanediol **3h** (1.0 equiv) was added to a stirred suspension of a 2-formylbenzene boronic acid **2** (1.1 equiv) in CHCl<sub>3</sub> (0.10 M). After 15 min, the reaction was diluted with an equivalent amount of CH<sub>2</sub>Cl<sub>2</sub> and passed through a silica plug. The plug was washed with CH<sub>2</sub>Cl<sub>2</sub> until no more product eluted, and the solvent was removed *in vacuo* to afford the desired boronate ester as a clear oil.

**2-((3*aS*,4*S*,6*S*,7*aR*)-3*a*,5,5-Trimethylhexahydro-4,6-methanobenzo[d][1,3,2]dioxaborol-2-yl)benzaldehyde 6.** General procedure 4 was followed using 2-FPBA **2** (83 mg, 0.55 mmol) and (1*S*,2*S*,3*R*,5*S*)-pinanediol **3h** (85 mg, 0.50 mmol), affording the title compound (3*aS*,4*S*,6*S*,7*aR*)-**6** (110 mg, 0.39 mmol) as a clear oil in 70% yield.  $[\alpha]_D^{23} = +18$  (c 1.0, CHCl<sub>3</sub>); IR (neat): 2921, 2870, 1693, 1593, 1488, 1370, 1337, 1236, 1076, 754, 666 cm<sup>-1</sup>; <sup>1</sup>H NMR (500 MHz, CDCl<sub>3</sub>)  $\delta$  10.55 (s, 1H, OCH), 7.98–7.95 (m, 1H, ArH), 7.90–7.86 (m, 1H, ArH), 7.62–7.53 (m, 2H, ArH), 4.52 (dd, 1H, *J* = 8.8, 1.9 H-7*a*), 2.48–2.39 (m, 1H, H-7), 2.32–2.23 (m, 1H, H-8), 2.16 (dd, 1H, *J* = 6.0, 4.9, H-4), 2.04–1.94 (m, 2H, H-6 + H-7), 1.53 (s, 3H, H-9), 1.33 (d, 1H, *J* = 10.8, H-8), 1.32 (s, 3H, H-10/11), 0.90 (s, 3H, H-10/11); <sup>13</sup>C{<sup>1</sup>H} NMR (126 MHz, CDCl<sub>3</sub>)  $\delta$ <sub>C</sub> 194.7, 141.4, 135.7, 133.1, 131.9 (deduced from HMBC, confirmed by –15 °C VT NMR), 130.8, 128.0, 86.9, 78.6, 51.5, 39.7, 38.4, 35.5, 28.7, 27.2, 26.6, 24.2; <sup>11</sup>B NMR (375.5 MHz, CDCl<sub>3</sub>)  $\delta$ <sub>B</sub> 30.7; HRMS (ESI<sup>+</sup>): calculated for [M + Na]<sup>+</sup> C<sub>17</sub>H<sub>21</sub>BO<sub>3</sub>Na, 307.1479; found, 307.1493.

**2-Fluoro-6-((3*aS*,4*S*,6*S*,7*aR*)-3*a*,5,5-Trimethylhexahydro-4,6-methanobenzo[d][1,3,2]dioxaborol-2-yl)benzaldehyde 3-F-6.** General procedure 4 was followed using 3-fluoro-2-FPBA **10a** (47 mg, 0.28 mmol) and (1*S*,2*S*,3*R*,5*S*)-pinanediol **3h** (96 mg, 0.25 mmol), affording the title compound (3*aS*,4*S*,6*S*,7*aR*)-3-F-**6** (73 mg, 0.39 mmol) as a clear oil in 96% yield.  $[\alpha]_D^{23} = +20$  (c 1.0, CHCl<sub>3</sub>); IR (neat): 2918, 2869, 1695, 1568, 1480, 1439, 1339, 1238, 1029, 794, 666 cm<sup>-1</sup>; <sup>1</sup>H NMR (500 MHz, CDCl<sub>3</sub>)  $\delta$  10.43 (d, 1H, *J* = 1.0, OCHC), 7.58 (ddd, 1H, *J* = 8.3, 7.2, 5.2, ArH), 7.40 (d, 1H, *J* = 7.2, ArH), 7.17 (ddd, 1H, *J* = 10.6, 8.3, 1.0, ArH), 4.55 (dd, 1H, *J* = 8.8, 2.0, H-7*a*), 2.48–2.38 (m, 1H, H-7), 2.37–2.27 (m, 1H, H-8), 2.17–2.11 (m, 1H, H-4), 2.06–1.96 (m, 2H, H-6 and H-7), 1.58 (s, 3H, H-9), 1.55 (d, 1H, *J* = 10.8, H-8), 1.34 (s, 3H, H-10/11), 0.91 (s, 3H, H-10/11); <sup>13</sup>C{<sup>1</sup>H} NMR (126 MHz, CDCl<sub>3</sub>)  $\delta$ <sub>C</sub> 189.0 (d, *J*<sub>F–C</sub> = 6.2), 164.3 (d, *J*<sub>F–C</sub> = 259.8), 135.7 (d, *J*<sub>F–C</sub> = 8.7), 129.1 (d, *J*<sub>F–C</sub> = 3.8), 127.8 (d, *J*<sub>F–C</sub> = 6.9), 121.6 (deduced from HMBC), 117.5 (d, *J*<sub>F–C</sub> = 20.9), 86.6, 78.8, 51.7, 39.7, 38.5, 35.5, 28.4, 27.3, 26.5, 24.2; <sup>11</sup>B NMR (375.5 MHz, CDCl<sub>3</sub>)  $\delta$ <sub>B</sub> 30.9; <sup>19</sup>F NMR (470 MHz, CDCl<sub>3</sub>)  $\delta$ <sub>F</sub> –121.0 (dd, *J* = 10.5, 5.3); HRMS (ESI<sup>+</sup>): calculated for [M + Na]<sup>+</sup> C<sub>17</sub>H<sub>20</sub>BO<sub>3</sub>FNa, 325.1385; found, 325.1381.

**General Procedure 5 for the Synthesis of *tert*-Butyl Sulfiniminoboronates 4h and 5h.** *tert*-Butyl sulfinamide **1a** (61 mg, 0.50 mmol, 1.0 equiv) was added to a stirred suspension of 2-formylbenzene boronic acid **2** (90 mg, 0.60 mmol, 1.2 equiv) and MgSO<sub>4</sub> (1.00 g) in CHCl<sub>3</sub>, and the reaction was stirred for 2 h, before (1*R*,2*R*,3*S*,5*R*)-pinanediol **3h** (111 mg, 0.65 mmol, 1.3 equiv) was added. After 10 min, the reaction was filtered and concentrated to dryness *in vacuo*, and the residue was purified by chromatography (0.5% MeOH in 1:1 DCM/*n*-hexane), affording the desired sulfiniminoboronate ester as a clear oil. The low stability of these complexes to the purification conditions employed meant that small amounts of 2-formyl boronate ester **6** remained.

**(*R*)-2-Methyl-N-((*E*)-2-((3*aR*,4*R*,6*R*,7*aS*)-3*a*,5,5-trimethylhexahydro-4,6-methanobenzo[d][1,3,2]dioxaborol-2-yl)-benzylidene)propane-2-sulfinamide 4h.** General procedure 5 was followed using (*R*)-Ellman's sulfinamide **1a**, affording the title compound (*R*<sub>S</sub>,3*aR*,4*R*,6*R*,7*aS*)-**4h** (24 mg, 0.062 mmol) as a clear oil in 12% yield, as a 89:11 mixture with the related formyl boronate ester (3*aR*,4*R*,6*R*,7*aS*)-**6**. <sup>1</sup>H NMR (500 MHz, CDCl<sub>3</sub>)  $\delta$ <sub>H</sub> 9.36 (s, 1H, NCH), 8.13–8.06 (m, 1H, ArH), 7.94–7.88 (m, 1H, ArH), 7.54–7.46 (m, 2H, ArH), 4.51 (dd, 1H, *J* = 8.8, 2.0, H-7*a*), 2.48–2.37 (m, 1H, H-7), 2.29–2.21 (m, 1H, H-8), 2.18 (dd, 1H, *J* = 6.1, 5.1, H-4),



2.02 (ddd, 1H,  $J = 14.7, 3.4, 2.0$ , H-7), 1.97–1.97 (m, 1H, H-6), 1.51 (s, 3H, H-9), 1.30 (s, 3H, H-10/11), 1.26 (s, 9H, *tert*-butyl), 1.23 (d, 1H,  $J = 10.9$ , H-8), 0.88 (s, 3H, H-10/11);  $^{11}\text{B}$  NMR (375.5 MHz,  $\text{CDCl}_3$ )  $\delta$  30.5; HRMS (ESI+): calculated for  $[\text{M} + \text{H}]^+$   $\text{C}_{21}\text{H}_{31}\text{BNO}_3\text{S}$ , 388.2116, Found 388.2118; calculated for  $[\text{M} + \text{Na}]^+$   $\text{C}_{21}\text{H}_{30}\text{BNO}_3\text{SNa}$ , 410.1936; found, 410.1940. IR and specific rotation data were not acquired due to the presence of significant residual (3aR,4R,6R,7aS)-6.  $^{13}\text{C}$  NMR spectra are not reported, as this impurity and the adjacent  $^{11}\text{B}$  nucleus led to unassignable spectra.

**(S)-2-Methyl-N-((E)-2-((3aR,4R,6R,7aS)-3a,5,5-trimethylhexahydro-4,6-methanobenzo[d][1,3,2]dioxaborol-2-yl)-benzylidene)propane-2-sulfonamide 5h.** General procedure 5 was followed using (S)-Ellman's sulfinamide **1a**, affording the title compound ( $S_S$ , 3aR,4R,6R,7aS)-**5h** (37 mg, 0.096 mg) as a clear oil in 19% yield, as a 96:4 mixture with the related formyl boronate ester (3aR,4R,6R,7aS)-6.  $^1\text{H}$  NMR (500 MHz,  $\text{CDCl}_3$ )  $\delta$  9.27 (s, 1H, NCH), 8.08–8.03 (m, 1H, ArH), 7.90–7.83 (m, 1H, ArH), 7.54–7.47 (m, 2H, ArH), 4.51 (dd, 1H,  $J = 8.7, 1.9$ , H-7a), 2.49–2.38 (m, 1H, H-7), 2.32–2.21 (m, 1H, H-8), 2.17 (dd, 1H,  $J = 6.0, 5.0$ , H-4), 2.09–1.91 (m, H-7 + H-6), 1.51 (s, 3H, H-9), 1.31 (s, 3H, H-10/11), 1.28–1.22 (m, 12H, *tert*-butyl + H-8), 0.88 (s, 3H, H-10/11);  $^{11}\text{B}$  NMR (375.5 MHz,  $\text{CDCl}_3$ )  $\delta$  31.2; HRMS (ESI+): calculated for  $[\text{M} + \text{H}]^+$   $\text{C}_{21}\text{H}_{31}\text{BNO}_3\text{S}$ : 388.2116, Found 388.2112; calculated for  $[\text{M} + \text{Na}]^+$   $\text{C}_{21}\text{H}_{30}\text{BNO}_3\text{S}$ , 410.1936; found, 410.1937; IR and specific rotation data were not acquired due to the presence of significant residual (3aR,4R,6R,7aS)-6.  $^{13}\text{C}$  NMR spectra are not reported, as this impurity and the adjacent  $^{11}\text{B}$  nucleus led to unassignable spectra.

**General Procedure 6 for the Three-Component Chiral Derivatization of Sulfinamides.** A 2-Formylbenzene boronic acid (0.12 mmol, 1.2 equiv) and anhydrous  $\text{MgSO}_4$  (200 mg) were added to a stirred solution of sulfinamide **1a–h** (0.10 mmol, 1.0 equiv) in  $\text{CDCl}_3$  (1.0 mL, TMS internal standard). The reaction was stirred at room temperature for 1 h, before addition of (1R, 2R, 3S, 5R)-pinanediol **3h** (1.0 M in  $\text{CDCl}_3$ , 130  $\mu\text{L}$ , 1.3 equiv). The reaction was then stirred for a further 10 min, before the reaction was filtered and the 500 MHz  $^1\text{H}$  NMR spectrum and/or 470 MHz  $^{19}\text{F}$  spectrum of the resultant iminoboronate esters were acquired. The acquired  $^1\text{H}$  and  $^{19}\text{F}\{^1\text{H}\}$  NMR spectra can be found in the associated [Supporting Information](#).

Scaemic and racemic samples of Ellman's sulfinamide **1a** were prepared from commercially available enantiopure samples of (R)- and (S)-*tert*-butyl sulfinamide **1a**. 0.1 M solutions of enantiopure **1a** in  $\text{CDCl}_3$  were prepared and then combined to produce scaemic samples of **1a**, the *ee* of which was determined by the ratio of enantiopure stock solutions.

## ■ ASSOCIATED CONTENT

### Supporting Information

The Supporting Information is available free of charge at <https://pubs.acs.org/doi/10.1021/acs.joc.9b02473>.

$^1\text{H}$ ,  $^{13}\text{C}$ ,  $^{19}\text{F}$ , and  $^{11}\text{B}$  NMR spectra of all compounds and spectra of three-component mixtures (PDF)

## ■ AUTHOR INFORMATION

### Corresponding Authors

\*E-mail: [s.d.bull@bath.ac.uk](mailto:s.d.bull@bath.ac.uk).

\*E-mail: [t.d.james@bath.ac.uk](mailto:t.d.james@bath.ac.uk).

### ORCID

Robin R. Groleau: 0000-0003-0213-5198

Tony D. James: 0000-0002-4095-2191

Steven D. Bull: 0000-0001-8244-5123

### Notes

The authors declare no competing financial interest.

## ■ ACKNOWLEDGMENTS

This work was supported by the EPSRC Centre for Doctoral Training in Catalysis (EP/L016443/1).

## ■ REFERENCES

- (1) (a) Davis, F. A.; Reddy, R. E.; Szweczyk, J. M.; Reddy, G. V.; Portonovo, P. S.; Zhang, H.; Fanelli, D.; Reddy, R. T.; Zhou, P.; Carroll, P. J. Asymmetric Synthesis and Properties of Sulfinimines (Thiooxime S-Oxides). *J. Org. Chem.* **1997**, *62*, 2555–2563. (b) Dong, H.-Q.; Xu, M.-H.; Feng, C.-G.; Sun, X.-W.; Lin, G.-Q. Recent applications of chiral *N-tert*-butanesulfinyl imines, chiral diene ligands and chiral sulfur-olefin ligands in asymmetric synthesis. *Org. Chem. Front.* **2015**, *2*, 73–89. (c) Davis, F. A. Adventures in sulfur-nitrogen chemistry. *J. Org. Chem.* **2006**, *71*, 8993–9003. (d) Zhou, P.; Chen, B.-C.; Davis, F. A. Recent advances in asymmetric reactions using sulfinimines (*N*-sulfinyl imines). *Tetrahedron* **2004**, *60*, 8003–8030.
- (2) (a) Robak, M. T.; Herbage, M. A.; Ellman, J. A. Synthesis and Applications of *tert*-Butanesulfinamide. *Chem. Rev.* **2010**, *110*, 3600–3740. (b) Zhang, Y.; Chitale, S.; Goyal, N.; Li, G.; Han, Z. S.; Shen, S.; Ma, S.; Grinberg, N.; Lee, H.; Lu, B. Z.; Senanayake, C. H. Asymmetric Synthesis of Sulfinamides Using (–)-Quinine as Chiral Auxiliary. *J. Org. Chem.* **2012**, *77*, 690–695.
- (3) (a) Evans, J. W.; Ellman, J. A. Stereoselective Synthesis of 1,2-Disubstituted-Amino Alcohols by Nucleophilic Addition to *N-tert*-Butanesulfinyl  $\alpha$ -Alkoxyaldimines. *J. Org. Chem.* **2003**, *68*, 9948–9957. (b) Liu, Z.-J.; Mei, Y.-Q.; Liu, J.-T. A practical diastereoselective synthesis of  $\beta$ -hydroxy- $\beta$ -trifluoromethyl imines. *Tetrahedron* **2007**, *63*, 855–860. (c) Lee, Y.; Akiyama, K.; Gillingham, D. G.; Brown, M. K.; Hoveyda, A. H. Highly Site- and Enantioselective Cu-Catalyzed Allylic Alkylation Reactions with Easily Accessible Vinylaluminum Reagents. *J. Am. Chem. Soc.* **2008**, *130*, 446–447. (d) Barrow, J. C.; Ngo, P. L.; Pellicore, J. M.; Selnick, H. G.; Nantermet, P. G. A facile three-step synthesis of 1,2-amino alcohols using the Ellman homochiral *tert*-butylsulfinamide. *Tetrahedron Lett.* **2001**, *42*, 2051–2054. (e) Viso, A.; Fernández De La Pradilla, R.; López-Rodríguez, M. L.; García, A.; Flores, A.; Alonso, M. Fine-Tuned Aminal Cleavage: A Concise Route to Differentially Protected Enantiopure  $\gamma,\delta$ -Diamino Esters. *J. Org. Chem.* **2004**, *69*, 1542–1547. (f) Kells, K. W.; Chong, J. M. Addition of  $\text{Bu}_3\text{SnLi}$  to *tert*-Butanesulfinimines as an Efficient Route to Chiral, Nonracemic  $\alpha$ -Aminoorganostannanes. *Org. Lett.* **2003**, *5*, 4215–4218. (g) Jayatilaka, L. P.; Deb, M.; Standaert, R. F. Asymmetric Synthesis and Translational Competence of L- $\alpha$ -(1-Cyclobutenyl)glycine. *Org. Lett.* **2004**, *6*, 3659–3662. (h) Tang, T. P.; Ellman, J. A. Asymmetric synthesis of  $\beta$ -amino acid derivatives incorporating a broad range of substitution patterns by enolate additions to *tert*-butanesulfinyl imines. *J. Org. Chem.* **2002**, *67*, 7819–7832.
- (4) (a) Oldenhuis, N. J.; Dong, V. M.; Guan, Z. From Racemic Alcohols to Enantiopure Amines: Ru-Catalyzed Diastereoselective Amination. *J. Am. Chem. Soc.* **2014**, *136*, 12548–12551. (b) Diné, P.; Sadhukhan, A.; Blomkvist, B. Chiral Sulfinamides as Highly Enantioselective Organocatalysts. *ChemCatChem* **2014**, *6*, 3063–3066. (c) Zhang, Z.-M.; Chen, P.; Li, W.; Niu, Y.; Zhao, X.-L.; Zhang, J. A New Type of Chiral Sulfinamide Monophosphine Ligands: Stereodivergent Synthesis and Application in Enantioselective Gold-(I)-Catalyzed Cycloaddition Reactions. *Angew. Chem., Int. Ed.* **2014**, *53*, 4350–4354.
- (5) Viswanadhan, V. N.; Ghose, A. K.; Hanna, N. B.; Matsumoto, S. S.; Avery, T. L.; Revankar, G. R.; Robins, R. K. Analysis of the in Vitro Antitumor Activity of Novel Purine-6-sulfenamide, -sulfinamide, and -sulfonamide Nucleosides and Certain Related Compounds Using a Computer-Aided Receptor Modelling Procedure. *J. Med. Chem.* **1991**, *34*, 526–532.
- (6) (a) Keceli, G.; Toscano, J. P. Reactivity of Nitroxyl-Derived Sulfinamides. *Biochemistry* **2012**, *51*, 4206–4216. (b) Keceli, G.; Moore, C. D.; Labonte, J. W.; Toscano, J. P. NMR Detection and Study of Hydrolysis of HNO-Derived Sulfinamides. *Biochemistry*

2013, 52, 7387–7396. (c) Keceli, G.; Toscano, J. P. Reactivity of C-Terminal Cysteines with HNO. *Biochemistry* **2014**, 53, 3689–3698.

(7) (a) Cogan, D. A.; Liu, G.; Kim, K.; Backes, B. J.; Ellman, J. A. Catalytic Asymmetric Oxidation of *tert*-Butyl Disulfide. Synthesis of *tert*-Butanesulfinamides, *tert*-Butyl Sulfoxides, and *tert*-Butylsulfinimines. *J. Am. Chem. Soc.* **1998**, 120, 8011–8019. (b) Weix, D. J.; Ellman, J. A. (*R*<sub>S</sub>)-(+)-2-Methyl-2-propanesulfinamide [*tert*-Butanesulfinamide]. *Org. Synth.* **2005**, 82, 157–165.

(8) Liao, J.; Sun, X.; Cui, X.; Yu, K.; Zhu, J.; Deng, J. Facile Optical Resolution of *tert*-Butanethiosulfinate by Molecular Complexation with (*R*)-BINOL and Study of Chiral Discrimination of the Diastereomeric Complexes. *Chem. - Eur. J.* **2003**, 9, 2611–2615.

(9) Savile, C. K.; Magloire, V. P.; Kazlauskas, R. J. Subtilisin-Catalyzed Resolution of *N*-Acyl Arylsulfinamides. *J. Am. Chem. Soc.* **2005**, 127, 2104–2113.

(10) Revankar, G. R.; Hanna, N. B.; Imamura, N.; Lewis, A. F.; Larson, S. B.; Finch, R. A.; Avery, T. L.; Robins, R. K. Synthesis and *in Vivo* Antitumor Activity of 2-Amino-9*H*-purine-6-sulfenamide-, sulfinamide, and sulfonamide and Related Purine Ribonucleosides. *J. Med. Chem.* **1990**, 33, 121–128.

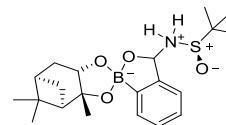
(11) (a) Pirkle, W. H.; Beare, S. D.; Muntz, R. L. Optically Active Solvents for Nuclear Magnetic Resonance. X. Enantiomeric Non-equivalence of Sulfinamides, Sulfinates, Sulfites, Thiosulfinates, Phosphine Oxides, and Amine Oxides. *J. Am. Chem. Soc.* **1969**, 91, 4575. (b) Ema, T.; Tanida, D.; Sakai, T. Versatile and Practical Macrocyclic Reagent with Multiple Hydrogen-Bonding Sites for Chiral Discrimination in NMR. *J. Am. Chem. Soc.* **2007**, 129, 10591–10596.

(12) (a) Pérez-Fuertes, Y.; Kelly, A. M.; Johnson, A. L.; Arimori, S.; Bull, S. D.; James, T. D. Simple Protocol for NMR Analysis of the Enantiomeric Purity of Primary Amines. *Org. Lett.* **2006**, 8, 609–612. (b) Kelly, A. M.; Pérez-Fuertes, Y.; Arimori, S.; Bull, S. D.; James, T. D. Simple Protocol for NMR Analysis of the Enantiomeric Purity of Diols. *Org. Lett.* **2006**, 8, 1971–1974. (c) Kelly, A. M.; Bull, S. D.; James, T. D. Simple chiral derivatisation protocols for NMR analysis of the enantiopurity of 1,2-diphenylethane-1,2-diamine and *N*-Boc-cyclohexane-1,2-diamine. *Tetrahedron: Asymmetry* **2008**, 19, 489–494. (d) Powell, M. E.; Kelly, A. M.; Bull, S. D.; James, T. D. A simple chiral derivatisation protocol for <sup>1</sup>H NMR spectroscopic analysis of the enantiopurity of *O*-silyl-1,2-amino alcohols. *Tetrahedron Lett.* **2009**, 50, 876–879. (e) Pérez-Fuertes, Y.; Kelly, A. M.; Fossey, J. S.; Powell, M. E.; Bull, S. D.; James, T. D. Simple protocols for NMR analysis of the enantiomeric purity of chiral primary amines. *Nat. Protoc.* **2008**, 3, 210–214. (f) Kelly, A. M.; Pérez-Fuertes, Y.; Fossey, J. S.; Lozano Yeste, S.; Bull, S. D.; James, T. D. Simple protocols for NMR analysis of the enantiomeric purity of chiral diols. *Nat. Protoc.* **2008**, 3, 215–219. (g) Tickell, D. A.; Mahon, M. F.; Bull, S. D.; James, T. D. Simple Protocol for NMR Analysis of the Enantiomeric Purity of Chiral Hydroxylamines. *Org. Lett.* **2013**, 15, 860–863. (h) Tickell, D. A.; Lampard, E. V.; Lowe, J. P.; James, T. D.; Bull, S. D. A Protocol for NMR Analysis of the Enantiomeric Excess of Chiral Diols Using an Achiral Diboronic Acid Template. *J. Org. Chem.* **2016**, 81, 6795–6799.

(13) (a) Su, H. Y.; Gorelik, D.; Taylor, M. S. Chiral phosphine ligand libraries based on the Bull-James three-component supramolecular assembly. *Supramol. Chem.* **2019**, 31, 190–202. (b) Fossey, J. S.; Anslyn, E. V.; Brittain, W. D. G.; Bull, S. D.; Chapin, B. M.; Cécile, C.; Le Duff, S.; James, T. D.; Lees, G.; Lim, S.; Lloyd, J. A. C.; Manville, C. V.; Payne, D. T.; Roper, K. A. Rapid Determination of Enantiomeric Excess via NMR Spectroscopy: A Research-Informed Experiment. *J. Chem. Educ.* **2017**, 94, 79–84. (c) Chapin, B. M.; Metola, P.; Lynch, V. M.; Stanton, J. F.; James, T. D.; Anslyn, E. V. Structural and Thermodynamic Analysis of a Three-Component Assembly Forming *ortho*-Iminophenylboronate Esters. *J. Org. Chem.* **2016**, 81, 8319–8330.

(14) Higashibayashi, S.; Tohmiya, H.; Mori, T.; Hashimoto, K.; Nakata, M. Synthesis of Sulfinimines by Direct Condensation of Sulfinamides with Aldehydes Using Cs<sub>2</sub>CO<sub>3</sub> as an Activating and Dehydrating Reagent. *Synlett* **2004**, 3, 457–460.

(15) It is possible that the lack of reactivity of the aldehyde functionality of boronate ester **6** toward imine formation in the three-component reaction may be due to the increased Lewis acidity of its boronic ester group (relative to boronic acid **2**) which acts to stabilize the carbinolamine intermediate **12** through an intramolecular B–O bond that prevents its subsequent dehydration to afford an imine.



**12**  
(Derived from (*R*)-**1a**)

(16) (*rac*)-Sulfinamides **1c–h** were synthesized using the methods described by: Di, J.; He, H.; Wang, F.; Xue, F.; Liu, X.-Y.; Qin, Y. Regiospecific alkyl addition of (hetero)arene-fused thiophenes enabled by a visible-light-mediated photocatalytic desulfuration approach. *Chem. Commun.* **2018**, 54, 4692–4695.

(17) Yeste, S. L.; Powell, M. E.; Bull, S. D.; James, T. D. Simple Chiral Derivatization Protocols for <sup>1</sup>H NMR and <sup>19</sup>F NMR Spectroscopic Analysis of the Enantiopurity of Chiral Diols. *J. Org. Chem.* **2009**, 74, 427–430.

(18) Hamaguchi, N.; Okuno, Y.; Oe, Y.; Ohta, T. A simple quantitative chiral analysis of amino acid esters by fluorine-19 nuclear magnetic resonance using the modified James-Bull method. *Chirality* **2019**, 31, 34–40.

(19) Fluorinated 2-FPBA analogues **10a–d** were synthesized using methods described by: Kowalska, K.; Adamczyk-Woźniak, A.; Gajowiec, P.; Gierczyk, B.; Kaczorowska, E.; Popenda, Ł.; Schroeder, G.; Sikorski, A.; Sporyński, A. Fluoro-substituted 2-formylphenylboronic acids: Structures, properties and tautomeric equilibria. *J. Fluorine Chem.* **2016**, 187, 1–8.

(20) Wang, L.; Dai, C.; Burroughs, S. K.; Wang, S. L.; Wang, B. Arylboronic Acid Chemistry under Electrospray Conditions. *Chem. - Eur. J.* **2013**, 19, 7587–7594.

(21) Ma, L.; Li, G.; Huang, J.; Zhu, J.; Tang, Z. Synthesis of asymmetrical thioethers with sulfinamides as the sulfonylation agent under metal-free conditions. *Tetrahedron Lett.* **2018**, 59, 4255–4258.

(22) Kowalczyk, R.; Edmunds, A. J. F.; Hall, R. G.; Bolm, C. Synthesis of CF<sub>3</sub>-Substituted Sulfoximines from Sulfonimidoyl Fluorides. *Org. Lett.* **2011**, 13, 768–771.

(23) Wang, B.; Xu, T.; Zhu, L.; Lan, Y.; Wang, J.; Lu, N.; Wei, Z.; Lin, Y.; Duan, H. Highly Enantioselective Nitro-Mannich Reaction of Ketimines Under Phase-Transfer Catalysis. *Org. Chem. Front.* **2017**, 4, 1266–1271.

(24) Lulinski, S. L.; Madura, I.; Serwatowski, J.; Szatyłowicz, H.; Zachara, J. A tautomeric equilibrium between functionalized 2-formylphenylboronic acids and corresponding 1,3-dihydro-1,3-dihydroxybenzo [*c*][2,1]oxaboroles. *New J. Chem.* **2007**, 31, 144–154.